ISSN 0021-9673

VOL. 542 NO. 2 APRIL 12, 1991

THIS ISSUE COMPLETES VOL. 542

JOURNAL OF CHROMATOGRAPHY

INCLUDING ELECTROPHORESIS AND OTHER SEPARATION METHODS

ELSEVIER

JOURNAL OF CHROMATOGRAPHY

Scope. The *Journal of Chromatography* publishes papers on all aspects of chromatography, electrophoresis and related methods. Contributions consist mainly of research papers dealing with chromatographic theory, instrumental development and their applications. The section *Biomedical Applications*, which is under separate editorship, deals with the following aspects: developments in and applications of chromatographic and electrophoretic techniques related to clinical diagnosis or alterations during medical treatment; screening and profiling of body fluids or tissues with special reference to metabolic disorders; results from basic medical research with direct consequences in clinical practice; drug level monitoring and pharmacokinetic studies; clinical toxicology; analytical studies in occupational medicine.

Submission of Papers. Manuscripts (in English; *four* copies are required) should be submitted to: Editorial Office of *Journal of Chromatography*, P.O. Box 681, 1000 AR Amsterdam, The Netherlands, Telefax (+31-20) 5862 304, or to: The Editor of *Journal of Chromatography, Biomedical Applications*, P.O. Box 681, 1000 AR Amsterdam, The Netherlands. Review articles are invited or proposed by letter to the Editors. An outline of the proposed review should first be forwarded to the Editors for preliminary discussion prior to preparation. Submission of an article is understood to imply that the article is original and unpublished and is not being considered for publication elsewhere. For copyright regulations, see below.

Subscription Orders. Subscription orders should be sent to: Elsevier Science Publishers B.V., P.O. Box 211, 1000 AE Amsterdam, The Netherlands, Tel. (+31-20) 5803 911, Telex 18582 ESPA NL, Telefax (+31-20) 5803 598. The *Journal of Chromatography* and the *Biomedical Applications* section can be subscribed to separately.

Publication. The *Journal of Chromatography* (incl. *Biomedical Applications*) has 38 volumes in 1991. The subscription prices for 1991 are:

J. Chromatogr. (incl. *Cum. Indexes, Vols. 501–550*) + *Biomed. Appl.* (Vols. 535–572):
Dfl. 7220.00 plus Dfl. 1140.00 (p.p.h.) (total *ca.* US$ 4976.25)

J. Chromatogr. (incl. *Cum. Indexes, Vols. 501–550*) only (Vols. 535–561):
Dfl. 5859.00 plus Dfl. 810.00 (p.p.h.) (total *ca.* US$ 3969.75)

Biomed. Appl. only (Vols. 562–572):
Dfl. 2387.00 plus Dfl. 330.00 (p.p.h.) (total *ca.* US$ 1617.25).

Our p.p.h. (postage, package and handling) charge includes surface delivery of all issues, except to subscribers in Argentina, Australia, Brasil, Canada, China, Hong Kong, India, Israel, Malaysia, Mexico, New Zealand, Pakistan, Singapore, South Africa, South Korea, Taiwan, Thailand and the U.S.A. who receive all issues by air delivery (S.A.L. — Surface Air Lifted) at no extra cost. For Japan, air delivery requires 50% additional charge; for all other countries airmail and S.A.L. charges are available upon request. Back volumes of the *Journal of Chromatography* (Vols. 1–534) are available at Dfl. 208.00 (plus postage). Claims for missing issues will be honoured, free of charge, within three months after publication of the issue. Customers in the U.S.A. and Canada wishing information on this and other Elsevier journals, please contact Journal Information Center, Elsevier Science Publishing Co. Inc., 655 Avenue of the Americas, New York, NY 10010, U.S.A., Tel. (+1-212) 633 3750, Telefax (+1-212) 633 3990.

Abstracts/Contents Lists published in Analytical Abstracts, Biochemical Abstracts, Biological Abstracts, Chemical Abstracts, Chemical Titles, Chromatography Abstracts, Clinical Chemistry Lookout, Current Contents/Life Sciences, Current Contents/Physical, Chemical & Earth Sciences, Deep-Sea Research/Part B: Oceanographic Literature Review, Excerpta Medica, Index Medicus, Mass Spectrometry Bulletin, PASCAL-CNRS, Pharmaceutical Abstracts, Referativnyi Zhurnal, Research Alert, Science Citation Index and Trends in Biotechnology.

See inside back cover for Publication Schedule, Information for Authors and information on Advertisements.

0021-9673/91/$03.50

Printed in The Netherlands

VOL. 542, NO. 2 JOURNAL OF CHROMATOGRAPHY APRIL 12, 1991

CONTENTS

(Abstracts/Contents Lists published in Analytical Abstracts, Biochemical Abstracts, Biological Abstracts, Chemical Abstracts, Chemical Titles, Chromatography Abstracts, Current Contents/Life Sciences, Current Contents/Physical, Chemical & Earth Sciences, Deep-Sea Research/Part B: Oceanographic Literature Review, Excerpta Medica, Index Medicus, Mass Spectrometry Bulletin, PASCAL-CNRS, Referativnyi Zhurnal, Research Alert and Science Citation Index)

REGULAR PAPERS

Liquid Chromatography

(Continued overleaf)

In articles with more than one author, the name of the author to whom correspondence should be addressed is indicated in the article heading by a 6-pointed asterisk (*)

For Superior Chiral Separation From Analytical To Preparative.

The finest from DAICEL……

Why look beyond DAICEL? We have developed the finest CHIRALCEL, CHIRALPAK and CROWNPAK with up to 17 types of HPLC columns, all providing superior resolution of racemic compounds.

NEW CHIRALPAK AS

● CHIRALPAK AS

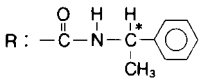

for β-Lactam antibiotics

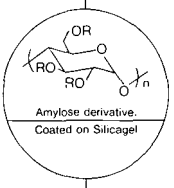

NEW CHIRALPAK AD

● CHIRALPAK AD

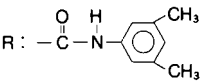

4-Acetoxy-2-azetidine

Eluent : Hexane/Ethanol = 8/2
Flow rate : 1.0mℓ/min
Temperature : r.t.
Detection : UV 254nm

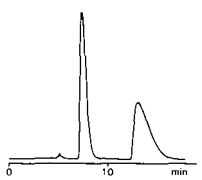

Oxyphencyclimine

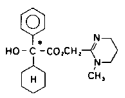

Eluent : Hexane/2-Propanol = 9/1
Flow rate : 1.0mℓ/min
Temperature : r.t.
Detection : UV 254nm

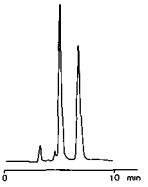

Ofloxacine methyl ester

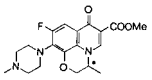

Eluent : Hexane/EtOH = 8/2
Flow rate : 1.2mℓ/min
Temperature : 40°C
Detection : UV 254nm

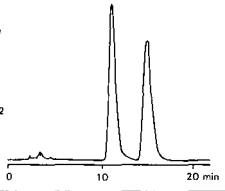

Verapamil

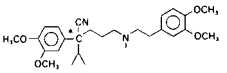

Eluent : Hexane/2-Propanol = 9/1
Flow rate : 1.0mℓ/min
Temperature : r.t.
Detection : UV 254nm

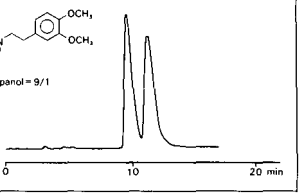

Analytical column 0.46cm × 25cm(10μm)

CHIRALCEL OA
OB
OC
OD
OJ
OF
OG
OK

CHIRALPAK AS
AD

Normal Phase

Semi-preparative column 2cm × 25cm(10μm)

You can have Pure enantiomer quickly!!

■Separation Service

- A pure enantiomer separation in the amount of 100g~10kg is now available.
- Please contact us for additional information regarding the manner of use and application of our chiral columns and how to procure our separation service.

DAICEL CHEMICAL INDUSTRIES, LTD.

chiral chemicals division.
8-1, Kasumigaseki 3-chome, Chiyoda-ku, Tokyo 100, Japan Phone: 03 (507) 3151 FAX: 03 (507) 3193

DAICEL(U.S.A.), INC.
Fort Lee Executive Park
Two Executive Drive, Fort Lee,
New Jersey 07024
Phone: (201) 461-4466
FAX: (201) 461-2776

DAICEL(U.S.A.), INC.
23456 Hawthorne Blvd.
Bldg. 5, Suit 130
Torrance, CA 90505
Phone: (213) 791-2030
FAX: (213) 791-2031

DAICEL(EUROPA)GmbH
Oststr. 22
4000 Düsseldorf 1, F.R. Germany
Phone: (211) 369848
Telex: (41) 8588042 DCEL D
FAX: (211) 364429

DAICEL CHEMICAL(ASIA)PTE. LTD.
65 Chulia Street #40-07
OCBC Centre, Singapore 0104
Phone: 5332511
FAX: 5326454

Journal of Chromatography, 542 (1991) 205–220
Elsevier Science Publishers B.V., Amsterdam

CHROM. 23 084

Characterization of cyano bonded silica phases from solid-phase extraction columns

Correlation of surface chemistry with chromatographic behavior

R. S. SHREEDHARA MURTHY and L. J. CRANE*
J. T. Baker Inc., 222 Red School Lane, Phillipsburg, NJ 08865 (U.S.A.)
and
C. E. BRONNIMANN
Regional NMR Center, Department of Chemistry, Colorado State University, Fort Collins, CO 80523 (U.S.A.)
(First received October 31st, 1990; revised manuscript received January 15th, 1991)

ABSTRACT

Cyano bonded phases from six solid-phase extraction cartridge vendors (identified as A to F) have been characterized by elemental analysis, chromatography of probe molecules, and infrared and solid-state nuclear magnetic resonance spectroscopy. The results indicate that cyano solid-phase extraction cartridges from different vendors possess diverse surface properties presumably arising from differences in bonding chemistry and manufacturing methods. For example, nuclear magnetic resonance and infrared spectra indicate that vendors E and F use mono- and difunctional cyanopropyl silane, respectively, while all others use trifunctional. A wide range of hydrophobicities (determined using the alkylarylketone retention index scale) was observed among these bonded phases, determined primarily by degree of cyano group loading, whether the product has been endcapped or not and ratio of cyano functional group to endcapping reagent. Products from vendors A and D showed the presence of carboxyl groups, possibly arising from hydrolysis of cyano groups during silane bonding, thus imparting them with ion-exchange character. One would expect that extraction properties of cyano cartridges from different vendors may be very different. These results help explain the difficulty in transfer of procedures from cyano cartridges of one vendor to another and lend insight into the possible origin of lot-to-lot variability of cyano bonded phase from a single vendor.

INTRODUCTION

Solid-phase extraction has become an important step in the analysis of complex biological, environmental and industrial matrices. The end user has a wide range of surface chemistries to choose from. Although C_{18} is the most often used surface chemistry, there is an increasing trend to use less hydrophobic surfaces [1] that require weaker solvents to elute retained analytes. The cyano bonded phase is being increasingly used as a short alkyl chain alternative to C_{18}.

0021-9673/91/$03.50

De Smet and Massart [2] have been extending their pioneering work on the development of expert high-performance liquid chromatography (HPLC) systems using cyano columns to solid-phase extraction processes. Musch and Massart [3] have chosen a cyano solid-phase extraction cartridge for the extraction of basic drugs from plasma prior to analysis on a cyano HPLC column. They [3] have shown that the cyano solid-phase extraction cartridge has enough hydrophobicity to retain basic drugs with carbon number $\geqslant 11$. Extension of this work has shown [4] that neutral and acidic drugs with carbon number > 10 and < 25 can also be extracted on a cyano solid phase extraction column. It has also been used to extract cyclosporin [5] and/or its metabolites [6], β-blockers [7] and catecholamines [8] from many biological matrices.

In spite of the many advantages, cyano solid-phase extraction columns have not found widespread acceptance. This is perhaps because of lot-to-lot variability in performance often experienced by users. Experience in our laboratory indicated that the methods used to routinely analyze our bonded phases did not reveal the lot-to-lot variability observed in sensitive solid-phase extraction methods. Therefore, we initiated a study to not only understand the basis of retention of analytes on the cyano bonded phase but also develop methods to monitor the various surface characteristics that affect retention.

Considerable work has been done to understand the basis of retention in normal- and reversed-phase chromatography with cyanopropyl silica in HPLC columns which can also be extended to the cyano bonded phase present in solid-phase extraction columns. A number of conclusions have been reached. In the normal-phase mode, the cyano column acts essentially as a deactivated silica surface resulting in the interaction of analytes with residual silanols [9]. If the polarity of the solvent in the normal phase mode is increased, the effect from the silanols is suppressed leaving the cyano groups as the principal adsorption site [10]. In the reversed-phase mode, the cyano column acts like a short chain alkyl silica [11]. The primary interaction of the analyte with the bonded phase is through the cyano groups whose concentration (or surface coverage) determines the hydrophobicity of the surface. The residual silanols also play a key role in determining the overall adsorptive property.

Differences in silica and bonding chemistry may explain the differences in the properties of HPLC columns with the same principal functional group from different vendors. Smith and Miller [12] compared the performance of cyano HPLC columns from three vendors. They obtained retention indices (based on the alkylarylketone scale [13]) for a series of test compounds in water–methanol medium. Although the carbon loading for the three columns prepared by using monofunctional silane were comparable (3.5, 3.9 and 4.4% C), the retention indices for *p*-cresol and 2-phenylethanol on the CPS-Hypersil column were considerably higher than that for the Spherisorb CN and Ultrasphere CN columns. The retention indices for the CPS-Hypersil cyano column were comparable to those obtained for ODS-Hypersil. The difference among brands was larger than that observed for the same test compounds on different brands of ODS silicas [14]. This suggests that carbon loading alone cannot be used to explain the hydrophobic nature of cyano bonded phases. Such chromatographic evaluations only reveal that columns from different vendors exhibit differences in retention behavior but does not explain why. Spectroscopic analysis of the bonded phases should reveal the nature of the chemical species, the relative population of primary and endcapping siloxane groups and their functionalities.

Infrared (IR) and nuclear magnetic resonance (NMR) spectroscopy have been extensively used to characterize chemically modified silica surfaces. Diffuse reflectance (DR) Fourier transform (FT) infrared spectroscopy was used to study the hydrolytic stability of cyano bonded silica samples [13]. The characteristic infrared bands from the cyano, amide and carboxyl groups can be used to determine the functional group purity of cyano bonded phases used in solid phase extraction columns from different vendors. Solid-state ^{13}C and ^{29}Si NMR spectroscopy is being increasingly used to understand the nature of the alkyl chain, confirm the presence of an endcapping agent, and also determine the functionality of the silane used to modify the silica surface. Recent publications have shown that chromatographic evaluations combined with spectroscopic data result in more complete understanding of the modified surface. Solid-state NMR studies on a series of commercially available C_{18} columns provided data regarding surface structure, silane loading and endcapping confirmation that agreed well with the chromatographic retention behavior method using large polycyclic aromatic hydrocarbons as probe molecules [16]. Two independent groups used solid-state NMR spectroscopy and extensive leaching followed by chromatography of probe molecules to show that trifunctional octyl [17] and octadecyl [18] silanes are bound more strongly to silica than di- or monofunctional silanes. This confirms earlier data obtained by HF-digestion followed by GC analysis of bonded phases [19].

This paper describes the use of elemental analysis, chromatography of probe molecules and IR and NMR spectroscopy to characterize cyano bonded phases from commercially available solid-phase extraction cartridges.

EXPERIMENTAL

Reagents

The cyano solid-phase extraction columns from J. T. Baker, Burdick & Jackson, Fisher, Supelco, Analytichem and Waters were purchased. The plastic housing of each column was cut open and the bonded phase recovered. A micro riffler was used to obtain a representative sample. Each sample was identified by a letter code A to F chosen at random. "Baker analyzed"-grade reagents such as potassium chloride, salts, triethylamine, HPLC-grade solvents and water were used. Acetophenone, valerophenone, octanophenone and dopamine were purchased from Aldrich.

Instrumentation

The cyano bonded phase being tested was packed dry into HPLC columns (250 × 4.6 mm I.D.). The column was equilibrated with methanol, water and then with the mobile phase being used.

A Varian HPLC pump (Model 9010), variable-wavelength detector (Model 9050) and an integrator (Model 4400) were used. Absorbance was measured at 254 nm while the mobile phase was being pumped at a flow-rate of 1 ml/min. The back pressure for each column was monitored.

To determine the hydrophobic nature of the cyano bonded phase, the test compounds used were a set of alkylarylketones such as acetophenone, valerophenone and octanophenone. They were diluted (usually 0.25–0.5 μl in 1 ml of methanol–water, 50:50) and injected onto the cyano column (20-μl loop). The void volume of

the column was established by injecting acetone. The average retention time for each test compound was obtained from at least three injections from which the capacity factors were calculated. The process was repeated for three columns packed with cyano bonded phase B (chosen because it had the highest percent nitrogen value) to obtain the average capacity factors which were plotted against carbon number ($\times$ 100) for each test compound. The regression equation obtained from this plot was used to calculate the retention index for the test compounds for other cyano columns.

To determine the ion-exchange properties of the cyano phases, a 4 m*M* solution of dopamine (pK_a 8.8) in 0.1 *M* phosphate buffer at pH 6.0 was used. To overcome severe peak tailing due to interaction of dopamine with residual silanols, 1% triethylamine was added to the mobile phase. To obtain reasonable retention times on all the cyano columns by reducing hydrophobic interactions, the mobile phase used was buffer–methanol (80:20). Capacity factors (k') were obtained from the measured retention time for dopamine for each column.

DR-FT-IR spectra were recorded using a Nicolet 740 spectrometer (Madison, WI, U.S.A.). A 10% dispersion of the bonded phase in finely ground KCl was filled in the sample cup of a Harrick diffuse reflectance accessory (Ossining, NY, U.S.A.). The sample spectrum, recorded at 8 cm^{-1} resolution, was ratioed to that of pure KCl and converted to Kubelka–Munk units. The area of the cyano and other bands of interest were ratioed to that of the silica reference band [20].

Solid-state NMR spectra of ^{13}C at 37.74 MHz and of ^{29}Si at 29.81 MHz were obtained on a Nicolet NT 150 spectrometer that has been modified for cross polarization magic angle spinning (CP-MAS) experiments. Approximately 0.6-g samples were spun at 3.5–4.0 kHz using Delrin rotors based on the design of Wind *et al.* [21]. In both ^{13}C and ^{29}Si experiments, rf field strengths were matched at 50 kHz. For ^{13}C cross-polarization, a contact time of 2 ms was used. A 5-ms contact time was used in the ^{29}Si measurements. In neither case were the observed intensities corrected for distortions that can arise from non-uniform cross-polarization dynamics. Therefore, the relative intensities within a spectrum are semiquantitative.

RESULTS AND DISCUSSION

Bonded phase variability has been a continuing concern throughout the development of HPLC and its companion technique, solid-phase extraction. Of the widely used bonded phases, the cyano phase has the unenviable reputation of being the most variable and especially prone to reproducibility problems. In spite of this, a number of solid-phase extraction applications have been routinely performed using Bakerbond cyano solid-phase extraction columns with no apparent problems. However, a particular production lot (A39081) that appeared normal by our routine analytical procedures, failed to perform for some of these applications. Table I gives the elemental analysis data for some recent lots of cyano bonded phase along with that for lot A39081. Clearly, from elemental analysis or C/N ratio, one cannot conclude why this lot should behave differently from others. This prompted us to investigate various aspects of surface structure that determine analyte retention on a cyano bonded phase and the actual surface composition of cyano bonded phases using a number of techniques. As only a limited amount of the material from lot A39081 was available, we chose to use a later lot for an in-depth analysis. We also decided to investigate cyano

TABLE I

ELEMENTAL ANALYSIS DATA FOR SOME LOTS OF CYANO PHASES FROM J.T. BAKER

Lot No.	%CHN	C/N Ratio
A39081	9.6%C, 1.8%H, 2-3%N	4.17
A48117	10.8%C, 1.9%H, 2.4%N	4.50
C04125	9.2%C, 1.5%H, 2.5%N	3.68
C07102	10.9%C, 2.0%H, 2.6%N	4.19
D04106	9.8%C, 1.7%H, 2.3%N	4.26

bonded phases from solid-phase extraction cartridges from Analytichem, Burdick & Jackson, Fisher, Supelco and Waters to extend the study to better understand the basis for retention differences. These vendors were thought to be representative of a variety of cyano bonded phase types. In the discussions that follow, each sample is identified by a letter code (A to F) chosen at random to represent each vendor. The identity of each sample (vendor and lot number) is available to the reader upon request.

Chemical characterization

Table II gives the chemical analysis data for the various cyano bonded phases. Products A and B form a group with the highest carbon loading while the rest have comparable but lower silane loading. The C/N ratio for these products vary over a wide range.

Chromatographic characterization

The retention indices of three alkylarylketones were determined as described in the Experimental section to establish the hydrophobic properties of the different cyano bonded phases. Fig. 1 shows the average (from three columns) log k' values obtained for acetophenone, valerophenone and octanophenone plotted against the number of carbon atoms in these molecules ($\times$ 100) for the cyano bonded phase from vendor B. The regression equation calculated from this data was used to determine the retention index (calculated carbon number $\times$ 100) for all the cyano bonded phases after determining k' values for the three alkylarylketones. The data are given in Table III. A plot of the theoretical carbon numbers (x 100) against the experimentally determined values is shown in Fig. 2. If the bonded phase is more hydrophobic in a reversed-phase mode than that from vendor B, the regression line should fall above that of B and *vice versa*. It is clear that the cyano phase from E has the most hydrophobic surface even though it has lower %C than B. Products A and B have comparable hydrophobicity while that from vendor D is the least hydrophobic. This behavior cannot be explained simply based on carbon and nitrogen content if cyano groups are responsible for the hydrophobic character.

Dopamine was used as a probe molecule to determine the ion-exchange properties of the cyano phases. The mobile phase pH was fixed at 6.0 to ensure that dopamine (pK_a 8.8) was present as a positively charged species capable of interacting with acidic groups. Severe peak tailing was observed for all the columns due to the interaction of dopamine with residual silanols. This was overcome by adding 1% triethyl-

TABLE II

COMPARATIVE CHEMICAL AND SPECTROSCOPIC DATA FOR CYANO BONDED PHASES

Vendor code	%CHN	C/N Ratio	IR CN band ratio	Peak positions (ppm) in the	
				^{13}C NMR spectrum	^{29}Si NMR spectrum
A	9.05C, 1.86H, 0.66N	13.71	0.15	−0.1, 12.9, 19.2, 36.8, 50.9, 176.4	15, −56, −66, −100, −110
B	9.18C, 1.53H, 2.52N	3.64	1.23	−0.2, 12.7, 19.1, 50.7, 120.5	15, −56, −66, −100, −110
C	7.06C, 1.42H, 1.60N	4.41	0.74	−0.2, 12.4, 19.7, 51.1, 121.6	15, −57, −66, −100, −110
D	6.88C, 1.34H, 1.61N	4.27	0.82	−, 12.4, 19.7, 36.6, 50.8, 120.3	−45, −55, −66, −100, −110
E	7.24C, 1.64H, 1.16N	6.24	0.43	−0.4, 16.1, 19.7, 118.9	15, −100, −110
F	6.66C, 1.18H, 1.34N	4.97	0.38	−0.4, 16.1, 19.8, 50.6, 118.9	15, −9, −16, −100, −110

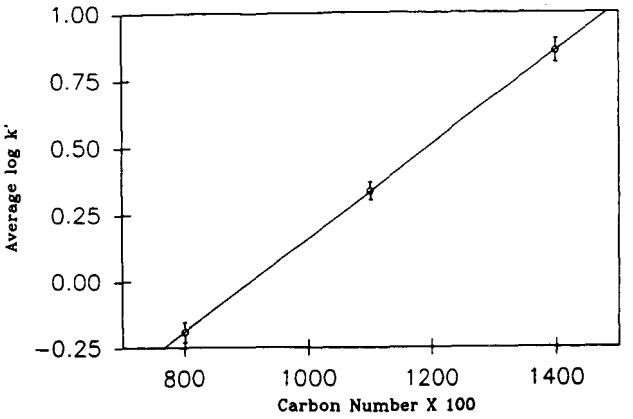

Fig. 1. Plot of average log k' values *versus* carbon number ($\times$ 100) of acetophenone (800), valerophenone (1100) and octanophenone (1400). Slope: $1.74.10^{-3}$; intercept: -1.587; correlation coefficient: 0.999. Error bars represent 3σ.

amine to the mobile phase. Under these conditions, dopamine was not expected to be retained on the column unless the surface had ion-exchange properties. Capacity factors given in Table III indicates that samples C, E and F did not have ion-exchange properties. The ion-exchange capacity (based on k' for dopamine) for other phases decreased in the order A > D > B.

The back pressure was generally 5–10 atm for all the columns during chromatographic evaluations, except for the sample from vendor E which gave a back pressure of 90–100 atm. When the bonded phase was suspended in methanol, the supernatant layer was turbid indicating the presence of fine silica particles. After decanting this layer several times to remove most of the fine silica, the column back pressure was 8–10 atm while the k' values for the test compounds were unchanged.

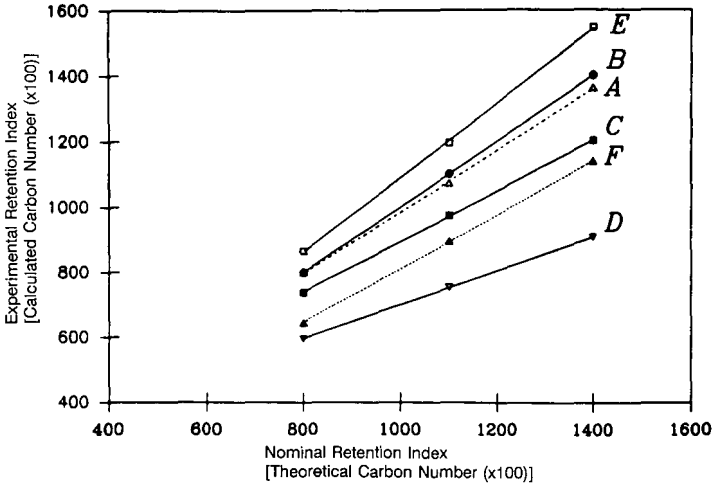

Fig. 2. Plot of theoretical carbon number ($\times$ 100) *versus* the number calculated from regression equation from Fig. 1 for samples A to F.

TABLE III

COMPARATIVE CHROMATOGRAPHIC DATA FOR CYANO BONDED PHASES

Vendor code	Retention index for			Capacity factor for Dopamine
	Aceto	Valero	Octano	
A	799	1073	1362	0.97
B	800	1101	1400	0.15
C	738	975	1201	0.02
D	557	754	907	0.24
E	866	1196	1547	0.01
F	645	896	1138	0.01
Theoretical	800	1100	1400	

Spectroscopic characterization

Fig. 3 shows the DR-FT-IR spectrum of the cyano bonded phase B. It shows the expected cyano group stretch band at 2252 cm^{-1} and the silica substrate Si–O–Si combination band at 1871 cm^{-1}. The ratio of the cyano to silica band area for each sample was obtained. This ratio was used to compare the relative concentration of the cyano groups. Table II lists the ratios obtained, which follows the same trend as the %N data. Trace levels of amide groups, produced by the hydrolysis of cyano groups in the presence of hydrochloric acid (which is a by-product of the reaction with chlorosilanes) and water give rise to two bands at 1666 and 1624 cm^{-1} (amide I and II bands, respectively) shown in Fig. 3. IR spectra of samples A and D (spectra A and B in Fig. 4) showed carboxyl carbonyl bands at 1720 cm^{-1}, presumably produced by further hydrolysis of the amide groups, in addition to the amide and cyano bands. Fig. 4 also shows the IR spectra of samples from (C) vendor B and (D) J.T. Baker (lot

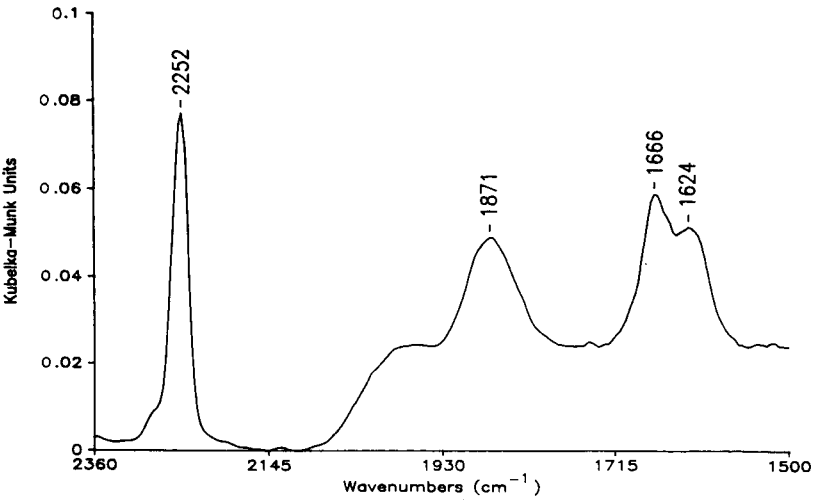

Fig. 3. DR-FT-IR spectrum of cyano bonded phase from vendor B. See text for band assignments.

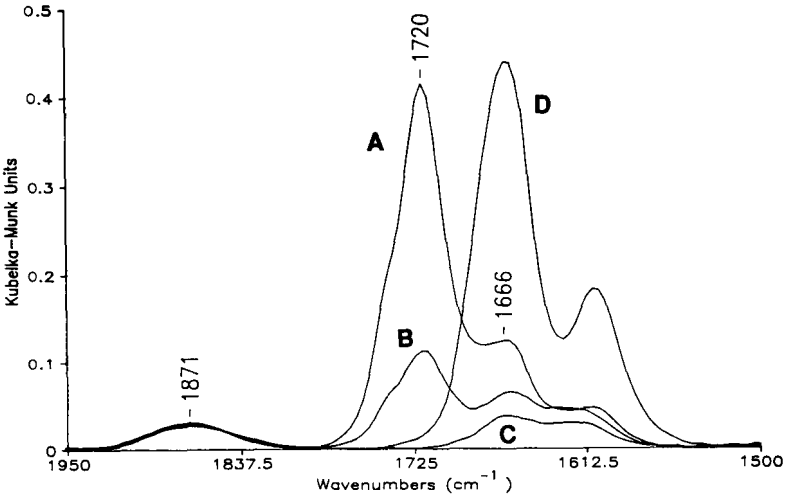

Fig. 4. IR spectra of cyano bonded phase samples from vendors (A) A, (B) D, (C) B and (D) J.T. Baker (lot No. A39081).

No. A39081). These spectra have been normalized to the silica band area for easy comparison of carbonyl band intensities. Spectra of samples from other vendors showed carbonyl band intensities similar to spectrum C.

Fig. 5 shows the solid-state ^{13}C NMR spectra of cyano bonded phases A, B and D as spectra A, B and C, respectively. The solid-state ^{13}C NMR spectrum of the cyano bonded phase C was very similar to that from vendor B and hence is not shown. A resonance located at about 0 ppm is from methyl carbon directly attached to silicon such as the trimethyl silyl group. Resonances at 12.4 and 19.2 ppm arise from methylene carbon while that at 121.5 ppm is from the cyano carbon. A peak at 50 ppm has been attributed [22] to methoxy carbon, presumably produced during the washing of the bonded phase with methanol. In addition to the aliphatic, cyano and methoxy carbon resonances, the spectrum of a sample from vendor D (C in Fig. 5) shows a peak at 36.7 ppm which has been attributed to the carbon adjacent to an amide carbon. The carboxyl carbonyl carbon peak should occur at 176 ppm and is barely visible above the instrumental noise. The absence of a peak at 0 ppm indicates that the sample does not have methyl groups directly attached to silicon as would be expected from an endcapped product or from a monofunctional silane. The solid-state ^{13}C NMR spectrum of the cyano bonded phase A (A in Fig. 5) shows, in addition to the aliphatic and methoxy carbon resonances, two intense peaks at 36.7 and 176.4 ppm. They have been attributed to the amide and carboxyl carbonyl carbons, respectively. The NMR spectrum shows virtually no cyano carbon peak, which is confirmed by the low cyano band area ratio in the infrared spectrum and by the low analysis for nitrogen. The peak at 0 ppm suggests that either a monofunctional silane has been used or the product has been endcapped.

The alkyl carbon resonances of samples A to D all occur at the same position (Table II) indicating that the silane with the same alkyl chain structure has probably been used. Readily available silanes containing the cyano groups are the cyanopropyl

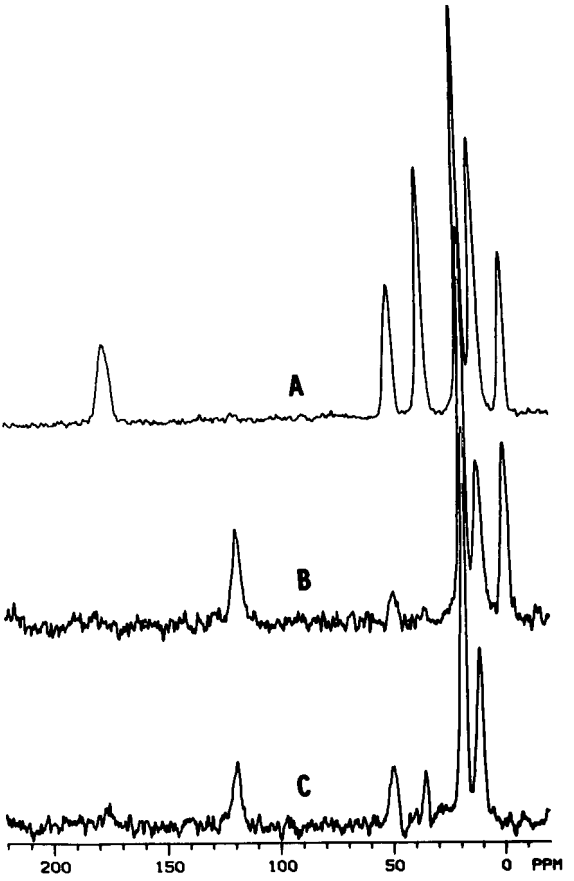

Fig. 5. Solid-state ^{13}C NMR spectra of cyano bonded phases (A) A, (B) B and (C) D. See text for band assignments.

or cyanoethyl trichloro (or trimethoxy) silanes. A ^{13}C NMR spectrum of cyanopropyltrichloro silane, used by J.T. Baker to make its product showed four peaks. A resonance at 18.9 ppm was assigned to the methylene carbon adjacent to silicon while the peaks at 19.2 and 23.2 ppm arise from the α- and β-methylene carbons, respectively: the cyano carbon resonance occurs at 118.5 ppm. Based on these assignments, the peak at 12.4 ppm in the solid-state ^{13}C NMR spectrum of the bonded phases (Fig. 5) is attributed to the methylene carbon adjacent to silicon while the peak at 19.7 ppm is a combination of peaks from the α- and β-methylene carbons. Curves B and C in Fig. 5 confirm the presence of cyano groups in samples B and D, respectively.

Solid-state ^{13}C NMR spectra of samples E and F are shown as spectrum A and B, respectively, in Fig. 6. The aliphatic carbon resonances are at 16.1 and 19.8 ppm. Both samples have a peak at 118.9 ppm from the cyano group. The resonance at 0 ppm can arise from any siloxane surface that has one or more methyl groups attached directly to silicon atoms. Hence, it cannot be conclusively determined from ^{13}C NMR spectra whether these samples have been endcapped. The relative intensity of the peak

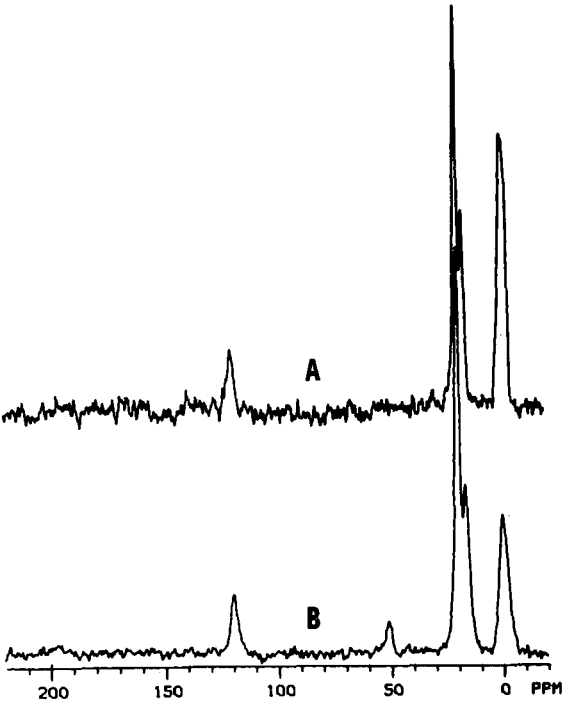

Fig. 6. Solid-state ^{13}C NMR spectra of cyano bonded phases (A) E and (B) F. See text for band assignments.

at 0 ppm arising from $\equiv SiO\text{–}Si(CH_3)_xR$ (where $x = 2$ or 3) is higher for a sample from vendor E compared to that from vendor F. This may suggest that sample E is more thoroughly endcapped or that vendor F may have used a different silane. Table II gives the positions of the observed resonances in the ^{13}C NMR spectra of all the samples.

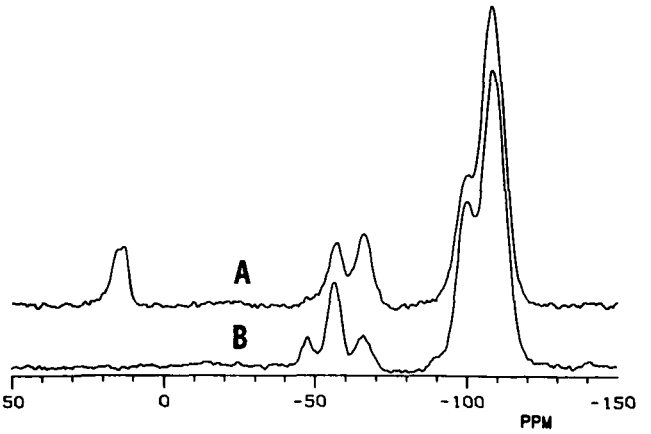

Fig. 7. Solid-state ^{29}Si NMR spectra of cyano bonded phases (A) B and (B) D. See text for band assignments.

TABLE IV

STRUCTURAL ELEMENTS AT THE SURFACE OF BONDED PHASES

Monofunctional	Difunctional	Trifunctional
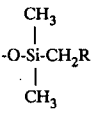	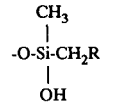	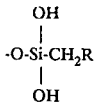
a	*c*	*e*
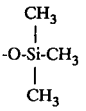	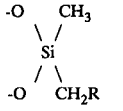	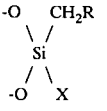
b	*d*	*f*
	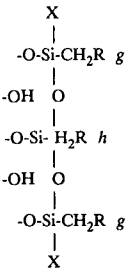	

Fig. 7 shows the solid-state ^{29}Si NMR spectra of cyano bonded phases (A) B and (B) D. The ^{29}Si NMR spectrum of sample A was very similar to B and hence is not shown. However, peak positions are listed in Table II for all the samples. Table IV gives the structural elements that give rise to different peaks. The resonance at 15 ppm arises from Si atoms with two or three methyl groups directly attached (such as the trimethylsilane) as shown by *a* or *b* in Table IV. A resonance at -55 ppm is assigned to the silicon atom with the environment shown as *f* or *g*, and the peak at -66 ppm is assigned to the silicon atom with environment shown as *h*. The other resonances at -100 and -110 ppm arise from the silicon atoms in the silica matrix. These data confirm that the cyano bonded phase B is made using a trifunctional silane, as it is bound to silica with di- and trisiloxane bonds, and that it has been endcapped.

The solid-state ^{29}Si NMR spectrum of sample D (B in Fig. 7) has no resonance at 15 ppm, confirming the absence of an endcapping agent. The presence of three peaks in the -45 to -66 ppm region confirms the use of a trifunctional silane. The relative intensity of the three peaks indicates that the cyano silane is bound to silica with more disiloxane bonds than trisiloxane bonds. It even has a resonance at -48 ppm attributed to a silicon atom with only one siloxane bond and two free silanols as shown by *e* in Table IV.

The ^{29}Si NMR spectrum of sample E has only one resonance at 15 ppm (A in Fig. 8) arising from silicon atoms with environment shown as *a* + *b* in Table IV. As

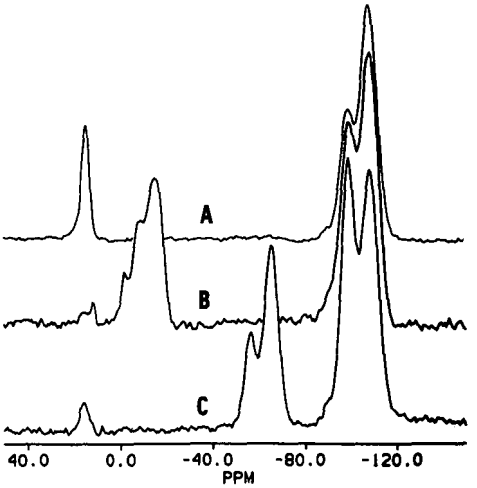

Fig. 8. Solid-state ^{29}Si NMR spectra of cyano bonded phases (A) E (monofunctional), (B) F (difunctional) and (C) C (trifunctional).

there are no peaks in the -45 to -65 ppm region, it has no silicon atoms with one or more siloxane bonds with other than methyl groups attached to them. This implies that a monofuntional cyano silane has been used. It does not confirm whether the sample has been endcapped or not. The ^{29}Si NMR spectrum of sample F (B in Fig. 8) has two peaks which can be attributed to silicon atoms with environment shown as *c* (-9.0 ppm) and *d* (-15.9 ppm). This suggests the use of a difunctional cyano silane for the primary bonding. From the intensity of the peak at 15 ppm, one can conclude that the product has been very lightly endcapped. For comparison, curve C in Fig. 8 is the ^{29}Si NMR spectrum of sample C which is identical to that from vendor B. Both samples have been made with a trifunctional silane and have been endcapped.

CONCLUSIONS

The retention of analytes (such as basic drugs) on a cyano bonded phase is achieved by a combination of hydrophobic, hydrophilic and ion-exchange mechanisms. The relative contribution of each of these mechanisms is affected by the relative population of cyanopropyl and endcapping silanes, presence of residual silanols and other ionizable groups. The six cyano bonded phases compared here have widely different hydrophobic and ion-exchange properties. They can be classified into groups depending on the nature of the bonding chemistry. Vendors of samples A to D all apparently use a trifunctional silane with cyanopropyl groups. The C/N ratio for this silane is 3.4. Vendor E uses a monofunctional silane, most probably functionalized with cyanopropyldimethyl groups. The C/N ratio for this compound is 5.1. Vendor F apparently uses a difunctional silane. If it is cyanopropylmethylsilane, the C/N ratio will be 4.3. The extent of deviation from the theoretical C/N ratio can be used to determine the relative population of the cyano and endcapping silanes if it is known that no cyano group hydrolysis has occurred. Based on the above assump-

TABLE V

COMPARATIVE SUMMARY OF CYANO PHASES

Vendor code	Cyano silane functionality	End cap	Remarks
A	Tri	Yes	High amide/carboxyl content
B	Tri	Yes	High cyano group content and purity
C	Tri	Yes	High cyano group purity
D	Tri	No	Amide/carboxyl groups present
E	Mono	Yes	Higher level of silica fines
F	Di	Yes	Lightly endcapped

tions and the experimental results, the following conclusions can be drawn about each cyano bonded phase (also summarized in Table V).

Sample A

This product has high carbon loading which is comparable to that from vendor B. It has the lowest cyano group content and hence the highest C/N ratio. Most of the cyano groups appear to have been hydrolyzed to amide and carboxyl groups giving the bonded phase the highest ion-exchange properties. The alkylarylketones used to determine the hydrophobicity are not retained by ion-exchange mechanisms and hence are not affected by the presence of these ionizable groups. The product is made with a trifunctional silane and has been endcapped. The silane is bound to silica with mostly di- and trisiloxane bonds.

Sample B

This cyano product has the highest carbon loading, cyano group content and functional group purity. It is also made with a trifunctional silane and has been endcapped. The C/N ratio is the closest to theoretical value for a trifunctional silane, from which it can be concluded that only 7% of the carbon loading is from the endcapping agent. The silane is bound with only di- and trisiloxane bonds.

Sample C

This product belongs to a set of bonded phases with lower carbon content, about 7% carbon, even though it is made with a trifunctional silane. It has been endcapped and thoroughly cured to bond the silane with di- and trisiloxane bonds. It has good cyano functional group purity. The C/N ratio indicates that about 29% of the carbon loading is from the endcapping agent. The lower population of cyanopropyl groups on the surface makes it less hydrophobic than B but more hydrophobic than D and F.

Sample D

Carbon loading is relatively low for a product that is made with a trifunctional silane. Failure to endcap has left residual silanols making it the least hydrophobic phase. Some of the cyano groups have been hydrolyzed to amide and carboxyl groups thus increasing the C/N ratio and heterogeneity in surface characteristics.

Sample E

This cyano phase is made with a monofunctional silane leading to only 7% carbon loading. From the C/N ratio, one can conclude that 22% of the carbon loading is from the endcapping agent. The relatively higher population of trimethylsilyl groups renders this product to be the most hydrophobic in the reversed-phase mode. However, the retention properties of this product for basic drugs may be quite different from one that has predominantly cyanopropyl groups. It has high levels of fine silica particles possibly restricting the flow during solid-phase extraction.

Sample F

This product is made with a difunctional silane and has been lightly endcapped. These facts explain why the relative intensity of the peak at 0 ppm in the ^{13}C NMR spectrum (Fig. 6, curve B) is much lower than that for sample E (curve A). From the C/N ratio, one can conclude that only 12% of the carbon loading arises from the endcapping agent. However, the presence of silicon atoms with residual silanols makes this product only slightly more hydrophobic than that from vendor D.

General

This study expands the results of earlier studies [2,3,9–12] in demonstrating that a number of variables determine the surface properties of the cyano bonded phase. Although chromatographic evaluations reveal differences in the overall retention properties [12–14], chemical and spectroscopic data support and explain why these differences arise. Failure to control particle size distribution in the final product can result in contamination of samples with finely divided silica and prevent reproducible flow-rates during solid-phase extraction. The functionality and functional group purity of the cyano silane present on the silica surface markedly affects the hydrophobic properties of the final bonded phase. Failure to cure or endcap leave the often undesirable silanols which are known to interact strongly with basic compounds. Improper conditions during the manufacturing process that permit the hydrolysis of cyano groups to amide/carboxyl groups produces a surface with ion-exchange properties. It was concluded from this study that the performance problems found with the J.T. Baker cyano phase (lot No. A39081) apparently occurred because it had a relatively high concentration of amide groups resulting from the first step in the hydrolysis of cyano groups (curve D in Fig. 4). A detailed study [15] of the hydrolytic stability of the cyano group has revealed reaction conditions that lead to hydrolysis. As a result of these studies, cyano bonded phases now meet strict specifications for their cyano and amide group content determined by FT-IR spectrometry.

The above study supports the perception that cyano bonded silica phases contained in solid phase extraction columns from different vendors possess widely varying properties. It is, hence, not surprising that transfer of extraction procedures from one vendor's product to another is often difficult. Understanding the actual surface composition should aid both in development of and in modification of solid phase extraction procedures if it is necessary to transfer to another vendor's product. It should be emphasized that the results described here apply only to specific lots of product from each vendor. Deviation from the theoretical surface structure observed for some of the products could have occurred during aberrations in the manufacturing process for a particular lot.

ACKNOWLEDGEMENT

The authors are grateful to the Colorado State University Regional NMR Center funded by National Science Foundation Grant No. CHE 78-18581.

REFERENCES

1 R. S. Shreedhara Murthy, R. E. Paschal and L. J. Crane, *Am. Lab.*, in press.
2 M. De Smet and D. L. Massart, *J. Chromatogr.*, 410 (1987) 77.
3 G. Musch and D. L. Massart, *J. Chromatogr.*, 432 (1988) 209.
4 G. Musch, T. Hamoir and D. L. Massart, *J. Chromatogr.*, 495 (1989) 215.
5 R. E. Kates and R. Latini, *J. Chromatogr.*, 309 (1984) 441.
6 D. J. Gmur, P. Meier and G. C. Yee, *J. Chromatogr.*, 425 (1988) 343.
7 G. Musch, Y. Buclens and D. L. Massart, *J. Pharm. Biomed. Anal.*, 7 (1989) 483.
8 R. Dixon, J. Hsiao, W. Caldwell, *Res. Commun. Pathol. Pharmacol.*, 59 (1988) 395.
9 E. L. Weiser, A. W. Salotto, S. M. Flach and L. R. Snyder, *J. Chromatogr.*, 303 (1984) 1.
10 J. F. Schabron, R. J. Hurtubise and H. F. Silver, *Anal. Chem.*, 50 (1978) 1911.
11 R. E. Majors, *J. Chromatogr. Sci.*, 18 (1980) 488.
12 R. M. Smith and S. L. Miller, *J. Chromatogr.*, 464 (1989) 297.
13 R. M. Smith, *J. Chromatogr.*, 236 (1982) 313.
14 M. C. Pietrogrande, F. Dondi, G. Blo, P. A. Borea and C. Bighi, *J. Liq. Chromatogr.*, 10 (1987) 1065.
15 R. S. Shreedhara Murthy and J. P. Berry, in D. E. Leyden and W. T. Collins (Editors), *Chemically Modified Oxide Surface*, Vol. 3, Gordon & Breach, New York, 1990, p. 151.
16 K. Jinno, *J. Chromatogr. Sci.*, 27 (1989) 729.
17 S. O. Akapo and C. F. Simpson, *J. Chromatogr. Sci.*, 28 (1990) 186.
18 M. Hetem, L. van de Ven, J. de Haan, C. Cramers, K. Albert and E. Bayer, *J. Chromatogr.*, 479 (1989) 269.
19 N. Sagliano, Jr., T. R. Floyd, R. A. Hartwick, J. M. Dibussolo and N. T. Miller, *J. Chromatogr.*, 443 (1988) 155.
20 R. S. Shreedhara Murthy and D. E. Leyden, *Anal. Chem.*, 58 (1986) 1228.
21 R. A. Wind, F. E. Anthonio, M. J. Duijvestijn, J. Smint, J. Trommel and G. M. C. deVette, *J. Magn. Reson.*, 52 (1983) 424.
22 E. Bayer, K. Albert, J. Reiners, M. Nieder and D. Muller, *J. Chromatogr.*, 264 (1983) 197.

Journal of Chromatography, 542 (1991) 221–237
Elsevier Science Publishers B.V., Amsterdam

CHROM. 23 053

Efficiency in chiral high-performance ligand-exchange chromatography

Influence of the complexation process, flow-rate and capacity factor

ANDREAS M. RIZZI
Institute of Analytical Chemistry, University of Vienna, Währingerstrasse 38, A-1090 Vienna (Austria)
(First received December 15th, 1989; revised manuscript received December 21st, 1990)

ABSTRACT

Chromatographic separations of enantiomers by ligand-exchange mechanisms are performed either by using chiral stationary phases (CSPs) or chiral mobile phase additives (CMAs). The two modes differ significantly with respect to their efficiency. It is shown that the process of chelate formation and dissociation at the CSP is the main source of enhanced plate height values when employing CSPs. When using highly soluble CMAs as selector ligands, the rate-determining ligand-exchange process takes place mainly in the mobile phase and therefore does not contribute much to the plate heights. These fundamental differences in the kinetics of the two modes of ligand-exchange chromatography are reflected in different dependences of the plate height data on the flow-rates. It is shown that for CSPs the plate height depends on the structure and configuration of the analyte and the composition of the mobile phase. Within a series of homologous amino acids a pronounced positive correlation is found between the kinetic plate height contribution and the capacity factor. However, this positive correlation is not a general dependence: on changing the capacity factor by changing the eluent composition, a negative correlation is found.

INTRODUCTION

Ligand-exchange chromatography (LEC) is a powerful tool for the separation of chiral analytes that form chelate complexes with heavy metals [1,2]. Many applications have illustrated the high enantioselectivity and the great separation power inherent in this method [1–28]. The probable structures of various types of complexes and the correlation of these structures with the observed enantioselectivities have been the topics of extensive investigations, and the results have been reviewed several times [1,2].

Chiral selectors in LEC are either immobilized at the surface of the packing or are components of the mobile phase. The immobilization can be done by binding the selectors chemically to the support material or by dynamically generating an adsorption layer on the support surface. In the latter instance a long hydrophobic

0021-9673/91/$03.50

group acts like an anchor in the alkyl chains of alkylsilica packings. In both instances, chiral stationary phases (CSPs) are obtained. A chiral mobile phase is produced by adding a highly soluble chiral additive to the mobile phase. Whether a chiral mobile phase additive (CMA) is adsorbed or remains predominantly in the mobile phase depends strongly on its activity coefficient in the eluent mixture.

This paper reports the first part of a broader investigation dealing with peak dispersion in high-performance ligand-exchange chromatography (HPLEC). It focuses on differences in peak dispersion found when applying different modes of ligand exchange, either with CSPs or with CMAs. It discusses the effects of flow-rate, the capacity factor and the structural features of the analytes.

THEORETICAL

Plate height equations

The theoretical background for the discussion of plate height data within this paper is provided by the plate height theories for packed columns as given by Huber [29,30] and Giddings [31] (see also a review [32]). These theoretical treatments belong to the most rigorous types usually applied in chromatography.

According to Huber [29,30], we assume that the total reduced plate height, h, is the sum of four different contributions, h_d, h_c, h_f and h_b, originating from different dispersion proceses as follows:

$$h_d = \varphi_d \cdot \frac{D_m}{u d_p} \tag{1a}$$

$$h_c = \frac{\varphi_c'}{1 + \varphi_c'' \left(\frac{D_m}{u d_p}\right)^{\frac{1}{2}}} \tag{1b}$$

$$h_f = \varphi_f \left(\frac{u d_p}{D_m}\right)^{\frac{1}{2}} \left(\frac{k''}{1 + k''}\right)^2 \tag{1c}$$

$$h_b = h_{b,mt} = \varphi_b \cdot \frac{u d_p}{D_m} \cdot \frac{k''}{(1 + k'')^2} \tag{1d}$$

where the subscripts d, c, f and b indicate dispersion due to axial diffusion, convection (including eddy dispersion), resistance to mass exchange in the mobile zone and resistance to mass exchange in the fixed bed, respectively, mt indicates the mass transfer contribution in the stagnant zone, d_p is the mean particle size, u the flow velocity, k' the capacity factor and D_m the diffusion coefficient in the mobile phase; k'' denotes the zone capacity factor, which is related to the phase capacity factor, k', by $k'' = (V_m/V_f)(k' + 1) - 1$, V_m being the mobile phase volume and V_f the interparticle volume; the parameters φ_d, φ_c, φ_f and φ_b are geometric factors depending on the packing material and packing geometry.

Since eqn. 1d accounts mainly for the resistance to mass exchange by the stagnant mobile phase, we have added a particular kinetic term, $h_{b,kin}$, for systems

involving slow adsorption–desorption processes. Following Giddings [31], we assume that $h_{b,kin}$ is given by

$$h_{b,kin} = \varphi_{kin} \frac{u}{d_p k_d} \frac{k'}{(1 + k')^2} \quad (2)$$

where k_d is the rate constant for the desorption of the solute from the surface and φ_{kin} is a geometric factor.

Equilibria involved in ligand-exchange chromatography

We assume that various equilibrium steps are involved in ligand-exchange chromatography, as shown in Fig. 1. Some of these steps are complexation reactions, others adsorption steps without complexation. The rate constants of these two types of equilibrium reactions are expected to differ considerably[a]. Fig. 1 contains those equilibria which we assume to be primarily important for the two different modes of LEC, using either CSPs or highly soluble CMAs. Other equilibria, not specified in Fig. 1 by a number, are assumed either to be of minor importance or not to influence significantly the peak dispersion. Buffer ions, counter ions and solvent molecules involved in the complexes are omitted from Fig. 1 for the sake of clarity. Nevertheless, they may be of great importance as ligand binding is always associated with the dissociation of another ligand. The following equilibria are of most importance:

Equilibria in ligand exchange at CSPs:

(1) Loading of the CSP with metal ions. Usually this loading is already achieved on equilibrating the CSP with a copper-containing eluent before starting chromatography.

(2) Ligand-exchange step of the analyte on the adsorbed metal (we assume this to be the essential rate-determining step).

(3) Adsorption–desorption of the pure analyte without any complexation, *e.g.*, by hydrophobic adsorption (we assume this process to be decisively more rapid than the ligand-exchange process).

(4) Adsorption of the pure analyte onto the stationary phase.

(5) Adsorption of the analyte–metal–analyte complex onto the stationary phase.

Ligand exchange employing highly soluble CMAs:

(1) Formation of the diastereomeric analyte–metal–selector complex in the mobile phase.

(2) Formation of the analyte–metal–analyte complex in the mobile phase.

If these two processes take place almost completely in the mobile phase, the ligand-exchange kinetics do not have much influence on the plate height.

(3) Adsorption of the diastereomeric analyte–metal–selector complex on the stationary phase.

---

[a] Free energies of binding for hydrophobic adsorption are about 20 kJ/mol [33], whereas those for chelate formation with amino acids are about 80–100 kJ/mol [34,35]. Activation energies for the desorption from hydrophobic binding sites are estimated to be *ca.* 35 kJ/mol [36]. This value is less than the complex binding energy itself and thus in any case much less than the activation energy of complex dissociation. Note that activation free energies for ligand-exchange reactions at surface immobilized ligands might be higher than those for bulk solutions.

(a) CSP:

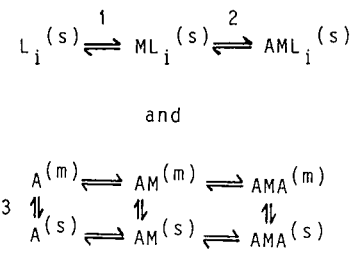

(b) CMA:

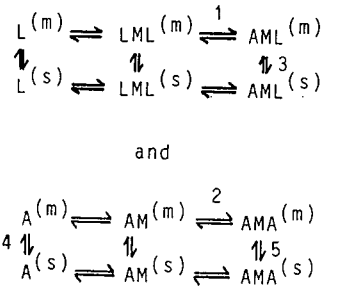

Fig. 1. Schematic representation of complex building and adsorption equilibria involved in LEC: (a) LEC with CSPs; (b) LEC with highly soluble CMAs and metal ion additives. The most important equilibria referred to in the text are indicated by numbers. A = Analyte; M = metal ion; L = chiral selector ligand. Subscript i indicates immobilization; m and s denote species in mobile and stationary phase, respectively.

The three adsorption steps (3)–(5) in Fig. 1b do not involve chelate formation or dissociation steps. They are assumed to proceed with the usual rates of reversed-phase adsorption.

This model implies significant differences in plate heights for the two different ligand-exchange modes (using either CSPs or CMAs). The experimental data on the kinetics of the systems are interpreted in the light of the model described.

EXPERIMENTAL

Apparatus

The chromatographic system consisted of a high-performance liquid chromatographic pump (Model L-6200 intelligent pump; Merck–Hitachi, Tokyo, Japan), a syringe–valve injector (Model 7161; Rheodyne, Cotati, CA, U.S.A.) equipped with a 20-μl loop (in specified instances 5 μl), a column oven (Model 655A-52; Merck–Hitachi), a UV detector (Model L-4000; Merck–Hitachi) or a spectrofluorimetric detector (Model F-1000; Merck–Hitachi) equipped with a 2-μl detection cell and an integrator (Model D-2000 chromato-integrator; Merck–Hitachi).

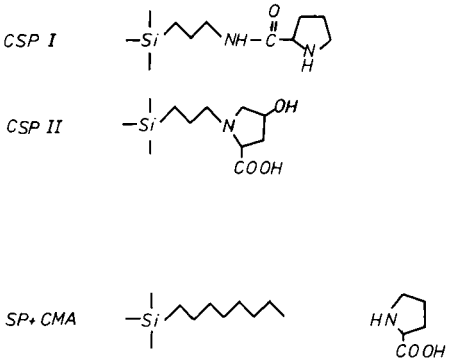

Fig. 2. Structures of the chiral stationary phases CSP I and II and the chiral mobile phase additive.

Columns

Two different CSPs (Fig. 2) were tested:

(i) CSP I: L-proline amide according to Lindner [5]; spacer, propylsilyl, 7-μm particles, material obtained from Loba Chemie (Austria); column dimensions, 125 mm × 4 mm I.D.

(ii) CSP II: L-hydroxyproline according to Unger and co-workers [12,13]; spacer, propylsilyl, 5-μm particles; column dimensions, 125 mm × 4 mm I.D.; this column was obtained prepacked from Macherey, Nagel & Co. (Düren, Germany).

Three different columns packed with CSP I were tested.

Non-chiral alkylsilica phases RP-2 and RP-8 (LiChrosorb; Merck) were used for the measurements with CMAs; column dimensions, 125 mm × 4 mm I.D.

Mobile phases

The organic eluent components methanol, ethanol and acetonitrile were of LiChrosolv grade and tetrahydrofuran (THF) of analytical-reagent-grade from Merck. Water was distilled twice from a quartz apparatus and additionally purified by passage through an RP-8 column before eluent preparation. The eluent mixtures were filtered and degassed by ultrasonic treatment.

The buffer salts, ammonium and sodium acetate and sodium hydrogensulphate, and also copper acetate and copper sulphate were obtained from Merck. The pH of the buffer solutions was adjusted by adding acetic acid or dilute sulphuric acid, and dilute ammonia or sodium hydroxide solution.

Analytes

Mono-, bi- and tridentate ligands of the types benzoic acid, D,L-amino acids and N-dansylated D,L-amino acids were investigated.

Chromatographic conditions

Flow-rates of 1 ml/min and a temperature of 30°C were applied unless indicated otherwise. Careful thermostating was necessary in order to keep the amount of copper adsorbed constant. Generally, UV detection was performed at 254 nm. Fluorescence detection (excitation at 340 nm and emission measurement at 480 nm) was used for

systems with CMAs only. An injection volume of 20 μl was used for experiments employing CSPs and 5 μl for the experiments with CMAs. Void volumes of the columns were determined from the system peaks in copper-free systems. Their values were about 1.20 ml for the given column dimensions.

Significance of data

Plate height values were calculated from peak widths determined at 0.607 of the peak heights and, for control purposes, from the distance between the inflection tangents at the base line [37].

The precision [relative standard deviation (R.S.D.)] of the capacity factor determination was about 3%. The precison (R.S.D.) of plate height determinations was about 10% in LEC systems with bonded selectors and about 7% in reversed-phase systems with CMAs.

The precision and accuracy of plate height determinations in LEC systems with bonded selectors are generally inferior to those in common reversed-phase systems. This is caused by three main factors: (i) with many LEC stationary phases, peak tailing occurs down to low concentrations of analytes, and often one has to balance between systematic errors caused by tailing peaks and statistical errors caused by the scatter of the baseline; (ii) mobile phases in LEC usually contain several components which give rise to several system peaks not all of which are detectable, and system peaks may affect the peak width of the analytes [38], even if the system peaks are undetected; (iii) when detection is performed at a wavelength where mobile phase components absorb, UV-monitored system peaks sometimes interfere with the analyte peaks or disturb the baseline (for this reason some entries in the data tables are blank).

RESULTS AND DISCUSSION

Plate heights in LEC as a function of flow-rate

The dependence of the plate height on the flow-rate is shown for ligand-exchange chromatography with chemically bonded selectors (CSPs) in Fig. 3 and for a system employing a highly soluble chiral selector as CMA in Fig. 4. The curves show significant differences between these two LEC modes.

Plate height curve for the CSP mode. With bonded selector ligands (CSP), the plate heights of most analytes decrease strongly and fairly linearly with the flow-rate, w. The plate height minimum is located at very low values of w. Flow-rate is thus one of the most important and practical parameters for improving the resolution in ligand-exchange chromatography with CSPs.

The strong flow-rate dependence of h supports the assumption that enhanced peak dispersion in LEC with CSPs results primarily from kinetic sources and does not originate from energetic inhomogeneity of adsorption sites and the resulting non-linear adsorption isotherm [39].

The data in Fig. 3 indicate the following pattern:

The plate height is most strongly determined by the dentation number: the monodentate ligand benzoic acid has lower plate height values than the bidentate ligands alanine, valine and leucine. Histidine often acts as a tridentate ligand [6]. The effect of dentation is observed to be predominant over the influence of capacity factors (*cf.*, benzoic acid, D-alanine, D-histidine).

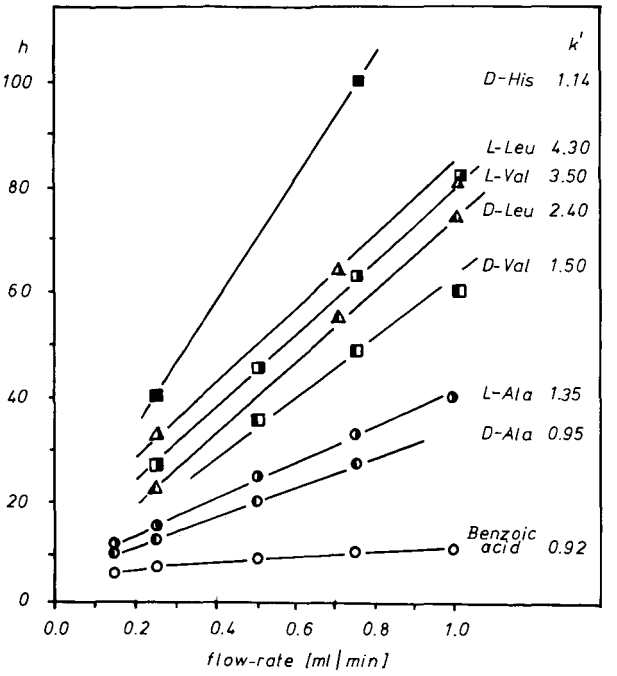

Fig. 3. Influence of flow-rate on the plate height in systems with bonded selectors. Chromatographic conditions: stationary phase, CSP II; mobile phase, aqueous buffer solution [$4 \cdot 10^{-4}$ *M* copper(II) acetate–$5 \cdot 10^{-2}$ *M* ammonium acetate, pH 5.5]; temperature, 30°C.

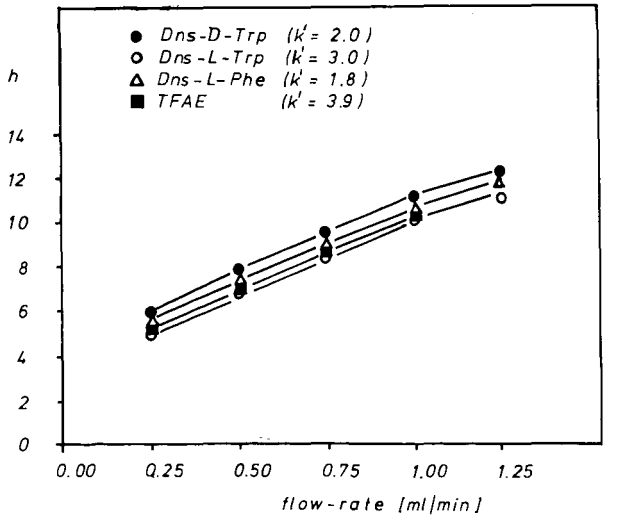

Fig. 4. Influence of flow-rate on the plate height in systems with chiral mobile phase additives. Chromatographic conditions: RP-2 column; mobile phase, aqueous buffer solution [$5 \cdot 10^{-3}$ *M* L-proline–$2.5 \cdot 10^{-3}$ *M* copper(II) sulphate–$1 \cdot 10^{-3}$ *M* ammonium acetate, pH 7]–acetonitrile (75:25, v/v); temperature, 30°C; mobile phase for TFAE, aqueous buffer (10^{-3} *M* ammonium acetate, pH 7)–acetonitrile (60:40, v/v); injection volume, 5 μl.

For the series of bidentate amino acids, the plate heights seem to increase with increasing capacity factors. More detailed investigations concerning the influence of k', however, revealed that the influence of k' is not simple. This point is discussed below.

In all instances investigated, the enantiomer eluted later shows a larger value of h.

Systems employing chiral ligands as CMA. In ligand-exchange systems working with highly soluble chiral mobile phase additives, the dependences of the plate height on the flow-rate are very similar to those usually observed in simple reversed-phase chromatography (Fig. 4). In our experiments, trifluoranthrylethanol (TFAE) was selected as a reference compound in copper-free systems to account for the simple reversed-phase adsorption mode (dansylamino acids have very small capacity factors under these conditions). In comparison with Fig. 3, the slope of the h *vs.* w plot is much smaller, the dependence of h on the capacity factor is marginal[a] and one can only detect a very small, probably insignificant, influence of the optical configuration on h.

The data in Figs. 3 and 4 are the main source for our conclusion that in the CMA mode employing highly soluble chiral additives, and under the chosen conditions, the ligand-exchange equilibrium (equilibrium 1 in Fig. 1b) is not rate determining. It is likely that complexation takes place in both phases, but mainly in the mobile phase, and that the diastereomeric complexes are adsorbed and desorbed from the alkylsilica surface (equilibrium 3 in Fig. 1b) with the rapid kinetics typical of reversed-phase chromatography. Under these conditions slow ligand-exchange kinetics should not have much effect on h, in contrast to the case where the ligand is bound at the surface. Moreover, it is likely that ligand exchange is even more rapid if performed in the mobile phase, owing to fewer steric constraints.

Influence of capacity factor on plate height in the CSP mode

Capacity factors influence the plate height in the CSP mode by a number of mechanisms, which are reflected both in theory (eqns. 1 and 2) and in experimental data.

Experimental data. Within the series of the homologous amino acids investigated and under constant phase system conditions, the plate heights increase from alanine, serine, methionine to valine, leucine and phenylalanine parallel to the increase in the k' values (Table I and the broken lines in the Figs. 5 and 6).

When changing the capacity factors by varying the content of organic modifier in the mobile phase, the h values for a given analyte decrease with increasing k' (full lines in Fig. 5). However, within the series of amino acids, the previously mentioned correlation is maintained (broken lines).

When changing the capacity factors by varying the pH of the eluent, the h values either increase (CSP I) or decrease (CSP II) with increasing k' (Fig. 6 and Table II). In all instances, however, the increase within the series of homologous amino acids is maintained (broken line).

Within the series of free amino acids investigated, the h *vs.* k' correlations are found to be similar in type for the two differing CSPs (Figs. 5 and 6). Within the series

[a] The slight decrease in h observed with increasing capacity factors might originate at least partly from extra-column contributions.

TABLE I

CAPACITY FACTORS, k', AND REDUCED PLATE HEIGHTS, h, AS A FUNCTION OF THE ANALYTE STRUCTURE AND THE VOLUME FRACTION OF ETHANOL IN THE MOBILE PHASE

Stationary phase, CSP II; mobile phase, aqueous buffer [0.05 M sodium acetate–$5 \cdot 10^{-4}$ M copper(II) acetate, pH 5.5]–ethanol as indicated; temperature, 30°C; flow-rate, 1 ml/min.

Amino acid		Ethanol (%, v/v)							
		0		20		40		70	
		k'	h	k'	h	k'	h	k'	h
Non-derivatized									
Benzoic acid		0.70	15	0.38	12				
Ala	I	0.75	31	1.66	28				
	II	0.95	38	2.20	31				
Met	I	1.82	38	3.09	38				
	II	2.52	47	3.79	44				
Val	I	1.36	50	2.39	43				
	II	2.86	58	4.70	47				
Leu	I	1.85	50	2.64	46				
	II	2.98	61	3.94	55				
Phe	I	3.44	53	4.65	50				
	II	4.88	60	5.80	58				
Dansylated									
Dns-Val	I			1.76	32	1.53	42	1.98	46
	II			3.61	41	3.18	52	4.25	61
Dns-Leu	I			1.78	29	1.06	25	1.51	38
	II			2.71	37	1.85	35	2.33	41
Dns-Ser	I			3.12	38	3.72	56	5.50	80
	II			5.82	50	5.65	96		
Dns-Phe	I			4.15	51	4.14	62	4.30	53
	II			8.09	76	10.42	130	12.80	110

of dansylated amino acids these h *vs.* k' correlations are different between CSP I and CSP II (Fig. 7).

For CSP II, the plate heights of dansyl amino acids increase strongly with increasing k' (like free amino acids), but for CSP I, h is nearly independent of k' (unlike free amino acids). This independence is also seen from the data in Table III, where the influence of different types of organic modifiers in the eluent is reported.

This difference between the two CSPs is of interest for investigations concerning differences in the predominant adsorption mechanisms in LEC phases. A more detailed discussion of the influence of organic modifiers and pH on the plate height will be given in a future paper in the broader context of a study on mixed adsorption mechanisms. With regard to the influence of the capacity factor, which is the primary concern here, the experimental finding is that no simple dependence of h on k' can be observed.

Theoretical expectations. From eqns. 1 and 2 we expect an increase in h with increasing capacity factors via the contribution h_f, a decrease in h via the contribution

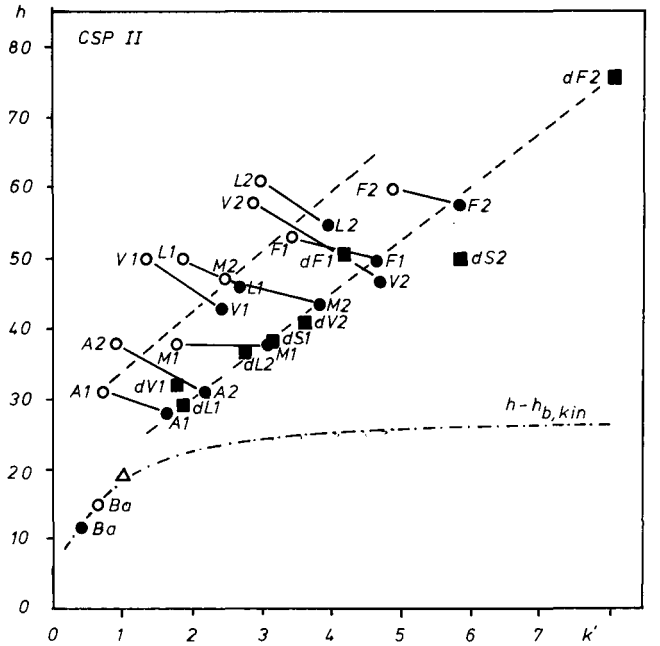

Fig. 5. Plate height *vs.* capacity factor correlation: influence of analyte structure and ethanol concentration in the mobile phase. Stationary phase, CSP II; mobile phase, aqueous buffer solution [$4 \cdot 10^{-4}$ *M* copper(II) acetate–$5 \cdot 10^{-2}$ *M* ammonium acetate, pH 5.5] with various concentrations of ethanol; temperature, 30°C; flow-rate, 1 ml/min. Circles, free amino acids; squares, dansylated amino acids; open symbols, no ethanol present; full symbols, 20% (v/v) ethanol. Analyte symbols: A = alanine; V = valine; L = leucine; S = serine; M = methionine; F = phenylalanine; W = tryptophan; T = threonine; Ba = benzoic acid; A1 = first-eluted enantiomer of alanine, A2 = second-eluted enantiomer, etc.; dA = dansylalanine; dV = dansylvaline, etc. Triangle: data point obtained for Dns-Phe in a phase system without copper ions; the dot-dashed line indicates plate height values without kinetic contributions, $h - h_{b,kin}$, obtained by extrapolation.

$h_{b,mt}$ and, depending on the values of the dissociation rate constant, k_d, and of k', an increase or a decrease via the kinetic contribution $h_{b,kin}$. Typical values for the k'-related factors in these terms in the investigated k' range are given in Table IV. An approximate evaluation of the relative contributions of the mentioned plate height terms gives the following:

For $h_{b,mt}$ we know from previous investigations that this term is small [40–42]. In a reasonable approximation one can therefore neglect this term in this discussion.

h_f might be important. Between $k' = 1$ and 10 this contribution increases by about 60% (*cf.*, Table IV). From data for copper-free systems we are able to calculate approximate h values for the case of insignificant kinetic contributions (in this instance the dependence on k' is mainly due to the h_f term). For CSP I experimental h *vs.* k' data in copper-free systems are available between $k' = 3$ and 14 and are given in Fig. 8. These data are plotted as the $h - h_{b,kin}$ curve at the bottom of Fig. 6b. For CSP II fewer experimental h data in copper-free systems are available. The extrapolated $h - h_{b,kin}$ curve at the bottom of Fig. 5 is obtained by assuming that under the given conditions at

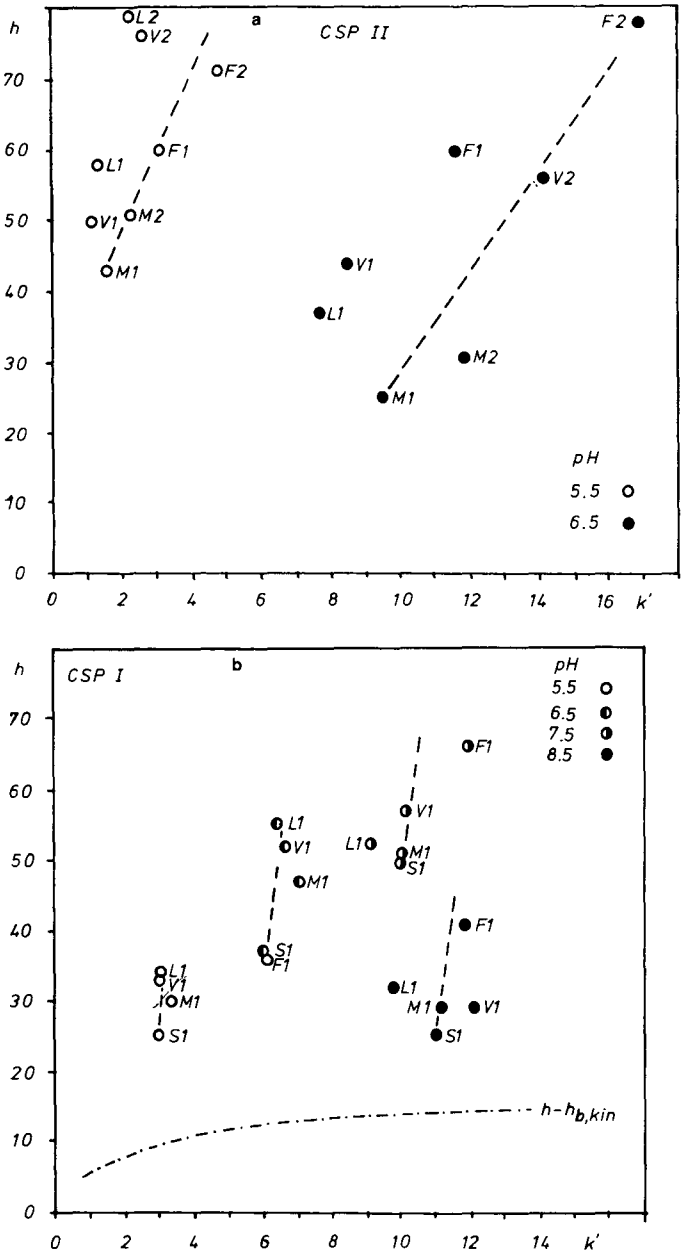

Fig. 6. Plate height *vs.* capacity factor correlation: influence of analyte structure and pH of the mobile phase. (a) Stationary phase, CSP II; mobile phase, aqueous buffer solution [$4 \cdot 10^{-4}$ *M* copper(II) acetate–$5 \cdot 10^{-2}$ *M* ammonium acetate, pH as indicated] with no organic modifier. (b) Stationary phase, CSP I; mobile phase, aqueous buffer solution [$4 \cdot 10^{-4}$ *M* copper(II) acetate–$5 \cdot 10^{-2}$ *M* ammonium acetate, pH as specified]–methanol (70:30, v/v); temperature, 30°C; flow-rate, 1 ml/min. Abbreviations of analytes as in Fig. 5. The dot-dashed line indicates the extrapolated total plate height curve without kinetic contributions, $h - h_{b,kin}$, obtained by use of the data in Fig. 8.

TABLE II

CAPACITY FACTORS, k', AND REDUCED PLATE HEIGHTS, h, AS A FUNCTION OF THE ANALYTE STRUCTURE AND THE pH OF THE ELUENT

(A) Stationary phase, CSP I; mobile phase, aqueous buffer [0.05 *M* ammonium acetate–4 · 10^{-4} *M* copper(II) acetate, pH values as indicated]–methanol (70:30, v/v); temperature, 30°C; flow-rate, 1 ml/min. (B) Stationary phase, CSP II; mobile phase, aqueous buffer [0.05 *M* ammonium acetate–5 · 10^{-4} *M* copper(II) acetate, pH values as indicated] with no organic modifier; temperature, 30°C; flow-rate 1 ml/min.

Conditions	Analyte		pH							
			5.5		6.5		7.5		8.5	
			k'	h	k'	h	k'	h	k'	h
A	L-Ser		2.98	25	6.04	37	10.01	49	10.97	25
	L-Met		3.42	30	7.09	47	10.04	49	11.16	29
	L-Val		3.10	33	6.72	52	11.98	57	12.18	29
	L-Leu		3.04	34	6.50	55	8.74	52	9.78	32
	L-Phe		6.08	36	10.30	–	11.94	66	11.86	41
	Dns-L-Val		6.47	25	16.18	56	13.71	82	5.00	103
	Dns-D-Val		9.89	28	29.30	54	23.73	79	8.02	–
	Dns-L-Leu		6.56	23	13.30	52	12.42	67	6.15	94
	Dns-D-Leu		10.74	25	28.00	–	23.74	55	10.06	93
	Dns-L-Ser		17.58	29	25.87	–	26.40	66	7.98	–
	Dns-D-Ser		33.06	24	47.80	–	42.46	56	10.54	–
B	DL-Met	I	1.6	43	9.5	25				
		II	2.3	51	11.9	31				
	DL-Val	I	1.2	50	8.5	44				
		II	2.6	76	14.2	56				
	DL-Leu	I	1.3	58	7.7	37				
		II	2.2	79	12.6	–				
	DL-Phe	I	3.1	60	11.6	60				
		II	4.8	71	16.9	78				

$k' = 1$ about half of the total plate height value originates from h_c (which is not dependent on k'), and about half from h_f, which can be extrapolated by means of eqn. 1c. On the basis of this rough approximation, the $h - h_{b,kin}$ curve can serve in this instance as a semi-quantitative guide only.

$h_{b,kin}$ is influenced by k' in two ways (*cf.*, eqn. 2): by the factor $k'/(k' + 1)^2$ and by the dissociation rate constant k_d. The k'-containing factor has its maximum value at $k' = 1$ and decreases to half of this value when k' increases from 1 to 6. In this capacity factor range, this is a negative dependence.

Considering the dissociation rate constant, it should be noted that k_d is determined by the activation free energy of complex dissociation and not by the binding energy of the complex, which determines k'. We expect, however, that under certain conditions (*e.g.*, considering a series of homologous compounds) the activation energy for this "reaction" and the binding energy are correlated to a certain extent. In these instances h will be positively correlated with k' via k_d, and this correlation may

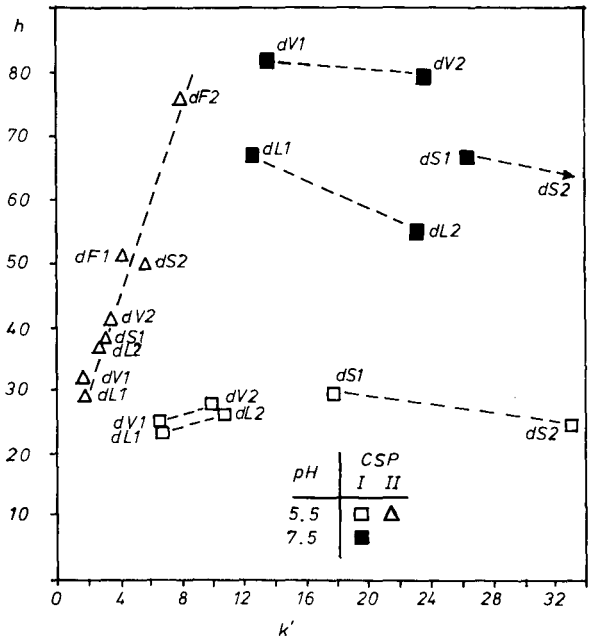

Fig. 7. Plate height *vs.* capacity factor correlation: influence of analyte structure of dansylated amino acids, pH and type of stationary phase. Stationary phases, CSP I and II; mobile phases, aqueous buffer solution [$4 \cdot 10^{-4}$ *M* copper(II) acetate–$5 \cdot 10^{-2}$ *M* ammonium acetate, pH as indicated]–methanol (70:30, v/v) for CSP I and aqueous buffer solution–ethanol (80:20, v/v) for CSP II; temperature, 30°C; flow-rate, 1 ml/min. Abbreviations of analytes as in Fig. 5.

TABLE III

CAPACITY FACTORS, k', AND REDUCED PLATE HEIGHTS, h, AS A FUNCTION OF THE TYPE OF ORGANIC MODIFIER IN THE ELUENT

Stationary phase, CSP I; mobile phase, aqueous buffer [0.05 *M* ammonium acetate–$5 \cdot 10^{-4}$ *M* copper(II) acetate, pH 5.5]–organic modifier (30:70, v/v); temperature, 30°C; flow-rate, 1 ml/min.

Compound		Modifier							
		Acetonitrile		Methanol		Ethanol		THF	
		k'	h	k'	h	k'	h	k'	h
Phe		2.27	13	2.61	14	2.00	15	1.33	14
Ile		2.12	11	3.32	17	2.57	17	1.58	17
Dns-Nval	I	1.50	5.1	8.58	6.6	4.80	6.5		
	II	2.05	5.8	11.74	7.6	6.00	6.0		
Dns-Leu	I	1.40	6.3	7.74	5.6	4.54	6.7	2.37	7.4
	II	1.95	6.2	10.12	6.1	5.54	6.5	2.60	6.1
Dns-Met	I	2.30	5.4	12.0	6.7	6.63	8.1	0.50	6.7

TABLE IV

NUMERICAL VALUES FOR THE CAPACITY FACTOR-RELATED FACTORS IN THE EQNS. 1c, 1d AND 2

k'	k''	$[k''/(k'' + 1)]^2$ in h_f	$k''/(k'' + 1)^2$ in $h_{b,mt}$	$k'/(k' + 1)^2$ in $h_{b,kin}$
0.1	1.2	0.30	0.24	0.08
0.5	2.0	0.44	0.22	0.22
1.0	3.0	0.56	0.19	0.25
3.0	7.0	0.77	0.11	0.19
5.0	11.0	0.84	0.08	0.14
10.0	21.0	0.91	0.04	0.08
20.0	41.0	0.95	0.02	0.05

mimic a strict and direct dependence of k_d (and thus h) on k', although a strict dependence is neither implied by theory nor found generally in the experiments (*cf.*, Table 7 in ref. 35). This positive correlation can be so significant that it far overcompensates for the negative correlation via the factor $k'(k' + 1)^2$.

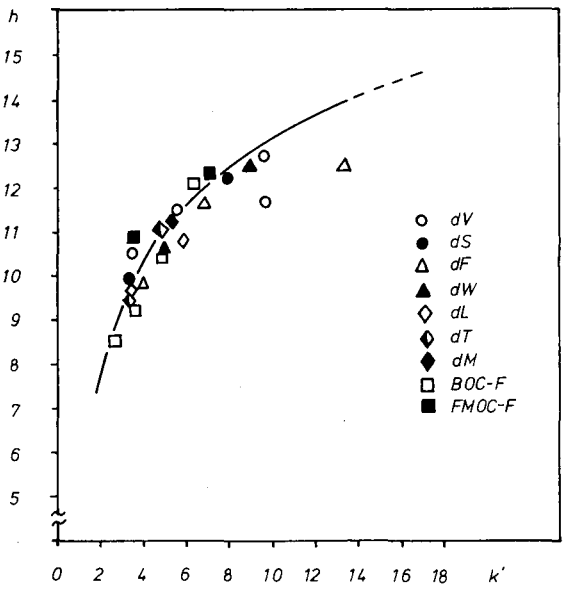

Fig. 8. Plate height *vs.* capacity factor correlation in copper-free systems. Stationary phase, CSP I; mobile phase, aqueous buffer solution ($5 \cdot 10^{-2}$ *M* ammonium acetate, pH 5.5) with various concentrations of acetonitrile; temperature, 30°C; flow-rate, 1 ml/min. Abbreviations of analytes as in Fig. 5. BOC = butyloxycarbonyl-; FMOC = fluorenyloxycarbonyl-.

CONCLUSIONS

From the data reported above, the following conclusions can be drawn:

In systems where ligand-exchange processes are operative at the surface, we found that plate heights for the bi- or tridentate analytes investigated are significantly higher than in systems without ligand-exchange processes (*cf.*, the $h - h_{b,kin}$ lines in Figs. 5 and 6 and the data in Fig. 8 obtained in the absence of metal ions). We attribute this effect to the slow ligand-exchange rates for a ligand-exchange step taking place at the surface of the stationary phase.

LEC systems using CMAs generally have better efficiencies than systems with CSPs. No significant difference in plate heights is observed between ligand-exchange and the usual reversed-phase adsorption chromatography. We conclude that in this mode the dominant mechanism is the adsorption of the diastereomeric complexes, which are formed in the mobile phase, by a simple reversed-phase adsorption mechanism. In this instance, slow ligand-exchange kinetics do not have much effect on h.

The plate height dependences on the flow-rate have different strengths for the two LEC modes. This is in agreement with the given model. As the ligand-exchange specific contribution to h is high with CSPs, the plate height minimum is situated at very low flow velocities. Using LEC with CSPs, there is great potential for improving the resolution by reducing the flow velocity.

When using immobilized selector ligands, the kinetic contribution, $h_{b,kin}$, depends on several parameters:

The most important influence originates from the dentation number of the analyte ligands. This is in accord with the fact that binding energy and the resulting activation energy for dissociation increase strongly with increase in the number of ligand–metal bonds involved.

The influence of the capacity factor on h is not simple. Within a series of amino acids we observe a certain positive correlation between the plate heights and the capacity factors, although there is a fairly reproducible fine structure of systematic deviations from this correlation. Plate heights, however, may also decrease with increasing k', *e.g.*, when varying the eluent composition. However, the positive correlation within the amino acid series mentioned is always maintained, and to a great extent even the "fine structure" of deviations (Figs. 5 and 6). The conservation of these fine structure on variation of the mobile phase precludes its origination from a statistical scatter of data.

From these observations, we conclude that h is not simply determined by the capacity factor itself[a], but rather by a parameter that is related to the length, shape, steric size and bulkiness of the side-chains and to the configuration at the chiral carbon atom of the amino acids, all of which affect the reaction rate constant and thus $h_{b,kin}$ via the free energy of activation. This conclusion is supported by the fact that in general an increase in h with increasing "bulkiness" of the side-chains has been found in all experiments (which measure for "bulkiness" will be most appropriate in this context is not yet clear). It is likely that bulkiness plays an even more important role for the

[a] Note in addition that the experimental h values are not really linearly correlated with the formation constants of the amino acid–copper complexes [35].

chelating reactions at surface-immobilized complexes than for those in a bulk phase.

For the amino acids investigated, the increasing steric size of the side-chains is also correlated with enhanced k' values. We therefore conclude that the observed positive correlation between h and k' within the series of amino acids basically originates from this correlation between binding energy and free energy of activation. It is in good agreement with this explanation that a different dependence of h on k' is detected when k' is increased not by varying the length of the side-chain but by varying the eluent composition.

Similar explanations may hold for the dependence of the reaction rate on the optical configuration. This influences k' and, in the way mentioned before, the energy of the transition state for the complexation reaction.

The different patterns in the h *vs.* k' curves observed for the dansylated amino acids at the two chiral stationary phases probably originate from a mixed mechanism of adsorption on at least one of these phases (CSP I). We have seen from capacity factor data in copper-free systems (triangle symbol in Fig. 5 and data in Fig. 8) that the hydrophobic adsorption of dansylamino acids without complexation is significant with CSP I, unlike the situation with CSP II. We argue that the approximate invariance of h with k', shown for CSP I in Fig. 7, might result from the reduced contributions of complexation for these analytes under the given conditions. This problem is the subject of a broader investigation to be presented in a subsequent paper.

We conclude that the predominant plate height-determining parameters are the dentation number of the analyte and the steric size and the optical configuration of the interacting groups in the chelate complex, all of which influence the dissociation rate constant, k_d. The plate height is not primarily determined by the value of the capacity factor itself. Capacity factors are often correlated with k_d, especially within a homologous series of analytes, but not necessarily.

ACKNOWLEDGEMENT

This study was supported by a grant from the Austrian Fond zur Förderung der wissenschaftlichen Forschung (FWF), project number P6300C. The author appreciates this support.

REFERENCES

1 V. A. Davankov, *Adv. Chromatogr.*, 18 (1980) 139.
2 V. A. Davankov, A. A. Kurganov and A. S. Bocklov, *Adv. Chromatogr.*, 22 (1983) 71.
3 J. N. LePage, W. Lindner, G. Davies, D. E. Seitz and B. L. Karger, *Anal. Chem.*, 51 (1979) 433.
4 W. Lindner, J. N. LePage, G. Davies, D. E. Seitz and B. L. Karger, *J. Chromatogr.*, 185 (1979) 323.
5 W. Lindner, *Naturwissenschaften*, 67 (1980) 354.
6 Y. Tapuhi, N. Miller and B. L. Karger, *J. Chromatogr.*, 205 (1981) 325.
7 B. Feibush, M. J. Cohen and B. L. Karger, *J. Chromatogr.*, 282 (1983) 3.
8 G. Gübitz, W. Jellenz, G. Löffler and W. Santi, *J. High Resolut. Chromatogr. Chromatogr. Commun.*, 2 (1979) 145.
9 G. Gübitz, W. Jellenz and W. Santi, *J. Chromatogr.*, 203 (1981) 377.
10 G. Gübitz, W. Jellenz and W. Santi, *J. Liq. Chromatogr.*, 4 (1981) 701.
11 G. Gübitz, *J. Liq. Chromatogr.*, 9 (1986) 519.
12 P. Roumeliotis, K. K. Unger, A. A. Kurganov and V. A. Davankov, *Angew. Chem.*, 94 (1982) 928.
13 P. Roumeliotis, K. K. Unger, A. A. Kurganov and V. A. Davankov, *J. Chromatogr.*, 255 (1983) 51.

14 A. Foucault, M. Caude and L. Oliveros, *J. Chromatogr.*, 185 (1979) 345.
15 H. Engelhard and S. Kromidas, *Naturwissenschaften*, 67 (1980) 353.
16 H. Engelhardt, Th. König and St. Kromidas, *Chromatographia*, 21 (1986) 205.
17 H. G. Kicinski and A. Kettrup, *Fresenius' Z. Anal. Chem.*, (1985) 51.
18 H. Brückner, *Chromatographia*, 24 (1987) 725.
19 P. E. Hare and E. Gil-Av, *Science (Washington, D.C.)*, 204 (1979) 1226.
20 V. A. Davankov, A. S. Bochkov, A. A. Kurganov, P. Roumeliotis and K. K. Unger, *Chromatographia*, 13 (1980) 677.
21 S. Lam, F. Chow and A. Karmen, *J. Chromatogr.*, 199 (1980) 295.
22 S. Lam and G. Malikin, *J. Chromatogr.*, 368 (1986) 413.
23 C. Gilon, R. Leshem and E. Grushka, *J. Chromatogr.*, 203 (1981) 365.
24 E. Grushka, R. Leshem and C. Gilon, *J. Chromatogr.*, 255 (1983) 41.
25 S. Weinstein, M. H. Engel and P. E. Hare, *Anal. Biochem.*, 121 (1982) 370.
26 R. Wernicke, *J. Chromatogr. Sci.*, 23 (1985) 39.
27 E. Armani, A. Dossena and R. Marchelli and R. Virgili, *J. Chromatogr.*, 441 (1988) 275.
28 E. Armani, L. Barazzoni, A. Dossena and R. Marchelli, *J. Chromatogr.*, 441 (1988) 287.
29 J. F. K. Huber, *J. Chromatogr. Sci.*, 7 (1969) 85.
30 J. F. K. Huber, *Ber. Bunsenges. Phys. Chem.*, 77 (1973) 179.
31 J. C. Giddings, *Dynamics of Chromatography, Part I, Principles and Theory*, Marcel Dekker, New York, 1965.
32 S. G. Weber and P. W. Carr, in P. R. Brown and R. A. Hartwick (Editors), *High Performance Liquid Chromatography*, Wiley-Interscience, New York, 1989.
33 W. R. Melander and Cs. Horváth, in Cs. Horváth (Editor), *High Performance Liquid Chromatography, Advances and Perspectives*, Vol. 2, Academic Press, New York, 1980, p. 119.
34 M. J. Nicol, C. A. Fleming and J. S. Preston, in G. Wilkinson, R. D. Gillard and J. A. McCleverty (Editors), *Comprehensive Coordination Chemistry, the Synthesis, Reactions, Properties and Applications of Coordination Compounds*, Vol. 6, Pergamon Press, Oxford, 1987, Ch. 63.3.
35 S. H. Laurie, in G. Wilkinson, R. D. Gillard and J. A. McCleverty (Editors), *Comprehensive Coordination Chemistry, the Synthesis, Reactions, Properties and Applications of Coordination Compounds*, Vol. 2, Pergamon Press, Oxford, 1987, Ch. 20.2.
36 Cs. Horváth and H.-J. Lin, *J. Chromatogr.*, 149 (1978) 43.
37 L. R. Snyder and J. J. Kirkland, *Introduction to Modern Liquid Chromatography*, Wiley-Interscience, New York, 2nd ed., 1979, Ch. 2.
38 T. Fornstedt, D. Westerlund and A. Sokolowski, *J. Liq. Chromatogr.*, 11 (1988) 2645.
39 L. R. Snyder and J. J. Kirkland, *Introduction to Modern Liquid Chromatography*, Wiley-Interscience, New York, 2nd ed., 1979, Ch. 15.2.
40 J. F. K. Huber and A. Rizzi, *J. Chromatogr.*, 384 (1987) 337.
41 R. W. Stout, J. J. DeStefano and L. R. Snyder, *J. Chromatogr.*, 282 (1983) 263.
42 J. H. Knox and H. P. Scott, *J. Chromatogr.*, 282 (1983) 297.

Journal of Chromatography, 542 (1991) 239–245
Elsevier Science Publishers B.V., Amsterdam

CHROM. 23 037

Determination of size limits of membrane separation in vesicle chromatography by fractionation of polydisperse dextran

RUDOLF EHWALD*, PETRA HEESE and ULRICH KLEIN
Humboldt-Universität zu Berlin, Sektion Biologie, Invalidenstr. 42, Berlin 1040 (Germany)
(First received June 26th, 1990; revised manuscript received October 9th, 1990)

ABSTRACT

A recently described vesicular chromatographic packing material (VP), consisting of purified plant cell walls with vesicular and cellular morphology, was characterized with respect to the minimum Stokes' diameter necessary for complete exclusion (size limit of exclusion = SLE) and the maximum Stokes' diameter permitting permeation into the whole stationary liquid volume (size limit of permeation = SLP). Using vesicle chromatography, the size fractionation of a polydisperse dextran preparation with a defined size distribution was carried out to determine the percentages of completely excluded (P_{ex}) and completely permeable (P_{perm}) dextran molecules. SLE may be derived from P_{ex} and SLP from P_{perm} taking into account the molecular size range of the fractionated polydisperse dextran sample. Values determined for the size limits of the vesicle membrane with the help of dextran 35 (calibrated on Sephadex G-200) were nearly equal to those determined with the help of dextran 15 (calibrated on Sephadex G-75). The SLP of the standard VP is 5.6 nm. However, negatively charged proteins with a Stokes' diameter slightly below the SLP (pepsin and ovalbumin) are excluded from the VP. The method may be applied in controlling the separation limits of VPs with altered ultrafiltration properties.

INTRODUCTION

The solid structure of the vesicular packing material (VP) [1] commercially available as Permselekt or Vesipor is the purified cell wall framework developed by cell clusters grown in a higher plant suspension culture. It consists of a cellulose–pectin (cellin) matrix [2] with a mechanically and chemically unaltered structure. The separation mechanism in vesicle chromatography (VC) is membrane permeation (dialysis) between the mobile phase and the stationary liquid phase which is kept in vesicles (cells, microcapsules). The cell walls act as dialysis membranes with a sharp separation limit. Chromatography with the VP permits a rapid separation of two size groups of macromolecules on short columns. The absence of an extended fractionation range in VC, which is the main difference from gel permeation chromatography (GPC), is an advantage for size fractionations in a narrow molecular size range. VP consisting of unaltered cellin walls separates excluded macromolecules (*e.g.*, proteins of $>50\,000$ dalton) from slightly smaller molecules and other permeable molecules [1]. We have found (unpublished work) that the separation limits of the cellin membranes may be increased by depolymerization of the protopectin matrix with different methods.

0021-9673/91/$03.50

In this paper, we describe a procedure for determining the the size limits of separation by VC. Such a method is necessary for controlling the preparation of VPs with different separation properties.

PRINCIPLE OF METHOD

In VC, a mixture of macromolecules with a continuous and broad distribution of molecular size, *e.g.*, polydisperse dextran, may be separated into two main fractions, a permeable and an unpermeable (excluded) fraction [1]. The method is based on such a separation using a dextran standard of defined molecular size distribution.

A polydisperse dextran standard is fractionated by GPC on a suitable gel, the bed having been calibrated by proteins of defined Stokes' diameter. GPC results in a broad, continuous elution profile of the fractionated dextran. Using a calibrated gel column, the dependence of dextran concentration in the eluate on the elution volume, V_e, is transformed into a calibration graph giving the dependence of the Stokes' diameter on the percentage of dextran eluted, P_e. Both the excluded percentage, P_{ex}, obtained from VC of the standard dextran and the percentage P_e obtained from GPC are related to the sum of monodisperse fractions with Stokes' diameter, d_s, larger than a certain size. If $P_e = P_{ex}$, then d_s, coordinated to P_e, is also the Stokes' diameter of the smallest dextran molecules excluded by the VP. Therefore, once P_{ex} has been determined experimentally, d_s may be read off the calibration graph. The value determined in this way is designated as the size limit of exclusion (SLE) of the VP. Similarly, the permeable percentage P_{perm} obtained from VC and the non-eluted percentage $(100 - P_e)$ obtained from GPC refer to the sum of dextran fractions with molecular size smaller than a certain value. If P_{perm} is equated to $100 - P_e$, the Stokes' diameter allied to P_e is the diameter of the largest permeable dextran molecules in the permeable fraction obtained by VC. This Stokes' diameter is designated as the size limit of permeation (SLP) of the VP. The interval between these two limits is the size range of dextran molecules eluted after the excluded fraction and before the permeable fraction (fractionation range).

EXPERIMENTAL

Dextran 15 and 35 were supplied by Serva (Germany). Both preparations were used from the same package for all experiments. Blue Dextran 2000, Dextran T 250 and Sephadex G-75 and G-200 were supplied by Pharmacia (Sweden).

The chromatographic system consisted of a peristaltic pump from Unipan (Poland) and a Perkin-Elmer Model 141M recording polarimeter (volume of microcuvette 1 ml, light path 10 cm) for recording dextran concentration. Peaks of polyethylene glycol and proteins were recorded by means of an RIDK differential refractometer (Czechoslovakia). Permselekt vesicular packing material as ethanol-moist or dry material was washed with distilled water and dispersed in the elution buffer.

Glass columns of 2.9 cm I.D. with end frits (polyamide cloth, mesh width 80 μm, supported by a polyethylene sieve plate) were packed using a slurry containing about 10 mg/ml of dry packing material. After the liquid above the sedimented material had been absorbed, the chromatographic bed was allowed to shrink to about 80% of its original sedimentation volume by slow draining with mild suction (2–3

kPa). The chromatographic bed was covered with a polyamide cloth and a polyethylene sieve plate, which was fixed by a tight-fitting rubber ring. Column contained 23 to 27 mg of the dry packing material per millilitre of bed volume. Between chromatographic experiments, the columns were equilibrated with a stabilizing medium (0.5% KH_2PO_4–0.05% NaN_3). Before use they were saturated with the elution buffer (0.05 *M* phosphate buffer containing 0.05% NaN_3). Glass columns for GPC were packed by the usual procedure.

Planimetry of the chromatograms was carried out gravimetrically using suitable transparent paper. The excluded percentage was determined as twice the percentage of the dextran sample that was eluted up to the maximum of the first (excluded) peak and the permeable percentage as twice the dextran percentage after the second peak maximum. Elution volumes and K_{av} values (the fraction of the gel volume that is available for the sample) were determined as described by Laurent and Killander [3].

RESULTS AND DISCUSSION

For the investigation of the molecular size distribution, dextran elution profiles representing more than 2000 theoretical plates were considered. Ranges of the elution volume, V_e, which are characterized by small variations in concentration within the peak variance of a monodisperse molecule were selected for use in calibration graphs (region a–b in Fig. 1). With respect to calibration of the Sephadex beds (G-75 and

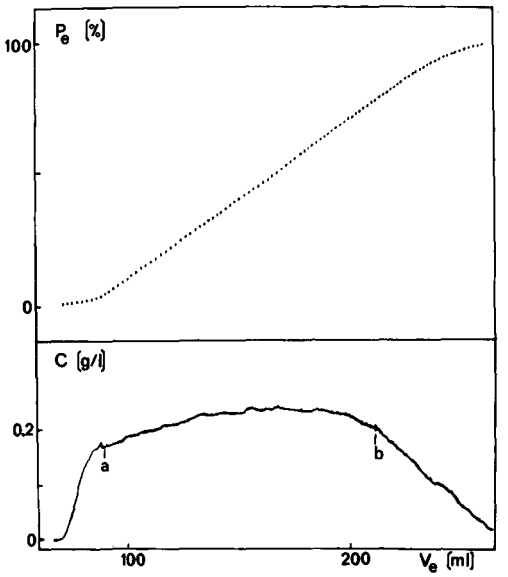

Fig. 1. GPC of dextran 35. Lower curve: trace for dextran 35 obtained by means of a Sephadex G-200 column (bed length 27.0 cm, bed volume 263 ml, particle size 40–120 μm, exclusion volume 84 ml). Sample (dissolved in 2 ml of eluent buffer), 40 mg; a–b, section of the elution curve with an approximately symmectrical influence of monodisperse neighbour fractions on the recorded dextran concentration. Trace recorded with a Perkin-Elmer Model 141 M polarimeter; wavelength = 436 nm. Upper curve: percentage of eluted dextran 35 derived by integration of the lower trace.

G-200) used for dextran fractionation, we did not find significant deviations of protein K_{av} values from the originally published curves [3]. Fig. 2 shows the corresponding curve from ref. 3, respresented by the line, together with the positions of the standard proteins determined with the applied column. In consequence, the calibration graphs (dependence of Stokes' diameter on eluted dextran percentage, Fig. 3) were derived from the dextran elution profile (Fig. 1) and the data in ref. 3. The investigation was carried out using two polydisperse dextrans (dextran 15 and 35) which were calibrated on different Sephadex gels. The size group fractionation of the two dextrans on the VP demonstrates the sharpness of separation ((Fig. 4).

Columns much larger than necessary for complete separation of the permeable from the excluded fraction were used in order to consider the possible influence of bed length and separation time. We have argued in a preceeding paper [1] that the small but significant share of a polydisperse sample eluting between the peaks may be an expression of non-uniformity of the cells (vesicles) with respect to their individual separation limit. If every cell in the chromatographic bed of the VP had an ultrafiltration membrane (cell wall) with a sharp transition from the highly permeable to the completely impermeable state at a certain molecular size (separation limit) but the cells varied to some extent with respect to the value of this limit, then molecules of a size within the statistical variance of cellular separation limits would have an intermediate elution volume between the exclusion volume and the total bed volume (statistical explanation of the fractionation range). Alternatively, permeable molecules with a size near the separation limit might be eluted before the second peak as their permeability is too low to reach the diffusional equilibrium (kinetic explanation). The results shown in Fig. 4 and Table I favour the statistical explanation, as both SLE and SLP were not clearly dependent on column length and separation time. As shown

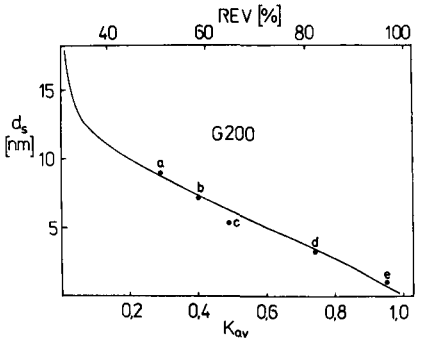

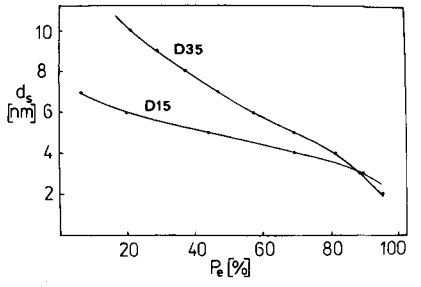

Fig. 2. Dependence of Stokes' diameter on K_{av} and relative elution volume (REV) as determined by chromatography of proteins on the Sephadex G-200 column used for fractionation of dextran 35. The positions of proteins used for calibration [(a) yeast alcohol dehydrogenase; (b) human serum albumin; (c) ovalbumin; (d) bovine cytochrome *c*; (e) sucrose] fit the original curve published for Sephadex G-200 [3]. Column as in Fig. 1.

Fig. 3. Calibration graphs used for the determination of the separation limits SLE and SLP from the percentage of excluded and permeable dextran. The curves represent the dependence of the molecular Stokes' diameter of the dextran fraction eluted from the GPC column at a certain volume V_e on the percentage of the sample eluted up to this volume. The curve for dextran 15 results from its fractionation by Sephadex G-75 and that for dextran 35 is based on fractionation by Sephadex G-200.

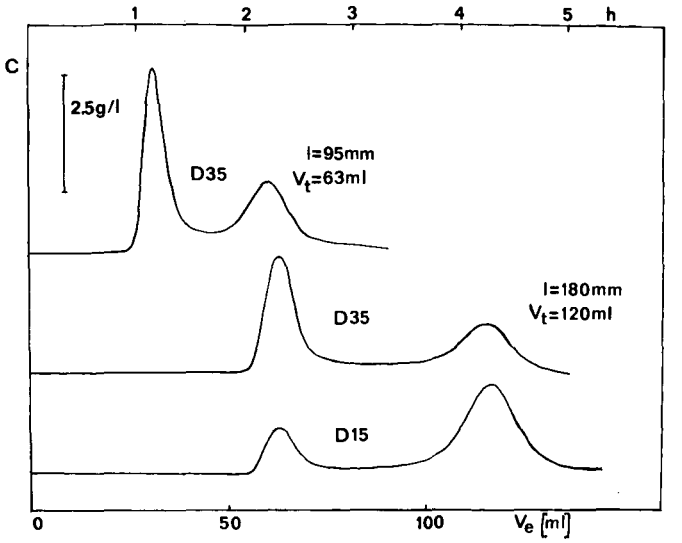

Fig. 4. Size group fractionation of two polydisperse dextran materials by VC on Permselekt. A 50-mg amount of dextran 35 or 15, dissolved in 2 ml of eluent solution, was fractionated on a column packed with the VP Permselekt (unaltered material). Beds of different lengths and volumes (as indicated) were eluted with 0.05 *M* PBS (pH 6.5). Column I.D., 29 mm. Detection as in Fig. 1.

previously [1], the elution volume of monodisperse samples (proteins) tested so far is either in the range 40–50% or 90–100% of the bed volume. It is interesting, however, that proteins with Stokes' diameters below the SLP determined for dextran may be excluded, presumably because of the increase in their apparent hydrodynamic molecular size by electrical interaction with the negatively charged matrix [4] (Fig. 5).

Although the cellin walls carry negative charges in high concentration (about 0.7 mequiv./g dry material), P_{ex} and P_{perm} for the neutral dextran molecules were found to be almost independent of the buffer pH (Table II).

Advantages of the described method for the determination of SLP and SLE are its simplicity and rapidity. As the size distribution of suitable polydisperse dextran

TABLE I

SIZE LIMITS OF EXCLUSION AND PERMEATION DETERMINED WITH THE HELP OF TWO CALIBRATED DEXTRAN MATERIALS

Details as described in the legend of Fig. 1.

Fractionated material	Column length (cm)	Elution time (h)	P_{perm} (%)	P_{ex} (%)	SLE (nm)	SLP (nm)
Dextran 35	9.5	2.5	39.7	49.3	6.8	5.7
	18	5	36.7	49.7	6.8	5.5
Dextran 15	9.5	2.5	67.4	22.3	6.0	5.5
	18	5	70.9	15.1	6.4	5.6

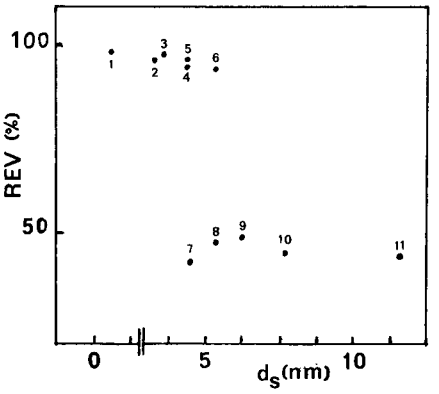

Fig. 5. Relative elution volumes (REV) of different proteins and polyethylene glycol preparations determined by VC with Permselekt columns as a function of their Stokes' diameter. 1 = Myoglobin; 2 = ribonuclease A; 3 = trypsin; 4 = chymotrypsinogen; 5 = polyethylene glycol 4000; 6 = polyethylene glycol 6000; 7 = pepsin; 8 = ovalbumin; 9 = peroxidase; 10 = human serum albumin; 11 = phycocyanin. Stokes' diameters of proteins were taken from ref. 3. Polyethylene glycol fractions of narrow size dispersion (Merck-Schuchardt) were analyzed by GPC on calibrated Sephadex G-75 for their mean Stokes' diameter.

samples is known (Fig. 2), only one size fractionation of such a sample by VC is sufficient for the determination of SLE and SLP. The SLE and SLP define the completely excluded and completely permeable fractions of a neutral hydrocolloid in terms of the minimum and maximum Stokes' diameter, respectively. Both dextran 15 and 35 are suitable materials for the determination of these limits if the VP has not been strongly altered in comparison with that consisting of the native cellin wall.

The reliability of the method is demonstrated by the nearly identical results on separation limits obtained with two dextran samples, the molecular size range of which was determined independently on different Sephadex gels (Table I). Dextran 15 is especially suitable for the size range of Stokes' diameter between 4 and 6 nm (Fig. 3). Dextran 35 (and other dextran materials with even larger mean molecular sizes)

TABLE II

EXCLUDED AND PERMEABLE PERCENTAGES OF DEXTRAN 35 AT DIFFERENT pH VALUES

The dextran was fractionated on the same bed with the pH of the elution buffer varied. Column length 9 cm; for other details, see legend of Fig. 1.

pH	P_{perm} (%)	P_{ex} (%)
5.5	38.1	50.0
6.5	41.9	48.5
7.0	40.9	51.8
5.5	41.8	51.6
6.5	42.3	49.0
7.0	41.3	48.3
5.5	40.3	52.1

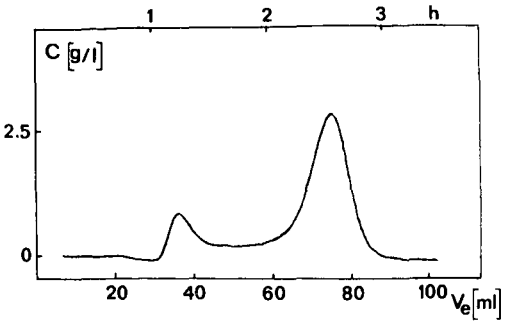

Fig. 6. Size group fractionation of dextran 35 on a column (29 mm I.D., bed length 116 nm) packed with VP Permselekt that had been treated before use with 2% sodium carbonate (3 days at room temperature). Details as in Fig. 4. The determined SLP and SLE are 8.1 and 11.5 nm, respectively.

would be preferred if the separation limits of the vesicle membrane have been increased.

As an example of application, the method was used to determine the separation limits of an alkali-treated VP. It is possible to increase the separation limits of the VP without changing the character of the fractionation (Fig. 6). The preparation of VPs with different but defined separation limits is important for their application in the preparative size fractionation of proteins, nucleic acids and other polymers. Papers on the variability and stability of the separation limits and the application of VPs with increased separation limits are in preparation.

REFERENCES

1 R. Ehwald, G. Fuhr, M. Olbrich, H. Göring, R. Knösche and R. Kleine, *Chromatographia*, 28 (1989) 561–564.
2 M. McNeil, A. G. Darvill, St. Fry and P. Albersheim, *Annu. Rev. Biochem.*, 53 (1984) 625–663.
3 T. C. Laurent and J. Killander, *J. Chromatogr.*, 14 (1964) 317–329.
4 P. I. Dubin, C. M. Speck and J. I. Kaplan, *Anal. Chem.*, 60 (1988) 895–900.

Journal of Chromatography, 542 (1991) 247–261
Elsevier Science Publishers B.V., Amsterdam

CHROM. 23 007

Computer spectrochromatography

Principles and practice of multi-channel chromatographic data processing

Yu. A. KALAMBET* and Yu. P. KOZMIN
Scientific and Technical Cooperative "Ampersand", P.O. Box 439, Moscow 123060 (U.S.S.R.)
and
M. P. PERELROYSEN
Novosibirsk Institute of Bioorganic Chemistry, Siberian Branch of the Academy of Sciences of the U.S.S.R., Pr. Lavrientieva 8, Novosibirsk 630090 (U.S.S.R.)
(First received June 6th, 1990; revised manuscript received November 23rd, 1990)

ABSTRACT

A new approach to multi-channel chromatographic data processing is introduced, based on the treatment of a chromatogram as a curve in multi-dimensional space. Each coordinate in this space is the signal-to-noise ratio for one detector. Every point in the space represents one spectrum-set of detector responses. Multi-dimensional space mathematics applied to the analysis of the chromatogram allows one to obtain individual substance detection profiles for overlapped peaks in the case of known spectra of each component, analyse peaks for homogeneity and determine the number of substances in overlapped peaks and their elution profiles without a prior knowledge of their spectra. All these tasks are solved with maximum accuracy owing to the principles of space coordinates construction. Theoretical considerations are illustrated by the results obtained for multi-wavelength chromatograms measured with a Milichrom chromatograph.

INTRODUCTION

The development of a wide range of ultraviolet (UV) spectral detection devices for chromatography probably started with the OB-4 chromatograph designed in the late 1970s in Novosibirsk [1]. This device is equipped with a rapid scanning UV detector with a forward optics double-beam measurement scheme. It has a 15-bit measurement accuracy and covers the absorbance range up to 12.8 (1.56 mm optical path cuvette). It was also the first microbore system with a column I.D. of 2 mm and a syringe pump volume of 2.5 ml.

We have been developing software for this device since 1983 and gained some experience in multi-wavelength data processing (*e.g.*, ref. 2) that may be useful when applied to other multi-wavelength or multi-channel chromatographic systems.

In particular, we succeeded in the analysis of unresolved peaks by spectral

0021-9673/91/$03.50

criteria. Two types of such an analysis are distinguished. The first is applied to peak analysis in the case when the spectra of all components are known. In this instance a least-squares method allows individual elution profiles and good estimates of the amounts of each component to be obtained. The second type helps in analysis when none of the component spectra are known in advance. In this instance multiple regression and factor analysis methods allows estimates of substance spectra, elution profiles and amounts to be obtained, but the results may be less accurate than in the first type of analysis.

THEORY

We use the term "spectrochromatography" for all kinds of chromatographic systems where the result of measurement is a set of values instead of one detector response as in traditional chromatography. This may be UV–VIS spectrum measurement (SM) systems, mass spectrometer (MS) systems or just a set of different detectors measuring different characteristics of the single gas or liquid chromatographic flow. From the very beginning of problem formulation we stress that different detector outputs may be mixed, thus changing the view from uniform chromatographic systems where all of the channels have the same physical units of measurement.

Detector response space

Apart from the three-dimensional view of a chromatogram offered by many photodiode-array detection software systems, we use a different approach. We consider a spectrochromatogram to be a curve in multi-dimensional space, where each coordinate represents an individual detector response, *e.g.*, the response of one diode of an array (SM) or one mass (MS). One point in the detector response (DR) space represents one spectrum. In this DR space the chromatogram looks like a curve where successive measurements are connected by the line. In the case of a "spectrum" consisting of only two wavelengths, this will be a curve on the plane where one axis represents the absorbance for one wavelength and the other axis the absorbance at the other wavelength. If we subtract the baseline in such a chromatogram, the curve will become tightly grouped around zero with peaks looking like curve fragments starting from zero and returning back to zero. The analysis of curves in this space is not convenient, as the value of a signal given by each coordinate depends on, *e.g.*, the units of measurements.

Noise-normalized detector response space

The main reason why curve analysis in DR space is complicated is that many curve analysis techniques use the root-mean-square (RMS) approach. This approach minimizes the sum of squares of distances for each coordinate. Therefore, if we wish to use this approach, the expected errors should be comparable for all axes, otherwise the result will not be accurate. Even more, DR space coordinates may have different physical units of measurement and we may add square absorbance units to square millivolts.

There is one natural way to find unified space coordinates suitable for all kinds of curve analysis, *viz.*, we can use units of measurement equal to the noise (or the expected measurement error). In this instance each coordinate axis will represent the

signal-to-noise ratio (S/N) for one channel. Let us call this space a noise-normalized detector response (NNDR) space. NNDR and DR spaces may be transformed into one another by linear transformation:

$$D = RW \tag{1}$$

where D = normalized spectrum from NNDR space (detection vector), W = weight matrix with $W_{ij} = 0$ $(i \neq j)$ and $W_{ii} = 1/E_i$, E_i = expected error for the channel i, $R = (R_1, \ldots, R_N)$ = detector response vector and N = number of channels (detectors).

NNDR space is very useful, as with its help one can analyse in a unified way physically different signals, *e.g.*, conductivity and radioactivity. One point in the NNDR space represents the normalized spectrum.

Hence NNDR space is just such a space where one coordinate represents one channel and expected errors for all coordinates are equal.

Total S/N ratio profile

The NNDR space chromatogram presentation contains additional information that can be easily extracted and successfully used.

Before the baseline subtraction, we need to find the peak beginning and end. However, in a multi-detector system it is very difficult to use any one channel for this purpose. An effective and consistent way is to use a "summary report" of a chromatogram, *i.e.*, the profile of the total S/N for all detectors (see Fig. 1). The S/N profile gives a good visual representation of the chromatographic curve end eliminates the question of "which channel is better".

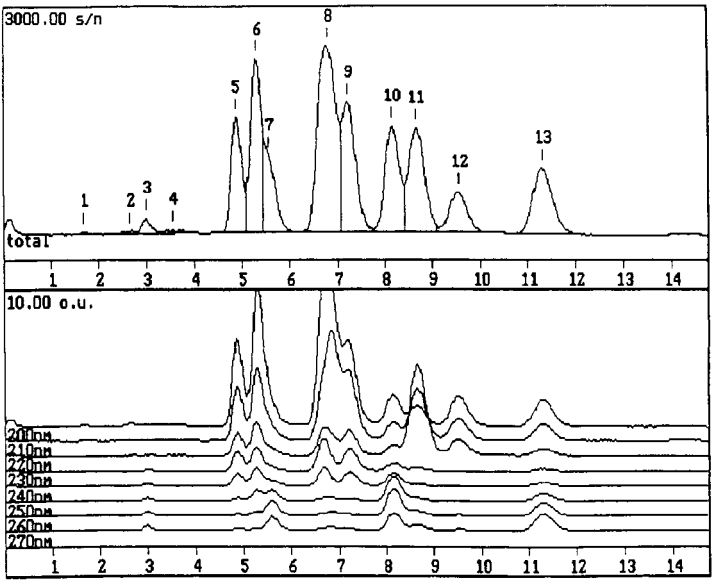

Fig. 1. Multi-channel chromatogram (bottom) and signal-to-noise ratio profile for this chromatogram (top). Abscissa in microlitres; ordinates are different and labelled at the top left corners. Output of Chrom&Spec software.

Peak shape in NNDR space

Hereafter, unless specially noted, we shall consider a chromatogram with a subtracted baseline, *i.e.*, each detector response will be substituted with the difference between the actual detector response value and the estimated baseline value at that point. The method of baseline estimation implemented in our program is described under Discussion.

In the case of a homogeneous peak and fulfillment of a detector response proportionality law (the detector response is proportional to substance concentration), all points belonging to the same peak should be positioned along the straight line with an average distance from the line close to 1:

$$D = cQ + e \tag{2}$$

where D = detection vector, c = concentration of substance, $Q = SW$ = substance spectrum S transformed into NNDR space and e = normalized error of measurement. Eqn. 2 is valid for all peak spectra with different concentration c and error vector e values.

A multi-component peak in NNDR space will be a linear combination of several detection vectors, one for each pure component:

$$D = c_1Q_1 + c_2Q_2 + \ldots + e \tag{3}$$

where c_k = concentration of the kth component and

$$Q_k = S_kW \tag{4}$$

is transformed to the NNDR space kth pure component spectrum S_k. As before, eqn. 3 can be written for every point within a peak.

Substance quantification

In the case when pure spectra for all substances within an overlapped peak are known in advance, one can use the RMS approach to decompose every measured spectrum of the peak into spectra of this pre-defined basis. In the case of known spectra, eqn. 3 represents a set of N equations with K unknowns, where K is the number of individual components and N, as before, is the number of channels. In the case when $K \leqslant N$ we can apply the RMS approach (see, *e.g.*, ref. 3) which will give solution of eqn. 3 in the form

$$C = DQ^T(QQ^T)^{-1} \tag{5}$$

where $C = (c_1, c_2, \ldots, c_K)$ is a concentration vector, D = detection vector and $Q = (NK)$ matrix composed of K detection vectors made from pure component spectra by eqn. 4.

Of course, the spectra of pure components should be linearly independent (not too similar), otherwise matrix inversion in eqn. 5 cannot be applied. If these conditions are fulfilled, decomposition is allowed and gives a unique concentration vector C.

By making a spectrum decomposition for every peak point, we can obtain

a concentration profile for each component. To present results it is usually more convenient to use an absorbance profile instead of a concentration profile. The absorbance profile may be reconstructed as

$$A_k(t) = c_k(t)S_k \tag{6}$$

where $A_k(t)$ = evaluated absorption (DR space!) vector of the kth component, $c_k(t)$ = concentration profile of the kth component obtained by eqn. 5 and S_k = kth component spectrum. Eqn. 6 should be evaluated at every peak point. To stress this fact, we introduced a time dependence into eqn. 6. Note that no peak shape considerations were used!

In the case when $K = N$, eqn. 5 will give an exact solution of N equations with N unknowns instead of the RMS approach, and this exact solution can be found for *any* N linearly independent basis spectra, no matter whether correct ones or taken as an arbitrary choice! To obtain reliable results the number of channels should be at least twice the number of detected substances, so that the residual error could help in the validation of results.

Use of NNDR space angle

To help in visual NNDR space chromatogram analysis, we can use angles between time-adjacent vectors in NNDR space, *i.e.*, we can associate additional characteristics with each peak point: an angle between NNDR vectors for that and the preceding point. These angles can be plotted as an angle profile of the peak. In the case of a homogeneous peak, NNDR space points are located along the line and angles inside the peak should be close to zero. At the very beginning and at the end of the peak the signal value is low, and the predicted angles are large in comparison with those inside the peak. Non-homogeneous peaks will show more complex structures (see Figs. 5–7).

In some instances we can also use the NNDR space inter-vector angle as a measure in comparisons of spectra. Comparisons of spectra should be performed taking into account the measurement error for each channel. Hence we can use the NNDR space angle as a measure of spectral similarity in the case of a spectral library search and other cases of spectral comparisons.

Many useful criteria may be introduced using angles. For example, in the case of spectrum decomposition for two known spectra, the angle between basis vectors should be much greater than the expected inter-vector angle caused by noise.

One argument for or against correct basic spectra selection is the residual error of spectrum decomposition. The problem is that the decomposed spectrum may differ from the sum of basis spectra with coefficients obtained by the RMS approach and an angle between initial and resynthesized vectors may be calculated. To obtain a numerical value of the angle we can use the tangent, *i.e.*, the ratio of the length of the residual vector to the length of initial vector (see Fig. 4, residual error value).

We shall mention one of the reasons why the angle is so attractive and why we consider it as an alternative to the correlation coefficient in spectra comparison: the angle is a natural measure, easily understandable by most people, and psychologically it is much easier to imagine an angle than a correlation coefficient.

Further chromatogram analysis

As a chromatogram is considered as a curve in a multi-dimensional space, we can try to analyse a curve without any *a priori* knowledge such as substance spectra. To do so we have to apply multi-dimensional space mathematics, *i.e.*, principal component and factor analysis. The theory and a detailed description of the algorithms for this type of analysis will be published elsewhere; here we shall only present an overview of the calculations made by our program. At this stage of curve analysis we apply the following.

(a) We obtain a subspace with a minimum number of dimensions that contain the entire peak curve within admissible error by principal component analysis. The number of subspace dimensions will represent the number of components in the peak and pure spectra should be linear combinations of subspace basis vectors (eigenvectors).

(b) We filter noise by placing the whole curve for the peak into subspace.

(c) We find the best candidates for the role of "pure spectrum" for each component among all of the vectors in the peak. That is, we assume that there exists some point within the peak where the first component is "pure" and assume the spectrum at this point to be a true pure first-component spectrum, and so on.

(d) We obtain elution profiles of each component within the peak and their amounts.

To apply this type of curve analysis, one should note the propositions made: (a) eluted substances have linearly independent (different) spectra; and (b) the elution profiles are shifted with respect to each other so that for each component there is a point within an analysed chromatogram region where only this component is present. The spectrum at this point will be taken as a pure spectrum of this component.

EXPERIMENTAL

Equipment and software

All measurements were performed using a Milichrom chromatograph (Nautchpribor, Orel, U.S.S.R.), which is an industrial version of the OB-4 chromatograph [1].

Two software systems were used. The first was developed at the Institute of Molecular Genetics of the Academy of Sciences of the U.S.S.R. for the ISKRA-226 computer (U.S.S.R.) with a special interface unit. The system was written in BASIC and Assembly languages. The second chromatographic data processor, Chrom&Spec, is a product of the "Ampersand" Cooperative (Moscow, U.S.S.R.) for IBM PC-compatible computers. With the Milichrom chromatograph data acquisition is performed by a special interface board, otherwise several analog-to-digital converting (ADC) devices are supported. Data import from LKB WaveScan primary data files and ASCII text files is also possible. The system is written in C and Assembly languages.

RESULTS

Peak analysis in the case of known pure spectra

One of the applications of this possibility was the evaluation of the amount of protein (RNA polymerase) crosslinked to DNA [2]. In this case the chromatographic column was used for the partial separation of the DNA–protein complex from

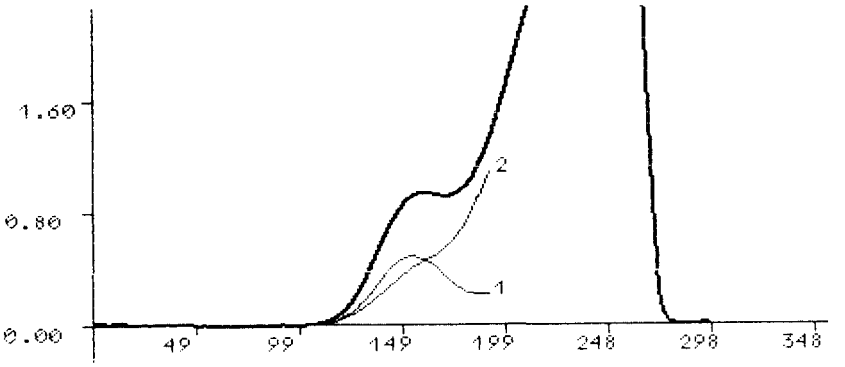

Fig. 2. Gel chromatogram of DNA–protein complex monitored at 230 nm and profiles of individual component elution: (1) DNA; (2) protein. Abscissa shows volume in microlitres, ordinate the absorption in o.u. Individual elution profiles were evaluated by eqn. 6. Output of ISKRA-226 software.

unbound protein (Fig. 2) by gel chromatography. We analysed the first part of the peak corresponding to the complex. The results of the spectrum decomposition are shown in Fig. 3, and associated numerical information in Fig. 4. Individual substance spectra were measured in advance and for the purpose of analysis they were loaded from disk files.

Factor analysis: what is visible to the user?

We have tried to provide a simple and convenient user interface in our software. We shall therefore try to illustrate how peak factor analysis is implemented to show that even an inexperienced user may extract some new information from the chromatogram.

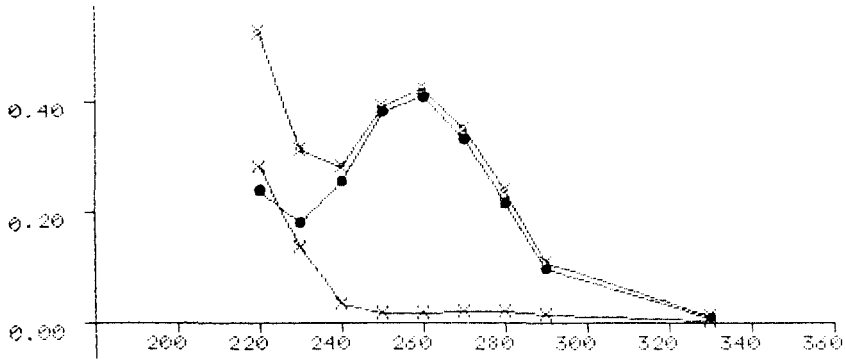

Fig. 3. Illustration of spectrum decomposition. Abscissa shows wavelength in nanometres, ordinate the absorption. The higher curve shows the chromatogram region spectrum and the lower curves (●) DNA and (×) protein library spectra. Associated textual program output is shown in Fig. 4. Output of ISKRA-226 software.

Chromatogram:
Date 18.05.85; 9 wavelengths; flow 10 mcl/min; User Burova;
Sample: pAO3 plasmid DNA: RNA polymerase complex;
Column: TSK-gel HW65, volume 300 mcl;
Eluent: 10mM TEA, 10 mM MgCl2, 100 mM KCl in water;
Wavelengths: 220 230 240 250 260 270 280 290 330 nm;

Section: volume 110-145 mcl.
Volume 35.8 mcl; Integral $8.29*10^{-4}$ o.u.*ml;
Mean absorption at 260 nm 0.41 o.u.

a) Spectrum:

Wavelength nm	Weight	Ratio
220	0.31	1.23
230	0.43	0.78
240	0.53	0.70
250	0.42	0.93
260	0.60	1.00
270	0.49	0.83
280	0.49	0.57
290	0.46	0.28
330	0.51	0.04

b) Spectral decomposition:

Substance name	Signal	Concentration mcg/ml	Concentration M/l	Amount mcg	Molecular mass Dalton
pAO3 DNA	79.1%	20.6	$1.96*10^{-8}$	0.74	1050000
RNA polymerase	19.4%	31.7	$7.05*10^{-8}$	1.13	450000

Residual RMS error 3.1%

Fig. 4. Spectral analysis of a chromatogram region. Weight column in the spectrum printout (a) stands for the reverse of the baseline noise. The weight equals 1 if the baseline noise is absent and hence the expected error equals the discretization error, 0.0004 o.u. in the case of the Milichrom device. Hence in the above example the baseline noise equals approximately 3 discretes for 220 nm (where discrete stands for the smallest voltage change that can be measured by the device) and is less than 2 discretes for 260 nm. The spectrum is normalized for the response at one wavelength (260 nm in this instance), called the reference wavelength. Spectrum decomposition is made by eqn. 5 with weights for DR-NNDR space transformation listed in Table (a). Molar ratio of DNA to protein amounts shows that 3–4 RNA polymerase molecules are bound to DNA, which was confirmed by electron microscopy [2]. Output of "ISKRA-226" software.

The option that performs peak factor analysis is called "Analyse". Before its activation it is necessary to mark a region of interest with the help of a vertical bar

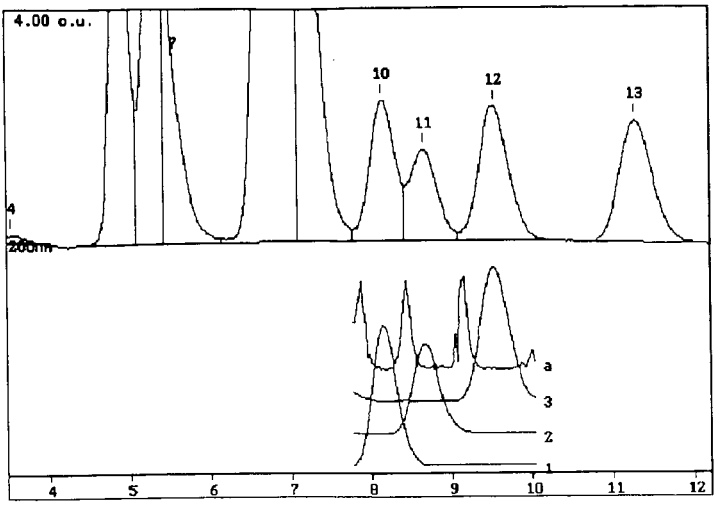

Fig. 5. Factor analysis of a chromatogram region. Here and in Figs. 6 and 7 the abscissa is in minutes, and the ordinate in absorbance units with full-scale labelled at the top left corner. Chromatogram at 200 nm and individual elution profiles for each component (curves 1, 2 and 3) are shown. Angle curve (a) is shown in arbitrary ordinate units. Output of Chrom&Spec software.

cursor. After the activation of the option the program performs some calculations and shows sets of numbers (NNDR space covariation matrix eigenvalues) to the user (an experienced user can use this set of numbers to select a number of substances in the region). Subsequently the program asks for the number of components and offers some value. The user can accept this value or enter his or her own. For the case of Milichrom data usually there is no need to change the value.

As the value is entered or confirmed, the program asks for the "pure spectrum"

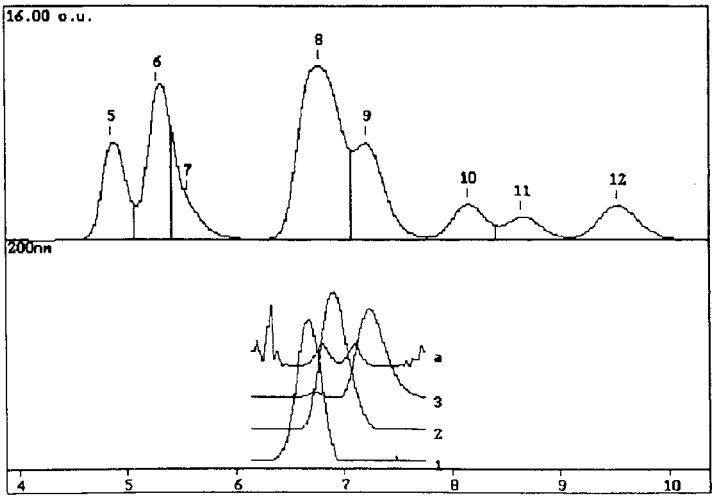

Fig. 6. Factor analysis of a chromatogram region. All notations as in Fig. 5.

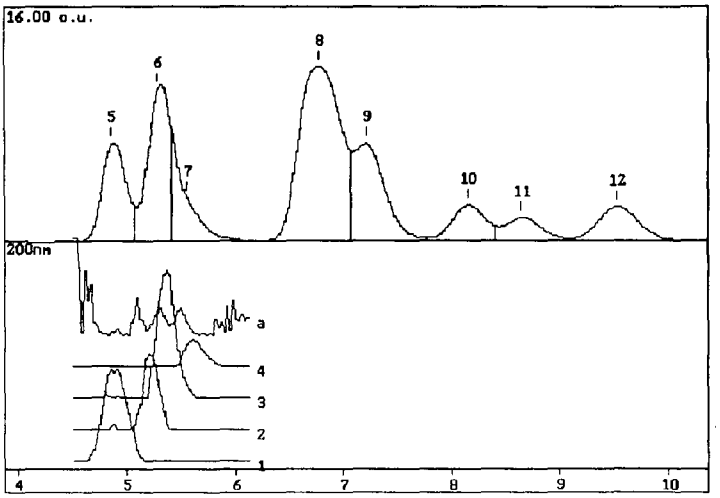

Fig. 7. Factor analysis of a chromatogram region. All notations as in Fig. 5.

selection mode (automatic or manual). In the case of the manual "pure spectrum" selection mode, one has to set the cursor to the position of the first "pure component" and press the Enter key and so on for every "pure component" position. In the case of the automatic mode the program selects these positions itself. Our experience shows that the spectrum selection algorithm works quite well and even if the user sees an angle function for the peak on the screen he or she usually cannot select better "pure spectrum" positions than those selected by the program.

After the end of the spectrum selection dialogue the program shows elution profiles for each component for the first wavelength (Figs. 5–7). Then it asks for the next wavelength to show. The sum of elution profiles is approximately equal to the peak profile for the channel shown on the screen (with subtracted baseline, of course). At this moment the scale factor can be changed so that peaks with different signal levels can be investigated and more details examined.

If the user presses the Escape key to quite the elution profile display loop, the program lists (in numerical form) each substance spectrum normalized for the reference wavelength (selected previously by the user) and the area for the peak normalized for the total area of the selected region (Fig. 8).

The final question is whether it is necessary to adjust peaks boundaries in accordance with the results of factor analysis. If the user replies positively, peak boundaries are shifted so that the number of peaks in the region equals the number of pure components and the resulting area of each peak at the reference wavelength is the same as that calculated by factor analysis. After this procedure, area estimates obtained by the "Analyse" option are permanently stored in the peak pattern.

```
Chromatogram: test1-i.ODS
Data: 31/07/1989 13:05:10
Operator: Nagaev I.
File: 97311306.CHM
Flow rate: 50.0 mcl/min
Column: LiChrospher C18, 5 um
Eluent: 80% MeOH: 20% water
Sample: mixture of methyl esters of benzoic acid, benzene,
        toluene, etc.
8 channel(s)
Reference channel: 200nm
```

No	200nm	210nm	220nm	230nm	240nm	250nm	260nm	270nm	Q-ty	Conc.%
1	1.000	0.560	0.347	0.250	0.417	0.794	0.870	0.564	26.03	34.83
2	1.000	2.527	4.568	0.162	0.078	0.149	0.239	0.285	18.03	24.12
3	1.000	0.720	0.544	0.015	0.004	0.014	0.037	0.046	30.68	41.05

Fig. 8. Table produced as a result of peak factor analysis. It includes estimated spectrum for each component (ratio of absorption at a given wavelength to absorption at the reference wavelength), amount (amount units are the same as quantity (area in arbitrary units) and not shown here) and relative amount. The relative amount is calculated as an area percentage with respect to the total area of the region for the reference wavelength.

Results of peak deconvolution

In some instances, as for peaks 10, 11 and 12, a regional structure is evident and the user gains only a better quantitative estimate of each peak area, as can be seen from Figs. 5 and 8. Curves 1, 2 and 3 show elution profiles for each component at a wavelength of 200 nm, curve a–angle profile. The angle profile shows three distinct minima that correspond to fairly pure component regions where one component is changed by the other and the spectra at adjacent points differ significantly or at the peak boundaries, where S/N is low.

In other instances, as with peaks 8 and 9, a regional structure is not so evident and only an experienced user can "find" more than one peak in peak 8. Evidence for the complex peak structure is the slightly shifted position of the peak 8 maximum at different wavelengths and the peak shape at a wavelength of 210 nm (Fig. 1). In fact, when we start to analyse this region we find three separate peaks as shown at Fig. 6.

The most impressive example of peak analysis is the group of peaks 5–7. Three peaks can be distinguished in this region and operator reflected this when marking the peak boundaries in the manual mode. Besides, factor analysis of the region detects four substances with different spectra. Their estimated elution profiles are shown in Fig. 7, curves 1–4. In fact, if we consider the angle curve [see Fig. 7, curve (a)], two distinct local minima within peak 6 are found. These minima show that the peak structure is complex, and at least two components are present. Of course, as these minima do not reach zero, there is no point where an appropriate substance is pure and the spectrum at the minimum of the angle function reflects the real substance spectrum with a significant error, but nevertheless it can be used to prove the presence of extra

components and to estimate the elution profile and the amount of the component by the order of magnitude.

DISCUSSION

None of the methods described under Theory is new and they have been applied to multi-channel chromatographic data previously [4–10]. What is new in our approach is that we introduced normalization of data for the expected error prior to data analysis (NNDR space), which allowed us (a) to perform all calculations with maximum accuracy, (b) to introduce and use the total signal-to-noise profile and (c) to introduce and use the angle profile of the chromatogram.

Although the methods used have long been known, they have not received the attention they deserve, and we hope that in the future their contribution will increase. We shall now discuss some of the advantages the user may gain from a wider application of these methods.

User gain

The user of a multi-channel chromatographic system gains the following from spectral detection: first, an estimate of peak purity; if the peak fits along a straight line within admissible error, then the peak can be considered pure; second, peak deconvolution for the known spectra; this task may be performed manually or in an automated mode depending on user needs; and third, analysis of a peak with unknown composition. These attributes lead to simpler method development, faster solvent optimization procedures, quantification of chromatographically unresolved peaks, additional information on the number of substances in the unknown peak, etc.

Another application direction is in the routine determination of amounts of components in repetitive chromatographic analyses of the same mixture. In this instance a simpler chromatographic system may be used, as the spectra are known in advance and spectrum decomposition partially replaces chromatographic separation. Individual elution profiles may also be useful in preparative chromatography. Many other areas of application are possible.

Sources of error

Usually no benefit can be gained without drawbacks. In this instance, the drawback is a potential error caused by improper use of the software. We shall outline here some of the problem areas.

An estimate of peak purity may be wrong because (a) spectral analysis cannot distinguish substances with identical spectra and (b) different errors of spectrum evaluation discussed below may be treated as spectral impurities.

Spectrum decomposition for the known spectra may be wrong because of (a) wrong basis spectra, (b) identical or almost identical basis spectra, (c) too many substances in a region and (d) errors in spectra evaluation.

Analysis of an unknown chromatographic peak may be wrong because (a) spectral analysis cannot distinguish substances with identical or very similar spectra, (b) there are too many substances in a region, (c) chromatographic separation of peaks is poor and (d) errors in spectra evaluation.

Estimate of expected error

There are several potential error sources in spectral measurement. Strictly we do not measure the spectrum of the substance that elutes within a peak. We try to evaluate this spectrum based on measured chromatographic data. This evaluation produces errors, and here we try to list and discuss some of them which are important from our point of view. We deal with evaluation and measurement errors only, ignoring other error sources, such as substance spectrum changes in different solvents.

To obtain NNDR space spectrum coordinates, one should know the expected error for each channel. At present we use high-frequency baseline noise instead of expected error throughout the program. Errors from other sources in many instances seem to be proportional to the baseline noise, so we consider normalization for the baseline noise to be the first greatest step in the direction of equal measurement errors by each channel. Further steps are possible, but they will not provide such an increase in accuracy as the first step did.

Spectrum correction for measurement timing

This is one type of error that in some instances can be precisely corrected. Its source is that measurements at different wavelengths of the same spectrum are made at different moments in time. The first wavelength response is measured first, and by the time of measurement of the last wavelength the absorption of the first may have changed significantly. This error source is important for PDA detectors but with the Milichrom device it is especially important because of the long minimum measurement time per wavelength (0.15 s). We solve this problem by data interpolation. That is, we substitute measured values for new ones, calculated for the time that corresponds to the middle of the spectrum measurement cycle. This is done once when the chromatogram finishes, as we use three-point quadratic interpolation and need previous and subsequent measurements at the same wavelength. We found that this type of interpolation gives adequate results and more complex interpolation methods are not required.

With multiple detectors in series, when measurements are separated not only by time but also in space, this error may be the greatest error source, because in addition to time adjustment difficulties the peaks change their shape from detector to detector.

Baseline subtraction

Correct baseline detection is one of the most important conditions of precise spectrum measurement. There is no sense in measuring an absolute absorbance value, as different solvent and gradient absorbance profiles may change the spectrum considerably. Therefore, absorbances should be measured with respect to the baseline and the spectrum should be constructed from these difference absorbances. In our system there are baseline points on the chromatogram and the baseline itself is linear under the peaks. Baseline points are considered to belong to the baseline on all channels/wavelengths. Hence the baseline for each channel is determined in the traditional way for chromatography, but the time positions of baseline points are common for all channels. To provide the best choice of baseline points we use for peak detection purposes our synthetic "total" channel (Fig. 1) by default.

The baseline subtraction error is theoretically always greater than or equal to the baseline noise error. To decrease its value, visual investigation of peak detection results

can be recommended and in some instances baseline noise filtration by a noise filtration algorithm may help. In all instances non-linear baseline changes cannot be accounted for and we consider this error as one of the greatest error sources.

Measurement error

From the very beginning we estimate the minimum measurement error. This error is equal to one discrete of signal conversion or baseline noise for the channel, whichever is greater. The expected error of the measured detector response at any point within a chromatogram cannot be less than this value. Also, with high absorbances another error source is important: the small amount of light passed through the cuvette increases the expected error owing to statistical fluctuations in the number of light quanta. The error increases to infinity in the case of signal overflow.

Because of different error sources, pure peak fits along the straight line not within baseline noise accuracy, but slightly worse. Most of the errors mentioned increase as the baseline noise increases and therefore the use of baseline noise for calculations at least makes the expected errors for each channel comparable and allows the RMS approach to be used adequately.

Spectral slit width and accuracy

The spectral slit width is a very important system characteristic: the wider the spectral slit, the lower is the noise. On the other hand, a change in spectral slit width will cause a change in the spectral ratio for most wavelengths and will require recalculation or measurement of another copy of a library spectrum. Further, a wide spectral slit gives undesirable effects. Thus, it is possible to show that with a wide rectangular spectral slit and a narrow absorption band the measured spectral ratio on the upslope and downslope of the absorption band will depend on the substance concentration, *i.e.*, the Lambert–Beer law will be violated. This effect is due to the fact that the physically measured value is not the absorbance, but the amount of light passed through the cuvette, and absorbance is obtained after non-linear conversion of that value. The error in absorption measurement caused by the spectral slit width in the case of a constant spectral intensity of the light source and a rectangular spectral slit may be evaluated as

$$A_{app} - A \approx (dA/dL)^2 w^2 l/12 \tag{7}$$

where A_{app} = measured (apparent) absorption, A = real absorption, l = optical path length, dA/dL = first derivative of absorption for the wavelength and w = spectral slit width. More discussion of this equation will be published elsewhere. Note that eqn. 7 shows that the measured spectrum depends on substance concentration.

The effect of the spectral slit width is more pronounced with visible light detection than with UV detection because of narrow bands and hence higher values of dA/dL (unpublished data). Thus a wider spectral slit may cause a change in the library spectrum and an additional risk of treatment of homogeneous peaks as non-homogeneous because of violation of the Lambert–Beer law.

To minimize the effect of the spectral slit width it is possible to select wavelengths for detection and calculations near the absorption band maxima and minima. Another

possibility is to use a narrow spectral slit width detector and a short optical path cuvette.

Rapid scanning vs. diode-array detectors

There are some additional considerations on different measurement schemes implemented in different SM detector types. A comparison of forward and reverse optics schemes shows that the high total S/N level obtained with PDA reverse optics, in addition to its advantages, also has some drawbacks: (a) lower S/N characteristics per channel and (b) very high light intensity inside the cuvette. The former effect makes our type of data analysis less informative but may be partially compensated for by a greater number of channels. The latter may play a critical role in some instances, producing, *e.g.*, depurinization of DNA or some other kind of degradation of analyte substances. It is also necessary to understand that 512 signals from an array in the case of a UV spectrum are not independent and *ca.* 20 channels are more than sufficient to reconstruct the full UV spectrum of a substance with high accuracy. In many instances the number of channels needed for spectrum reconstruction may be significantly smaller.

On the other hand, the PDA detector may provide an optimum selection of wavelengths for correct data analysis.

The benefits of rapid scanning detectors such as the Milikhrom are that they provide a better S/N per channel, they provide almost all the information that diode arrays do, they produce less substance degradation and they save disk storage space.

Use of different hardware

Our software allows different hardware configurations to be used for data acquisition owing to the support of several ADC types. We are only starting to gain experience in the field of multi-detector systems. Two of the most obvious problems are adjustment of data from different detectors and peak shape changes.

ACKNOWLEDGEMENTS

The authors are grateful to Dr. A. A. Alexandrov for support with the first stages of investigations. They also thank Dr. I. Nagaev for his excellent unresolved chromatogram, which he indicated was much easier to obtain than a well resolved chromatogram.

REFERENCES

1 G. I. Baram, M. A. Grachev, N. I. Komarova, M. P. Perelroysen, Yu. A. Bolvanov, F. V. Kuzmin, V. V. Kargaltsev and E. A. Kuper, *J. Chromatogr.*, 264 (1983) 69–90.
2 Yu. A. Kalambet, E. I. Burova, A. A. Zhuchkov, V. L. Knorre and A. A. Alexandrov, in H. Kalasz and L. S. Ettre (Editors), *Chromatography '87*, Akadémiai Kiadó, Budapest, 1988, pp. 251–268.
3 G. E. Forsythe, M. A. Malcolm and C. B. Moler, *Computer Methods for Mathematical Computations*, Prentice Hall, Englewood Cliffs, NJ, 1977.
4 J. C. Nicolson, J. J. Meister, D. R. Patil and L. R. Field, *Anal. Chem.*, 56 (1984) 2447–2451.
5 E. R. Malinowski and D. G. Howery, *Factor Analysis in Chemistry*, Wiley, New York, 1980.
6 F. J. Knorr and J. H. Futrell, *Anal. Chem.*, 51 (1979) 1236–1241.
7 M. A. Sharaf and B. R. Kowalski, *Anal. Chem.*, 54 (1982) 1291–1296.
8 M. F. Delaney, *Anal. Chem.*, 56 (1984) 261R–277R.
9 S. D. Brown, T. Q. Barker, R. J. Larivee, S. L. Monfre and H. R. Wilk, *Anal. Chem.*, 60 (1988) 252R–273R.
10 S. D. Brown, *Anal. Chem.*, 62 (1990) 84R–101R.

Journal of Chromatography, 542 (1991) 263–275
Elsevier Science Publishers B.V., Amsterdam

CHROM. 23 035

Analysis of biomass pyrolysis liquids: separation and characterization of phenols

GEORGE E. ACHLADAS
Chemical Process Engineering Research Institute, P.O. Box 1517, 54006 University City, Thessaloniki (Greece)

(First received September 6th, 1990; revised manuscript received December 10th, 1990)

ABSTRACT

The liquid products derived from biomass (fir wood) pyrolysis were separated by silica gel open-column chromatography. A fraction rich in *ortho*- and non-*ortho*-substituted alkylarylphenols was isolated. This fraction was characterized by thin-layer chromatography and gas chromatography and was identified by IR, ^{1}H and ^{13}C NMR spectroscopy and was subjected to gas chromatographic–mass spectrometric analysis. About 12–17% (w/w) of the pyrolysis liquid products consisted of phenols, and the fraction rich in phenols contained phenol and other substituted phenols (85–95%, w/w). Aryl ethers can be produced by catalytic alkylation of the phenolic compounds.

INTRODUCTION

Phenols found in coal and biomass pyrolysis liquids are important compounds of increasing interest [1–5]. Phenols can be used as pure substances, as food antioxidants and gasoline additives or as precursors for the production of other chemicals, such as colorants, pesticides and aromatic ethers. Phenols are among the main constituents of biomass pyrolysis liquids [6].

Several methods have been used for separating and obtaining phenol-rich fractions. The most important are liquid–liquid extraction [7], ion-exchange chromatography [8] and silica gel column chromatography [9]. For the chemical characterization and identification of the phenolic components, chromatographic techniques [thin-layer chromatography (TLC), gas chromatography with flame ionization detection (GC–FID), high-performance liquid chromatography (HPLC)] [10–13] and spectroscopic methods (IR, ^{1}H and ^{13}C NMR, Fourier transform IR) have been applied [6,14,15]. Also analysis with gas chromatography–mass spectrometers (GC–MS) have also proved very versatile for this purpose [16,17].

In this work, a modified method was applied for separating the phenolic fraction from biomass pyrolysis liquids by silica gel open-column chromatography. Owing to the small amounts of pyrolytic liquids obtained, a phenol-rich fraction was isolated and not individual phenols. Alkaline extraction of the phenol-rich fraction was applied. Analysis and characterization of the phenolic fraction obtained were performed by TLC, GC–FID, IR, ^{1}H and ^{13}C NMR spectroscopy and GC–MS. For the first time, the phenolic compound 2,6-bis(1,1-dimethylethyl)-4-methylphenol was identified among the alkylphenols present in fir wood pyrolysis phenolic liquids.

0021-9673/91/$03.50

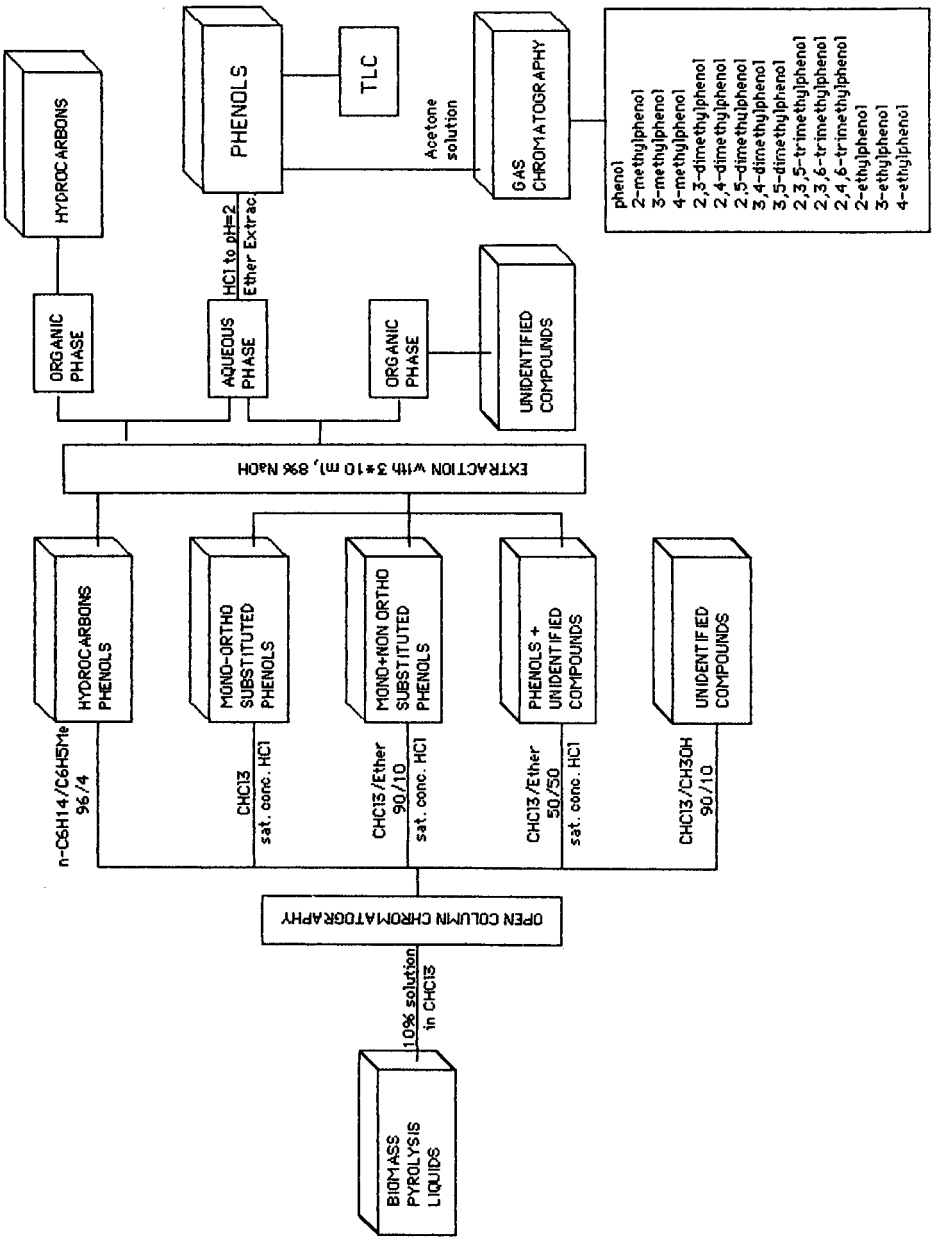

Fig. 1. Scheme for separation of phenols from biomass pyrolysis liquids.

EXPERIMENTAL

Materials

All solvents used were Merck LiChrosolv products. The biomass pyrolysis liquids were obtained by the reported procedure [18]. Phenol standards were obtained commercially (Merck, Supelco) and were used without further purification.

Silica gel open-column chromatography

A slurry column packed with 20 g of silica gel (70–140 mesh) in *n*-hexane–toluene (96:4) was prepared according to the method described by Schabron *et al.* [9]. This was carried out under a nitrogen atmosphere, with a silica-to-biomass pyrolysis liquids ratio of 20:0.1 [18]. As shown in Fig. 1 a procedure involving successive elutions with solvents of increasing polarity was followed. The first fraction was extracted with 10 ml of 8% sodium hydroxide solution. After phase separation and solvent removal, a yellow residue remained, which was weighed to an accuracy of 0.0001 g and was defined as "hydrocarbons". This residue was not characterized. The other three fractions were combined and extracted three times with 10 ml of 8% sodium hydroxide solution. This procedure was followed by acidification with concentrated hydrochloric acid. Extraction with diethyl ether gave a brown liquid rich in phenols, which was weighed and defined as the "phenolic fraction". This technique was first tested with model mixtures that contained representative phenolic components. The recovery of phenols was over 95% [19].

Instrumentation

A LECO CHN-800 microanalyser was used for elemental analysis of the phenolic fraction.

^{1}H NMR spectra were recorded on a Varian T-60 NMR spectrometer in deuterochloroform (C^2HCl_3)–tetramethylsilane (TMS) as internal standard, and ^{13}C NMR spectra were obtained on a Bruker WP-80 NMR spectrometer in C^2HCl_3–TMS.

The phenolic fraction was spot tested on plastic TLC sheets with silica gel 60 F_{254} and observed under long-wavelength ultraviolet light [10]. In addition, TLC was applied to the product of the characteristic reaction of diazotized *p*-nitroaniline with phenols, performed according to Crump's method [11]. The same method was applied using pure alkylphenols.

IR spectra of the biomass pyrolysis liquid samples were recorded on a Beckman IR 18-A spectrophotometer in C^2HCl_3 and tetrahydrofuran (THF). IR spectra (KBr) of the phenolic fraction were measured on a Model 1430 ratio recording IR spectrometer.

GC of the pyrolysis liquids was carried out on a Hewlett-Packard Model 5710A gas chromatograph equipped with a flame ionization detector and an Autolab computing integrator. A stainless-steel 6 ft. × $\frac{1}{8}$ in. I.D. column was used with 0.1% SP-1000 on 80–100-mesh Carbopack C. The carrier gas was helium at a flow-rate of 20 ml/min. The temperature programme was 170°C for 16 min, increased to 220°C at 2°C/min and maintained at that temperature for the remainder of the run.

GC–MS was performed on a QMD 1000 GC–MS system (Carlo Erba) equipped with a J&W DB-WAX fused-silica capillary column (60 m × 0.32 mm I.D.)

with a film thickness of 0.5 μm. The temperature was programmed as follows: 66°C for 1 min, 66–200°C at 20°C/min, for 10 min and 200–300°C at 10°C/min. For MS the scan rate was 1 s per scan with electron impact ionization at 70 eV, 200 μA. GC–MS as also performed on an ITD system (Finnigan MAT), equipped with a 25-m SE-54 capillary column directly coupled to the ITD.

RESULTS AND DISCUSSION

Analysis of the biomass pyrolysis liquids

Table I lists the average composition of typical biomass (fir wood) liquids [20], obtained from pyrolysis reactors described recently [18].

The IR spectra of the soluble portion from the biomass pyrolysis liquids, C^2HCl_3 (3380–3880 cm^{-1}) and THF (1500–1800 cm^{-1}), revealed strong absorptions. At 3690 cm^{-1} water absorption was observed, whereas at 3600 cm^{-1} free phenolic OH was indicated. Also, the peak at 3470 cm^{-1} showed the presence of pyrrolic NH. Three carbonyl bands were observed in THF solutions, similar to those reported by Dooley *et al.* [14]. These carbonyl bands are believed to show the presence of carboxylic acids (1735 cm^{-1}), associated acids or ketones (1700 cm^{-1}) and aromatic amides (1680 cm^{-1}).

The ^1H NMR spectra contained two major regions of signals around δ 1–5 ppm and δ 6–9 ppm, due to aromatic and aliphatic protons, indicating concentrations of methoxyl or other alkyl and aryl ethers. The same region of signals was observed by Boocock *et al.* [7] in oil fractions derived from hydrogenation of aspen wood.

Analysis of the phenolic fraction

Elemental analysis of the phenolic fraction gave the results shown in Table II. The oxygen content appeared to be very high, possibly owing to phenols and other oxygen-containing compounds (keto acids, esters, alkyl aryl ethers, etc.).

TLC gave for this fraction 4–7 populations that can be observed under long-wavelength UV light and can be detected with a spray reagent, *e.g.*, Folin's reagent.

Reaction of the phenolic fraction with diazotized 4-nitroaniline according to the method proposed by Crump [11] produced a mixture of 2- and 3-coupled stable dyes of yellow-orange colour. This reaction forms the basis of many well known quantitative methods for the determination of phenols.

The mobile phase used was benzene–cyclohexane–dipropylene glycol (30:70:3, v/v/v) and the papers were impregnated with formamide (Fig. 2). TLC single spots

TABLE I

AVERAGE COMPOSITION OF PYROLYSIS LIQUIDS

Compound	Concentration (%, w/w)
Hydrocarbons	14 ± 3
Phenols	15 ± 2
Unidentified (by difference)	71 ± 6

TABLE II

ELEMENTAL ANALYSIS OF THE PHENOLIC FRACTION

Element	Concentration (%, w/w)
C	72.3
H	8.3
O	18.8
N	0.6

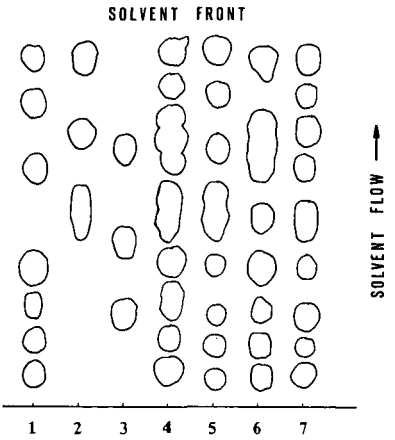

Fig. 2. Thin-layer chromatography. 1 = Mixture of phenol and methyl- and ethylphenols; 2 = mixture of dimethylphenols; 3 = mixture of trimethylphenols; 4 = mixture of pure phenols; 5 = sample A; 6 = sample B; 7 = sample C.

TABLE III

TLC R_F VALUES AND IDENTIFICATION OF PURE ALKYLPHENOLS (SINGLE SPOTS)

Phenol	2-Nitrophenylazo dyes			3-Nitrophenylazo dyes		
	R_F	Colour		R_F	Colour	
		Before ammonia treatment	After ammonia treatment		Before ammonia treatment	After ammonia treatment
Phenol	0.15	Orange-yellow	Yellow	0.14	Yellow	Rose
2-Methylphenol	0.35	Orange-yellow	Rose	0.34	Yellow	Mauve
3-Methylphenol	0.30	Orange-yellow	Orange	0.28	Yellow	Magenta
4-Methylphenol	0.98	Orange-yellow	Red	0.99	Orange	Purple
2-Ethylphenol	0.61	Orange-yellow	Orange	0.57	Yellow	Mauve
3-Ethylphenol	0.50	Orange-yellow	Yellow	0.48	Yellow	Magenta
4-Ethylphenol	1.00	Orange-yellow	Red	1.00	Orange	Purple
2,3-Dimethylphenol	0.57	Orange-yellow	Rose	0.47	Yellow	Lilac
2,5-Dimethylphenol	0.64	Orange-yellow	Red	0.50	Yellow	Lilac
2,6-Dimethylphenol	0.90	Orange-yellow	Rose	0.74	Yellow	Lilac
3.5-Dimethylphenol	0.46	Orange-yellow	Orange	0.42	Yellow	Brown
2,3,6-Trimephenol	0.60	Orange-yellow	Red	0.61	Yellow	Red
2,4,6-Trimephenol	0.36	Orange-yellow	Orange	0.38	Yellow	Mauve
2,3,5-Trimephenol	0.85	Orange-yellow	Rose	0.84	Orange	Purple

TABLE IV

MAIN BANDS OF THE IR SPECTRA OF THE PHENOLIC FRACTION

Wavenumber (cm^{-1})	Origin
3600–3200	O–H stretching vibration
2920–2940	C–H substituted on aromatic ring stretching vibration
1710	Carbonyl stretching, unconjugated
1595–1497	Common benzene skeletal vibration
1359	O–H bending vibration
1220	Characteristic C–OH stretching vibration of phenolics

following ammonia treatment gave a variety of colours including purple, rose, lilac and red-brown due to the reaction of 2- and 3-nitrophenylazo dyes with ammonia (Table III).

The main bands of the IR spectra of the phenolic fraction are given in Table IV.

Integration of the peaks in the ^{13}C NMR (δ, C^2HCl_3–TMS) spectra showed carbons attached to the phenolic hydroxyls. On the basis of these observations, the carbons appearing in the region δ 150–155 ppm indicate the presence of monophenols, whereas those in the region δ 140–146 ppm show the presence of heavy phenols. These observations are in good agreement with the literature [7].

In addition to the qualitative spectroscopic techniques applied to the phenolic fraction, GC analysis was also carried out using anisole and eugenol as internal standards. Identification and determination of phenolic components was based on matching relative response factors (RRF) of pure phenol standards. The results shown in Table V correspond to the phenolic fraction, the phenol separation of which appears in Fig. 3. There are some unidentified peaks because it was not possible to

TABLE V

CHEMICAL COMPOSITION OF THE PHENOLIC FRACTION DERIVED FROM GC ANALYSIS

Compound	Absolute amount (g)	RRF	Weight% (av.)
Phenol	0.00561	0.3637	3.4657
2-Methylphenol	0.00228	2.3800	1.4096
3-Methylphenol	0.00199	0.5163	1.2271
4-Methylphenol	0.00193	0.4836	1.1925
2-Ethylphenol	0.00005	0.5469	0.0291
3-Ethylphenol	0.00020	0.6272	0.1217
4-Ethylphenol	0.00013	0.6634	0.0810
2,6-Dimethylphenol	0.00017	0.5141	0.1037
2,4- and 2,5-Dimethylphenol	0.00117	0.5371	0.7231
2,3- and 3,5-Dimethylphenol	0.00076	0.6075	0.4679
3,4-Dimethylphenol	0.00028	0.6796	0.1736
2,4,6-Trimethylphenol	0.00023	0.5872	0.1426
2,3,6-Trimethylphenol	0.00022	0.6138	0.1377
2,3,5-Trimethylphenol	0.00025	0.7857	0.1512

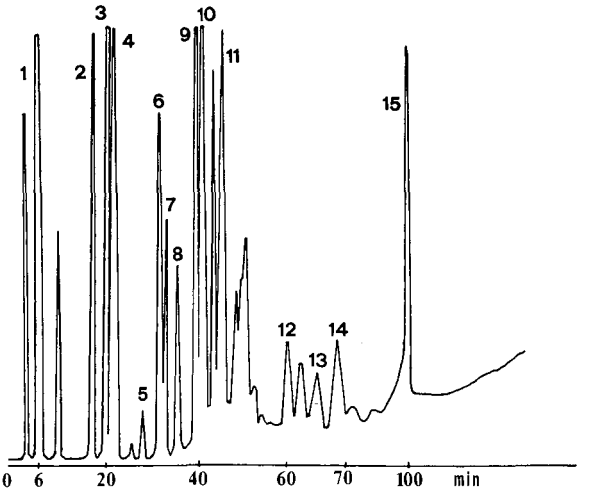

Fig. 3. Phenol separation on 6 ft. × 1/8 in. I.D. stainless-steel GC column of 0.1% SP-1000 on Carbopack C. Carrier gas, helium at a flow-rate of 20 ml/min. Temperature programme: 170°C for 16 min, 170–220°C at 2°C/min. Peaks: 1 = phenol; 2 = 2-methylphenol; 3 = 3-methylphenol; 4 = 4-methylphenol; 5 = 2-ethylphenol; 6 = 3-ethylphenol; 7 = 4-ethylphenol; 8 = 2,6-dimethylphenol; 9 = 2,4- and 2,5-dimethylphenol; 10 = 2,3- and 3,5-dimethylphenol; 11 = 3,4-dimethylphenol; 12 = 2,4,6-trimethylphenol; 13 = 2,3,6-trimethylphenol; 14 = 2,3,5-trimethylphenol; 15 = eugenol (internal standard).

find other commercially available phenol standards. The total proportion of light alkylphenols listed in Table V was calculated to be 9% (w/w) of the phenolic fraction [21].

The impossibility of finding more phenol standards for GC led to more sophisticated methods of analysis. Samples of phenolic fractions were also subjected to GC–MS. Figs. 4 and 5 show the total ion currents (TIC) for the same selected sample.

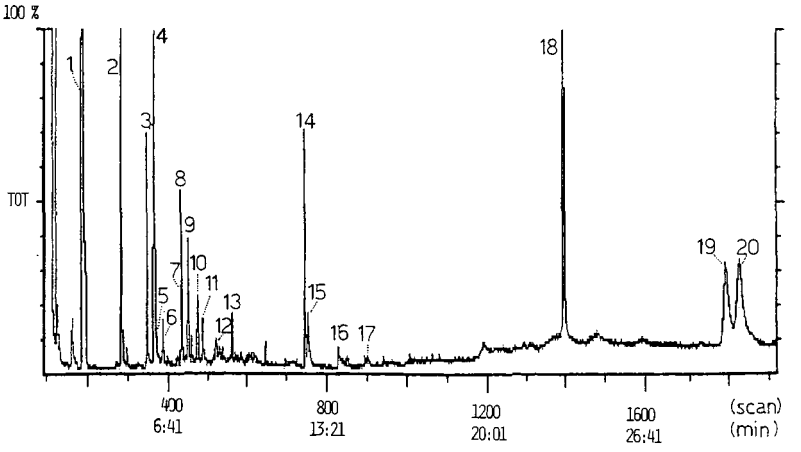

Fig. 4. Total ion current GC–MS (Carlo Erba) of the phenolic fraction of biomass pyrolysis liquids. For peak identification see Table VI.

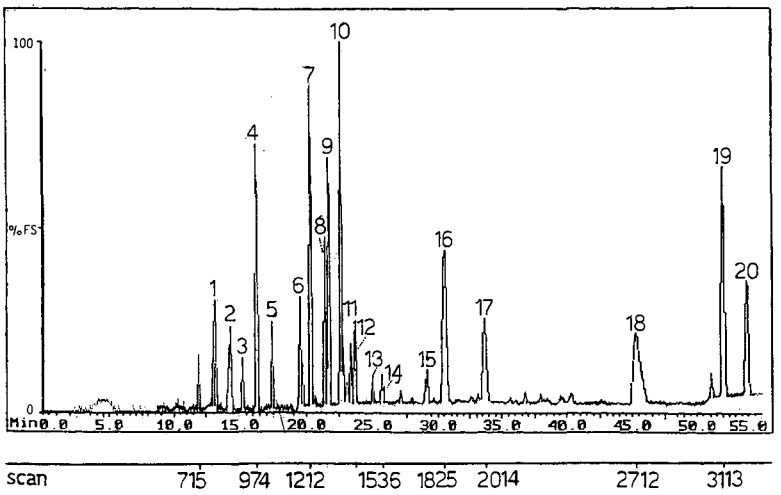

Fig. 5. Total ion current GC–MS (Finnigan Mat) of the phenolic fraction of biomass pyrolysis liquids. For peak identification see Table VII.

TABLE VI

COMPOUNDS IDENTIFIED BY GC–MS OF PHENOLIC FRACTION OF BIOMASS PYROLYSIS LIQUIDS (CARLO ERBA INSTRUMENT)

Peak No.[a]	Scan	Compound	*m/z*	Formula	Fragment ions[b]	Confirmation by comparison with standards[c]
1	187	2,3-Dimethyl-2-pentanol	78	C_7H_6O	59,101,83	×
2	282	Phenol	94	C_6H_6O	94,66,65	×
3	345	2-Methylphenol	108	C_7H_8O	108,107,79	×
4	362	4-Methylphenol	108	C_7H_8O	107,108,79	×
5	385	2,4-Dimethylphenol	122	$C_8H_{10}O$	107,122,121	×
6	390	3-Methylphenol	108	C_7H_8O	107,108,77	×
7	429	2,3-Dimethylphenol	122	$C_8H_{10}O$	107,122,121	×
8	446	2-Ethylphenol	122	$C_8H_{10}O$	107,122,77	×
9	455	3,5-Dimethylphenol	122	$C_8H_{10}O$	107,122,77	×
10	482	Ethenyloxybenzene	120	C_8H_8O	91,120,65	×
11	487	1-Octanol	130	$C_8H_{18}O$	41,56,43	×
12	546	2,6-Dimethylphenol	122	$C_8H_{10}O$	107,122,77	×
13	573	Methyl octanoate	158	$C_9H_{18}O$	74,87,43	×
14	741	2,6-Bis(1,1-dimethylethyl)-4-methylphenol	220	$C_{15}H_{24}O$	205,115,57	×
15	750	2-Naphthol	144	$C_{10}H_8O$	115,144,117	
16	823	2-Methyl-1-naphthol	158	$C_{11}H_{10}O$	158,129,115	
17	887	(1,1-Biphenyl)-3-ol	170	$C_{12}H_{10}O_2$	170,141,115	×
18	1400	2,3,6-Trimethylphenol	136	$C_9H_{12}O$	45,121,136	×
19	1780	3-(2-Hydroxyphenyl)-2-propenoic acid	164	$C_9H_8O_3$	120,91,65	
20	1840	1-(2-Hydroxyphenyl)ethanone	148	$C_8H_8O_2$	121,136,93	

[a] Peak numbers refer to the chromatogram in Fig. 4.

[b] The three most intense fragment ions from each 70-eV electron impact (EI) mass spectrum are given in order of decreasing intensity.

[c] Intensities were confirmed by comparing the retention indices and EI fragmentation patterns with those of standard compounds. Agreement between retention indices of the standard and sample species was typically within 1 unit.

Peak identification was performed partly by GC–MS and partly by the use of appropriate GC standards (Tables VI and VII). Twenty compounds were identified in the phenolic fraction. Good agreement of the two separate GC–MS analyses was observed (Tables VI and VII). It is important to mention here that 2,3-bis(1,1-dimethylethyl)-4-methylphenol was identified in both GC–MS analyses.

Of these twenty compounds the characteristic mass spectra of two representative phenols are considered here. The computer library matches of the mass spectra in many instances appeared fairly good (Figs. 6b, 7b and 8b). Fig. 6a displays the mass spectra of an unknown compound of the phenolic fraction. The fragment of *m/z* 94 is very stable and characteristic of the phenol parent ion $[M]^+$. In addition, the fragments of *m/z* 66, 65 and 39 derived from $[M-CO]^+$, $[M-CHO]^+$ and $[M-C_3H_3]^+$ are also characteristic ion fragments of this phenol. The computer library search (Fig. 6b) shows that phenol was the unknown compound. Phenol was also identified by TLC (Fig. 2) and GC (Fig. 3).

Similarly, in Figs. 7 and 8, the fragments of *m/z* 205, 220, 177, 119 and 57 indicate the presence of 2,6-bis(1,1-dimethylethyl)-4-methylphenol. In addition to the

TABLE VII

COMPOUNDS IDENTIFIED BY GC–MS ANALYSIS OF A PHENOLIC FRACTION OF BIOMASS PYROLYSIS LIQUIDS (FINNIGAN MAT INSTRUMENT)

Peak No.[a]	Scan	Compound	*m/z*	Formula	Fragment ions[b]	Confirmation by comparison with standards[c]
1	870	Phenol	94	C_6H_6O	94,66,65	×
2	885	2-Methylphenol	108	C_7H_8O	108,107,79	×
3	974	4-Methylphenol	108	C_7H_8O	108,107,79	×
4	1100	3-Methylphenol	108	C_7H_8O	108,107,79	×
5	1180	2-Ethylphenol	122	$C_8H_{10}O$	107,122,77	×
6	1212	2,4-Dimethylphenol	122	$C_8H_{10}O$	107,122,77	×
7	1250	2,3-Dimethylphenol	122	$C_8H_{10}O$	107,122,77	×
8	1311	3,5-Dimethylphenol	122	$C_8H_{10}O$	107,122,77	×
9	1358	2,6-Dimethylphenol	122	$C_8H_{10}O$	107,122,77	×
10	1420	1-Octanol	130	$C_8H_{18}O$	41,56,43	×
11	1465	Methyl octanoate	158	$C_9H_{18}O$	74,87,43	×
12	1484	2-Naphthol	144	$C_{10}H_8O$	115,144,177	×
13	1536	2-Methyl-1-naphthol	158	$C_{11}H_{10}O$	158,129,115	×
14	1770	2,6-Bis(1,1-dimethylethyl)-4-methylphenol	220	$C_{15}H_{24}O$	205,115,57	×
15	1800	2,3,6-Trimethylphenol	136	$C_9H_{12}O$	45,121,136	×
16	1826	(1,1-biphenyl)-3-ol	170	$C_{12}H_{10}O_2$	170,141,115	
17	2014	2,4,6-Trimethylphenol	136	$C_9H_{12}O$	45,121,136	
18	2712	1-(2-Hydroxyphenyl)ethanone	148	$C_8H_8O_2$	121,136,93	
19	3113	3-(2-Hydroxyphenyl)-2-propenoic acid	164	$C_9H_8O_3$	121,136,93	
20	3180	1-(3-Hydroxyphenyl)ethanone	148	$C_8H_8O_2$	121,136,93	

[a] Peak numbers refer to the chromatogram in Fig. 5.

[b] The three most intense fragment ions are given in order of decreasing intensity.

[c] Intensities were confirmed by comparing the retention indices and EI fragmentation patterns with those of standard compounds. Agreement between retention indices of the standard and the phenolic sample was the same as with the Carlo Erba instrument.

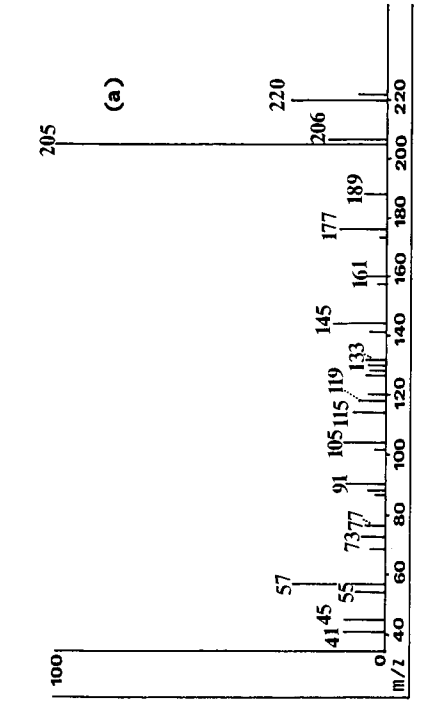

Fig. 6. (a) Mass spectrum of unknown compound in scan 282 and (b) its computer library search.

Fig. 7. (a) Mass spectrum of unknown compound in scan 741 and (b) its computer library search.

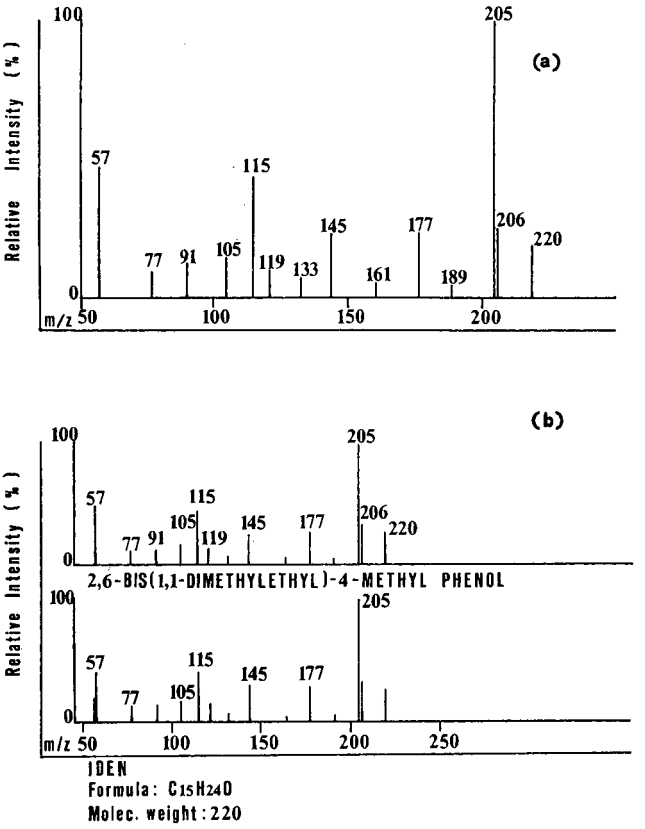

Fig. 8. (a) Mass spectrum of unknown compound in scan 1770 and (b) its computer library search.

two separate computer library searches of the phenolic fraction, the mass spectrum of the pure phenol in question was measured. It appeared that the pure phenol gave exactly the same fragments as those shown in the GC–MS analyses of the phenolic sample. It is important to mention that the aforementioned phenol was identified for the first time in fir wood pyrolysis liquids. In the same way, other phenolic compounds characterized and found to be present in decreasing abundance were 2-, 3- and 4-methylphenols, ethenylphenol, ethenyloxybenzene, dimethylphenols, 2-naphthol, 1-(2-hydroxyphenyl)ethanone, (1,1-biphenyl)-3-ol, 3-(2-hydroxyphenyl)-2-propenoic acid and 2,3,6- and 2,4,6-trimethylphenols. The methylphenols, dimethylphenols, ethylphenols and trimethylphenols were also identified by TLC and GC (Figs. 2 and 3). These compounds have also been reported by other workers [1–5].

Lack of high-field NMR equipment restricted our analysis to the techniques mentioned above. However, high-field NMR analysis is desirable in future work.

It was estimated qualitatively that non-*ortho*- and *ortho*-substituted alkylphenols comprise 70% and 30% of the phenolic fraction, respectively. The amount of non-removable solvents, from the pyrolysis liquids and from the phenolic fraction in the different separation techniques was about 4% as determined by GC.

CONCLUSIONS

The recovery of phenols using acidified silica gel column chromatography was over 95% (w/w). Good separation and characterization of the phenolic fraction was achieved after combining open-column chromatography with alkaline extraction.

The phenol content in biomass pyrolysis liquids was found to be 12–17% (w/w). The phenolic fraction of biomass pyrolysis liquids consisted mainly (85–95%, w/w) of light and heavy non-*ortho*- and *ortho*-substituted alkylphenols, with a non-*ortho*-to-*ortho* ratio of 2:3. The light alkylphenol content was calculated to be about 9% (w/w) of the phenolic fraction. 2,6-Bis(1,1-dimethylethyl)-4-methylphenol was identified in the phenolic fraction.

ACKNOWLEDGEMENTS

This work was financially supported by the EEC under Contract No. EN3B-0052-GR and the Greek Ministry of Energy and Industry. The author gratefully thanks Miss M. Samolada for the biomass pyrolysis liquid samples and Dr. M. Christianopoulou of the College of Chemical Engineers and Dr. A. Geronikaki of the Pharmaceutical Department of the University of Thessaloniki for the IR, ^{1}H and ^{13}C NMR spectra. The author is indebted to Carlo Erba and Finnigan MAT for the GC–MS analyses.

REFERENCES

1 H. G. Davis, M. A. Eames, C. Figueroa, R. R. Gansley, L. L. Schaleger and D. W. Watt, in R. P. Overend, T. A. Milne and L. K. Mudge (Editors), *Fundamentals of Thermochemical Biomass Conversion*, Elsevier Applied Science, Barking, 1985, p. 1027.
2 E. Churin, R. Maggi, P. Grange and B. Delmon, in A. V. Bridgwater and J. L. Kuester (Editors), *Research in Thermochemical Biomass Conversion*, Elsevier Applied Science, Barking, 1988, p. 896.
3 K. Ogan and E. Katz, *Anal. Chem.*, 53 (1981) 160.
4 R. J. Evans and T. A. Milne, *Energy & Fuels*, 1, March–April (1987) 123.
5 D. C. Elliott, L. J. Sealock and R. S. Butner, in E. J. Soltes and T. A. Milne (Editors), *Pyrolysis Oils from Biomass, Producing, Analyzing and Upgrading (ACS Symposium Series*, No. 376.), American Chemical Society, Washington, DC, 1988.
6 I. A. Vasalos, T. Stoicos, M. Samolada, G. Achladas and C. Paramargaritis, *Production and Utilization of Synthetic Liquid Fuels, Progr. Rep., C.P.E.R.I., Contr. No. EN3B-0052-GR, Brussels, July/August 1987*, Elsevier Applied Science, Barking, p. 357.
7 D. G. B. Boocock, R. K. M. R. Kallury and T. T. Tidwell, *Anal. Chem.*, 55 (1983) 1689.
8 C. D. Chriswell, R. C. Chang and J. S. Fritz, *Anal. Chem.*, 47 (1975) 1325.
9 J. F. Schabron, R. J. Hurtubise and H. F. Silver, *Anal. Chem.*, 51 (1979) 1426.
10 F. K. Schweighardt, H. L. Retcofsky and R. A. Friedel, *Fuel*, 85 (1976) 313.
11 G. B. Crump, *J. Chromatogr.*, 10 (1963) 21.
12 D. Meier, R. D. Larimer and O. Faix, *Fuel*, 65 (1986) 916.
13 J. F. Schabron, R. J. Hurtubise and H. F. Silver, *Anal. Chem.*, 50 (1978) 1911.
14 J. E. Dooley, C. J. Thompson and S. E. Scheppele, *Analytical Methods for Coal and Coal Products*, Vol. 1, Academic Press, New York, 1978, p. 467.
15 H. Pakdel, C. Roy and K. Zeidan, in A. V. Bridgwater, J. L. Kuester (Editors), *Research in Thermochemical Biomass Conversion*, Elsevier Applied Science, Barking, 1987, p. 572.
16 P. Chandal, S. Kaliaguine, J. L. Grandmaison and A. Mahay, *Appl. Catal.*, 10 (1984) 317.
17 D. C. Elliott, paper presented at *14th Meeting on Biomass Thermochemical Conversion, Arlington, VA, June 23–24, 1982.*
18 I. A. Vasalos, M. C. Samolada, and G. E. Achladas, paper presented at the *Research in Thermochemical Biomass Conversion Congress, Phoenix, AZ, May 2–6, 1988.*

19 I. Vasalos, T. Stoikos, M. Samolada, G. Achladas and K. Papamargaritis, *Production and Utilization of Synthetic Liquid Fuels, Prog. Rep., C.P.E.R.I., Contr. No. EN3B-0052-GR, Naples, January/June 1988.*
20 I. A. Vasalos, M. Samolada, G. Achladas and T. Stoikos, paper presented at *International Congress on Production and Utilization of Synthetic Liquid Fuels, Saarbrücken, October 24–28, 1988.*
21 G. E. Achladas, paper presented at the *12th Greek Congress of Chemistry, Thessaloniki, November 21–25, 1978.*

Journal of Chromatography, 542 (1991) 277–293
Elsevier Science Publishers B.V., Amsterdam

CHROM. 23 024

Optimized isocratic separation of major carboxylic acids in wine

R. M. MARCÉ*, M. CALULL, J. C. OLUCHA, F. BORRULL and F. X. RIUS
Department of Chemistry, University of Barcelona, Pça. Imperial Tarraco 1, 43005 Tarragona (Spain)
(First received July 18th, 1990; revised manuscript received October 23rd, 1990)

ABSTRACT

The reversed-phase high-performance liquid chromatographic separation of major carboxylic acids in wine was optimized. The separation was carried out by isocratic elution, and the optimization of the mobile phase composition with a constant solvent strength was studied. The optimization was carried out by using the overlapping resolution mapping approach employing previously developed software. The best mobile phase consisted of tetrahydrofuran, methanol and acetonitrile as organic modifiers and water as a carrier solvent to maintain a constant solvent strength.

INTRODUCTION

The determination of carboxylic acids in wine has considerable importance in enology as these compounds are used to control the vinification process. Carboxylic acids also have a great influence on the biological stability and organoleptic properties of wines, and are therefore determined routinely in many enological laboratories.

Various chromatographic methods offer alternatives to the time-consuming traditional methods of analysis, especially high-performance liquid chromatography (HPLC) employing either reversed-phase partition equilibria or ion-exchange equilibria [1–3]. Of the methods based on reversed-phase chromatography, the direct method, without derivatization and detection by UV spectrophotometry at about 210 nm, and the derivatization method, using different reagents such as phenacyl [4,5], naphthacyl [6], *p*-nitrophenyl [7] or *p*-nitrobenzyl [8] bromides and detection at 254 nm, are commonly used. The method using derivatized compounds is preferred to the direct method owing to the higher sensitivity achieved.

Good resolution between the different peaks is usually obtained when using a gradient of solvent strength, but isocratic elution has two basic advantages in routine analysis, *viz.*, the equipment is simpler and the overall time of analysis for a series of samples is shorter. In this paper, an optimized isocratic method for determining carboxylic acids in wine with precolumn derivatization with phenacyl bromide is reported.

Two factors that depend on the mobile phase composition, the capacity factor k' and the separation factor α, influence the resolution in isocratic systems. The

0021-9673/91/$03.50

separation factor is influenced by solvent composition and, for a constant solvent strength, different resolutions are obtained when different solvents are used. Three solvents (methanol, acetonitrile and tetrahydrofuran) as organic modifiers and water as the carrier to maintain a constant solvent strength have been used to find the optimum solvent composition by using the overlapping resolution mapping (ORM) [9,10] technique, which gives the best overall separation for a chosen resolution level.

Although some software implementing overlapping resolution mapping has been reported [11], in this work we used our own program that includes high-quality graphics for this application. The program runs on an IBM PC or compatible computer and is available from the authors.

EXPERIMENTAL

Equipment

A Hewlett-Packard Model 1050 modular chromatograph with a Hewlett-Packard Series 1050 variable-wavelength detector and a workstation with a Model 35900 interface was used. The chromatographic separation was carried out with a Spherisorb ODS-2 column (250 × 4.6 mm I.D.) of 5-μm particle size and a precolumn (30 × 3.9 mm I.D.) filled with Bondapak C_{18}/Corasil (37–50-μm particle size).

Reagents and standards

Phenacyl bromide (Fluka), 18-crown-6 (Fluka) and phosphate buffer solution (pH 6.8) were used in the derivatization reaction. All solvents in the derivatization process (acetone) and in the chromatographic separation (methanol, acetonitrile and tetrahydrofuran) were of HPLC quality from Merck and water was purified in a Milli-Q apparatus (Millipore).

The study was carried out with the most frequent carboxylic acids found in wine, *i.e.* tartaric, malic, acetic, lactic, succinic and citric acid (Aldrich). Methylmalonic acid was used as an internal standard.

Chromatographic conditions

The derivatization procedure has been optimized elsewhere [12] and the chromatographic conditions (flow-rate, 1 ml/min; detection, UV absorption at 254 nm; volume injected, 5 μl; and temperature, 30°C) were chosen on the basis of previous work [12].

RESULTS AND DISCUSSION

The first step in the optimization of the solvent composition for isocratic elution consists in determining a suitable solvent strength that gives acceptable values of k' for all the carboxylic acids considered. Among different approaches developed for determining an adequate solvent strength [13–15], one based on an initial gradient separation was chosen [13]. From the chromatogram obtained by using a binary water–methanol linear gradient, sufficient information can be extracted to calculate the percentage of methanol in the mobile phase that gives acceptable values of k' and, from this value, three different mixtures of acetonitrile, methanol and tetrahydrofuran with water were derived that define the three vertices of an optimization triangle [16].

Taking into account the experience from previous work in our laboratory on the optimization of a linear gradient separation of carboxylic acids present in wine [12], a linear gradient from 30 to 90% methanol in 20 min allowed good resolution to be obtained for all the peaks studied (Fig. 1). The sample injected consisted of a white wine to which pure carboxylic acids had been added because some of them were not present naturally in the actual wine sample analysed. The injected sample was obtained by mixing 1 ml of the white wine sample with 1 ml of a 0.5 g/l standard solution of carboxylic acids.

In the optimization process, peaks 1 (system peak), 2 (lactic acid), 3 (acetic acid), 4 (reagent peak, phenacyl bromide), 5 (tartaric acid), 6 (malic acid), 7 (succinic acid), 8 (internal standard, metylmalonic acid) and 9 (citric acid) were considered. The first peak appearing in Fig. 1 corresponds to acetone, the solvent used in the derivatization solution, and as its retention time is shorter than those of the system peaks, it was not considered.

From the chromatographic data, the program calculates the percentage of the first isocratic solution derived from the gradient elution which determines the solvent strength from the expression [13]

$$c_o = (c_1 c_2 ... c_n)^{1/n}$$

where c_i is the solvent composition at which each solute i leaves the column, calculated from the following equation [13]

c_i = initial concentration of selectivity-adjusting solvent + (time of elution for each peak − distance between gradient generator and column inlet in time units) × (gradient rate in % of selectivity-adjusting solvent per minute)

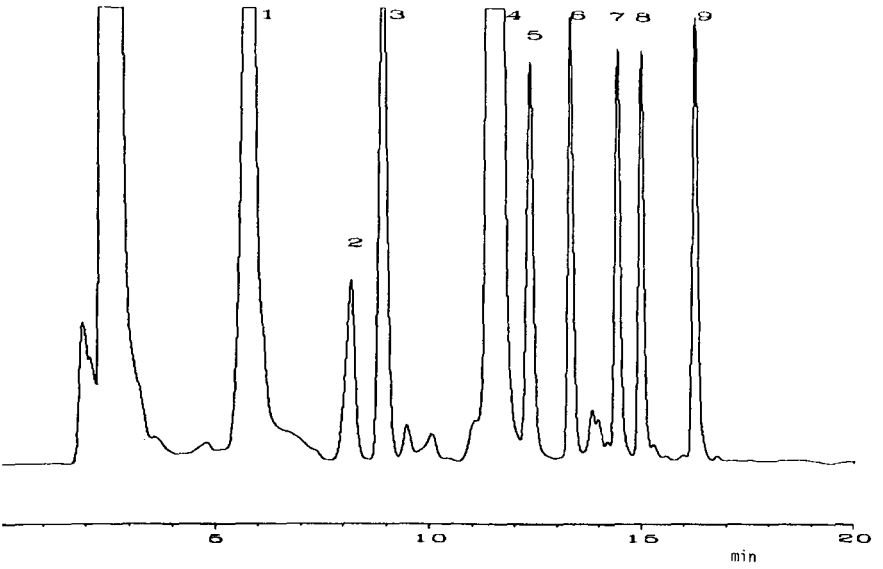

Fig. 1. Chromatogram of the carboxylic acids obtained with linear gradient elution from 30 to 90% of methanol in 20 min.

TABLE I

EXPERIMENTAL CONDITIONS FOR THE DIFFERENT EXPERIMENTS TO BE CARRIED OUT TO DEFINE THE RESPONSE SURFACE

Experiment	Methanol (%)	Acetonitrile (%)	Tetrahydrofuran (%)	Water (%)
1	52.75	0.00	0.00	47.25
2	0.00	42.86	0.00	57.14
3	0.00	0.00	30.48	69.52
4	26.38	21.43	0.00	52.19
5	0.00	21.43	15.24	63.33
6	26.38	0.00	15.24	58.38
7	17.58	14.29	10.16	57.97
8	35.17	7.14	5.08	52.61 Validation[a]
9	8.79	28.57	5.08	57.55 Validation[a]
10	8.79	7.14	20.32	63.74 Validation[a]

[a] These experimental conditions were used on the validation of the mathematical expression found.

However, as poor retention of solutes is sometimes found with this value, it is multiplied by a correction factor [13]. The c_o value found using the software developed was 63.3% of methanol, which was multiplied by a factor of 5/6 [13], resulting a mobile phase constituted by 52.8% methanol and 47.2% water.

The compositions of all other experimental points were computed by the program (Table I) by using the expression

$$S = \sum s_i \varphi_i$$

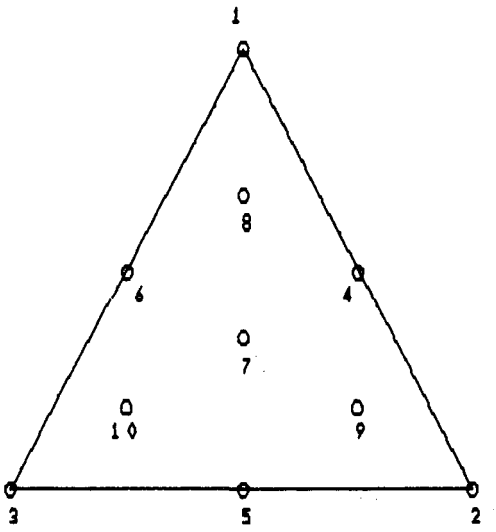

Fig. 2. Simplex lattice experimental design used. Point 1 (52.8% methanol, 47.2% water), point 2 (42.9% acetonitrile, 57.1% water) and point 3 (30.5% tetrahydrofuran, 69.5% water).

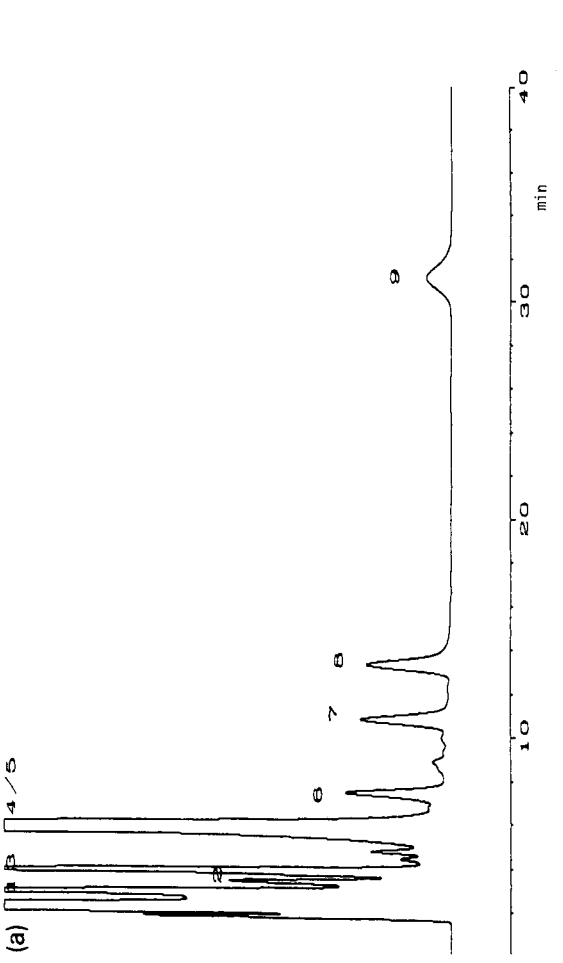

Fig. 3.

(Continued on p. 282)

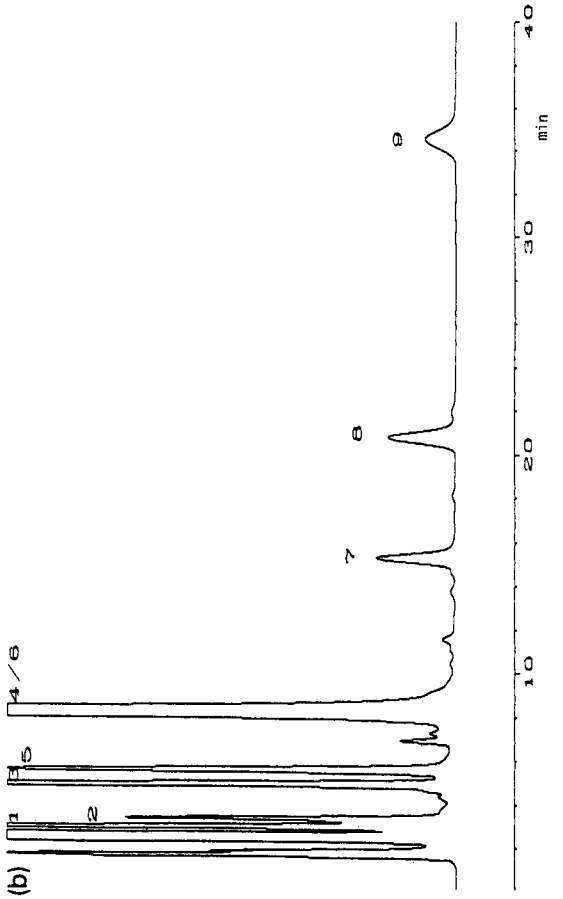
(b)
1
2
3
4/6
7
8
9
10
20
30
40
min

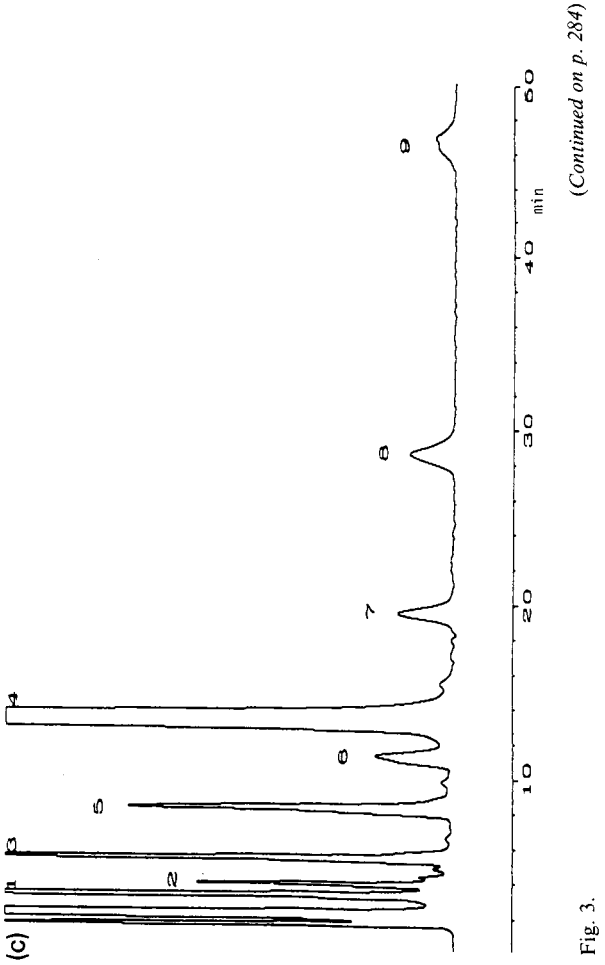

Fig. 3.

(Continued on p. 284)

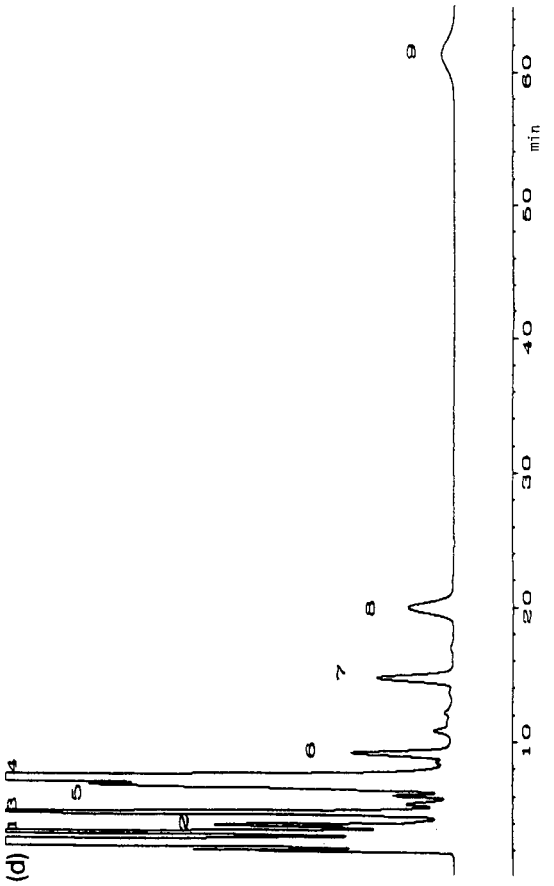
(d)
1
2
3
4
5
6
7
8
9
10
20
30
40
50
60
min

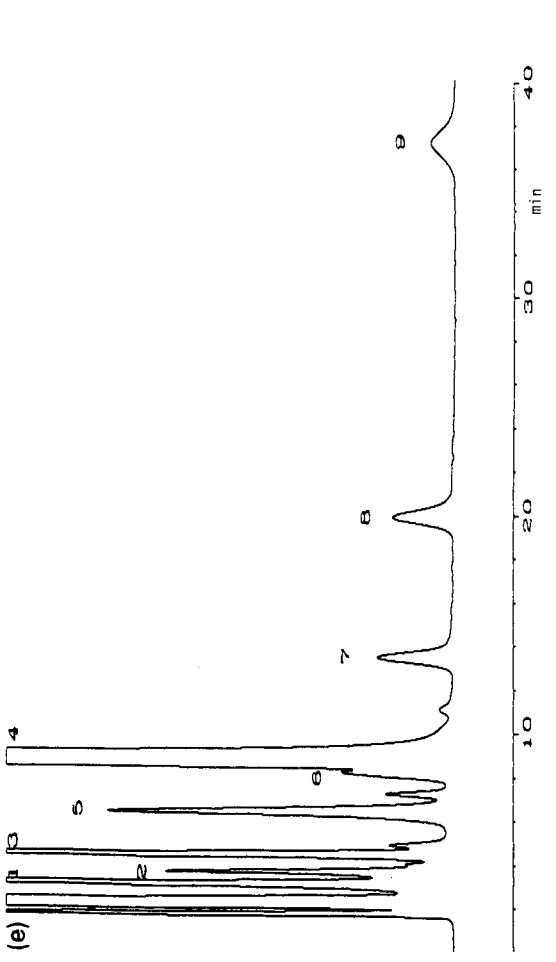

Fig. 3.

(*Continued on p. 286*)

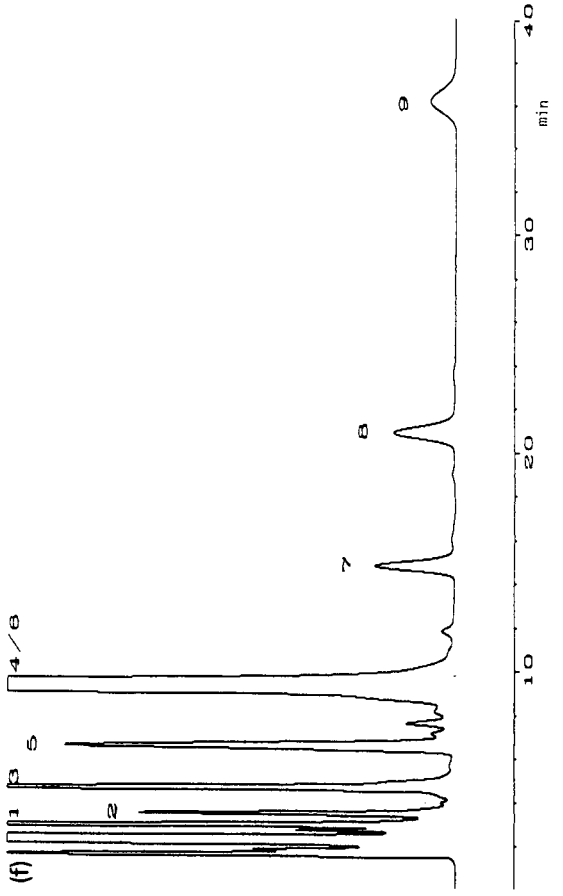
(f)
1
2
3
5
4/6
7
8
9
10
20
30
40
min

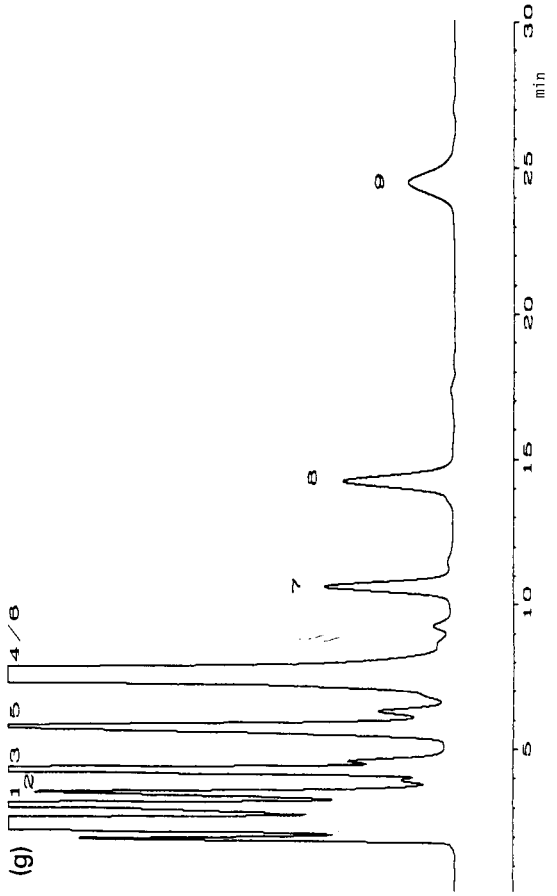

Fig. 3. Chromatograms obtained for the different isocratic mobile phase compositions.

where S is the solvent strength of the mobile phase, s_i is the solvent strength weighting factor of each solvent i (2.6, 3.2 and 4.5 for methanol, acetonitrile and tetrahydrofuran, respectively) and φ_i is the solvent fraction.

Fig. 2 shows the parameter space defined in which the optimization will take place. The three binary mobile phases derived are the vertices of a simplex lattice experimental design and points 4, 5 and 6 define the compositions of the ternary mobile phase and point 7 defines the quaternary mobile phase. Points 1–7 were used to calculate the response surface and points 8–10 to check the lack of fit between the model and the experimental results. All mobile phase compositions involved will give rise to approximately the same solvent strength, although specific retention times and therefore orders of elution and selectivities will change.

The different chromatograms obtained for each experiment are shown in Fig. 3. Peaks 1, 2, 3, 7, 8 and 9 do not change their elution orders in any of the experiments carried out, whereas peaks 4, 5 and 6 change their position when the composition of the mobile phase varies.

The seven chromatograms were evaluated by using the overlapping resolution mapping approach by using the SMR[a] program. The program models the resolution between each pair of peaks as a function of the percentages of methanol, acetonitrile and tetrahydrofuran along the parameter space defined by the experimental design used. The following equation has been considered:

$$R_{m,n} = a + bx + cy + dz + ex^2 + fy^2 + gz^2 + hxy + ixz + jyz$$

where x, y and z are the percentages of methanol, acetonitrile and tetrahydrofuran, respectively, m and n refer to the pairs of peaks 1–2, 2–3, 3–4, 4–5, 5–6, 6–7, 7–8, 8–9, 3–5, 4–6 and 4–7 and a, b, c,...,j are the coefficients of the model.

First, the different peaks of each pair are tracked by the software by comparing the different retention times. Prior to the introduction of the retention time and width, each peak of the chromatogram is assigned to a compound. The order with the first composition is considered to be the initial order and the elution order obtained for the other compositions are compared with this one. When the elution order obtained changes in a composition, a crossover is considered.

Taking into account the seven experiments carried out, the computer program calculates the coefficients of the model by a non-linear multivariate regression algorithm.

Once a minimum threshold value for the resolution between all peaks has been defined, the SMR program allows the visualization of those areas (unshaded zones) in which the mobile phase compositions give rise to chromatograms in which the resolution is higher than the fixed resolution value. In Fig. 4 the different response surfaces obtained for a resolution higher than 1.5 for each pair of peaks can be observed. It can be seen that the pairs of peaks 3–4, 5–6, 6–7, 7–8, 8–9, 3–5 and 4–7 have a resolution higher than the minimum established value of 1.5 for all possible compositions at the solvent strength considered. At this resolution value, the pairs of peaks 1–2, 2–3, 4–5 and 4–6 have a resolution lower than 1.5 for some mobile phase compo-

[a]SMR is the name of the program used. They are the initials of the Catalan translation of ORM (overlapping resolution map).

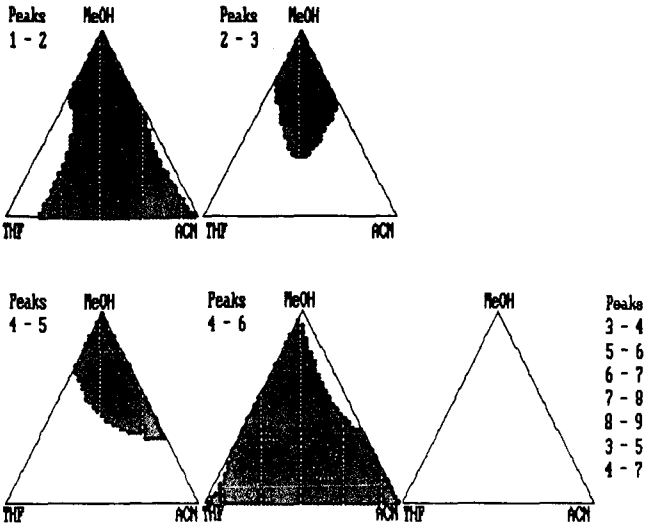

Fig. 4. Peak-pair resolution map for a resolution higher than 1.5. Here and in subsequent figures, MeOH = methanol, ACN = acetonitrile and THF = tetrahydrofuran.

sitions. The pair of peaks 2–3 and 4–5 have a resolution lower than 1.5 when the percentage of methanol in the mobile phase is higher and the pairs of peaks 1–2 and 4–6 have only a small zone where the resolution is higher than 1.5. These two zones are localized when a high percentage of tetrahydrofuran is present in the mobile phase and when the mobile phase is composed of a mixture of methanol and acetonitrile.

By superposing all the computed response surfaces, a unique overlapping resolution map is obtained in which the unshaded zones indicate the mobile phase compo-

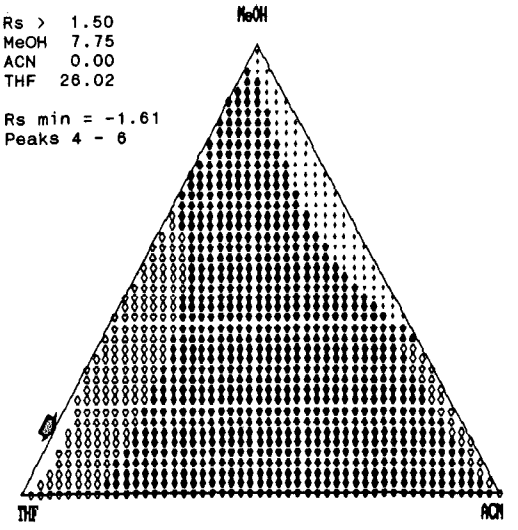

Fig. 5. Overlapping resolution map for a resolution of 1.5.

TABLE II

THEORETICAL RESOLUTION VALUES OBTAINED UNDER THE OPTIMUM CONDITIONS

Mobile phase: methanol–tetrahydrofuran (7.75:26.02).

Resolution, R_s	Peaks	Resolution, R_s	Peaks
2.0661	1–2	5.1407	7–8
2.8516	2–3	7.4442	8–9
6.7576	3–4	4.0742	3–5
−3.8675	4–5	1.6138	4–6
2.7942	5–6	3.2587	4–7
6.0116	6–7		

sitions which give rise to resolutions higher than 1.5 for all pairs of peaks considered (Fig. 5). This zone is located in the present instance at a high concentration of tetrahydrofuran and low concentrations of both acetonitrile and methanol. The optimum conditions for the isocratic analysis can be deduced from the graph obtained. The program allows the identification by means of an arrow of the optimum zone and it calculates the concentrations of each solvent in the mobile phase at each considered point, and the pair of peaks with the lowest resolution which is indicated at the top left of the figure. The optimum conditions considered for isocratic elution are 26% of tetrahydrofuran, 7.8% of methanol and 66.2% of water. Under these conditions the lowest resolution of 1.6 is obtained for peaks 4–6. The program allows one to see all other resolution values obtained under these conditions for the remainder of the peaks. The values obtained can be seen in Table II. Under these conditions all other peaks show a resolution higher than 2.7. The chromatogram obtained under these conditions is shown in Fig. 6.

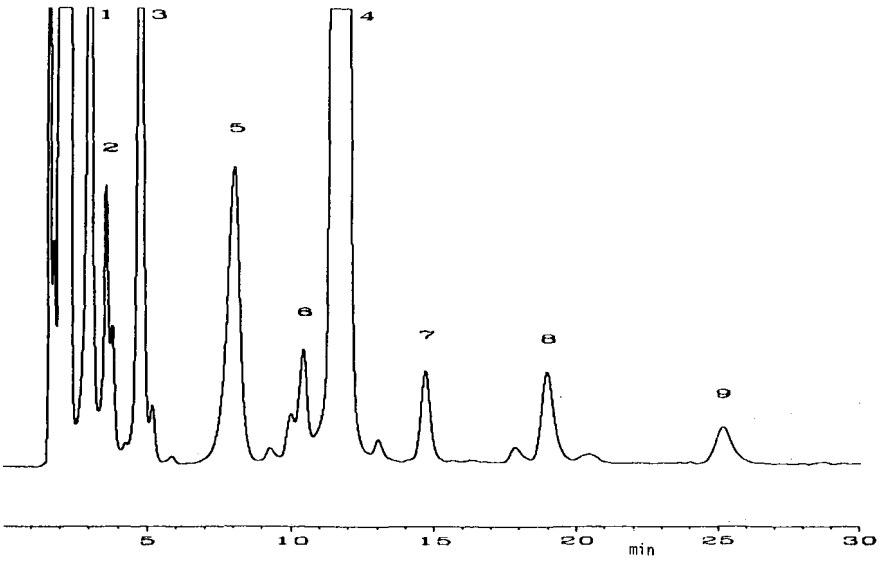

Fig. 6. Chromatogram obtained under the optimum conditions.

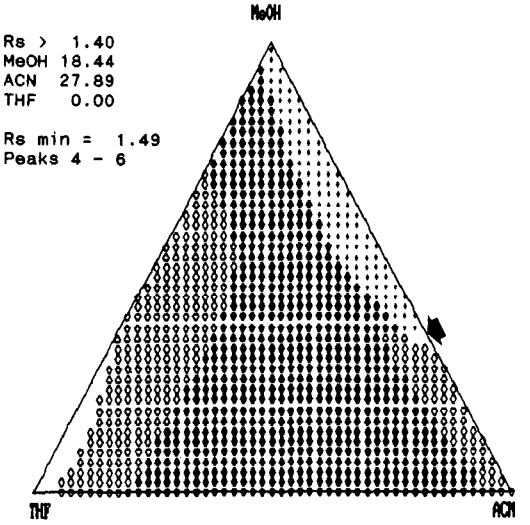

Fig. 7. Overlapping resolution map for a resolution of 1.4 without tetrahydrofuran in the mobile phase.

An alternative mobile phase composition can be found by slightly reducing the minimum value of the resolution between peaks. If the threshold value is set to 1.4, the response surface depicted in Fig. 7 is obtained. As indicated by the arrow, a solvent composition which does not include tetrahydrofuran can be used in an isocratic elution (18.4% methanol, 27.9% acetonitrile and 53.7% water), giving rise to the chromatogram shown in Fig. 8. Clearly, peaks 1 and 2 and 5 and 4 are coeluted to

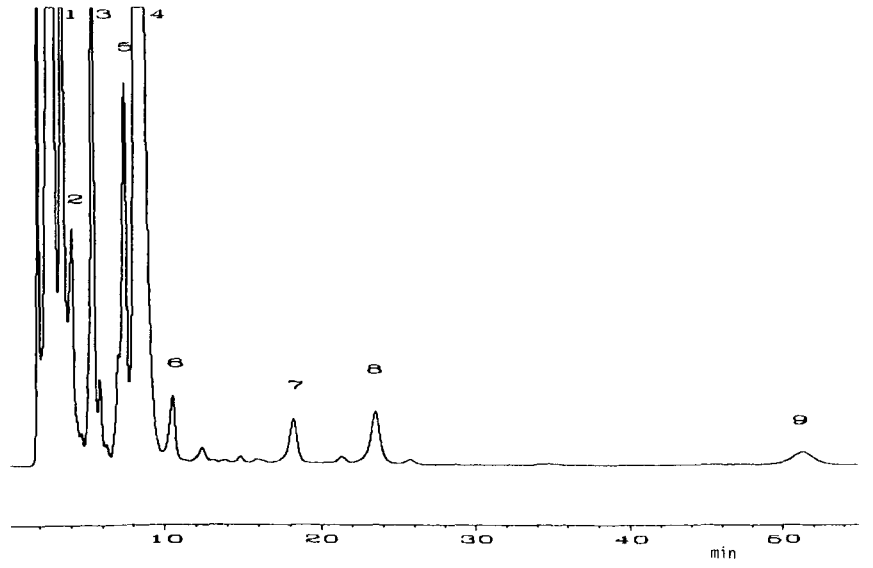

Fig. 8. Chromatogram obtained with the conditions in Fig. 7.

TABLE III

EXPERIMENTAL AND THEORETICAL RESOLUTION VALUES AND RESIDUAL VALUES FOR THE PAIR OF PEAKS 1–2 FOUND WITH THE FIRST SEVEN EXPERIMENTS

Experiment	Exptl. response, $R_{exp.}$	Calc. response, $R_{calc.}$	$R_{calc.} - R_{exp.}$
1	0.966	0.963	0.0030
2	1.560	1.557	0.0030
3	2.188	2.184	0.0030
4	1.683	1.695	0.0120
5	1.514	1.526	0.0120
6	0.800	0.812	0.0120
7	1.297	1.270	0.0271
			$\sum(R_{calc.} - R_{exp.})^2 = 0.0012$

a greater extent than in the previous zone and the retention time of citric acid (peak 9) has greatly increased.

When the first seven experimental points are used to check the lack of fit, the values of the residuals obtained for each pair of peaks by subtracting the experimental from the theoretical values are very similar and the error calculated, the sum of squared residuals, is acceptable for the method used. An example of the residuals obtained for the pair of peaks 1–2 can be seen in Table III. When replications of the three points corresponding to experiments 8, 9 and 10 are considered in the analysis of lack of fit of the computed model, the sum of squared residuals obtained increases but its value is acceptable for the method used. Different values obtained in the statistical analysis are given in Table IV.

CONCLUSIONS

The optimum mobile phase composition for determining carboxylic acids in wine by reversed-phase HPLC using precolumn derivatization with phenacyl bromide and isocratic elution has been found. A resolution greater than 1.5 between all

TABLE IV

VALIDATION OF THE RESPONSE SURFACE FOR THE PAIR OF PEAKS 1–2 WITH EXPERIMENTS 8, 9 and 10.

Each experimental value is the mean of three determinations.

Experiment	Exptl. response, $R_{exp.}$	Calc. response, $R_{calc.}$	$R_{calc.} - R_{exp.}$
8	1.306	1.320	0.014
9	1.392	1.224	0.168
10	1.531	1.489	0.042
			$\sum(R_{calc.} - R_{exp.})^2 = 0.0302$

pairs of peaks was considered as the optimization criterion. The mobile phase found consists of tetrahydrofuran (26%), methanol (7.8%) and water (66.2%) and the retention time for the last peak is 26 min.

An alternative mobile phase which avoids the use of tetrahydrofuran is composed of acetonitrile (27.9%), methanol (18.4%) and water (53.7%) and the resolution for all the peaks is greater than 1.4, but the retention time of the last peak increases to 52 min.

When the developed method is compared with that employing gradient elution, a shorter time for elution of all compounds is observed for the latter, but it must be taken into account that the overall analysis time can increase considerably because of the time to adapt the column between to determinations.

The SMR program has been used to determine the optimum mobile phase composition which gives a minimum resolution for all the peaks of interest and allows one to visualize the overlapping resolution maps with satisfactory results.

ACKNOWLEDGEMENTS

The authors thank CICYT (project 86-0029) for financial support given and R. M. M. gratefully acknowledges a research grant from CIRIT (project AR89) of Catalonia.

REFERENCES

1 R. F. Frayne, *Am. J. Enol. Vitic.*, 37 (1986) 4.
2 A. Schneider, V. Gerbi and M. Redoglia, *Am. J. Enol. Vitic.*, 38 (1987) 2.
3 J. P. Goiffon, A. Blachere and C. Reminiac, *Analusis*, 13 (1985) 218.
4 E. Mentasti, M. C. Gennaro, C. Sarzanini, C. Baiocchi and M. Savigliano, *J. Chromatogr.*, 322 (1985) 177.
5 F. Caccamo, G. Carfagnini, A. Di Corcia and R. Samperi, *J. Chromatogr.*, 362 (1986) 47.
6 M. J. Cooper and M. W. Anders, *Anal. Chem.*, 46 (1974) 1849.
7 E. Grushka, H. D. Durst and E. J. Kikta, *J. Chromatogr.*, 112 (1975) 673.
8 R. Badoud and G. Pratz, *J. Chromatogr.*, 360 (1986) 119.
9 J. L. Glajch, J. J. Kirkland and K. M. Square, *J. Chromatogr.*, 199 (1980) 57.
10 P. J. Schoenmakers, *Optimization of Chromatographic Selectivity*, Elsevier, Amsterdam, 1986.
11 J. L. Glajch, J. L. Kirkland and J. M. Minor, *J. Liq. Chromatogr.*, 10 (1987) 1727.
12 R. M. Marcé, M. Calull, F. Borrull and F. X. Rius, *Am. J. Enol. Vitic.*, 41 (1990) 289.
13 M. D. Smet, G. Hoogewijs, M. Putemans and D. L. Massart, *Anal. Chem.*, 56 (1984) 2662.
14 J. C. Berridge, *Techniques for the Automated Optimization of HPLC Separations*, Wiley, Chichester, 1985.
15 L. R. Snyder, J. L. Glajch and J. J. Kirkland, *Practical HPLC Method Development*, Wiley-Interscience, New York, 1988.
16 R. Leher, *Int. Lab.*, Nov.–Dec. (1981) 76.

Journal of Chromatography, 542 (1991) 295–306
Elsevier Science Publishers B.V., Amsterdam

CHROM. 23 029

Luminarin 4 as a labelling reagent for carboxylic acids in liquid chromatography with peroxyoxalate chemiluminescence detection

MICHEL TOD* and MICHEL PREVOT
Department of Pharmacotoxicology, Avicenne Hospital, 125 Route de Stalingrad, 93000 Bobigny (France)
JOSEPH CHALOM
Eurobio, ZA Courtaboeuf, 7 Avenue de Scandinavie, 91953, Les Ulis (France)
and
ROBERT FARINOTTI and GEORGES MAHUZIER
Laboratoire de Chimie Analytique II, Faculty of Pharmaceutical Sciences, Rue J. B. Clément, 92290 Chatenay Malabry (France)
(First received July 19th, 1990; revised manuscript received December 11th, 1990)

ABSTRACT

Luminarin 4 is a labelling reagent with a quinolizinocoumarin structure, which reacts with carboxylic acids after their activation by N-hydroxysuccinimide for 12 h at 20°C and dicyclohexylcarbodiimide for 60 min at 70°C. Small fatty acids were derivatized and separated by reversed-phase liquid chromatography. The fluorescence detection threshold was 300 fmol injected. The limit of chemiluminescence detection, which required a post-column reaction with an oxalic ester and hydrogen peroxide, was 50 fmol injected. The reaction was used to measure prostaglandin E_2, whose detection limit was 32 fmol injected, but the derivatization limit was 60 pmol. Linearity was observed in the range 0.1–10 nmol of prostaglandin E_2.

INTRODUCTION

Peroxyoxalate chemiluminescence (CL) detection was first used in liquid chromatography by Kobayashi and Imai [1] and further investigated by a number of others [2–11]. An oxalic ester reacts with hydrogen peroxide to form a proposed energetic intermediate, peroxyoxalate, which transfers its energy to a fluorescer, resulting in the emission of a photon. This mechanism has been applied to polycyclic and aminopolycyclic aromatic hydrocarbons [2,3], fluorescamine-labelled catecholamines [4], dansylated amino acids [5] and steroid [6], rhodamine-labelled chlorophenols [7] and coumarinic derivatives [8]. The main reason for the interest in this technique is that, for certain fluorophores, the CL detection limits are lower than those obtained with photoexcitation, but only a few fluorophores are better detected by chemiexcitation. In previous studies [9–11], we showed that, among various amino coumarins, the chemiluminescent intensity of the quinolizinocoumarin moiety was stronger [10], and the molecule was suitable for both normal and reversed-phase liquid chromatography with CL detection [11], affording femtomole detection limits.

0021-9673/91/$03.50

Quinolizinocoumarin served as the basis for the development of a series of chemiluminescent labels, called luminarins. In this study, luminarin 4 was investigated as a derivatizing reagent for carboxylic acids.

Many kinds of precolumn fluorescent derivatization reagents have been developed for the determination of carboxylic acids [12–25] by high-performance liquid chromatography (HPLC). They can be subdivided into two classes: those involving direct reaction between the acid and the labelling reagent, and those requiring the activation of the carboxylic acid before reaction with the fluorescer. To the first category belong halogenomethyl aromatics such as 4-bromomethyl-7-methoxycoumarin [12] and related compounds. These compounds had high limits of derivatization (L.D.) (about 200 pmol) and lacked selectivity, because they reacted with phenols, thiols and imides [16]. Aryldiazoalkanes were highly reactive (L.D. = 1 pmol) but were usually unstable when exposed to heat and light, with the exception of 1-pyrenyldiazomethane [14]. Derivatization with *o*-diamines, *e.g.* 9,10-diaminophenanthrene, to form 2-substituted phenanthrimidazoles [15] afforded a favourable L.D. (10 pmol) but necessitated the preparation of methylpolyphosphate as the solvent and the derivatives were quenched by dissolved oxygen.

To the second category belong the carboxylic acids activated by 1-methyl-2 halogenopyridinium iodide [16], N,N′-carbonyldiimidazole [16] and carbodiimides [17,18]. The activated acid was then condensed with an alcohol, *e.g.*, hydroxymethylanthracene (16), or a hydrazine, 2-nitrophenylhydrazine [17]. Among these methods, activation by 1-methyl-2-bromopyridinium iodide proved to be useful, with an L.D. in the subpicomole range. On the other hand, although activation by carbodiimides has been widely used in synthesis [19], application to the derivatization of amounts of carboxylic acids smaller than 1 nmol has not been reported. Owing to the attractive features of this activation reaction, including mild derivatization conditions and stability of the reagent and the derivatives, its application to fatty acids was investigated using luminarin 4 (Fig. 1) as a luminophore.

EXPERIMENTAL

Reagents

Isovaleric and nonanoic acid were purchased from Prolabo (Paris, France). Prostaglandin E_2 was a gift from Upjohn (Kalamazoo, MI, U.S.A.). N-Hydroxysuccinimide (NOHS) and bis-(2,4,6-trichlorophenyl) oxalate (TCPO) were bought from Fluka (Buchs, Switzerland). Dicyclohexylcarbodiimide (DCC), tetrahydrofuran (THF), imidazole, methyl acetate, dimethylformamide (DMF) and dimethyl sulphoxide (DMSO) were purchased from Merck (Darmstadt, Germany). Coumarin 102, laser grade, was obtained from Eastman-Kodak (Rochester, NY, U.S.A.) and luminarin 4 from Eurobio (Les Ulis, France). Hydrogen peroxide (30% aqueous solution) was supplied by Janssen (Beerse, Belgium).

All reagents and solvents were of analytical-reagent grade, unless stated otherwise, and were used as supplied. N-Succinimidoxyisovalerate was synthesized by dissolving 57.5 mg of NOHS and 123.6 mg of DCC in 2 ml of DMF and mixing with 55 μl of pure isovaleric acid. The solution was left for 1 h at 4°C and then for 1 h at room temperature. Precipitated dicyclohexylurea was removed by centrifugation and the solution was used diluted 1:100 in DMF.

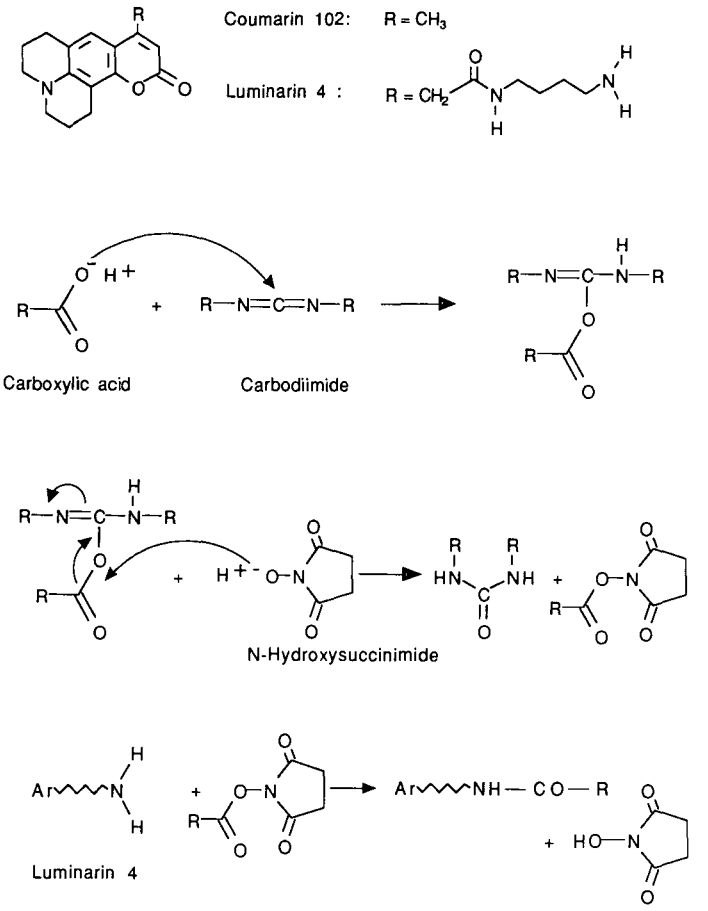

Fig. 1. Derivatization of carboxylic acids by luminarin 4.

Instrumentation

The liquid chromatograph consisted of a Chromatem 380 pump (Touzart et Matignon, Vitry, France), a Rheodyne Model 7125 injector with a 20-μl sample loop, a Kratos FS970 fluorescence detector (Applied Biosystems, Rungis, France) and a Shimadzu CR3A integrator (Touzart et Matignon). For chemiluminescence measurements, a Shimadzu CTO-6A column oven (Touzart et Matignon) and a Kratos URS051 post-column reactor (Applied Biosystems) were added, with a 292-μl capillary placed in the oven for mixing TCPO and hydrogen peroxide, and a 60-μl capillary for mixing these reagents with the eluent before entering the detector.

For on-line absorbance measurements, a Shimadzu diode-array SPD-M6A detector was used. Excitation, emission and synchronous excitation spectra were recorded on a Model LS-5 spectrofluorimeter (Perkin-Elmer, Norwalk, CT, U.S.A.), with the slits adjusted to 2.5 nm. All spectra were fully corrected.

For the determination of the relative fluorescence quantum yield, a Shimadzu

SPD2A absorbance detector was connected to the outlet of the fluorescence detector. The signal from each detector was recorded on a double-trace integrator.

Chromatographic conditions

Four sets of conditions were used, as follows. System 1 consisted of an Ultrasphere ODS-2 (5 μm) column (250 × 4.6 mm I.D.) (Beckman, Les Ulis, France) and the mobile phase was acetonitrile–DMSO–5 m*M* imidazole nitrate buffer (pH 6.5) (60:10:30, v/v/v) pumped at 1 ml/min. In system 2, a Spherisorb ODS-2 (5 μm) column (150 x 4.6 mm) [Société Française de Chromatographie sur Colonne (SFCC), Neuille-Plaisance, France] was used with a mobile phase of acetonitrile–DMSO–5 m*M* imidazole nitrate buffer (pH 7) (45:5:50, v/v/v) at a flow-rate of 1.5 ml/min. System 3 was identical with system 2 except that the buffer concentration was 10 m*M*. System 4 used a Spherisorb ODS-2 (5 μm) column (250 × 4.6 mm I.D.) (SFCC) with a mobile phase of acetonitrile–10 m*M* imidazole nitrate buffer (pH 7.7) (45:55, v/v) pumped at 1.2 ml/min.

For all systems, fluorimetric detection was performed with the excitation wavelength set at 390 nm and a 470-nm emission cut-off filter. When chemiluminescence detection was used, the lamp was turned off. The reagent solutions (1 mg/ml TCPO in methyl acetate and 0.4 *M* hydrogen peroxide in THF) were each pumped by the post-column system at a flow-rate of 0.25 ml/min and the oven was set at 40°C. The conditions were optimized as described previously [11].

The fluorescence quantum yield was calculated as the ratio of the total fluorescence intensity to the absorbance of the corresponding peak, in arbitrary units [20]. The two detectors were set at 360 nm for excitation and absorbance, respectively, whereas a 419-nm cut-off filter was used to collect all the emission bands of the fluorescers.

Derivatization procedure

Luminarin 4 derivatives were prepared by mixing 0.1 ml of 62.5 m*M* NOHS in DMF, 0.1 ml of 75 m*M* DCC in DMF and 0.05 ml of a solution of the carboxylic acid to be tested in DMF. The activation reaction was complete after 12 h at 20°C. Then 0.05 ml of a 2 m*M* coumarin 102 solution (internal standard) in DMSO and 0.5 ml of a 1 m*M* luminarin 4 solution in DMSO were added. After 60 min at 70°C, the derivatives were diluted 1:10 or more in DMSO before injection, so that the amount of derivative injected ranged from 0.5 to 20 pmol.

RESULTS AND DISCUSSION

Luminarin 4 isomerism

The first attempts to optimize the chromatographic conditions for luminarin 4 revealed an unusual feature of this product compared with other quinolizinocoumarins: the injection of luminarin 4 solutions, even when freshly prepared, resulted in several peaks of unequal heights when assessed by fluorescence detection. Various treatments of the luminarin 4 powder (recrystallization, acid–alkali extraction) yielded no modifications, and the luminarin 4 structure was confirmed by mass, ^{1}H NMR and IR spectrometry and C, H, O, N and S determinations [21]. Before trying purification by preparative chromatography, it was necessary to ensure that no peak was

retained on the column (*i.e.*, that recovery was complete), and that the fractions were stable. To achieve these goals, three chromatographic systems (1–3) were optimized and five peaks were detected as reported in Table I. Peaks 2 and 5 were the major components, representing 80% of the total area of the five peaks. A "recovery test" was made using system 1, by comparing the total areas of the absorbance signal with and without a column. The absorbance of the five peaks of luminarin 4 was not significantly different from that of the luminarin 4 solution when the mean areas of five injections were compared: 109 ± 11 *vs.* 127 ± 13 ($p > 0.05$), in arbitrary units.

TABLE I

RETENTION TIMES OF LUMINARIN 4 ISOMERS IN THREE CHROMATOGRAPHIC SYSTEMS

System	Retention time (min)				
	Peak 1	Peak 2	Peak 3	Peak 4	Peak 5
1	2.8	6.9	6.3	ND[a]	8.8
2	3.0	4.8	5.4	9.7	12.8
3	2.0	2.8	5.8	ND[a]	7.0

[a] Not detectable.

The stability of the fractions was then determined using system 2. Luminarin 4 (10^{-5} *M*) in DMSO was injected repeatedly and the five peaks were collected. Immediate reinjection of the fractions allowed the verification of their chromatographic purity and after 24 h of convervation at room temperature, each of them gave the same five peaks. This demonstrated the establishment of an equilibrium between the five components of luminarin 4 which are isomers and eliminated the possibility of preparing a "single peak" of luminarin 4.

Before applying luminarin 4 to carboxylic acid derivatization, it was necessary to ensure that its isomerism would not complicate the procedure unnecessarily. Three questions had to be answered: which of the isomers can derivatize the acids, do the isomers have similar excitation and emission spectra and does the derivatization lead to a single derivative? The first point was examined by looking for the isomers reacting with acetic anhydride, *i.e.*, containing a terminal amino group. The equimolar reaction of luminarin 4 with acetic anhydride for 60 min at 70°C in DMSO showed that peaks 1, 2 and 5 disappeared completely whereas peak 3 remained unchanged. No conclusion could be drawn regarding peak 4, which was too small. It follows that the two major components of luminarin 4 (peaks 2 and 5) are able to react with activated acids.

It was important to determine the excitation and emission spectra of the isomers because their positions are related to the singlet excitation energy, which is a major factor governing the chemiluminescent intensity [22]. Owing to the rapid interconversion of the isomers, these data could not be obtained in the usual way by spectrofluorimetry.

The absorbance spectra, determined using a diode-array detector, for the three

TABLE II

ABSORPTION SPECTRA[a] OF THREE LUMINARIN 4 ISOMERS AND COUMARIN 102

Parameter	Peak 1	Peak 2	Peak 5	Coumarin 102
λ_{max} (nm)	254 and 445	254 and 400	254 and 400	254 and 400
Peak-height ratio[b]	0.42	0.55	0.50	0.45

[a] In the mobile phase of system 2.
[b] Ratio of absorbance at 254 nm to absorbance at 400 (or 445 nm).

peaks giving sufficiently high absorbance (1, 2 and 5) and that of coumarin 102 are shown in Table II. It could be concluded that the two major components (peaks 2 and 5) probably contain the intact quinolizinocoumarin moiety, whereas peak 1 does not because its band at 400 nm is shifted to 445 nm. The occurence of distinct emission bands was then investigated using synchronous fluorescence spectrometry, with wavelength intervals between monochromators equal to those of the known intervals between excitation and emission bands of coumarin 102, *i.e.*, 80, 100, 125, 218 and 236 nm. The spectra of luminarin 4 and coumarin 102 showed no differences, and consisted of a single band in each instance. Hence the emission of the major components was similar to that of coumarin 102, with an emission maximum at 490 nm in the mobile phase of system 2. Finally, relative fluorescence quantum yields (another major factor controlling the chemiluminescence intensity) were similar for peaks 1, 2 and 5 and coumarin 102, whereas the yield of peak 3 was three times lower (Table III). Thus, in answer to the second question, the major components of luminarin 4 have similar fluorescence properties.

The third point concerned the derivatization of luminarin 4 isomers. With all the carboxylic acids labelled to date (fatty acids and prostaglandin E_2), a single peak of a derivative was obtained. It seems that the amidification of the terminal amino group supresses the interconversion between the isomers. Finally, ^1H NMR studies in several solvents gave an insight into the probable structure of four out of five isomers (Fig. 2) [21]. The structure of "peak 3" remains controversial, but the absence of reaction with acetic anhydride and the low fluorescence quantum yield could be explained by an interaction between the terminal amino group and the lactone ring. In conclusion, luminarin 4 isomerism is not a major obstacle to its use as a derivatization reagent.

TABLE III

RELATIVE FLUORESCENCE YIELDS OF LUMINARIN 4 ISOMERS AND COUMARIN 102

Parameter	Peak 1	Peak 2	Peak 3	Peak 5	Coumarin 102
Absorbance[a]	7	25	7	32	31
Fluorescence[a]	14	43	4.5	58	58
Ratio	2.00	1.72	0.64	1.81	1.87

[a] In arbitrary units. See text for details.

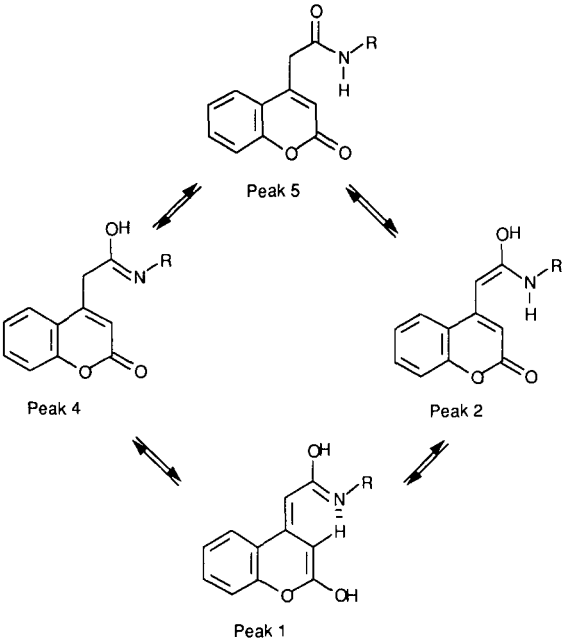

Fig. 2. Probable structures of luminarin 4 isomers. The quinolizine ring has been omitted for convenience.

HPLC analysis

Isovaleric acid, nonanoic acid and prostaglandin E_2 (PGE_2) were labelled according to the procedure described above, and were fractioned in different chromatographic systems, as shown in Table IV and Fig. 3. Derivatives of homologous fatty acids could be easily separated by varying the acetonitrile-to-buffer ratio.

Suprisingly, the isovaleric derivative was retained less than luminarin 4 itself, even though it is less polar. This was attributed to a strong interaction between the free silanol groups of the stationary phase and the terminal amino group of luminarin 4, by electrostatic attraction and/or hydrogen bonding. This hypothesis is supported by the strong effect of ionic strength on retention, as demonstrated by the comparison of the retention times in systems 2 and 3.

The mobile phase components (acetonitrile, imidazole nitrate buffer) were chosen according to their ability to promote a high chemiluminescence intensity and their miscibility with the excitation reagent solution.

Time and temperature of reaction

The kinetics of the first phase of the reaction were determined at −20, 4, 20 and 30°C. Carboxylic acids have often been activated by NOHS and DCC, or DCC alone, at low temperature [19], because the dicyclohexylurea thus formed is insoluble and precipitates, displacing the equilibrium to the right. However, when used for analytical purposes, dicyclohexylurea precipitation is not likely, because the reagent concentrations are low. In contrast, a higher temperature will promote a faster reaction. For these reasons, the reactions were carried out at the four temperatures mentioned

TABLE IV

RETENTION TIMES OF LUMINARIN 4 DERIVATIVES

System	Retention time (min)				
	Luminarin 4[a]	Luminarin 4–C 5[b]	Luminarin 4–C 9[c]	Luminarin 4–PGE_2	Coum 102
1	8.8	4.8	7.2	ND[d]	10.3
2	12.8	12.6	17.0	4.5	9.0
3	7.0	ND[d]	11.5	3.5	8.0
4	14.0	ND[d]	16.0	10.5	15.0

[a] Only peak 5 is given.
[b] Luminarin 4 derivative of isovaleric acid.
[c] Luminarin 4 derivative of nonanoic acid.
[d] Not determined.

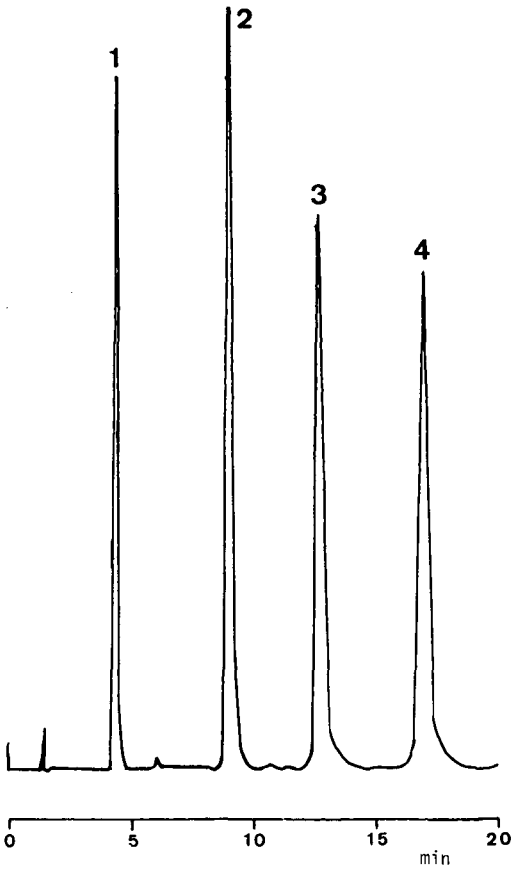

Fig. 3. Separation of some luminarin 4 derivatives with system 2 and fluorescence detection. Peaks: 1 = luminarin 4–PGE_2; 2 = coumarin 102; 3 = luminarin 4–isovaleric acid; 4 = luminarin 4–nonanoic acid. Peaks represent 10 pmol of each derivative injected onto the column. Range, 0.1 μA full-scale.

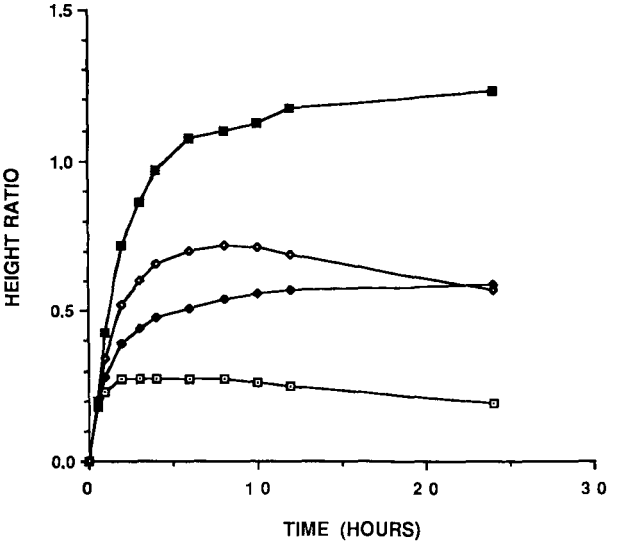

Fig. 4. Kinetics of derivatization (first phase: activation of the carboxylic acid) at four temperatures: □ = −20; ◆ = 4; ■ = 20; ◇ = 30°C. Ordinate is the ratio of the luminarin 4–isovaleric acid peak height to the coumarin 102 peak height.

above, and the results are shown in Fig. 4, with the highest yield being obtained at 20°C for 12 h.

The kinetics of the second phase of the labelling reaction were studied, using the N-succinimidoxyisovalerate prepared as described above. The formation of the luminarin 4 derivative was examined over 240 min at 50 or 70°C, as shown in Fig. 5.

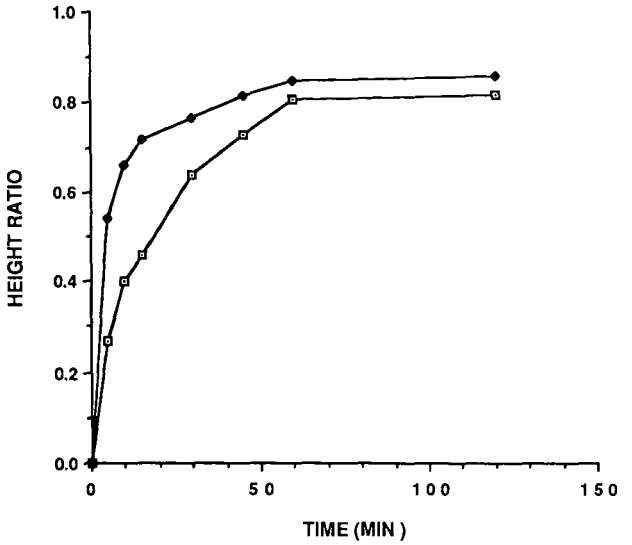

Fig. 5. Kinetics of derivatization (second phase: condensation with luminarin 4) at two temperatures: □ = 50; ◆ = 70°C. Ordinate is the ratio of the luminarin 4–isovaleric acid peak height to the coumarin 102 peak height.

Higher yields were obtained in shorter times at 70°C, the temperature at which the reaction was complete in 60 min. The overall yield, measured at a level of 50 nmol of nonanoic acid with reference to known amounts of the isolated derivative, was 91%. A larger excess of luminarin 4 or NOHS and DCC did not improve this yield but resulted in larger interfering peaks. As the linearity and reproducibility of the derivatization were found to be satisfactory, no further attempts were made to increase the reaction yield.

Linearity and sensitivity

The calibration graphs obtained with this method showed good linearity; the equation for the calibration line was $y = ax + b$ with $a = 0.016 \pm 0.001$ (mean ± S.D.) and $b = 0.083 \pm 0.027$ ($r = 0.995$, $p < 0.01$) after analysing five samples of each standard containing 12.5–125 nmol of isovaleric acid, detected fluorimetrically. For PGE_2, the calibration graphs were linear from 0.1 to 10 nmol of PGE_2 ($r = 0.995$, $p < 0.01$). Under the prevailing conditions, the detection limits for the luminarin 4 derivatives of isovaleric and noanoic acid were 300 fmol injected (signal-to-noise ratio = 3) for fluorescence detection and 50 fmol injected for peroxyoxalate CL detection.

The former detection limit (300 fmol) was similar to that found in our previous study on luminarin 1 derivatives [11], whereas the latter was higher than that obtained previously (50 *vs.* 6 fmol). The main explanation lies in the difference between the excitation conditions. In the present investigation, the mobile phase was much more aqueous (50 *vs.* 30%). In order to prevent the precipitation of the oxalic ester TCPO in the system, three precautions were taken: the TCPO concentration was reduced (1 vs. 4.5 mg/ml), TCPO and hydrogen peroxide were mixed and heated at 40°C so that TCPO was almost completely transformed before being added to the mobile phase and the pH of the mobile phase was raised to 7.7 in order to accelerate oxalic ester hydrolysis and to increase the solubility of the trichlorophenol formed. The low concentration of TCPO resulted in a lower excitation level [9] and a higher limit of detection. Precipitation could also have been avoided if a more soluble oxalate ester such as TDPO, bis[4-nitro-2-(3,6,9-trioxadecyloxycarbonyl)phenyl] oxalate, had been applied [5,23,24]. However, in this work TCPO was used to allow comparison with our previous results, and was found to work satisfactorily. Further, our results are in the same range as those reported by Grayeski and De Vasto [8] with aminocoumarinic derivatives.

For PGE_2, in order to improve the limit of derivatization (L.D.), only 0.05 ml of 0.5 m*M* luminarin 4 solution was added to the mixture after the activation step. This resulted in a higher concentration of activated PGE_2 in the reaction medium and a diminution in the amplitude of interfering peaks on the chromatogram. Further, the sample loop volume was reduced to 10 μl, to improve the separation (Fig. 6). The interfering peaks could also have been reduced by a preliminary extraction of the derivatives before injection onto the HPLC column, but this procedure was not investigated in this work. The L.D. was 60 pmol and the CL detection limit was 32 fmol injected (signal-to-noise ratio = 3).

Although there have been many papers [25–30] on the separation and measurement of prostaglandins by HPLC, it remains a difficult analysis, because physiological levels are very low; taking PGE_2 as an example, the levels are about 100 pmol/l

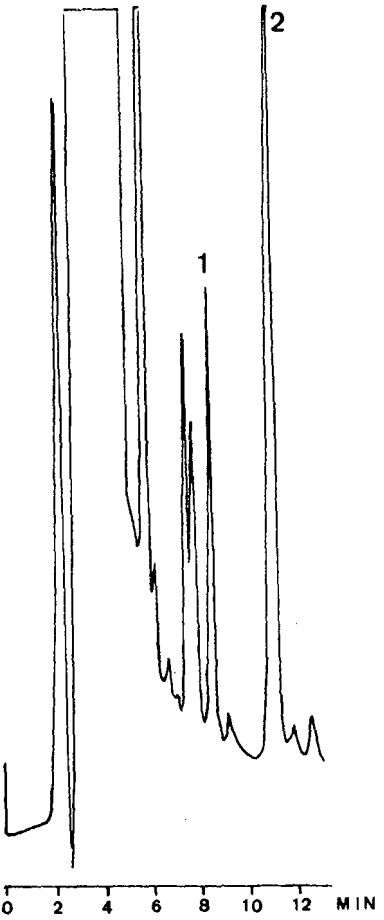

Fig. 6. Separation of luminarin 4–prostaglandin E_2 derivative with system 4 and chemiluminescence detection. Peaks: 1 = luminarin 4–PGE_2, 2 pmol injected onto column; 2 = luminarin 4 (last peak). See text for details. Range, 0.1 μA full-scale.

in human plasma and 0.3–40 nmol/l in human urine [25], the highest levels, 25–750 μmol/l, being in seminal fluid [26]. It is generally accepted that gas chromatography–mass spectrometry provides the most sensitive and specific method available, especially when using negative-ion chemical ionization [27], and that liquid chromatography lacks sensitivity. With UV detection in the 190–210-nm range [28,29], the limit of detection was about 60 pmol injected.

CONCLUSIONS

Luminarin 4 appears to be a promising reagent for carboxylic acid derivatization. Luminarin 4 isomerism was not a real drawback, as a single derivative was formed and was easily separated from the excess of reagent. Linearity and quantita-

tive yields demonstrated the reactivity of luminarin 4 with activated acids. Activation by NOHS and DCC was not a fast reaction, but the mildness of the conditions allowed its application to unstable compounds, such as PGE_2. Chemiluminescence detection sensitivity was better than that of fluorescence, although the mobile phase was very aqueous (50%), and this depended on the properties of the quinolizinocoumarin structure of luminarin 4. A gap remains between the very low limit of detection and the much higher limit of derivatization, which is the limiting factor in the application of the method, but others have reported that sensitivity was increased by derivatization of the ketone [23] or carboxylic function [28], achieving a limit of derivatization of 0.3 pmol for PGE_2.

Work is in progress to improve the limit of derivatization, in order to take advantage of the low detection limit. Otherwise, CL detection could be applied in immunological assays, where the labelling reaction does not need to be carried out at a low carboxylic acid concentration.

REFERENCES

1 K. Kobayashi and K. Imai, *Anal. Chem.*, 52 (1980) 424.
2 K. W. Sigvardson and J. W. Birks, *Anal. Chem.*, 55 (1983) 432.
3 K. W. Sigvardson, J. M. Kennish and J. W. Birks, *Anal. Chem.*, 56 (9184) 1096.
4 S. I. Kobayashi, J. Sekino, K. Honda and K. Imai, *Anal. Biochem.*, 112 (1981) 99.
5 K. Imai, Y. Matsunaga, Y. Tsukamoto and A. Nishitani, *J. Chromatogr.*, 400 (1987) 169.
6 T. Koziol, M. L. Grayeski and R. Weinberger, *J. Chromatogr.*, 317 (1984) 355.
7 P. J. M. Kwakman, J. G. J. Mol, D. A. Kamminga, R. W. Frei, U. A. Th. Brinkman and G. J. De Jong, *J. Chromatogr.*, 459 (1988) 139.
8 M. L. Grayeski and J. K. De Vasto, *Anal. Chem.*, 59 (1987) 1203.
9 M. Tod, R. Farinotti and G. Mahuzier, *Analusis*, 14 (1986) 271.
10 M. Tod, R. Farinotti, G. Mahuzier and I. Gaury, *Anal. Chim. Acta*, 217 (1989) 11.
11 M. Tod, M. Prevot, M. Poulou, R. Farinotti, J. Chalom and G. Mahuzier, *Anal. Chim. Acta*, 223 (1989) 309.
12 S. Lam and E. Grushka, *J. Chromatogr.*, 158 (1978) 207.
13 J. A. Secrist, J. R. Barrio and N. J. Leonard, *Biochem. Biophys. Res. Commun.*, 45 (1971) 1262.
14 N. Nimura, T. Kinoshita, T. Yoshida, A. Uetake and C. Nakai, *Anal. Chem.*, 60 (1988) 2067.
15 J. B. F. Lloyd, *J. Chromatogr.*, 189 (1980) 359.
16 H. Lingeman, A. Hulshoff, W. J. M. Hunderberg and F. B. J. M. Offermann, *J. Chromatogr.*, 290 (1984) 215.
17 J. Miwa, C. Hiyama and M. Yamamoto, *J. Chromatogr.*, 321 (1985) 165.
18 H. Miwa, *J. Chromatogr.*, 333 (1985) 215.
19 H. G. Khorana, *Chem. Rev.*, 53 (1953) 145.
20 C. A. Parker and W. T. Rees, *Analyst (London)*, 85 (1960) 587.
21 M. Tod, *Ph.D. Thesis*, Université-Paris Sud, Faculté de Pharmacie, Paris XI, 1990, No. 138.
22 K. Honda, K. Miyaguchi and K. Imai, *Anal. Chim. Acta*, 177 (1985) 111.
23 K. Imai, H. Nawa, M. Tarraka and H. Ogata, *Analyst (London)*, 111 (1986) 209.
24 K. Imai, A. Nishitani and Y. Tsukamoto, *Chromatographia*, 24 (1987) 77.
25 K. Yamada, M. Onodera and Y. Aizawa, *J. Pharmacol. Methods*, 9 (1983) 93.
26 K. Svanborg, M. Bygdeman, P. Eneroth and E. Bendwold, *Prostaglandins*, 24 (1982) 636.
27 S. E. Barrow, K. A. Waddel, M. Enmis, C. T. Dollery and I. A. Blair, *J. Chromatogr.*, 239 (1982) 71.
28 A. Terragno, R. Rydzik and N. A. Terragno, *Prostaglandins*, 21 (1981) 101.
29 D. M. Desiderio, M. D. Cunningham and J. A. Trimble, *J. Liq. Chromatogr.*, 4 (1981) 1261.
30 K. Wessel, V. Kaever and K. Resh, *J. Liq. Chromatogr.*, 11 (1988) 1273.

Journal of Chromatography, 542 (1991) 307–316
Elsevier Science Publishers B.V., Amsterdam

CHROM. 23 062

Purification of galactolipids by high-performance liquid chromatography for monolayer and Langmuir–Blodgett film studies

JUDITH GALLANT and ROGER M. LEBLANC*

Centre de Recherche en Photobiophysique, Université du Québec à Trois-Rivières, 3351 Boulevard des Forges, C.P. 500, Trois-Rivières, Québec, G9A 5H7 (Canada)

(First received July 30th, 1990; revised manuscript received November 9th, 1990)

ABSTRACT

In order to obtain pure galactolipids usable for monolayer work at the nitrogen–water interface, and also for fluorescence intensity measurements in Langmuir–Blodgett films when mixed with chlorophyll *a*, purification procedures for mono- and digalactosyldiacylglycerol were established using high-performance liquid chromatography. The rapid and efficient methods described were applied to commercial samples and enriched extracted fractions of lipids obtained by preparative liquid chromatography. Surface pressure–area isotherms at the nitrogen–water interface of purified and unpurified samples are also reported. The fluorescence spectra of chlorophyll *a* mixed with purified and unpurified galactolipids in Langmuir–Blodgett films clearly show the necessity for the purification.

INTRODUCTION

An important factor controlling the activity of the photosynthetic apparatus of plants and algae is the lipid composition of membranes in which the photosynthetic proteic complexes are embedded [1–4]. In thylakoids of higher plants, galactolipids comprise *ca.* 80% of the total lipid content [5]. Interestingly, this lipid class is found almost exclusively in the photosynthetic membranes. A useful technique in the investigation of the physico-chemical properties of pure galactolipids is the determination of surface pressure–area isotherms in monolayers [6].

Before monolayer work can be performed, it is necessary to establish a rapid and efficient method to purify thoroughly monogalactosyldiacylglycerol (MGDG) and digalactosyldiacylglycerol (DGDG), the two most abundant galactolipids in thylakoids [5]. Two of the most common methods used to purify these lipids are thin-layer chromatography (TLC) [6–9] and liquid chromatography (LC) [6,10]. These techniques are generally time consuming and therefore inconvenient. Moreover, with TLC, it is difficult to avoid the degradation of lipid fatty acids, which are easily oxidized by oxygen present in the air and/or dissolved in solvents.

This paper presents rapid and simple high-performance liquid chromatographic (HPLC) purification procedures for MGDG and DGDG. Surface pressure–area

0021-9673/91/$03.50

isotherms are also presented and compared with those reported in the literature. These measurements are useful for cross-checking the separation before using the lipids in monolayer fluorescence experiments in a mixture with chlorophyll *a*. To emphasize the significance of the purification of galactolipids, the excitation fluorescence spectrum of a pheophytin *a*–phospholipid mixture in a Langmuir–Blodgett film is compared with that of monolayers of chlorophyll *a* mixed with purified and unpurified MGDG.

EXPERIMENTAL

Glassware cleaning procedure

As the purified lipids were to be analyzed using surface pressure–area isotherms, great care was taken to ensure clean glassware throughout the experiments. All glassware was cleaned according to an adapted version [11] of the method published by Tancrède *et al.* [6]. Quartz slides were cleaned according to the method published by Munger *et al.* [12].

Samples and reagents

Commercial samples of MGDG extracted from whole wheat flower were purchased from Serdary (London, Canada). These samples were used to establish the HPLC method prior to the purification of the extracted MGDG.

The extraction of galactolipids from barley leaves (*Hordeum vulgare* L.) and the preparative LC procedures to obtain enriched fractions of MGDG and of DGDG are described elsewhere [11]. For LC, a Sepharose CL-6B gel (Pharmacia, Uppsala, Sweden) saturated with *n*-hexane was used. The elution scheme, reported in Table I, started with *n*-hexane, which was then gradually enriched in isopropanol (IPA). This

TABLE I

ELUTION SCHEME AND GALACTOLIPID-ENRICHED FRACTIONS COLLECTED IN LIQUID CHROMATOGRAPHY

Column, 11 × 2 cm I.D.; stationary phase, Sepharose CL-6B.

Eluent	Proportions (v/v)	Volume (ml)	Collected fractions
n-Hexane		50	Pigments
n-Hexane–IPA	90:10	100	Pigments
n-Hexane–IPA	85:15	100	Pigments
n-Hexane–IPA	80:20	100	Pigments
n-Hexane–IPA	75:25	100	MGDG
n-Hexane–IPA	70:30	100	MGDG
n-Hexane–IPA	60:40	100	MGDG
n-Hexane–IPA	50:50	100	–
n-Hexane–acetone	50:50	100	–
Acetone		100	DGDG
Acetone–methanol	50:50	100	DGDG, SQDG and PG[a]
Methanol		300	PC[b]

[a] Phosphatidylglycerol.
[b] Phosphatidylcholine.

permitted the collection of most of the pigments. The MGDG emerged from the column when the concentration of IPA was between 25 and 40% (v/v). The removal of *n*-hexane, leaving acetone as the mobile phase, permitted the elution of DGDG. Sulfoquinovosyldiacylglycerol (SQDG) was recovered by the addition of 50% methanol to the acetone mobile phase. All solvents used in these procedures were of chromatographic or spectrophotometric grade.

Chlorophyll *a* from spinach was extracted and crystallized using the dioxane method of Iriyama *et al.* [13]. It was then purified by LC according to the method reported by Omata and Murata [14,15]. Pheophytin *a* was obtained by an acid treatment of the previously purified chlorophyll *a* [16].

Dioleoylphosphatidylcholine (DOPC) was purchased from P.L. Biochemicals (Milwaukee, WI, U.S.A.).

TLC procedures

All extraction, preparation and purification steps were verified by TLC. The precoated silica gel 60 plates, 50 × 200 × 0.250 mm (BDH, Toronto, Canada, or E. Merck, Darmstadt, Germany) were washed according to Tancrède *et al.* [6]. Two different elution systems were used to prevent misinterpretation for the case of DGDG. The first was acetone–benzene–water (91:30:8, v/v/v), as described by Pohl *et al.* [7]. The R_F of MGDG and DGDG are 0.56 ± 0.06 and 0.24 ± 0.05, respectively. The second migration mixture was chloroform–methanol–water (70:30:4, v/v/v), as described by Siebertz *et al.* [8]. MGDG and DGDG were then identified by the presence of spots, using iodine, at R_F values of 0.7 ± 0.1 and 0.43 ± 0.06, respectively.

HPLC procedures

The HPLC system used was purchased from Waters Assoc. (Milford, MA, U.S.A.). It was composed of two Model 510 pumps, a Model 680 automatic gradient controller, a Rheodyne (Cotati, CA, U.S.A.) Model 7126 injector equipped with a 200-μl loop and a Model 490 programmable UV–visible detector set at 205 nm. Two similar columns were used. The Altex Ultrasphere-Si silica gel column (Beckman, San Ramon, CA, U.S.A.), with dimensions 250 × 4.6 mm I.D., was used to purify MGDG. The column used to separate DGDG measured 250 × 10 mm I.D. The gel consisted of particles with an average diameter of 5 μm. No guard column was used.

All solvents used for the procedure were of HPLC grade (Burdick & Jackson Labs., Muskegon, MI, U.S.A.). Mixtures of solvents used in the mobile phase were filtered through Millipore (Bedford, MA, U.S.A.) membrane filters with pores of 0.2 μm and degassed under vacuum prior to their introduction into the HPLC system. The mobile phases were composed of mixtures of *n*-hexane, IPA and water. The optimum proportions found for isolating MGDG, were 85:15:0.4 (v/v/v), with a flow-rate of 4.00 ml/min, and for DGDG 70:30:2 (v/v/v), with a flow-rate of 9.00 ml/min. All elutions were isocratic.

The concentration of lipid solutions prepared for injection into the HPLC system was *ca.* 0.2 mg/ml. The dry-weighed lipid was dissolved in the elution mixture. Because of the low solubility of the lipid in the eluent, 200 μl of the lipid solution were injected into the HPLC column, corresponding to *ca.* 40 μg of lipid. As a precautionary measure, all lipids to be used in monolayer work were purified twice.

GLC procedure

The determination of the molecular weight of the galactolipid prior to surface pressure measurements is very important. This was done, in this work, by methylation of the lipid fatty acids, followed by analysis by gas–liquid chromatography (GLC). The complete methylation procedure is reported elsewhere [11]. The Model 3700 GLC system from Varian (Sunnyvale, CA, U.S.A.) was equipped with a flame ionization detector and a 2.4-m GP 10% SP2330 on 100–120-mesh Chromosorb W AW column (Supelco, Bellefonte, PA, U.S.A.). The column temperature programme was as follows: 2 min at 170°C, increased to 235°C at 3°C/min, held at 235°C for 10 min. The injector and detector temperatures were 260 and 300°C, respectively. The nitrogen carrier gas flow-rate was 20 ml/min. Standard mixtures of methylated fatty acids (Supelco Canada, Oakville, Canada) were used to identify the peaks. A Shimadzu (Kyoto, Japan) C-R3A Chromatopac integrator was used to analyze the chromatograms.

Langmuir trough

The laboratory-built aluminum trough, 52.0 cm long × 14.0 cm wide × 4.4 cm deep, was covered with an adhesive PTFE film (Fluorocarbon Dielectrix Division, Lockport, NY, U.S.A.). An in-wall, closed water circuit was set at 20°C using a Lauda Model k-21R thermostated bath from Brinkmann Instruments (Rexdale, Canada). An in-wall, open circuit of nitrogen was flushed over the buffer surface at low flow-rates, to prevent oxygen from reaching the spread molecules on the interface. The on and off positions of the mobile barrier were set by the position of two switches and barrier movement was controlled by an electric motor activated by an external control box. The surface pressure was detected by a Milar float from DuPont (Montréal, Canada). The float was attached to a torsion wire of 0.05 cm diameter (Fender Musical Instruments, Fullerton, CA, U.S.A.). This wire was connected to a metallic bar which was free of movement inside a magnetic transducer (Model 7 DCDT-050, Hewlett-Packard, Boeblengen, Germany). The displacement of the float was converted by the transducer into a voltage detected by a multimeter (Model 4060, Brunelle Instruments, St. Elie d'Orford, Canada). The sensitivity of the Langmuir balance, calibration and recording of the isotherms were calculated by an in-house program adapted for an Apple IIc computer.

The subphase used for the surface pressure–area isotherms and the Langmuir–Blodgett film preparation was a purified 10^{-3} *M* phosphate buffer adjusted to pH 8.00. The water used to prepare the subphase was doubly distilled in quartz; its specific resistivity and surface tension were 18 MΩ cm and 71 mN/m (as determined by Du Nouy's method), respectively. Purification of the anhydrous Na_2HPO_4 (ACP Chemicals, Montréal, Canada) was made possible by six repetitive washes of the salt in chloroform (Anachemia Accusolv, Montréal, Canada), agitated each time for 10–15 min. The fresh subphase was flushed with nitrogen before it was put in the trough. A waiting period of 60 min was applied to the buffer standing in the trough, so that all surface-active contaminants might reach the interface. The surface was cleaned by suction before deposition of the lipid.

The concentration of the lipid solution used to measure surface pressure–area isotherms was in the range $3 \cdot 10^{-4}$ *M*. This concentration was found to be optimum for the spreading of $1.8 \cdot 10^{16}$–$2.2 \cdot 10^{16}$ molecules in 80–100 μl of solution. Benzene

used as the deposition solvent was freshly distilled and free from gaseous oxygen by flushing with a stream of nitrogen or argon. The solution was kept in a 3.5-ml glass vial closed by a screw-capped PTFE Mininert valve from Pierce (Rockford, IL, U.S.A.). This permitted removal of a fraction of the solution without exposing it to excessive evaporation.

To prepare Langmuir–Blodgett films for fluorescence measurements, cleaned quartz slides were dipped into the subphase on which a mixture of pigment and lipid (in a 1:100 molar ratio) had been spread. The vertical movement was controlled by a hydraulic system described elsewhere [12]. The surface pressure was kept at 20 mN/m throughout film deposition on the quartz slide.

Spectrofluorimeter

The apparatus used to measure the excitation fluorescence spectra of pigments mixed with lipids was a Fluorolog II, Model 1870 (Spex Industries, Metuchen, NJ, U.S.A.). The emission wavelength was set at 678 nm and the excitation ranged from 350 to 500 nm. The two slits at excitation were set at 4 mm, with the two others at the emission adjusted to 1.5 mm. Emission was polarized in order to avoid Wood's anomaly. The monochromators were controlled by a Spex Datamate computer. The spectra were corrected for lamp emission and sensitivity of the water-cooled photomultiplier tube (Model R 928/115, Products for Research, Danvers, MA, U.S.A.) [17].

RESULTS AND DISCUSSION

MGDG was established to be best isolated using *n*-hexane–IPA–water (85:15:0.4, v/v/v). The chromatograms obtained for commercial and extracted lipids are shown in Fig. 1. Isocratic elution was chosen because of some difficulties when the column was not in complete equilibrium with the mobile phase. This was probably due to the presence of water, necessary in the elution solvents, forming a hydration coating surrounding the gel particles. MGDG was eluted from the column in less than 5 min. The injections could therefore be done in a 10-min sequence. As the capacity factors (k') of MGDG and the following product were in a good range, selectivity was within the desired margin of 1.5–2.0. Resolution was also acceptable.

In the chromatograms, the products eluted in the first 2 min are the porphyrin pigments, such as chlorophyll *a* and *b* and pheophytin *a* and *b*. During the next 2 min, some carotenoids are eluted, characterized by their yellow-orange color. As indicated below, the peak following MGDG is believed to be a saturated lipid.

To evaluate the approximate yield of the purification, the weight of the lipid sample before and after purification was measured. The injection of 1.901 mg of crude material gave 0.572 mg of light-colored MGDG, indicating the presence of pigments. This corresponds to a 30% yield. This value is surprisingly low when compared with the calculated yield obtained from the area ratio of the MGDG peak to the total chromatogram, which gave 59%. Therefore, one of the eluted products, which is believed to be of similar molecular weight, has a very small absorption coefficient, and the area under its peak is not proportional to the amount eluted. It is possibly the product following MGDG which behaves as a lipid, but has not been identified. This eluted component is likely to be a more saturated derivative of MGDG or of another lipid, as the absorption at 205 nm is related to the unsaturated bonds in the fatty acids.

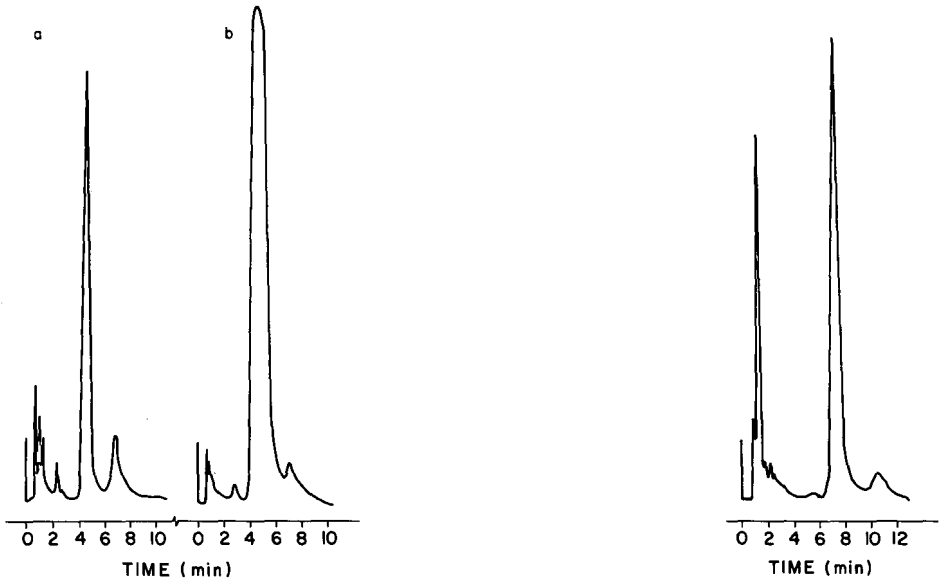

Fig. 1. HPLC of MGDG using an Altex Ultrasphere-Si column (250 × 4.6 mm I.D.). Mobile phase, *n*-hexane–IPA–water (85:15:0.4, v/v/v); flow-rate, 4.00 ml/min. (a) Commercial sample (retention time, t_R = 4.9 ± 0.2 min); (b) extracted sample (t_R = 4.6 ± 0.2 min).

Fig. 2. HPLC of extracted DGDG using an Altex Ultrasphere-Si column (250 × 10 mm I.D.). Mobile phase, *n*-hexane–IPA–water (70:30:2, v/v/v); flow-rate, 9.0 ml/min. t_R = 7.2 ± 0.1 min.

The best mobile phase found for purifying DGDG was *n*-hexane–IPA–water (70:30:2, v/v/v), giving the chromatogram shown in Fig. 2. During the first 4 min, pigments, carotenoids and MGDG (the second strongest peak in the chromatogram) are eluted. The small peak eluting before DGDG is an unknown lipid, and that following DGDG is probably SQDG. The conditions permitted a new injection every 15 min. As there is half as much DGDG as MGDG in the extracts, it is evident that the DGDG peak is less concentrated with regard to the amount of contaminants present in the sample.

Other methods that involve the use of HPLC to identify and quantify galactolipids have been published. Of these reported techniques, reversed-phase columns were employed to determine the fatty acid composition of one particular isolated type of lipid [18–22]. Therefore, these methods were not applicable for the separation of an individual class of galactolipid from a complex pigment–lipid matrix. The other published procedures for determining the galactolipid content of plant tissues used polar columns. In two of these reports, the mobile phase contained small amounts of acid [23,24]. This is undesirable, as acids may degrade lipids. Furthermore, traces of acid inevitably destroy the chlorophyll *a* pigments that are in the pigment-purified lipid mixture. In the third procedure [22], total lipid extracts were injected on to a silica gel column and, using a gradient elution scheme, all the major lipid components in the samples could be separated. Unfortunately, this method did not adequately resolve MGDG from pigments and so was unsuitable for MGDG

purification. Moreover, DGDG was not isolated from SQDG, so this analytical method cannot be used to purify DGDG either. Finally, an HPLC method has been published that used a gradient elution extending up to 50 min [25]. This method was excellent for separating MGDG and DGDG, although SQDG was indefinitely adsorbed on the column. However, as the total galactolipid extracts obtained from barley contained appreciable amounts of pigments and phospholipids, it became advantageous to include preparative liquid chromatography in the experimental procedure. This step separated the sample into enriched fractions of MGDG, DGDG and SQDG. The sequential separation into individual classes of galactolipids permitted the development of HPLC purification procedures for each lipid that were much more rapid than the method involving a lengthy gradient elution [25].

Table II presents the fatty acid composition of each sample studied using surface pressure–area isotherms. The lipid fatty acid composition is a very important factor controlling the reproducibility of surface pressure measurements. The differences between the commercial and extracted MGDG are due to their different origins. The isotherms reflect these differences (see Fig. 3, curves a and b). However, the similarity of fatty acids in the purified and unpurified extracted MGDG is evident. The largest difference in the chromatograms (not shown) is the presence of a contaminant peak in unpurified MGDG. This contaminant is due to the esterification of the phytol side-chain of chlorophyllic pigments. This contaminant peak was calculated in the total chromatogram area of the unpurified MGDG, lowering the relative amount of 18:3 fatty acid in the sample compared with the purified lipid that does not show this peak.

TABLE II

FATTY ACID COMPOSITION AND MOLECULAR WEIGHT OF COMMERCIAL MGDG AND EXTRACTED MGDG AND DGDG

Column, GP 10% SP 2230 on 100–120-mesh Chromosorb W AW; Column dimensions, 2.4 m × 6.0 mm I.D., carrier flow-rate, 20 ml/min.

Lipid	Fatty acid (%)				Molecular weight (g/mol)
	16:0	18:1	18:2	18:3	
MGDG, Serdary	21	16	50	10	770
MGDG, extracted:					
Unpurified	Trace	–	5.9	88	773
Purified	Trace	–	4.4	95	775
DGDG, extracted	14.5	2.5	4.0	78.9	931

The first surface pressure–area isotherm presented in Fig. 3 was measured with the purified commercial MGDG. The principal characteristics of these measurements are shown in Table III. The first isotherm was almost identical with that published by Tancrède *et al.* [26], who used the same experimental conditions. The only difference was the origin of their commercial MGDG sample. However, they did not verify the fatty acid composition of their sample.

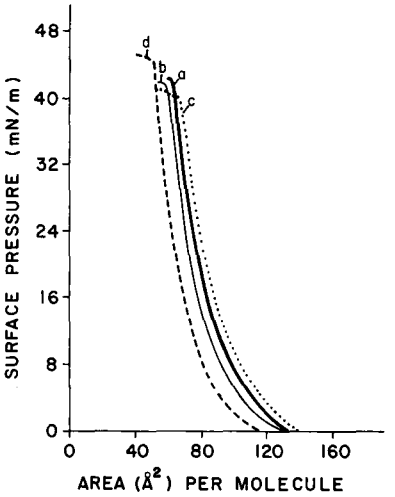

Fig. 3. Surface pressure–area isotherms of galactolipids using 10^{-3} *M* phosphate buffer (pH 8.00). (a) Purified commercial MGDG; (b) purified extracted MGDG; (c) unpurified extracted MGDG; (d) purified extracted DGDG.

The second and third measured isotherms were from the purified and unpurified extracted MGDG. The purified lipid isotherm was identical with that reported by Tancrède *et al.* [6] for MGDG purified by TLC. If their lipid source was actually from spinach, which is rich in linolenic acid (18:3), this similarity clearly shows that our reported HPLC purification procedures are as effective as the TLC method. Compared with the purified sample, the unpurified material has a lower collapse value, and the curve is observed to be displaced to the right, indicating the presence of contamination, mostly pigments that occupy more space than lipids at the interface. As pointed out by Tancrède *et al.* [6], the highest collapse of the purified MGDG is always relative to the highest purity.

The last isotherm shown in Fig. 3 is of the purified, extracted DGDG. This curve

TABLE III

MOLECULAR AREA AT THREE DIFFERENT SURFACE PRESSURES AND COLLAPSE PRESSURE OF GALACTOLIPIDS

Subphase, 10^{-3} *M* phosphate buffer (pH 8.00).

Lipid	Molecular area (Å²/mol) at			Collapse pressure (mN/m)
	10 mN/m	20 mN/m	30 mN/m	
MGDG, Serdary, purified	94	78	70	42
MGDG, extracted:				
Purified	87	73	66	42
Unpurified	100	83	74	40
DGDG, extracted, purified	77	65	58	44

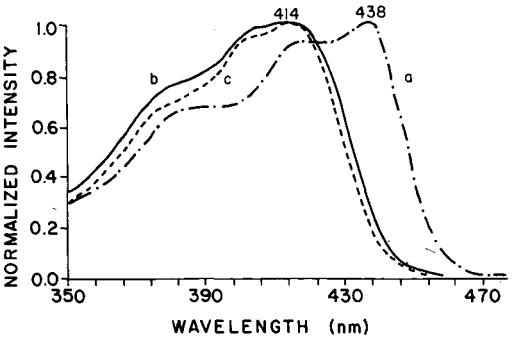

Fig. 4. Excitation fluorescence spectra of pigment–lipid mixtures in Langmuir–Blodgett films (molar ratio 1:100), with detection at 678 nm. (a) Chlorophyll *a*–purified MGDG; (b) chlorophyll *a*–unpurified MGDG; (c) pheophytin *a*–DOPC.

(d) is similar to that published by Trosper and Sauer [27], who used identical experimental conditions. However, the collapse of the DGDG isotherm in Fig. 3 was 4 mN/m higher than that reported in the literature. As mentioned previously, this higher value is usually interpreted as an indication of a greater lipid purity.

From a comparison of their isotherms, it can be seen that DGDG uses less molecular area at the interface than MGDG. Although the polar head of DGDG is twice as large as that of MGDG, this does not increase the occupied space at the interface. On the contrary, a combination of a higher degree of interaction between the DGDG polar heads, favored by the increased number of hydroxyl groups, and a lower unsaturation index in the fatty acids which are more easily ordered, may be responsible for that effect.

The importance of the purification of the galactolipids was evident in the excitation fluorescence spectra shown in Fig. 4. When purified MGDG was used in the chlorophyll *a*–galactolipid mixture, the spectrum showed a maximum at 438 nm, characteristic of the chlorophyll *a* pigment [17]. However, the use of unpurified MGDG shifted the maximum to 414 nm. This value is usually interpreted as a pheophytinization of the pigment, which has lost the central Mg atom in the process. To verify this interpretation, the measurement of a mixture of pheophytin *a* and DOPC was performed. The close resemblance of the two curves is unmistakable. The unpurified MGDG contained a contaminant that was capable of destroying the chlorophyll *a* pigment in the monolayer. Therefore, the proposed MGDG purification method was shown to be successful in eliminating all contaminants that might produce the degradation of chlorophyll *a*.

CONCLUSIONS

The rapid isocratic purification procedures described in this paper were efficient for isolating MGDG and DGDG, prior to their characterization by the surface pressure–area isotherms at the nitrogen–water interface. These measurements were in good agreement with those found in the literature. The procedures reported in this work employed no acid, and minimized all contacts between the lipids and oxygen,

a source of lipid degradation often encountered when purifying lipids by TLC or LC. Finally, the excitation fluorescence spectra in Langmuir–Blodgett films of different mixtures of pigment and lipid showed the importance of a good purification procedure. The unpurified MGDG induced the degradation of the chlorophyll *a* pigment, characterized by the disappearance of the 438-nm band, shifting the maximum to 414 nm.

ACKNOWLEDGEMENTS

The assistance of Drs. G. Picard and B. Zelent is greatly appreciated. Special thanks are due to Dr. F. Bellemare and to Mr. G. Munger for their preliminary work on chloroplast lipids purified by liquid chromatography. This work was supported by grants from the Natural Sciences and Engineering Research Council of Canada (NSERC) and the Fonds pour la Formation de Chercheurs et l'Aide à la Recherche (FCAR). Financial support as postgraduate scholarships came from FCAR to J.G.

REFERENCES

1 D. G. Bishop and J. R. Kenrick, in P. Mazliak, P. Benveniste, C. Costes and R. Douce (Editors), *Biogenesis and Function of Plant Lipids*, Elsevier, Amsterdam, 1980, p. 415.
2 J. M. Anderson, *Biochim. Biophys. Acta*, 416 (1975) 191.
3 A. Rawyler, L. E. A. Henry and P.-A. Siegenthaler, *Carlsberg Res. Commun.*, 45 (1980) 443.
4 S. G. Sprague, *J. Bioenerg. Biomembr.*, 19 (1987) 691.
5 P.-A. Siegenthaler, A. Rawyler and C. Giroud, in P. K. Stumpf, J. B. Mudd and W. D. Nes (Editors), *The Metabolism, Structure and Function of Plant Lipids*, Plenum Press, New York, 1987, p. 161.
6 P. Tancrède, G. Chauvette and R. M. Leblanc, *J. Chromatogr.*, 207 (1981) 387.
7 P. Pohl, H. Glasl and H. Wagner, *J. Chromatogr.*, 49 (1970) 488.
8 H. P. Siebertz, E. Heinz, M. Linscheid, J. Joyard and R. Douce, *Eur. J. Biochem.*, 101 (1979) 429.
9 A. H. Reine and S. J. Stegink, *J. Chromatogr.*, 437 (1988) 211.
10 M. S. Webb and B. R. Green, in J. Biggins (Editor), *Progress in Photosynthesis Research, Proceedings of the 7th International Congress on Photosynthesis, 1986*, Vol. 2, Nijhoff, Dordrecht, 1987, p. 197.
11 J. Gallant, *M.Sc. Thesis*, Université du Québec à Trois-Rivières, 1990.
12 G. Munger, L. Lorrain, G. Gagné and R. M. Leblanc, *Rev. Sci. Instrum.*, 58 (1987) 285.
13 K. Iriyama, N. Ogura and A. Takamiya, *J. Biochem.*, 76 (1974) 901.
14 T. Omata and N. Murata, *Photochem. Photobiol.*, 31 (1980) 183.
15 T. Omata and N. Murata, *Plant Cell Physiol.*, 24 (1983) 1093.
16 H. J. Perkins and D. W. A. Roberts, *Biochim. Biophys. Acta*, 58 (1962) 486.
17 G. Picard, *Ph.D. Thesis*, Université du Québec à Trois-Rivières, 1990.
18 J. Kesselmeier and E. Heinz, *Methods Enzymol.*, 148 (1987) 650.
19 J. Kesselmeier and E. Heinz, *Anal. Biochem.*, 144 (1985) 319.
20 D. V. Lynch, R. E. Gundersen and G. A. Thompson, Jr., *Plant Physiol.*, 72 (1983) 903.
21 D. G. Bishop, *J. Liq. Chromatogr.*, 10 (1987) 1497.
22 C. Demandre, A. Trémolières, A.-M. Justin and P. Mazliak, *Phytochemistry*, 24 (1985) 481.
23 D. Marion, R. Douillard and G. Gandemer, *Rev. Fr. Corps Gras*, 35 (1988) 229.
24 W. W. Christie and W. R. Morrison, *J. Chromatogr.*, 436 (1988) 510.
25 J. W. M. Heemskerk, G. Bogemann, M. A. M. Scheijen and J. F. G. M. Wintermans, *Anal. Biochem.*, 154 (1986) 85.
26 P. Tancrède, G. Munger and R. M. Leblanc, *Biochim. Biophys. Acta*, 689 (1982) 45.
27 T. Trosper and K. Sauer, *Biochim. Biophys. Acta*, 162 (1968) 97.

Journal of Chromatography, 542 (1991) 317–326
Elsevier Science Publishers B.V., Amsterdam

CHROM. 23 058

High-performance liquid chromatography of abietane-type compounds

NOBUYUKI OKAMURA*, KEIZO KOBAYASHI and AKIRA YAGI
Faculty of Pharmacy and Pharmaceutical Sciences, Fukuyama University, Hiroshima, 792-02 (Japan)
and
TAKASHI KITAZAWA and KOICHIRO SHIMOMURA
Tsukuba Medicinal Plant Research Station, National Institute of Hygienic Sciences, 1 Hachimandai, Yatabe, Tsukuba, Ibaraki, 305 (Japan)
(First received August 5th, 1990; revised manuscript received December 13th, 1990)

ABSTRACT

A sensitive, quantitative procedure was developed for the simultaneous determination of tanshinone IIA and I, cryptotanshinone and dihydrotanshinone I by high-performance liquid chromatography (HPLC) employing a normal-phase column. In addition, a method for the determination of the polar tanshinones tanshinone V and VI by reversed-phase HPLC, an HPLC method for ferruginol and a qualitative procedure for other tanshinones were also developed. These methods were applied to identify abietane-type compounds in various tissues of *Salvia miltiorrhiza* Bung, including cultured cells, fresh roots and regenerated plant roots.

INTRODUCTION

Dried roots (Tan-Shen in Chinese) of *Salvia miltiorrhiza* Bung (Labiatae), an ancient Chinese drug, have been used to treat haemorrhages, menstrual disorders and miscarriages [1]. Tan-Shen is known to contain abietane-type diterpenes (tanshinones), such as tanshinone I [2], cryptotanshinone [3] and tanshinone VI [4], which protect the myocardium against ischaemia [4], and also related orange-red pigments (shown in Fig. 1).

Usually, tanshinones have been resolved by thin-layer chromatography and cryptotanshinone and ferruginol determined by gas chromatography [5]. Recently, a reversed-phase high-performance liquid chromatographic (HPLC) method was applied to the determination of several tanshinones from *Salvia* species [6,7]. However, tanshinones are hydrophobic compounds and tanshinone IIA and cryptotanshinone, the major tanshinones, can be completely eluted from a silica gel column with chloroform. The objective of this study was to develop a simple method for the determination of tanshinones and ferruginol in various tissues using isocratic normal-phase HPLC. This procedure involves the extraction of tanshinones followed by fractionation and analysis by HPLC. Both qualitative and quantitative procedures for the polar tanshinones were accomplished by reversed-phase HPLC. With these

0021-9673/91/$03.50

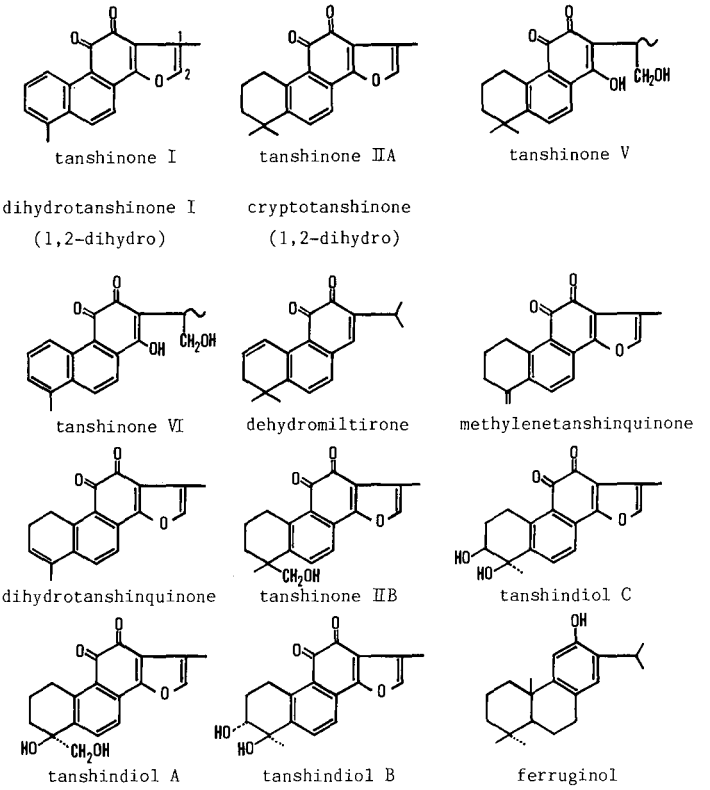

Fig. 1. Structures of abietane-type compounds.

methods it was possible to study the production of bioactive tanshinones in cultured cells and regenerated plants.

EXPERIMENTAL

Materials

Tan-Shen grown in China was purchased from Nakai-Koshindo (Kobe, Japan). *S. miltiorrhiza*, regenrated plants, water-cultured plants and callus derived from *S. miltiorrhiza* were supplied by Tsukuba Medicinal Plant Research Station (Ibaraki, Japan).

Adventitious root cultures were derived on Murashige-Skoog medium supplemented with 1-naphthaleneacetic acid (0.5 ml/l) and benzyladenine (0.1 ml/l) from segments of stems and petioles after 8 weeks in the dark at 25°C. Differentiated shoots were induced when the stem pieces were placed on Murashige-Skoog medium containing 3-indoleacetic acid (0.5 mg/l) and kinetin (1 mg/l) for 8 weeks under 16 h light (4000 lux) at 25°C. Young plantlets were derived from stem tips of differentiated shoots on hormone-free Murashige-Skoog medium for 8 weeks under 16 h light (4000 lux) at 25°C and transferred to a field in May. Regenerated plants were harvested in November and January. Water-cultured plants were grown in a greenhouse for

3 months. Ferruginol was kindly provided by Tomita (Niigata, Japan) and tanshinones were isolated from Tan-Shen [4]. The HPLC solvents were of HPLC grade and other solvents and chemicals were of analytical-reagent grade, all of which were obtained from Wako (Osaka, Japan). Iatrobeads (silica gel, 100-μm particle size) were from Iatron Laboratories.

Apparatus

The HPLC system consisted of two Tosoh CCPD pumps equipped with a Tosoh CCP controller connected to a dynamic mixer, a 5-μl sample loop and a Tosoh UV-8000 UV–VIS detector. The data were processed by means of a SIC Chromatocorder-11 integrator to evaluate the peak areas. The purity of the chromatographic peaks was estimated using a Waters M990J photodiode-array detector.

Extraction and fractionation of tanshinones and ferruginol

All procedures for the extraction, fractionation and analyses were performed in the dark as much as possible because some tanshinones readily undergo photo-oxidation [8]. The lyophilized sample was homogenized with ten volumes or more of chloroform–methanol (2:1, v/v). The homogenate was then centrifuged and the supernatant was transferred to a test-tube by decantation. The remaining insoluble material was sonicated in a sonic cleaning bath for 10 min with half the volume of the above homogenate. The pooled supernatant was washed according to the method of Folch *et al.* [9] and evaporated to dryness under nitrogen. An appropriate amount of extract, containing less than 14 mg, was taken up in a small volume of hexane–chloroform (1:1, v/v) and placed on a silica gel column containing 0.4 g of Iatrobeads. The column was eluted with 4 ml each of the above solvent and chloroform. The first fraction contained ferruginol and tanshinones were recovered in the second fraction. Both fractions were evaporated to dryness under nitrogen, dissolved in a known small volume of chloroform and then a portion was injected into the HPLC system. For the analysis of only tanshinones, the Iatrobeads chromatography was omitted.

Preparation for determination of tanshinone VI

The extract (10–100 mg) prepared by the method of Folch *et al.* [9] described above was dissolved in 2 ml of ethyl acetate and extracted with 2 ml of 5% aqueous sodium carbonate. The ethyl acetate layer was further extracted twice with 1 ml of the same solvent. Hydrochloric acid (1 *M*, 3.5 ml) was added to the pooled sodium carbonate layer and the mixture was extracted with 3 ml of ethyl acetate. The residual layer was further extracted once more in the same manner. The pooled ethyl acetate layer was washed three times with 1 ml of water and evaporated to dryness under nitrogen. The residue was dissolved in acetonitrile and an appropriate aliquot was used for reversed-phase HPLC analysis.

Normal-phase HPLC procedures

Normal-phase HPLC was performed on a stainless-steel column (250 × 4.6 mm I.D.) of Tosoh TSKgel silica 150 (5-μm particle size). The determinations of tanshinones and ferruginol was carried out under two sets of HPLC conditions. Elution was performed in an isocratic mode with two ratios of hexane to dioxane at a flow-rate of 1.0 ml/min throughout. HPLC system A for tanshinones employed

dioxane–hexane (8:92) and was monitored at 260 nm, whereas system B for ferruginol used dioxane–hexane (2.4:97.6) and was monitored at 285 nm. After use, the column was washed with dioxane–hexane (15:85) overnight.

Reversed-phase HPLC procedures

The reversed-phase column was made of stainless-steel (150 × 4.6 mm I.D.) and packed with a Tosoh TSKgel ODS-120T (5-μm particle size). The analytical procedures were performed with two HPLC systems, both of which utilized two solvents, (A) acetonitrile–0.01 *M* acetate buffer (pH 5.2) (20:80) and (B) acetonitrile. The flow-rate was maintained at 1.0 ml/min throughout. The qualitative and quantitative analysis of tanshinones was carried out with HPLC system C (see below), whereas the quantitative determination of tanshinone VI was accomplished by the use of system D following the pretreatment described above.

With system C, the elution programme was as follows: 0–3 min, 86% B; 3–20 min, linear change to 75% B; 20–30 min, 75% B (monitored at 275 nm). In order to prevent the peaks of tanshinone V and VI from broadening, the column was rinsed with 30 ml or more of 0.5% trifluoroacetic acid in acetonitrile prior to use.

With system D, the elution programme was as follows: 0–29 min, linear change from 14 to 33% B; 29–30 min, linear change to 90% B; 30–50 min, 90% B (monitored at 290 nm).

Partial synthesis of tanshinone VI

Dihydrotanshinone (169 mg) was dissolved in 1 ml of 1 *M* hydrochloric acid–50% methanol and heated for 1 h at 80°C. This reaction mixture was extracted with 4 ml of 5% aqueous sodium carbonate and washed three times with 1 ml of ethyl acetate. The residual layer was neutralized with 1 *M* hydrochloric acid and extracted three times with 1 ml of ethyl acetate. The pooled ethyl acetate extract was rinsed three times with 1 ml of water and evaporated to dryness under nitrogen. The residue was analysed using system C.

RESULTS AND DISCUSSION

Normal-phase HPLC

Table I gives the retention times (t_R) and capacity factors (k') of tanshinones and ferruginol standards in two systems with normal- and reversed-phase columns.

System A separated tanshinone IIA and I, cryptotanshinone and dihydrotanshinone I, but methylenetanshinquinone and 1,2-dihydrotanshinquinone eluted as a single peak (shown in Fig. 2). There was good linearity from 30 pmol to 10 nmol of tanshinone IIA and I, cryptotanshinone and dihydrotanshinone I with a correlation coefficient (r) of 0.999–1.000 with system A. In system A ferruginol emerged at 5.6 min, overlapping peaks corresponding to an impurity, and could not be detected. Pretreatment with Iatrobeads and the use of system B facilitated the detection of ferruginol (t_R = 12.0 min, k' = 2.00; shown in Fig. 3). A linear calibration graph for ferruginol with system B was obtained over the concentration range 0.1–100 nmol (r = 1.000). Tanshinones cannot be detected with system B.

TABLE I

RETENTION TIMES AND CAPACITY FACTORS FOR TANSHINONES AND FERRUGINOL STANDARDS

Compound	System A		System C	
	t_R (min)	k'	t_R (min)	k'
Ferruginol	5.6	0.49		
Dehydromiltirone	6.4	0.71	22.2	12.21
Tanshinone IIA	7.3	0.95	23.4	12.93
Methylenetanshinquinone	8.2	1.19	22.2	12.21
1,2-Dihydrotanshinone	8.2	1.19	22.2	12.21
Tanshinone I	9.6	1.56	21.2	11.62
Cryptotanshinone	16.4	3.37	20.4	11.14
Dihydrotanshinone I	19.6	4.23	18.0	9.71
Tanshinone V			16.0	8.52
Tanshinone IIB			14.6	7.69
Tanshinone VI			13.0	6.74
Tanshindiol C			8.4	4.00
Tanshindiol B			6.8	3.05
Tanshindiol A			6.4	2.81

Reversed-phase HPLC

Tanshinone V and VI, tanshindiol A–C and tanshinone IIB, the polar tanshinones, cannot be detected using normal-phase HPLC. Therefore, we developed

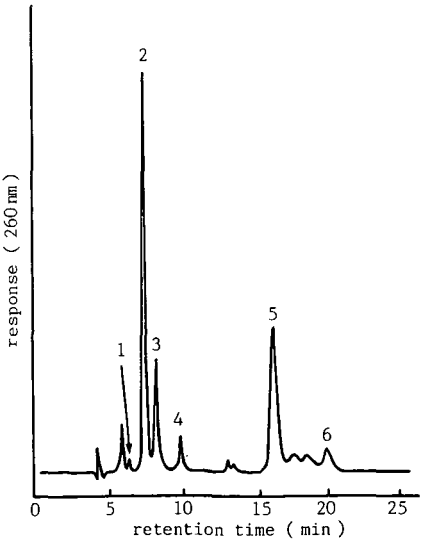

Fig. 2. Separation of tanshinones in the root of *S. miltiorrhiza* using system A. Peaks: 1 = dehydromiltirone; 2 = tanshinone IIA; 3 = methylenetanshinquinone and 1,2-dihydrotanshinquinone; 4 = tanshinone I; 5 = cryptotanshinone; 6 = dihydrotanshinone I.

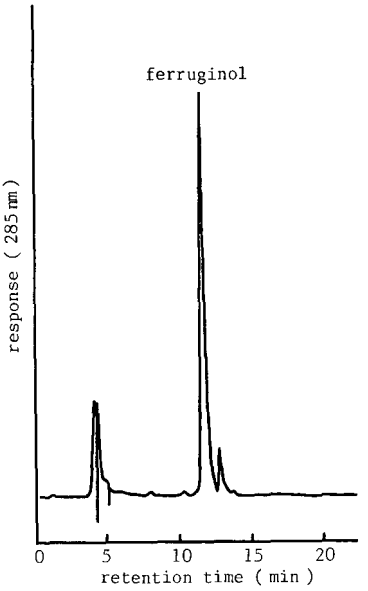

Fig. 3. Separation of ferruginol in Tan-Shen using system B.

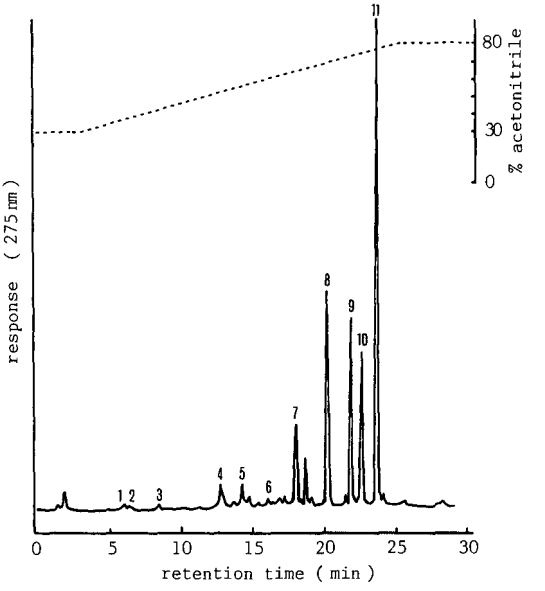

Fig. 4. Separation of tanshinones in Tan-Shen using system C. Peaks: 1 = tanshindiol A; 2 = tanshindiol B; 3 = tanshindiol C; 4 = tanshinone VI; 5 = tanshinone IIB; 6 = tanshinone V; 7 = dihydrotanshinone I; 8 = cryptotanshinone; 9 = tanshinone I; 10 = dehydromiltirone, methylenetanshinquinone and 1,2-dihydrotanshinquinone; 11 = tanshinone IIA.

a reversed-phase HPLC procedure by which the polar tanshinones can be studied both quantitatively and qualitatively.

System C resulted in the separation of most tanshinones, except dehydromiltirone, methylenetanshinquinone and 1,2-dihydrotanshinquinone, which completely overlapped each other (shown in Fig. 4). The calibration graphs for tanshinone V and VI and the less polar tanshinones (tanshinone IIA and I, cryptotanshinone, dihydrotanshinone I) in the concentration range 0.03–5 nmol followed a straight line (r = 0.999–1.000) with system C. Tanshindiol A–C and tanshinone IIB also yield distinct peaks, although the linear range was not examined.

Tanshinone VI is the most effective of the tanshinones in protecting the myocardium against ischaemia-induced derangements. It is difficult to measure tanshinone VI in tissues with system C, because it cannot be separated from impurities. It can be achieved, however, by using a sample pretreated with 5% aqueous sodium carbonate, even for low concentrations in tissues, with system D (t_R = 22.0 min, k' = 14.71), as shown in Fig. 5. Good linearity was obtained at levels of 0.1–2 nmol (r = 0.999).

We recommend system A for the less polar tanshinones and system C for the highly polar tanshinones. A sample containing tanshinones of high and low polarities can best be analysed by using a combination of both methods. Similar results were obtained with both systems A and C with the less polar tanshinones. The determination of tanshinone VI and ferruginol are achieved best with systems B and D, respectively.

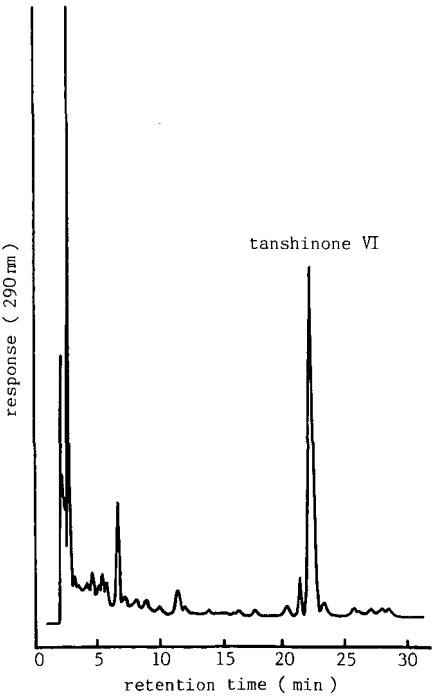

Fig. 5. Separation of tanshinone VI in the root of *S. miltiorrhiza* using system D.

TABLE II

RECOVERY AND PRECISION FOR TANSHINONES AND FERRUGINOL

Compound	System	Initial amount (μg)	Added (μg)	Recovery (%)[a]	Relative standard deviation (%)[b]
Ferruginol	B	108.1	66.0	97.1 ± 5.7	1.53
Tanshinone IIA	A	707.4	316.7	99.2 ± 0.9	0.53
Tanshinone I	A	116.6	55.6	96.5 ± 1.0	0.60
Cryptotanshinone	A	241.1	102.9	101.2 ± 2.7	0.54
Dihydrotanshinone I	A	46.3	18.5	96.3 ± 1.2	0.73
Tanshinone VI	D	22.5	9.6	89.8 ± 3.0	1.92

[a] Results are means ± standard deviation from three independent extractions.
[b] $n = 10$.

Recovery experiments

Recovery experiments were carried out by adding known amounts of tanshinones and ferruginol to the homogenate of regenerated plants. The mixture was extracted and assayed according to the above procedure. Table II summarizes the percentage recoveries and the statistical evaluation for tanshinones and ferruginol.

Determination of tanshinones and ferruginol

Ferruginol is found only in the roots of intact plants, as are tanshinones [10]. The contents of tanshinones and ferruginol in the roots of regenerated plant, the parent plant, water-cultured plant and Tan-Shen are given in Table III. One-year-old roots of regenerated plants contained 3–7 times more tanshinones than Tan-Shen, an amount similar to that in the parent plant (about 1 year old). This study on plant regeneration suggests useful and relatively rapid culture methods for the production of tanshinones; currently, commercial Tan-Shen is obtained from the roots of *S. miltiorrhiza* cultured for 4–5 years.

TABLE III

CONTENT OF TANSHINONES IN REGENERATED PLANT, PARENT PLANT, WATER-CULTURED PLANT AND TAN-SHEN DETERMINED USING SYSTEMS A AND B

Material	Concentration (% dry weight)				
	Tanshinone IIA	Tanshinone I	Cryptotanshinone	Dihydrotanshinone I	Ferruginol
Regenerated plant[a]	1.102	0.172	0.335	0.077	0.089
Parent plant[b]	1.524	0.141	1.141	0.104	0.117
Water-cultured plant[c]	0.011	0.007	0.018	0.015	0.012
Commercial Tan-Shen	0.150	0.050	0.050	0.025	0.074
Callus[d]	0.116	0.034	0.106	0.037	0.052

[a] Cultured in Tsukuba since May 1988 and harvested in June 1989.
[b] Cultured in Tsukuba and harvested in November 1987 (about 1 year old).
[c] Cultured for 3 months.
[d] Obtained by adventitious root culture.

TABLE IV

CONTENT OF TANSHINONES IN REGENERATED PLANT AND PARENT PLANT BY SYSTEMS A AND B

Material	Concentration (% fresh weight)				
	Tanshinone IIA	Tanshinone I	Crypto-tanshinone	Dihydro-tanshinone I	Ferruginol
Regenerated plant[a]:					
Nov. 1988[b]	0.31	0.04	0.07	0.01	0.06
Jan. 1989[b]	0.14	0.02	0.03	0.01	0.04
Parent plant[c], Tsukuba	0.48	0.04	0.36	0.03	0.12

[a] Cultured in Tsukuba since May 1988.
[b] Harvest time.
[c] Cultured in Tsukuba and harvested in November 1988 (about 1 year old).

Table IV shows a comparison of the contents of the tanshinones and ferruginol in the roots of regenerated plants harvested at different times. The content in tissue harvested in November was approximately twice that in tissue harvested in January. It appears that the production of tanshinones and ferruginol is greatly influenced by the season.

Determination and partial synthesis of tanshinone VI

Tanshinone VI is one of the most effective components of *S. miltiorrhiza*, as described previously. It is difficult to isolate sufficient for analysis because of the low levels found in various sources (Table V). Therefore, we studied the partial synthesis of tanshinone VI from dihydrotanshinone I with the use of system C. Dihydrotanshinone I was treated with 1 *M* hydrochloric acid in 50% methanol for 1 h at 80°C, giving a yield of tanshinone VI of 69.5%.

ACKNOWLEDGEMENTS

We express our appreciation to Dr. Motoyoshi Satake (Tsukuba Medicinal Plant Research Station) for the provision of plants and cultured cells and Professor

TABLE V

CONTENT OF TANSHINONE VI IN COMMERCIAL TAN-SHEN, FRESH ROOT AND CALLUS DETERMINED USING SYSTEM D

Material	Concentration (% dry weight)
Fresh root[a]	0.0034
Callus[b]	0.0018
Commercial Tan-Shen	0.0072

[a] Cultivated in Fukuyama and harvested in November 1988.
[b] Obtained by adventitious root culture.

Yutaka Tomita (Niigata College of Pharmacy) for the supply of ferruginol. We also thank Miss Michiko Okamoto, Akiko Fujii and Noriko Uotani and Mr. Masahiko Tsujikawa for excellent technical assistance.

REFERENCES

1 A. R. Lee, W. L. Wu, W. L. Ching, H. C. Lin and M. L. King, *J. Nat. Prod.*, 50 (1987) 157.
2 M. Nakano and T. Fukushima, *Yakugaku Zasshi*, 54 (1934) 154.
3 K. Takiura, *Yakugaku Zasshi*, 61 (1941) 475.
4 A. Yagi, K. Fujimoto, K. Tanonaka, K. Hirai and S. Takeo, *Planta Med.*, 55 (1989) 51.
5 T. Nakanishi, H. Miyasaka, M. Nasu, H. Hashimoto and K. Yoneda, *Phytochemistry*, 22 (1983) 721.
6 M. Wang, F. Yan, F. Gao and B. Li, *Yaowu Fenxi Zazhi*, 5 (1985) 348.
7 G. Chen and Y. Tong, *Zhongyao Tongbao*, 12 (1987) 269.
8 T. Kusumi, T. Kishi and H. Kakisawa, *J. Chem. Soc., Perkin Trans. 1*, (1976) 1716.
9 J. Folch, M. Lees and G. H. Sloane-Stanley, *J. Biol. Chem.*, 226 (1957) 497.
10 H. Miyasaka, M. Nasu, T. Yamamoto, K. Matsumura and K. Yoneda, *Plant Tissue Cult. Lett.*, 1 (1984) 57.

Journal of Chromatography, 542 (1991) 327–336
Elsevier Science Publishers B.V., Amsterdam

CHROM. 23 055

Liquid chromatographic characterization of the triterpenoid patterns in *Ganoderma lucidum* and related species

RONGSUEY CHYR and MING-SHI SHIAO*
Department of Medical Research, Veterans General Hospital-Taipei, Shih-pai, Taipei 11217 (Taiwan)
(First received August 27th, 1990; revised manuscript received December 14th, 1990)

ABSTRACT

Reversed-phase high-performance liquid chromatography was applied to the determination of the triterpenoids compositions in the Chinese medicinal fungus *Ganoderma lucidum* (Fr.) Karst and several taxonomically related species. Twenty-five well-characterized reference triterpenoids were selected for compositional comparison. It was found that characterization based on triterpenoid profile mapping was compatible with the morphological classification. The very unique oxygenated triterpenoids, which up to now have only been identified in the genus *Genoderma*, provided supporting evidence for classification. The triterpenoid profiles also gave characteristic information for distinguishing this medicinal fungus from other taxonomically related species. The method was also applicable to screening of specific triterpenoids with particular biological activities.

INTRODUCTION

Many secondary metabolites, such as terpenoids, flavonoids and phenolic natural products, have been used as marker compounds for the characterization and classification of taxonomically related fungi and higher plants [1,2]. These metabolites can provide useful information for chemical taxonomy provided that their occurrence and compositions are characteristic of a single, unique genus or are restricted to only a few closely related species. Common natural products or secondary metabolites which are greatly subjected to seasonal variations or subtle changes in culture conditions are not suitable for this purpose. In addition, the determination of these marker metabolites is essential for elucidating their compositions and abundance. Gas chromatography (GC) and high-performance liquid chromatography (HPLC) are nowadays the most commonly employed methods for this purpose [3,4].

Ganoderma lucidum (Fr.) Karst (Polyporaceae) and related species are fungi used in traditional Chinese medicine [5]. Recent studies on this fungus have demonstrated many interesting biological activities, inlcuding antitumour, anti-inflammatory and cytotoxicity to hepatoma cells [6,7]. Inhibitory activities of histamine release, platelet aggregation, cholesterol biosynthesis and angiotensin-converting enzyme (ACE) have also been reported [8–10]. Accumulated evidence supported the suggestion that these biological activities are mainly associated with oxygenated triterpenoids [11–21].

0021-9673/91/$03.50

Particularly interesting from the taxonomical point of view is the natural occurrence of over 100 species of oxygenated triterpenoids, which have been identified recently from the culture mycelia and fruiting bodies of *G. lucidum*. These triterpenoids have several structural features of particular note. Their common lanostanoid skeleton contains highly oxygenated functionalities, namely hydroxyl, acetoxyl and oxo groups at C-3, C-15, C-22, C-23, and many other positions [12–16]. The C-26 carbon is also functionalized to the hydroxyl or carboxyl status in many triterpenoids of *G. lucidum* (Fig. 1). Most of these oxygenated triterpenoids have not been reported in other genera of Polyporaceae, although extensive screening has not yet been carried out for detailed comparison. To pave the way for the later application of these triterpenoids in the chemical taxonomy of the genus *Ganoderma*, the structural determination of many triterpenoids in this fungus has been accomplished recently. Screening of better producing strains for those biologically active triterpenoids is also desirable in pharmacological studies.

Both these two aspects rely heavily on the determination of these triterpenoids by chromatographic methods. We have previously elucidated the chromatographic behaviour of these oxygenated triterpenoids using silica gel thin-layer chromatography and normal-phase HPLC [22]. As multiple and different polar functional groups can occur, the volatilities of these triterpenoids are low. GC is less practical for direct measurement. It is also worth mentioning that many pairs of stereo- and positional isomers can appear simultaneously in the culture mycelia and fruiting bodies of *G. lucidum*. We have determined the contributions to molecular polarity of the hydroxy (OH) and acetoxy (OAc) substituents at the C-3 and C-15 positions in governing the retention behaviour (capacity factors) by using reversed-phase HPLC [23]. The trend of their weighing factors is as follows: 3β-OH > 3α-OH, 15α-OH > 3α-OAc > 3β-OAc. The chromatographic behaviour of these oxygenated triterpenoids allowed us to apply a binary solvent system of acetonitrile and water with gradient elution for optimum resolution of many pairs of stereo- and positional isomers [23]. The aim of this study was to explore the applicability of triterpenoid patterns, based on reversed-phase HPLC, to the chemical taxonomy of the fungus *G. lucidum*. The determination and comparison of production yields of several desired triterpenoids in the genus *Ganoderma* were also tested. The triterpenoid profiles of *G. lucidum* and several taxonomically related species are reported.

EXPERIMENTAL

Cultures of Ganoderma and related species

Two strains of *G. lucidum* (ATCC 32471 and 32472) were obtained from the American Type Culture Collection (Rockville, MD, U.S.A.). Strains CCRC 36111, 36114, 36143, 36144, 36110, 36125 and 36021 were obtained from the Culture Collection and Research Centre (CCRC), Food Industry Research and Development Institute (Hsinchu, Taiwain). Strains TP-1 and G.l.-chen were collected locally. Strains ATCC 64251 and CJ-3 were obtained from the Institute of Botany, Academia Sinica (Taiwan). All strains were maintained on potato–dextrose–agar slants. For mycelial culture, fungi were inoculated in 1-l culture flasks containing 300 ml of medium consisting of 30 g of dextrose, 20 g of malt extract, and 1 g of peptone per litre of distilled water at pH 6.5. Each strain was inoculated into three culture flasks and stationary cultures were maintained at 28 ± 1.5°C for 30 days [12,24].

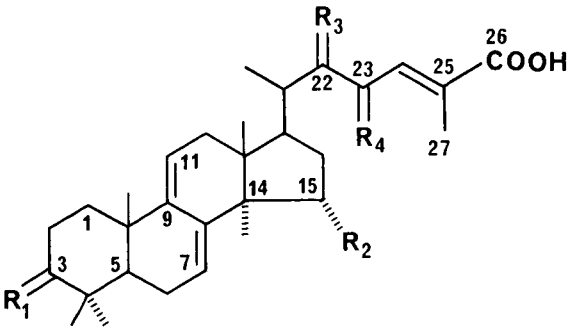

	R_1	R_2	R_3	R_4
1	α-OAc	OAc	H_2	H_2
2	β-OAc	OAc	H_2	H_2
3	α-OH	OAc	H_2	H_2
4	α-OAc	OH	H_2	H_2
5	β-OH	OAc	H_2	H_2
6	β-OAc	OH	H_2	H_2
7	=O	OAc	H_2	H_2
8	α-OH	OH	H_2	H_2
9	β-OH	OH	H_2	H_2
10	α-OAc	OH	β-OAc	H_2
11	β-OH	OAc	β-OAc	H_2
12	α-OAc	OAc	β-OAc	H_2
13	β-OAc	OAc	β-OAc	H_2
14	α-OH	OAc	H_2	O
15	α-OAc	OAc	H_2	O
16	α-OAc	OH	H_2	O
17	α-OAc	OH	α-OH	H_2
18	α-OAc	OAc	α-OH	H_2
19	β-OAc	OAc	α-OH	H_2
20	β-OH	OH	β-OAc	H_2
21	α-OH	OH	β-OAc	H_2
22	β-OH	OH	β-OH	H_2
23	α-OH	OH	α-OH	H_2
24	α-OH	H	H_2	H_2
25	α-OAc	H	H_2	H_2

Fig. 1. Structures of marker triterpenoids (**1**–**25**) isolated from *Ganoderma lucidum* (strains ATCC 32471 and TP-1).

General procedure for the isolation of oxygenated triterpenoids

Mycelia were harvested by filtration through four layers of cheesecloth and were gently washed with water. The dry weight was obtained by heating the mycelia at 45°C in darkness for 48 h. About 1 g of mycelia from each sample was precisely weighed, ground into powder and extracted three times with 15 ml of methanol. The pooled extracts were concentrated on a rotary evaporator. Each concentrated preparation was suspended in 1.5 ml of methanol and passed through glass-wool in a disposable pipette to remove insoluble matter. To remove lipophilic metabolites, the filtrate was passed slowly through a Sep-Pak cartridge column [Waters Assoc. (Milford, MA, U.S.A.), C_{18} reversed phase]. Columns was eluted with acetonitrile and 5-ml volumes of eluates were collected. The solvents were evaporated to dryness at 45°C with a stream of nitrogen in darkness. The concentrated residues were weighed and dissolved in 1 ml of acetonitrile for the determination by HPLC.

Determination of triterpenoids by reversed-phase HPLC

A Model 1084B solvent-delivery system (Hewlett-Packard, Avondale, PA, U.S.A.) equipped with a Rheodyne Model 7125 sample injector, a Model 440 variable-wavelength UV detector (Waters Assoc.) and a Model 79850B integrator (Hewlett-Packard) was used in the HPLC analysis. Separation was performed on a prepacked reversed-phase column (Cosmosil 5 C_{18}, 5 μm, 25 × 0.46 cm I.D.; Nacalai Tesque, Kyoto, Japan). Multi-step linear gradient elution with a binary solvent system of acetonitrile and water was employed [23]. To achieve better resolution in the separation of triterpenoids containing a C-26 carboxyl group, a constant concentration of acetic acid (0.5%, v/v) was used to suppress the ionization. These oxygenated triterpenoids all contain a transoid diene skeleton and showed very strong and almost identical UV absorption at 235 nm ($\log \varepsilon = 4.14$), 243 nm ($\log \varepsilon = 4.16$) and 251 nm ($\log \varepsilon = 3.97$) in methanol [12]. Routinely, post-column UV detection at 243 nm was used. Quantification was based on the peak areas of the corresponding triterpenoids. At least ten reference triterpenoids (compounds **1**–**10** in Table I) were used to construct the calibration graphs.

Identification of oxygenated triterpenoids

Identification of triterpenoids in the HPLC profiles was based on their co-migration with the authentic triterpenoid standards. The reference standards were purified from *G. lucidum* (strains ATCC 32471 and TP-1). Their structures were completely identified by the spectroscopic methods reported previously [12–16]. To confirm the identity of these oxygenated triterpenoids produced in species which were not *G. lucidum*, several representative peaks in HPLC were also collected for UV and mass spectrometric identification.

RESULTS AND DISCUSSION

The compositional study of oxygenated triterpenoids in *G. lucidum* and related species was conducted in a comparable manner. We cultured these fungi under identical conditions for 30 days. Based on a previous study of strains TP-1 and ATCC 32471, this culture period was long enough to reach the stationary phase as judged by the mycelial biomass [24]. Under these conditions, the concentrations of the two most

abundant triterpenoid metabolites, namely lanosta-7,9(11),24-trien-3α,15α-diacetoxy-26-oic acid (compound **1** in Fig. 1) and lanosta-7,9(11),24-trien-3β,15α-diacetoxy-26-oic acid (compound **2**), which are epimers at C-3 in pairs, reached their plateau on day 28. The triterpenoid patterns remained unchanged in the reference strains (ATCC 32471 and TP-1) at least until day 50 [12]. In the culture of *G. lucidum*, the yellowish to brownish yellow pigments appeared between days 14 and 20, which was also the vigorous production period of these two major oxygenated triterpenoids. Ergosterol and other lipophilic metabolites were also produced in significant amounts by these fungi.

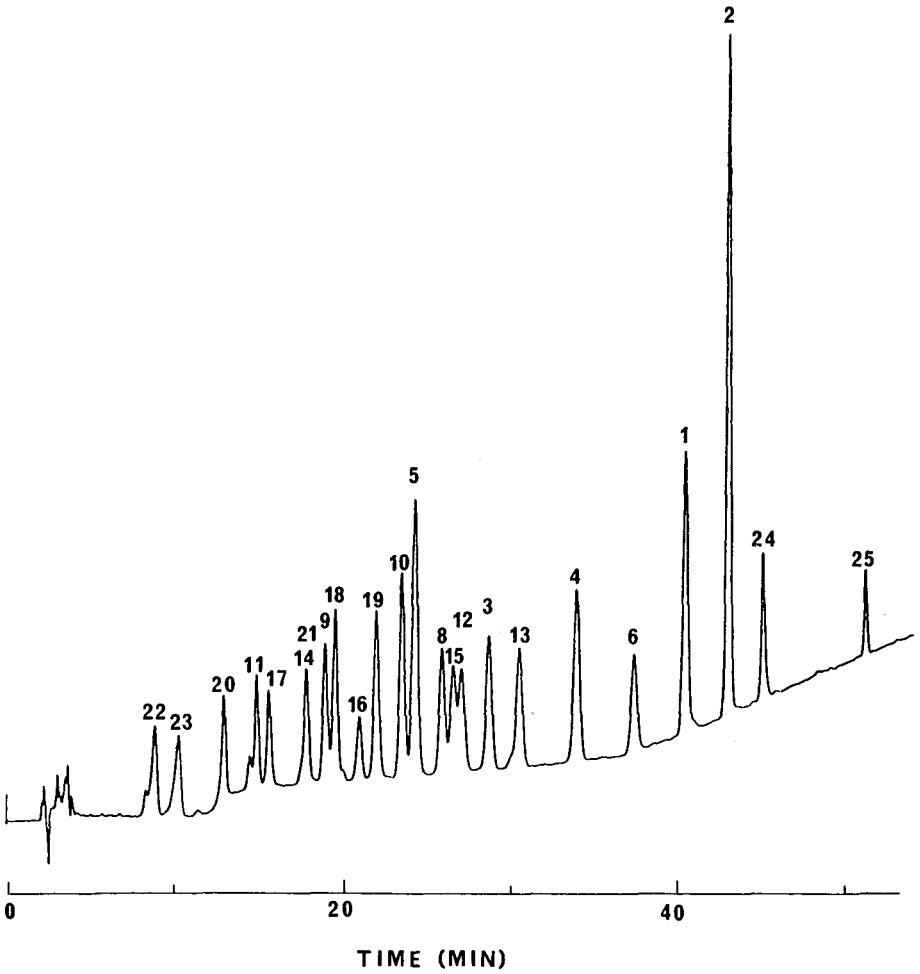

Fig. 2. Reversed-phase HPLC trace of reference triterpenoids (compounds **1–6** and **8–25**). Column, Cosmosil 5 C_{18}, 25 × 0.46 cm I.D. Eluent A, methanol–acetic acid (100:0.5, v/v); eluent B, methanol–water–acetic acid (80:20:0.5, v/v/v); flow-rate, 1.0 ml/min; UV detection at 243 nm. Gradient elution was started with 80% methanol, increased linearly to 84% in 15 min, to 86% in a further 15 min, to 88% in 10 min, to 94% in a further 10 min and finally to 100% in 20 min.

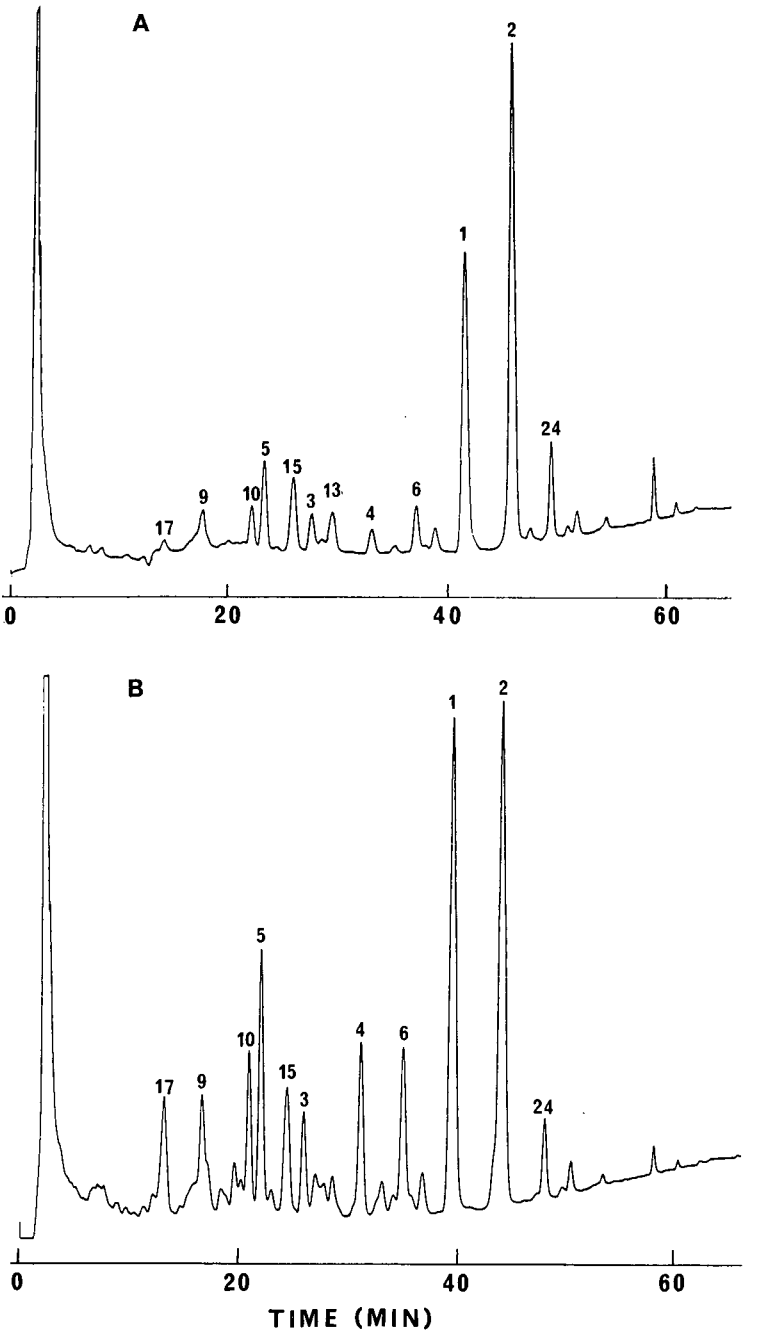

Fig. 3. Reversed-phase HPLC of triterpenoids of *G. lucidum*. (A) strain TP-1; (B) CCRC 36021. Conditions as in Fig. 2.

TABLE I

RELATIVE MOLAR PERCENTAGES OF MAJOR TRITERPENOIDS IN *GANODERMA* SPECIES AS DETERMINED BY HPLC

Strain	Triterpenoid[a] (mol%)[b]											
	17	**9**	**10**	**5**	**15**	**3**	**13**	**4**	**6**	**1**	**2**	**24**
TP-1	1.7	3.1	2.8	6.2	5.6	2.8	3.8	1.6	3.3	23.8	40.7	4.8
CCRC 36021	5.7	4.5	6.1	9.8	6.1	3.8	ND[c]	5.3	4.0	25.2	26.1	3.3
ATCC 64251	3.4	7.0	4.5	2.4	19.0	6.8	15.0	7.6	ND	18.6	3.3	12.4
CCRC 36111	10.1	6.0	9.1	0.7	5.3	5.7	3.9	28.0	ND	15.5	3.6	11.8
CCRC 36144	2.2	2.3	2.4	0.6	1.0	ND	4.1	31.8	ND	3.1	12.6	40.1
CCRC 36143	13.2	8.7	25.9	ND	20.7	ND	7.7	9.0	3.1	6.0	4.0	1.7
G.l.-chen	5.3	8.0	13.3	ND	35.3	ND	35.2	0.6	ND	1.5	0.4	0.5

[a] For structures, see Fig. 1.

[b] The total number of moles of these twelve triterpenoids was assigned a value of 100%. Results are mean values of three HPLC determinations.

[c] ND, not detectable.

The methanolic extracts of mycelia were passed through reversed-phase cartridge columns to reduce the interferences. This clean-up procedure was tested to ensure quantitative recoveries of the oxygenated triterpenoids listed in Fig. 1, which are all more polar than ergosterol (data not shown). Twenty-five triterpenoids were isolated from two reference strains of *G. lucidum* for this study (Fig. 1). Compound **7** is a minor metabolite and was therefore not used in the HPLC analysis.

The resolution of these triterpenoids by reversed-phase HPLC and their elution sequence are illustrated in Fig. 2. The triterpenoid profiles of these two reference strains of *G. lucidum* (TP-1 and ATCC 32471) were well characterized previously in our laboratory [23]. Their profiles were very similar to each other. It was found that many strains of *G. lucidum*, exemplified by CCRC 36021, gave triterpenoid patterns very close to those of TP-1 and ATCC 32471 (Fig. 3). The profiles of both CCRC 36021 and TP-1 showed that compounds **1** and **2** were predominant (Fig. 1). More than twelve major triterpenoid components in strians TP-1 and ATCC 32471 also appeared in strain CCRC 36021 (Table I). Strain CCRC 36021 was recently also confirmed to be *G. lucidum* by detailed morphological study at CCRC (data not shown). This fingerprint mapping of triterpenoid patterns determined by reversed-phase HPLC was in agreement with the morphological characterization.

The triterpenoid profiles were also determined in several taxonomically related species. For example, strain CCRC 36114 was a species of *Ganoderma*. This strain did not show the typical ovate double-walled basidiospores of *G. lucidum*. We found that strain CCRC 36114 also gave a completely distinct HPLC profile. The triterpenoid patterns of strains CJ-3 and CCRC 36110 were almost identical with each other (data not shown). However, their patterns were also completely different from those of characterized strains of *G. lucidum* (TP-1 and ATCC 32471). The strain CJ-3 has been classified as *G. tsugae* by other investigators [25]. It was therefore suspected that strain CCRC 36110 was also a species of *G. tsugae*. However, more detailed morphological information is needed to clarify this point. Strain CCRC 36143 and strain

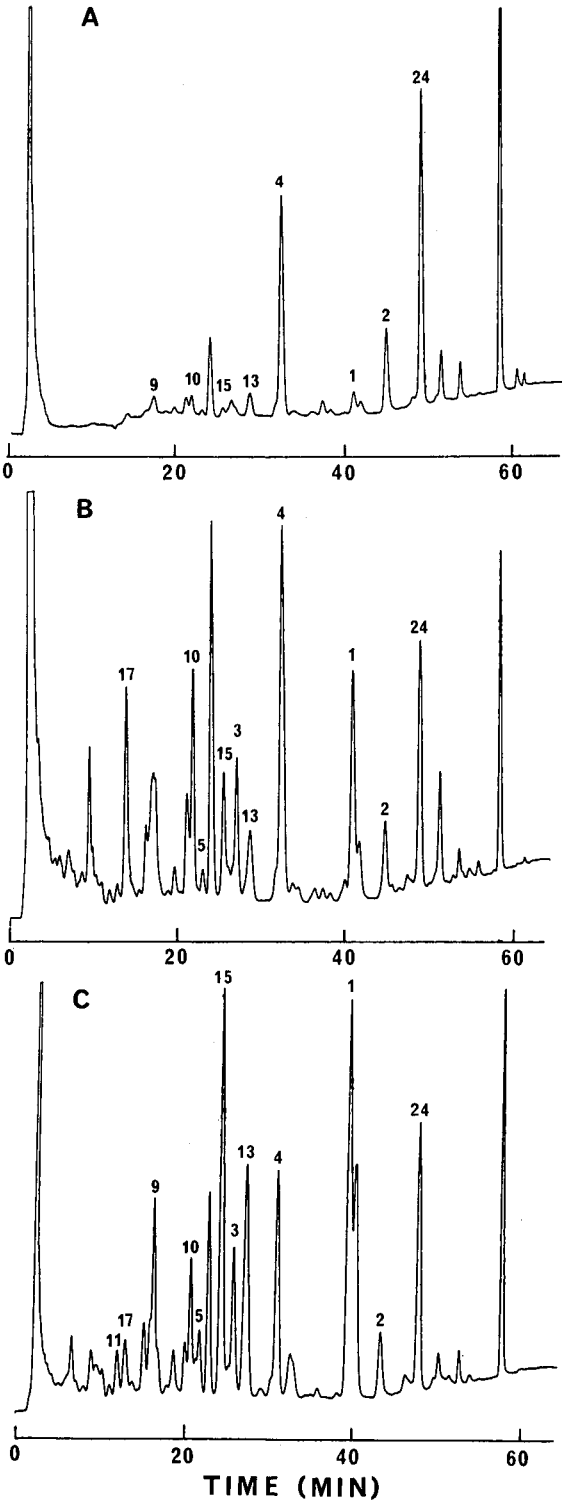

Fig. 4. Reversed-phase HPLC of triterpenoids of *Ganoderma* species. (A) CCRC 36144; (B) CCRC 36111; (C) ATCC 64251. Conditions as in Fig. 2.

G.l.-chen gave very similar triterpenoid patterns (Table I). These two strains also produced many common triterpenoids which also appeared in the reference strains of *G. lucidum* (TP-1 and ATCC-32471). The major difference between these two groups of *Ganoderma* species was that strains CCRC 36143 and G.l.-chen produced more polar triterpenoids listed in Fig. 1, which were eluted in front of triterpenoids **1** and **2** in reversed-phase HPLC. We confirmed that their major metabolites were compounds **10**, **13** and **15**. However, compounds **1** and **2** were still detectable in strains CCRC 36143 and G.l.-chen (Table I). The strains CCRC 36111 and 36144 were listed as *G. lucidum* by CCRC. They produced many triterpenoids which were common to those of reference strains ATCC 32471 and TP-1 (Fig. 4). However, their relative abundances were different (Table I). Interestingly, strain ATCC 64251, which was originally collected in Taiwan, also showed a triterpenoid pattern almost identical with that of CCRC 36111 (Fig. 4). The taxonomic classification of these strains remained to be clarified.

This study has illustrated the potential application of triterpenoid patterns in the chemical taxonomy of the genus *Ganoderma*. The information about triterpenoid patterns provided by HPLC and morphological characterization was generally in good agreement. This profile analysis should also be useful for the screening of particular triterpenoids with known biological activities. Both applications rely heavily on the precise determination of marker triterpenoids, which has been achieved.

ACKNOWLEDGEMENTS

Financial support from the National Science Council and Veterans General Hospital–Taipei, Taiwan, is gratefully acknowledged. We thank Prof. T.-C. Tseng, Institute of Botany, Academia Sinica, Mr. B.-C. Wang, Culture Collection and Research Centre, Hsinchu, Taiwan, and Dr. L.-J. Lin for fungal strains and valuable discussions.

REFERENCES

1 T. Swain (Editor), *Chemical Plant Taxonomy*, Academic Press, New York, 1963.
2 H. Yokokawa, *Phytochemistry*, 19 (1980) 2615.
3 T. Nishitoba, H. Sato, S. Shirasu and S. Sakamura, *Agric. Biol. Chem.*, 50 (1986) 2151.
4 H.-J. Busse, T. El-Banna and G. Auling, *Appl. Environ. Microbiol.*, 55 (1989) 1578.
5 T. Miyazaki and M. Nishijima, *Chem. Pharm. Bull.*, 29 (1981) 3611.
6 J. O. Toth, B. Luu and G. Ourisson, *Tetrahedron Lett.*, 24 (1983) 1081.
7 H. Kohda, W. Tokumoto, K. Sakamoto, M. Fujii, Y. Hirai, K. Yamasaki, Y. Komoda, H. Nakamura, S. Ishihara and M. Uchida, *Chem. Pharm. Bull.*, 33 (1985) 1367.
8 A. Shimizu, T. Yano, Y. Saito and Y. Inada, *Chem. Pharm. Bull.*, 33 (1985) 3012.
9 A. Morigiwa, K. Kitabatake, Y. Fujimoto and N. Ikekawa, *Chem. Pharm. Bull.*, 34 (1986) 3025.
10 Y. Komoda, M. Shimizu, Y. Sonoda and Y. Sato, *Chem. Pharm. Bull.*, 37 (1989) 531.
11 T. Usui, Y. Iwasaki, K. Hayashi, T. Mizuno, M. Tanaka, K. Shinkai and M. Arakawa, *Agric. Biol. Chem.*, 45 (1981) 323.
12 M.-S. Shiao, L.-J. Lin, S.-F. Yeh and C.-S. Chou, *J. Nat. Prod.*, 50 (1987) 886.
13 M.-S. Shiao, L.-J. Lin and S.-F. Yeh, *Phytochemistry*, 27 (1988) 873.
14 L.-J. Lin, M.-S. Shiao and S.-F. Yeh, *Phytochemistry*, 27 (1988) 2269.
15 M.-S. Shiao, L.-J. Lin and S.-F. Yeh, *Phytochemistry*, 27 (1988) 2911.
16 L.-J. Lin, M.-S. Shiao and S.-F. Yeh, *J. Nat. Prod.*, 51 (1988) 918.
17 M. Hirotani and T. Furuya, *Phytochemistry*, 25 (1986) 1189.

18 M. Hirotani, C. Ino, T. Furuya and M. Shiro, *Chem. Pharm. Bull.*, 34 (1986) 2282.
19 M. Hirotani, I. Asaka, C. Ino, T. Furuya and M. Shiro, *Phytochemistry*, 26 (1987) 2797.
20 T. Nishitoba, H. Sato, S. Shirasu and S. Sakamura, *Agric. Biol. Chem.*, 51 (1987) 619.
21 T. Nishitoba, H. Sato and S. Sakamura, *Agric. Biol. Chem.*, 51 (1987) 1149.
22 L.-J. Lin and M.-S. Shiao, *J. Chromatogr.*, 410 (1987) 195.
23 M.-S. Shiao, L.-J. Lin and C.-S. Chen, *J. Lipid Res.*, 30 (1989) 287.
24 T.-C. Tseng, M.-S. Shiao, Y.-S.- Shieh and Y.-Y. Hao, *Bot. Bull. Acad. Sin.*, 25 (1984) 149.
25 T.-C. Tseng and L.-L. Lay, *Bot. Bull. Acad. Sin.*, 29 (1988) 189.

Journal of Chromatography, 542 (1991) 337–344
Elsevier Science Publishers B.V., Amsterdam

CHROM. 23 057

Allergenic fragments in *Parietaria judaica* pollen extract

EZIO BOLZACCHINI, PATRIZIA DI GENNARO, GIUSEPPINA DI GREGORIO and BRUNO RINDONE*

Dipartimento di Chimica Organica e Industriale, Università di Milano, Via Venezian 21, I-20133 Milan (Italy)

PAOLO FALAGIANI and GIOVANNI MISTRELLO

Lofarma Allergeni, Reparto Ricerche, Viale Cassala 40, I-20146 Milan (Italy)

and

IB SONDERGAARD

Royal Veterinary and Agricultural University, 40 Thorvaldsenvej, DK-1871 Frederiksberg C, Copenhagen (Denmark)

(First received July 31st, 1990; revised manuscript received November 16th, 1990)

ABSTRACT

High-performance ion-exchange chromatography and immunoaffinity chromatography suggest that Par jI, the principal allergenic component of *Parietaria judaica* pollen, is a very unstable molecule, which tends to fragment in solution. Several fragments were obtained from Par jI and some of them show positivity toward the anti-Par jI monoclonal antibody, suggesting that they retain the entire structure of the allergenic determinant. These fragments could be the target for sequence and conformation studies.

INTRODUCTION

Parietaria pollen allergenic extracts are used in the immunotherapy of allergic diseases. As these extracts consist of a mixture of heterogeneous proteins, studies aimed to improve their standardization and their chemical composition are needed.

A variety of chromatographic [1–7], electrophoretic and immunochemical [8–11] techniques have been attempted. In particular, the combination of sodium dodecyl sulphate–polyacrylamide gel electrophoresis (SDS-PAGE) and reversed-phase high-performance liquid chromatography (RP-HPLC) led to the isolation of an allergenic protein with a molecular weight of 10 000 dalton, called Par jI [12], which can polymerize spontaneously. On the other hand, using high-performance ion-exchange chromatography (HPIEC) we obtained at high elution volume a fraction containing a single component, probably derived from the dissociation of a homopolymer as a result of the dissociating effect of the ionic strength gradient used. This component seems similar to Par jI allergen, as demonstrated by SDS-PAGE, isoelectric focusing (IEF) and crossed immunoelectrophoresis (CIE) [13].

Recent evidence suggests the importance of studies on the molecular structure

0021-9673/91/$03.50

of allergens, in order to define epitopes that may represent targets of the human allergic response. The fragmentation with cyanogen bromide of the major allergen of *Festuca elatior* (Fes eI) allowed a peptide fragment with immunoglobulin E (IgE)-binding ability to be obtained. This was also able to induce an IgG response which cross-reacted with the entire allergen when used as an immunogen in mice [14]. This could occur also with *Parietaria*, as a low-molecular-weigth peptide having allergenic activity has been isolated [15].

In order to isolate allergenic peptides from *Parietaria* pollen extract, we used alternatively a combination of HPIEC and high-performance size-exclusion chromatography (HPSEC), or a combination of affinity chromatography and HPSEC or a combination of methanol extraction and HPSEC.

EXPERIMENTAL

Preparation of Parietaria pollen extract

A 10-g sample of defatted dry pollen obtained from Allergon (Engelholm, Sweden) was extracted with 200 ml of 0.15 *M* phosphate buffer (pH 7.2) for 24 h at 4°C. After centrifugation at 28 000 *g* for 40 min the solution was filtered on a Sephadex G-25 gel column (ratio of sample to adsorbent = 1:5) with 20 m*M* phosphate buffer (pH 6.8) as the eluent. The exclusion peak corresponding to blue dextran was collected and lyophilized.

HPLC analyses

HPSEC was performed by dissolving lyophilized pollen extracts in 0.15 *M* phosphate buffer (pH 6.8)–0.5 *M* potassium chloride and injecting the solution through a Rheodyne 100-μl loop. A Varian (Palo Alto, CA, U.S.A.) 5500 HPLC gradient instrument was used equipped with a Synchropak 100 column (SynChrom, Lafayette, IN, U.S.A.) with 0.15 *M* phosphate buffer (pH 6.8)–0.5 *M* potassium chloride as eluent at a flow-rate of 0.8 ml/min. The detector was a Hewlett-Packard (Palo Alto, CA, U.S.A.) Model 1040 diode-array detector.

HPIEC with an ionic strength gradient was performed by dissolving the material in 10 m*M* Tris–acetic acid buffer (pH 7.0)–100 m*M* sodium acetate at the required molarity and injecting the solution through a Rheodyne 5-ml loop. A Waters Delta Prep 3000 HPLC instrument equipped with a TSK DEAE-5 PW ion-exchange column (15 cm × 21.5 mm I.D.) was used, eluting with a 50-min gradient from solvent A to B, where A was 10 m*M* Tris–acetic acid buffer of the required pH plus sodium acetate of the required molarity and B was 10 m*M* Tris–acetic acid buffer of the required pH containing 500 m*M* sodium acetate. The flow-rate was 6 ml/min. The fractions were then analysed by the direct radio-allergo-sorbent test (RAST).

Reversed-phase (RP) HPLC was performed using a LiChrosorb RP-C_{18} column (25 cm × 4 mm I.D.) (Merck-Bracco, Milan, Italy). The material was dissolved in methanol and injected into the Waters instrument previously described using a 100-μl loop, then eluted with a 30-min linear gradient from A [0.1% aqueous trifluoroacetic acid (TFA)–acetonitrile (70:30)] to B [0.1% aqueous TFA–acetonitrile (10:90)]. The individual fractions were lyophilized and the residue was analysed by direct RAST.

Monoclonal antibody to Par jI

Cells producing monoclonal antibody to Par jI were expanded *in vivo* by injecting $2 \cdot 10^6$ cells intraperitoneally into Balb/c mice pretreated with pristane. The ascitic liquid was separated from cells by centrifugation at 1680 *g* for 10 min, precipitated with 50% saturated ammonium sulphate and extensively dialysed against 0.1 *M* sodium hydrogencarbonate (pH 8.3).

The ascitic liquid was further purified on protein Sepharose G, eluting IgG fractions with 0.1 *M* glycine hydrochloride (pH 2.7). The fractions corresponding to the peak were pooled and dialysed against 0.1 *M* sodium hydrogencarbonate (pH 8.3).

Immunoabsorbent preparation for conventional affinity chromatography

The purified immunoglobulin fraction from ascitic liquid was covalently coupled to a properly activited support (Affi-Gel 10; Bio-Rad Labs., Segrate, Milan, Italy) by continuous stirring for 4 h at room temperature. After blocking residual reactive sites by 1 *M* ethanolamine hydrochloride (pH 8), the gel was transferred to a 10 × 1.2 cm I.D. Bio-Rad column and washed with coupling buffer until the absorbance at 280 nm was close to zero.

Conventional affinity chromatography

The immunoabsorbent column prepared as above was used for the purification of 10 ml of a gel-filtered *Parietaria judaica* extract with a protein content of 0.8 mg/ml. After washing with phosphate-buffered saline (PBS) (pH 7.2) until the absorbance at 280 nm was close to zero in the eluent, the antibody-bound fraction was eluted with 2 *M* sodium chloride in PBS buffer (pH 7.2). The eluted fraction was dialysed against 10 m*M* PBS, lyophilized and tested by direct RAST, then further analysed by HPSEC.

Immunoabsorbent preparation for high-performance affinity chromatography

The purified immunoglobulin fraction from ascitic liquid was covalently coupled to a properly activated support using an Affi-prep 10 affinity cartridge (25 × 15 mm I.D. (Bio-Rad Labs., Segrate, Milan, Italy) according to the procedure recommended by the producer (Bulletin 1237).

High-performance affinity chromatography

The extract of *Parietaria judaica* (1 ml, protein content 0.8 mg/ml) was applied to the column which was eluted with 2 *M* sodium chloride in 0.15 *M* phosphate-buffered saline (PBS) (pH 7.2). The eluted fraction was dialysed against 10 m*M* PBS, lyophilized and tested with direct RAST, then further analysed by HPSEC.

Methanol extraction

A sample of 40 mg of gel-filtered *Parietaria judaica* extract was treated with 10 ml of methanol with stirring for 15 min at room temperature. The soluble fraction was then separated by centrifugation at 4200 *g* for 15 min. The solvent was evaporated at reduced pressure at room temperature and the residue was analysed by direct RAST, then analysed by HPSEC.

Radio-allergo-sorbent test (RAST)

The fractions were bound to cyanogen bromide-activated paper discs, and direct RAST or RAST inhibition was performed according to Yman *et al.* [16] using a pool of sera from 95 patients with high sensitivity to *Parietaria judaica* pollen and polystyrene beads as solid phase (Sferikit, Laboratorio Farmaceutico Lofarma, Milan, Italy).

For immunocapture RAST, the purified immunoglobulin fraction derived from ascite was bound to activated polystyrene beads, then used for a direct RAST.

RESULTS AND DISCUSSION

The HPIEC purification of the *Parietaria* extract could give better results if performed at different pH values and with different ionic strength gradients. These could act as better dissociating conditions for the homopolymerized allergen and allow the enrichment into the monomer to be optimized.

The first experiment was performed using a pH 7 buffer and a linear gradient of ionic strength from 250 to 500 m*M* sodium acetate, in order to have the maximum dissociating power of the eluent throughout the chromatography. The result is shown in Fig. 1a. Direct RAST analysis of all the fractions showed that the allergenic activity was spread over the chromatogram. IEF analysis of the fractions indicated that most components were eluted in the first part of the chromatogram. Fractions 23 and 25 had mainly a band at p*I* 4.5, which could correspond to the major allergenic protein of *Parietaria* pollen extract, *i.e.*, Par jI. Hence this chromatographic region was analysed by HPSEC.

The result from fraction 26 is shown in Fig. 2a and a RAST test using a monoclonal anti-Par jI antibody was performed. This showed that both the main peak in Fig. 2a and the peak at a 15.6-min elution time were allergens, suggesting that Par jI was eluted in the main peak (centred at about mol. wt. 11 000 dalton), and that in the minor peak a peptide of lower molecular weight that contained the allergenic determinant was eluted. This peak was analysed with a diode-array detector and showed a sharp absorption at 278 nm.

A further experiment was effected using a pH 5 buffer and a linear ionic strength gradient from 100 to 500 m*M* sodium acetate and the fractions were analysed by direct RAST. The result is shown in Fig. 1b. The individual fractions were analysed by HPSEC and most of these had the chromatographic profile shown in Fig. 2b for fraction 8. Also in this instance, RAST analysis was performed with the monoclonal anti-Par JI antibody. Again the major peak containing Par jI was accompanied by the peak at a 15.5-min elution time. Calibration of the column suggested an apparent molecular weight slightly higher than 5000 dalton which contained the allergenic determinant and absorbed at 278 nm. Diode-array detection showed that no contaminant was coeluted in this peak in most fractions. The experiments reported in Fig. 1a and b showed that a pH 5 mobile phase allowed fractions to be obtained from which this peptide could be recovered by purification using HPSEC.

These results suggested that the structure of the allergenic determinant in Par jI could be obtained by isolating peptides positive to the monoclonal anti-Par jI antibody, instead of isolating the very elusive Par jI itself.

Confirmation of these data was obtained submitting the *Parietaria* total extract

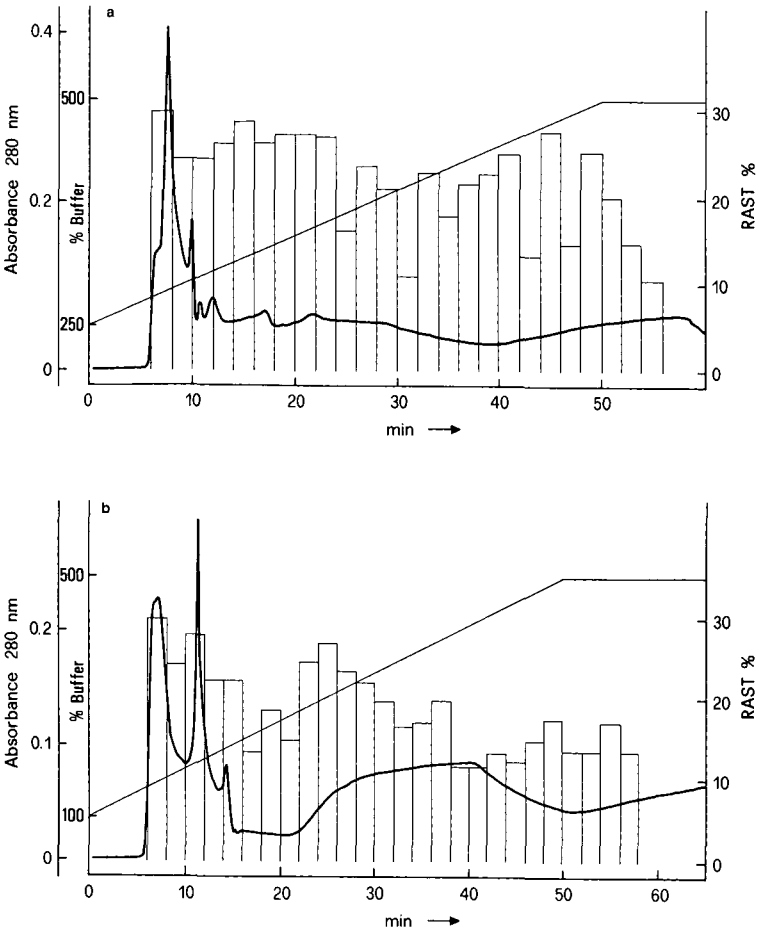

Fig. 1. Preparative HPIEC separation of *Parietaria* pollen extract and RAST analysis of the fractions. Column: DEAE-5PW. Ionic strength gradient: (a) 10 m*M* Tris–acetic acid buffer (pH 7.0)–250 m*M* sodium acetate (eluent A), 10 m*M* Tris–acetic acid buffer (pH 7.0) containing 500 m*M* sodium acetate (eluent B); (b) 10 m*M* Tris–acetic acid buffer (pH 5.0)–100 m*M* sodium acetate (eluent A), 10 m*M* Tris–acetic acid buffer (pH 7.0) containing 500 m*M* sodium acetate (eluent B). Flow-rate, 6 ml/min; 12-ml fractions were collected.

to immunoaffinity chromatography. In a first attempt, a monoclonal anti-Par jI antibody purified by ammonium sulphate precipitation was coupled to the stationary phase in conventional affinity chromatography. Elution with sodium chloride solution gave an eluate which was analysed by HPSEC. Several peaks appeared in the chromatographic region where Par jI was expected.

In order to improve the separation efficiency of the immunoaffinity approach, a further immunoaffinity chromatographic experiment was then performed using an HPLC column, and the same monoclonal anti-Par jI antibody was used. Elution with sodium chloride solution gave an eluate which was analysed by HPSEC. Several components were present in the eluate; these were collected, submitted to immuno-

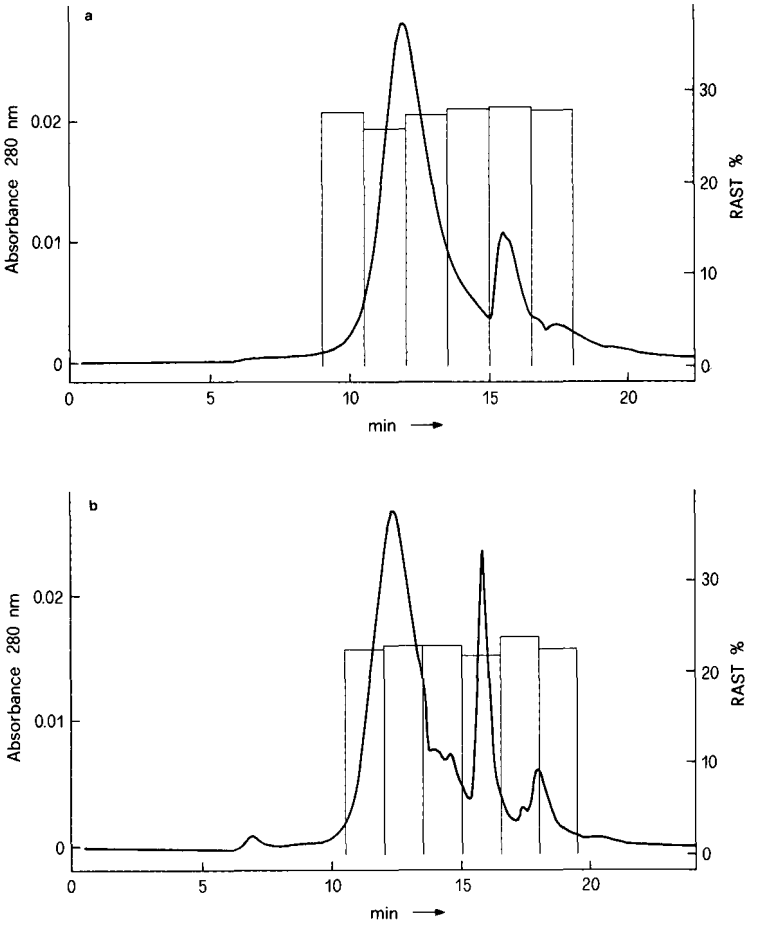

Fig. 2. (a) HPSEC analysis of fraction 26 from the run in Fig. 1a and RAST analysis of the fractions. (b) HPSEC analysis of fraction 8 from the run in Fig. 1b and RAST analysis of the fractions. Column, Synchropak 100; eluent, 0.15 *M* PBS (pH 6.8)–0.5 *M* KCl; flow-rate, 0.8 ml/min; 1.2-ml fractions were collected.

capture RAST and all the fractions were positive to RAST except one. Hence the allergenic determinant of Par jI was contained in a family of fragments.

Small peptides are sometimes extracted from complex proteic material by solvent extraction. Hence, some of these allergenic fragments could possibly be obtained by methanol extraction from the crude extract.

The gel-filtered extract of *Parietaria* pollen was extracted with methanol and centrifuged in order to eliminate the insoluble part of the extract. The solution obtained was analysed by HPSEC. The chromatogram showed a major peak at 18 min, which was positive in the RAST with monoclonal antibodies. Moreover, diode-array detection showed only a shoulder at 270 nm. The fractions containing this peak were further analysed using a reversed-phase C_{18} column with a 30-min linear gradient

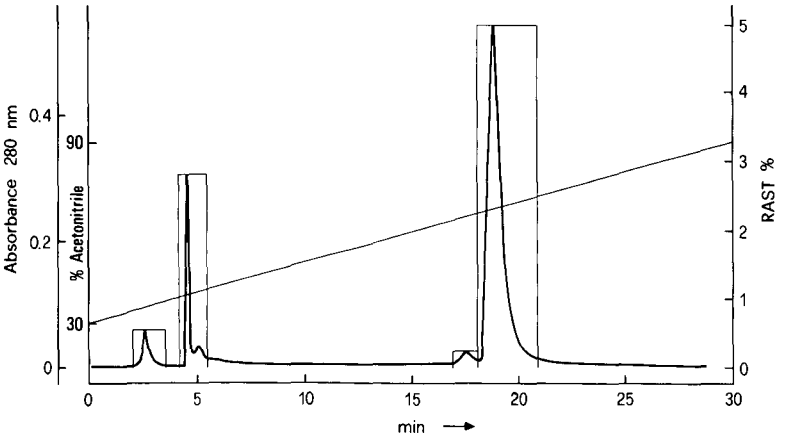

Fig. 3. RP-C_{18} HPLC analysis of the methanolic extract of *Parietaria* pollen and RAST analysis of the fractions. Column, Merck LiChrosorb RP-C_{18}; 30-min gradient from 0.1% aqueous TFA–acetonitrile (70:30) (eluent A) to 0.1% aqueous TFA–acetonitrile (10:90) (eluent B).

from 0.1% aqueous TFA–acetonitrile (70:30) to 0.1% aqueous TFA–acetonitrile (10:90). In this way we isolated the peak at a 20-min elution time, which was positive to the RAST test (Fig. 3). Diode-array detection of the peak showed a high purity.

In conclusion, these chromatographic experiments suggest that Par jI is a very unstable allergen, which tends to fragment when in solution. Several peptides were obtained from Par jI, and some of them show positivity toward the anti-Par jI monoclonal antibody, suggesting that they retain the entire structure of the allergenic determinant. These peptides could then be the target of further studies and the optimization of their isolation could lead to sufficient material for sequence and conformation studies.

ACKNOWLEDGEMENTS

We thank our students F. Farina and M. Odiardo for their collaboration. This work was supported by a CNR grant, Progetto Finalizzato Chimica Fine II, by the Danish Natural Science Research Council and the Danish Agricultural and Veterinary Research Council.

REFERENCES

1 P. Falagiani, E. Cavallone, M. Nali, B. Rindone, S. Tollari and G. Crespi, *J. Chromatogr.*, 328 (1985) 425.
2 E. Bolzacchini, G. Di Gregorio, M. Nali, B. Rindone, S. Tollari, P. Falagiani, G. Riva and G. Crespi, *J. Chromatogr.*, 397 (1987) 299.
3 N. Rubio and A. Brieva, *J. Chromatogr.*, 407 (1987) 408.
4 A. Giuliani, C. Pini, S. Bonini, N. Mucci, L. Ferroni and G. Vicari, *Allergy*, 42 (1987) 434.
5 E. Bolzacchini, G. Di Gregorio, M. Nali, B. Rindone, S. Tollari, P. Falagiani, G. Riva and G. Crespi, *Allergy*, 42 (1987) 743.

6 A. Bassoli, E. Bolzacchini, F. Chioccara, G. Di Gregorio, B. Rindone, S. Tollari, P. Falagiani and G. Riva, *J. Chromatogr.*, 446 (1988) 179.
7 A. Bassoli, F. Chioccara, G. Di Gregorio, B. Rindone, S. Tollari, P. Falagiani, G. Riva and E. Bolzacchini, *J. Chromatogr.*, 444 (1988) 209.
8 S. A. Ford, B. A. Baldo, D. Geraci and D. Bass, *Int. Arch. Allergy Appl. Immunol.*, 79 (1986) 120.
9 D. Geraci, K. B. Billesbolle, R. Cocchiara, R. Lowenstein and H. Ipsen, *Int. Arch. Allergy Appl. Immunol.*, 78 (1985) 421.
10 A. L. Corbi and J. Carreira, *Int. Arch. Allergy Appl. Immunol.*, 74 (1984) 318; 76 (1985) 156.
11 A. Ruffilli, U. Oreste, V. Santonastaso, A. Scotto D'Abusco, and G. Sacerdoti, *Mol. Immunol.*, 24 (1987) 305.
12 R. Cocchiara, G. Locorotondo, A. Parlato, G. Guarnotta, S. Ronchi, G. Albeggiani, S. Amoroso, P. Falagiani and D. Geraci, *Int. Arch. Allergy Appl. Immunol.*, 90, (1989) 84.
13 I. Sondergaard, P. Falagiani, E. Bolzacchini, P. Civaroli, G. Di Gregorio, V. Madonini, A. Morelli and B. Rindone, *J. Chromatogr.*, 512 (1990) 115.
14 R. E. Esch and D. G. Kappler, *J. Immunol.*, 142 (1989) 179.
15 S. Feo, R. Cocchiara and D. Geraci, *Mol. Immunol.* 21 (1984) 25.
16 L. Yman, G. Ponterius and R. Brand, *Dev. Biol. Stand.*, 29 (1975) 1551.

Journal of Chromatography, 542 (1991) 345–350
Elsevier Science Publishers B.V., Amsterdam

CHROM. 23 077

Electrochemical detection of oligopeptides through the precolumn formation of biuret complexes

HWEIYAN TSAI and STEPHEN G. WEBER*
Chevron Science Center, Department of Chemistry, University of Pittsburgh, Pittsburgh, PA 15260 (U.S.A.)
(First received August 1st, 1990; revised manuscript received November 27th, 1990)

ABSTRACT

The relatively slow kinetics of formation of the electroactive Cu(II)–peptide complexes from larger (>6 amino acids) peptides requires relatively high temperature and long reaction times for a postcolumn reactor. The precolumn incubation of bradykinin, Tyr^8-bradykinin and insulin A chain with biuret reagent for 20 min at 60°C leads to the formation of biuret complexes which can be subjected to chromatography in acidic or basic eluents. These complexes are detected electrochemically with a sensitivity similar to the Cu(II)–$(ala)_3$ complex (1 nC/pmol at 1.0 ml/min). The influence of the column-packing material on the electrochemical detector response of the Cu–peptide complexes has also been studied.

INTRODUCTION

Reaction detection in liquid chromatography [1] has been used to increase detection sensitivity by the introduction of suitable chromophores or fluorophores, and to increase detection selectivity by using specific reactions. While certainly less convenient than detection by means of the native property of a compound, the gain in detection limit, sensitivity or selectivity is often substantial.

Recently, we [2,3] have introduced a method for the detection of peptides following their liquid chromatographic separation. The postcolumn reaction is the biuret reaction [4] which has been employed in an absorbance scheme for detection [5]. The poor detection limits in the latter technique do not recommend it for trace determinations. However, the electrochemical approach yields detection limits for small peptides (3–6 amino acids) of around 0.2 pmol in a 20-μl injection into a 15 cm × 4.6 mm I.D. reversed-phase column [2] (10 n*M*).

The detection system is based on the formation of Cu(II)–peptide complexes in the classical biuret reaction. The chemistry of Cu(II)–tripeptide complexes has recently been studied in great detail in a series of papers by Margerum [6] who showed in particular that these coordination compounds are easily oxidized to the Cu(III) form. Dual-electrode electrochemical detection can be used because the biuret electrochemistry is reversible. The first electrode in the series of two electrodes acts as an anode, or generator, by oxidizing the solutes passing by it in the flowing stream. The second electrode acts as a cathode or collector, reducing the products of the first electrode that are carried across its surface by the flow stream.

0021-9673/91/$03.50

We reported previously [2] that a tetradecapeptide, fibrinopeptide A, was about 100-fold less sensitively detected than a model tripeptide, A_3. This note demonstrates that precolumn formation of the complex leads to sensitivity equal to or better than the model compound for three larger peptides.

EXPERIMENTAL

The measurements were carried out on an apparatus consisting of two Waters M45 pumps, a Rheodyne 7125 injection valve with a 20-μl sample loop, a BAS detection cell with a dual glassy carbon electrode, a BAS LC-4B amperometric detector and a BBC Goerz dual channel recorder. A stainless-steel auxiliary electrode and a silver–silver chloride reference electrode (purchased from BAS) were used. With no chromatographic column, this is a flow-injection system. C_{18} columns (15 cm long, Waters Nova-Pak) and ZrO_2-polybutadiene (PBD) columns (a kind gift from Professor P. W. Carr, University of Minnesota) were also used. Control over postcolumn reactor temperature was by placement of knotted PTFE tubing into a BAS column heater.

Optical absorbance measurements were carried out with an IBM Model 9420 UV–visible spectrophotometer equipped with a cell holder, the temperature of which could be controlled with a recirculating bath (Haake). Reagents were brought to the appropriate temperature before mixing and spectrophotometric observation.

The following reagents were used without further purification: potassium phosphate monobasic and dibasic GR crystals, acetonitrile (HPLC grade), and phosphoric acid (E.M. Science, Cherry Hill, NJ, U.S.A.), sodium carbonate anhydrous and sodium bicarbonate (Fisher Scientific, Pittsburgh, PA, U.S.A.), sodium hydroxide pellets (J.T. Baker, Phillipsburgh, NJ, U.S.A.). All peptides were purchased from Sigma (St. Louis, MO, U.S.A.). Potassium sodium tartrate (Aldrich, Milwaukee, WI, U.S.A.) was recrystallized from water before use. Water was doubly deionized and passed through an activated carbon column before distillation in a Corning system. All the solutions were filtered through nylon-66 filters (pore size 0.2 μm, purchased from Rainin, Woburn, MA, U.S.A.) before use.

Aqueous peptide solutions containing 4 nmol in a 20-μl injection were injected for the postcolumn experiment; 0.2–0.4 nmol of the Cu–peptide complexes were injected in the precolumn reaction system.

RESULTS AND DISCUSSION

Temperature and biuret reaction time effects

We reason that the lower sensitivity to the larger peptide is kinetic in origin. The visible absorbance from the biuret complex measured *vs.* time at 20.8°C shows that bradykinin (nonapeptide) requires at least 2 min for complete reaction (Fig. 1). Fig. 2 shows that increasing the postcolumn reaction time from 0.1 to 0.7 min and increasing the temperature of the reactor up to 70°C increases the sensitivity of the system to bradykinin, but only by a factor of at most five (up to 0.1 nC/pmol). This still leaves one order of magnitude to be gained compared to smaller peptides like A_3 (typical sensitivity 1.0 nC/pmol). The reaction time was increased by using longer knotted PTFE tubing (0.01 in. I.D.) after the mixing "T". It is unlikely that the

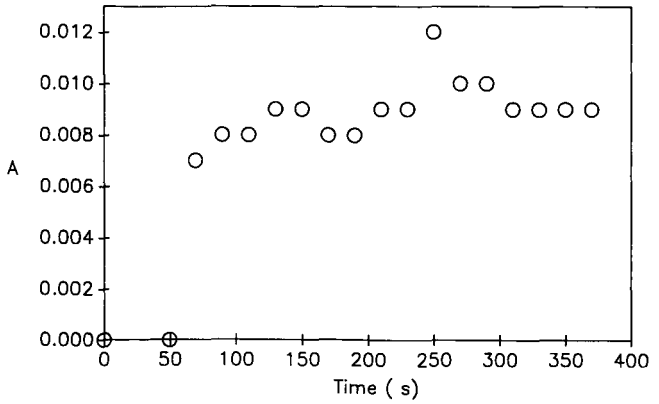

Fig. 1. Color development of bradykinin–Cu reaction *vs.* time. Concentrations are 0.1 m*M* bradykinin, 0.7 m*M* Cu^{2+}, 4.2 m*M* tartrate, pH 10.0 ± 0.1, wavelength set at 530 nm.

reaction solution heated up from room temperature to 70°C in 0.1 min, so the temperatures shown here must be regarded as those of the column heater, not measured reaction temperatures. Even so, it is evident that dramatic increases in reaction time would be required to obtain a sensitivity equivalent to A_3 for the larger oligopeptides.

An alternate approach is to use precolumn reaction. The incubation of peptides (bradykinin, Tyr^8-bradykinin, insulin A chain) with biuret reagent for 20 min at 60°C leads to the formation of the complex. These complexes yield good sensitivity in a flow-injection experiment (Table I). The eluent contained 1.0 m*M* Cu^{2+}, 3.0 m*M*

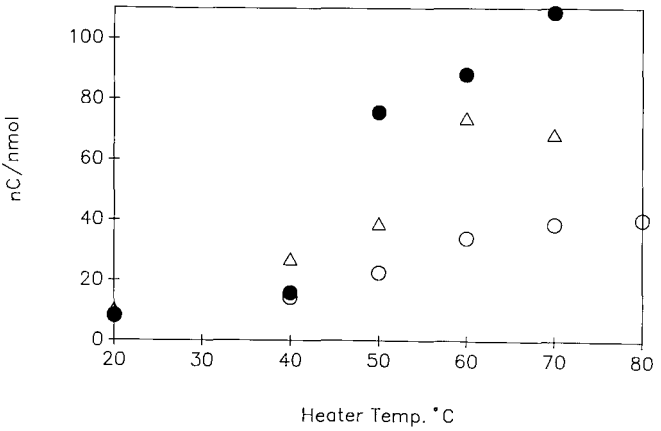

Fig. 2. Temperature and biuret reaction time effects on the electrochemical detector response of bradykinin–Cu complex. Postcolumn biuret reaction time: 0.1 min (○), 0.6 min (△), 0.7 min (●). Chromatographic conditions: column, Waters Nova-Pak C_{18}; mobile phase, 0.1% trifluoroacetic acid in acetonitrile–H_2O (3:7); postcolumn reagent, 0.25 *M* $NaHCO_3$, 0.25 *M* Na_2CO_3, 0.1 m*M* Cu^{2+}, 2.0 m*M* tartrate. Mobile phase: postcolumn reagent ratio is 60:40, flow-rate is 2.0 ml/min. Anodic potential is 0.80 V *vs.* Ag/AgCl in 3 *M* NaCl reference electrode.

TABLE I

ANODIC SENSITIVITIES (nC/pmol) *VS.* POTENTIAL

Data from flow injection. The eluent contains 1.0 m*M* Cu^{2+}, 3.0 m*M* KNa tartrate, 0.10 *M* Na_2CO_3 and 0.02 *M* $NaHCO_3$. The pH is 10.5 ± 0.1 and the flow-rate is 1.0 ml/min. The peptides were prepared in the eluent and incubated for 20 min at 60°C.

Peptide	Potential (V *vs.* Ag/AgCl in 3 *M* NaCl)			
	0.5	0.6	0.7	0.8
Bradykinin	0.17	0.66	3.70	6.14
Tyr^8-bradykinin	0.10	1.08	1.82	2.28
Insulin A chain	0.08	0.21	0.41	0.54

KNa tartrate, 0.10 *M* Na_2CO_3 and 0.02 *M* $NaHCO_3$. The pH was 10.5 ± 0.1 and the flow-rate was 1.0 ml/min. Note that the sensitivities of bradykinin and Tyr^8-bradykinin are greater than for the A_3 (*ca.* 1.0 nC/pmol at 0.80 V) implying that more than one copper binds to each molecule of these peptides. Signals at the cathode for bradykinin and insulin A chain are in the range of 20% of those at the anode just as for the smaller peptides [2]. It is somewhat lower, *ca.* 10%, for Tyr^8-bradykinin.

Column packing material effects

Fig. 3 shows sensitivity for bradykinin in three systems. Two of the sets of data are from injection of the biuret complex of bradykinin into a flowing stream of basic copper tartrate; one is flow injection while the other is chromatography on the PBD

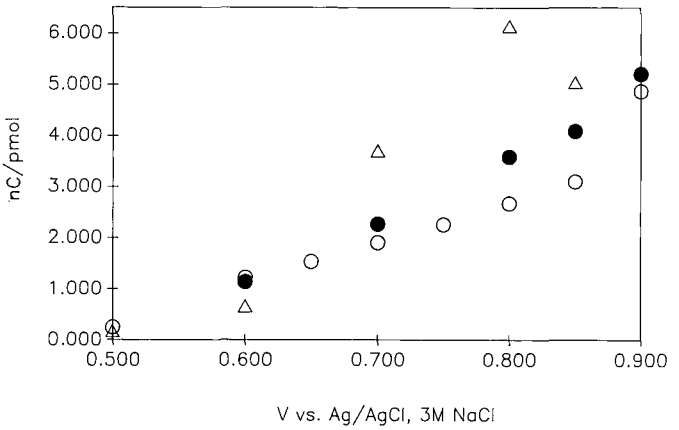

Fig. 3. Hydrodynamic voltammograms for bradykinin. Chromatographic conditions: (○) PBD column, eluent containing 1.0 m*M* Cu^{2+}, 3.0 m*M* KNa tartrate, 50 m*M* Na_2HPO_4, 0.1 *M* NaOH is added for adjusting the pH to 10.5 ± 0.1. Flow-rate is 1.0 ml/min. (△) Flow injection (*i.e.*, no column), eluent containing 1.0 m*M* Cu^{2+}, 3.0 m*M* tartrate, 0.10 *M* Na_2CO_3 and 0.02 *M* $NaHCO_3$, pH is 10.5 ± 0.1, flow-rate is 1.0 ml/min. (●) Waters Nova-Pak C_{18} column; mobile phase is 25 m*M* KH_2PO_4, 2 g/l H_3PO_4 in acetonitrile–water (6:94); postcolumn reagent is the same as the eluent for the flow injection. Flow-rate is 2.0 ml/min; mobile phase, postcolumn reagent ratio is 1:1. Note: the sensitivities have been corrected for the postcolumn reagent dilution factor.

column which is stable to base [7]. The third set of data is for chromatography on a C_{18} phase with an acidic mobile phase (pH 2.5 phosphate buffer–acetonitrile, 94:6) followed by the introduction of basic copper tartrate after the column as before. There is no electrochemical response if the basic copper tartrate is not introduced after the column. Signals at the cathode resulting from upstream oxidation at 0.6–0.7 V are in the range of 20–30% of those at the anode, just as for the smaller peptides.

The sensitivities for the two chromatographic experiments are equivalent. This indicates that the complex is kinetically stable in acid, and it can survive the chromatographic step. Thus, although the chromatography will be different than the chromatography of native peptides, the practitioner has the choice of whether to use C_{18} columns with an acidic eluent, or a base-stable column with a basic eluent. A chromatogram of bradykinin and Tyr^8-bradykinin copper complexes on the C_{18} column is shown in Fig. 4; the top trace is the response of the cathode and the bottom one is the response of the anode.

Two other points have been noted. The PBD column caused fouling. Table II shows the effect of the PBD column on the response of the electrochemical detector to the Cu–peptide complexes. Column A in Table II has the data from flow injection; the eluent was 1.0 m*M* Cu^{2+}, 3.0 m*M* KNa tartrate, 50 m*M* Na_2HPO_4, and NaOH was added for adjusting the pH to 10.5 $\pm$ 0.1; the flow-rate was 1.0 ml/min. Column B has the data from flow injection with the PBD column before the injector. The last column (C) has the data from chromatography with the PBD column. The sensitivity was lower even when the column was not used for chromatography (B). Also, the

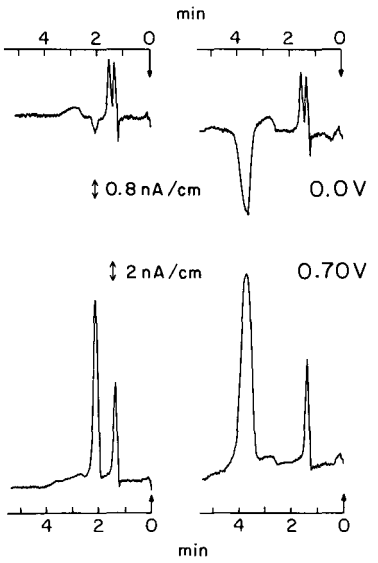

Fig. 4. Chromatogram of bradykinin– and Tyr^8-bradykinin–copper complexes. To the right: 0.48 nmol bradykinin–copper complex; to the left: 0.42 nmol Tyr^8-bradykinin–copper complex. Chromatographic conditions: mobile phase, 25 m*M* KH_2PO_4, 2 g/l H_3PO_4 in acetonitrile–water (6:94, v/v), postcolumn reagent, 1.0 m*M* Cu^{2+}, 3.0 m*M* tartrate, 0.10 *M* Na_2CO_3 and 0.02 *M* $NaHCO_3$. Flow-rate is 2.0 ml/min; mobile phase, post column reagent ratio is 1:1. The peptides were incubated in the post column reagent for 20 min at 60°C before being injected into the chromatography system.

TABLE II

Cu–peptide complex	Anodic sensitivity at 0.8 V (nC/pmol)		
	A	B	C
Bradykinin	6.3	4.7	2.9
Tyr^8-bradykinin	1.4	1.1	0.53
Insulin A chain	0.53	0.21	0.12

drawn-out shape of the voltammetry with the PBD column should be compared to the voltammetry in flow-injection analysis (Fig. 3). This indicates electrode fouling by the column. The electrode fouling problem has been noted before when using C_{18} columns [2], and it is lessened by operating at pH $\gtrsim$ 10. However, it is even less of a problem in flow injection than in chromatography, so we speculate that the columns are responsible for this. The other point to note is that the tyrosine-containing peptide, Tyr^8-bradykinin, has a lower collection efficiency than bradykinin, and insulin A chain has a lower sensitivity. Recently, we have begun to study the influence of an electroactive functional group on the electrochemical detector response to the Cu–peptide complexes. These results will be reported in due course.

It is thermodynamically feasible that the Cu(II)–peptide complexes can be oxidized by oxygen. The following casual observations suggest that the oxidation is slow, and therefore not a problem. The Cu(II)–tripeptide complexes are stable for at least several months. The Cu(II)–bradykinin complex in the biuret reagent containing Na_2HPO_4 buffer is still purple after 7 months. On the other hand, the purple color of a Cu(II)–polylysine complex disappeared after 20 days.

ACKNOWLEDGEMENTS

The donation of the column heater by BAS is gratefully acknowledged. Partial support of this work through the National Institute of General Medical Sciences, Grant GM28112, is also gratefully acknowledged.

REFERENCES

1 I. S. Krull (Editor), *Reaction Detection in Liquid Chromatography*, Marcel Dekker, New York, Basel, 1986.
2 A. M. Warner and S. G. Weber, *Anal. Chem.*, 61 (1989) 2664.
3 H. Tsai and S. G. Weber, *J. Chromatogr.*, 515 (1990) 451.
4 A. G. Gornall, J. Bardawill and M. David, *J. Biol. Chem.*, 177 (1949) 751.
5 T. Schlabach, *Anal. Biochem.*, 139 (1984) 309.
6 D. W. Margerum, *Pure Appl. Chem.*, 55 (1983) 23.
7 M. P. Rigney, T. P. Weber and P. W. Carr, *J. Chromatogr.*, 484 (1989) 273.

Journal of Chromatography, 542 (1991) 351–363
Elsevier Science Publishers B.V., Amsterdam

CHROM. 23 060

Factors influencing the retention of rare earth–tetraphenylporphine complexes in reversed-phase high-performance liquid chromatography

KOICHI SAITOH, YOSHIHIKO SHIBATA and NOBUO SUZUKI*
Department of Chemistry, Faculty of Science, Tohoku University, Sendai, Miyagi 980 (Japan)
(First received July 23rd, 1990; revised manuscript received December 13th, 1990)

ABSTRACT

The high-performance liquid chromatographic (HPLC) retention behaviour of the complexes of tetraphenylporphine (TPP) with twelve rare earths (REs), *viz.*, Y(III), Nd(III), Sm(III), Eu(III), Gd(III), Tb(III), Dy(III), Ho(III), Er(III), Tm(III), Yb(III) and Lu(III), on an octadecyl-bonded silica gel column is described. All these metal complexes can be chromatographed without undesirable demetallation in their migration process along the column with a methanol–water mixture containing a small amount of acetylacetone and an amine. The elution sequence for the RE complexes depends on the amine added to the mobile phase. With trialkylamines and dialkylamines possessing branched alkyl structures, the capacity factors of the RE–TPP complexes increase monotonously in the order of increasing atomic number of the REs. With di-*n*-alkylamines, the capacity factor tends to decrease in the order of increasing atomic number of the REs for light to moderate lanthanides, whereas the reverse tendency occurs for the complexes of heavier lanthanides. In all instances, the capacity factor of the Y(III) complex lies between those of the Dy(III) and Ho(III) complexes. The effects of the amine are discussed in terms of the adduct complex formation of RE–TPP with the amine. Successful separation of the Nd, Gd, Tb, Dy, Ho, Er and Lu complexes in 15 min using triethylamine is demonstrated.

INTRODUCTION

In recent years, there has been increased interest in the separation of metalloporphyrins. Some metalloporphyrins are used for biomedical diagnosis of diseases or as therapeutic agents [1,2]. The metalloporphyrins found in petroleum have been important for the characterization and processing of the petroleum [3]. Highly sensitive spectrophotometric determination has been successful for some trace metal ions as their porphyrin complexes [4]. Various non-chromatographic methods such as electrophoresis, extraction, precipitation and sublimation have been useful for the separation of metalloporphyrins and also metal-free porphyrins [5]. However, high-performance liquid chromatography (HPLC) is the most powerful candidate for the separation for these compounds today, because of its wide applicability to compounds in solution state, the flexibility in the choice of separation modes and conditions and the facility for on-line combination with various detectors and spectrometers. In most HPLC studies on the separation of porphyrins and/or metalloporphyrins, the reversed-phase mode has been employed successfully.

0021-9673/91/$03.50

There are two types of HPLC separation of metalloporphyrins: the separation of different porphyrin complexes of a certain metal and the separation of metalloporphyrins with respect to their central metal ions. The HPLC of the vanadium and/or nickel porphyrins in petroleum samples is an example of the former type of separation [6–8]. The latter type of HPLC separations has been difficult, because each metal ion is surrounded by a bulky macrocyclic porphyrin structure to which various organic functional groups are further bonded. The difficulty in the separation of metalloporphyrins increases with an increase in the chemical similarity of the central metal ions. The HPLC separation of metalloporphyrins has been investigated on the Ni(II), Cu(II) and Pd(II) complexes of porphine (the compound with the simplest porphyrin stucture [9], the Fe(III), Co(II), Cu(II) and Zn(II) complexes of meso- and protoporphyrins [10], Ni(II), Cu(II) and Zn(II) haematoporphyrins [11] and the Mg(II), V(IV), Ni(II), Cu(II), Zn(II) and Pd(II) complexes of tetraphenyl- [12] and tetrakis(*p*-tolyl)porphines [13].

This paper deals with the reversed-phase HPLC retention behaviour of the porphyrin complexes of rare earth (RE) metals. About 100 papers have dealt with RE complexes of porphyrins, mostly in the last decade. However, no HPLC study of RE porphyrins has been reported, although classical alumina column chromatography has been briefly reported for the preparation of RE porphyrin complexes [14]. RE(III) porphyrin complexes are considerably less stable than those of other metals, *e.g.*, Fe(II), Fe(III), Ni(II) and Cu(II), owing to the large ionic radii of the RE(III) ions (larger than 100 pm at coordination number >6) compared with the best fit (64 pm) for the hole in the N-4 moiety of porphyrin [15]. The suppression of undesirable demetallation of the complexes in the chromatographic process is the prime requisite for the successful LC separation of RE–porphyrins. It was previously found that RE(III) complexes of tetraphenylporphine (TPP) could be successfully developed without demetallation of the complexes on an octadecyl-bonded silica thin-layer chromatographic plate with a developing solvent containing both acetylacetone and diethylamine [16].

This work was undertaken to examine the feasibility of reversed-phase HPLC for the separation of the porphyrin complexes of RE(III) metals, which have very similar chemical properties. The retention behaviour of twelve RE(III)–TPP complexes was investigated on an octadecyl-bonded silica gel column with mobile phases containing different amines.

EXPERIMENTAL

Materials

The preparation of the free acid form of TPP (H_2tpp) and its complexes with RE(III) (RE = Y, Nd, Sm, Eu, Gd, Tb, Dy, Ho, Er, Tm, Yb, Lu) was described previously [16]. The RE complexes thus prepared were in the mixed-ligand forms with tetradentate tpp and bidentate acetylacetonato (acac) anions, RE(tpp) (acac), with the structure illustrated in Fig. 1 [17,18]. The term RE–TPP hereafter refers to this mixed-ligand complex, unless indicated otherwise.

Acetylacetone (Hacac), diethylamine (DEA), dipropylamine (DPA), diisopropylamine (DIPA), dibutylamine (DBA), dihexylamine (DHA), triethylamine (TEA), tripropylamine (TPA), tributylamine (TBA), piperidine (pip), 2,6-dimethyl-

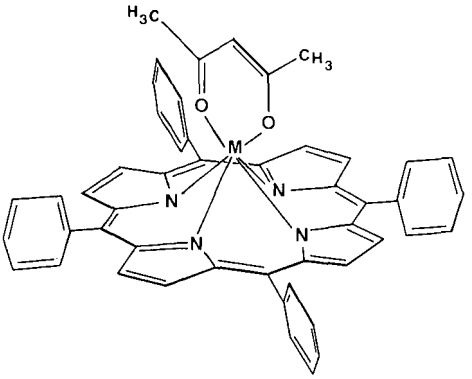

Fig. 1. Structural formula of an RE–TPP complex. M indicates the RE(III) ion.

piperidine (DMpip), dichloromethane and sodium hydroxide (NaOH) were of guaranteed reagent grade (Wako, Osaka, Japan). Methanol and water were distilled in glass.

HPLC

A Twincle solvent-delivery pump, a Model VL-611 sample-injection valve (Jasco, Tokyo, Japan) and a Model SPD-M6A photodiode-array UV–visible spectrophotometric detector (Shimadzu, Kyoto, Japan) were assembled into a liquid chromatographic system. The column (Model TSK ODS-80TM) packed with octadecyl-bonded silica gel (particle diameter 5 μm) in a 150 mm × 4.6 mm I.D. stainless-steel tube was obtained from Tosoh (Tokyo, Japan).

The mobile phase was prepared, unless indicated otherwise, by addition of an amine to methanol–water–Hacac (95:5:1, v/v/v) so that the amine was of equimolar concentration with respect to Hacac in the final solution (about 0.1 *M*). The flow-rate of the mobile phase was 1.0 ml/min.

A sample solution of each RE–TPP complex was prepared at a concentration about 0.1 m*M* in dichloromethane containing DEA (2%, v/v), and 10 μl or less of the solution were injected into the column. The chromatograms were recorded using the so-called three-dimensional mode (absorbance *versus* wavelength *versus* time) in the visible region and also the conventional fixed-wavelength mode at 555 nm. All experiments were carried out at 25 ± 1°C.

RESULTS AND DISCUSSION

Sample solutions

Some RE–TPP complexes, particularly of Nd(III), Sm(III) and Eu(III), were so unstable in common solvents such as methanol, acetone, acetonitrile, benzene and dichloromethane that demetallation of the complexes occurred within 1 h after the preparation of the solutions (at about the 0.1 m*M* level). These complexes were stabilized by addition of a small amount of an amine, such as DEA, to the solutions [16]. In this work, the solution of an RE–TPP complex to be applied to HPLC was prepared in dichloromethane–DEA (50:1, v/v).

Capacity factors of RE–TPP complexes

All RE–TPP complexes could be eluted without undesirable tailing by using a mobile phase containing both Hacac and an amine, which implied that no demetallation or irreversible adsorption of injected complexes occurred in the migration process along the column. The possibility of ligand-exchange reactions occurring between the injected complexes and the metal components of the HPLC system is generally taken into account in the HPLC of metal complexes. In this work, it was confirmed by means of real-time photodiode-array spectrophotometric monitoring of the UV–visible absorption profile of the eluate that such a ligand-exchange reaction did not occur to any extent that could be detected.

For calculation of the capacity factor (k') of an RE–TPP complex, sodium nitrate was used as an unretained reference substance. The k' value was determined from triplicate measurements in each instance with a relative standard deviation of less than 1%.

Effect of the composition of the mobile phase

In each instance, the mobile phase consisted of methanol–water as the principal solvent, to which Hacac and amine were added as modifiers. The capacity factor of each RE–TPP complex increases with increase in the water content of the mobile phase, as illustrated in Fig. 2 as an example, which shows the result with a mobile phase containing DEA. The effect of the water content on the capacity factor of such a metal complex is consistent with general retention trends for non-electrolytes in reversed-phase liquid chromatography.

The free ligand, H_2TPP, showed such a large retention that it could not be eluted in a short time (about 20 min, for example) with a water-containing mobile phase.

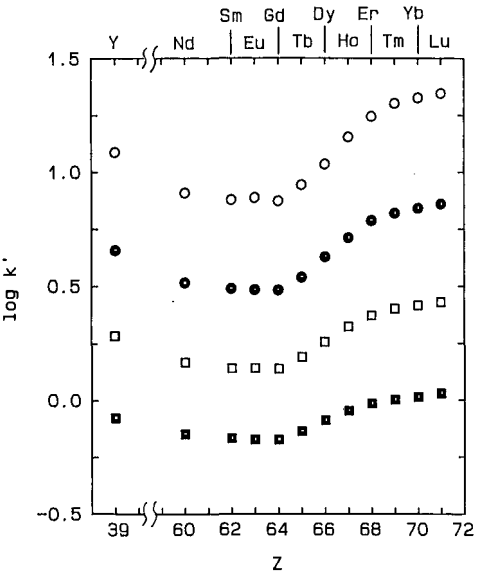

Fig. 2. Retention of RE–TPP complexes. Mobile phase system, methanol–water–Hacac–DEA: ○ = 85:15:1:1; ● = 90:10:1:1; □ = 95:5:1:1; ■ = 100:0:1:1 (v/v).

Even with water-free mobile phases, the k' values of H_2TPP were more than eight times as large as those of RE–TPP complexes. The retention data for H_2TPP are omitted from this paper.

The variation in the water content caused little change in the retention sequence of the RE–TPP complexes. The water-to-methanol ratio in the mobile phase was fixed hereafter at 5:95 (v/v) unless noted otherwise.

In the mobile phase system containing trialkylamines, such as TEA, TPA and TBA, the capacity factor of RE–TPP increased with increasing atomic number (Z) of the RE within the lanthanide series, as shown in Fig. 3. The capacity factor of the Y(III) complex was found to be between those of the Ho(III) and Dy(III) complexes.

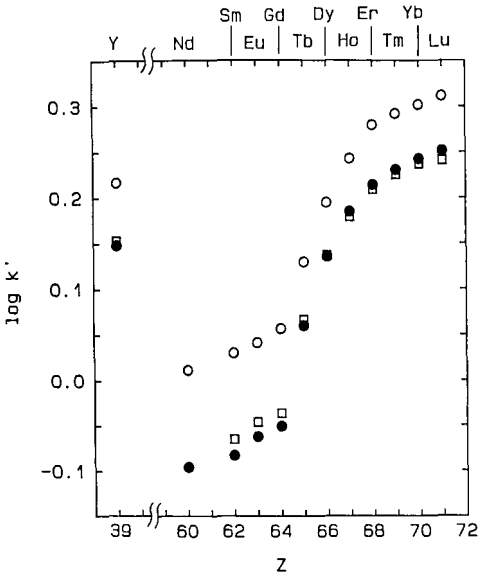

Fig. 3. Relationship between the retention of RE–TPP complexes and the atomic number (Z) of RE. Mobile phase: ○ = methanol–water–Hacac–TEA (95:5:1:1.3, v/v); ● = methanol–water–Hacac–TPA (95:5:1:1.8, v/v); □ = methanol–water–Hacac–TBA (95:5:1:2.3, v/v).

When dialkylamines such as DPA, DBA and DHA were used as the mobile phase additives, the retention of the RE–TPP complex varied with the Z of the RE, as shown in Fig. 4. The results with DEA are shown in Fig. 2. Among the complexes of relatively light lanthanides, the capacity factor tends to decrease in the order of the Z of the RE, whereas the reverse trend, which is similar to the results obtained with trialkylamines, is found for the complexes of heavy lanthanides. Minimum retentions are found for the Gd(III), Tb(III) and Ho(III) complexes when using DEA, DPA, DBA and DHA as the mobile phase additives, respectively. The k' value of the Y(III) complex is found to be between those of the Dy(III) and Ho(III) complexes, which is similar to the results obtained with trialkylamines.

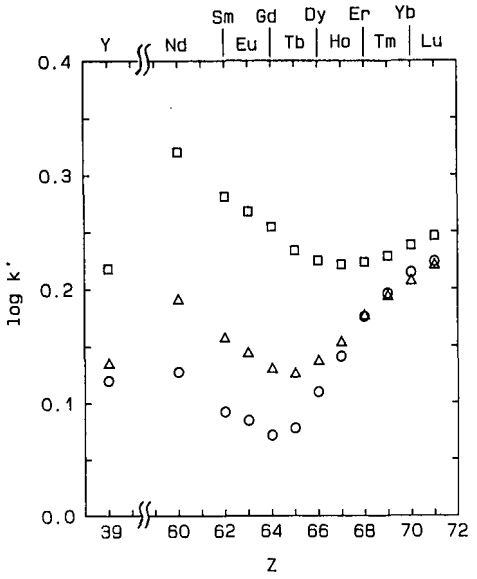

Fig. 4. Relationship between the retention of RE–TPP complexes and the atomic number (Z) of RE. Mobile phase: ○ = methanol–water–Hacac–DPA (95:5:1:1.3, v/v); △ = methanol–water–Hacac–DBA (95:5:1:1.6, v/v); □ = methanol–water–Hacac–DHA (95:5:1:2.3, v/v).

Functions of the mobile phase additives

In order to examine the necessity for the addition of Hacac and an amine to the mobile phase, the elution of RE–TPP complexes was attempted with pure methanol. In each instance neither RE–TPP nor H_2tpp (the metal-free form of TPP) was eluted from the column. If demetallation of the metal complex had occurred in the column process, H_2TPP should be detected in the eluate under this mobile phase condition.

It has been reported that the TPP complexes of trivalent metals (M), such as Mn(tpp)Cl and Co(tpp)Cl, showed a large retention in reversed-phase HPLC using ethanol as the mobile phase, whereas the retention was reduced considerably on addition of a salt to the mobile phase [19]. This phenomenon was explained in terms of the dissociation of Cl^- from the initial form of the complex, M(tpp)Cl, followed by adsorption of the positively charged form, $[M(tpp)]^+$, on an ion-exchangeable site (presumably a silanol group) existing on the surface of the octadecyl-bonded material packed in the column.

In this work, the complexes in the form RE(tpp)(acac) were injected onto the column. When the dissociation of the anionic ligand, $acac^-$, from the initial form of an RE–TPP complex occurred in the mobile phase, a large retention of the RE complex was probable owing to the adsorption of the cationic form $[RE(tpp)]^+$ on the active site located on the surface of the column packing material. Increasing of the concentration of the $acac^-$ anion in the mobile phase was a reasonable way to reduce the anomalous retention of the RE–TPP complexes caused by the dissociative reaction:

$$RE(tpp)(acac) \rightleftharpoons [RE(tpp)]^+ + acac^-$$

In practice, the RE–TPP complexes other than Er–, Tm–, Yb– and Lu–TPP were not eluted with an Hacac-containing mobile phase [typically, methanol–water–Hacac (95:5:1, v/v/v)], but were eluted successfully with a mobile phase containing an amine such as TEA together with Hacac. It is considered that the amine functioned as a base which promoted the dissociation of weakly acidic Hacac and effectively increased the $acac^-$ concentration in the mobile phase. All amines used in this work were found to be effective as basic mobile phase additives for the elution of RE–TPP complexes.

According to the above argument, it was expected that all RE–TPP complexes would be eluted successfully by using a simple inorganic base such as NaOH in place of an amine. In practice, NaOH was added to methanol–water–Hacac (95:5:1, v/v/v) so as to be approximately half the equimolar concentration with respect to Hacac in the final composition of the mixture in order to avoid damaging the column. When using this base, the capacity factors of the RE–TPP complexes increased in the order of the atomic numbers of the REs within the lanthanide series as shown in Fig. 5, which was the same retention trend as those found with trialkylamines (Fig. 3) but different from those with dialkylamines (Fig. 4).

Usually, RE(III) is able to have coordination numbers (CN) larger than 6 [20]. In an RE–TPP complex, the coordination sphere of the RE(III) ion is not necessarily saturated by tetradentate tpp and bidentate acac in the mobile phase. The possibility of coordination with additional ligands in the mobile phase, such as water, methanol and amine, is taken into account. Amines have stronger Lewis basic characteristics than water and methanol, and they have hydrophobic alkyl moieties in their molecules. When the coordination of an amine to the RE atom in RE(tpp)(acac) occurs in an amine-containing mobile phase, the retention of the RE–TPP complex may be different to that observed without the amine. It was observed that the retention

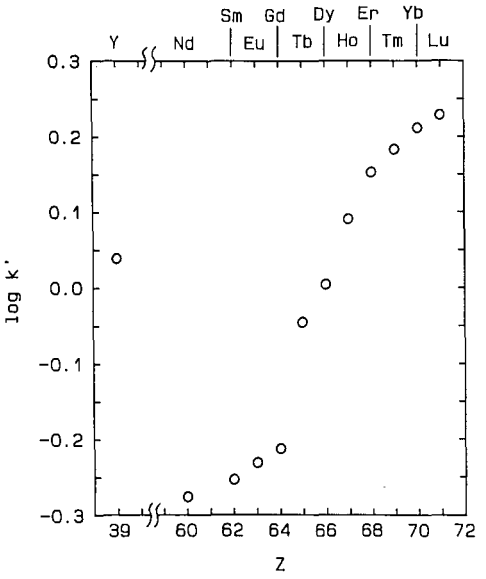

Fig. 5. Relationship between the retention of RE–TPP complexes and the atomic number (Z) of RE. Mobile phase: 0.045 M NaOH in methanol–water–Hacac (95:5:1, v/v/v).

sequences for the RE–TPP complexes obtained with the mobile phases containing dialkylamines (Fig. 4) were different from those obtained with NaOH instead of an amine (Fig. 5), whereas no clear difference was found among the retention sequences observed with trialkylamines (Fig. 3) and NaOH.

The visible absorption spectrum of a metal–TPP complex is affected by additional coordination of a neutral ligand to the central metal of the complex [21,22]. In this work, in order to examine whether they depended on the mobile phase additives, such as amines and NaOH, the visible spectra of RE–TPP complexes in various mobile phases were recorded by using the photodiode-array detector placed at the column outlet. The spectra recorded for every complex in the mobile phases containing trialkylamines, such as TEA, TPA and TBA, were almost same not only as each other but also as the spectrum recorded with the NaOH-containing mobile phase. The results obtained with mobile phases containing dialkylamines, such as DEA, DPA, DBA and DHA, were complicated, as follows. For the complexes of light REs, such as Nd, Sm, Eu, Gd, Tb, Dy and Y, the spectra recorded in an amine-containing mobile phase were different from those in the NaOH-containing mobile phase. However, for the complexes of heavy REs, such as Ho, Er, Tm, Tb and Lu, the spectra of the complexes were independent of the amine used and the same as those recorded in the NaOH-containing mobile phase, which was similar to the results found with trialkylamine-containing mobile phases.

The visible spectra of the TPP complexes of typical light and heavy REs in mobile phases containing different basic additives are compared in Fig. 6(a) and (b).

According to these results, it is considered that the trialkylamines coordinate to the central metals of RE–TPP complexes with low stability, and that the additional coordination of dialkylamines to the metal is considerable in the TPP complexes of relatively light lanthanides between Nd and Dy and also Y, whereas such coordination is negligible with heavy lanthanides from Ho to Lu.

Effects of the central metal

The central metal atom in a solid RE–TPP complex is displaced considerably from the porphyrin plane towards the extra-ligand acac; the estimated out-of-plane distance increases with increasing ionic radius and decreases in the order of the atomic numbers within the lanthanides [for example, 1.8 Å for Eu(III) and 1.6 Å for Yb(III)] [8,23]. It is assumed that the longer the out-of-plane distance, the greater is the extent of the interaction that occurs between the metal ion and an additional ligand in the mobile phase. The interaction with water or methanol reduces the retention of an RE–TPP complex in the reversed-phase mode, whereas that with a ligand containing hydrophobic alkyl moieties, such as an amine, probably enhances the retention.

The retention trends of RE–TPP complexes observed with different amines or NaOH are represented as a function of the ionic radius ($r_{i,RE}$) of the RE(III) in Fig. 7, where the $r_{i,RE}$ values [24] for a coordination number (CN) of 8 are conveniently applied. A decreasing tendency of the retention in the order of $r_{i,RE}$ is observed with trialkylamines and NaOH, which is considered to result from the additional coordination of hydrophilic ligand(s) such as water and/or methanol with the RE atom. Similar arguments are applied in discussing the decreasing tendency of the retentions of several RE–TPP complexes observed with dialkylamines. The reverse retention trends are observed with dialkylamines for the complexes of REs(III) having

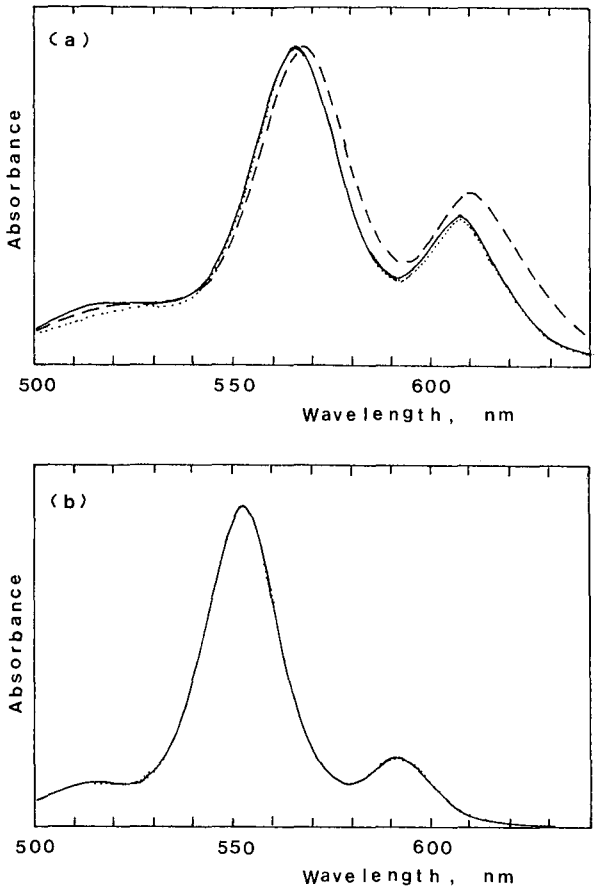

Fig. 6. Visible absorption spectra of the (a) Nd–TPP and (b) Lu–TPP in their eluting zones. Mobile phase: dotted line, 0.045 *M* NaOH in methanol–water–Hacac (95:5:1, v/v/v); solid line, methanol–water–Hacac–TEA (95:5:1:1.3, v/v); dashed line, methanol–water–Hacac–DPA (95:5:1:1.3, v/v).

relatively large $r_{i,RE}$ values, which is considered to result from the enhancement of the retention due to the formation of hydrophobic amine adducts of the RE–TPP complexes. The retention-enhancing effect becomes more significant with increase in the length of the alkyl side-chains inherently in dialkylamines (see also Fig. 4).

It is noted that the plot for the complex of Y(III) lies between those of Dy(III) and Ho(III), whose ionic radii are close to that of Y(III).

Effect of the molecular structure of the amine

It is notable that the retention sequence of RE–TPP complexes depends on the amine added to the mobile phase together with Hacac; trialkylamines and dialkylamines in particular give distinct retention sequences.

In an RE–TPP complex, RE(tpp)(acac), the central metal ion is situated significantly out of the porphyrin plane, where it is coordinated with four nitrogen

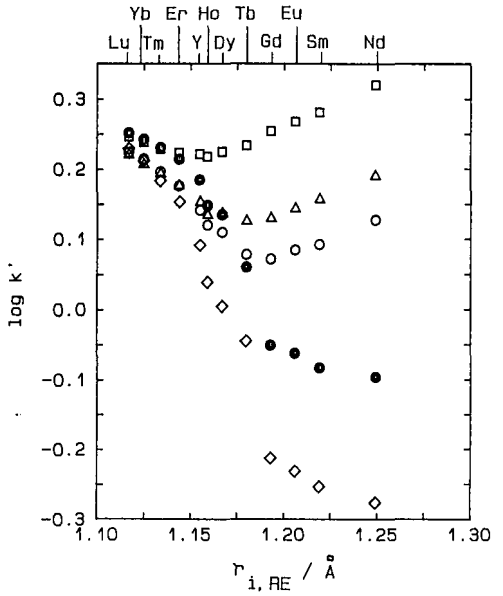

Fig. 7. Retention of RE–TPP complexes as a function of the ionic radius ($r_{i,RE}$) of RE(III) ($r_{i,RE}$ values for $CN = 8$). Basic mobile phase additives: ● = TPA; ○ = DPA; △ = DBA; □ = DHA; ◇ = NaOH. For the mobile phase compositions, see Figs. 3–5.

atoms in tpp and two oxygen atoms in acac and probably also with other coordination atom(s) belonging to additional ligand(s) contained in the mobile phase. In a tpp molecule, four phenyl groups are bonded with four meso-carbons in the porphyrin structure, respectively, with a significant bond angle between the phenyl and porphyrin planes. Accordingly, when the amine used as the mobile phase additive has a bulky alkyl moiety in the molecule, a steric hindrance effect of the alkyl moiety is possible on the coordination of the amine to the RE ion in the RE–TPP complex. Such a steric effect is regarded as being responsible for the difference between trialkylamines and dialkylamines in the coordination ability. According to this hypothesis, the steric effects must be significant even with a dialkylamine if it has alkyl groups with a bulky stucture in the vicinity of the nitrogen atom.

The steric effects of the alkyl moieties in amines were examined by comparing DIPA with DPA and DMpip with pip. The results are represented in Figs. 8 and 9. With amines possessing branched alkyl side-chains, such as DIPA and DMpip, the retention of the RE–TPP decreased with increase in the radius of the RE ion, which was similar to the trend observed with a trialkylamine (see Fig. 7). These results support the hypothesis that the little coordinative interaction between a trialkylamine and RE–TPP is due to the steric effects of bulky alkyl moieties of the amine.

Separation of RE–TPP complexes

The retention of each RE–TPP complex depends on the composition of the mobile phase. When the methanol-to-water ratio in the mobile phase was decreased, the capacity factors of the complexes increased monotonously, whereas little change

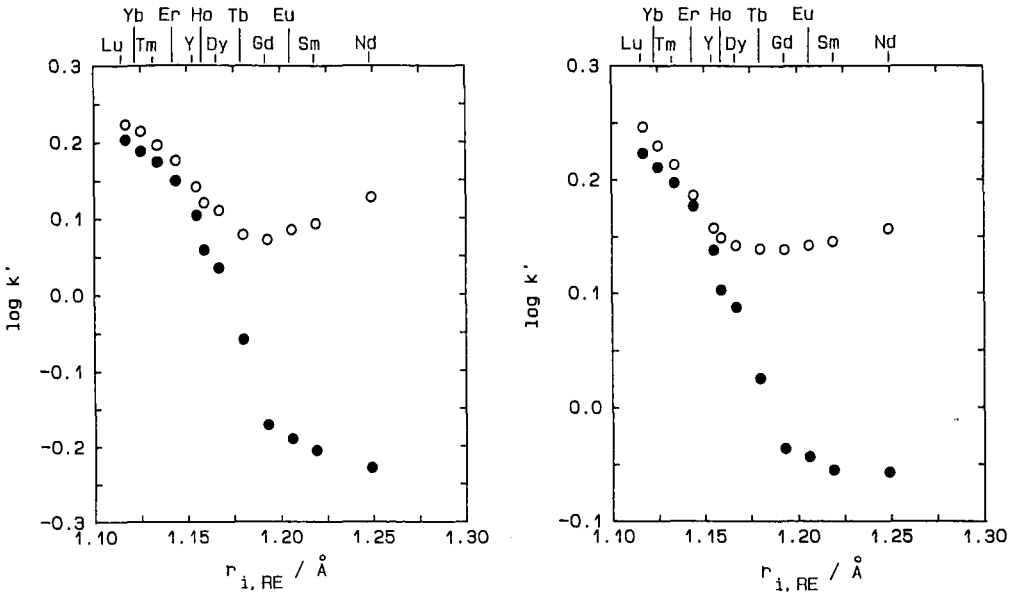

Fig. 8. Retention of RE–TPP complexes as a function of the ionic radius ($r_{i,RE}$) of RE with $CN = 8$. Mobile phase: ● = methanol–water–Hacac–DIPA (95:5:1:1.4, v/v); ○ = methanol–water–Hacac–DPA (95:5:1:1.3, v/v).

Fig. 9. Retention of RE–TPP complexes as a function of the ionic radius ($r_{i,RE}$) of RE with $CN = 8$. Mobile phase: ● = methanol–water–Hacac–DMpip (95:5:1:0.96, v/v); ○ = methanol–water–Hacac–pip (95:5:1:1.3, v/v).

occurred in the retention selectivities among the complexes, as shown in Fig. 2. This means that the elution sequence for the RE–TPP complexes shows little variability with either the methanol or the water content of the mobile phase. However, according to the results illustrated in Fig. 7, the retention selectivities for the RE–TPP complexes

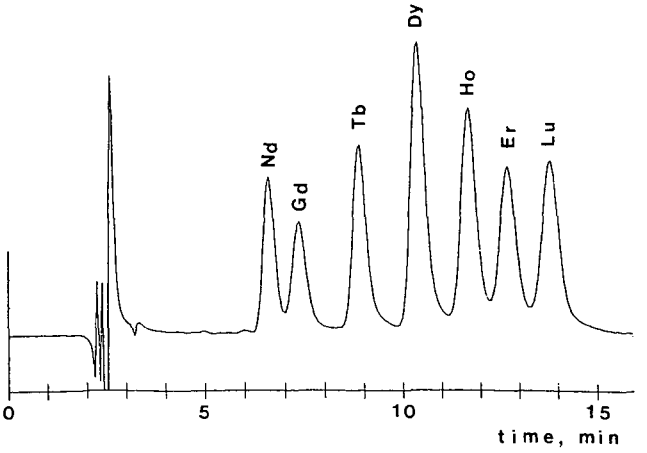

Fig. 10. HPLC separation of RE–TPP complexes. Column, TSK Gel ODS-80TM (50 μm) (150 mm × 4.6 mm I.D.); mobile phase, methanol–water–Hacac–TEA (90:10:0.5:0.68, v/v); flow-rate, 0.8 ml/min.

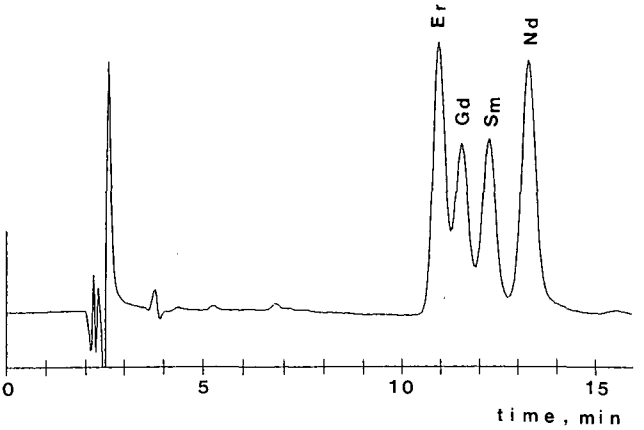

Fig. 11. HPLC separation of RE–TPP complexes. Mobile phase, methanol–water–Hacac–DHA (90:10:1:2.3, v/v); other conditions as in Fig. 10.

can be changed by varying the amine used as the basic mobile phase additive. When trialkylamines, DIPA and DMpip are used, the TPP complexes are eluted in the order of the atomic numbers of the RE. The separation in the reverse elution sequence is possible particularly for the complexes of relatively light lanthanoids when using a di-*n*-alkylamine. Separation of RE–TPP complexes using trialkylamine- and dialkylamine-containing mobile phases are demonstrated in Figs. 10 and 11, respectively. In Fig. 10 seven RE–TPP complexes are separated successfully in the order of the atomic numbers of the REs within 15 min. The elution sequence of the complexes shown in Fig. 11 is the reverse of that shown in Fig. 10.

CONCLUSION

The TPP complexes of REs can be chromatographed in a reversed-phase system with octadecyl-bonded silica and an aqueous methanolic mobile phase. Hacac and an amine are effective mobile phase additives for successful elution of these RE–porphyrin complexes. The retention selectivity for the RE–TPP complexes varies with the amine added to the mobile phase. The amine functions as a base which promotes the dissociation of Hacac to $acac^-$ ion, and accordingly the mixed ligand complex, RE(tpp)(acac), is stabilized. Amines, particularly di-*n*-alkylamines, function as hydrophobic neutral ligands with which an RE–TPP can form an adduct complex, and accordingly the retention is enhanced. The effect of the latter function depends on the amine used, which is explained in terms of a steric effect of the alkyl moiety in the amine molecule.

It is expected that the results of this study will be useful in porphyrin chemistry where the separation or purification of RE–TPP complexes is required. For application to the HPLC determination of RE(III) ions in aqueous samples, the development of a successful procedure for the quantitative formation of RE–TPP complexes is urgently needed.

REFERENCES

1 D. Kessel and M.-L. Cheng, *Cancer Res.*, 45 (1985) 3053.
2 A. Kappas and G. D. Drummond, *J. Clin. Invest.*, 77 (1986) 335.
3 R. H. Filby and J. F. Branthaver (Editors), *Metal Complexes in Fossil Fuels*, American Chemical Society, Washington, DC, 1986.
4 K. L. Cheng, K. Ueno and T. Imamura, *Handbook of Organic Analytical Reagents*, CRC Press, Boca Raton, FL, 1982, p. 355.
5 V. Varadi, F. R. Longo and A. D. Adler, in D. Dolphin (Editor), *The Porphyrins*, Vol. I, Academic Press, New York, 1978, p. 581.
6 S. K. Hajibrahim, P. J. C. Tibbetts, C. D. Watts, J. R. Maxwell, G. E. Eglinton, H. Colin and G. Guiochon, *Anal. Chem.*, 50 (1978) 549.
7 P. Sundararaman, *Anal. Chem.*, 57 (1985) 57.
8 C. J. Boreham and C. J. R. Fookes, *J. Chromatogr.*, 467 (1989) 195.
9 Y. Wakui, K. Saitoh and N. Suzuki, *Chromatographia*, 22 (1986) 160.
10 C. K. Lim, J. M. Rideout and T. J. Peters, *J. Chromatogr.*, 317 (1984) 333.
11 N. Suzuki, K. Saitoh and Y. Sugiyama, *Chromatographia*, 21 (1986) 509.
12 K. Saitoh, M. Kobayashi and N. Suzuki, *J. Chromatogr.*, 243 (1982) 291.
13 M. Kobayashi, K. Saitoh and N. Suzuki, *Chromatographia*, 20 (1985) 72.
14 C. P. Wong, *Inorg. Synth.*, 22 (1983) 152.
15 W. Buchler, in K. M. Smith (Editor), *Porphyrins and Metalloporphyrins*, Elsevier, Amsterdam, 1975, p. 191.
16 N. Suzuki, K. Saitoh and Y. Shibata, *J. Chromatogr.*, 504 (1990) 179.
17 C. P. Wong and W. D. Horrocks, Jr., *Tetrahedron Lett.*, 31 (1975) 2637.
18 W. D. Horrocks, Jr. and C. P. Wong, *J. Am. Chem. Soc.*, 98 (1976) 7157.
19 N. Suzuki, T. Takeda and K. Saitoh, *Chromatographia*, 22 (1986) 43.
20 A. Zalkin, D. H. Templeton and D. G. Karraker, *Inorg. Chem.*, 8 (1969) 2680.
21 M. Nappa and J. S. Valentine, *J. Am. Chem. Soc.*, 100 (1978) 5075.
22 F. A. Walker, E. Hui and J. M. Walker, *J. Am. Chem. Soc.*, 97 (1975) 2390.
23 C.-P. Wong, R. F. Venteicher and W. D. Horrocks, Jr., *J. Am. Chem. Soc.*, 96 (1974) 7149.
24 R. D. Shannon, *Acta Crystallogr., Sect. A*, 32 (1975) 751.

Journal of Chromatography, 542 (1991) 365–372
Elsevier Science Publishers B.V., Amsterdam

CHROM. 23 054

High-performance liquid chromatographic determination of biotin in pharmaceutical preparations by post-column fluorescence reaction with thiamine reagent

TOSHIO YOKOYAMA*
Central Research Laboratory, SS Pharmaceutical Co. Ltd., 1143 Nanpeidai, Narita-shi, Chiba 286 (Japan)
and
TOSHIO KINOSHITA
School of Pharmaceutical Sciences, Kitasato University, 9–1 Shirokane-5, Minato-ku, Tokyo 108 (Japan)
(First received July 5th, 1990; revised manuscript received December 6th, 1990)

ABSTRACT

A high-performance liquid chromatographic method for the determination of biotin was devised utilizing a post-column reaction in which the amide bond of biotin was chlorinated and allowed to react with thiamine to give fluorescent thiochrome. A linear relationship was observed between the peak height of biotin in the range 20 ng–3 μg per injection. The limit of detection was 10 ng per injection. The relative standard deviations for 40 and 200 ng per injection of biotin were 3.1 and 1.2% ($n = 10$), respectively. The method could be applied directly to pharmaceutical preparations without any sample pretreatment for the elimination of interfering materials as is required in the conventional methods.

INTRODUCTION

Since biotin was first identified in 1940 by Gyorgy *et al.* [1], many workers have investigated its biochemical functions. The biochemical role of biotin has been revealed to be as the coenzyme of four carboxylases involved in lipid, amino acid, carbohydrate and energy metabolism.

Biotin in biological fluids and pharmaceutical preparations has generally been determined by microbiological methods [2–5], because it has no particular functional group that facilitates sensitive detection, and its contents in such samples are extremely small. Although microbiological methods provide excellent sensitivity, they require long incubation periods and give variable results because they are readily affected by different contaminants. On the other hand, several workers have reported chemical and physico-chemical methods, such as spectrophotometric methods based on the perturbation of dye–protein complexes [6], reaction with 4-dimethylaminocinnamaldehyde [7,8] or oxidation with potassium iodate [9]. However, these methods are neither as sensitive nor as specific as the microbiological methods. Although gas chromatographic methods [10,11] have also been proposed, they require tedious pre-column derivatization and the only method for sensitive detection is mass spectrom-

0021-9673/91/$03.50

etry, which is not readily available in ordinary laboratories. Radiodilution assay [12,13] and radiometric–microbiological assay [14] methods are not as specific and require the manipulation of radioisotopes.

Recently, high-performance liquid chromatographic (HPLC) methods have been applied to the simultaneous determination of various vitamins. As biotin does not show UV absorption suitable for its detection, it was detected either electrochemically [15] or fluorimetrically with precolumn derivatization using reagents such as 4-bromomethyl-7-methoxycumarin (Br-Mmc) [16], 9-anthryldiazomethane (ADAM) [17] and 1-pyrenyldiazomethane (PDAM) [18]. Although highly sensitive and specific, these methods are laborious, because the electrochemical detector requires careful conditioning and the precolumn fluorescence derivatization methods are not easily automated and are prone to interference from contaminants.

We have previously reported [19,20] the fluorimetric assay of proteins in which the amide (peptide) bonds of proteins were chlorinated and allowed to react with thiamine to give fluorescent thiochrome. This paper deals with the application of this principle to the determination of biotin by HPLC.

EXPERIMENTAL

Chemicals

Biotin, thiamine hydrochloride, riboflavin, pyridoxine hydrochloride, nicotinamide and folic acid were obtained from Nippon Roche (Tokyo, Japan). Analytical-reagent grade $Na_2HPO_4 \cdot 12H_2O$, $NaH_2PO_4 \cdot H_2O$, 10% sodium hypochlorite solution (Antiformin), sodium nitrite, sodium hydroxide and Brij-35 and HPLC-grade acetonitrile were obtained from Wako (Osaka, Japan). Sodium 1-butanesulphonate and the tetrapeptide Val–Ala–Ala–Phe were purchased from Tokyo Kasei (Tokyo, Japan) and Sigma (St. Louis, MO, U.S.A.), respectively.

Mobile phase and derivatization reagents

The mobile phase for HPLC was 50 m*M* phosphate buffer (pH 4.5)–acetonitrile (9:1) containing 25 mmol/l of 1-butanesulphonate as the ion-pair reagent. The hypochlorite reagent was prepared by adding 120 ml of 1 *M* sodium hydroxide solution and 4 ml of 25% Brij-35 solution to 80 ml of Antiformin and diluting the resulting mixture with 0.1 *M* phosphate buffer to 1000 ml. The final concentration of available chlorine in the reagent should be 0.8%. Thiamine reagent was prepared by dissolving sodium nitrite and thiamine hydrochloride in 0.1 *M* phosphate buffer (pH 7.5) as described previously [20]. The mobile phase and reagents were filtered through a 0.45-μm microfilter (Fuji Photo Film, Tokyo, Japan) and degassed prior to use.

Chromatographic system

Fig. 1 shows a schematic diagram of the HPLC system. Chromatographic separation was carried out on a 15 cm × 6.0 mm I.D. TSKgel ODS-80TM column (Tosoh, Tokyo, Japan) at 50°C. The mobile phase and the two post-column derivatization reagents were pumped with a Shimadzu LC-6A HPLC solvent-delivery system.

The mobile phase was delivered at a flow-rate of 1.0 ml/min, and 20 μl of the sample solution were injected into the chromatograph using a KMT-60A HPLC

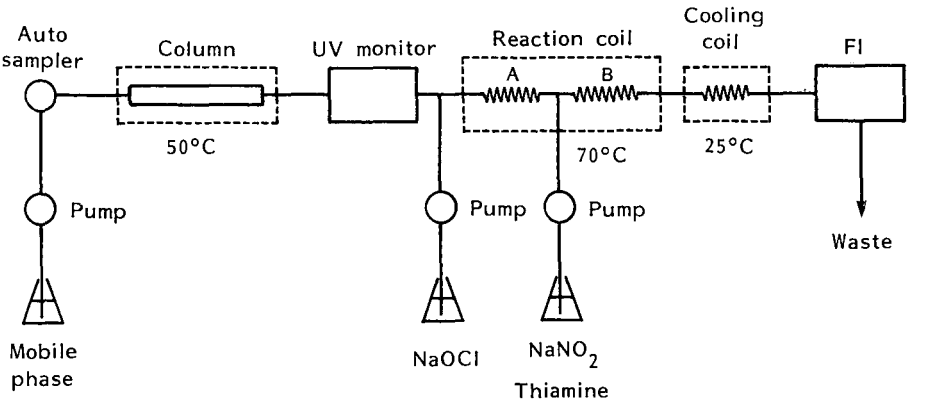

Fig. 1. Schematic diagram of the system for HPLC and fluorescence detection of biotin. Fl = Spectrofluorimeter.

autosampler (Kyowa-Seimitu, Tokyo, Japan). The eluate from the column was first passed through a Shimadzu SPD-6A UV detector equipped with a 20-μl flow cell set at 210 nm, then it was introduced into the fluorescence reactor system. The hypochlorite reagent was delivered to the eluate stream at a flow-rate of 0.3 ml/min and the stream was allowed to flow through the PTFE tubing reaction coil A (3 m × 0.5 mm I.D.) immersed in a water-bath at 70°C (Thermo-minder, Type Ace-80, Taiyo Service Centre, Tokyo, Japan). The eluate was mixed with the thiamine reagent delivered at a flow-rate of 0.3 ml/min, and the resulting mixture was passed through the PTFE tubing reaction coil B (5 m × 0.5 mm I.D.) also in the 70°C water-bath. The effluent from coil B was passed through the PTFE tubing cooling coil (1 m × 0.5 mm I.D.) and its fluorescence intensity was measured at excitation and emission wavelengths of 370 and 440 nm, respectively, using a Shimadzu RF-535 spectrofluorimeter equipped with a 20-μl flow cell.

Analysis of multivitamin tablets and capsules

Twenty tablets and capsules containing biotin were weighed and finely powdered. An accurately weighed portion of the powder equivalent to about 200 μg of biotin was transferred into a centrifuge tube, and 10 ml of the internal standard solution, containing 40 μg/ml of Val–Ala–Ala–Phe in 0.1 *M* Na_2HPO_4, was pipetted into the centrifuging tube. The mixture was shaken for 3 min, ultrasonicated for 20 min and centrifuged at 2000 *g* for 10 min. The supernatant obtained was filtered through a 0.45-μm membrane filter and a 20-μl aliquot of the filtrate was injected into the chromatograph.

Analysis of frozen multivitamin infusion

The multivitamin infusion was determined in the same manner as for tablets and capsules except that ultrasonication and centrifugation were omitted.

RESULTS AND DISCUSSION

Chromatographic separation

Figs. 2 and 3 show the reversed-phase HPLC profiles of a mixture containing biotin and five water-soluble vitamins, *i.e.*, thiamine, riboflavin, pyridoxine, nicotinamide and folic acid, which are usually contained in multivitamin preparations.

The separation was considerably influenced by the pH and composition of the mobile phase. Biotin was well retained on the ODS column in the low pH range, and its peak appeared in the vicinity of riboflavin.

The retention time of biotin decreased with increase in the concentration of acetonitrile in the mobile phase, and it was eluted together with thiamine, pyridoxine, nicotinamide and folic acid. Further, six water-soluble vitamins were not well separated at an acetonitrile concentration of 15% in the mobile phase. When it was decreased to 5%, the biotin was to well retained, giving a retention time over 60 min. Consequently, the pH of the mobile phase was adjusted to 4.5 and the concentration of acetonitrile in the mobile phase to 10%.

In addition to the column used in the standard procedure in the present method, silica-NH_2 and ion-exchange columns were examined for the separation of biotin from the additives in the preparations. However, the former column did not retain biotin and the latter gave poor separations.

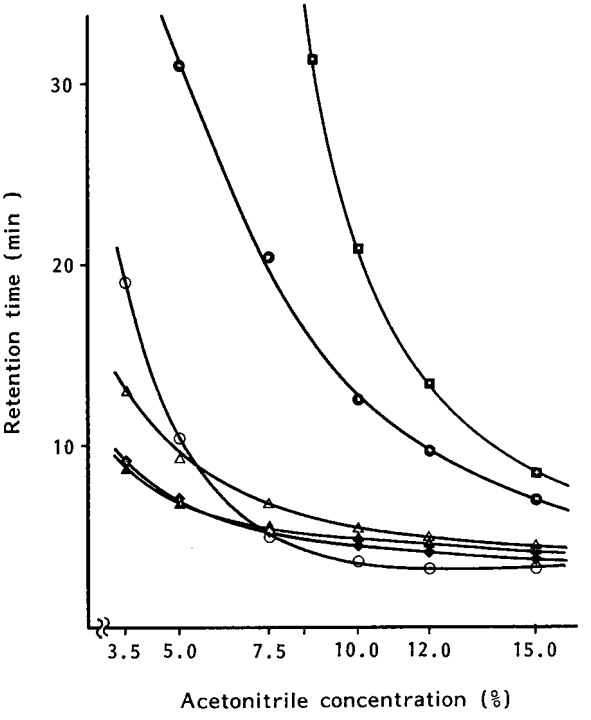

Fig. 2. Retention times of (●) biotin, (△) thiamine hydrochloride, (■) riboflavin, (▲) pyridoxine hydrochloride, (◆) nicotinamide and (○) folic acid plotted against the concentration of acetonitrile in the mobile phase (pH 4.5). HPLC conditions as in the text, except for the acetonitrile concentration.

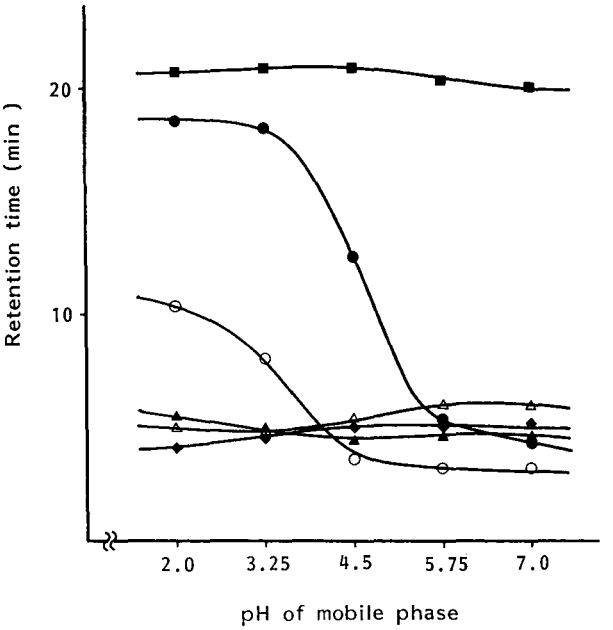

Fig. 3. Retention times of (●) biotin, (△) thiamine hydrochloride, (■) riboflavin, (▲) pyridoxine hydrochloride, (◆) nicotinamide and (○) folic acid plotted against the pH of the buffer in the mobile phase at an acetonitrile concentration of 10%. HPLC conditions as in the text, except for the buffer pH.

Optimization of post-column reaction conditions

The conditions of the reaction were approximately the same as those described previously [20] except for the composition of the hypochlorite reagent. It was necessary to increase the alkalinity of this reagent as the eluate from the chromatograph was acidic whereas the fluorescence reaction requires slightly alkaline conditions. Fig. 4 shows the relationship between the fluorescence intensity and the amount of 1 *M* sodium hydroxide added to the hypochlorite reagent. The maximum fluorescence intensity was observed when 12 ml of 1 *M* sodium hydroxide solution were added to 100 ml of the reagent solution. Acetonitrile or an ion-pair reagent, such as sodium dodecyl sulphate, in the mobile phase did not affect the reaction.

System performance

A linear relationship was observed between the peak height and the amount of biotin injected in the range 20 ng–3 μg, with a correlation coefficient of 0.998. The limit of detection for biotin was 10 ng per injection at a signal-to-noise ratio of 2, which was equal to that of the absorbance at 210 nm, with a relative standard deviations of the fluorescence intensity of 14.1% (n = 10). The relative standard deviations of the fluorescence intensity for 40 and 200 ng per injection of the standard samples of biotin were 3.1 and 1.2% (n = 10), respectively.

Commercial biotin pharmaceutical preparations were assayed utilizing the fluorescence and the absorbance at 210 nm. Fig. 5 shows the chromatograms of several biotin preparations. Table I shows the labelled contents of these preparations. Excel-

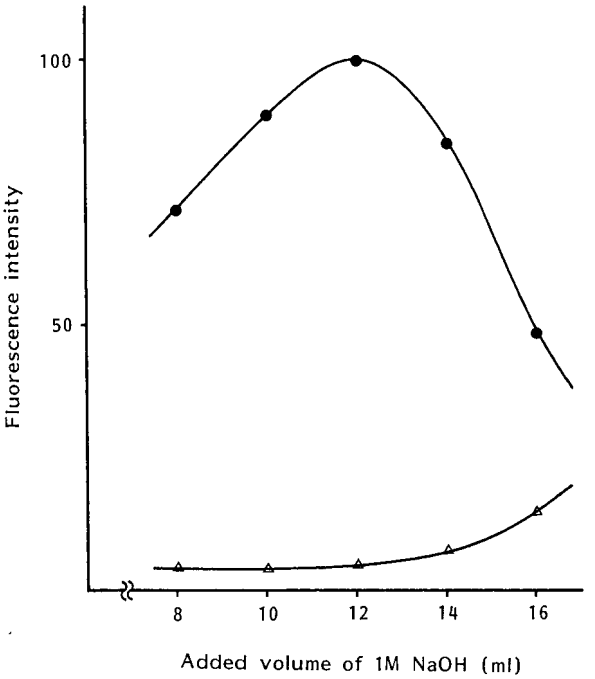

Fig. 4. (●) Fluorescence intensity of biotin (1 μg per injection) and (△) background plotted against the volume of 1 *M* NaOH added to 100 ml of the hypochlorite reagent. HPLC and post-column reaction conditions as in the text, except for the volume of 1 *M* NaOH added.

lent recoveries of biotin were observed with satisfactory reproducibility, as shown in Table II.

As a pretreatment, biotin was extracted from the pharmaceutical products with 0.1 *M* Na_2HPO_4 containing the tetrapeptide Val–Ala–Ala–Phe as an internal standard, and the extract was injected directly into HPLC system. This procedure is much simpler than the methods using Br-Mmc, ADAM or PDAM [16–18].

Absorption at 210 nm, although widely used for detecting substances such as

TABLE I

LABELLED CONTENTS OF BIOTIN IN PHARMACEUTICAL PREPARATIONS

Preparation	Labelled contents
Tablet	Biotin 0.02 mg, bisbenthiamine 8.33 mg, riboflavin 2 mg, pyridoxine · HCl 8.33 mg, nicotinamide 16.67 mg, folic acid 0.13 mg, ascorbic acid 50 mg, cyanocobalamin 0.02 mg, retinol palmitate 666.67 IU, ergocalciferol 66.67 IU, tocopherol calcium succinate 3.46 mg, calcium carbonate 50 mg per tablet
Capsule	Biotin 0.01 mg, L-cysteine 30 mg, riboflavin 15 mg, pyridoxine · HCl 50 mg, nicotinamide 25 mg, calcium pantothenate 15 mg per capsule
Frozen infusion	Biotin 0.06 mg, thiamine · HCl 3.9 mg, riboflavin · Na 4.6 mg, pyridoxine · HCl 4.9 mg, nicotinamide 40 mg, folic acid 0.4 mg, pantothenol 14 mg, ascorbic acid 100 mg per vial

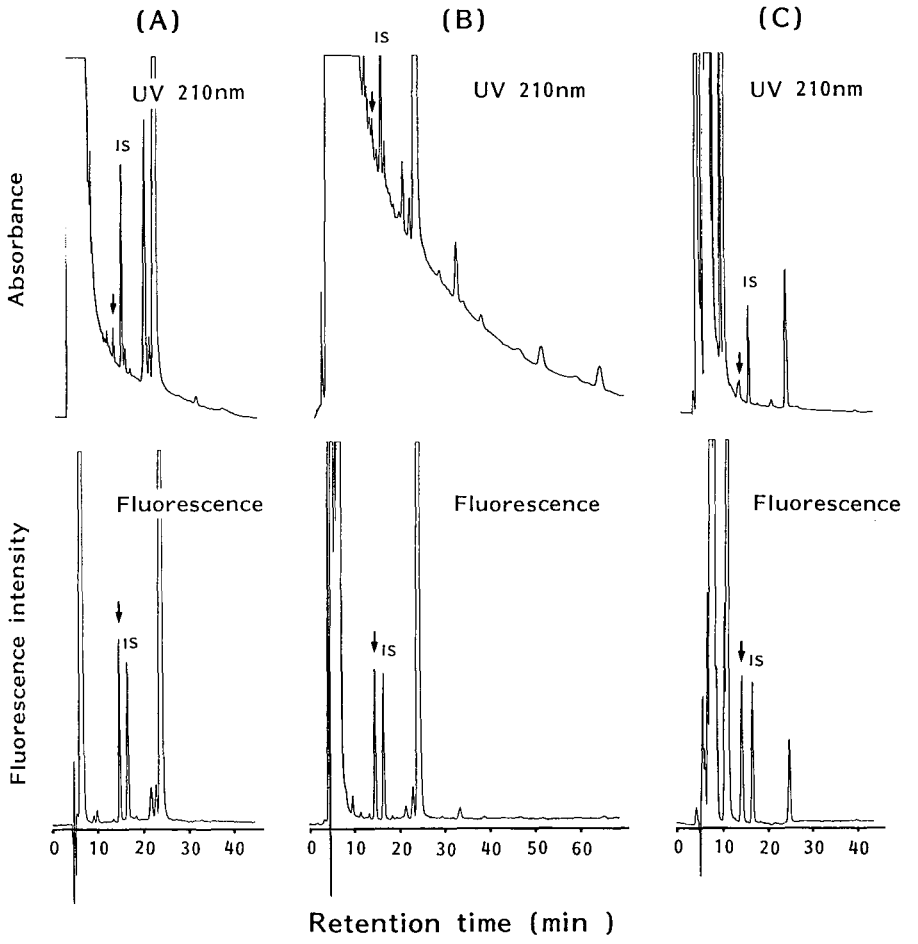

Fig. 5. Comparison of chromatograms for (A) the multivitamin tablet, (B) capsule and (C) frozen infusion obtained by the UV (210 nm) method (top) and the present fluorescence method (bottom). HPLC and post-column reaction conditions as in the text.

TABLE II

RECOVERIES OF BIOTIN FROM COMMERCIAL PHARMACEUTICAL PREPARATIONS

Preparation[a]	Biotin added (μg)	Biotin found[b] (μg)	Recovery (%)	Relative standard deviation (%)
Tablet	200	199.4 ± 5.3	99.7	2.63
Capsule	200	195.6 ± 4.4	97.8	2.18
Frozen infusion	200	194.2 ± 6.1	97.1	3.04

[a] See Table I.

[b] Each preparation was analysed five times; results are means ± S.D.

biotin, which are generally insensitive to UV at longer wavelengths, is seriously affected by various UV-absorbing substances, as the biotin peak appears in the tailing part of the large peaks of rapidly eluting compounds. This effect reduces the reliability of the determination. In contrast, the present method is less subject to interference from contaminants, because it is specific to the amide bonds. The chromatograms obtained by the present fluorescence method are simpler and give higher biotin peaks than those obtained using absorption at 210 nm. In addition, the peaks originating from the rapidly moving components are small enough that their tailing effect is negligible. Moreover, the present method shows only small fluctuations of the baseline and the chromatography is completed within 30 min.

The proposed method is expected to be useful for the sensitive and specific determination of biotin in various pharmaceutical products.

REFERENCES

1 P. D. Gyorgy, B. Melville, D. Burk and V. DuVigneaud, *Science (Washington, D.C.)*, 91 (1940) 243.
2 L. D. Wright and H. R. Skeggs, *Proc. Soc. Exp. Biol. Med.*, 56 (1944) 95.
3 K. Dittmer and V. du Vigneaud, *J. Biol. Chem.*, 169 (1947) 63.
4 L. D. Wright, E. L. Cresson and C. A. Driscoll, *Proc. Soc. Exp. Biol. Med.*, 91 (1956) 248.
5 M. N. Voigt, R. R. Eitenmiller and G. O. Ware, *J. Food Sci.*, 44 (1979) 729.
6 N. M. Green, *Biochem. J.*, 94 (1965) 23C.
7 K. Shimada, Y. Nagase and U. Matsumoto, *Yakugaku Zasshi*, 89 (1969) 436.
8 D. B. McCormick and J. A. Roth, *Anal. Biochem.*, 34 (1970) 226.
9 C. Plinton, F. P. Mahn, M. Hawrylyshyn, V. S. Venturella and B. Z. Senkowski, *J. Pharm. Sci.*, 58 (1969) 875.
10 V. Viswanathan, F. P. Mahn, V. S. Venturella and B. Z. Senkowski, *J. Pharm. Sci.*, 59 (1970) 400.
11 H. Janecke and H. Voege, *Fresenius' Z. Anal. Chem.*, 254 (1971) 355.
12 K. Shimada, U. Matsumoto and Y. Nagase, *Yakugaku Zasshi*, 92 (1972) 575.
13 K. Dakshinamurti, A. D. Landman, L. Ramamurti and R. J. Constable, *Anal. Biochem.*, 61 (1974) 225.
14 T. R. Guilarte, *Nutr. Rep. Int.*, 31 (1985) 1155.
15 K. Kamata, T. Hagiwara, M. Takahashi, S. Uehara, K. Nakayama and K. Akiyama, *J. Chromatogr.*, 356 (1986) 326.
16 P. L. Desbene, S. Coustal and F. Frappier, *Anal. Biochem.*, 128 (1983) 359.
17 K. Hayakawa and J. Oizumi, *J. Chromatogr.*, 413 (1987) 247.
18 T. Yoshida, A. Uetake, C. Nakai, N. Nimura and T. Kinoshita, *J. Chromatogr.*, 456 (1988) 412.
19 T. Yokoyama, N. Nakamura and T. Kinoshita, *Anal. Biochem.*, 184 (1990) 184.
20 T. Yokoyama and T. Kinoshita, *J. Chromatogr.*, 518 (1990) 141.

Journal of Chromatography, 542 (1991) 373–383
Elsevier Science Publishers B.V., Amsterdam

CHROM. 23 074

High-performance liquid chromatography–continuous-flow fast atom bombardment mass spectrometry of chlorophyll derivatives

RICHARD B. VAN BREEMEN*
Department of Chemistry, Box 8204, North Carolina State University, Raleigh, NC 27695 (U.S.A.)
and
FATIMA L. CANJURA and STEVEN J. SCHWARTZ
Department of Food Science, North Carolina State University, Raleigh, NC 27695 (U.S.A.)
(First received August 21st, 1990; revised manuscript received December 18th, 1990)

ABSTRACT

Nine chlorophyll derivatives from different spinach preparations were separated and identified using reversed-phase high-performance liquid chromatography–mass spectrometry (HPLC–MS). These pigments included chlorophylls *a* and *b*, chlorophyllides *a* and *b*, pheophorbide *a*, pheophytins *a* and *b*, and pyropheophytins *a* and *b*. HPLC–MS measurements were carried out using HPLC–frit-fast atom bombardment (FAB)-MS, which is a continuous-flow FAB-MS interface. The highly hydrophobic chlorophyll derivatives were eluted from a reversed-phase HPLC column using a gradient of increasing ethyl acetate concentration. Glycerol was included in the mobile phase to serve as the matrix for FAB ionization. During analysis by positive-ion HPLC–frit-FAB-MS, abundant protonated molecules, $[M + H]^+$, were detected for all nine chlorophyll derivatives. Fragment ions were observed in the mass spectra that were similar to those produced during standard probe FAB-MS. These HPLC–MS procedures were shown to be useful for the rapid separation and identification of a variety of chlorophyll derivatives from natural sources.

INTRODUCTION

The importance of chlorophyll pigments in photosynthesis and plant physiology has prompted enormous research efforts spanning almost 100 years that have resulted in the complete structural determination of chlorophyll [1]. Nevertheless, numerous questions remain regarding the catabolism of chlorophyll during senescence in plant tissues and the structures and functions of chlorophyll derivatives involved in ripening [2]. Previous studies of chlorophyll pigments have been hindered by the lack of sensitive techniques for the analysis and identification of small quantities of their metabolic intermediates in plant tissues and degradation products formed during heat processing of food products.

Since the development of desorption methods suitable for the ionization of non-volatile and thermally labile compounds, mass spectrometry (MS) has been ap-

0021-9673/91/$03.50

plied to the characterization and identification of a variety of chlorophyll derivatives. Mass spectra of chlorophylls have been obtained using laser desorption [3–7], field desorption [8,9], plasma desorption [10–12], fast atom bombardment (FAB) [13–18] and "in beam" (desorption) electron impact ionization [19]. Because FAB facilitates the continuous formation of chlorophyll ions, this ionization technique has been the method of choice for tandem mass spectrometric (MS–MS) studies of chlorophylls [15–18]. Among the ionization methods used to obtain mass spectra of chlorophylls, FAB is the only technique that has been coupled with high-performance liquid chromatography (HPLC) in a routine analytical instrument. However, no HPLC–MS studies of chlorophylls have yet been reported.

During FAB, sample ions are desorbed into the gas phase from a liquid matrix of low volatility (usually glycerol) as a result of bombardment by a beam of energetic atoms (usually xenon or argon at 3–10 keV) [13,20]. If fast ions are substituted for the fast atoms, then the technique is called liquid secondary-ion mass spectrometry. FAB-MS has been interfaced to HPLC in the HPLC–MS system called continuous-flow FAB-MS [21] or a variation of this technique known as HPLC–frit-FAB-MS [22]. In these HPLC–MS systems, the FAB matrix is typically mixed with the mobile phase prior to being pumped into the ion source of the mass spectrometer [22,23]. Small amounts (up to 10% by volume) of a matrix such as glycerol in the mobile phase have been shown to slightly increase band widths during reversed-phase (RP-) HPLC separations of peptides [24]. Instead of mixing the matrix with the mobile phase prior to chromatographic separation, coaxial flow of matrix and column effluent onto the FAB probe has been used to improve chromatographic resolution [24]. Alternatively, post-column addition of matrix has been carried out without significantly reducing chromatographic resolution [25].

During frit-FAB, the HPLC effluent is pumped through a fused-silica capillary and then through a stainless-steel frit located inside the ion source of the mass spectrometer [22]. The fast atom beam is focused onto the opposite side of the frit from the capillary, so that sample ions are desorbed into the gas phase as they flow through the frit. The HPLC solvent rapidly evaporates and is pumped away by the vacuum system of the mass spectrometer.

Our recent chlorophyll studies have involved the development of RP-HPLC procedures to separate and identify chlorophyll derivatives contained in complex mixtures extracted from spinach leaves. In one study, chlorophyll detection and identification was based on visible light absorption using an array detector [26]. Subsequently, structural confirmation of the HPLC-purified chlorophyll derivatives was obtained using FAB-MS combined with collisional activation and MS–MS analysis [18]. In the present investigation, HPLC separation of chlorophyll derivatives contained in extracts from spinach leaves was combined on-line with mass spectrometric detection using HPLC–frit-FAB-MS. The structures of the chlorophylls and chlorophyll derivatives discussed in this paper are shown in Fig. 1.

EXPERIMENTAL

Identification of chlorophyll derivatives in spinach leaf extracts was based on comparison to standards isolated from leaves and purified by RP-HPLC [26]. The identity of each standard compound was determined by its visible light absorbance

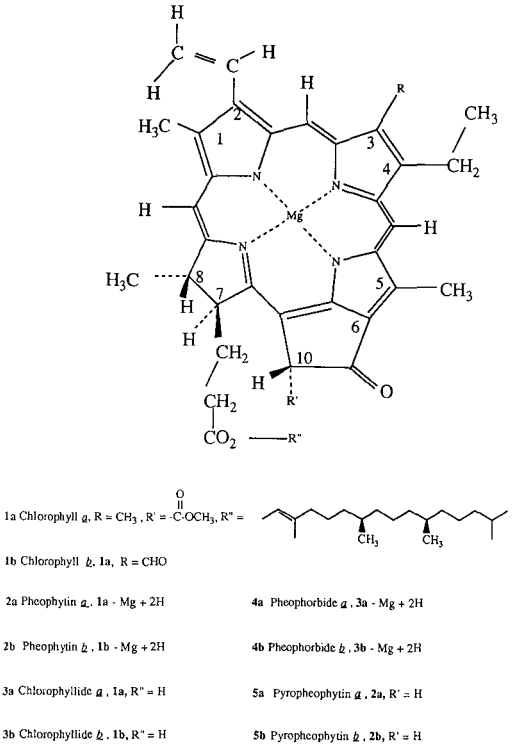

Fig. 1. Structures of chlorophylls and chlorophyll derivatives.

spectrum recorded on a diode-array detector [26] and confirmed using FAB-MS–MS [18]. Fresh spinach leaves containing chlorophylls *a* and *b* (**1a** and **1b** in Fig. 1) were incubated at 65°C for 30 min to activate the enzyme chlorophyllase. During this incubation period, the chlorophylls were partially converted into chlorophyllides *a* and *b* (**3a** and **3b**). Next, the mixture of chlorophylls and chlorophyllides was extracted from the spinach leaves using acetone as previously described [26] and then analyzed by HPLC–MS as described below. In another procedure, pheophytins *a* and *b* (**2a** and **2b**) were extracted using diethyl ether from an acidified chlorophyll extract [18]. The pheophytin extract was then analyzed by HPLC–MS. Pyropheophytins *a* and *b* (**5a** and **5b**) were prepared from heat-processed (145°C for 7 min) spinach puree as previously described [27] and then analyzed by HPLC–MS. Although pheophorbide *a* (**4a**) was detected in several samples, pheophorbides *a* and *b* (**4a** and **4b**) were obtained by acidification (1.0 *M* HCl) of a chlorophyllide extract. Prior to analysis by HPLC–MS, the chlorophyll derivatives contained in each sample extract were identified by RP-HPLC based on their visible light absorbance spectra recorded on a diode-array detector [26]. All samples containing chlorophyll derivatives were handled under subdued light.

HPLC separations were carried out using an Applied Biosystems (Foster City, CA, U.S.A.) Model 140A dual syringe solvent delivery system, that had been mod-

ified so that the dynamic mixer was replaced with a "T" union to minimize dead volume. The HPLC system was equipped with a Rheodyne (Cotati, CA, U.S.A.) Model 8125 injector and Vydac (Hesperia, CA, U.S.A.,) C_{18} narrow-bore column (15 cm × 2.1 mm) packed with 300 Å pore size, 5-μm diameter silica particles. The solvent flow-rate was 70 μl/min for all separations. Each extract was dissolved in diethyl ether or acetone (approximately 1 μg/μl), and 15 μl (15 μg) were injected onto the reversed-phase column per analysis.

The mixture of chlorophylls and chlorophyllides, extracted from spinach leaves that had been incubated at 65°C, was separated by RP-HPLC using a procedure modified from that of Canjura and Schwartz [26]. The solvent system consisted of a 20-min linear gradient from 100% solvent A to 100% solvent B. Solvent A consisted of ethyl acetate–methanol–water–glycerol (15:65:20:0.5, v/v/v/w), and solvent B contained the same solvents in a ratio of 60:30:10:0.5 (v/v/v/w). In order to shorten the retention times of the more hydrophobic pheophytins in the acid-treated spinach extract, a 10-min linear gradient was used from 50 to 100% solvent B. For extracted mixtures of pheophytins and pyropheophytins from heat-treated tissue, the original 20-min gradient from 100% solvent A to 100% solvent B was used, but mass spectra were recorded beginning 15 min after sample injection. Otherwise, recording of frit-FAB mass spectra was begun 5 min after sample injection, and the solvent front eluted approximately 7 min after injection or at approximately 2 min on the total-ion chromatograms. The delay before recording mass spectra minimized the use of computer disk memory to store background scans during HPLC–MS.

Positive-ion FAB mass spectra were obtained using a JEOL (Tokyo, Japan) JMS-HX110HF double-focusing mass spectrometer equipped with a JMA-DA5000 data system and HPLC–frit-FAB-MS interface. Xenon fast atoms at 6 kV were used for FAB ionization. The accelerating voltage was 10 keV, and the resolving power was 1000 for all measurements. The range m/z 300–1000 was scanned over approximately 7 s except during the analysis of pyropheophytins, in which this mass range was scanned in approximately 15 s. Although standard FAB mass spectra were recorded in profile mode (Fig. 2 A and B), centroided data were recorded during HPLC–frit-FAB-MS (Fig. 2C) because of limited computer disk space.

For compatibility with the vacuum system of the mass spectrometer, the HPLC column eluate was split so that approximately 5 μl/min entered the HPLC–frit-FAB-MS interface. At a column flow-rate of 70 μl/min, this resulted in a split ratio of 1:14. Because approximately 15 μg of each sample was injected, approximately 1 μg reached the mass spectrometer per analysis. Operation of the column at higher flow-rates would have resulted in a smaller split ratio and loss of sensitivity. The ion source temperature was maintained at 40°C, which was sufficient to prevent solvent from freezing in the frit. Glycerol contained in the mobile phase functioned as the FAB matrix.

RESULTS AND DISCUSSION

In recent studies of chlorophylls by positive-ion FAB-MS using a standard FAB probe [17,18], abundant molecular ions, $M^{+\cdot}$, were detected using 3-nitrobenzylalcohol as the FAB matrix. Protonated and deprotonated molecules, $[M+H]^+$ and $[M-H]^+$, were also observed although at lower relative abundance. The use of more

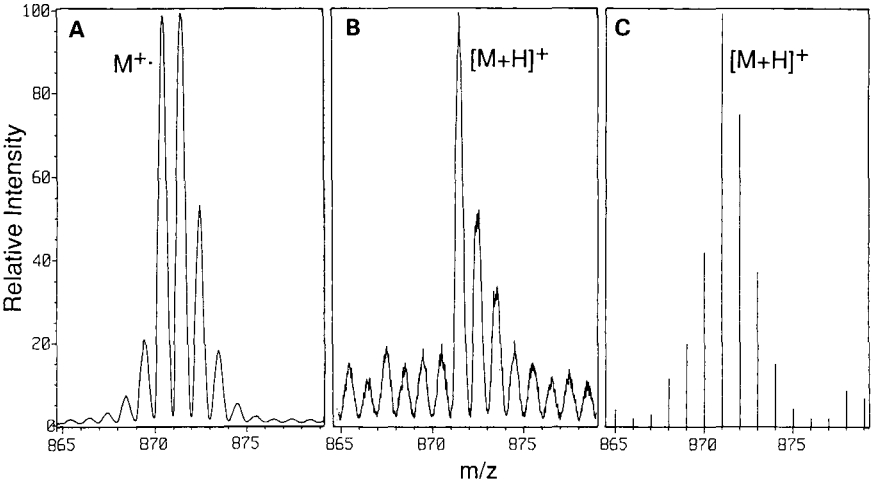

Fig. 2. Comparison of molecular-ion species of pheophytin *a* obtained using (A) standard probe FAB-MS with neat 3-nitrobenzylalcohol as the matrix, (B) standard probe FAB using neat glycerol as the matrix, or (C) HPLC–frit-FAB-MS with a mobile phase containing ethyl acetate–methanol–water–glycerol. In each positive-ion FAB mass spectrum, note the relative abundances of the radical cation, $M^{+\cdot}$, and the protonated molecule, $[M+H]^+$.

acidic matrices such as dithiothreitol–dithioerythritol or thioglycerol resulted in an increase in the relative abundance of protonated molecules of chlorophyll *a* [17].

Because of its greater volatility and proven compatibility with continuous-flow FAB-MS [28], glycerol instead of 3-nitrobenzylalcohol was added to the mobile phase for HPLC–MS analysis of chlorophyll derivatives. However, neat glycerol is a poor solvent for hydrophobic compounds and is not an ideal matrix for standard probe FAB-MS of chlorophylls. For example, the molecular-ion species for 1-μg aliquots of pheophytin *a* are compared in Fig. 2 using a matrix of either 3-nitrobenzylalcohol or glycerol on a standard FAB probe. In these mass spectra, the use of 3-nitrobenzylalcohol (Fig. 2A) produced $M^{+\cdot}$ ions with a signal-to-noise ratio that was approximately 10-fold higher than that of the $[M+H]^+$ ions obtained using glycerol (Fig. 2B). However, HPLC–frit-FAB-MS of approximately 1 μg pheophytin *a* (after split, Fig. 2C) produced protonated molecules with a signal-to-noise ratio comparable to that of the molecular-ion radicals obtained using standard probe FAB with 3-nitrobenzylalcohol.

Abundant protonated molecules, $[M+H]^+$, were detected for all chlorophyll derivatives investigated using RP-HPLC separation in combination with positive-ion frit-FAB-MS. The compounds investigated by HPLC–frit-FAB-MS included chlorophylls *a* and *b*, chlorophyllides *a* and *b*, pheophytins *a* and *b*, pheophorbide *a*, and pyropheophytins *a* and *b* (see chlorophyll structures in Fig. 1). During HPLC–frit-FAB-MS, the combination of glycerol with large proportions of ethyl acetate and methanol in the HPLC–MS mobile phase provided both a good solvent for the chlorophylls and a protic environment for the formation of $[M+H]^+$ ions.

The total-ion chromatogram and mass chromatograms for the HPLC–MS

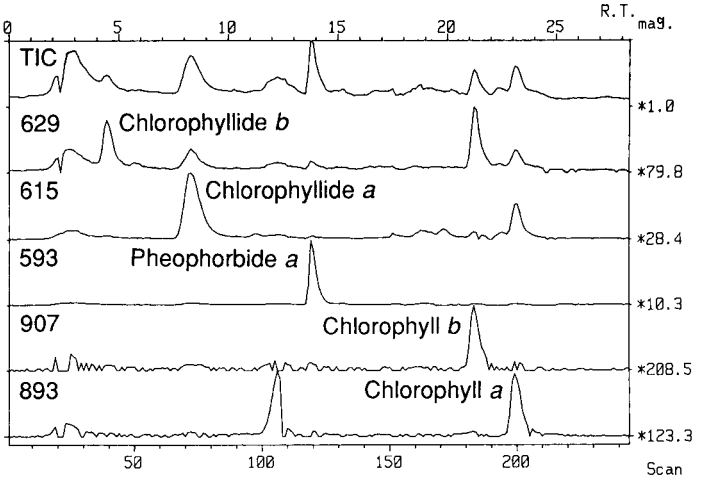

Fig. 3. Total-ion chromatogram and mass chromatograms obtained by positive-ion HPLC–frit-FAB-MS showing the detection of chlorophyllides *a* and *b*, pheophorbide *a*, and chlorophylls *a* and *b*, extracted from spinach that had been incubated to activate chlorophyllase. R.T. = Retention time in min. Right-hand scale: mag = magnification factor.

analysis of a mixture of chlorophylls *a* and *b*, chlorophyllides *a* and *b*, and pheophorbide *a* are shown in Fig. 3. Chlorophyllides *a* and *b* (retention times 8.2 and 4.3 min, respectively) were formed by chlorophyllase action on chlorophyll prior to extraction from the spinach. Intact chlorophylls *a* and *b* were detected at 23.2 and 21.2 min, respectively. Pheophorbide *a* and chlorophyllides *a* and *b* eluted before their more hydrophobic precursors, chlorophylls *a* and *b* (Fig. 3). Pheophorbide *a*, detected at a

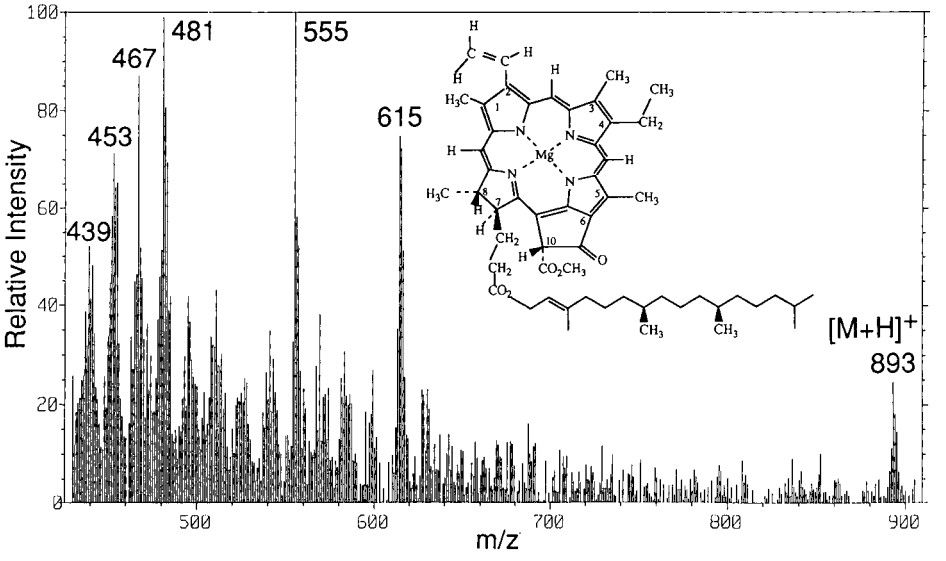

Fig. 4. Positive-ion frit-FAB mass spectrum of chlorophyll *a* (retention time 23.2 min) from the HPLC–MS analysis shown in Fig. 3.

retention time of 13.8 min, was formed by decomposition of chlorophyllide *a* during handling and extraction. No pheophorbide *b* was detected in this sample because of the greater stability of its precursor, chlorophyll *b*.

In addition to protonated molecules, fragment ions were detected in all mass spectra. The fragmentation patterns corresponded to those reported by Grese *et al.* [17] and van Breemen *et al.* [18]. For example, the positive-ion frit-FAB mass spectrum of chlorophyll *a*, recorded during the HPLC–MS analysis discussed above, is presented in Fig. 4. In this mass spectrum, fragment ions of chlorophyll *a* were detected at *m/z* 439, 453, 467, 481, 555 and 615. The most abundant fragment ion in the mass spectrum of chlorophyll *a* was detected at *m/z* 555, which was formed either by loss of $HCOOCH_3$ from *m/z* 615, $[MH-C_{20}H_{38}-HCOOCH_3]^+$, or by loss of $CH_3COOC_{20}H_{39}$ from the $[M+H]^+$ ion [17]. The ion detected at *m/z* 615, indistinguishable from the protonated molecule of chlorophyllide *a*, was formed by loss of the phytyl chain ($C_{20}H_{38}$) from the $[M+H]^+$ ion of chlorophyll *a* with transfer of a hydrogen from the leaving group back to the ester oxygen [17,18]. Therefore, the mass chromatogram of *m/z* 615 in Fig. 3 shows two bands, one corresponding to the protonated molecule of chlorophyllide *a* (retention time 8.2 min) and the other formed by fragmentation of chlorophyll *a* (retention time 23.2 min). Similarly, the mass chromatogram of *m/z* 629 (Fig. 3) shows two major bands corresponding to the $[M+H]^+$ ion of chlorophyllide *b* (retention time 4.3 min) and a fragment ion of chlorophyll *b* (retention time 21.2 min). The origin of the extra band in the mass chromatogram of chlorophyll *a* at a retention time of 12 min was not determined. However, the mass spectrum corresponding to this unknown band contained no fragment ions indicative of known chlorophylls or their derivatives. Instead, ions were detected at *m/z* 520, 571, 737, 765, 781, 839, 855, 877 and 893 (data not shown).

The total-ion chromatogram generated from the HPLC–frit-FAB-MS analysis of the pheophytin extract is shown in Fig. 5. Mass chromatograms corresponding to

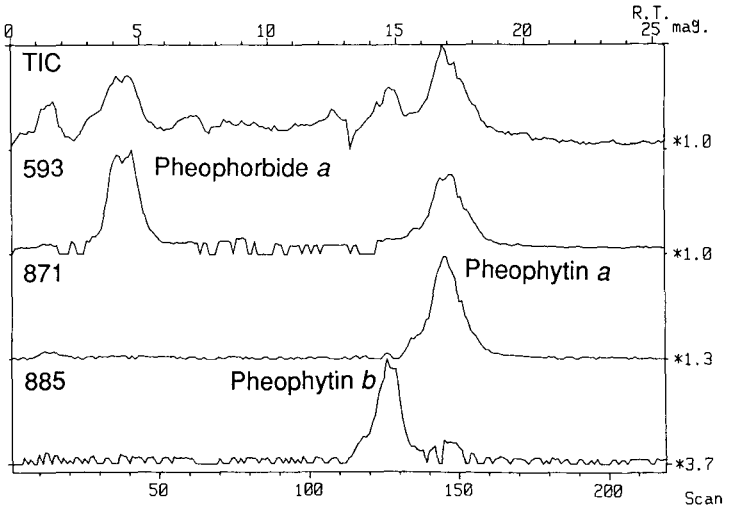

Fig. 5. Total-ion chromatogram and selected-ion chromatograms using positive-ion HPLC–frit-FAB-MS showing the detection of pheophytins *a* and *b*, and pheophorbide *a* from an acid-treated spinach extract. R.T. = Retention time in min. Right-hand scale: mag = magnification factor.

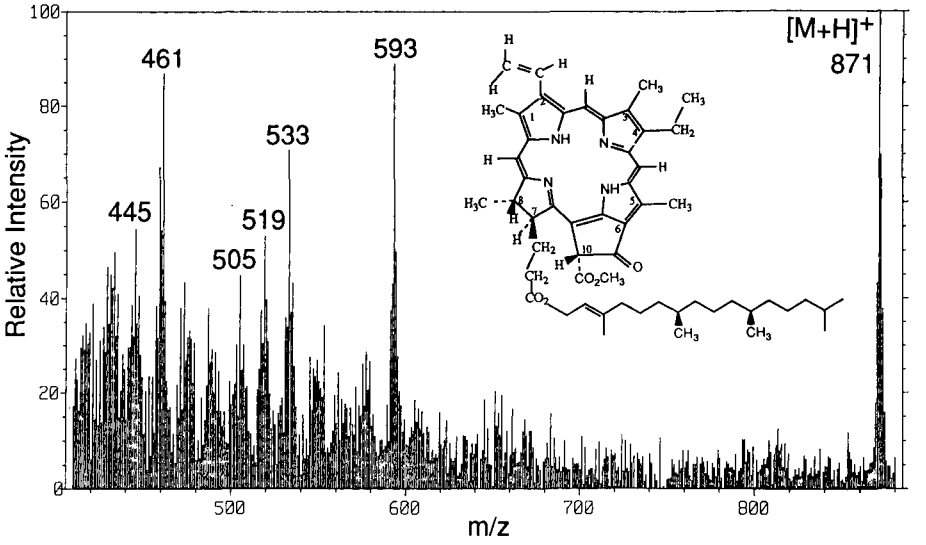

Fig. 6. Positive-ion frit-FAB mass spectrum of pheophytin *a* corresponding to a retention time of 19.1 min in the HPLC–MS chromatogram shown in Fig. 5.

the protonated molecules of pheophytins *a* and *b* and pheophorbide *a* are also plotted. These bands appeared wider than those of the chlorophylls and chlorophyllides shown in Fig. 3 or the pheophytins and pyropheophytins shown in Fig. 7. The primary explanation for the broader bands was the different gradient used for this elution. The mass spectrum of pheophytin *a*, showing an abundant protonated molecule at *m/z* 871 and several fragment ions, is shown in Fig. 6.

Pyropheophytins *a* and *b*, formed by heat treatment of spinach leaves, were extracted and then analyzed by HPLC–MS. The total-ion chromatogram and mass chromatograms for this analysis are shown in Fig. 7. A mixture of pheophytins and pyropheophytins was detected, since the conversion of pheophytin to pyropheophytin is incomplete during thermal treatments [29]. The mass spectrum of pyropheophytin *b* obtained during HPLC–MS is shown in Fig. 8. An abundant protonated molecule was detected at *m/z* 827 as well as fragment ions at *m/z* 461, 475, 489, 503 and 549. These fragment ions were similar to those observed using standard probe FAB-MS [18]. For example, the ion at *m/z* 549 was formed by loss of the phytyl chain with hydrogen transfer and is analogous to the ion at *m/z* 615 in the mass spectrum of chlorophyll *a* discussed above.

A contributing factor to the broadening of pheophytin and pheophorbide bands in the chromatograms shown in Figs. 5 and 7 was epimerization at C-10 caused by acid treatment of chlorophylls *a* and *b* to generate the pheophytins and pheophorbides. The pairs of epimers have been completely resolved using a different chromatographic column, mobile phase, and gradient [26]. There was no difference between the mass spectra of each pair of the epimers, however.

Several bands were detected by HPLC–MS that did not correspond to chlorophyll derivatives. The major contaminants in the chlorophyll and chlorophyllide ex-

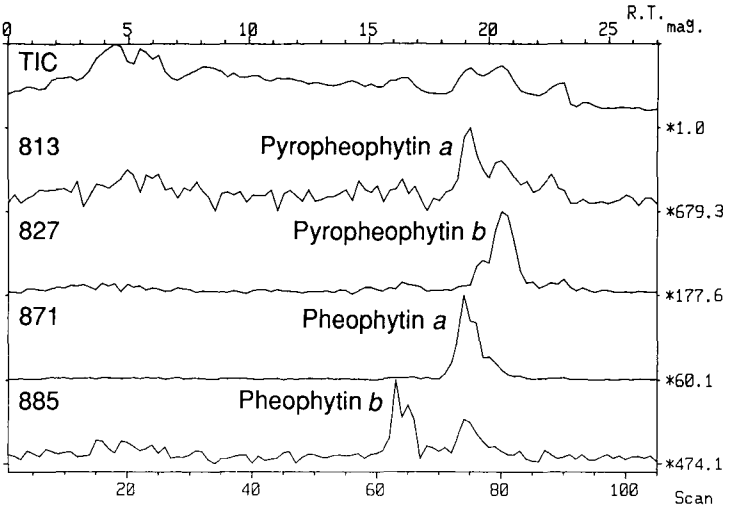

Fig. 7. Total-ion chromatogram and mass chromatograms for a mixture of pyropheophytins *a* and *b* and pheophytins *a* and *b* obtained using positive-ion HPLC–frit-FAB-MS. Mass spectra were recorded beginning 15 min after injection instead of 5 min as in Figs. 3 and 5. R.T. = Retention time in min. Right-hand scale: mag = magnification factor.

tract (Fig. 3) eluted at the solvent front (approximately 2 min), and at 3, 12 and 22.3 min. The most abundant contaminant band, eluting at 3 min, produced a base peak that corresponded to a protonated molecule at *m/z* 521. In the pheophytin extract (Fig. 5), the major bands that did not correspond to chlorophyll derivatives were

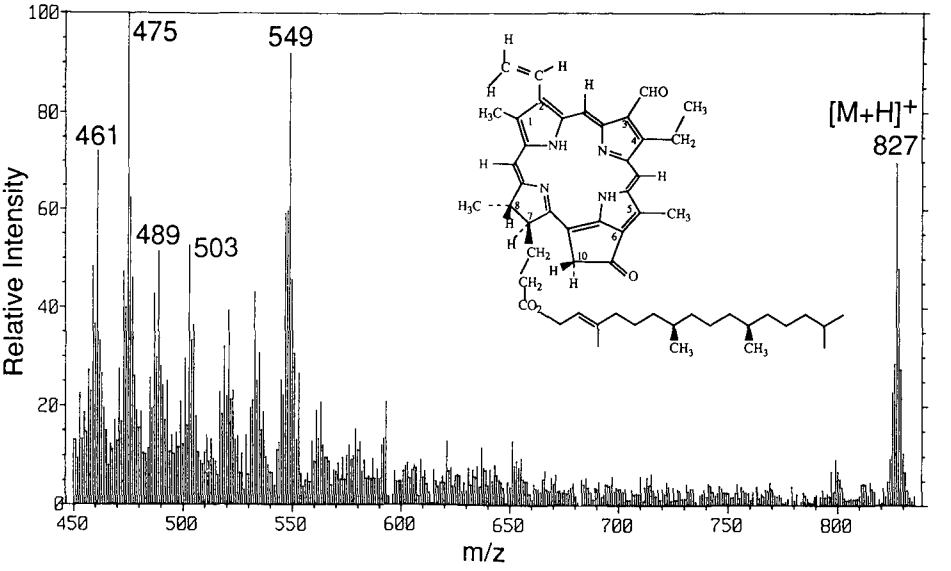

Fig. 8. Positive-ion frit-FAB mass spectrum of pyropheophytin *b* recorded at a retention time of 20.6 min in the HPLC–MS chromatogram shown in Fig. 7.

observed at 1.5, 6.8 and 12.3 min. Because these samples were prepared as crude extracts of spinach, the presence of hydrophobic compounds other than chlorophyll derivatives was expected. No further characterization of these contaminants was undertaken.

Grese *et al.* [17] have suggested and other investigators have shown [30,31] that formation of radical species in solution such as chlorophyll $M^{+\cdot}$ ions or perhaps radical matrix species can result in chlorophyl allomerization. These products typically form by oxidation of chlorophyll to a radical cation followed by nucleophilic attack at the C-10 position [31]. The longer chlorophylls are exposed to the FAB beam, the more oxidized by-products are produced [17]. During HPLC–frit-FAB-MS analysis of nine chlorophyll derivatives, no evidence of chlorophyll allomerization was observed. Because fresh sample and matrix are continuously flowing onto the frit-FAB probe, degradative processes such as reactions between chlorophyll and matrix are minimized compared to standard probe FAB-MS. Furthermore, the use of protic matrices such as glycerol minimizes the formation of radical ions and promotes the formation of protonated molecules instead.

CONCLUSIONS

The first HPLC–MS separation and identification of chlorophylls and their chlorophyllide, pheophytin, pheophorbide and pyropheophytin derivatives is reported here. The on-line combination of HPLC with FAB-MS provides a rapid and specific method to characterize chlorophyll derivatives. Although not used in this investigation, a UV–VIS absorbance detector could be added between the HPLC column and the mass spectrometer for further characterization of the pigments.

Compared to our previous HPLC analyses of chlorophyll derivatives using visible absorbance detection [26], HPLC–MS chromatograms showed the same order of elution for each chlorophyll derivative but with different retention times and lower chromatographic resolution. These differences were the result of the addition of glycerol to the mobile phase for HPLC–MS, the use of a shorter HPLC column, and a faster gradient program. Glycerol matrix was added to the mobile phase instead of post-column or coaxial addition for convenience and technical simplicity. The HPLC column and gradient were selected to increase the speed of each HPLC–MS analysis, which was important because of the high demand for MS analyses in our laboratory.

Compared to HPLC fraction collection, sample concentration *in vacuo*, and then analysis by MS or other techniques, HPLC–MS is much faster and reduces the time the sample might be exposed to light or atmospheric oxygen during handling. Furthermore, HPLC–frit-FAB-MS minimizes chlorophyl allomerization that occurs during standard probe FAB as a result of exposure to the FAB beam in the presence of nucleophilic matrix. Unlike moving-belt or thermospray HPLC–MS, the HPLC eluate is heated only slightly during HPLC–frit-FAB-MS so that pyrolysis of chlorophyll pigments does not occur. (The ion source was heated to 40°C to prevent freezing of solvent in the frit.) Given the ease of use and numerous advantages of the method, HPLC–frit-FAB-MS can be a powerful technique for the identification of new chlorophyll derivatives from natural sources and for biochemical studies of chlorophyll degradation products formed during senescence of leaves.

ACKNOWLEDGEMENTS

This material is based upon work supported by the North Carolina Biotechnology Center. Preliminary results were presented at the *38th ASMS Conference on Mass Spectrometry and Allied Topics, Tucson, AZ, June 3–8, 1990.*

REFERENCES

1 T. W. Goodwin, *Chemistry and Biochemistry of Plant Pigments*, Academic Press, New York, 2nd ed., 1976.
2 J. Gross, *Pigments in Fruits*, Alden Press, Oxford, 1987.
3 M. A. Posthumus, P. G. Kistemaker, H. L. C. Meuzelaar and M. C. Ten Noever de Brauw, *Anal. Chem.*, 50 (1978) 985.
4 J.-C. Tabet, M. Jablonski, R. J. Cotter and J. E. Hunt, *Int. J. Mass Spectrom. Ion Processes*, 65 (1985) 105.
5 R. S. Brown and C. L. Wilkins, *J. Am. Chem. Soc.*, 108 (1986) 2447.
6 J. Grotemeyer, U. Boesl, K. Walter and E. W. Schlag, *J. Am. Chem. Soc.*, 108 (1986) 4233.
7 J. Grotemeyer and E. W. Schlag, *Angew. Chem. Eng. Ed.*, 27 (1988) 447.
8 R. C. Dougherty, P. A. Driefuss, J. Sphon and J. J. Katz, *J. Am. Chem. Soc.*, 102 (1980) 416.
9 A. H. Jackson, *Phil. Trans R. Soc. Lond. A*, 293 (1979) 21.
10 J. E. Hunt, R. D. Macfarlane, J. J. Katz and R. C. Dougherty, *J. Am. Chem. Soc.*, 103 (1981) 6775.
11 B. T. Chait and F. H. Field, *J. Am. Chem. Soc.*, 104 (1982) 5519.
12 B. T. Chait and F. H. Field, *J. Am. Chem. Soc.*, 106 (1984) 1931.
13 M. Barber, R. S. Bordoli, G. J. Elliot, R. D. Sedgwick and A. N. Tyler, *Anal. Chem.*, 54 (1982) 645A.
14 R. G. Brereton, M. B. Bazzaz, S. Santikarn and D. H. Williams, *Tetrahedron Lett.*, 24 (1983) 5775.
15 D. L. Bricker and D. H. Russell, *J. Am. Chem. Soc.*, 108 (1986) 6174.
16 R. Guevremont and R. K. Boyd, *Int. J. Mass Spectrom. Ion Processes*, 84 (1988) 47.
17 R. P. Grese, R. L. Cerny, M. L. Gross and M. Senge, *J. Am. Soc. Mass Spectrom.*, 1 (1990) 72.
18 R. B. van Breemen, F. L. Canjura and S. J. Schwartz, *J. Agric. Food Chem.*, (1990) submitted for publication.
19 E. Constantin, Y. Nakatani, G. Teller, R. Hueber and G. Ourisson, *Bull. Soc. Chim. Fr.*, 7/8 (1981) II303.
20 C. Fenselau and R. J. Cotter, *Chem. Rev.*, 87 (1987) 501.
21 R. M. Caprioli, T. Fan and J. S. Cottrell, *Anal. Chem.*, 58 (1986) 2949.
22 Y. Ito, T. Takeuchi, D. Ishi and M. Goto, *J. Chromatogr.*, 346 (1985) 161.
23 R. M. Caprioli, W. T. Moore, B. Dague and M. Martin, *J. Chromatogr.*, 443 (1988) 355.
24 S. Pleasance, P. Thibault, M. A. Moseley, L. J. Deterding, K. B. Tomer and J. W. Jorgenson, *J. Am. Soc. Mass Spectrom.*, 1 (1990) 312.
25 D. E. Games, S. Pleasance, E. D. Ramsey and M. A. McDowall, *Biomed. Environ. Mass Spectrom.*, 15 (1988) 179.
26 F. J. Canjura and S. J. Schwartz, *J. Agric. Food Chem.*, (1991) in press.
27 F. J. Canjura, S. J. Schwartz and R. V. Nunes, *J. Food Sci.*, (1991) in press.
28 R. M. Caprioli, *Anal. Chem.*, 62 (1990) 477A.
29 S. J. Schwartz, S. L. Woo and J. H. von Elbe, *J. Agric. Food Chem.*, 29 (1981) 533.
30 J. E. Hunt, P. M. Schaber, T. J. Michalski, R. C. Dougherty and J. J. Katz, *Int. J. Mass Spectrom. Ion Phys.*, 53 (1983) 45.
31 P. M. Schaber, J. E. Hunt, R. Fries and J. J. Katz, *J. Chromatogr.*, 316 (1984) 25.

Journal of Chromatography, 542 (1991) 385–395
Elsevier Science Publishers B.V., Amsterdam

CHROM. 23 051

Determination of chlorophenoxy acids using high-performance liquid chromatography–particle beam mass spectrometry

M. J. INCORVIA MATTINA

Department of Analytical Chemistry, Connecticut Agricultural Experiment Station, 123 Huntington Street, New Haven, CT 06511 (U.S.A.)

(First received August 28th, 1990; revised manuscript received December 4th, 1990)

ABSTRACT

An isocratic mobile phase of methanol containing phenoxyacetic acid–dilute acetic acid (70:30) achieved a good high-performance liquid chromatographic (HPLC) separation of 2,4-dichlorophenoxyacetic acid (2,4-D), 2,4,5-trichlorophenoxyacetic acid (2,4,5-T) and 2-(2,4,5-trichlorophenoxy)propionic acid (Silvex). The HPLC eluate was introduced into a mass spectrometer operated under methane-enhanced electron-capture negative ionization conditions through the particle beam interface. With the mass spectrometer operated in selected-ion monitoring mode, detection limits in the low μg/l range were attained for all three acids. This is one of the first reports of liquid chromatography coupled with mass spectrometry through the particle beam interface for the detection of chlorophenoxy acid herbicides.

INTRODUCTION

The widespread use of chlorophenoxy acid herbicides has resulted in their detection as residues in surface water and ground water [1]. For this reason, there is a need for the development of sensitive methods for the analysis of water samples for the presence of these herbicides. The original methods for the detection of the chlorophenoxy acids in water utilized liquid–liquid extraction followed by esterification to permit analysis by gas chromatography (GC) with electron-capture detection [2–6]. Recently, it has been demonstrated that the liquid–liquid extraction step may be replaced by solid-phase extraction (SPE) of the water sample using SPE cartridges. SPE and elution are followed either by high-performance liquid chromatography (HPLC) with UV detection of the intact acids [7] or by methylation of the acids followed by GC–mass spectrometric (MS) analysis of the methyl esters [8].

Because of its specificity, MS detection is preferable to the use of other detectors, such as the variable-wavelength UV detector used by Hoke *et al.* [7]. On the other hand, the derivatization required in the GC–MS approach of Infante and Peréz [8] prolongs the analysis. Obviously, the coupling of LC with MS for the detection of the intact acids can achieve both the specificity and the speed of analysis desirable for non-volatile analytes such as chlorophenoxy acids.

0021-9673/91/$03.50

The particle beam interface permits LC–MS to be attained relatively simply [9]. Among the additional advantages of this interface is its ability to generate classical electron impact (EI) and chemical ionization (CI) mass spectra. This is an asset over other types of LC–MS interfaces such as thermospray (TSP), which yield spectra with little or no fragmentation [10]. The relatively poor sensitivity of the particle beam interface, however, has been a drawback in its application to environmental analyses [11]. The disappointing sensitivity has been attributed to reduced transport efficiency of the analytes through the desolvation chamber and the momentum separator. Improved transport efficiency, as evidenced by MS signal enhancement, has been attained through the addition of a "carrier" to the mobile phase. For example, ammonium acetate has been used as a carrier for several different classes of compounds, such as phenylureas and carbamates [12]. Alternatively, isotopically labelled analogues of each analyte of interest have also been reported as carriers [13]. One analysis has been reported using a carrier, malic acid, specific for one target analyte, alar, which has a structure similar to that of the carrier [14].

The method reported here combines the particle beam interface for LC–MS analysis together with the time-saving use of SPE for three intact chlorophenoxy acids: 2,4-dichlorophenoxyacetic acid (2,4-D), 2,4,5-trichlorophenoxyacetic acid (2,4,5-T) and 2-(2,4,5-trichlorophenoxy)propionic acid (Silvex). Picogram amounts of the acids can be detected by using the carrier, phenoxyacetic acid, as a component in the mobile phase. The detection limit was also improved by operating the mass spectrometer in the selected ion monitoring (SIM) mode under methane-enhanced electron-capture negative ionization (ECNI) conditions. Recovery data for each analyte spiked into distilled water ranged from 89% to 109%. Linear calibration graphs were obtained with approximately 8–60 ng of each analyte injected on-column.

EXPERIMENTAL

Reagents

The chlorophenoxy acids at $\geq 99\%$ purity were obtained from Dow Chemical (Midland, MI, U.S.A.). Phenoxyacetic acid (PAA) was purchased from Aldrich (Milwaukee, WI, U.S.A.). Solvents were of HPLC grade or Resi-Analyzed grade (J. T. Baker, Phillipsburg, NJ, U.S.A.). Water was distilled and passed through a Barnstead (Newton, MA, U.S.A.) NANOpure II system followed by 0.2-μm filtration. Acidified water was prepared by adding 0.2 ml of concentrated HCl to 250 ml of distilled, dionized water. SPE cartridges were C_{18} high-capacity 6-ml cartridges from J. T. Baker.

Helium for the nebulizer on the particle beam interface was of ultra-high purity grade (Union Carbide–Linde Division, Danbury, CT, U.S.A.) and was filtered through an Oxyclear disposable gas purifier (Labclear, Oakland, CA, U.S.A.), followed by a Supelco (Bellefonte, PA, U.S.A.) OMI-1 filter. Methane for chemical ionization was of ultra-high purity grade (Union Carbide–Linde Division) and was filtered through an OMI-1 filter.

Apparatus

A Hewlett-Packard Model 1090 liquid chromatograph fitted with a Rheodyne (Cotati, CA, U.S.A.) Model 7010 injector equipped with a Rheodyne Model 7012

loop filler port and a 20-μl loop was coupled to a Hewlett-Packard Model 5988A quadrupole mass spectrometer through the HP 59980A particle beam interface. Data acquisition and processing were under the control of the HP 59970C MS Pascal ChemStation (Rev. 3.2). A Waters Assoc. (Milford, MA, U.S.A.) 300 mm × 2.1 mm I.D. stainless-steel μBondapak (10 μm) C_{18} column was protected by a Supelco LC 18 guard column.

Acrodisc polytetrafluoroethylene (PTFE) 0.2-μm filters (Gelman, Ann Arbor, MI, U.S.A.) were washed with HPLC-grade methanol prior to use.

Calibration graphs

A 1000 μg/ml stock solution of each herbicide was prepared in methanol, and diluted to give a 10.00 ng/μl methanolic solution of each herbicide. Appropriate volumes of the 10.00 ng/μl solutions were diluted with methanol to prepare 2.00 ml of four calibration solutions, each of which contained a mixture of the three herbicides. The concentrations of each herbicide in the calibration solutions were as follows: solution 1, 0.500 ng/μl; solution 2, 1.00 ng/μl; solution 3, 2.00 ng/μl; and solution 4, 3.00 ng/μl. Each calibration solution was well mixed and filtered through a 0.2-μm PTFE filter. To each filtered solution 300 μl of acidified water were added.

Solid-phase extraction

A sample of water was spiked with the 10.00 ng/μl methanolic solution of each herbicide to achieve a 20.00 μg/l concentration level of each herbicide when the final volume of the spiked solution was 100.00 ml. To the spiked water was added 0.08 ml of concentrated HCl and the volume was adjusted to 100.00 ml. The 6-ml C_{18} high-capacity SPE cartridge was conditioned with 5 ml of ethyl acetate, followed by 5 ml of methanol, then 20 ml of distilled, dionized water and finally 5 ml of acidified water. The solvents were drawn through the cartridge under gentle vacuum (5 in. Hg) and the cartridge was not permitted to run dry after addition of the acidified water. A 75-ml reservoir was fitted to the top of the cartridge and the water spiked with the herbicides was drained through the cartridge under gentle vacuum at the rate of *ca.* 5 ml/min. After the solution had drained completely through the cartridge, the cartridge was washed with 5 ml of acidified water. The cartridge was then air dried for 5 min. The herbicides were eluted with 2.00 ml of methanol under very gentle vacuum. To the methanolic eluate 300 μl of acidified water were added.

Liquid chromatography

An isocratic mobile phase consisting of a 70:30 mixture of methanol, which contained PAA at a concentration of 1.7 ng/μl, and 1% acetic acid eluted 2,4-D, 2,4,5-T and Silvex in under 10 min. The injection size was 20 μl and the flow-rate was 0.4 ml/min.

RESULTS AND DISCUSSION

Fig. 1 shows a typical particle beam–methane-enhanced ECNI chromatogram acquired in the SIM mode under the LC conditions specified above for 52 ng of each herbicide injected on-column. 2,4-D was eluted at 5.3 min, 2,4,5-T at 6.7 min and Silvex at 8.6 min. These retention times were steady to within 6 s for all injections

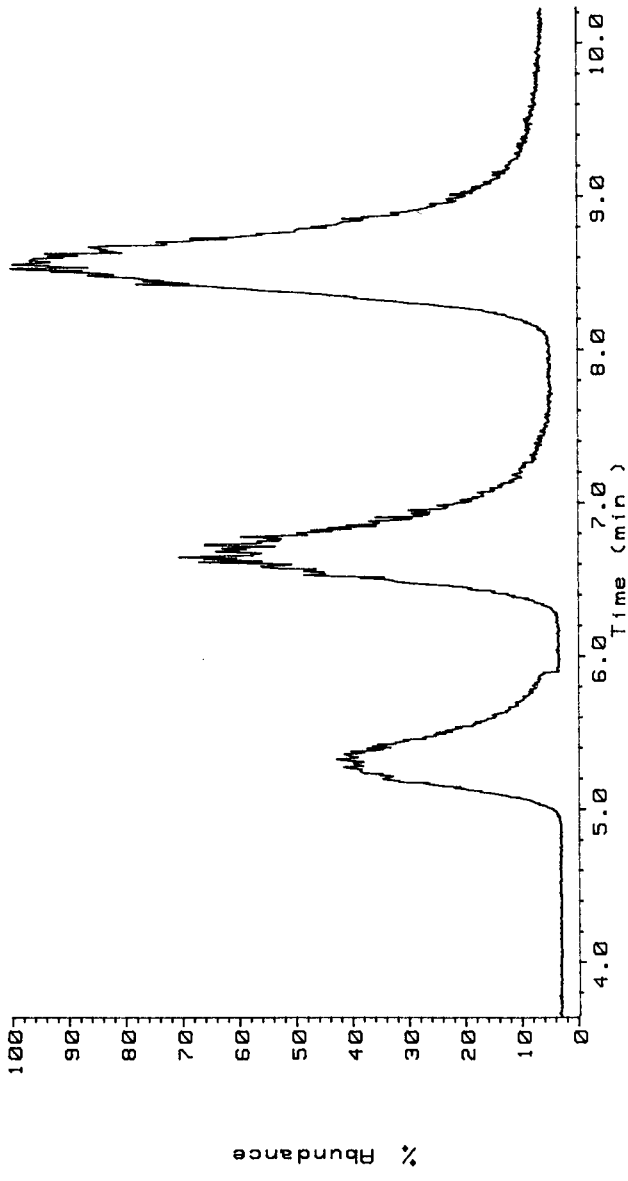

Fig. 1. Chromatogram obtained from HPLC–particle beam MS of 2,4-D, 2,4,5-T and Silvex in the methane-enhanced ECNI mode under SIM conditions.

performed over the course of 5 h. The isocratic elution of 2,4-D, 2,4,5-T and Silvex (in that order) from a C_{18} LC column by means of a mobile phase composed of methanol containing 1.7 ng/μl phenoxyacetic acid–1% acetic acid (70:30) is similar to earlier observations using methanol–1% acetic acid (68:32) as the mobile phase [7]. The addition of phenoxyacetic acid to the mobile phase has no apparent adverse effect on the chromatography.

The initial attempt to use the carrier effect for the improvement of detection limits in the analysis of 2,4-D using HPLC–particle beam mass spectrometry in our laboratory focused on the addition of ring [$^{13}C_6$]-2,4-D to water samples previously spiked with native 2,4-D. The results of this experiment indicated that the native 2,4-D, present in the isotopically labelled material at a 1% impurity level interfered with the 2,4-D concentrations added to the water sample.

It was determined subsequently that PAA can serve as a generic carrier for all three herbicides examined. Another advantage of using PAA as the carrier for the chlorophenoxy acid herbicides derives from the smaller electron-capture cross-section of PAA relative to that of the chlorophenoxy acid herbicides. This means that in the MS source PAA has a lower tendency to capture thermal electrons during the ECNI process than the chlorinated phenoxy acid herbicides [15]. Hence there is no reduction in the ionization efficiency of the analytes or the sensitivity of the analytes to ECNI in the presence of PAA.

PAA was added to the methanol component of the mobile phase at a concentration of 1.7 ng/μl. Using flow-injection analysis (FIA) it was determined that higher concentrations of PAA did not improve the detection limits and lower concentrations did not maximize the signal enhancement. For example, without the PAA carrier in the mobile phase, 20 μl of a 100 ppb solution of 2,4-D (2000 pg) injected in FIA was undetectable by LC–particle beam MS with methane ECNI in the SIM mode. With the phenoxyacetic acid carrier at 1.7 μg/ml in the methanol component of the mobile phase, it was possible to detect 20 μl of a 25 ppb solution of 2,4-D (500 pg) in FIA. With the LC column in place, 20 μl of a 50 ppb solution of each herbicide (1000 pg) injected on-column was detectable at a signal-to-noise ratio of 3:1 when PAA was present in the mobile phase. Beginning with an original sample size of 100 ml and adhering to the procedure outlined above, this detection limit translates into a concentration of 1.1 μg/l (1.1 ppb) for each herbicide in the original sample.

The MS conditions employed are summarized in Table I. Although LC–particle beam MS for 2,4-D and Silvex in the EI mode has been reported [16, 17], the molar response factors for the chlorophenoxy acids, determined by FIA, are approximately ten times larger in the methane ECNI mode than in the EI mode (unpublished results). A similar observation has been made for other chlorinated herbicides [18]. Although the mass spectrometer is tuned at a source temperature of 200°C using perfluorotributylamine (PFTBA)–perfluorobenzonitrile (PFBN) (1000:1), the optimum sensitivity for the chlorophenoxy acid herbicides is achieved with the source at 300°C. The full-scan methane-enhanced ECNI spectra for 200 ng of each herbicide injected on-column are shown in Fig. 2–4. The ions monitored in the SIM analysis correspond to the $[M - HOCl]^{-\cdot}$ fragment for each herbicide.

The settings for the particle beam parameters required for optimum sensitivity, such as the helium nebulizer pressure and the nebulizer position, were determined by means of FIA of the chlorophenoxy acids.

TABLE I

PARTICLE BEAM AND MASS SPECTROMETER CONDITIONS FOR THE ANALYSIS OF CHLOROPHENOXY ACIDS

Parameter	Conditions
Desolvation chamber temperature	47°C
He nebulizer pressure	26 p.s.i.
Ionization mode	Methane ECNI
Source temperature	300°C
Source pressure	0.5 Torr[a]
Acquisition mode	SIM
	m/z 168[b], 170; 4.0–5.9 min
	m/z 202[b], 204; 5.9–7.8 min
	m/z 216[b], 218; 7.8–10.2 min

[a] Pressure as measured with the thermocouple gauge at the GC–MS interface.
[b] The quantification ion for each herbicide is designated.

The well-defined peak shape for all three herbicides in the particle beam–methane-enhanced ECNI chromatogram shown in Fig. 1 was achieved with the addition of acidified water to the calibration solutions. Without this addition the peaks for all three herbicides were broad and poorly resolved. It should be noted that the pH of the mobile phase employed was 3.5. When acidified water was added to the LC mobile phase in the proportion specified under Experimental, the pH dropped to 2.8. As the pK_a values of the three chlorophenoxy acids are in the range 2.8–3.0 [19], the acidified water is necessary to assure that the compounds are in the acid form in the calibration solutions. Under the experimental conditions employed, conversion of the free chlorophenoxy acids to the corresponding methyl esters is unlikely. A preliminary study of the LC–particle beam MS of the methyl esters of 2,4-D, 2,4,5-T and Silvex showed that they do not interfere with the LC or the MS of the free acids.

The calibration graphs for the three herbicides, constructed by performing duplicate injections of each calibration solution in random order and plotting the peak height of the calibration ion *versus* the amount injected, are shown in Fig. 5.
The correlation coefficients were calculated to be 0.994 for 2,4-D, 0.990 for 2,4,5-T and 0.996 for Silvex. In contrast to the linear calibration graphs in Fig. 5, calibration graphs for LC–particle beam MS determined using the methane ECNI mode for chlorinated phenylurea herbicides without the use of a carrier in the mobile phase were non-linear [20]. The reports of other workers confirm that without a carrier in the mobile phase, the calibration graphs obtained with particle beam MS in both the EI [13] and CI [14] modes tend to be non-linear.

The SPE recovery data are summarized in Table II. The spiking level was chosen to be within the range of the maximum contaminant levels set by the EPA National Primary Drinking Water Regulations, *i.e.*, 100 μg/l for 2,4-D and 10 μg/l for Silvex [21]. The data were obtained by making duplicate injections in random order of each recovery solution, three solutions prepared with tap water and three solutions prepared with distilled, deionized water. The recovery results were similar when either 2 μg were added to a 100-ml water sample or 1 μg was added a 50-ml water sample. Whereas the recovery data from the distilled, deionized water samples are acceptable,

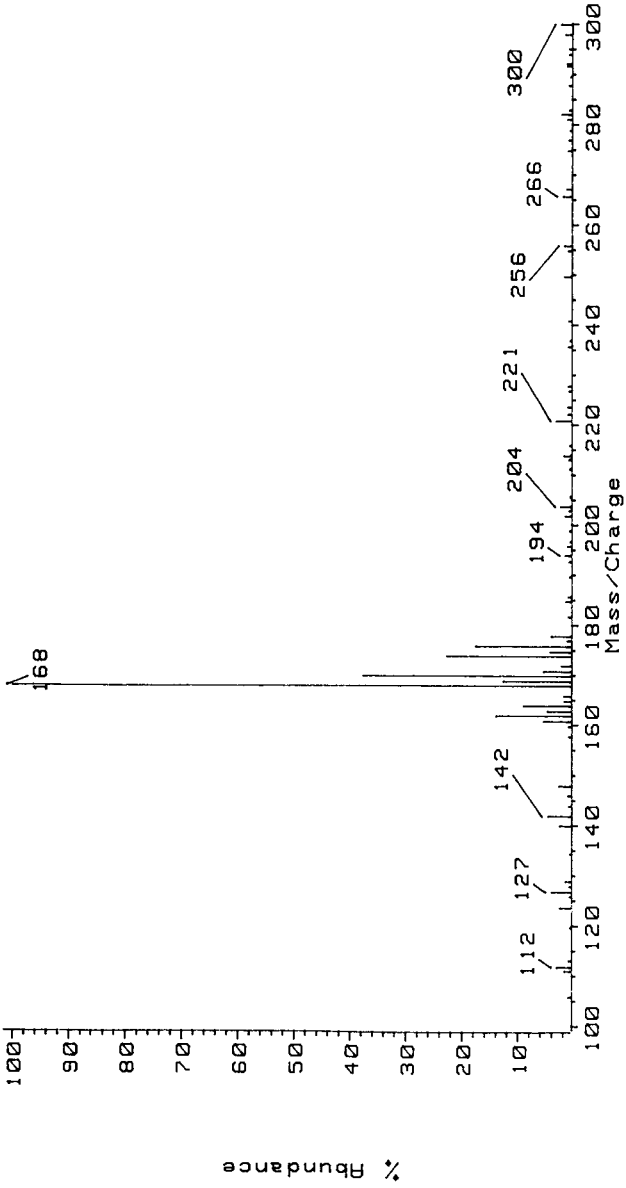

Fig. 2. Full-scan HPLC–particle beam methane-enhanced ECNI mass spectrum for 2,4-D.

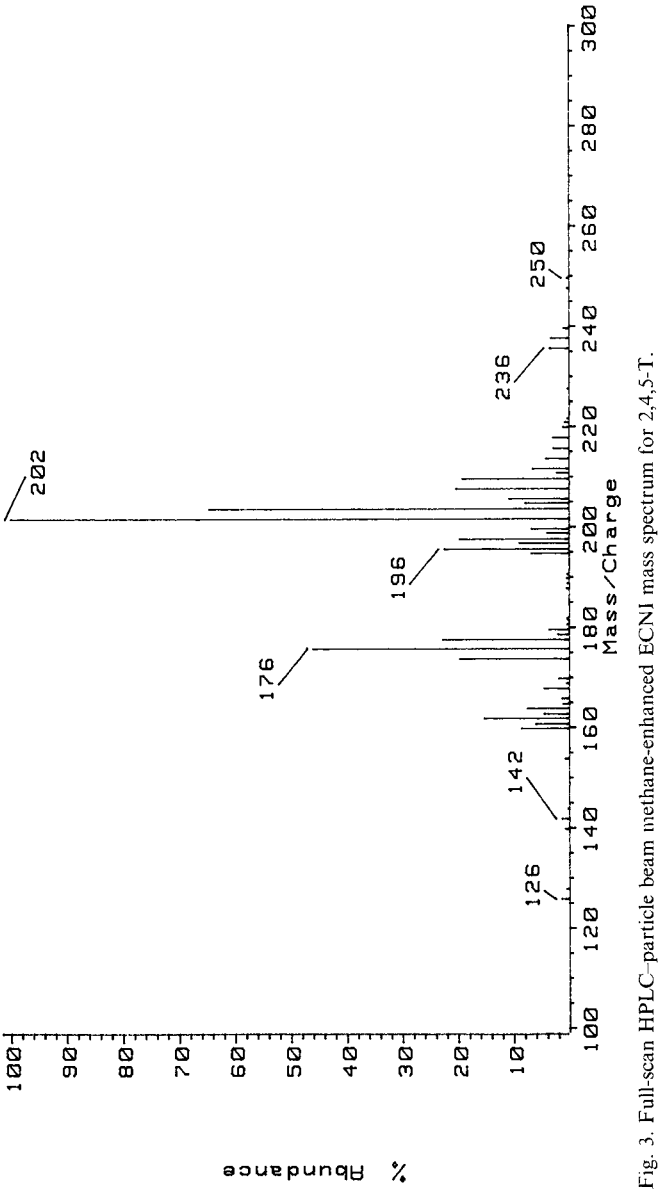

Fig. 3. Full-scan HPLC–particle beam methane-enhanced ECNI mass spectrum for 2,4,5-T.

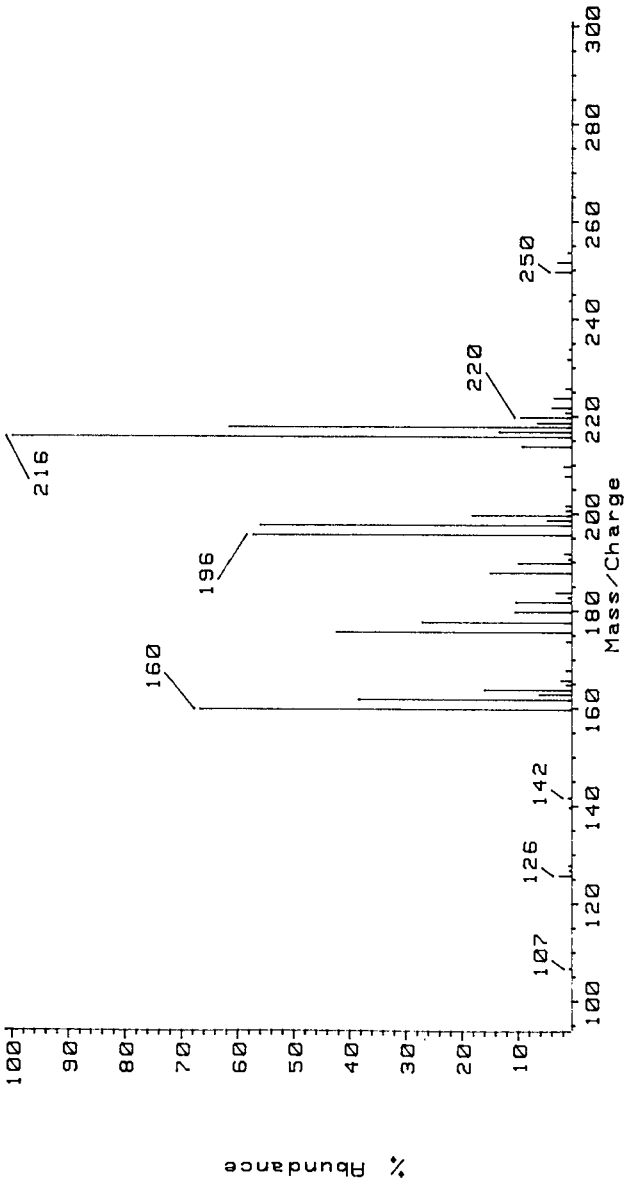

Fig. 4. Full-scan HPLC–particle beam methane-enhanced ECNI mass spectrum for Silvex.

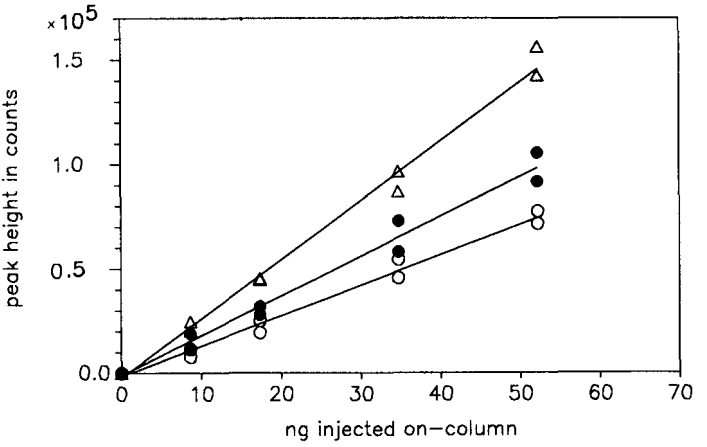

Fig. 5. Calibration graphs for (○) 2,4-D, (●) 2,4,5-T and (△) Silvex using HPLC–particle beam methane-enhanced ECNI in the SIM mode.

those from the tap water samples are consistently high. SPE recovery data reported by other investigators for chlorophenoxy acids in environmental waters range from 29% to 76% [7] and in drinking water recoveries of 31% and 156% have been reported [8].

In summary, HPLC–particle beam mass spectrometry in the methane-enhanced ECNI mode has been shown to provide the sensitivity, accuracy and precision necessary for the determination of three chlorophenoxy acid herbicides in water. The method can be coupled with SPE to provide the rapid analysis of water samples for these herbicides. Further studies are in progress to extend the method to additional compounds in this class and to investigate the higher recoveries observed for environmental water samples.

TABLE II
SPE RECOVERY FOR CHLOROPHENOXY ACIDS FROM WATER AS DETERMINED BY HPLC–PARTICLE BEAM MS IN THE METHANE-ENHANCED ECNI MODE

Spiking level (μg/l)	Recovery (%)			Water
	2,4-D	2,4,5-T	Silvex	
20 (n = 6)	89.3 ± 10.5	109.1 ± 15.4	99.5 ± 8.7	DDI[a]
20 (n = 6)	109.2 ± 6.9	134.8 ± 25.0	123.8 ± 12.9	Tap
0 (n = 3)	0	0	0	DDI[a]
0 (n = 3)	0	0	0	Tap

[a] Distilled, deionized water.

REFERENCES

1 N. Masuda, Y. Kondo, H. Motomura and M. Yamaguchi, *Nagasaki-ken Eisei Kogai Kenkyushoho*, 26 (1984) 170.
2 A. E. Greenberg, R. R. Trussell and L. S. Clesceri (Editors), *Standard Methods for the Examination of Water and Wastewater*, American Public Health Association, Washington, DC, 16th ed., 1985, Method 509 B.
3 V. Lopez-Avila, P. Hirata, S. Kraska and J. H. Taylor, *J. Agric. Food Chem.*, 34 (1986) 530.
4 S. M. Waliszewski and G. A. Szymczynski, *Fresenius' Z. Anal. Chem.*, 322 (1985) 510.
5 B. A. Olson, T. C. Sneath and N. C. Jain, *J. Agric. Food Chem.*, 26 (1978) 640.
6 A. S. Y. Chau and K. Terry, *J. Assoc. Off. Anal. Chem.*, 59 (1976) 633.
7 S. H. Hoke, E. E. Brueggemann, L. J. Baxter and T. Trybus, *J. Chromatogr.*, 357 (1986) 429.
8 R. Infante and C. Peréz, in R. M. Caprioli (Editor), *Proceedings of the 38th ASMS Conference on Mass Spectrometry and Allied Topics, Tucson, AZ, June 3–8, 1990*, American Society for Mass Spectrometry, East Lansing, MI, 1990, p. 645.
9 R. C. Willoughby and R. F. Browner, *Anal. Chem.*, 56 (1984) 2626.
10 T. A. Bellar and W. L. Budde, *Anal. Chem.*, 60 (1988) 2076.
11 T. D. Behymer, T. A. Bellar and W. L. Budde, *Anal. Chem.*, 62 (1990) 1686.
12 T. A. Bellar, T. D. Behymer and W. L. Budde, *J. Am. Soc. Mass Spectrom.*, 1 (1990) 92.
13 L. McLaughlin, T. Wachs, R. Pavelka, G. Maylin, and J. Henion, paper presented at the 1990 Pittsburgh Conference and Exposition on Analytical Chemistry and Applied Spectroscopy, New York, March 5–9, 1990.
14 I. S. Kim, F. I. Sasinos, R. D. Stephens and M. A. Brown, *J. Agric. Food Chem.*, 38 (1990) 1223.
15 S. Erharde-Zabik, J. T. Watson and M. J. Zabik, *Biomed. Environ. Mass Spectrom.*, 19 (1990) 101.
16 W. L. Budde, T. D. Behymer, T. A. Bellar and J. S. Ho, *J. Am. Water Works Assoc.*, 82 (1990) 60.
17 M. A. Brown, I. S. Kim, F. I. Sasinos and R. D. Stephens, in M. A. Brown (Editor), *Liquid Chromatography/Mass Spectrometry: Applications in Agricultural, Pharmaceutical, and Environmental Chemistry*, American Chemical Society, Washington, DC, 1990, Ch. 13, p. 198.
18 M. J. I. Mattina, in R. M. Caprioli (Editor), *Proceedings of the 38th ASMS Conference on Mass Spectrometry and Allied Topics, Tucson AZ, June 3–8, 1990*, American Society for Mass Spectrometry, East Lansing, MI, 1990, p. 1091.
19 D. Barceló, *Org. Mass Spectrom.*, 24 (1989) 219.
20 M. J. I. Mattina, *J. Chromatogr.*, submitted for publication.
21 *Code of Federal Regulations*, U.S. Government Printing Office, Washington, DC, 7–1–89 edition, 1989, Title 40, Ch. I, Part 141.12.

Journal of Chromatography, 542 (1991) 397–411
Elsevier Science Publishers B.V., Amsterdam

CHROM. 23 069

Partitioning of cells in dextran–poly(ethylene glycol) aqueous phase systems

A study of settling time, vessel geometry and sedimentation effects on the efficiency of separation

HARRY WALTER*, EUGENE J. KROB and LOUIE WOLLENBERGER[a]
Laboratory of Chemical Biology –151, Veterans Affairs Medical Center, Long Beach, CA 90822 (U.S.A.)
(Received November 6th, 1990)

ABSTRACT

The effect of prolonged settling times (up to 2 h), in high- and low-phase columns, on the cell partition ratios measured and on the separability of cell populations was examined. With closely related cell populations, modelled by rat erythrocytes in which subpopulations of red blood cells of distinct age were labeled isotopically, it was found that partitioning proceeds over the entire time period examined as evidenced by the continuous change in relative specific activity of cells in the top phase as the partition ratio falls. In control cell sedimentation experiments in top phase there was almost no change in the quantity of cells present when vertical settling (*i.e.*, high-phase columns) was used and no separation of specific subpopulations was found. In the horizontal settling mode the initially higher cell partition ratio, as compared to vertical settling, decreased to a greater extent with longer time intervals; a given purity of cells only being obtained at a lower partition ratio than in the vertical settling mode. Cell sedimentation in top phase was appreciable with time in the horizontal settling mode but did not result in a separation of cell subpopulations.

The effect of relative cell partition ratios and sizes in high- and low-phase columns on the efficiency of separation was examined by use of rat or sheep ^{51}Cr-labeled red cells mixed with an excess of human unlabeled erythrocytes. Rat and sheep red cells are appreciably smaller than human erythrocytes. Rat red cells have higher, and sheep red cells lower partition ratios than human erythrocytes. With vertical settling, over a 2-h period, there is no appreciable contribution to the change in relative specific activities by cell sedimentation. However, the more rapid sedimentation of the larger human red cells has, with time, a measurable effect on the relative specific activities obtained during cell partitioning when run in the horizontal mode: enhancing the rat–human and diminishing the sheep–human cell separations.

Partitioning cells in high-phase columns is of advantage with respect to increasing separation efficiency and virtually eliminating the influence of other physical parameters (*e.g.*, cell size). Since the cell partitioning process continues for long periods of time, yielding ever-lower partition ratios with increasing proportions of cells with higher P values, a time may be selected which balances desired relative cell purity and yield.

INTRODUCTION

Partitioning in dextran–poly(ethylene glycol) aqueous-phase systems is an established, sensitive method for the separation and fractionation of cell populations

[a] Present address: Department of Biochemistry, Chemical Center, University of Lund, S-221 00 Lund, Sweden.

0021-9673/91/$03.50

based on differences in their surface properties (for some recent reviews see refs. 1–3). Unlike the partitioning of soluble materials which occurs between the bulk phases and depends on the materials' relative solubility, the partitioning of cells generally takes place between one of the bulk phases and the interface and is time-dependent [4,5]. Early events in the partitioning process which involve characteristic kinetics of cell- and phase-specific interactions and phase separation have previously been described [4,6,7]. A relation between phase-column height, a factor in the rapidity of phase settling, and the efficiency of cell separation has also been detailed [8]. In the current work we explore the effect of prolonged settling times, in high- and low-phase columns, on the cell partition ratios measured and on the separability of closely related cell populations as well as of cell mixtures. The contribution of cell sedimentation on the partitions obtained is also examined. Our results indicate that partitioning proceeds over a period of (at least two) hours; that with time one can obtain more purified cells at lower yield; that a given purity of cells is attained at higher yield when phase columns are high rather than low, and that cell sedimentation has no appreciable effect on the yield or separation obtained with high-phase columns but can affect both with low-phase columns.

The reported enhancement of cell separation by partitioning by extending settling times in low-phase columns [9,10] is thus: (a) a consequence of cell sedimentation superimposed on the partitioning process and (b) not to be taken as a general rule since a reduction of a partitioning separation by sedimentation can occur equally well.

EXPERIMENTAL

Reagents

Dextran T500 (lot No. 01 06905) was obtained from Pharmacia LKB (Piscataway, NJ, U.S.A.) and poly(ethylene glycol) 8000 (PEG, "Carbowax 8000") from Union Carbide (Long Beach, CA, U.S.A.). [^{59}Fe]Ferrous citrate and [^{51}Cr]-sodium chromate were products of ICN (Irvine, CA, U.S.A.). All salts used were of reagent grade.

Bleeding of rats, sheep and of human donors

Male Sprague–Dawley rats (Charles River, Wilmington, DE, U.S.A.), weighing between 250 and 400 g, were bled by heart puncture. Sheep blood (UCI Medical Center, Orange, CA, U.S.A.) was obtained by use of an indwelling catheter in the femoral vein or by venipuncture of the jugular. A 10-ml volume of blood was collected in 3 ml acid–citrate–dextrose (ACD) anticoagulant. Human blood from presumably normal individuals was obtained by venipuncture using the same ratio of blood to anticoagulant as indicated for rat and sheep blood. Red cells were used in experiments within one week of collection.

In vivo radioisotopic labeling of rat erythrocytes of different age

Some of the rats were injected with 10–20 μCi [^{59}Fe]ferrous citrate via the saphenous vein. These were then bled at 4, 12 or 13 and 42 or 43 days after injection. This gave rise to erythrocyte populations in which cells, corresponding in age to the time which elapsed between injection and bleeding, were radioactively labeled.

Aliquots of the erythrocyte populations were washed three times with at least ten times the cell volume of isotonic aqueous salt solution (saline) before being used in the partitioning experiments described below.

In vitro radioisotopic labeling of rat or sheep erythrocytes and the preparation of mixtures of rat or sheep labeled red cells plus human unlabeled erythrocytes to test cell separation efficiency by partitioning

Labeling of erythrocytes with [^{51}Cr]sodium chromate has previously been described [11]. Approximately 10–20 μCi ^{51}Cr was used per ml of an aliquot of anticoagulated rat or sheep blood. Labeled rat or sheep blood and an aliquot of unlabeled human blood were then washed five times with saline.

To test the efficiency of the separation of human plus rat or sheep erythrocytes by partitioning under various conditions (see below) a mixture of ^{51}Cr-labeled rat or sheep erythrocytes and an excess of unlabeled human erythrocytes was prepared. Into a centrifuge tube containing four ml of saline was pipetted 0.5 ml of washed, packed, labeled rat or sheep red cells and 2.0 ml of washed, packed, unlabeled human erythrocytes. The tube was capped, inverted a few times to mix the cells, and centrifuged. The supernatant solution was discarded and the packed cell mixture used in some of the partition experiments described below.

Preparation of two-polymer aqueous phase systems

Four dextran–PEG aqueous two-phase systems having different polymer and/or salt compositions were prepared as previously reported [5]. System I was composed of 5% (w/w) dextran, 3.6% (w/w) PEG, 0.15 *M* sodium chloride and 0.01 *M* sodium phosphate buffer, pH 6.8; system II contained 5% (w/w) dextran, 4.4% (w/w) PEG and 0.11 *M* sodium phosphate buffer, pH 6.8; system III, 5% (w/w) dextran, 3.4% (w/w) PEG with the same salt composition as system I; and system IV, 5% (w/w) dextran, 3.9% (w/w) PEG and the same salt composition as system II. Systems II and IV in which phosphate predominates have an electrostatic potential difference between the phases (top phase positive) and are deemed charge-sensitive [5]. Phases in which sodium chloride is the main salt have virtually no potential difference between the phases and are non-charge-sensitive [5].

Partitioning of erythrocytes in aqueous two-phase systems as a function of vessel geometry and time

The phase system which was to be used for partitioning, at 21–24°C, was mixed and about 12 ml were poured into each of 14 partition tubes (*i.e.*, calibrated tubes, 125 mm × 16 mm). The tubes were centrifuged to speed-up phase separation and the top- and bottom-phase volumes were adjusted to be equal at 5 ml. A 0.05-ml volume of washed, packed rat erythrocytes (containing ^{59}Fe-labeled red cells of distinct age) or a rat or sheep (^{51}Cr-labeled) plus human (unlabeled) erythrocyte mixture which was to be partitioned was added to each of the fourteen tubes containing the same phase system and mixed. As soon as a tube had been mixed the timing of its cells' partitioning commenced. One set of seven tubes was permitted to remain in a vertical position while the phases settled and the tubes were sampled at different times. A 4.5-ml volume of the top phase was withdrawn at 20, 30, 40, 50, 60, 90, or 120 min. The second set of seven tubes was capped (with parafilm) and permitted to settle in a horizontal position. One

tube was gently raised to a vertical position (without agitating the contents) after 7.5, 15, 30, 45, 60, 90 or 120 min and permitted to settle for one additional min. A 4.5-ml volume of top phase was then withdrawn. The quantity of cells in each top phase was determined by lysing the cells and measuring the hemoglobin absorbance at 540 nm as previously described [12]. The quantity of cells initially added to the partition tubes was similarly determined. Aliquots of the lysates were counted on a Beckman scintillation well-counter using the ^{59}Fe or ^{51}Cr setting (depending on the isotope used in the experiment).

Sedimentation of erythrocytes in top phase as a function of vessel geometry and time

Phase systems, at 21–24°C, in a separatory funnel, were mixed and permitted to settle overnight. Top and bottom phases were then separated. Top phase was centrifuged in a Sorvall RC-5 centrifuge (set to the same temperature range) at 12 000 *g* for 10 min to remove any remaining bottom-phase droplets. A 5-ml volume of bottom phase was pipetted into each of fourteen partition tubes as used above. A 0.75-ml volume of washed, packed erythrocytes (*i.e.*, aliquots of the same cells as used in the partitioning experiments described in the previous section) was pipetted into 70 ml of the centrifuged, absolutely clear top phase. The top phase was gently shaken so as to obtain a homogeneous cell suspension. A 5-ml volume of the latter was carefully layered over each of the bottom phases in the tubes without mixing or agitation. (This is best done by holding the tubes at an angle and permitting the cell suspension in top phase to run slowly down the inner wall of each tube.) Seven tubes were left standing in a vertical position and were sampled at various time intervals and were analyzed in a manner analogous to that described for vertical tube partitioning. Seven tubes were capped and carefully placed in a horizontal position (again without mixing or agitating the systems) and were then sampled at various time intervals and were analyzed in a manner analogous to that described for horizontal tube partitioning.

Presentation of data

The cell partition ratio, *P*, is defined as the quantity of cells in the top phase, at the time of sampling, as a percentage of the total quantity of cells added [5]. The relative specific activity (RSA), a measure of the relative extent of labeled and unlabeled cell separation in a cell population or mixture, is [6].

$$\frac{\text{counts/min per hemoglobin absorbance in the top phase}}{\text{counts/min per hemoglobin absorbance in the original, unfractionated cell population (or mixture)}}$$

In the figures we present plots of the partition ratio *vs.* the RSA value obtained at the different times of phase sampling. Sedimentation results are given in an analogous manner: percentage of added cells found in the top phase *vs.* RSA at the different sampling times. The figures show data typical of that which was obtained in at least three separate experiments using blood from different animals and individuals (with the exception of sheep blood with which only two experiments were conducted).

RESULTS

Our studies were undertaken with closely related cell populations (rat erythrocytes containing ^{59}Fe-labeled cell subpopulations of different but distinct age) and with cell mixtures (*i.e.*, ^{51}Cr-labeled rat or sheep erythrocytes plus human red blood cells). From previous studies [13,14] it is known that, in both non-charge-sensitive and charge-sensitive phase systems, rat young and middle-aged (*e.g.*., 4 and 12–13 days old) red cells have higher, and old (*e.g.*, 42–43 days) cells have lower partition ratios than the mean partition ratio of the whole cell population. Rat red cells have higher partition ratios than human erythrocytes in both non charge-sensitive and charge-sensitive phases while sheep red cells have much lower partition ratios than those from humans in non charge-sensitive phases and slightly lower partition ratios in charge-sensitive phases [5]. Furthermore, rat and sheep erythrocytes have appreciably smaller volumes than human red blood cells [15,16].

Partition and sedimentation studies on rat red blood cell populations containing ^{59}Fe-labeled erythrocytes of distinct age. Experiments in vertically-placed tubes (high-phase columns)

In the figures we show the effect of sampling time on the percentage of cells in the top phase and on the cells' RSA value. Figs. 1 (top left panel) and 2 (top left and right panels) depict results obtained with rat red cell populations containing isotopically labeled 4, 13 and 42 days old cells, respectively, partitioned in non-charge-sensitive phase system I. The points in each graph represent, in sequence from right to left samples obtained after 20, 30, 40, 50, 60, 90 and 120 min of vertical-phase settling. As the time is extended, the percentage of cells in the top phase diminishes from about 65 to 20% while the RSA values continue to change (increasing from 1.04 to 1.62 with erythrocytes containing 4 days old labeled cells, 1.00 to 1.23 with 13 days old cells, and decreasing from 0.88 to 0.60 with 42 days old cells). The ever-changing RSA values (in the absence of appreciable cell sedimentation, see below) indicate that cell partitioning continues over the entire time course of the experiment.

In Fig. 1, upper right panel, the results of a sedimentation experiment with rat erythrocytes containing 4 days old labeled cells are depicted. Cells suspended in top phase (system I) were permitted to stand in a vertical position and sampled at times and analyzed in a manner analogous to that described above for the partitioning experiments. The percentage of cells in the top phase hardly diminishes (from about 97 to 90%) over the 2-h sedimentation period and the RSA values remain virtually constant at 1.00. Identical results on sedimentation are obtained with rat red blood cells irrespective of the age of the labeled cell subpopulation they contain. Thus there is no evidence of separation in the different-aged rat erythrocytes upon sedimentation in the top phase.

Figs. 3 (top left panel) and 4 (top left and right panels) present results analogous to those in Figs. 1 and 2, respectively, except that charge-sensitive phase system II was used. In these experiments the percentage of cells in the top phase diminishes, with time, from about 60 to 50% while the RSA values change (increasing from 1.51 to 1.67 with erythrocytes containing 4 days old labeled cells, 1.50 to 1.57 with 12 days old cells, and decreasing from 0.70 to 0.56 with 43 days old cells). Thus, the initial RSA values are much higher (lower in the case of 43 days old cells) than in the non charge-sensitive

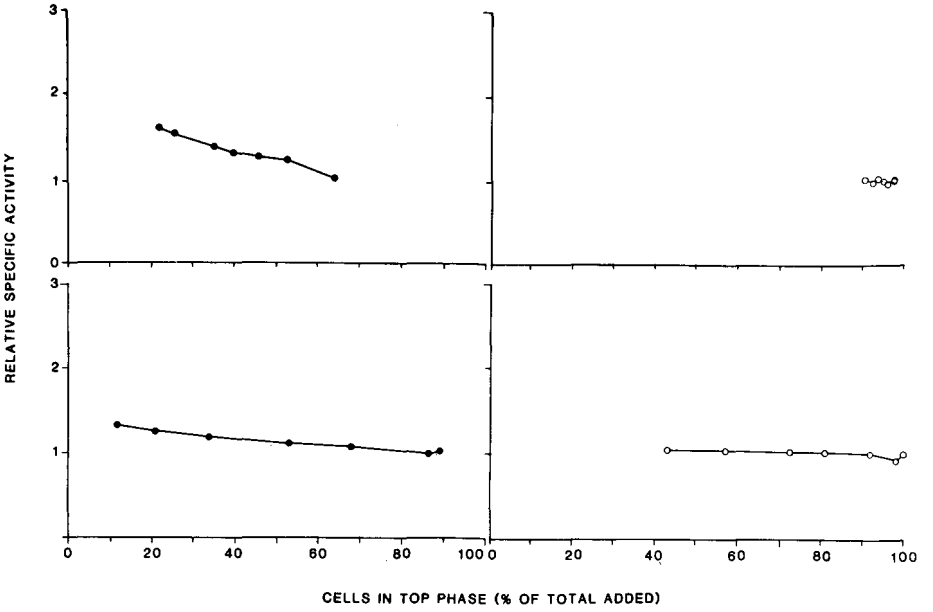

Fig. 1. Rats were injected with [^{59}Fe]ferrous citrate and bled at different times thereafter. This gave rise to red cell populations in which the bulk of labeled cells corresponds in age to the time elapsed between injection and bleeding. Rat erythrocytes of different ages have characteristic partition ratios (see text). Aliquots of such cell populations were partitioned in a dextran–poly(ethylene glycol) aqueous-phase system *or* permitted to sediment in the top phase of the same system. A series of tubes, seven in the vertical (high-phase column) and seven in the horizontal (low-phase column) mode, was used and the top phase withdrawn at different times (*i.e.*, at 20, 30, 40, 50, 60, 90 and 120 min for high- and at 7.5, 15, 30, 45, 60, 90 and 120 min for low-phase column experiments). The top phase was analyzed for the quantity of cells present as a percentage of the total cells added and for the cells' relative specific activity, RSA. In this figure data are shown in which rat blood obtained four days after isotope injection (rat No. 90-1) and non-charge-sensitive phase system I were used. The upper left panel gives results of partitioning cells in the vertical mode. The points indicate, from right to left, the time course of the decrease of cells in the top phase accompanied by an increase in RSA value (*i.e.*, enrichment of 4 days old rat red cells). The upper right panel shows the corresponding sedimentation experiment. Note that here the decrease of cells in the top phase is negligible and that the RSA value remains constant at 1.00. We conclude that cell partitioning continues over the entire 2-h period of the experiment. The lower left panel presents partitioning data in the horizontal mode. Again the time course of the decrease of cells in the top phase is accompanied by an increase in the RSA value. In the lower right panel, low-phase column sedimentation, the decrease of cells in the top phase is appreciable. The RSA value remains, however, constant at 1.00. Note that at any given percentage of cells in the top phase, the RSA value is higher when partitioned in high- rather than low-phase columns indicating a greater separation efficiency in the former mode (compare left top and bottom panels). See text for discussion.

system [Figs. 1 (top left panel) and 2 (top left and top right panels)] while the subsequent changes in RSA values are smaller.

Fig. 3, upper right panel, depicts the results of a sedimentation experiment with rat erythrocytes containing 4 days old labeled cells in phase system II and conducted as described for Fig. 1. The percentage of cells in the top phase again diminishes only slightly (from 100 to 97%) over the 2-h sedimentation period and the RSA values remain constant at 1.00. As with phase system I, identical results for sedimentation are obtained with rat red blood cells irrespective of the age of the labeled cell

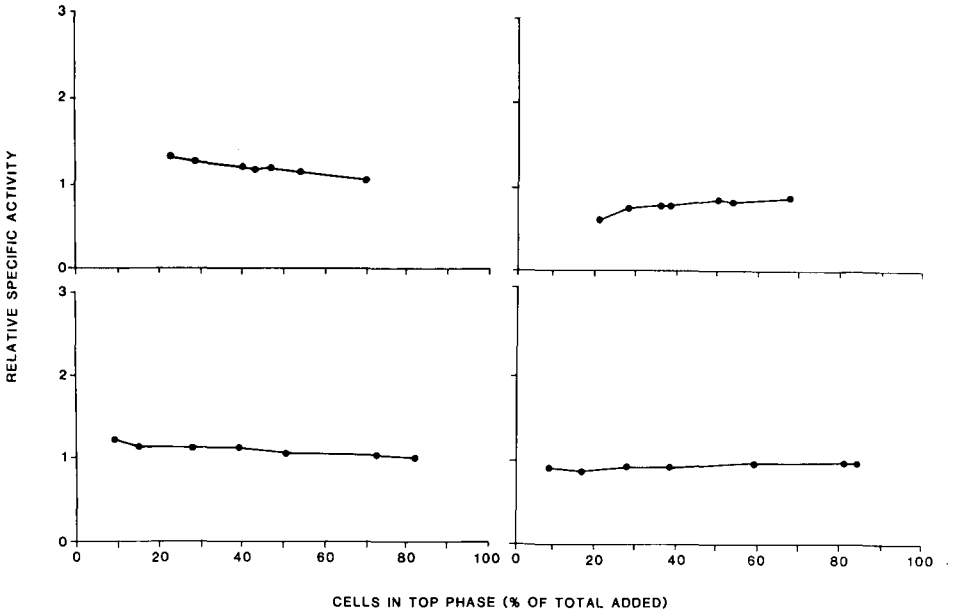

Fig. 2. Partitioning experiments (as in Fig. 1) with rat erythrocytes obtained 13 days (left panels, rat No. 90-5) or 42 days (right panels, rat No. 89-12) after ^{59}Fe injection. Top panels depict partitioning in high-phase columns; bottom panels partitioning in low-phase columns. See Fig. 1 and text for details.

subpopulation they contain. As in the case of the non-charge-sensitive phase system I, no fractionation can be detected for the different-aged rat erythrocytes upon sedimentation.

Partition and sedimentation studies on rat red blood cell populations containing ^{59}Fe-labeled erythrocytes of distinct age. Experiments in horizontally placed tubes (low-phase columns)

In the lower left panel of Fig. 1 and the lower panels of Fig. 2 the points represent, in sequence from right to left, partitioning samples in system I obtained after 7.5, 15, 30, 45, 60, 90 and 120 min of horizontal- plus 1 min of vertical-phase settling. As the sampling time is extented, the percentage of cells in the top phase diminishes markedly from about 85 to 10% while the RSA values change (increasing from 1.03 to 1.38 with erythrocytes containing 4 days old labeled cells, 1.00 to 1.23 with 13 days old cells, and decreasing from 0.98 to 0.89 with 42 days old cells).

In the lower right panel of Fig. 1 the results of a sedimentation experiment are depicted in which cells, suspended in top phase (system I), were permitted to be in a horizontal position and then in a vertical position for time intervals as described in the previous partitioning experiments and sampled and analyzed in a manner analogous to them. Unlike the small decrease in the percentage of cells in the top phase as a function of sedimentation when tubes are in the vertical position (Fig. 1, upper right), the decrease of cells in the top phase with tubes in a horizontal position is sizable over the 2 h period, 100 to 43%, and close in magnitude to the change in P values

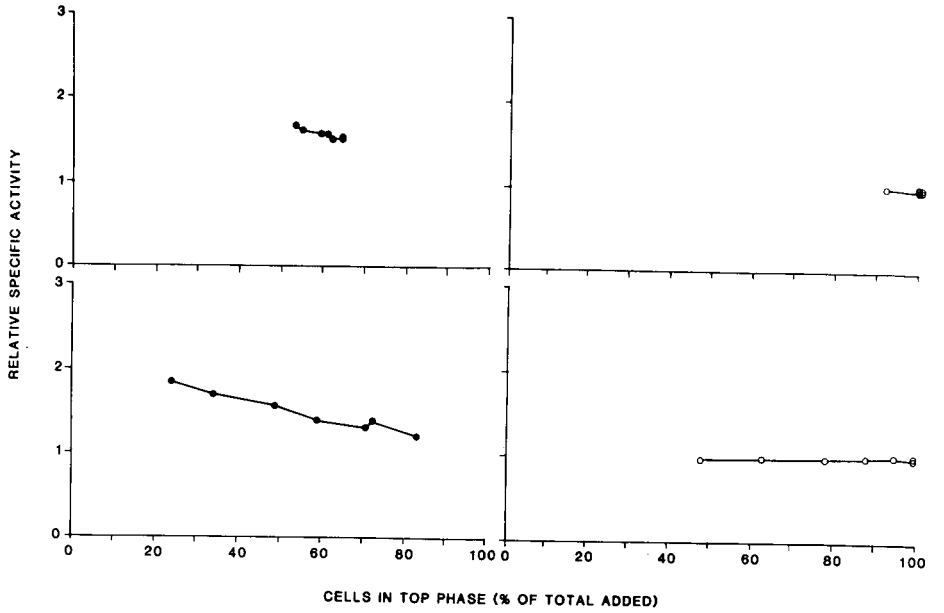

Fig. 3. Experiments as in Fig. 1 except that charge-sensitive phase system II was used. See discussion.

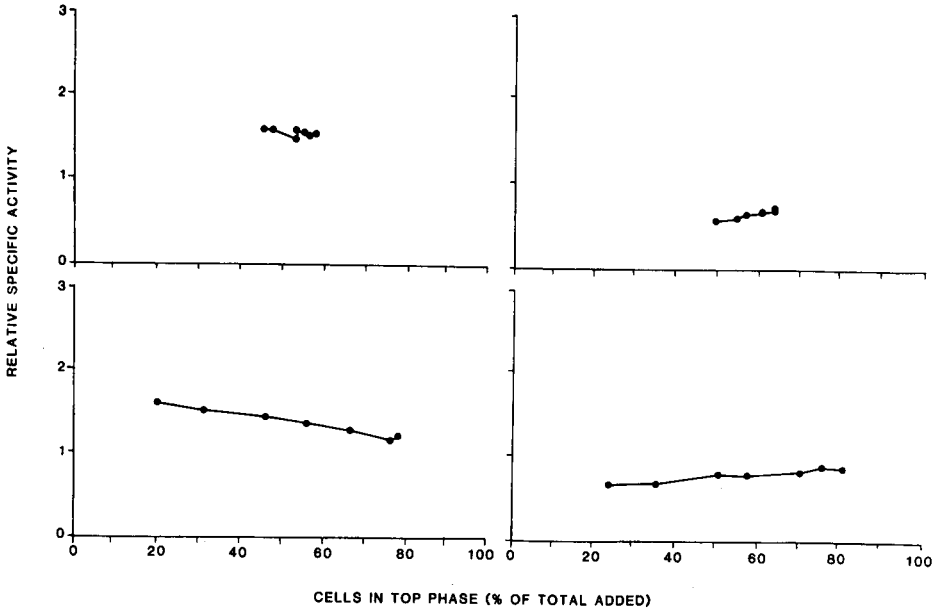

Fig. 4. Partitioning experiments similar to those in Fig. 2 except that charge-sensitive phase system II was used. Left panels: erythrocytes obtained 12 days after ^{59}Fe injection (rat No. 89-18) and, right panels, 43 days after isotope injection (rat No. 90-3). See Discussion.

observed with horizontal partitioning (compare Fig. 1, lower left and right panels). The RSA values remain constant at 1.00 again indicating that no fractionation of cells occurs during sedimentation.

In Figs. 3 and 4, lower panels, experiments analogous to those depicted in Figs. 1 and 2, respectively, were undertaken with the exception that charge-sensitive phase system II was used. The percentage of cells in the top phase again diminishes markedly with time, from about 80 to 20%, while the RSA values change (increasing from 1.39 to 1.85 with erythrocytes containing 4 days old labeled cells, 1.15 to 1.59 with 12 days old cells, and decreasing from 0.88 to 0.67 with 43 days old cells).

The accompanying sedimentation experiment (Fig. 3, lower right) again shows a decrease in the percentage of cells in the top phase over the time-course of the experiment, 100 to 48%, which is comparable in magnitude to that found on cell partitioning (Fig. 3, lower left), with the RSA values remaining constant at 1.00.

Partition and sedimentation studies on a mixture of rat ^{51}Cr-labeled red blood cells and an excess of human unlabeled erythrocytes. Experiments in high- and low-phase columns

Fig. 5 depicts superimposed partitioning and sedimentation results obtained with a mixture of ^{51}Cr-labeled rat red cells plus an excess of human unlabeled erythrocytes. In the top left panel the points represent, in sequence from right to left, samples obtained after 20, 30, 40, 50, 60, 90 and 120 min of vertical-phase settling in non-charge-sensitive phase system III. As in Figs. 1–4, the percentage of partitioned cells (solid symbols) in the top phase diminishes with time (from about 70 to 35%) while the RSA value increases dramatically (from 1.38 to 2.86). In the sedimentation experiment (open symbols), in which cells suspended in the top phase were permitted to stand in a vertical position and were sampled at time intervals and analyzed in a manner analogous to the partitioning experiment, the percentage of cells in the top phase diminishes very slightly during the 2-h experiment and the RSA values remain close to 1.00.

In the lower left panel, the points represent, in sequence from right to left, samples obtained after 7.5, 15, 30, 45, 60, 90 and 120 min of horizontal- plus 1 min of vertical-phase settling. With longer settling times the percentage of partitioned cells in the top phase again diminishes (from about 90 to 25%) and the RSA values increase (1.11 to 2.48). In the corresponding sedimentation experiment the decrease of cells in the top phase, as they sediment in a low-phase column, is appreciable over the 2-h period (from about 100 to 30%) and is comparable in magnitude to the change in the P value observed with horizontal partitioning. Unlike the results obtained with horizontal sedimentation of closely related cell populations (Figs. 1 and 3) the RSA value of a mixture composed of cells of appreciably different size also changes (in the present case from 0.85 to 1.85). This reflects the more rapid sedimentation of the larger human red cells in the mixture yielding an increasing ratio of radioactively labeled rat to human erythrocytes. The more rapid sedimentation of the human red cells thus serves to enhance the separation of human and rat erythrocytes by partitioning.

The upper and lower right panels of Fig. 5 show experiments conducted as in the respective left panels of the figure except that charge-sensitive phase system IV was used. In the top right panel (high-phase columns) the percentage of partitioned cells (solid symbols) in the top phase diminishes with time (from about 68 to 48%) while the RSA values increase (from 1.45 to 2.00). In the corresponding sedimentation

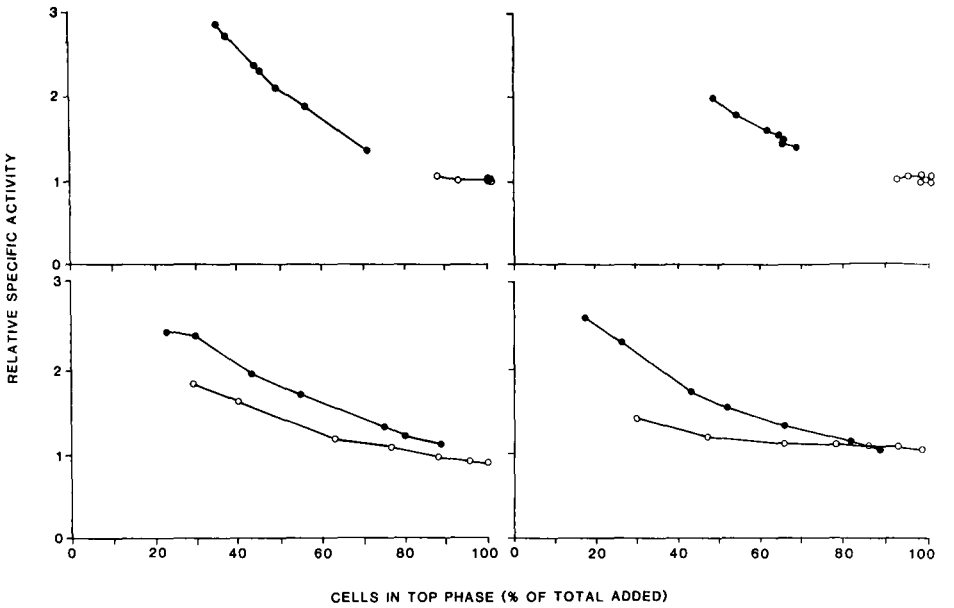

Fig. 5. Mixtures of ^{51}Cr-labeled rat red blood cells plus unlabeled human erythrocytes (1:4) were partitioned or permitted to sediment in a manner as described for Fig. 1. Partitioning (solid symbols) and sedimentation (open symbols) data are presented superimposed in the graphs. Left panels show experiments in non-charge-sensitive system III and right panels show experiments in charge-sensitive system IV. Top panels represent high-phase column partitioning or sedimentation; bottom panels, low-phase columns. Rat erythrocytes have higher partition ratios than human red cells in both systems III and IV. They are also smaller. Note that unlike the results obtained with the closely related rat red cells of different age (Fig. 1), sedimentation in low-phase columns also causes marked changes in the RSA values reflecting a more rapid sedimentation of human as opposed to rat red cells during the 2-h course of the experiment. For additional discussion see text.

experiment (open symbols), the percentage of cells in the top phase hardly diminishes over the 2-h experiment and the RSA values remain a constant 1.00.

In the bottom right panel (low-phase columns) the percentage of cells partitioned in the top phase again diminishes with time (from about 90 to 15%) and the RSA values increase (1.07 to 2.64). In the sedimentation experiment the decrease of cells in the top phase, as they form sediment in a low-phase column, is appreciable over the 2 h period (about 100 to 30%) and is comparable in magnitude to the change in the *P* value observed with low-phase partitioning. Again, as in Fig. 5, lower left panel, the RSA value of a mixture of cells of appreciably different sizes also changes on sedimentation (in the present case from 0.97 to 1.42) again reflecting a fractionation on the basis of size.

Partition and sedimentation studies on a mixture of sheep ^{51}Cr-labeled red blood cells and an excess of human unlabeled erythrocytes. Experiments in high- and low-phase columns

Fig. 6 depicts superimposed partitioning and sedimentation data obtained in a manner similar to that described for Fig. 5 but with a mixture of ^{51}Cr-labeled sheep

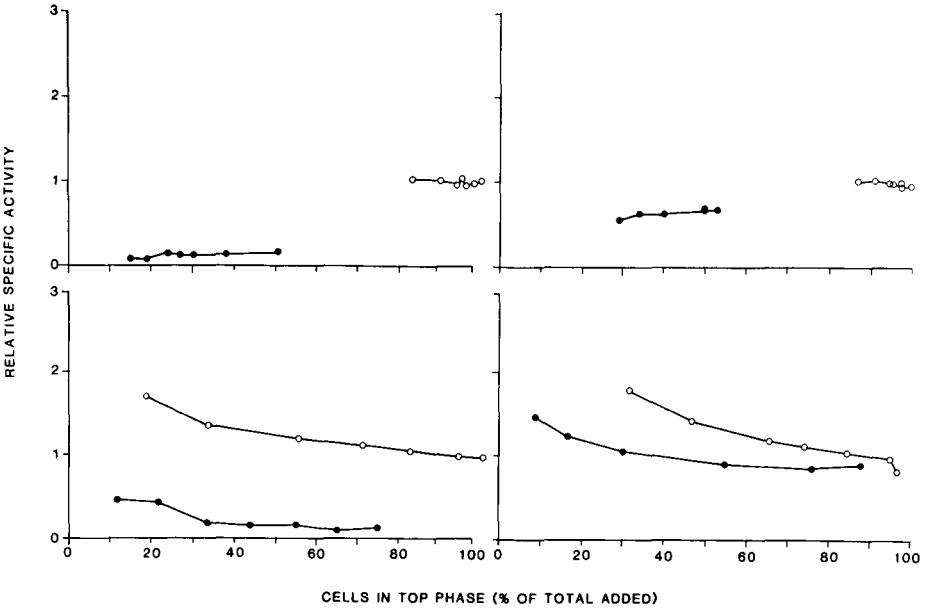

Fig. 6. Mixtures of ^{51}Cr-labeled sheep red blood cells plus unlabeled human erythrocytes (1:4) were partitioned or permitted to sediment in a manner as described for Fig. 1. Partitioning (solid symbols) and sedimentation (open symbols) data are presented superimposed in the graphs. Left panels show experiments in non-charge-sensitive system III and right panels show experiments in charge-sensitive system IV. Top panels represent high-phase column partitioning or sedimentation; bottom panels, low-phase columns. Sheep erythrocytes have much lower partition ratios than human red cells in system III and slightly lower partition ratios in system IV. They are also much smaller. Since the partition ratio of human red cells is higher than those from sheep but human red cells sediment more rapidly (shown by the increase in the RSA values on sedimentation in low-phase columns, lower panels), the initial low RSA value in the partitioning experiments increase with longer settling times (partitioning data in lower panels). For discussion see text.

red cells plus an excess of human unlabeled erythrocytes. In the top left panel vertical-phase settling results in non-charge-sensitive phase system III are shown. The percentage of partitioned cells (solid symbols) in the top phase diminishes with time (from about 50 to 15%) while the RSA value, reflecting the very low P value of the labeled sheep red cells, is and remains low (ranging from 0.17 to 0.08). In the sedimentation experiment (open symbols), the percentage of cells in the top phase diminishes only slightly over the 2 h experiment and the RSA values remain close to 1.00.

In the lower left panel, low-phase column partitioning and sedimentation data in system III are presented. With longer settling times the percentage of partitioned cells in the top phase again diminishes (from about 75 to 10%) and the RSA values at first remain low (0.12 to 0.20) but with extended sedimentation (*i.e.*, beyond 1 h) increase to 0.47. In the corresponding sedimentation experiment the decrease of cells in the top phase, as they sediment in a low-phase column, is appreciable over the 2-h period (about 100 to 20%). As with the results in Fig. 5, but unlike those in Figs. 1 and 3 which have closely related cell populations, the RSA value changes (in the present case from 0.99 to 1.69). This again reflects the more rapid sedimentation of the larger

human red cells in the mixture yielding an increasing ratio of radioactively labeled sheep to human erythrocytes. The increase in RSA values with prolonged partitioning times (*i.e.*, beyond 1 h) is due to the differential sedimentation of human and sheep red blood cells. Because both the sedimentation rate and the partition ratio of human red cells is greater than those of sheep erythrocytes, sedimentation tends to reduce the separation of human and sheep erythrocytes by partitioning. Sedimentation effects on the separation by partitioning of human and sheep red cells is shown even more dramatically in Fig. 6, right (see below).

The upper and lower right panels of Fig. 6 show experiments conducted as in the respective left panels of the figure except that charge-sensitive phase system IV was used. In the top right panel (high-phase columns) the percentage of partitioned cells (solid symbols) in the top phase diminishes with time (from about 55 to 30%) while the RSA values decrease minimally (from 0.68 to 0.54). In the corresponding sedimentation experiment (open symbols), the percentage of cells in the top phase hardly diminishes over the 2-h experiment and the RSA values remain a constant 1.00.

In the bottom right panel (low-phase columns) the percentage of cells partitioned into the top phase again diminishes with time (from about 90 to 10%) but, unlike the data in the upper right panel, the RSA values increase from less than to greater than 1.00 (0.90 to 1.46). (RSA values less than 1.00 reflect a smaller P value for sheep red cells than for human red cells while RSA values greater than 1.00 indicate the opposite.) The explanation for the change in RSA values is to be found in the corresponding sedimentation experiment in which the decrease of cells in the top phase, over the 2 h period in a low-phase column, is accompanied by an increase in RSA values all the way to 1.76. The increase in RSA values on prolonged sedimentation thus affects the apparent red cell P values. The larger human erythrocytes sediment more rapidly than the sheep red cells making it appear that the sheep red cell, which actually has a lower P value than the human red blood cell in phase system IV, has a higher P value.

DISCUSSION

It is known that cell partitioning is a kinetic process which depends on cell- and phase-specific interactions wherein cells bind to droplets of one phase (in the present case, the dextran-rich phase) suspended in the other (PEG-rich phase) after mixing followed by the delivery of droplet-bound cells to the bulk interface [4]. Thus the partition ratio, P, of cells depends on the time chosen for analysis. Furthermore, since the height of the phase column influences the speed of phase settling, with smaller heights resulting in faster settling, cell separation by partitioning is also affected by the geometry of the vessel used. More efficient fractionations are obtained in high rather than small phase columns [8]. The reason suggested for this finding is that with low-phase column heights, phase separation proceeds too rapidly for cells to attach to the phase droplets. (Hence the use of a Craig counter-current distribution apparatus [17] with high-phase columns is of more advantage when fractionating cells than the more commonly used Albertsson thin-layer unit [18].)

In the present work we have further explored the efficiency of cell fractionation by partitioning in two-polymer aqueous-phase systems in both high- and low-phase columns *vs.* time. The contribution of cell sedimentation in the phases (in the absence

of partitioning) was also examined. We studied both closely related cells (*i.e.*, rat erythrocytes containing ^{59}Fe-labeled cells of different ages) and mixtures of red blood cells of different sizes (*i.e.*, human plus rat, human plus sheep) in which the smaller cells (sheep or rat erythrocytes) were isotopically labeled with ^{51}Cr and mixed with an excess of the larger cells. Efficiency of fractionation was determined by measuring the changes in relative specific radioactivity (RSA) with time.

A surprising result of our experiments is the fact that cel partitioning proceeds for (at least two) hours. This is indicated by the change in RSA value (*e.g.*, Fig. 1, top left) with time in the absence of cell sedimentation (*i.e.*, without an appreciable change in the percentage of cells present in the top phase, see *e.g.*, Fig. 1, top right) or even in the presence of cell sedimentation where the latter does not result in changes in RSA values (*e.g.*, Fig. 1, bottom right). A practical result of the finding that the partitioning process continues for a long period of time, yielding ever-lower P values with higher proportions of separated cells, is that a time interval may be chosen which balances relative cell purity in a given phase and yield.

With high-phase columns and closely related cells (*i.e.*, cells of similar size) cell sedimentation is negligible (over the 2-h period of the experiment) and no fractionation of the cells due to sedimentation is observed. With low-phase columns and closely related cells sedimentation is appreciable, although without cell fractionation since the RSA value remains constant at 1.0, (*e.g.*, Figs. 1 and 3, bottom right). The decrease in the percentage of added cells due to sedimentation does not differ much from the percentage of cells in the top phase found on partitioning (see Figs. 1 and 3, bottom). The partitioning and sedimentation processes are thus not "additive" and it is tempting to speculate that cell partitioning actually slows the sedimentation of some cells.

As previously reported [8] the RSA value obtained with the same cell population in the same phase system at a given partition ratio, P value, is always higher in vertical- (high) than in horizontal- (low) phase columns (see *e.g.*, Figs. 1, left; 2; 3 left). The current data show that one can, in some phases (see the left side of Fig. 3 as well as Fig. 4), attain the same RSA values with horizontal-phase settling as with vertical-phase settling but then only at a lower P value (*i.e*, lower cell yield).

With high-phase columns and mixtures of cells of different sizes, cell sedimentation is not significant (over the 2 h period of the experiment) and no fractionation of the cells due to sedimentation occurs (Figs. 5, top and 6, top). With low-phase columns and such cell mixtures, sedimentation is appreciable and affects cell separation. In the case of rat red blood cells which are smaller than human ones but have a higher partition ratio in these phases [5], the more rapid sedimentation of the larger human erythrocytes leaves more rat red cells in the top phase. Sedimentation, in this case, would thus serve to enhance the separation (Fig. 5, bottom). Sheep red blood cells are also smaller than human erythrocytes but have a slightly lower P value in charge-sensitive phases and a much smaller P value in non charge-sensitive phases [5]. The RSA value of sheep red blood cells should therefore be less than 1.0 and diminish with time. The removal of human red blood cells by sedimentation actually increases the observed RSA values (see Fig. 6, bottom).

The reports that increasing the settling time in low-phase columns (as on a thin-layer countercurrent distribution apparatus) improves the fractionation of cells by partitioning [9,10] was unexpected in light of the cell partitioning mechanism [8].

Our current studies show that the enhanced fractionation of bone marrow cells by partitioning [9,10] must be a function not of enhanced partitioning but of differential cell sedimentation. Such an improvement in separation cannot, however, be taken as a general rule [9,10], since a partitioning separation can equally well be diminished by cell sedimentation (see *e.g.*, Fig. 6).

CONCLUSIONS

Cell partitioning in two-polymer aqueous-phase systems proceeds for (at least two) hours. With high-phase columns one obtains, with time, ever-lower cell partition ratios containing greater proportions of cells with a higher P value. With low-phase columns the partitioning of cells of different sizes is affected by cell sedimentation with extended times. Depending on the relative partition ratios of the larger and smaller cells being separated, sedimentation can serve to enhance or diminish the separation by partitioning.

Extending the settling time of phases in cell separation procedures using low-phase columns (*e.g*, on a thin-layer counter-current distribution apparatus), as has been reported [9,10], must result, when working with populations of different cell size, in fractionations which depend on both cell surface properties (partitioning) and size (sedimentation). Such separations *cannot* thus be interpreted on the basis of cell surface properties [9,10].

Partitioning cells in high-phase columns is not only of advantage with respect to increasing separation efficiency [8] but also with respect to virtually eliminating the influence of other physical parameters (*i.e.*, cell size) on the fractionation.

ACKNOWLEDGEMENT

This work was supported by the Medical Research Service of the Department of Veterans Affairs.

REFERENCES

1 H. Walter, D. E. Brooks and D. Fisher (Editors), *Partitioning in Aqueous Two-Phase Systems—Theory, Methods, Uses, and Applications to Biotechnology*, Academic Press, Orlando, FL, 1985.
2 P.-Å. Albertsson, *Partition of Cell Particles and Macromolecules*, Wiley-Interscience, New York, 3rd ed., 1986.
3 H. Walter and G. Johansson, *Anal. Biochem.*, 155 (1986) 215.
4 D. E. Brooks, K. A. Sharp and D. Fisher, in H. Walter, D. E. Brooks and D. Fisher (Editors), *Partitioning in Aqueous Two-Phase Systems —Theory, Methods, Uses, and Applications to Biotechnology*, Academic Press, Orlando, FL, 1985, pp. 11–84.
5 H. Walter, in H. Walter, D. E. Brooks and D. Fisher (Editors), *Partitioning in Aqueous Two-Phase Systems —Theory, Methods, Uses, and Applications to Biotechnology*, Academic Press, Orlando, FL, 1985, pp. 327–376.
6 F. D. Raymond and D. Fisher, *Biochim. Biophys. Acta*, 596 (1980) 445.
7 D. Fisher, F. D. Raymond and H. Walter, in P. Todd and D. D. Kompala (Editors), *Cell Separations (ACS Symposium Series)*, American Chemical Society, Washington, DC, in press.
8 H. Walter and E. J. Krob, *Biochim. Biophys. Acta*, 966 (1988) 65.
9 A. I. Garcia-Perez, P. Sancho and J. Luque, *J. Chromatogr.*, 504 (1990) 79.
10 P. Sancho, M. D. Delgado, A. I. Garcia-Perez and J. Luque, *J. Chromatogr.*, 380 (1986) 339.
11 H. Walter and E. J. Krob, *Biochem. Biophys. Res. Commun.*, 120 (1984) 250.

12 H. Walter and E. J. Krob, *J. Chromatogr.*, 479 (1989) 307.
13 H. Walter and F. W. Selby, *Biochim. Biophys. Acta*, 112 (1966) 146.
14 H. Walter and E. J. Krob, *Br. J. Haematol.*, 38 (1978) 43.
15 L. L. M. Van Deenen and J. de Gier, in C. Bishop and D. M. Surgenor (Editors), *The Red Blood Cell*, Academic Press, New York, 1964, pp. 243–307.
16 P. L. Altman and D. S. Dittmer (Editors), *Biology Data Book, Vol. III*, Federation of American Societies for Experimental Biology, Bethesda, MD, 2nd ed., 1974.
17 L. C. Craig and D. Craig, in A. Weissberger (Editor), *Techniques of Organic Chemistry*, Vol. 3, Part I, Wiley-Interscience, New York, 2nd ed., 1956, pp. 149–332.
18 P.-Å. Albertsson. *Anal. Biochem.*, 11 (1965) 121.

Journal of Chromatography, 542 (1991) 413–450
Elsevier Science Publishers B.V., Amsterdam

CHROM. 23 045

Analysis of volatile organic compounds in estuarine sediments using dynamic headspace and gas chromatography–mass spectrometry

ALEXANDER P. BIANCHI*
Exxon Chemical Co., Department of Environmental Affairs, Fawley, Southampton (U.K.)
MARK S. VARNEY
Department of Oceanography, University of Southampton, Southampton (U.K.)
and
JOHN PHILLIPS
Department of Earth Sciences, The Open University, Walton Hall, Milton Keynes (U.K.)
(First received June 28th, 1990; revised manuscript received December 4th, 1990)

ABSTRACT

In our previous paper (*J. Chromatogr.*, Vol. 467, p. 111) we reported a modified variant of the purge-and-trap gas chromatographic analysis of volatile organic carbon compounds in water. In this paper we report the application of the modified open-loop dynamic headspace technique for the stripping and trapping of volatile organic compounds (VOCs) from estuarine sediments. Sediment samples (*ca.* 300–400 g wet weight) are transferred into all-glass 1-l bottles and purged at 60°C for 70 min in an ultrapure helium gas stream. Volatile eluates are quantitatively trapped onto three different sorbent beds arranged in series. Analysis is then performed using thermal desorption with capillary column chromatography and simultaneous flame ionisation with ion-trap detection. As with water samples, stripping temperature had the greatest effect upon compound recovery, with smaller variances in recovery observed when comparing different sediment types.

The method is capable of quantifying many individual volatile organic compounds down to a detection limit between 10 and 100 ng kg^{-1} (dry weight). The linear dynamic range for a broad range of compounds fell between the lower limit of detection to approximately 500–700 $\mu g\ kg^{-1}$ (dry weight). The results of a case study on sediments taken from the Southampton Water estuary are presented as an example of the method application. A list of component concentration ranges are also presented.

INTRODUCTION

Within the past ten years much attention has been focused on the detection and quantification of volatile organic compounds (VOCs) in sludges, muds and sediments. Many types of VOC, originating from diverse sources ranging from oil spills [1,2] and industrial wastewaters [3], to natural, biogenic compounds [4] have been identified in estuarine sediments. Some of these compounds are mutagens, teratogens or carcinogens [5,6] and resistant to microbial or photochemical degradation [2]. Studies concerning their occurrence, behaviour and fate in estuarine sediments are comparatively limited, a fact which reflects the necessity for research and vigilance in this area.

0021-9673/91/$03.50

There has been extensive reporting of analytical methods for measuring low level concentrations of VOCs in surface waters. These are based mainly on static (equilibrium) and purge-and-trap (non-equilibrium) headspace analysis [7–12]. However, the direct application of these methods for analysing VOCs in sediments is not straightforward and must take account of complicating factors such as sediment composition, the physico-chemical properties of the sediments and the organic compound classes involved. These properties may also necessitate an appreciation of factors such as particle-size distribution, organic carbon content and the geographical variability of different sediment types [13].

Previous research on the composition of sediments as media for sorbing organic compounds has provided clues regarding the key factors which determine sorbability. Examples of such research included studies of the relationship between the partition coefficients (K_p) of hydrophobic organic compounds and the sediment matrix [14]. An important conclusion arising from this work stated that sorptive action by shallow estuarine sediments was directly involved in the removal of individual VOCs from overlying waters, regardless of the sediment type. Accordingly, much research has been aimed at studying the affinity of different sediment types for various classes of organic compounds [15].

Unfortunately, there are no universally recognised and approved methods for the analysis of VOCs in sediments, especially marine sediments. Rigorous analytical approaches have been used to evaluate the efficiency of static (equilibrium) headspace methods for determining VOCs in coastal sediments [16] and in estuarine sediments [17]. Similarly, purge-and-trap stripping methods have been applied with a degree of success to the laboratory analysis of sediments [18,19] and in field studies of sediment and fish tissues [20]. Purge-and-trap methods utilise purging of the sample matrix by purified inert gases, followed by trapping of the volatile compounds onto adsorbent beds, typically Tenax or carbon-based sorbents. Another interesting analytical variant used vacuum-extraction techniques to partition VOCs from solid materials, followed by transfer of the extracted organic vapour to a conventional purge-and-trap device. Analysis was then conducted according to standard gas chromatographic (GC) protocols [21].

One of the most commonly used purge-and-trap methods used for stripping VOCs from sediment matrices is the United States Environmental Protection Agency Method 5030. This method is used for volatile organics, defined as those organic compounds with boiling points below 200°C and which are insoluble or only slightly soluble in water. Method 5030 includes a low-level variant intended for samples containing less than 1 mg kg^{-1} of individual VOCs, although it is limited to sediment samples that are of a similar (granular and porous) consistency. Volatile water-soluble (*i.e.* alcohols and ketones) compounds can be included in this method. However, as a general observation, quantitation limits [by GC or gas chromatography–mass spectroscopy (MS)] were stated to be approximately ten times higher than non-polar hydrophobic organic compounds, because of their poor purging efficiencies.

In this sediment purge-and-trap method, VOC were purged from sediment samples at elevated temperatures onto a similar three-stage sorbent trap. After the purging step, the trapping tube arrangement was disconnected, and the individual tubes thermally desorbed using a Perkin-Elmer automated thermal desorber (ATD-50; Perkin-Elmer, Beaconsfield, U.K.). The ATD-50 is a multi-functional instrument

developed initially for the United Kingdom Health & Safety Executive environmental laboratories [22]. The principal role of the ATD-50 is for the analysis of organic vapours at low concentrations (sub-ppm). An integral two-stage desorption facility is available whereby organic compounds desorbed from adsorption tubes, within an oven held at 150°C, are then re-trapped inside an electronically cooled cold-trap packed with a secondary adsorbent bed, at a temperature down to −30°C. The cold-trap is then electronically heated at a rate exceeding 1000°C min^{-1} to an upper limit of 300°C, sending a discrete band of concentrated sample through the fused-silica transfer line to the GC capillary column where the transferred components are chromatographed.

The sediment purging method, which uses the ATD-50, has separated over 100 volatile organic compounds found mainly as trace contaminants or naturally occurring compounds in estuarine sediments within approximately 70 min. The method utilises flame ionisation detection (FID) with the added facility of ion-trap detection to provide confirmation of peak identity. This work conducted on VOCs in British estuarine sediment [23] and water samples [24] has revealed a wide range of volatile compounds to be present.

EXPERIMENTAL

The experimental details have been described previously [24]. However, this section shall include details pertinent to the analysis of sediment, as opposed to water samples.

Reagents

Standards were prepared using re-distilled analytical grade materials (Aldrich, Wimborne, U.K.). Stock standard mixtures were prepared gravimetrically in all-glass containers according to both EPA [25] and CONCAWE [26] methods. Replicate standards containing organic compounds covering materials varying in boiling point range from *n*-pentane to *n*-octadecane were prepared in 1-litre flasks, inverted, and spiked through aluminium-coated teflon septa using plunger-in-needle hypodermic syringes (SGE, Milton Keynes, U.K.). Sodium azide, recommended as a poison to prevent further biological reaction after sampling [27], was added to all samples. Internal standards, *i.e.* 1-chloroalkanes, were obtained from Aldrich.

Organic-free water was prepared by purging pure AnalaR grade water (BDH, Poole, U.K.) overnight in a stream of purified nitrogen. Aliquots (500 ml) were then heated at 95°C for 30 min to remove any remaining volatile components, cooled under a purified nitrogen blanket, and stored under zero-headspace immediately prior to use.

Standard sediment

The optimum standard matrix to use has been stated to be that of the sample matrix itself [28]. Sediment particle size distribution and organic matter content tend to vary between and within estuarial sites, and may affect the sorption and subsequent desorption of volatile organic compounds on sediments [14]. According to Bartlett [29], the majority of sediments within the 10-km length of Southampton Water exhibit seasonally constant physical characteristics which show little variation from year to year. Individual grain size properties of Southampton Water sediments were

determined using standard techniques developed and reported by Little *et al.* [30] and McLaren [31]. The organic matter content of the sediments was determined using the simple combustion method reported by Froelich [32].

Sediment grain size data for representative sediment samples taken from the head (sediment 1), mid-point (sediment 2) and mouth (sediment 3) of the estuary are presented in Table I. All three sites are composed of a mixture of good to moderately sorted fine silts (*e.g.* 70–80% silt), although some poorly sorted silts are found at the fringes of the estuarine mouth where the estuary opens into the Solent waterway. Clay contents increase from the head towards the mouth of the estuary, whereas silt contents follow the opposite trend. The organic matter content of the sediments follows the same pattern as silts, *i.e.* decreasing steadily from the head towards the mouth of the estuary.

TABLE I

SEDIMENT GRAIN SIZE DATA FOR SAMPLES TAKEN FROM THE HEAD (SEDIMENT 1), MID-POINT (SEDIMENT 2), AND MOUTH (SEDIMENT 3) OF THE ESTUARY

Sediment	Depth (cm)	Mud (%)	Gravel (%)	Organic matter (%)	Sorting index	Wentworth grade
1	0–10	94.56	0	20.79	Good	Fine silt
2	0–10	97.45	0	15.14	Good	Fine silt
3	0–10	94.70	0	13.21	Moderate	Fine silt

Grain size distribution[a]

Grain size	Sediment 1	Sediment 2	Sediment 3
Sand	1.35	2.18	5.31
Silt	80.29	72.78	70.35
Clay	18.36	20.04	24.34

[a] Grain size key: sand = $7.07 \cdot 10^{-1}$ to $6.25 \cdot 10^{-2}$ mm; silt = $6.25 \cdot 10^{-2}$ to $3.91 \cdot 10^{-3}$ mm; clay = $3.91 \cdot 10^{-2}$ to $1.38 \cdot 10^{-3}$ mm (Reference: *British Standards Institution*, (1975) BS 1377).

Sediments from the head, mid-point and mouth of the estuary were taken in order to prepare "blank" organic-free sediment suitable for spiking experiments. These were prepared according to protocols already described by Bianchi and Varney [17], and Lee *et al.* [33]. Procedures intended to remove volatile organics from sediments may modify adsorptive sites within the particle matrix. However, a suitable compromise was sought between the practical necessity to prepare "blank" sediment material and the retention of the basic physico-chemical integrity of the original, unaltered estuarine sediment.

Preparation of spiked blank sediment

Sub-samples of dried sediment (300 g) were gravimetrically added to a 1-litre glass vessel with a metal spoon. The vessels were prepared in a glass-blowing workshop from 1-litre "Dreschel" jars. These were fitted with 19/26 mm ground-glass necks and ground-glass stoppers. Aliquots (100 ml) of spiked standard water were added to the sample vessels, shaken vigorously for 10 min and let to stand under purified nitrogen

for 15 min at 4°C. Pure gaseous standards, *e.g.* chloromethane, (obtained from BDH) were added by injecting known aliquots of diluted gas from Tedlar gas bags (SKC, Shaftesbury, U.K.) directly into inverted vessels containing blank sediment slurry. These were injected through 1-litre glass vessels fitted with PTFE-coated silicone septa lined caps using 10-μl gas syringes (SGE) and shaken gently for 5 min. Samples were then purged according to the protocol described in the following section.

Sorbents and tubes

Tenax-TA, Chromosorb-106 and Spherocarb sorbents (all 60–80 mesh), obtained from Perkin-Elmer, were conditioned overnight according to manufacturers instructions in $\frac{1}{4}$ in. diameter stainless-steel tubes in a flow of purified nitrogen. After conditioning, sorbents were packed into desorption tubes (90 mm × 5 mm I.D.). Each tube set, containing sequentially, Tenax-TA, Chromosorb-106 and Spherocarb were inter-connected using standard $\frac{1}{4}$ in.–$\frac{1}{4}$ in. PTFE ferrules and $\frac{1}{4}$ in. stainless-steel Swagelok unions.

Sampling apparatus

The purge-and-trap stripping apparatus consists of an all-glass 1-litre bottle (nominal capacity, 1150 ml). A modified dreschel head assembly incorporating a ground-glass collar (19/24 mm) was inserted into the ground-glass neck of the sample bottle (19/24 mm) and locked using a PTFE cage. Ultrapure helium was metered via a metal-glass joint into a 7-mm O.D., 7-cm length of glass tubing fabricated onto the inlet of the purge head assembly. The internal glass tubing of the inlet purge head was fitted with a coarse porosity frit (Grade 2) suitable for producing sufficient agitation within the sediment slurry mixture. A schematic of this arrangement is shown in Fig. 1. The heated "jaws" unit consists of a thermostatically controlled, spring-loaded, heated metal block which clamps over the exit tubing. By heating the glass tubing the unit minimises the collection of water vapour droplets which condense out on the inner walls. The strip gas then passes directly through the three trapping tubes which are connected in series. The apparatus was immersed in a heated water bath (Grant Instruments, Cambridge, U.K.), and agitated at regular intervals allowing 30 min for thermostatic equilibrium to be attained.

Instrumentation and capillary column

The automated thermal desorber (ATD-50) was connected to a Perkin-Elmer 8700 gas chromatograph via a 1-m length of deactivated fused-silica transfer line, 0.22 mm I.D., held at 150°C [24].

The gas chromatograph was fitted with a cradle-mounted, 50 m × 0.22 mm I.D. OV-1701 wall coated open-tubular fused-silica capillary column, 0.5-μm film thickness (SGE). This column was found to offer satisfactory performance for the analysis of volatile compound in sediments and was used as the basis for many of the following experiments. The exit point of the column was connected to a twin-hole split ferrule permitting 50% of the column eluant to be routed to a flame ionisation detector. The remaining 50% is swept via a second 1-m length of transfer line at 250°C into an ion-trap detector (Finnigan MAT).

Carbon dioxide gas for cooling the chromatograph oven below ambient temperature was piped into the rear of the oven via a 4-m length of 3.0 mm O.D. copper

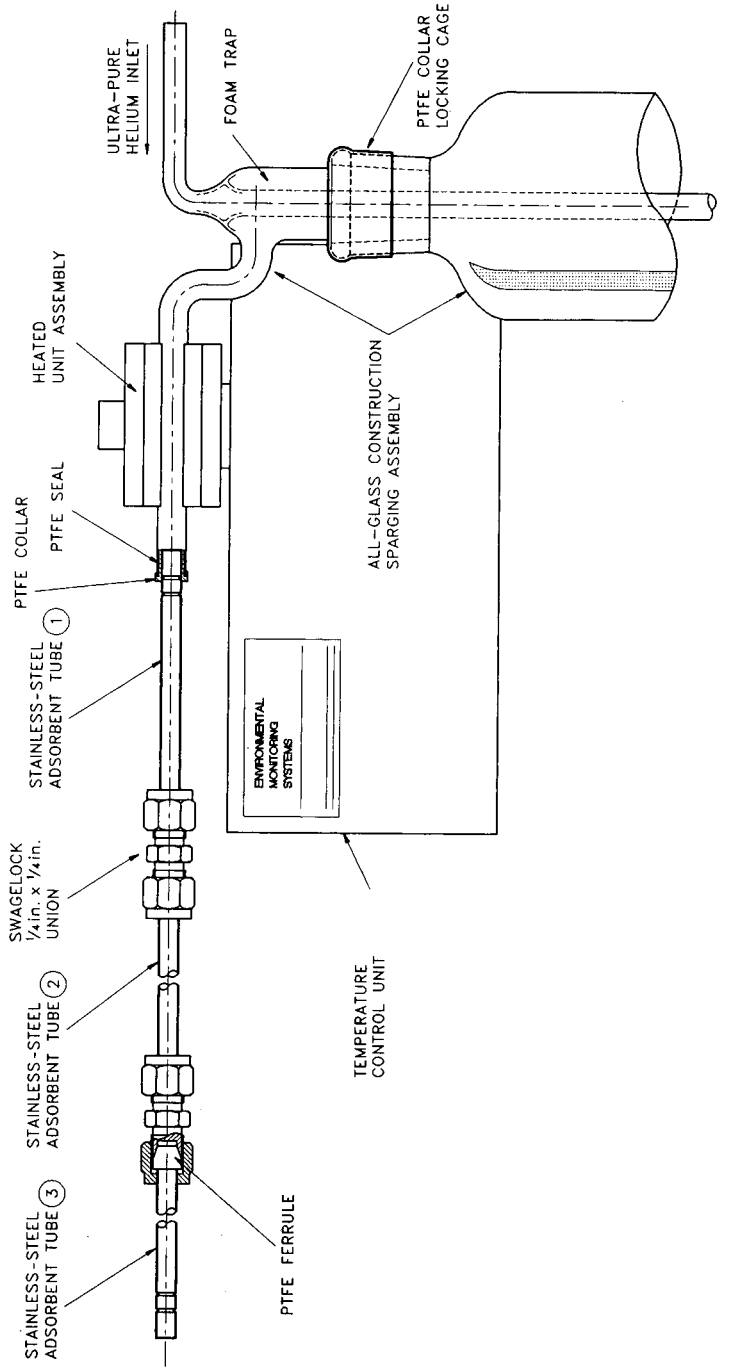

Fig. 1. Schematic of the modified open-loop stripping apparatus for analysing VOCs in sediments.

tubing. The feed rate for carbon dioxide gas is gauged by a microprocessor-controlled valve in the gas chromatograph.

Analytical operating conditions

Carrier gas. Ultrapure helium 5.5 grade (Air Products, Basingstoke, U.K.); carbon dioxide (Air Products, Southampton, U.K.).

ATD-50. Cold-trap packing, 10 mg Tenax-TA + 10 mg Chromosorb-106; cold-trap low temperature, −30°C; cold-trap high temperature, 250°C; split ratio (combined), 100:1; desorption oven temperature, 250°C; adsorbent tube desorption time, 10 min; desorption gas flow-rate, 10 ml min^{-1}, carrier gas pressure, 25 p.s.i. (*i.e.* 174 kPa).

Gas chromatograph. Detector temperature, 300°C; carrier gas flow-rate, 1 ml min^{-1} (20 cm s^{-1} at 10°C). Temperature conditions: oven temperature, 10°C; isothermal time 1, 10 min; ramp rate 1, 6°C min^{-1}; oven temperature 2, 300°C; final hold time 2, 10 min.

Ion trap detector. Ionisation voltage, 70 eV; s/scan, 1.0; mass range, 25–250 mass units; transfer temperature, 250°C; ion source temperature, 250°C; multiplier delay, 200 s; mass defect, 100 m.m.u./100 a.m.u.; acquire time, 70 min.

Collection of sediment samples

Since it is very difficult to assess the losses of volatile compounds from sediments after sampling, care and speed is necessary to transfer sediments into sealed glass containers as quickly as possible after sampling. Sediment samples [*ca.* 300–400 g (wet weight)] were immediately transferred after sampling into clean 1-litre glass purging vessels. Mid-estuarine samples were collected using a shipborne Wan-Ween sediment grab, cored with an all-glass cylinder, and inserted into the glass vessel. Solid materials such as stones or shells were quickly removed by hand before placing into the glass vessels. Intertidal mud samples were sampled using steel corers and inserted into the glass vessel. Sodium azide (*ca.* 0.5 g) was promptly added to sediment samples, and sample vessels immediately chilled on dry-ice inside sealed polystyrene lined "cool-boxes". As the sample storage vessels are then directly used for the purge analysis, volatilisation losses are kept to a practical minimum.

Analysis of sediment samples

After preliminary addition of (i) standard spiked water (100 ml) to standard blank sediment, or (ii) organic-free water (100 ml) to estuarine sediment samples, all samples were shaken gently for 10 min. Following this, standard samples were stood for 15 min under nitrogen at 4°C to allow mixing then settling of the spiked organic material into the sediment and the supernatant liquid. In order to determine longer term changes in composition arising from storage, duplicate standards were spiked with sodium azide, chilled in a refrigerator at −4°C and subsequently analysed after 24 and 48 h respectively.

After assembly of the apparatus, standard and estuarine sediment samples were immersed in the heated water bath. After 30 min equilibration, samples were purged in a flow of ultrapure helium (5.5 grade) for 70 min at 100 ml min^{-1}. All connections between the purge-gas line, purge-head and adsorbent "tube-train" were checked for leakage of purging gas using a soap solution. The effluent gas leaving the final tube of

the trapping arrangement was also connected to an on-line flowmeter (Chrompack U.K., London, U.K.). The initial purge rate through the purging apparatus was set at 100 ml min^{-1} and monitored throughout the purging cycle for loss of flow due to a leakage in the system.

The purging experiments were performed initially at 30°C, then at 60°C. Following the purge and trap cycle, the purge gas was switched off and disconnected. The trap tubes were removed from the sample vessel, disconnected and independently analysed on the thermal desorber–gas chromatographic system. This involves placing analytical end-caps on each tube, locating the tube in the desorber carousel and activating the desorption mechanism on the ATD. The tubes are analysed on the ATD-50 thermal desorber by placing stainless-steel pressure caps (or "analytical" end-caps) on the ends of the tubes [22]. These caps contain a small valve which opens when a discrete gas pressure is applied by the desorption unit on the ATD-50. The tubes are placed sequentially in a carousel arrangement which is pre-programmed to interface the tubes to the desorption mechanism according to a user-specified method. Before analysis, each tube is individually pressurised by the ATD-50 to check for leakage in the end-cap seals (if the leak check cycle identifies loss of pressure, the tube is rejected for analysis). If the leak-test is successful, the desorption cycle is automatically implemented. Basically, the tube is heated within the oven unit of the desorption unit whilst a flow of pure helium carrier gas is passed through each tube. Organic vapours are desorbed off the tube to be passed onto the cold-trap. Here, the organic vapours are cooled and re-trapped. Following a desorption time of 10 min, the cold trap is "fired", which sends the organic vapours to the GC column via the fused-silica transfer line.

The results of recoveries of VOCs from water, at these stripping temperatures, have already been reported [24], and were used as a basis for investigating similar effects on sediments. Following stripping, attention was paid to the identification of any apparent losses or thermal degradation effects on organic compounds with increasing stripping temperature. Internal standards, 1-chlorohexane and 1-chlorooctane were initially used as a means of monitoring recoveries. For routine analyses, an external standard calibration technique was used. The concentration of individual components were determined by multiplying component peak area by the external standard response factor. Response factors were calculated directly from calibration standard data. Hence, it was necessary to determine the linear dynamic range of the method before starting sample analyses.

Calculation of absolute dry weights (*i.e.* of sediments) and recovery data on actual samples were made by decanting off separated supernatant liquid several hours after the purging. The remaining slurry was then collected in a pre-weighed, wide-mouth pyrex glass dish (500 ml), cooled further and then evaporated to dryness in an oven held at 105°C for 8–12 h. The dried residue was then placed in a dessicator for 2 h, and re-weighed to obtain the absolute dry weight. The mean recovery for reweighed sediments was 99.41 $\pm$ 0.19%, based on 44 consecutive sediment samples.

RESULTS AND DISCUSSION

Detection limits

The lower detection limit in GC analysis is generally considered to be that amount of analyte which gives a peak area response three times as great as the standard

deviation of the response obtained from the blank. In equilibrium headspace experiments developed to detect trace organochlorine compounds in effluent water, Pizzie [28] defined the lower detection limit (*D.L.*) mathematically as:

$$D.L. = 3.o_b/m$$

where o_b is the standard deviation of the blank response, and m is the slope (or sensitivity) of the calibration curve for the analyte in question. Using this definition, the lower limits of detectability for a range of VOCs using the purge-and-trap stripping method were determined. These data are presented in Table II.

Linear dynamic range

The linear dynamic range of the method was investigated by preparing and analysing serial dilutions of master standard mixtures. The bottom of the range is set by the limits of detection for each component. However, at higher concentrations, diminishing recoveries and/or overloading of the sample tube with analyte occurs, leading to loss of linear response at the flame ionisation detector. To test for linearity, the response factor for each component was compared with the actual peak area and the known concentration in the calibration blends. The response factor should yield the correct concentration for the component (allowing for the accuracy and precison of the method) within the linear range of the component. Linear dynamic range data for a series of volatile organic compounds are also presented in Table II.

Repeatability

The short term precision (*i.e.* repeatability) of the purging method is expressed as the relative standard deviation (R.S.D.) over three concentration levels. This data is presented in Table III. The data illustrate that the R.S.D. decreases with increasing concentration for all the model VOC classes tested during these experiments. However, not all compound classes yielded similar values. For example, volatile alcohols and ketones exhibited R.S.D. values up to 12.2% for alcohols (*i.e.* *n*- and 2-butanol), and up to 24.2% for ketones (*i.e.* 2-decanone). Conversely, alkanes, aromatics and halogenated compounds exhibited R.S.D. values between 1.1 and 4.3% at the 100 μg kg^{-1} concentration level.

Accuracy

Accuracy is expressed as the bias. Bias is a directional value which shows how much the sample results differ from the reference value. This can be summarised as (bias = average value − reference value). The bias value can therefore be positive or negative. The bias values for the model VOC at three concentration levels are presented in Table IV. Accuracies were generally within $\pm$ 20% at the 100 ng kg^{-1} level, $\pm$ 3.8% at the 1000 ng kg^{-1} level, and $\pm$ 6% at the 100 μg kg^{-1} concentration level. This indicates that the method accuracy is highest mid-way between the dynamic linear range of the method, diminishing slightly towards the lower and upper limits respectively.

TABLE II

LIMITS OF DETECTION AND LINEAR DYNAMIC RANGE FOR SELECTED VOLATILE ORGANIC COMPOUNDS RECOVERED FROM SEDIMENTS AT 60°C

Compound Name	Limits of detection (ng kg^{-1}, dry weight)	Linear dynamic range (dry weight)	
		Lower limit (ng kg^{-1})	Upper limit (μg kg^{-1})
n-Pentane	10	10	550
n-Hexane	30	40	510
n-Heptane	30	60	510
n-Octane	40	75	500
n-Nonane	50	80	500
n-Decane	80	100	490
n-Undecane	100	115	490
n-Dodecane	100	120	480
n-Tridecane	100	120	480
n-Tetradecane	100	150	460
Isopentane	30	10	550
3-Methyl-1,3-butadiene	30	40	600
2,2-Dimethylbutane	40	50	520
2,3-Dimethylbutane	40	50	520
2-Methylpentane	45	60	520
3-Methylpentane	45	60	520
Cyclopentane	50	70	500
2,2,4-Trimethylpentane	70	90	450
2,4,4-Trimethylpentene-2	90	110	440
Benzene	10	10	650
Methylbenzene	10	10	660
1,3-Dimethylbenzene	20	25	600
1,2-Dimethylbenzene	20	25	600
Ethylbenzene	20	25	600
Isopropylbenzene	30	45	590
n-Propylbenzene	30	50	550
1,2,3-Trimethylbenzene	40	70	490
1,2,4-Trimethylbenzene	40	70	480
1,3,5-Trimethylbenzene	40	70	480
1,2,3,4-Tetramethylbenzene	70	110	460
1,2,3,5-Tetramethylbenzene	70	110	460
1,2-Dichlorobenzene	60	90	380
Dichloromethane	10	20	370
Trichloromethane	10	30	360
1,1,1-Trichloroethane	10	70	340
Trichloroethylene	15	130	340
Chloroethane	30	250	130
1,1,2-Trichlorotrifluoroethane	40	170	50
Dimethylsulphide	10	10	700
Dimethyldisulphide	10	10	700
Dimethyltrisulphide	20	40	670
2-Methylthiophene	60	90	580
Ethanol	200	280	200
Propanol	270	300	300
tert.-Butanol	270	330	380
n-Butanol	300	330	380
2-Butanol	300	370	370

TABLE II *(continued)*

Compound Name	Limits of detection (ng kg^{-1}, dry weight)	Linear dynamic range (dry weight)	
		Lower limit (ng kg^{-1})	Upper limit (μg kg^{-1})
Propanal	50	70	480
Pentanal	50	70	480
Hexanal	70	80	470
Heptanal	70	80	470
Benzaldehyde	70	90	450
2-Butanone	300	390	390
2-Pentanone	300	300	390
2-Heptanone	300	300	370
2-Decanone	320	350	290
Naphthalene	100	120	430
Indene	100	120	430
1,3-Dimethylnaphthalene	170	190	400
1,2-Dimethylnaphthalene	165	190	400
2-Methylfuran	40	70	450
2,5-Dimethylfuran	40	70	450
1-Chloroheptane	40	180	400
1-Chlorooctane	50	190	400

The effect of sediment type

The effect of different grain size distribution and organic matter content on the efficiency of the stripping method was examined. Analysis was performed on samples from the head (sediment 1), mid-point (sediment 2) and mouth of the estuary (sediment 3). The physical data was presented in Table I. Briefly, sediment 1 contains the lowest clay (18.36%) and sand (1.35%) content and highest organic carbon (20.79%) and silt (80.29%) content. Sediment 2 contains the highest proportion of mud (97.45%). Sediment 3 contains the highest proportion of sand (5.31%) and clay (24.34%) and the smallest proportion of organic matter (13.21%) and silt (70.35%).

The recoveries of volatile organic compounds from each of the three sediment types were measured. These experiments were conducted at 30°C and 60°C to determine the relative effect of sediment type and stripping temperature upon recovery. The results are presented in Table V.

Inspection of the data show that, in general, high clay and sand contents correspond with lowest recoveries, *i.e.* sediment 3 recoveries were up to 2–4% lower than sediment 1, which contains the highest proportion of silt. A similar observation was made by Karickhoff *et al.* [15] who stated that the linear partition coefficients (K_p) were directly related to organic carbon content for different particle size isolates in different sediments. In particular, the sand fraction (> 50 μm particle size) acts as a less effective sorbent. Less conclusive funtional relationships were found when comparing relative recoveries with the percentage of organic carbon and clays within the sediments. However, the general observation was made that the higher the silt contents, the better the recoveries. This observation was also reflected in data reported

TABLE III

THE REPEATABILITY OF MODEL VOLATILE ORGANIC COMPOUNDS PURGED FROM SEDIMENTS AT 60°C

Short term precision is expressed as % relative standard deviation (R.S.D.) at three concentration levels.

Compound name	Concentrations (dry weight)		
	100 ng kg^{-1}	1000 ng kg^{-1}	100 μg kg^{-1}
n-Pentane	5.5	4.6	1.9
n-Hexane	5.7	4.6	2.0
n-Heptane	5.7	4.7	2.0
n-Octane	5.9	4.8	2.2
n-Nonane	6.2	4.9	2.2
n-Decane	6.7	5.1	2.3
n-Undecane	–	5.0	2.5
n-Dodecane	–	5.2	2.6
n-Tridecane	–	5.2	2.9
n-Tetradecane	–	5.9	3.0
Isopentane	4.4	4.7	2.2
3-Methyl-1,3-butadiene	4.3	4.3	2.1
2,2-Dimethylbutane	4.4	4.1	2.1
2,3-Dimethylbutane	4.4	4.1	2.1
2-Methylpentane	4.3	4.1	2.0
3-Methylpentane	4.3	4.1	2.0
Cyclopentane	5.0	4.3	2.1
2,2,4-Trimethylpentane	5.6	4.5	2.2
2,4,4-Trimethylpentene-2	–	4.6	2.3
Benzene	3.3	2.6	1.1
Methylbenzene	3.3	2.7	1.2
1,3-Dimethylbenzene	3.4	2.9	1.3
1,2-Dimethylbenzene	3.4	2.9	1.4
Ethylbenzene	3.5	2.8	1.3
Isopropylbenzene	3.7	3.0	1.5
n-Propylbenzene	3.7	3.0	1.7
1,2,3-Trimethylbenzene	3.8	3.1	1.9
1,2,4-Trimethylbenzene	3.9	3.4	2.1
1,3,5-Trimethylbenzene	4.1	3.6	2.2
1,2,3,4-Tetramethylbenzene	–	3.6	2.5
1,2,3,5-Tetramethylbenzene	–	3.7	2.5
1,2-Dichlorobenzene	4.4	4.1	2.4
Dichloromethane	3.2	3.9	1.8
Trichloromethane	3.7	3.0	2.1
1,1,1-Trichloroethane	3.1	2.9	2.1
Trichloroethylene	–	2.9	2.2
Chloromethane	–	3.4	2.7
1,1,2-Trichlorotrifluoroethane	–	5.4	4.3
Dimethylsulphide	3.2	2.2	1.2
Dimethyldisulphide	3.3	2.3	1.4
Dimethyltrisulphide	3.4	2.5	1.6
2-Methylthiophene	3.7	2.3	1.9

TABLE III *(continued)*

Compound name	Concentrations (dry weight)		
	100 ng kg^{-1}	1000 ng kg^{-1}	100 μg kg^{-1}
Ethanol	–	9.9	8.4
Propanol	–	10.1	8.8
tert.-Butanol	–	11.2	9.0
n-Butanol	–	12.2	10.3
2-Butanol	–	12.2	10.3
Propanal	4.8	4.0	3.4
Pentanal	4.8	4.2	3.7
Hexanal	4.9	4.8	3.9
Heptanal	4.9	4.7	3.9
Benzaldehyde	4.0	3.4	2.2
2-Butanone	–	16.2	13.4
2-Pentanone	–	17.2	14.7
2-Heptanone	–	24.6	18.3
2-Decanone	–	30.1	24.2
Naphthalene	–	5.1	4.2
Indene	–	5.1	4.3
1,3-Dimethylnaphthalene	–	5.2	4.5
1,2-Dimethylnaphthalene	–	5.2	4.7
2-Methylfuran	5.4	4.6	3.9
2,5-Dimethylfuran	5.5	4.9	3.9
1-Chloroheptane	–	3.1	2.5
1-Chlorooctane	–	3.3	2.8

by Charles and Simmons [13]. In their report, which investigated the stripping of chlorinated solvents from sediments at ambient temperatures, the authors concluded that neither sediment weight, sediment type, nor the conductivity of the desorbing solution had noticeable effects on the recovery performance of a simple purge-and-trap method. Using their method, recoveries were quoted of 38% for trichloromethane, 48% for trichloroethylene and 54% for chlorobenzene. However, concern over the wide variance in reproducibility (*i.e.* between 4% and 55%) was expressed [13]. Our experiments using the modified open-loop stripping method [24], revealed an improvement in the recovery of the same compounds (*i.e.* trichloromethane, 84%; trichloroethene, 87%; and chlorobenzene, 84%, respectively), with a standard deviation ($n = 15$) for all compounds of less than 10%. These improvements reflect the comparative influence of method parameters on overall recoveries, relative to differences in sediment type.

The efficiency of multi-sorbent trapping

The use of a multi-sorbent trapping system for trace VOC analyses have been previously discussed by the authors [24]. The combination of sorbents, with individual affinities and retentive capacities for different compounds, traps those compounds

TABLE IV

THE ACCURACY OF MODEL VOLATILE ORGANIC COMPOUNDS PURGED FROM SEDIMENTS AT 60°C

The accuracy is expressed as the bias of the method for individual VOCs at three concentration levels.

Compound name	Concentrations (dry weight)		
	100 ng kg^{-1}	1000 ng kg^{-1}	100 μg kg^{-1}
n-Pentane	9	−15	6
n-Hexane	7	16	2
n-Heptane	7	19	2
n-Octane	− 9	19	2
n-Nonane	12	19	2
n-Decane	17	−11	−3
n-Undecane	–	20	5
n-Dodecane	–	22	6
n-Tridecane	–	−32	−9
n-Tetradecane	–	29	7
Isopentane	4	17	2
3-Methyl-1,3-butadiene	3	13	1
2,2-Dimethylbutane	− 9	−11	2
2,3-Dimethylbutane	12	−23	4
2-Methylpentane	9	28	5
3-Methylpentane	10	19	3
Cyclopentane	12	−23	4
2,2,4-Trimethylpentane	5	11	3
2,4,4-Trimethylpentene-2	10	23	−1
Benzene	8	4	−1
Methylbenzene	9	4	−1
1,3-Dimethylbenzene	11	− 5	2
1,2-Dimethylbenzene	12	− 4	1
Ethylbenzene	13	3	2
Isopropylbenzene	−16	7	−1
n-Propylbenzene	17	7	−1
1,2,3-Trimethylbenzene	−11	2	3
1,2,4-Trimethylbenzene	−12	7	3
1,3,5-Trimethylbenzene	18	23	3
1,2,3,4-Tetramethylbenzene	–	24	−2
1,2,3,5-Tetramethylbenzene	–	−30	2
1,2-Dichlorobenzene	10	19	1
Dichloromethane	16	19	−2
Trichloromethane	9	10	2
1,1,1-Trichloroethane	9	11	2
Trichloroethylene	–	16	−1
Chloromethane	–	−33	−5
1,1,2-Trichlorotrifluoroethane	–	−28	−3
Dimethylsulphide	2	5	1
Dimethyldisulphide	3	8	1
Dimethyltrisulphide	4	5	2
2-Methylthiophene	7	3	1

TABLE IV *(continued)*

Compound name	Concentrations (dry weight)		
	100 ng kg^{-1}	1000 ng kg^{-1}	100 μg kg^{-1}
Ethanol	–	– 9	–4
Propanol	–	– 1	–5
tert.-Butanol	–	– 3	–3
n-Butanol	–	– 2	–3
2-Butanol	–	– 2	–3
Propanal	5	4	1
Pentanal	8	– 2	1
Hexanal	11	– 3	2
Heptanal	–23	– 3	1
Benzaldehyde	21	5	2
2-Butanone	–	–23	–2
2-Pentanone	–	–24	–2
2-Heptanone	–	–35	–2
2-Decanone	–	–38	–3
Naphthalene	–	28	2
Indene	–	24	2
1,3-Dimethylnaphthalene	–	30	–1
1,2-Dimethylnaphthalene	–	28	–2
2-Methylfuran	7	10	–2
2,5-Dimethylfuran	– 5	–10	1
1-Chloroheptane	–	11	1
1-Chlorooctane	–	13	–1

which would otherwise be unretained by single adsorbent traps. Multi-sorbent trapping has therefore been an increasingly popular approach in purge-and-trap analysis in recent years. In general, Tenax-TA quantitatively retains most volatile compounds in a boiling-point range extending roughly from benzene and *n*-heptane upwards, although it will retain more volatile compounds at very low concentrations. Tenax has a limited retention volume capacity for low boiling organics and more efficient sorbents must be substituted [34] to achieve quantitative trapping. Although this method uses Chromosorb-106 and Spherocarb as the second and third traps respectively, newer sorbents such as Carbopack B, a graphitised carbon black, offer realistic alternatives. Multi-sorbent trapping also minimises overloading which is encountered when employing single tubes, with organics, and interferences which may occur between the sorbates. The practical value of employing this three-stage trapping arrangement was also discussed in more detail in the previous paper [24].

The effect of stripping temperature

The results of these experiments show that the stripping temperature of the sediments has a significant effect on compound recovery. When compared to the recoveries of VOCs from water samples [24], Table V shows that, in general, recoveries at both 30°C and 60°C are lower from sediments.

TABLE V

RECOVERIES OF VOLATILE ORGANIC COMPOUNDS FROM DIFFERENT SEDIMENT TYPES AT 30°C AND 60°C

Conditions: helium flow-rate, 100 ml min^{-1}; sampling time, 70 min.

Compound name	Sediment type	Molecular mass	Boiling point (°C)	Recovery	
				30°C	60°C
n-Pentane	1	72.1	35	84	97
	2			82	95
	3			81	93
n-Hexane	1	86.2	69	84	88
	2			83	87
	3			82	86
n-Heptane	1	100.2	98	76	85
	2			75	83
	3			75	82
n-Octane	1	114.2	126	73	79
	2			72	78
	3			71	77
n-Nonane	1	128.2	151	73	77
	2			72	76
	3			71	75
n-Decane	1	142.3	174	70	74
	2			69	73
	3			67	71
n-Undecane	1	156.3	196	65	71
	2			63	70
	3			61	69
n-Dodecane	1	170.3	216	59	67
	2			56	66
	3			55	64
n-Tridecane	1	198.4	234	53	65
	2			50	63
	3			47	61
n-Tetradecane	1	198.4	254	46	65
	2			65	62
	3			64	60
Isopentane	1	72.1	28	87	95
	2			86	94
	3			85	93
3-Methyl-1,3-butadiene	1	68.1	34	85	92
	2			84	91
	3			81	90
2,2-Dimethylbutane	1	86.2	50	79	84
	2			78	84
	3			78	83
2,3-Dimethylbutane	1	86.2	58	77	83
	2			76	82
	3			75	81
2-Methylpentane	1	86.2	62	76	85
	2			75	84
	3			73	83

TABLE V *(continued)*

Compound name	Sediment type	Molecular mass	Boiling point (°C)	Recovery	
				30°C	60°C
3-Methylpentane	1	86.2	64	75	84
	2			75	84
	3			74	83
Cyclopentane	1	70.1	50	77	85
	2			76	84
	3			74	82
2,2,4-Trimethylpentane	1	114.2	98	75	86
	2			73	85
	3			74	82
2,4,4-Trimethylpentene-2	1	112.2	102	73	84
	2			70	83
	3			69	82
Benzene	1	78	79	80	92
	2			80	90
	3			80	90
Methylbenzene	1	92.1	83	78	84
	2			77	83
	3			76	82
1,3-Dimethylbenzene	1	106.2	139	68	78
	2			67	77
	3			66	76
1,2-Dimethylbenzene	1	106.2	144	66	77
	2			65	76
	3			64	75
Ethylbenzene	1	116.2	135	59	78
	2			58	77
	3			57	76
Isopropylbenzene	1	120.2	153	57	76
	2			56	75
	3			55	74
n-Propylbenzene	1	120.2	159	55	74
	2			54	73
	3			50	71
1,2,3-Trimethylbenzene	1	120.2	176	57	74
	2			55	73
	3			53	71
1,2,4-Trimethylbenzene	1	120.2	168	54	73
	2			52	72
	3			49	70
1,3,5-Trimethylbenzene	1	120.2	163	54	75
	2			54	74
	3			52	71
1,2,3,4-Tetramethylbenzene	1	134.2	205	47	68
	2			45	68
	3			44	65
1,2,3,5-Tetramethylbenzene	1	134.2	199	48	69
	2			45	68
	3			44	65

(Continued on p. 430)

TABLE V *(continued)*

Compound name	Sediment type	Molecular mass	Boiling point (°C)	Recovery	
				30°C	60°C
1,2-Dichlorobenzene	1	147	179	56	73
	2			55	72
	3			53	71
Dichloromethane	1	86.9	40	85	92
	2			83	91
	3			80	89
Trichloromethane	1	120.4	61	69	85
	2			68	85
	3			68	84
1,1,1-Trichloroethane	1	133.4	75	73	87
	2			71	86
	3			69	85
Trichloroethylene	1	131.4	86.9	71	86
	2			69	85
	3			69	84
Chloromethane	1	51	−24	83	94
	2			80	92
	3			75	89
1,1,2-Trichlorotrifluoroethane	1	187.4	47	71	87
	2			68	87
	3			66	85
Dimethylsulphide	1	62	38	71	91
	2			70	90
	3			70	87
Dimethyldisulphide	1	94.2	109	69	79
	2			69	77
	3			67	77
2-Methylthiophene	1	98.2	113	68	84
	2			67	83
	3			65	82
Ethanol	1	46	78	45	70
	2			45	70
	3			42	67
2-Propanol	1	60	82	44	69
	2			45	69
	3			44	67
tert.-Butanol	1	75	118	38	61
	2			38	60
	3			35	58
n-Butanol	1	75	118	37	61
	2			37	60
	3			35	57
2-Butanol	1	74	98	37	69
	2			34	63
	3			34	60
Propanal	1	58	48	80	88
	2			77	86
	3			74	84

TABLE V *(continued)*

Compound name	Sediment type	Molecular mass	Boiling point (°C)	Recovery	
				30°C	60°C
Pentanal	1	86	103	70	84
	2			68	84
	3			66	80
Heptanal	1	114	153	65	76
	2			64	76
	3			60	74
Benzaldehyde	1	106	179	55	73
	2			55	72
	3			54	70
2-Butanone	1	72.1	80	38	73
	2			35	71
	3			33	67
2-Pentanone	1	86.1	101	37	70
	2			35	67
	3			31	65
2-Heptanone	1	114.2	150	29	59
	2			29	58
	3			27	55
2-Decanone	1	156	211	25	47
	2			25	46
	3			24	42
Naphthalene	1	128	217	46	62
	2			44	59
	3			40	57
Indene	1	116	182	49	64
	2			48	63
	3			47	60
1,3-Dimethylnaphthalene	1	156	263	38	54
	2			38	54
	3			36	50
1,2-Dimethylnaphthalene	1	156	267	35	53
	2			35	52
	3			34	50
Internal standards					
1-Chloroheptane	1	134.7	159–161	69	79
	2			67	78
	3			65	73
1-Chlorooctane	1	148.7	223	58	70
	2			57	69
	3			54	67

Total recoveries in excess of 50% were obtained for a broad range of organic compounds stripped at 30°C. Strip recoveries were increased by amounts ranging from 10–40% for most compounds when strip temperatures were raised to 60°C, regardless of differences in the physical composition of the sediments. This effect may be

important when very low concentrations (ng kg^{-1}) need to be purged from the sediment matrix or when poor recoveries are achieved when using ambient strip temperatures, as experienced by Charles and Simmons [13].

However, at temperatures above 60°C, recoveries of some volatile compounds such as chloromethane and 3-methyl-1,3-butadiene began to fall off with increasing temperature, regardless of their physical composition. This may have occurred as

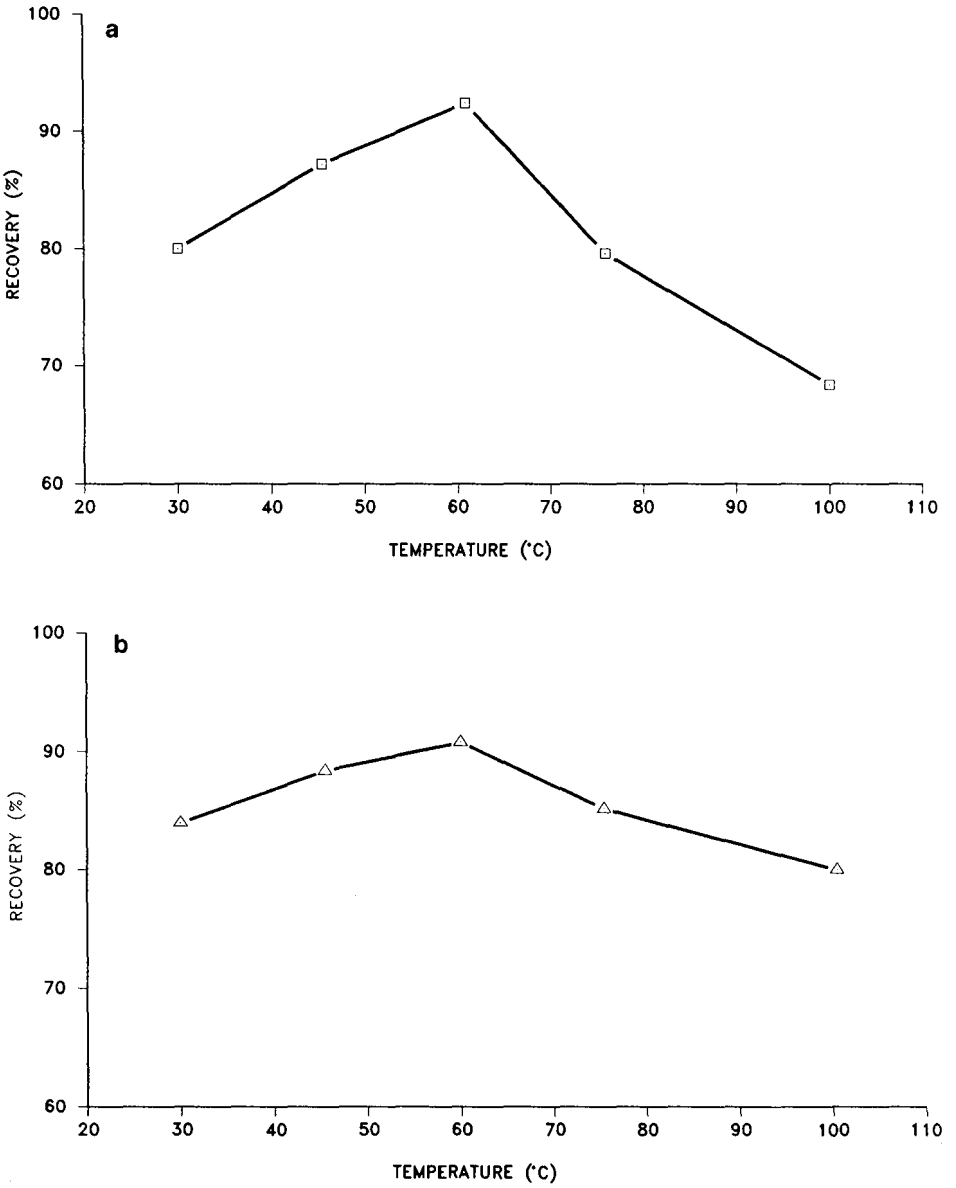

Fig. 2. The variation in recovery of (a) chloromethane and (b) 2-methyl-1,3-butadiene with increasing stripping temperature.

a result of thermal degradation or following reaction with other analytes. This effect is illustrated in Fig. 2 which shows the loss in recovery of both analytes as the stripping temperature is stepped above 60°C. There was no evidence of leakage from the stripping apparatus, and the selective removal of these compounds suggests a degradative pathway specific to these compounds.

The effect of boiling point on recovery

According to Charles and Simmons [13], the performance of sediment purge-and-trap methods are primarily dependent on the physico-chemical properties of the analytes, rather than intrinsic properties of the sediments. Three of the most common physico-chemical properties of VOCs are their boiling points, vapour pressures and aqueous solubilities. Table V included corresponding boiling points of the model VOCs used in this study listed alongside the recoveries of the same VOCs from the three different sediment matrices. When the recoveries of all 60 tabulated compounds (at 60°C) are plotted against their respective boiling points, the correlation coefficient ($R = -0.806$) suggests that a reasonably good correlation exists between both parameters. This is illustrated in Fig. 3a. However, most of the individual plotted data points which fall below the line in Fig. 3a correspond to the values for volatile alcohols and ketones. When the recovery values for the alcohols and ketones are excluded from the correlation data table, the modified correlation coefficient value ($R = -0.955$) shows a much higher correlation between boiling point and recovery for the remaining compounds. See Fig. 3b. This indicates that the relationship between recovery and boiling point depends significantly upon the functional organic compound class. Hence, comparatively non-polar, hydrophobic compounds such as the volatile alkanes, aromatics and organohalogens, for example, exhibit a more consistent and linear relationship between boiling point and recovery (*i.e.* at 60°C) than the polar, hydrophilic alcohols and ketones, especially when purging is carried out at above ambient temperatures.

The effect of vapour pressure on recovery

There are less data in the literature on the vapour pressures of organic compounds than corresponding boiling point data. However, when recovery was plotted against vapour pressure (mmHg at 20°C) for a representative group of the model VOCs (*i.e.* for which vapour pressure values are available, listed in Table VI), a moderate correlation coefficient ($R = 0.715$) was obtained. As a general observation, organic compounds with recoveries below 80% and/or vapour pressures below 30 mmHg at 20°C correlated only marginally (*i.e.* $R = <0.5$). As Table V and VI show, these compounds correspond mainly with the volatile alcohols, ketones or with those *n*-alkanes with boiling points above 100°C. However, by excluding compounds with recoveries below 80% and vapour pressures less than 30 mmHg at 20°C from the original data set, the correlation coefficient ($R = 0.733$) improves only slightly. Hence, the experimental data obtained from this study suggest that, in general, the higher the vapour pressure of the selected VOC, the better the recovery. The relationship between vapour pressure and recovery is, however, less well established than the relationship between boiling point and recovery.

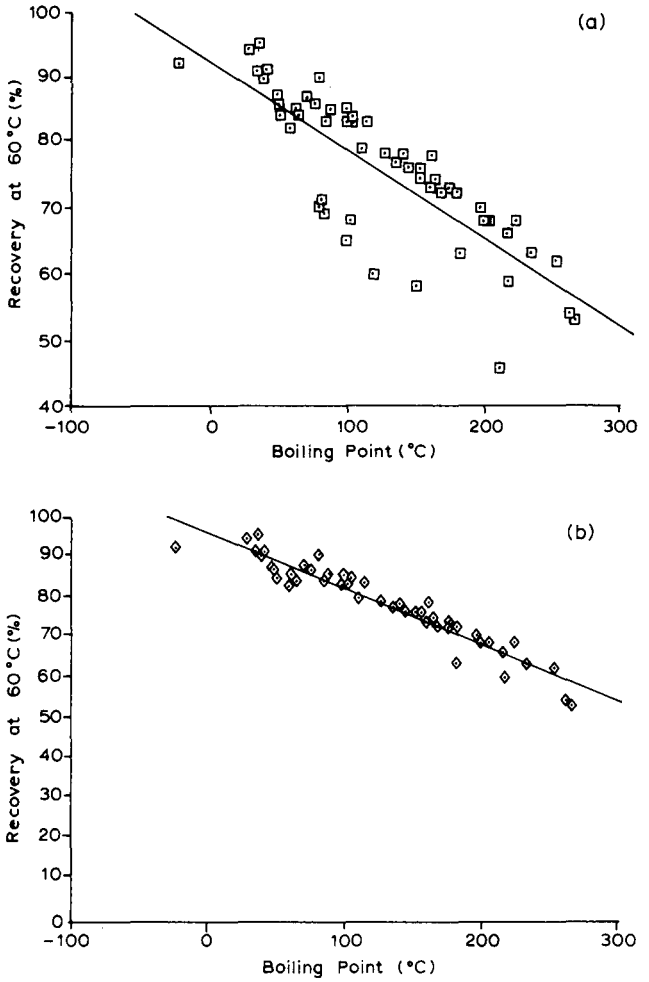

Fig. 3. (a) Correlation line obtained by plotting recovery (at 60°C) from sediment against the boiling points (°C) of 60 model VOCs listed in Table V; $y = 92.31 - (-0.1338)x$, $r = -0.806$. (b) Correlation line obtained by replotting the data in (a) excluding all the data points for the volatile alcohol and ketone compounds; $y = 95.10 - (-0.1364)x$, $r = -0.955$.

The effect of solubility on recovery

When recoveries were plotted against the corresponding aqueous solubility data (also presented in Table VI), a very low correlation coefficient ($R = -0.414$) was obtained. However, as Table VI shows, the solubilities of the model VOCs vary widely from, for example, 0.009 mg l^{-1} for *n*-decane to 353 000 mg l^{-1} for 2-butanone. According to McAuliffe [35], it is the nature of the chemical bonding and size of individual organic compounds which largely determines their solubility in water. Research by McAuliffe concluded that for each homologous series of hydrocarbons, the logarithm of the solubility in water is a linear function of the hydrocarbon molar

TABLE VI

SOLUBILITIES (AT 25°C) AND VAPOUR PRESSURES (AT 20°C) OF SELECTED VOLATILE ORGANIC COMPOUNDS

Data from refs. 35 and 40.

Compound	Vapour pressure (mmHg at 20°C)	Solubility (mg l^{-1} at 25°C)
n-Pentane	430	38.5
n-Hexane	120	9.5
n-Heptane	35	293
n-Octane	11	0.66
n-Nonane	3.22	0.07
n-Decane	2.70	0.009
n-Undecane	0.90	–
3-Methyl-1,3-butadiene	493	642.0
2,2-Dimethylbutane	–	18.4
2,3-Dimethylbutane	200	–
2-Methylpentane	190 (approximate)	13.8
3-Methylpentane	–	12.8
Cyclopentane	300 (approximate)	156.0
Isopentane	–	47.8
2,2,4-Trimethylpentane	–	2.44
Benzene	76	1780
Methylbenzene	22	515
1,3-Dimethylbenzene	6	–
1,2-Dimethylbenzene	5	175
Ethylbenzene	7	152
1,2,4-Trimethylbenzene	–	57
Isopropylbenzene	–	50
1,2-Dichlorobenzene	1	100
Dichloromethane	349	20000
Trichloromethane	160	8000
1,1,1-Trichloroethane	100	4400
Trichloroethylene	60	1100
1,1,2-Trichlorotrifluoroethane	270	–
Dimethylsulphide	420	6300
Ethanol	43.9	–
Propanol	14.5	–
tert.-Butanol	31	–
n-Butanol	4.4	–
2-Butanol	12	125000
Propanal	235	–
Pentanal	48	–
Heptanal	2	–
Benzaldehyde	0.8	–
2-Butanone	77.5	353000
2-Pentanone	12	–
2-Heptanone	2.6	–
Naphthalene	0.4 (approximate)	–
2-Methylfuran	142	–

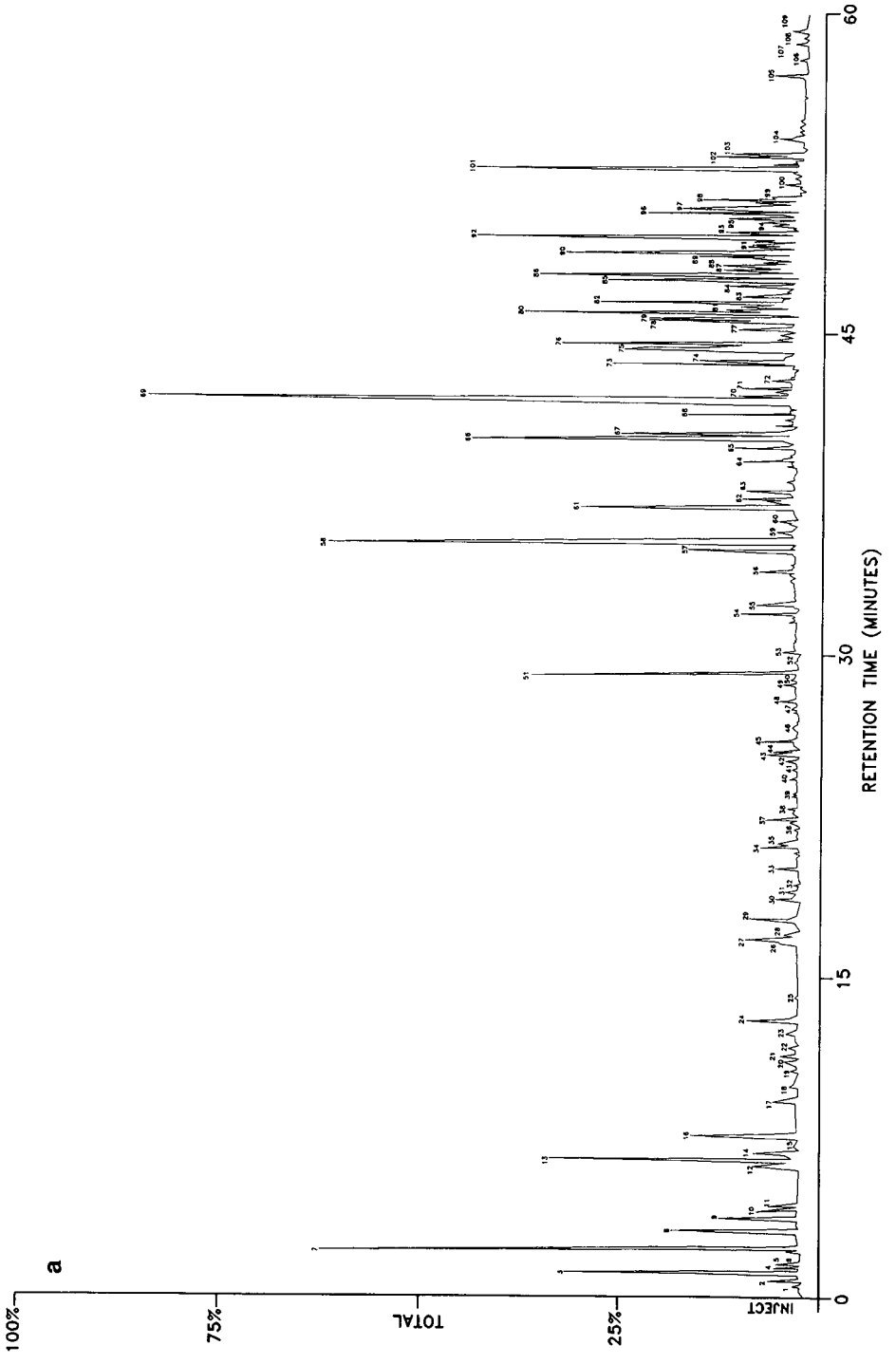
a
100%
75%
TOTAL
25%
INJECT
0
15
30
45
60
RETENTION TIME (MINUTES)

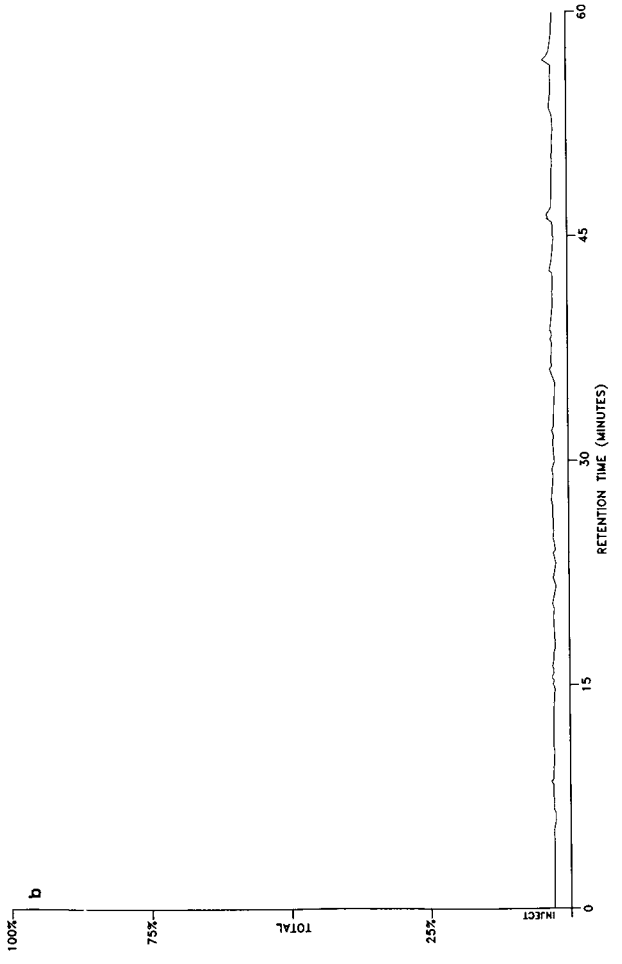

Fig. 4.

(Continued on p. 438)

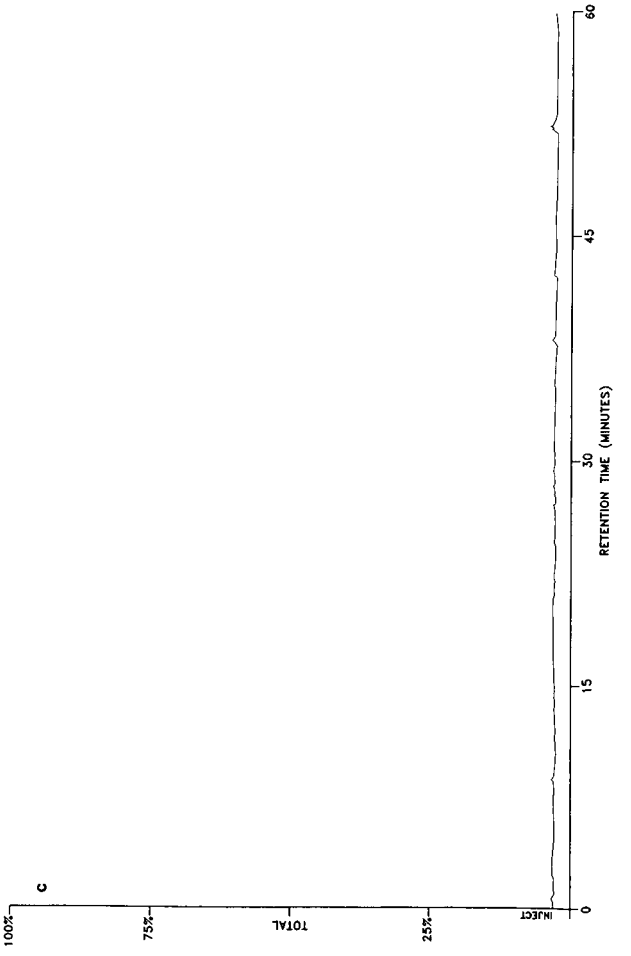
C
100%
75%
TOTAL
25%
INJECT
0
15
30
45
60
RETENTION TIME (MINUTES)

Fig. 4. (a) Reconstructed ion-chromatogram (RIC) of a gasoline contaminated sediment sample taken from the Itchen river in the Southampton Water estuary. This trace was obtained by desorbing the organic analytes trapped on the Tenax-TA tube. (b) Reconstructed ion-chromatogram (RIC) of "blank" water and sediment mixture purged onto the Tenax-TA tube prior to the sample analysis. (c) Reconstructed ion-chromatogram (RIC) of "blank" water and sediment mixture purged onto the Tenax-TA tube after the sample analysis. Peaks: 1 = Propane; 2 = *iso*-butane; 3 = *n*-butene; 4 = *trans*-butene-2; 5 = *cis*-butene-2; 6 = 3-methyl-butene-1; 7 = isopentane; 8 = *n*-pentane; 9 = 2-methylbutene-1; 10 = *trans*-pentene-2; 11 = *cis*-pentene-2 + 2,2-dimethylbutane; 12 = 2,3-dimethylbutane; 13 = 2-methylpentane; 14 = cyclopentane; 15 = 4-methylpentene-2; 16 = 3-methylpentane; 17 = *n*-hexane; 18 = 2-methylpentene-1; 19 = *trans*,*cis*-hexene-2; 20 = *trans*-hexene-2; 21 = 2-methylpentene-2; 22 = *cis*-3-methylpentene-2; 23 = 4-methylcyclopentane; 24 = *trans*-3-methylpentene-2 + *cis*-hexene-2 + 2,4-dimethylpentane; 25 = methyl cyclopentane; 26 = 4-methylcyclopentene; 27 = 2-methylhexane + cyclohexane; 28 = 2,3-dimethylpentane; 29 = 3-methylhexane; 30 = 2,2,4-trimethylpentane; 31 = *cis*-2,3-dimethylcyclopentane; 32 = *trans*-1,2-dimethylcyclopentane; 33 = cyclohexene; 34 = 2,3-dimethylpentene-2; 35 = *n*-heptane; 36 = 3-methylhexene-1; 37 = benzene; 38 = *trans*-1,2-dimethylcyclopentane; 39 = hexene-2; 40 = 3-methylhexene-2; 41 = C_4 olefin; 42 = methylcyclohexane; 43 = 2,5-dimethylhexane; 44 = 1,4-dimethylhexane; 45 = *n*-octane; 46 = octene; 47 = 2,3,4-trimethylpentane; 48 = 2,3,3-trimethylpentane; 49 = 2,3-dimethylhexane; 50 = 2,2-dimethylheptane; 51 = methylbenzene; 52 = 2,6-dimethylheptane; 53 = 3,5-dimethylheptane; 54 = 2- + 4-methyloctane; 55 = 3-methyloctane; 56 = *n*-nonane; 57 = ethylbenzene; 58 = 1,2- + 1,4-dimethylbenzene; 59 = dimethyloctane; 60 = C_{10} alkene + cyclodiene; 61 = 1,3-dimethylbenzene; 62 = 4-methylnonane; 63 = isopropylbenzene; 64 = *n*-decane; 65 = *n*-propylbenzene; 66 = 1-methyl-3-ethylbenzene + 1-methyl-4-ethylbenzene; 67 = 1,3,5-trimethylbenzene; 68 = 1-methyl-2-ethylbenzene; 69 = 1,2,4-trimethylbenzene + C_{11} alkene; 70 = secondary butylbenzene; 71 = C_{11} alkane; 72 = aromatic?; 73 = 1,2,3-trimethylbenzene; 74 = *n*-undecane; 75 = nonene-1; 76 = 1-methyl-3-propylbenzene; 77 = 1-methyl-2-propylbenzene; 78 = 1,4-dimethyl-3-ethylbenzene; 79 = 1,3-dimethyl-4-ethylbenzene; 80 = 2-dimethyl-4-ethylbenzene; 81 = C_{10} aromatic; 82 = substituted indene aromatic?; 83 = C_{12} alkane; 84 = 1,3-dimethyl-2-ethylbenzene; 85 = 1,2,4,5-tetramethylbenzene; 86 = 1,2,3,5-tetramethylbenzene; 87 = *n*-dodecane; 88 = C_{11} alkane + C_{11} alkene; 89 = C_{11} aromatic; 90 = C_{11} aromatic; 91 = C_{11} aromatic; 92 = 2,3-dihydro, 4-methyl-indene; 93 = dimethylpropylbenzene; 94 = C_{11} aromatic; 95 = 2,3-dihydro-1,3-dimethylindene; 96 = *n*-tridecane; 97 = 2,3-dihydro-1,6-dimethylindene; 98 = C_{12} aromatic; 99 = C_{12} aromatic; 100 = C_{12} aromatic; 101 = naphthalene; 102 = 2,3-dihydro-4,7-dimethylindene; 103 = C_{13} aromatic; 104 = dihydrodimethylindene; 105 = 1-methylnaphthalene; 106 = 2-methylnaphthalene; 107 = 1,3-dimethylnaphthalene; 108 = C_{13} alkene; 109 = 1,2-dimethylnaphthalene.

volume. Solubility decreases in the order alkynes > alkenes > alkanes. McAuliffe also stated that branching of the molecule increases the water solubility for alkane, alkene and alkyne hydrocarbons but not for cycloalkane, cycloalkene or aromatic hydrocarbons. However, for a given carbon number, ring formation increases water solubility. Double bond addition to a molecule, ring or chain also increases water solubility. The increased solubilities due to branching are not due to structural features of the molecules, but to the higher vapour pressure of the branched chain hydrocarbons relative to the corresponding alkane or alkene hydrocarbon.

Hence, it is more useful to compare the experimental recoveries of VOCs from sediments with the solubilities of VOCs from within their own particular functional class, rather than across compounds with, for example, similar boiling ranges. When this is done, the increased correlation coefficients obtained (*n*-alkanes, $R = 0.864$; aromatics, $R = 0.916$; organohalogens, $R = 0.721$) show that improved correlations between the recovery and solubilities of groups of compounds are obtained. Solubility is therefore a reasonable guide to recovery of VOCs from the sediments found in Southampton Water, second to the boiling points.

Once again, it is the nature of the individual functional class which determines the reliability and predictability of these relationships. This suggests that by developing sound, experimentally based performance models for groups of compounds within individual organic classes, purge-and-trap analysis of sediment matrices can be reliably performed to obtain good quality analytical data.

Losses of VOCs following storage of sediments

Analysis of standard samples stored for 48 h in the refrigerator at $-4°C$ were found to be within the repeatability (*i.e.* short term precision, R.S.D.) of the method for all 60 model volatile compounds at three concentration levels (as quoted in Table III). The retention of chilled sediment samples under zero headspace in all-glass vessels is therefore an effective short-term storage option should it not be possible to immediately analyse samples. We did not determine the lifetime of chilled samples beyond a 48-h storage period.

Since most samples were analysed within 24 h of sampling, losses due to microbial attack, respiration and chemical alteration were minimised. However, for sediment samples kept in the laboratory at ambient temperature which *were not spiked* with sodium azide, it was observed that volatile organosulphide concentrations began to increase with time. For example, after 48 h storage at 24°C, dimethylsulphide, dimethyldisulphide and dimethyltrisulphide were recovered at higher concentrations (*i.e.* typically by 5–10%) relative to spiked samples analysed shortly after sampling. This phenomenon was previously noticed by Schwarzenbach *et al.* [36] who considered the *in-situ* synthesis of volatile organosulphides to be due to ongoing anaerobic microbial activity taking place after the samples were taken.

The Solent estuary —a case study

The Solent estuary forms a body of water separating the Isle of Wight from the submerged channel of Southampton Water on the coastline of central southern England. Southampton Water is a semi-industrialised estuary accommodating a broad range of activities including oil-refining, petrochemical processing, electricity generation and intense recreational and merchant-marine activities. In addition, the

estuary receives input from six sewage treatment plants, agricultural run-off and flush-water from enclosed marinas. The latter developments present a growing pollution problem for estuarine ecosystems. For example, Bianchi *et al.* [37] found high levels of volatile aromatic compounds (*i.e.* $> 500\ \mu g\ l^{-1}$ per compound) in anoxic sediments adjacent to a new marina site in Southampton Water. Spillages of fuels occur from time to time and lead to localised contamination of water and underlying sediments. For example, Fig. 4a shows a reconstructed ion-chromatogram (RIC) obtained from the upper 5-cm of sediment in the River Itchen following the spillage of gasoline from a barge moored alongside fuel storage tanks. Fig. 4b and c show the respective ion-chromatograms obtained following purging of the Tenax-TA tube with a mixture of "blank" water and "blank" sediment before and after the Itchen sediment sample was analysed. The total mass of organic material (*i.e.* total area under the summed peaks) due to the petroleum spill was calculated to be 395 $\mu g\ kg^{-1}$. An interesting observation from this analysis is that some of the more volatile compounds (*e.g.* C_4 and C_5 compounds) have been recovered from the sediment and trapped/desorbed from the Tenax-TA tube. It was also noted that the comparatively high mass of gasoline components sorbed onto the surface sediments effectively "blanks-out" any natural, biogenic VOC present in the sediments at much lower concentrations from the analysis.

With so many potential sources of organic compounds it has become a major analytical challenge to identify, categorise and quantitate every single volatile compound found during purge-and-trap analysis of large numbers of water and sediment samples. Tables of concentration ranges of key compounds are a valuable aid in understanding how sediments act as repositories for VOCs. Sediments have the potential to accumulate and concentrate much higher levels of VOCs than might normally be found in the water column, especially within estuaries where large volumes of anthropogenic substances are channelled in the path from rivers to the open sea. Table VII shows the broad range of VOCs found in the estuarine sediments as well as the typical variation in concentrations which were observed between water and sediment samples over an 18-month period. The majority of the compounds listed in Table VII were found in all three sediments, *i.e.* head, mid-point and mouth of the estuary. This suggests that the many of the mechanisms responsible for their production and/or deposition in sediments behave similarly across the length of Southampton Water. Apart from random pollution related events (*i.e.* oil spills), the most significant variations in VOC concentrations occurred as a result of seasonal changes. For example, total VOC concentrations in sediments reach their minimum during July–August and their maximum from October–January. Higher summer temperatures accelerate evaporation from surface water relative to sorption and deposition processes. During autumn and winter, cooler sea-surface temperatures combined with significant increases in organic load to the estuary from its source rivers contribute to the build-up of VOCs in sediments from both synthetic and natural sources, *e.g.*, autumn leaf-fall. Increases in the anthropogenic input to the estuary during autumn (*i.e.* from increased rainfall run-off, increased use of fossil fuels and urban pollution) also contribute additional VOCs to the sediments. A gas chromatogram (*i.e.* Fig. 5a, obtained by desorption of a Chromosorb-106 trap tube) of surface sediment taken from the Test river during October illustrates the diversity of VOCs which can be recovered during the autumn cycle. Fig. 5b shows the respective "blank" analysis performed on the same tube prior to analysis of the sample.

TABLE VII

COMMON VOLATILE ORGANIC COMPOUNDS RECOVERED FROM WATER AND SEDIMENT SAMPLES IN SOUTHAMPTON WATER OVER AN 18-MONTH PERIOD

Compound	Concentration ranges	
	Water (ng l^{-1})	Sediment (ng kg^{-1})
Methanethiol	10–73	103–1950
n-Butane	28–60199[a]	55–86353[a]
2-Methylpropane	50–60100	70–80000
2-Methyl-1,3-butadiene	5–1233	28–97951
n-Pentane	25–327	50–35292[a]
Isopentane	25–250	70–10100
2-Methylbutene-1	50–700	100–1110
Propanone	<10–300	150–380
Dichloromethane	15–1004	20–2742
Dimethylsulphide	10–814[b]	10105–350900[c]
Carbon disulphide	10–100	10–747
Propanal	30–300	120–350
Propanol-1	60–430	350–980
Propanol-2	70–300	350–700
Freon-113	25–70	170–21550
Propanethiol	<10–70	200–3200
2,2-Dimethylbutane	33–94	68–12019
2,3-Dimethylbutane	38–109	60–13786
Methyl *tert.*-butyl ether	15–81	15–20645
Butanone-2	25–240	390–570
Butanone-1	25–200	400–450
n-Hexane	47–496	70–1335
Pentanone-2	35–230	100–380
2-Methylpentene-1	130–700	489–1590
Trichloromethane	10–7502	97–22940
2-Methylfuran	10–17	75–496
1,2-Dichloroethane	15–955	70–11045
1,1,1-Trichloroethane	< 5–2788	70–31031
Benzene	100–55380	298–96735
2,2,3-Trimethylbutane	85–290	200–580
Carbon tetrachloride	<10–311	75–1856
n-Butanol	<10–440	335–607
2-Butanol	<10–400	350–380
Thiophene	<10–190	95–174
4-Methyl-2,3-dihydrofuran	<10–200	90–550
3-Methyl-2-butenal	<10–180	100–390
1,2-Dibromoethane	<10–176	65–6442
Cyclohexane	30–801	100–1440
Trichloroethylene	<10–603	70–4005
Pentanal	<10–170	75–208
2,2,4-Trimethylpentane	<10–400	100–15150
2,4,4-Trimethylpentene-2	<10–490	170–3000
2,5-Dimethylfuran	<10–50	100–312
n-Heptane	50–260	80–19400
Methyl isobutylketone	<10–347	300–420
Dimethyldisulphide	<10–5250[b]	55–72000
Methylcyclohexane	<10–100	100–300
1,1,2,2-Tetrachloroethylene	<10–343	85–20177
Methylbenzene	10–48850	548–120200
3-Ethylhexane	50–110	200–400
Chlorodibromomethane	10–2200	150–27350
3-Methylthiophene	<10–50	120–410

TABLE VII *(continued)*

Compound	Concentration ranges	
	Water (ng l^{-1})	Sediment (ng kg^{-1})
Hexanal	<10–100	80–260
n-Octane	90–290	154–25700
Octene-1	25–75	10–130
1,3-Dimethylbenzene	10–402070	875–480200
1,2-Dimethylbenzene	10–400020	870–480560
Chlorobenzene	<10–120	95–550
Ethylbenzene	10–312008	505–201100
Tribromomethane	10–2597	75–62609
Styrene	30–296	50–2930
Dimethyltrisulphide	25–411	125–795
n-Nonane	95–357	100–41627
Nonene-1	90–300	130–150
Isopropylbenzene	10–47307	250–43370
1,5-Cyclooctadiene	<10–400	170–1000
Cyclooctene	<10–380	230–980
α-Pinene	25–412	150–506
Camphene	25–99	170–303
2,4-Dimethyl-4-vinylcyclohexane	45–31	155–290
n-Propylbenzene	15–2391	60–20004
Benzaldehyde	15–569	95–11937
p-Cymene	35–45	200–350
1,3,5-Trimethylbenzene	20–1500	80–7397
1,2,4-Trimethylbenzene	20–8000	100–1570
1,2,3-Trimethylbenzene	50–6200	90–11775
2,3-Dihydroindene	30–400	200–950
Limonene	25–633	105–807
Indene	55–277	125–1702
1,2-Dichlorobenzene	35–107	95–1055
n-Undecane	87–619	115–1056
1-Methyl-3-propylbenzene	25–550	120–3020
1-Methyl-2-propylbenzene	25–590	120–3010
1,4-Dimethyl-3-ethylbenzene	25–200	90–1000
1,3-Dimethyl-3-ethylbenzene	25–210	90–1120
2-Dimethyl-4-ethylbenzene	30–100	110–980
1,3-Dimethyl-4-ethylbenzene	35–120	135–1200
1,2,3,5-Tetramethylbenzene	25–1430	130–4205
1,2,3,4-Tetramethylbenzene	25–1247	150–8767
Naphthalene	45–894	125–25766
n-Dodecane	95–707	190–1966
Biphenyl	15–42	29–6052
2-Methylnaphthalene	15–490	87–11020
1-Methylnaphthalene	55–450	80–10202
1,3-Dimethylnaphthalene	55–403	200–20300
1,2-Dimethylnaphthalene	25–356	220–20530
n-Hexadecane	30–238	160–23040
n-Heptadecane	15–209	170–25035
n-Octadecane	35–300	200–18030
Pristane	30–155	170–1010
n-Nonadecane	35–250	200–14300
Phytane	30–200	180–1120
n-Eicosane	55–73	180–300

[a] High concentrations mainly from sewage outfalls.
[b] High concentrations associated with plankton blooms.
[c] High concentrations associated with anaerobic marsh sediments.

The functional organic distribution of the major VOCs in water and sediments fall into five major groups. These are (i) the volatile aromatics, (ii) alkanes and alkenes, (iii) oxygen-containing compounds such as alcohols, ketones, ethers and aldehydes, (iv) organosulphur compounds and (v) organohalogens. Although many of these compounds are of anthropogenic origin, many individual compounds such as the terpenes, aldehydes, organosulphides and some of the substituted alkanes (*e.g.* 2,2-dimethylbutane) are contributed to sediments by biological processes.

Volatile aromatics are ubiquitous in the estuary, accounting for between 48–74% of all VOCs found in water samples and 32–78% of all VOCs found in sediments, taking into account variability due to time and place of sampling. This explains why there are such broad concentration ranges for aromatic compounds listed in Table VII. Their sources are numerous and equally as diverse, ranging from exhaust gases from fossil fuel powered engines and ballast water from marine craft to inputs from raw sewage, road run-off and industrial effluents. Methylbenzene is the only volatile aromatic in Southampton Water which has a natural as well as anthropogenic source. The stepwise generation of biogenic methylbenzene has been determined previously in sediments at the bottom of anoxic lakes, showing that methylbenzene also has several discrete biological formation pathways via microbiological mechanisms [38]. Recent studies by the authors suggest that methylbenzene is generated by identical processes *in situ* within surface sediments in Southampton Water, especially in the weeks following the autumn leaf fall. Methylbenzene was also synthesised in river bed sediments 15 miles upstream of the Test river. This was monitored in an unpolluted rural area, in the complete absence of any other aromatic compounds.

Volatile alkane and alkene compounds comprise up to 40% of VOCs in both water and sediments throughout the estuary. They are therefore numerically the second major class of VOCs found in the estuary. Although many of these compounds originate from industrial effluents, they are also produced as a by-product following intense planktonic activity occurring in the estuary. During the midsummer "red-tide bloom" of the photosynthetic ciliate "*Mesodinium rubrum*", concentrations of substituted alkenes, including terpenes such as 2-methyl-1,3-butadiene (isoprene), α-pinene and limonene increase significantly to very high relative concentrations (*i.e.* 90 000, 500 and 800 ng kg^{-1} respectively, in sediments). During autumn, concentrations of isoprene show a second sharp seasonal increase, suggesting that this simple terpene compound is a major participant or intermediary in biologically related processes in Southampton Water.

Volatile organosulphides, notably dimethylsulphide, are consistently found at high concentrations (*i.e.* up to 360 000 ng kg^{-1}) in Southampton Water sediments. Dimethylsulphide is the single most abundant non-aromatic volatile compound occurring in sediments, rarely found in concentrations less than 1000 ng kg^{-1}. It is produced *in-situ* within the anoxic muds and sediments in Southampton Water by biological fermentation processes. However, it is also found in surface water samples (a) near sewage outfalls, and (b) during the mid-summer plankton "blooms". During the *Mesodinium rubrum* bloom, concentrations of the disulphide homologue, dimethyldisulphide, reach an annual maximum both in water and sediments, exceeding even the concentrations of dimethylsulphide in the water column. This annual peak in dimethyldisulphide concentration is uniquely due to the June–July proliferation of the plankton in the estuary. Dimethyldisulphide is formed by the oxidative coupling of

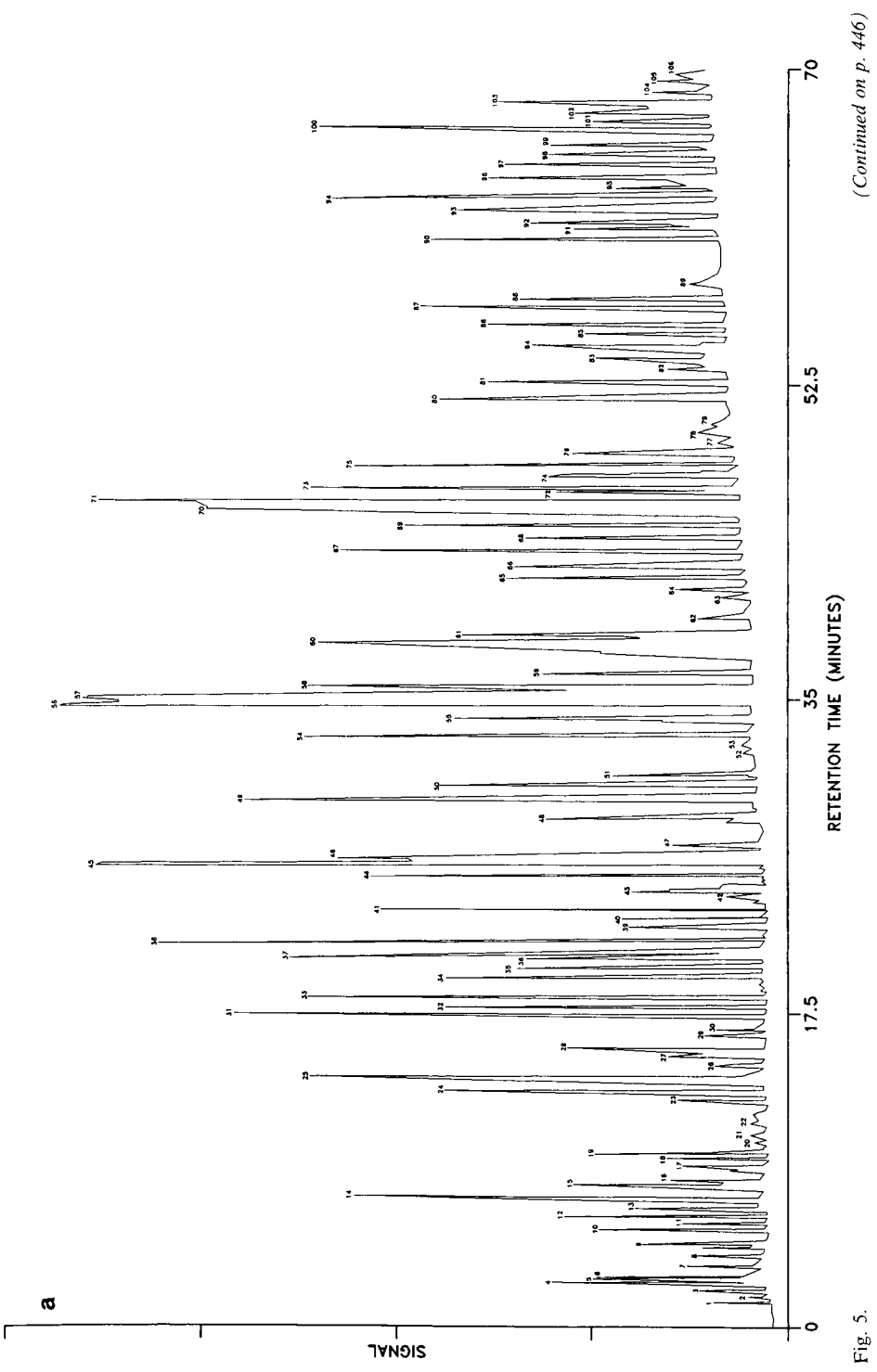

(Continued on p. 446)

Fig. 5.

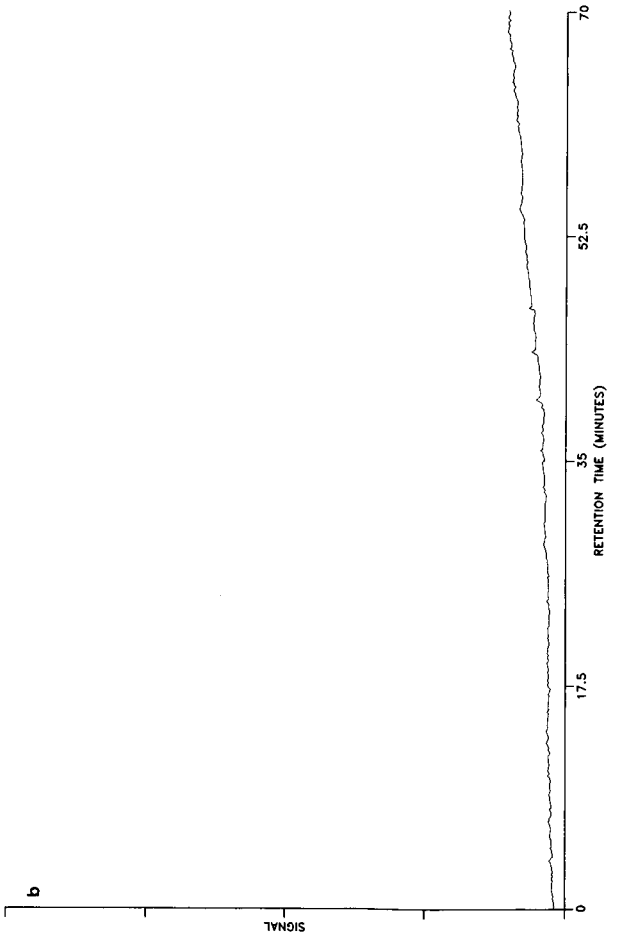
b
SIGNAL
0
17.5
35
52.5
70
RETENTION TIME (MINUTES)

Fig. 5. (a) Gas chromatogram of a sediment sample taken from the River Test. This chromatogram was obtained following thermal desorption of a Chromosorb-106 sorbent "trap" tube. Peak numbers: 1 = Propane; 2 = isobutane; 3 = *n*-butane + 2-methylpropane; 4 = *trans*- + *cis*-butene; 5 = isopentane + methanethiol; 6 = *n*-pentane; 7 = fluorotrichloromethane; 8 = 2-methyl-1,3-butadiene; 9 = 2,2-dimethylbutane; 10 = *trans*-1,2-dichloroethylene + 2,3-dimethylbutane; 11 = 2-methylbutene-2 + 2-methylpentane; 12 = 3-methylpentane; 13 = cyclopentane + 4,4-dimethylbutane; 14 = dimethylsulphide; 15 = *tert*.-butanol; 16 = carbon disulphide; 17 = 2-butanone; 18 = *n*-butanal; 19 = *n*-hexane; 20 = trichloromethane; 21 = methyl *tert*.-butyl ether; 22 = 2-methylfuran; 23 = *trans*- + *cis*-hexene-3; 24 = 2-methylpentene-2; 25 = *cis*-3-methylpentene-2; 26 = 3-methylcyclopentene; 27 = 4,4-dimethylpentene-1; 28 = *cis*-2-hexene; 29 = 2,3-dimethyl-1,3-butadiene; 30 = 3-methyl *trans*-2-heptene; 31 = ethylcyclobutane; 32 = 1,2-dichloroethane; 33 = 2,2-dimethylpentane; 34 = *n*-heptane; 35 = 3-methyl hexene-1; 36 = 1,1,1-trichloroethane; 37 = 3-methylbutanal; 38 = benzene; 39 = 2-methylhexene-2; 40 = 2,2,3-trimethylbutane; 41 = carbon tetrachloride; 42 = *n*-butanal; 43 = dimethyldisulphide; 44 = ethylcyclopentane; 45 = methylcyclohexane; 46 = 2,2,3-trimethylpentane; 47 = *n*-octane; 48 = 3,3-dimethylhexane; 49 = methylbenzene; 50 = 2,6-dimethylheptane; 51 = 3,5-dimethylheptane; 52 = 2- + 4-methyloctane; 53 = 3-methyloctane; 54 = *n*-nonane; 55 = chlorobenzene; 56 = ethylbenzene; 57 = 1,3- + 1,4-dimethylbenzene; 58 = styrene; 59 = C_9 alkene; 60 = 1,2-dimethylbenzene; 61 = C_9 alkene; 62 = dimethyltrisulphide; 63 = isopropylbenzene; 64 = α-pinene; 65 = *n*-decane; 66 = *n*-propylbenzene; 67 = 1-methyl-3-ethylbenzene; 68 = 1,3,5-trimethylbenzene; 69 = C_{11} alkane; 70 = 1-methyl-2-ethylbenzene; 71 = 1,2,4-trimethylbenzene; 72 = octanal; 73 = terpene (?); 74 = terpene (?); 75 = 1,2,3-trimethylbenzene; 76 = dimethyltetrasulphide; 77 = 1-methyl-2-propylbenzene; 78 = 2-dimethyl-4-ethylbenzene; 79 = *n*-undecane; 80 = 1,3-dimethyl-2-ethylbenzene; 81 = indene; 82 = C_{12} alkene; 83 = 1,2,4,5-tetramethylbenzene; 84 = 1,2,3,5-tetramethylbenzene; 85 = *n*-dodecane; 86 = C_{11} aromatic; 87 = dimethylpropylbenzene; 88 = *n*-tridecane; 89 = naphthalene; 90 = 2,2-dihydro-4,7-dimethyl indene; 91 = a substituted naphthalene (?); 92 = C_{13} aldehyde; 93 = *n*-tetradecane; 94 = 1-methylnaphthalene; 95 = 2-methylnaphthalene; 96 = C_{12} aldehyde; 97 = *n*-pentadecane; 98 = 1,3-dimethylnaphthalene; 99 = *n*-hexadecane; 100 = 1,2-dimethylnaphthalene; 101 = C_{14} aldehyde; 102 = *n*-heptadecane; 103 = pristane; 104 = pentadecanal; 105 = C_{14} alkene; 106 = phytane. (b) Gas chromatogram of a "blank" sediment sample analysed using the same purge-and-trap/thermal-desorption analytical method as used for samples. This chromatogram was obtained following thermal desorption of a Chromosorb-106 sorbent "trap" tube.

methyl mercaptan, a simple organosulphide which is bio-synthesised *in situ* by the organisms [39]. By early autumn, dimethyldisulphide concentrations dwindle rapidly to background concentration levels determined by constant low-level inputs supplied by sewage effluents and microbial fermentation processes in muds.

In contrast, volatile organohalogens in Southampton Water originate almost exclusively from the activities of man and are commonly found around both raw and treated-sewage outfalls. Highest concentrations are found in effluent discharge zones around the city of Southampton. Compounds such as carbon tetrachloride, 1,1,1-trichloroethane and 1,2-dichlorobenzene are consistently found at concentrations up to ten times higher in sediments than in water. Unlike many of the other volatile organic compound classes, these compounds are also found in deeper sediments (*i.e.* down to 50-cm in depth), suggesting that they can migrate readily through sediments and are comparatively resistant to biodegradation. As such, they are probably the most stable volatile compounds found in sediments.

Oxygen-containing volatiles, such as aldehydes, ketones and alcohols were found generally at lower concentrations than the VOCs mentioned in the foregoing discussion. Aldehydes, especially pentanal, hexanal and benzaldehyde were found all year round in water and sediments. Their concentrations varied mainly with planktonic activity, reaching their annual maxima in conjunction with the midsummer peak in *Mesodinium rubrum* and chlorophyll *a*.

This brief discussion of the VOCs found in Southampton Water shows that volatile organics are contributed from both man-made and natural sources. This field study also demonstrates how the application of the stripping method has revealed much detailed information about the occurrence and behaviour of VOCs in estuarine environments. Hence, it offers additional insight into geochemical and environmental processes.

CONCLUSIONS

This study shows that the modified purge-and-trap method, developed initially for the analysis of water samples, can be usefully applied to detect VOCs in estuarine sediments. The adoption of a simple purging apparatus with multi-sorbent trapping facilitates quantitative trapping of VOCs at very low concentrations. The sorbent traps are adapted for use from well established analytical methodologies. Thermal desorption analysis and gas chromatography can be automated, making it possible for laboratories to analyse significant numbers of samples with more efficient use of manpower.

Results of basic studies on the recovery of VOCs from different sediment matrices illustrate that desorption was marginally affected by differences in the physical composition of different sediment types representative of the Southampton Water estuary. This may not be the case when stripping different sediment matrices, *e.g.* those containing an exceptionally high clay or sand content. Major factors affecting the stripping of sediments include the efficiency of the method, the concentration of the VOCs and physico-chemical properties (*e.g.* boiling point, vapour pressures and aqueous solubilities) of the functional classes of organic compounds present. Consequently, it is the ability of the analytical method to quantitatively strip VOCs from the sediments that determines the efficiency and usefulness of the

technique to the environmental chemist. Knowing the composition of VOCs in sediments is potentially very useful for determining the pollution status of an estuary and for providing an improved understanding of the nature of both biogenic and anthropogenic inputs.

REFERENCES

1 S. R. Carlberg, in E. Olausson and I. Cato (Editors), *Chemistry and Biogeochemistry of Estuaries*, Wiley-Interscience, New York, 1980, Ch. 12.
2 A. H. Knap, *Ph.D. Thesis*, University of Southampton, Southampton, 1978.
3 L. S. Sheldon and R. A. Hites, *Environ. Sci. Technol.*, 13 (1979) 574–579.
4 R. B. Gagosian and C. Lee, in E. K. Duursma and R. Dawson (Editors), Marine Organic Chemistry, Elsevier, New York, 1981, Ch. 5.
5 E. Merian and M. Zander, in O. Hutzinger (Editor), *Handbook of Environmental Chemistry*, Vol. 3, Part B, Springer, New York, 1981, pp. 117–161.
6 L. Fishbein, *Sci. Total Environ.*, 11 (1979) 163–195.
7 T. A. Bellar, J. J. Lichtenberg and R. C. Kroner, *J. Am. Water Works Assoc.*, 66 (1974) 703–706.
8 W. L. Budde and J. W. Eichelberger, *Organics Analysis Using Gas Chromatography/Mass Spectrometry*, Ann Arbor Sci. Publ., Ann Arbor, MI, 1980, p. 39.
9 K. Grob, *J. Chromatogr.*, 84 (1973) 243–255.
10 J. P. Mieure, J. W. Mappes, E. S. Tucker and M. W. Dietrich, in L. A. Keith (Editor), *Identification and Analysis of Organic Pollutants in Water*, Ann Arbor Sci. Publ., Ann Arbor, MI, 1976, pp. 113–133.
11 A. Bianchi, *Int. Environ. Safety (UK)*, 6 (3) (1988) 8–10.
12 A. Bianchi and M. S. Varney, *Int. Environ. Safety (UK)*, 6 (4) (1988) 12–13.
13 M. J. Charles and M. S. Simmons, *Anal. Chem.*, 59 (1987) 1217–1221.
14 D. J. O'Connor and J. P. Connolly, *Water Res.*, 14 (1980) 1517–1523.
15 S. W. Karickhoff, D. S. Brown and T. A. Scott, *Water Res.*, 13 (1979) 241–248.
16 A. Y. Huc and J. W. Hunt, *Geochim. Cosmochim. Acta*, 44 (1980) 1081–1089.
17 A. Bianchi and M. S. Varney, *Analyst (London)*, 114 (1989) 47–51.
18 A. W. Elzerman and J. W. Coates, in R. A. Hites and S. J. Eisenreich (Editors), *Sources and Fates of Organic Pollutants (Advances in Chemistry Series*, Vol. 216), American Chemical Society, Washington, DC, 1987, Ch. 10.
19 K. Schellenberg, C. Leuenberger and R. B. Schwarzenbach, *Environ. Sci. Technol.*, 18 (1984) 652–657.
20 M. H. Hiatt, *Anal. Chem.*, 53 (1981) 1541–1543.
21 R. S. Brazell and M. P. Maskarinec, *J. High Resolut. Chromatogr. Chromatogr. Commun.*, 4 (1981) 404–405.
22 R. A. Hurrel, *Int. Environ. Safety (UK)*, June (1981) 18–21.
23 A. Bianchi and M. S. Varney, *J. High Resolut. Chromatogr. Chromatogr. Commun.*, 12 (1989) 184–186.
24 A. Bianchi, M. S. Varney and A. J. Phillips, *J. Chromatogr.*, 467 (1989) 111.
25 *Method-624. (Purgeables)*, United States Environmental Protection Agency, Environmental Monitoring and Support Laboratory, Cincinnati, OH, July, 1982.
26 *CONCAWE Report No 8/86*, CONCAWE (Oil Companies International Study Group for the Conservation of Clean Air and Water), The Hague, 1986.
27 G. Harvey, *Mar. Chem.*, 24 (2) (1988) 199–202.
28 R. Pizzie, *Ph.D. Thesis*, Univ. of Southampton, Southampton, 1984.
29 P. Bartlett, Senior Analytical Chemist, Oil Pollution Research Unit, Orielton, Dyfed, personal communication.
30 D. I. Little, M. F. Staggs and S. S. C. Woodman, in J. Parker and K. Kinsman (Editors), *Transfer Processes in Cohesive Sediment Matrices*, Plenum Press, New York, 2nd ed., 1984, p. 47.
31 P. McLaren, *Sediment Transport and Contaminant Disposal in Sullom Voe and Southampton Water, Report*, Institute of Petroleum, London, 1987, p. 81.
32 P. N. Froelich, *Limnol. Oceanogr.*, 25 (3) (1980) 564.
33 H. B. Lee, R. L. Hong-You and A. S. Y. Chau, *Analyst (London)*, 111 (1986) 81–84.
34 K. E. Murray, *J. Chromatogr.*, 135 (1977) 49.
35 C. McAuliffe. *J. Phys. Chem.*, 70 (1966) 1267.

36 R. P. Schwarzenbach, R. H. Bromund, P. M. Gschwend and O. C. Zafiriou, *Org. Geochem.*, 1 (1978) 93.
37 A. Bianchi, C. A. Bianchi and M. S. Varney, *Oil Chemical Pollution*, 5 (1989) 477–488.
38 F. Juttner and J. J. Henatsch, *Nature (London)*, 323 (1986) 797.
39 P. M. Gschwend, O. C. Zafiriou, R. F. C. Mantoura, R. P. Schwarzenbach and R. B. Gagosian, *Environ. Sci. Technol.*, 16 (1982 31.
40 K. Verscheuren, *Handbook of Environmental Data on Organic Chemicals*, Van Nostrand Reinhold, New York, 1983.

Journal of Chromatography, 542 (1991) 451–458
Elsevier Science Publishers B.V., Amsterdam

CHROM. 23 003

Gas chromatographic determination of monoterpenes in essential oil medicinal plants

S. V. SUR*, F. M. TULJUPA and L. I. SUR
Institute of Colloid Chemistry and Chemistry of Water, Ukrainian Academy of Sciences, Pr. Vernadskogo 42, 252142 Kiev (U.S.S.R.)
(First received May 14th, 1990; revised manuscript received November 8th, 1990)

ABSTRACT

Gas chromatographic (GC) techniques for the determination of the major biologically active monoterpenoids in peppermint, fennel, garden sage and creeping thyme plant material and water infusions were developed. The analysis requires 1–2 g of plant material or 100–200 g of infusion and takes no more than 1.5 h, including distillation and GC. The techniques allow the analysis of the herbs and infusions without the determination of the total essential oil content and weighing of isolated oils for chromatography. It was found that the essential oil component ratios were changed on dissolution in water during the preparation of infusions. The average values of the extraction factors for monoterpene alcohols, ketones, phenols and peroxides extracted from plant material are ten times those for related hydrocarbons and ethers extracted under the same conditions.

INTRODUCTION

Essential oil medicinal herbs are widely used in the U.S.S.R.in traditional and scientific medicine for treating many diseases [1,2]. The following components of essential oils are considered to be the most important biologically active substances in different medicinal herbs: menthol, menthyl acetate and methone for peppermint (*Mentha piperita* L.), fenchone and anethole for fennel (*Foeniculum vulgare* Mill.), cineole and camphor for garden sage (*Salvia officinalis* L.) and thymol and carvacrol for creeping thyme (*Thymus serpyllum* L.) [1].

Infusions are most often used for phytotherapy. According to the U.S.S.R. Pharmacopoeia [2], they represent aqueous extracts of plant materials and contain complex mixtures of water-soluble low- and high-molecular-weight compounds of various classes. It may be expected that infusions of the plant material are likely to contain only small amounts of essential oil constituents.

The aim of this work was to develop simple and rapid methods for the determination of the main biologically active terpenoids in plant material and infusions of peppermint, fennel, garden sage and creeping thyme, in order to allow us to determine objectively the quality of plant raw material and related medicines, to optimize their methods of production and to solve some other problems.

Terpenoids are usually determined by gas chromatography (GC) of essential

0021-9673/91/$03.50

oils isolated from samples by various methods. For essential oil isolation different methods are used, *e.g.*, extraction with organic solvents [3,4], hydrodistillation [5,6], the headspace method [7], retention by sorbents [8] or cooling traps [9], evaporation in a modified injector [10] and combinations of these methods.

For the isolation of essential oil components from plant materials and infusions we selected the hydrodistillation method, owing to its simplicity and rapidity, the relative stability of the analytes and the possibility of their quantitative isolation during distillation. Hydrodistillation can also be combined with GC using the internal standard method. As a result, we developed methods that are simpler and faster than those described in the literature for the determination of terpenoids in plant materials and water infusions.

EXPERIMENTAL

Distillation apparatus and distillation

The apparatus used is a modified version of that applied to for the determination of essential oils in plant materials according to the U.S.S.R. Pharmacopoeia [11] and the British Pharmacopoeia [12] methods. The modified apparatus is approximately half the size and has a more effective inverse condenser and other constructional improvements. The apparatus is shown in Fig. 1 (dimensions are given in millimetres). Condenser A is connected with chamber C, which is the oil and water condensate receiver. The receiver has orifice B closed with a stopper during distillation. The level of liquid in the receiver is maintained by arm D, which returns condensed water to flask.

Accurately weighed plant material (1–2 g) and 100 ml of water or 100–200 g of infusion, 20–40 g of sodium chloride (salting-out agent) and a few small pieces of porous earthenware were placed in a 500-ml flask, which was then joined to the apparatus. Before distillation, water was poured into the apparatus up to maximum level and 0.2–0.5 ml of a 4.95% (w/v) solution of methyl salicylate (internal standard) in hexane was accurately measured and introduced into receiver C through orifice B.

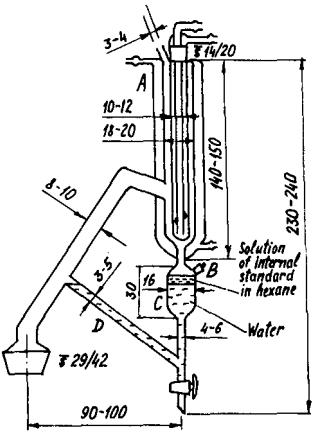

Fig. 1. Apparatus for essential oil isolation.

The internal standard solution was used as the collecting solvent for the hydrodistilled oil constituents.

During distillation, the essential oils and water vapour condensed in the condenser and the condensate dropped into the reciver. The terpenoids were dissolved in a mixture of hexane and internal standard but water was automatically returned through arm D into the flask with plant material or infusions. Because of the high partition coefficient between hexane and water, virtually full retention of oil components by hexane was achieved during distillation.

A distillation time of 45 min was estimated to be adequate for complete isolation of the analytes from all the herbs and infusions studied. After the end of distillation, 0.2–0.5 μl of the obtained mixture of isolated oils and internal standard were injected into the gas chromatograph.

To establish possible losses of analytes, the major components in peppermint, fennel, garden sage and creeping thyme oils were determined before and after distillation. Essential oils (0.2 g) with known composition were accuratley weighed and placed in a flask containing 100 ml of 20% sodium chloride solution when distilled for 45 min. A mixtgure of distilled essential oil with internal standard in hexane was chromatographed and the distillation recovery for the analytes was calculated. The results obtained (from 93.2 to 100.0%) indicated that the losses were insignificant.

The reproducibility of the isolation method was determined by distillation of five peppermint leaf samples with the same mass and composition. These samples were selected from well milled and mixed peppermint leaves. The essential oil from each sample was isolated and the determination of menthol, menthyl acetate and menthone was carried out. The results of statistical treatment [relative standard deviation (n = 5) for menthol = 1.98%, for menthyl acetate = 2.66% and for menthone = 3.57%)] confirm the high reproducibility of both isolation and analysis.

Gas chromatography

An LHM-80 (the 6th model) gas chromatograph equipped with a flame ionization detector was used. Thymol and carvacrol determinations were carried out on a 2 m × 3 mm I.D. stainless-steel column packed with 5% Superox 20M on Chromosorb W-HW (100–120 mesh) (Alltech) with temperature programming from 100 to 220°C at 4°C/min. In other instances a 3 m × 3 mm I.D. column with the same stationary phase was used and the temperature was programmed from 100 to 190°C at 3°C/min. The carrier gas (helium) and hydrogen flow-rates were 25 ml/min and the air flow-rate was 250 ml/min. The injector and detector were thermostated at 190 and 220°C, respectively.

The chromatography takes 30 min and full analyses, including hydrodistillation, not more than 1.5 h.

The determination of analytes was carried out by the internal standard method with methyl salicylate [4.95% (w/v) solution in hexane] as the internal standard. Mixtures of internal standard and essential oils isolated from each sample were chromatographed five times. The content was calculated by comparing the areas under the peaks of the analytes and internal standard and taking into account the response factors.

Menthol, camphor and thymol which corresponded to the U.S.S.R. Pharmacopoeia requirements, were used as standard substances. Menthone was obtained by

oxidation and menthyl acetate by acetylation of menthol. Other reference substances were isolated from essential oils: cineole from eucalyptus oil by *o*-cresol extraction, anethole by cooling from an ethanolic solution of fennel oil, fenchone from fennel oil by preparative column chromatography on silica gel using gradient elution with hexane–diethyl ether and carvacrol by alkaline extraction from thyme oils which are rich in carvacrol. Their authenticity was confirmed by IR spectrometry and their purity was determined by GC.

The response factors of analytes measured with respect to methyl salicylate under the conditions mentioned above were menthol 0.529, menthyl acetate 0.644, menthone 0.503, fenchone 0.498, anethole 0.531, cineole 0.497, camphor 0.504, thymol 0.513 and carvacrol 0.502.

Plant material and infusions

All the medicinal plant raw material samples investigated corresponded to the U.S.S.R. Pharmacopoeia [2] requirements and were bought in pharmacies. Fennel fruits were milled using a coffee grinder before analysis and preparation as infusions.

The infusions were prepared by the U.S.S.R. Pharmacopoeia [11] method: the plant material and water, taken in ratios appointed above, were heated in a special eathenware beaker for 15 min on a water-bath, then cooled by air to room temperature for 45 min and filtered. The ratios of plant material to water were taken according to the literature [13]: for leaves of peppermint and garden sage 1:40, for fennel fruits and for creeping thyme herb 1:20.

RESULTS AND DISCUSSION

It was found that complete distillation of analytes from all the species of plant materials and infusions investigated took 45 min. The dependences of the amounts of menthol, menthone and menthyl acetate isolated from peppermint leaves on distillation time are shown in Fig. 2.

Limonene has a retention time near to that of cineole using Superox 20M as stationary phase and would interfere in the determination of cineole. However, using

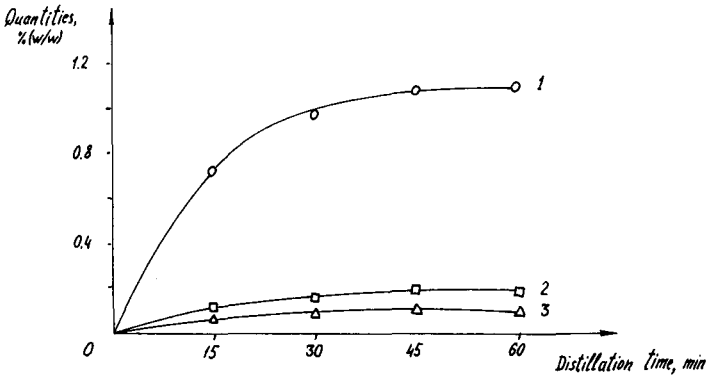

Fig. 2. Dependences of amounts of (1) menthol, (2) menthone and (3) methyl acetate isolated from peppermint leaves on duration of distillation.

a column with 3% OV-17 on Chromosorb W-HP (100–120 mesh) it was found that garden sage oils isolated from the investigated plant material samples contain only traces of limonene and cineole could be reliably determined.

The contents of major monoterpenoids in a set of peppermint leaves, fennel fruits, garden sage leaves and creeping thyme herb were determined by the developed methods. It can be seen from Table I that samples of one herb may have wideley differing contents and ratios of oil constituents. It is evident that medicinal preparations from these samples can vary in their medicinal efficacy.

The results of the determination of monoterpenoids in infusions (Table II) indicate that the contents of these compounds in infusions also differ significantly.

These methods allow the quantitative evaluation of the efficiency of the U.S.S.R. Pharmacopoeia method for infusion preparation. For this purpose we cal-

TABLE I

RESULTS OF MONOTERPENOID DETERMINATION IN PLANT MATERIAL

Plant material sample	Compound determined					
	Content (%, w/w)	R.S.D.[a] (%)	Content (%, w/w)	R.S.D.[a] (%)	Content (%, w/w)	R.S.D.[a] (%)
Peppermint leaf	*Menthol*		*Menthone*		*Menthyl acetate*	
20985	1.095	1.81	0.184	2.68	0.097	2.62
20986	0.277	2.64	0.149	3.53	0.137	2.82
1460987	0.843	1.65	0.098	1.30	0.175	2.18
81287	0.689	1.98	0.400	3.57	0.223	2.66
10188	1.351	1.71	0.188	1.45	0.192	2.59
Fennel fruits	*Anethole*		*Fenchone*			
80685	2.05	1.08	0.41	2.32		
10586	1.94	3.29	0.48	1.73		
80288	2.52	2.53	0.46	2.43		
90288	2.68	1.84	0.67	2.08		
100288	2.44	3.24	0.58	2.57		
240387	2.11	4.52	0.42	2.75		
Garden sage leaf	*1,8-Cineole*		*Camphor*			
50383	0.064	2.62	0.099	2.15		
31285	0.085	3.36	0.109	1.64		
70687	0.133	1.81	0.362	1.87		
181287	0.130	2.72	0.193	3.19		
161287	0.117	1.81	0.170	2.38		
20388	0.146	1.74	0.216	2.06		
Thyme herb	*Thymol*		*Carvacrol*			
10684	0.414	1.63	0.547	1.34		
20684	0.349	3.06	1.054	2.01		
50684	0.211	2.12	1.403	2.41		
130684	1.001	1.46	0.089	5.53		
150684	0.491	1.24	0.516	1.94		
470684	0.288	1.56	0.086	2.76		

[a] Relative standard deviation.

culated the extraction factor, which is the ratio between the amounts of a substance in the initial plant material and dissolved in water.

It was found that aqueous infusions of individual samples of herbs prepared under standard conditions show differing extraction efficiencies for the main constituents of the essential oils. Table II shows that the extraction factors for various substances are from only 1.0 to 45.2% at best. This illustrates the low efficiency of the infusion preparation method because the majority of the biologically active compounds is not used.

The extraction factors for a particular substance from different plant material samples are similar under the same conditions, indicating that the monoterpenoid content in infusions is approximately proportional to their content in the initial plant material and that infusions with higher concentrations of monoterpenoids can be preparated from herbs with high contents of these compounds.

Comparing the chromatograms of essential oils isolated from plant material and related infusions (Fig. 3), it can be noted that the ratio of the main components of

TABLE II

RESULTS OF MONOTERPENOID DETERMINATION IN INFUSIONS PREPARED BY U.S.S.R. PHARMACOPOEIA METHOD [2]

Plant material sample taken for infusion preparation	Compound determined								
	Content $\times 10^{-3}$ (%, w/w)	R.S.D.[a] (%)	E.F.[b] (%)	Content $\times 10^{-3}$ (%, w/w)	R.S.D.[a] (%)	E.F.[b] (%)	Content $\times 10^{-5}$ (%, w/w)	R.S.D.[a] (%)	E.F.[b] (%)
Infusions of peppermint (1:40)	*Menthol*			*Menthone*			*Menthyl acetate*		
20985	8.25	1.91	30.1	1.21	1.87	26.3	3.64	5.84	1.5
20986	2.62	2.34	37.7	1.02	1.44	27.3	4.11	6.78	1.2
1460787	7.82	1.02	37.1	0.69	3.52	28.4	4.37	7.12	1.0
Infusions of fennel (1:20)	*Anethole*			*Fenchone*					
80288	2.38	2.41	1.9	5.13	2.18	21.1			
90288	2.43	2.03	1.8	4.75	2.24	14.3			
100288	1.89	2.19	1.5	3.99	3.42	13.7			
Infusions of garden sage (1:40)	*Cineole*			*Camphor*					
50283	0.44	3.99	27.8	0.99	1.15	40.2			
70687	0.75	3.55	22.6	3.98	1.83	45.2			
161287	0.24	2.39	31.9	1.62	1.92	38.1			
181287	0.78	2.44	24.1	1.73	1.24	35.8			
20388	1.31	1.25	35.7	2.37	1.52	43.9			
Infusions of creeping thyme (1:20)	*Thymol*			*Carvacrol*					
10684	3.72	3.51	17.9	5.02	3.35	18.4			
20684	3.49	2.69	20.2	12.33	3.47	23.4			
150684	3.61	2.77	14.7	3.99	2.88	15.5			

[a] Relative standard deviation.
[b] Extraction factor.

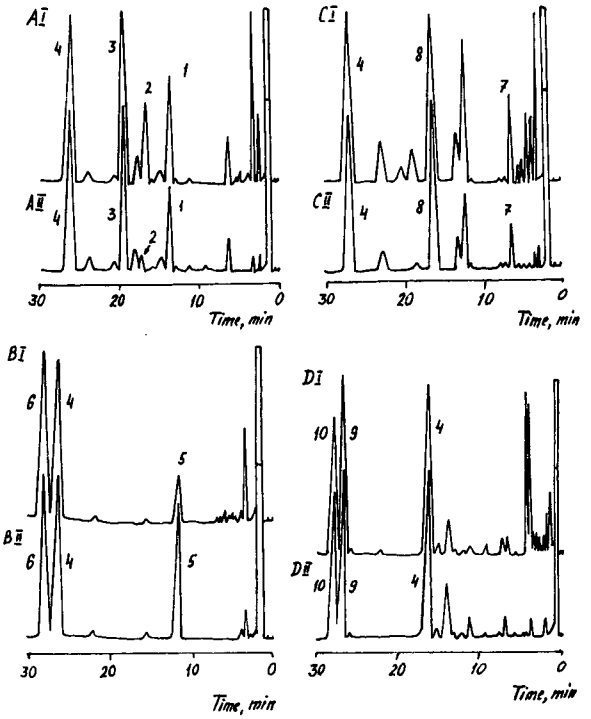

Fig. 3. Chromatograms of essential oils isolated from (A) peppermint, (B) fennel, (C) garden sage and (D) creeping thyme plant material samples (I) and infusions (II) prepared from them. Peaks: 1 = menthone; 2 = menthyl acetate; 3 = menthol; 4 = methyl salicylate (internal standard); 5 = fenchone; 6 = anethole; 7 = cineole; 8 = camphor; 9 = thymol; 10 = carvacrol.

essential oils is significantly changed when dissolved in water during the preparation of infusions. Fig. 3 and Tables I and II show that the preparation of infusions significantly lowers the proportion of menthyl acetate, menthone, etc., in peppermint oil, of anethole in fennel oil, of cineole and other constituents in garden sage oil and of monoterpene hydrocarbons and other constituents in creeping thyme oil.

The substances with an "open" oxygen-containing group such as the alcohols menthol, thymol and carvacrol and the ketones camphor, menthone and fenchone are more readily extracted by infusion than compounds where oxygen is "blocked" such as the ether anethole or the ester menthyl acetate. The epoxide cineole gives an anomalously high extraction factor.

To obtain comparable results we also studied the fennel and creeping thyme infusions made at a plant material-to-water ratio of 1:40. The extraction factors under these conditions were as follows: for fenchone 19.8–26.6%, for anethole 2.0–4.8%, for thymol 27.7–34.8% and for carvacrol 26.8–38.1%. The extraction factors of monoterpene hydrocarbons from all herbs were 0.7–2.1%.

Under these conditions the monoterpene alcohols, phenols, ketones and epoxides have extraction factors of more than 20%, on average ten times those of related hydrocarbons, ethers and esters.

REFERENCES

1 N. P. Maxjutina, N. F. Commissarenko, A. P. Procopenko, L. I. Pogodina and G. N. Lipkan, *Rastitelnjie Lekarstvennjie Sredstva* (*Plant Medicinal Remedies*), Zdorov'ya, Kiev, 1985.
2 *U.S.S.R. State Pharmacopoeia,* Vol. 2, Medicina, Moscow, 11th ed., 1989.
3 O. Hindaki and O. Yutaka, *J. Chromatogr.,* 286 (1983) 336.
4 G. G. Rosik, A. A. Vinchenko, I. P. Rosnichenko and I. P. Kovalev, *Khim.-Farm. Zh.,* 5 (1987) 632.
5 M. Goderfroot, P. Sandra and M. Verzele, *J. Chromatogr.,* 203 (1981) 325.
6 C. Bicchi, A. D'Amato, G. M. Nano and C. Frattini, *J. Chromatogr.,* 279 (1983) 409.
7 F. Chialva, G. Doglia, G. Garbi and F. Ulian, *J. Chromatogr.,* 279 (1983) 333.
8 R. A. Whitley and P. E. Coffey, *J. Geophys. Res.,* 82 (1977) 5928.
9 R. G. Buttery, R. A. Flath, T. R. Mon and L. C. Ling, *J. Agric. Food Chem.,* 34 (1986) 786.
10 Y. Z. Chen, Z.-L. Li, D.-Y. Xue and M.-L. Qi, *Anal. Chem.,* 59 (1987) 744.
11 *U.S.S.R. State Pharmacopoeia,* Vol. 1, Medicina, Moscow, 11th ed., 1987.
12 *British Pharmacopoeia 1988,* H. M. Stationery Office, London, 1988.
13 M. D. Mashkovskij, *Lekarstvennjie Sredstva* (*Medicinal Remedies*), Medicina, Moscow, 1986.

Journal of Chromatography, 542 (1991) 459–471
Elsevier Science Publishers B.V., Amsterdam

CHROM. 23 090

Separation of carbohydrate-mediated microheterogeneity of recombinant human erythropoietin by free solution capillary electrophoresis

Effects of pH, buffer type and organic additives

AN D. TRAN*, SUNGAE PARK and PETER J. LISI
BioAnalytical Research Department, R. W. Johnson Pharmaceutical Research Institute at Ortho Pharmaceutical Corporation, Route 202, Raritan, NJ 08869 (U.S.A.)
and
OANH T. HUYNH, RALPH R. RYALL and PHILIP A. LANE
Analytical R & D Department, R. W. Johnson Pharmaceutical Research Institute at Ortho Pharmaceutical Corporation, Route 202, Raritan, NJ 08869 (U.S.A.)

(First received August 13th, 1990; revised manuscript received December 27th, 1990)

ABSTRACT

Free solution capillary electrophoresis has been investigated as an alternative to isoelectric focusing for the separation of the glycoforms of recombinant human erythropoietin (r-HuEPO), a primary regulator of erythropoiesis. A systematic approach was used to study the effect of pH, buffer type and organic modifiers on the resolution of the microheterogeneity of erythropoietin. The main factors for improving the resolution were the regulation of the electroosmotic flow of the running buffer and the reduction of solute-wall interaction. The best resolution of the glycoforms of r-HuEPO was obtained with a mixed buffer pH 4.0 (100 m*M* acetate–phosphate, 10 h preequilibration time).

INTRODUCTION

Erythropoietin (EPO) is a glycoprotein hormone which is produced primarily in the kidney of adult mammals and which acts on bone marrow erythroid progenitor cells to promote development into mature red blood cells [1]. The molecular mass of EPO is in the range of 34 000–38 000 with approximately 40% of its weight attributed to its carbohydrate structure [2]. The molecule has a peptidic backbone of 165 amino acids (p*I* 4.5–5.0) and contains two types of carbohydrates: three N-linked complex polysaccharide antennaries at the asparagine positions 24, 38 and 83, and one O-linked polysaccharide chain at the serine position 126 [2].

Since EPO is present at picomolar levels in the serum and urine, it was not purified until 1977 [3] and it has only recently become available as recombinant human EPO (r-HuEPO). Like the naturally occurring hormone, r-HuEPO exhibits microheterogeneity[a] in the charged carbohydrate moieties bound to the protein. As the only

0021-9673/91/$03.50

major charge-bearing component of the r-HuEPO carbohydrate, sialic acid has been shown to be the origin of different charge classes of r-HuEPO (Fig. 1). These classes differ from each other in the degree of sialylation of the polysaccharide chains [4], where sialic acid is linked to the terminal end of the polysaccharide chain through the hydroxy group located at position 2 of the pyran ring.

The critical role of sialic acid in the *in vivo* activity of r-HuEPO has been well established [5]. Therefore, it is of interest to examine the relative proportion of the glycoforms[b] contained in the purified r-HuEPO.

Currently, the technique of isoelectric focusing (IEF) offers an unrivaled method for screening the pattern of glycoforms [6]. Because of the labor involved in IEF using conventional slab gels and the semi-quantitative nature of the assay, capillary electrophoresis (CE) has been investigated as an alternative method for determining the ratio of EPO glycoforms. This technique is based on the same principles as traditional slab gel electrophoresis, but offers on-line injection and detection. Although spectacular results have been reported in the use of the IEF mode in capillary electrophoresis [7,8], the technique does require the use of a coated capillary column (*i.e.* polyacrylamide or methylcellulose). Currently, because of the short lifetime of these columns under severe operating conditions such as wide pH range and high operating voltage, the IEF mode of electrophoresis in capillary columns is not yet suitable for routine analysis. Among different CE modes, free solution capillary electrophoresis (FSCE) is the simplest and the most widely used. We report here the use of FSCE as an alternative method to IEF for the separation of the glycoforms of r-HuEPO. The effects of separation variables such as pH, buffer type and organic modifiers (methanol, acetonitrile, ethylene glycol, polyethylene glycol) were evaluated as part of this study.

MATERIALS AND METHODS

Apparatus

Separations were carried out on a capillary electropherograph System P/ACE

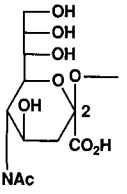

Fig. 1. Structure of sialic acid (N-acetyl neuraminic acid). Ac = Acetyl.

[a] Microheterogeneity, as used herein, is defined as variation in carbohydrate primary structure between molecules of a glycoprotein, such as variation in the number of terminal sialic acid residues with the same chain length or variation in the number of branches (*e.g.* di-, tri-, tetraantennary structures of N-linked chains).

[b] Glycoform, as used herein, is defined as a subset of glycoprotein molecules sharing an identical polypeptide backbone but differing in carbohydrate structure (*i.e.*, sequence or disposition).

2000 (Beckman Instruments, Palo Alto, CA, U.S.A.) equipped with a capillary cartridge, 75 μm I.D. × 375 μm O.D.; the total length of the capillary was 27 cm (20 cm effective length) for runs at low pH values (2.0, 3.0 and 4.0) and 57 cm (50 cm effective length) for runs at higher pH values (6.0, 7.0, 8.0 and 9.0). Prior to use the capillary was pretreated successively with 0.1 *M* HCl and 0.1 *M* NaOH for 10 min each, then rinsed with water and electrolyte. The column temperature was maintained at 25 ± 0.1°C by means of a fluorocarbon liquid continuously circulated through the cartridge. A deuterium light source with a 214-nm bandpass filter was used and absorbance was monitored at a range of 0.02 a.u.f.s. Injection was made by nitrogen pressure with sample concentrations ranging from 0.1–0.3 mg/ml. Data analysis and collection was accomplished using the Beckman System P/ACE 2000 software, version 1.0.

Materials

The phosphate buffers (100 m*M*, pH 2.0, 3.0 and 4.0) were prepared by titrating a solution of 0.1 *M* phosphoric acid (Baxter Health Care Corp., McGraw Park, IL, U.S.A.) with 0.1 *M* sodium hydroxide to the desired pH. The acetate buffer (100 m*M*, pH 4.0) was prepared by titrating a solution of 0.1 *M* of acetic acid (Mallinckrodt, Paris, KY, U.S.A.) with a solution of 0.1 *M* sodium acetate (Mallinckrodt) to a desired pH. The acetate–phosphate buffer (100 m*M*, pH 4.0) was prepared by titrating a solution of 0.1 *M* sodium acetate with a solution of 0.1 *M* phosphoric acid to the desired pH. The phosphate buffer (100 m*M*, pH 4.0) was prepared by titrating a solution of 0.1 *M* of phosphate monobasic with a solution of 0.1 *M* phosphoric acid. The 2-[N-morpholino]ethanesulfonic acid (MES) (50 m*M*, pH 6.0), bis[2-hydroxyethyl]imino–tris[hydroxymethyl]methane (Bis–Tris) (50 m*M*, pH 7.0), and tricine (50 m*M*, pH 8.0) were prepared by titrating a solution of 0.05 *M* of the corresponding product (Sigma, St. Louis, MO, U.S.A.) with a solution 1.0 *M* hydrochloric acid to the corresponding pH.

Viscosity measurements

The kinematic viscosities and densities of buffer solutions were measured using the Cannon-Ubbelohde viscometer and a Kimble pycnometer, respectively. The absolute viscosity of a solution is a product of the kinematic viscosity and density. All measurements were performed at 25 ± 0.05°C and are the mean of five independent measurements for each buffer solution.

RESULTS AND DISCUSSIONS

Effect of pH and organic modifiers in the separation of r-HuEPO glycoforms

In FSCE, ionic species are separated on the basis of the differential electrophoretic mobilities of the analytes. According to Jorgenson and Lukacs [9] the resolution (R_s) of two zones in FSCE can be given by eqn. 1:

$$R_s = 0.18\,\Delta u_{ep}[Vl/DL(u_{eo} + u_{ep})]^{1/2} \quad (1)$$

where u_{ep} is the electrophoretic mobility of an ionic solute, u_{eo} is the electroosmotic flow of the running buffer, V is the applied voltage, D is the diffusion coefficient of the

ionic solute in the running buffer system, l and L are the effective length of the capillary column between the inlet and the detector and the total length of the capillary respectively.

As indicated in eqn. 1, the resolution in FSCE could in principle be improved by increasing the difference in electrophoretic mobility of the two separated zones or by reducing the electroosmotic flow of the running buffer. To test this hypothesis, our initial attempts at separating the glycoforms of r-HuEPO were performed at pH 6.0, 7.0, 8.0 and 9.0 of the running buffer. At these pH values, r-HuEPO (pI 4.5–5.0) exists as a negative species and the interaction between solute and the capillary wall is minimized. Fig. 2 illustrates the overlayed electropherograms of r-HuEPO obtained at pH 6.0, 7.0, 8.0 and 9.0. At pH 9.0 where the osmotic flow is the fastest in the range of pH selected, r-HuEPO eluted as a sharp peak with no separation of glycoforms observed. Some sign of separation was observed at a lower pH of 8.0 or 7.0 and clearly improved at pH 6.0. At this pH, a combination of two effects, reduction in the electrophoretic flow and increase in differences in charge between glycoforms are presumably the origin for the separation observed.

To ascertain that these multiple peaks originate from the microheterogeneity of the product, r-HuEPO was incubated with neuraminidase, an enzyme known to selectively remove sialic acid from the polysaccharide backbone. The neuraminidase treated r-HuEPO converged into a single peak when subjected to capillary electrophoresis. These results strongly suggest that the multiple peaks observed at pH 6.0 originate from the microheterogeneity of r-HuEPO. To further improve the separation between glycoforms, the osmotic flow of the running buffer was reduced by increasing the viscosity of the solution. Several organic modifiers with different viscosities and dielectric constants were selected and are listed in Table I. The main consequences

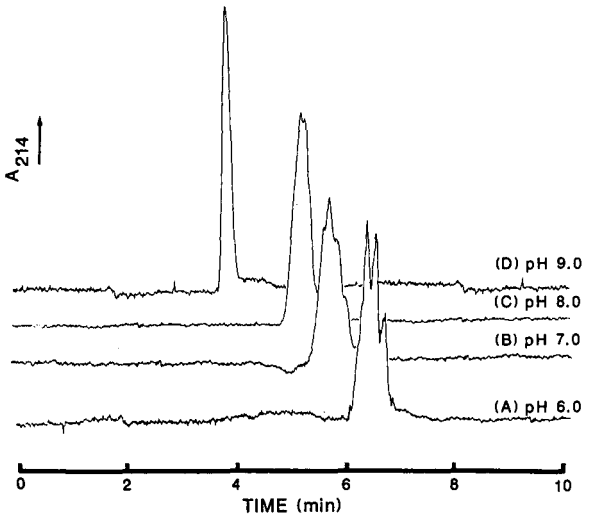

Fig. 2. High-performance capillary electrophoresis of r-HuEPO in free solution. The electropherograms were obtained using a fused-silica capillary tube 50 cm × 75 μm I.D. (A) pH 6.0 (50 mM MES, 25 kV, 44 μA); (B) pH 7.0 (50 mM Bis-Tris, 25 kV, 15 μA); (C) pH 8.0 (50 mM tricine, 25 kV, 70 μA); (D) pH 9.0 (50 mM tricine, 25 kV, 85 μA).

TABLE I

LIST OF DIFFERENT ORGANIC MODIFIERS USED IN THE MANIPULATION OF VISCOSITY OF THE RUNNING BUFFER

Alcohol	Diols	Others
Methanol [11]	Ethylene glycol	Acetonitrile [12,13]
Ethanol	Glycerol	Sucrose
1-Propanol [12]	1,2-Butanediol	
2-Butanol	1,3-Butanediol	
	1,4-Butanediol	
	trans-Cyclohexane-1,2-diol	
	cis,trans-Cyclohexane-1,2-diol	
	PEG-200	
	PEG-400	

resulting from the addition of an organic modifier to a running buffer consisted of multiple changes, *i.e.* of the viscosity and the ionic strength of the buffer. However, an effect such as the binding of the organic modifier to the capillary wall, through hydrogen bonding or dipole interaction, could induce a drastic change of the osmotic flow caused by the change of the net charge of the capillary surface or the local viscosity of the double layer [10]. To simplify the interpretation of the observed results, the ionic strength of the organic–buffer solution was kept constant during the addition of the organic modifier. Therefore the change of the osmotic flow induced by the presence of organic modifier in a capillary column is mainly due to the change of the viscosity of the resulting buffer, and the change of the net charge of the capillary wall resulting from the binding of the organic molecule to the capillary wall. The selection of organic modifiers (*i.e.* positional isomers 1,2-, 1,3- and 1,4-butanediol or isomers of *cis,trans*-cyclohexane-1,2-diol) was intended to detect the effect of binding of diol compounds onto the capillary wall since the viscosities of the neat solvent of the corresponding isomer compounds are identical. Different binding constants of corresponding isomers onto the wall could induce different changes of the osmotic flow of the running buffer.

Figs. 3 and 4 illustrate the effect of organic additives on the viscosity and the electroosmotic flow of the running buffer tricine buffer (50 m*M*, pH 8.0). In the series of organic additives selected (Table I), acetonitrile is the least efficient in modifying the viscosity of the running buffer. Acetonitrile could be added up to 30% (v/v) without inducing a significant change in the viscosity of the running buffer while a different pattern was observed for the osmotic flow (Fig. 4). With 5% (v/v) of acetonitrile added to the running buffer, a 10% change was observed for the osmotic flow which stayed constant within the range of 5–25% of acetonitrile added. The change of osmotic flow observed with 5% of acetonitrile could originate from the dipole interaction of acetonitrile with the capillary wall causing a change in the net charge and the local viscosity of the double layer. The binding of acetonitrile to the wall seems to be saturated at the 5% level of organic solvent added since the osmotic flow remained constant within the range of 5–25% of acetonitrile added. A significant reduction of the osmotic flow up to 40% was observed when the level of added acetonitrile reached 30% and the phenomena still remined unclear. These results are in agreement with the

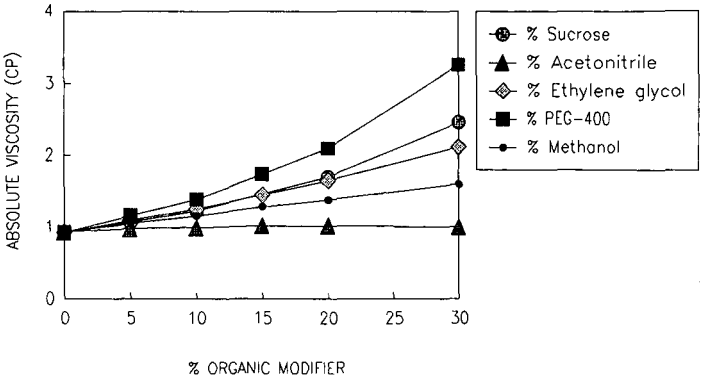

Fig. 3. Absolute viscosity as a function of the percentage of organic modifier. For conditions see Experimental.

recently reported results by VanOrman *et al.* [10]. On the other hand, methanol was shown to be clearly more efficient in increasing the viscosity and decreasing the electroosmotic flow of the buffer when compared to acetonitrile (Figs. 3 and 4). The dependency of the electroosmotic flow on the chain length of the alcohol follows the order: methanol < ethanol < propanol < butanol. Diol compounds are more efficient than alcohol in increasing the viscosity or decreasing the electroosmotic flow of the running buffer. As indicated by the viscosities of the neat solvent, the efficacy of all diol compounds selected increased from ethylene glycol < glycerol < 1,2-butanediol, 1,3- or 1,4-butanediol < *trans* or *cis,trans*-cyclohexane-1,2-diol < PEG-200 < PEG-400 and are clearly more efficient than methanol. The geometry or the location of the diol groups (*i.e.* 1,2-, 1,3- and 1,4-butanediol and *cis,trans*-cyclohexane-1,2-diol) does not play an important role in the binding to the capillary wall as indicated by their effect on the osmotic flow.

When acetonitrile was used as the organic modifier, the separation of the glycoforms of r-HuEPO was evident as illustrated in Fig. 5. At a level of 5%

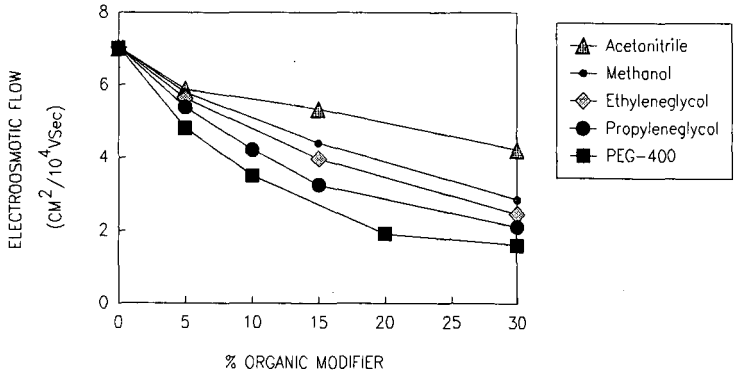

Fig. 4. Effect of organic modifier on the electroosmotic flow, u_{eo}, of the running buffer. Conditions: fused-silica capillary column 50 cm × 75 μm I.D.; voltage 25 kV.

acetonitrile in tricine buffer (50 m*M*, pH 8.0), the product eluted as a multiplet, however the resolution deteriorated when more organic modifier was added.

In contrast, when methanol or ethylene glycol was used as the organic modifier, the separation of glycoforms improved between 5% and 30% of organic modifiers (Figs. 6 and 7) and began to decrease at higher concentrations. When the percentage of methanol and ethylene glycol reached the 50% level, the resolution clearly deteriorated. These results were observed for all linear diols or polydiols selected (Table I). The same results were obtained at pH 6.0 (50 m*M*, MES).

Since the electrophoretic mobility is dependent on the osmotic flow of the running buffer (eqn. 2), a plot of the product of viscosity and the electrophoretic mobility *versus* the percent of organic solvent illustrates the effect of organic additives on the ionic state and shape of r-HuEPO during electrophoresis.

$$u_{ep} = v/E = q/6\pi r\eta \tag{2}$$

where u_{ep} is the electrophoretic mobility, v is the migration velocity, E is the electric field strength, q is the net charge on the molecule, η the solvent viscosity and r is the apparent Stokes radius of the molecule.

Fig. 8 shows the plot of $u_{ep} \cdot \eta$ *vs.* the percent of organic additives. The origin of a negative slope observed for acetonitrile may be due to the change in ionic state of r-HuEPO caused by the low dielectric constant of the solvent used or the change in conformation of the product. Measurement of the UV and UV second derivatives spectra of r-HuEPO in the presence of 30% of acetonitrile in 50 m*M* tricine buffer (pH 8.0) corroborate this hypothesis. A shift to the far UV was observed when the UV spectrum of r-HuEPO was recorded in 30% acetonitrile in tricine buffer (50 m*M*, pH 8.0).

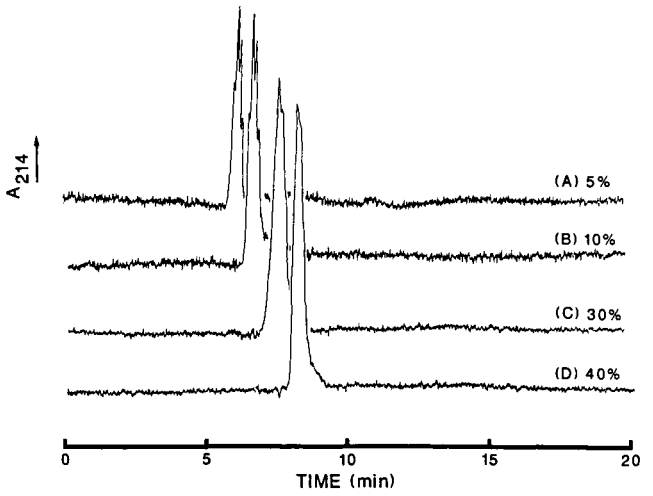

Fig. 5. High-performance capillary electrophoresis of r-HuEPO in free solution. The electropherograms were obtained using a fused-silica capillary tube 50 cm × 75 μm I.D. (A) 5% Acetonitrile in 50 m*M* tricine buffer pH 8.0 (25 kV; 18 μA); (B) 10% acetonitrile in 50 m*M* tricine buffer pH 8.0 (25 kV; 16 μA); (C) 30% acetonitrile in 50 m*M* tricine buffer pH 8.0 (25 kV; 14 μA), (D) 40% acetonitrile in 50 m*M* tricine buffer pH 8.0 (25 kV; 12 μA).

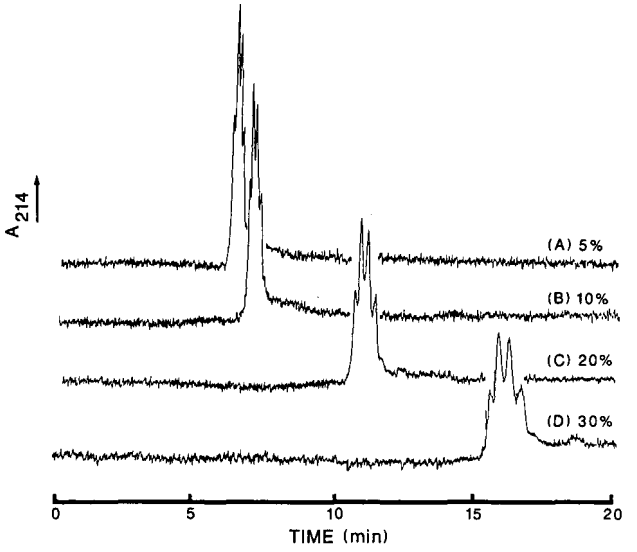

Fig. 6. High-performance capillary electrophoresis of r-HuEPO in free solution. The electropherograms were obtained using a fused-silica capillary tube 50 cm × 75 μm I.D. (A) 5% methanol in 50 m*M* tricine buffer pH 8.0 (25 kV; 20 μA); (B) 10% methanol in 50 m*M* tricine buffer pH 8.0 (25 kV; 18 μA); (C) 30% methanol in 50 m*M* tricine pH 8.0 (25 kV; 15 μA), (D) 30% methanol in 50 m*M* tricine buffer pH 8.0 (25 kV; 13 μA).

Similar to acetonitrile, the addition of methanol to the running buffer also induces a negative slope on the plot of the product of electrophoretic mobility and viscosity *versus* percent organic modifier (Fig. 8). However when compared to

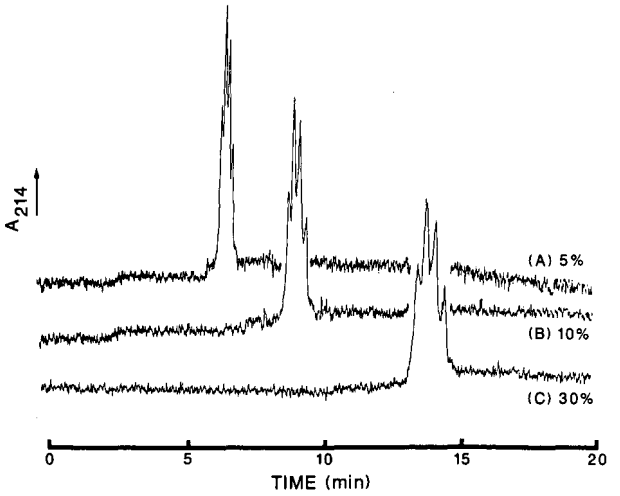

Fig. 7. High-performance capillary electrophoresis of r-HuEPO in free solution. The electropherograms were obtained using a fused-silica capillary tube 50 cm × 75 μm I.D. (A) 5% ethylene glycol in 50 m*M* tricine buffer pH 8.0 (25 kV; 27 μA); (B) 10% ethylene glycol in 50 m*M* tricine buffer pH 8.0 (25 kV; 21 μA); (C) 30% ethylene glycol in 50 m*M* tricine buffer pH 8.0 (25 kV; 10 μA).

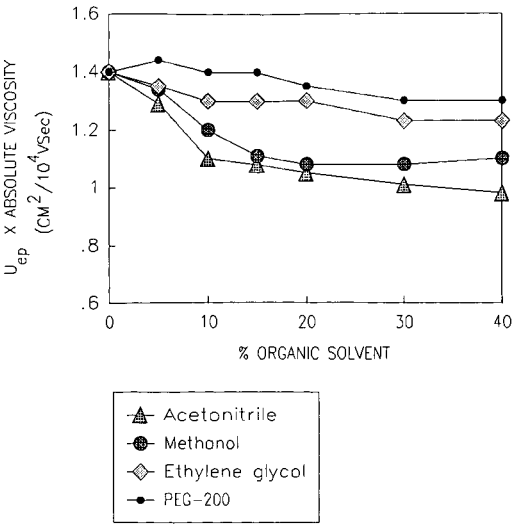

Fig. 8. Plot of the product of electroosmotic flow and viscosity of glycoforms of r-HuEPO as a function of the organic modifier. For conditions see Fig. 4.

acetonitrile, the slope is slightly less pronounced when compared to acetonitrile. A shift to the far UV was observed when the UV and its second derivative spectra of r-HuEPO were recorded in 30% methanol in tricine buffer (50 m*M*, pH 8.0). With polydiols, and especially polyethyleneglycol, the slope observed is clearly much less affected by increasing the concentration of organic modifier (Fig. 9). Unlike methanol and acetonitrile, the addition of PEG-200 to the running buffer does not cause a drastic change in the dielectric constant of the media, and provides less perturbation of the ionic state of the protein.

Effect of acetate, phosphate and sulphate ions in the separation of r-HuEPO at low pH

At low pH, the resolution in FSCE should in principle be improved since the electroosmotic flow of the bulk solution is drastically reduced [14,15]. Our initial attempts at separating the glycoforms of r-HuEPO were performed at pH 2.0, 3.0 and 4.0 of the running buffer. At these pH values r-HuEPO (p*I* 4.5–5.0) exists as a positive species. Fig. 9 shows an overlay of three electropherograms of r-HuEPO performed at pH 2.0 (100 m*M* phosphate buffer), pH 3.0 (100 m*M* phosphate buffer) and pH 4.0 (100 m*M* acetate buffer). At pH 2.0, where the osmotic flow is the slowest in the range of pH selected, r-HuEPO eluted as a sharp peak with some separation observed. The poor peak shape observed at pH 3.0 is not due to sample overload on the column but rather originates from the microheterogeneity of the product. A solute–capillary interaction is also possible since the operating pH is below the p*I* of the r-HuEPO.

At pH 4.0, the product eluted as a broad single peak. Unlike the migration of r-HuEPO occurred at the pH of 2.0 and 3.0, the product eluted behind the neutral marker. Since the operating pH is closer to the p*I* of the product, the overall positive charge of the molecule is reduced and the friction between solute and the buffer is dominant.

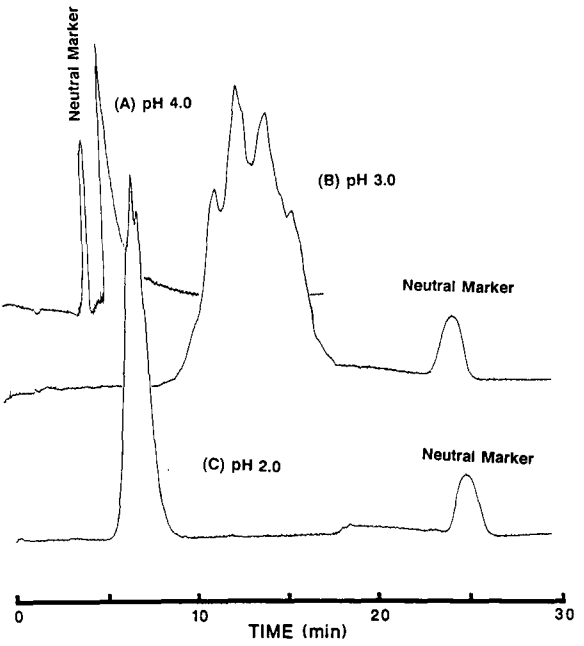

Fig. 9. High-performance capillary electrophoresis of r-HuEPO in free solution. The electropherograms were obtained using a fused-silica capillary tube 20 cm × 75 μm I.D. (A) pH 2.0 (100 m*M* phosphate buffer, 10 kV, 65 μA); (B) pH 3.0 (100 m*M* H_3PO_4, 10 kV, 80 μA); (C) pH 4.0 (100 m*M* acetate buffer, 10 kV, 3 μA). Phenol was used as neutral marker.

The critical role of the phosphate ion in improving the separation was demonstrated when a mixed buffer (100 m*M* acetate–phosphate, pH 4.0) was used. The sample was resolved into four different major and one minor glycoforms (Fig. 10B). The presence of phosphate resulted in a better separation. A decrease in the migration time of the product in the mixed buffer, as compared to the migration time obtained with the acetate buffer (100 m*M*, pH 4.0) was due to a change in electroosmotic flow. These results may indicate, as suggested by McCormick [15], that phosphate binds strongly to the silica surface of the capillary wall. Such binding could convert the residual acidic silanols to a more easily protonated silica–phosphate complex at pH 4.0, thereby reducing surface charge on the capillary wall. To obtain good and reproducible results (*e.g.* electrophoretic mobility, area counts and electroosmotic flow relative standard deviation $<2\%$) the column must be equilibrated in the mixed buffer for 4 h before use. Reproducible results can be achieved for at least 30 injections as long as no washing step with NaOH and waiting period are included into the running sequence. If the column starts to lose its performance, the phosphate layer can be regenerated by washing the column with NaOH (0.1 *M*). The capillary column must be equilibrated in the mixed buffer (100 m*M* acetate–phosphate buffer, pH 4.0) for 4 h before use.

The migration time of the product and the electroosmotic flow of the running buffer was further decreased with the mixed buffer (100 m*M* acetate–sulphate, pH 4.0) (Fig. 10C); however resolution of the glycoforms is not as good as observed with the acetate–phosphate buffer.

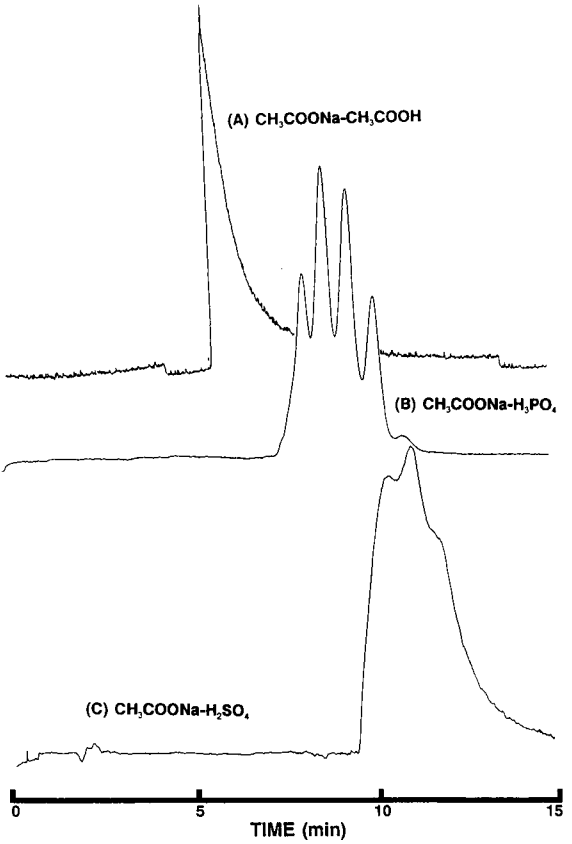

Fig. 10. High-performance capillary electrophoresis of r-HuEPO in free solution. The electropherograms were obtained using a fused-silica capillary tube 20 cm × 75 μm I.D. (A) pH 4.0 (100 m*M* acetate buffer, 10 kV, 30 μA); (B) pH 4.0 (100 m*M* acetate–phosphate buffer, 10 kV, 120 μA); (C) pH 4.0 (100 m*M* acetate–sulfate buffer, 10 kV, 200 μA).

Better separation was obtained when equilibration time of the column is extended to 10 h (Fig. 11) prior to use.

The long period required for equilibration time of the column before use is due to the presence of the acetate ions in the buffer. The same resolution can be achieved with much shorter preequilibration time (30 min) when phosphate buffer pH 4.0 is used. Since this buffer did not have a good buffering capacity, the inlet and outlet reservoir of the running buffer needs to be replaced after every three runs to avoid the pH drop. Such change will cause a lack of reproducibility from run to run. Because of the short equilibration time required, the pH 4.0 phosphate buffer is useful for proteins which need to be washed with NaOH after each run.

CONCLUSIONS

This work provides very encouraging results for the separation of the glycoforms of r-HuEPO using FSCE with a fused silica at low pH. The best condition found was

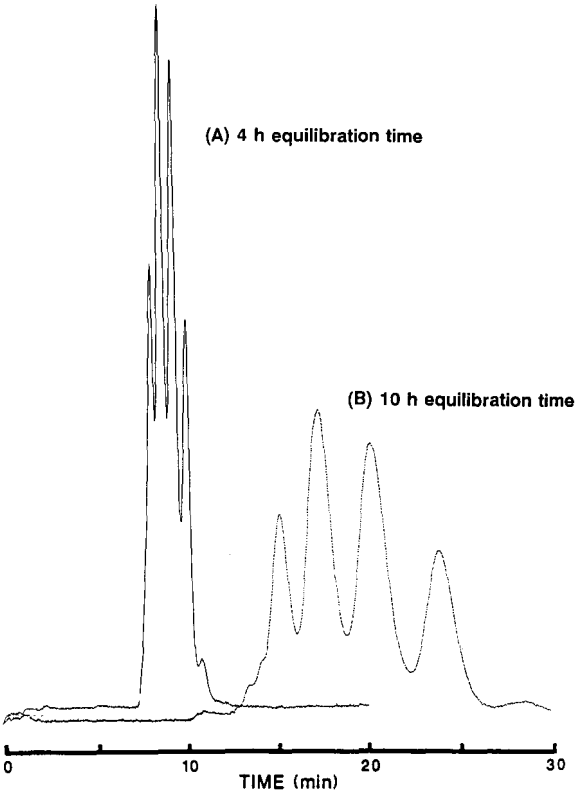

Fig. 11. High-performance capillary electrophoresis of r-HuEPO in free solution. The electropherograms were obtained using a fused-silica capillary tube 20 cm × 75 μm I.D. (A) pH 4.0 (100 m*M* acetate–phosphate buffer, 10 kV, 120 μA); the column was filled with the running buffer and equilibrated for 4 h prior to use. (B) same conditions as (A) with the column equilibrated in the running buffer for 10 h prior to use.

with buffer pH 4.0 (100 m*M* acetate–phosphate, 10 h preequilibration time). The resolution of glycoforms obtained by this technique is close to those obtained by conventional isoelectric focusing slab gel.

REFERENCES

1 J. Spivak, *Int. J. Cell Cloning*, 4 (1986) 139.
2 P.-H. Lai, R. Everett, F.-F. Wang, T. Arakawa and E. Goldwasser, *J. Biol. Chem.*, 261 (1986) 3116.
3 K. Jacobs, C. Shoemaker, R. Rudersdorf, S. D. Neill, R. J. Karfman, A. Mufson, J. Seehra, S. S. Jones, R. Hewick, E. F. Fritsch, M. Kawakita, T. Shimizu and T. Miyake, *Nature (London)*, 313 (1985) 806.
4 H. Sasaki, B. Bothner, A. Dell and M. Fukuda, *J. Biol. Chem.*, 262 (1987) 12 059.
5 P. Hirth, L. Wieczorek and P. Scigalla, *Contr. Nephrol.*, 66 (1988) 50.
6 P. G. Righetti, *Isoelectric Focusing: Theory, Methodology and Applications*, Elsevier, Amsterdam, 1983.
7 F. Kilar and S. Hjertén, *Electrophoresis*, 10 (1989) 23.
8 S. Hjertén and M.-D. Zhu, *J. Chromatogr.*, 492 (1989) 585.
9 J. Jorgenson and K. D. Lukacs, *Science (Washington, D.C.)*, 222 (1983) 266.

10 B. B. VanOrman, T. M. Olefirowicz, G. G. Liversidge, A. G. Ewing and G. L. McIntire, *J. Microcol. Sep.*, 2 (1990) 289.
11 A. S. Cohen, N. Grunberg and B. L. Karger, *J. Chromatogr.*, 448 (1988) 41–53.
12 M. J. Sepaniak, D. F. Swaile and C. Powell, *J. Chromatogr.*, 480 (1989) 185–196.
13 M. Zhu, D. L. Hansen, S. Burd and F. Gannon, *J. Chromatogr.*, 480 (1989) 311–319.
14 P. D. Grossman, J. C. Colburn and H. H. Lauer, *Anal. Biochem.*, 179 (1989) 28.
15 R. M. McCormick, *Anal. Chem.*, 60 (1988) 2322.

Journal of Chromatography, 542 (1991) 473–481
Elsevier Science Publishers B.V., Amsterdam

CHROM. 23 048

Separation of phthalates by micellar electrokinetic chromatography

C. P. ONG, H. K. LEE and S. F. Y. LI*
Department of Chemistry, National University of Singapore, Kent Ridge Crescent, 0511 (Republic of Singapore)
(First received October 11th, 1990; revised manuscript received December 11th, 1990)

ABSTRACT

Micellar electrokinetic chromatography (MEKC) of priority phthalate esters was investigated. A commercial photodiode-array ultraviolet–visible detector was modified for on-column detection in an MEKC system. For the separation of phthalate esters, electrophoretic media with sodium dodecyl sulphate in phosphate–borate buffer were used. The retention behaviour of the phthalate esters at different concentrations of micellar solution and at different pH values of the electrophoretic media was investigated. In addition, the effect of different voltages across the capillary tubing was examined. The results successfully demonstrated the application of MEKC for the separation of a group of six phthalate esters, five of which are priority pollutants.

INTRODUCTION

Interest in the use of high-performance capillary electrophoresis (CE) in separation science has been tremendous in recent years. The rapid developments in this area could be largely attributed to the many advantages of this technique, including its exceptionally high efficiency, rapid rate of separation and relatively simple instrumentation.

An example of the CE techniques is micellar electrokinetic chromatography (MEKC), first developed by Terabe *et al.* [1]. The instrumental set-up is the same as that in conventional capillary electrophoresis, but a micellar solution is usually employed as the electrophoretic medium. The main advantage of MEKC is that both neutral analytes and charged solutes can be separated. There have been numerous reports in which MEKC has been successfully used for separating chemical and biological compounds [2,3]. However, to the best of our knowledge MEKC has not been employed to separate phthalates.

Phthalates are used extensively as plasticizers in the formulation of polymers [4]. As these plasticizers are not chemically bonded to the polymer, they can migrate from the plastics into the environment under suitable conditions [5]. The widespread use of these compounds and their presence in the environment have promoted great interest in the development of chromatographic methods for their detection [6,7].

This paper describes the use of MEKC for the separation of six phthalate esters,

0021-9673/91/$03.50

five of which are listed by the United States Environmental Protection Agency (USEPA) as priority pollutants. In a previous study [8], five of the phthalates investigated were successfully separated using isocratic high-performance liquid chromatography (HPLC). However, the sixth phthalate, bis(2-ethylhexyl) phthalate, was found to be satisfactorily separated only with gradient elution [9].

In this application of MEKC, an on-column photodiode-array detector was used for detection. Sodium dodecyl sulphate (SDS) in borate–phosphate buffer was used as the electrophoretic medium. The effects of various experimental parameters, including the pH of the buffer, the SDS concentration in the electrophoretic medium and the voltage used, on the retentions of the phthalates were investigated.

EXPERIMENTAL

The experiments were performed on a laboratory-built MEKC instrument. The on-column detection of the peaks was effected on a Shimadzu (Kyoto, Japan) Model SPDM6A detector. The detector cell was modified according to the procedures described elsewhere [10]. Briefly, the laboratory-built cell was erected on two metal blocks between which the separation column was mounted. The window for the UV light path was made by removing a small portion of the polyimide layer on the capillary tubing. A fused-capillary tube, 50 cm × 50 μm I.D. (Polymicro Technologies, Phoenix, AZ, U.S.A.), was used as the separation column. The power supply was a Spellman Model RHR 30PN10/RVC capable of delivering up to 30 kV.

All chemicals were of analytical-reagent grade unless specified otherwise. The buffer solution was prepared by dissolving sodium dihydrogenphosphate dihydrate and sodium tetraborate in water purified with a Millipore system. The electrophoretic medium consisting of SDS micelles in phosphate–borate buffer was prepared as described previously [1]. The structures of the six phthalates studied are shown in Fig. 1. The standard solution of the phthalates and Sudan III was prepared in HPLC-grade methanol (J. T. Baker, Phillipsburg, NJ, U.S.A.) at a concentration of 500 ppm for each of the species. All of these chemicals were supplied by Fluka (Buchs, Switzerland).

Introduction of sample was made manually by gravity feed, by placing the tip of the capillary at the high-potential end into a sample vial at a level 5 cm higher than the buffer reservoir. The time for each injection was 5 s. The amount of sample injected by this method was typically about 1.5 nl. The capillary end was subsequently rinsed by dipping it in a rinsing solution similar to that of the reservoir. It was then returned to the buffer reservoir before the power was switched on.

RESULTS AND DISCUSSION

All six phthalates were successfully analysed in a single run by MEKC. The separation was achieved by optimizing the pH of the buffer, SDS concentration and voltage across the separating column.

Preliminary experiments were first conducted at pH 6.0 and 7.5 without SDS in the electrophoretic medium. These conditions are similar to those used in conventional capillary zone electrophoresis (CZE). In both instances, a single broad peak was observed for all the phthalates, indicating that all the solutes possess similar charges

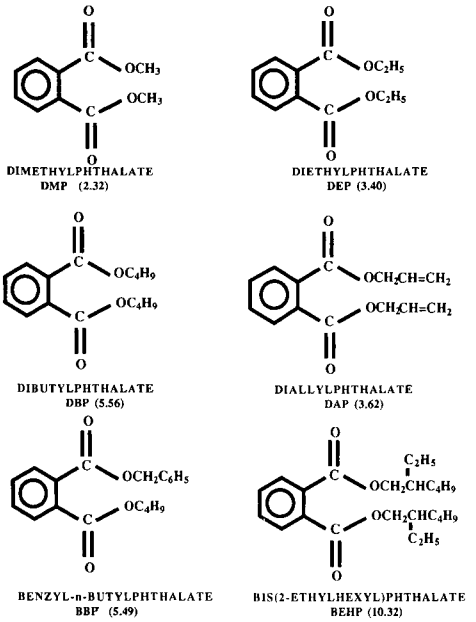

Fig. 1. Structures of the phthalates studied and their log P values.

under these pH conditions. The electrophoretic medium in the absence of the micelles does not seem to provide sufficient selectivity to separate the six phthalates. On the other hand, with SDS, the components in the mixture sample can be separated on the basis of the relative affinity for the micellar environment or the bulk aqueous phase. The more hydrophobic phthalates would tend to be strongly associated with the micelles and thus be eluted later than the hydrophilic species. This is one of the unique features of the MEKC system which enables the phthalates in the mixture to be separated.

Effect of pH

The experimental conditions used for the investigation of the effect of pH on the migration of the phthalates are listed in Table I. The results obtained are shown

TABLE I

EXPERIMENTAL CONDITIONS EMPLOYED TO INVESTIGATE THE EFFECT OF pH ON THE SEPARATION OF PHTHALATES AND EXPERIMENTAL t_0/t_{mc} RATIOS

Parameter	Experiment No.			
	1	2	3	4
pH	6.0	6.6	7.0	7.5
Applied voltage (kV)	15	15	15	15
Length (cm)	50	50	50	50
Tubing I.D. (μm)	50	50	50	50
Electrophoretic solution	10 mM SDS in 0.1 M borate–0.05 M phosphate buffer			
t_0/t_{mc}	0.21	0.21	0.20	0.22

graphically in Fig. 2. The capacity factor, k', used in this investigation was calculated using the equation [11]

$$k' = \frac{t_r - t_0}{t_0[1 - (t_r/t_{mc})]} \quad (1)$$

where t_r, t_0 and t_{mc} are the migration times for the solute, the insolubilized solute (methanol) and the micelles (measured using Sudan III as the marker), respectively.

Fig. 2 indicates that there was no change in the migration order for the six phthalates throughout the whole range of pH examined. The migration times for the phthalates increased in the order DMP < DEP < DAP < BBP < DBP < BEHP, and their hydrophobicities (log P) (see Fig. 1) in the order log P_{DMP} < log P_{DEP} < log P_{DAP} < log P_{BBP} < log P_{DBP} < log P_{BEHP}. By correlating these two series, it can be deduced that the phthalates might be in the neutral form in the pH range investigated. Consequently, their migration order would be dominated by their log P values, *i.e.*, the more hydrophobic phthalates are eluted later.

An interesting trend observed was that at higher pH (7.5), there was a marked increase in the migration times for some of the phthalates (DBP and BEHP in particular). This observation seems to contradict the fact that if the phthalates are in the neutral form they should not be affected by any changes in pH. A possible reason for this discrepancy could be that preferential dissociation of some of the phthalates

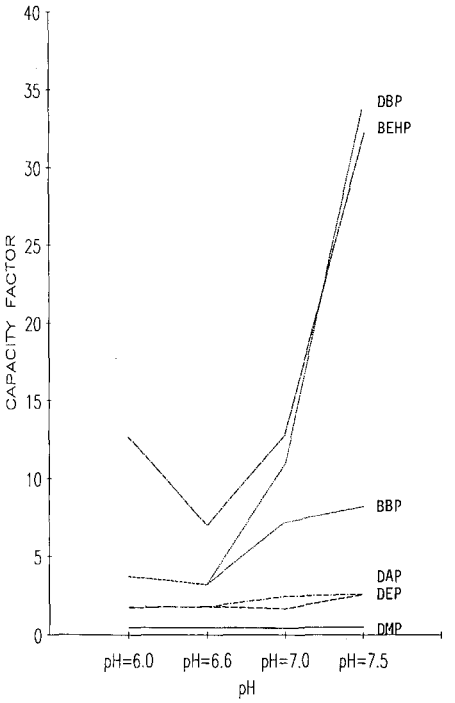

Fig. 2. Plot of capacity factors *versus* pH. Other conditions are given in Table I.

might occur at pH 7.5. These negatively charged phthalates would then be affected by the electrophoretic attraction towards the anode. Therefore, it is expected that there will be competition between the micelles and the anode for these partially negatively charged species. The electrophoretic attraction is a much stronger electrostatic type of interaction than the Van der Waal's type of interaction for micellar solubilization. Therefore, in spite of the fact that the SDS concentration remained constant in all these experiments, an increase in the migration times was observed for these species at pH 7.5.

Effect of SDS

Experiments at three different SDS concentrations were performed. The experimental conditions for these three experiments are listed in Table II. The results obtained are given in Fig. 3, where the capacity factors are plotted against SDS concentration.

There was an increase in the migration times of the phthalates when the SDS concentration in the electrophoretic solution increased. This increase can be accounted for by the fact that at higher SDS concentrations the phase ratio of the micelle to the aqueous phase would be larger. Hence the probability of solubilization of the phthalates by the micelles would be higher, resulting in an increase in the migration times for these compounds, as observed. This trend is also consistent with those observed previously by Terabe and co-workers [12,13].

Effect of voltage

The application of a higher voltage increases the resolution in CE [14]. As our attempts to optimize the separation of the phthalates based on SDS concentration and pH failed, the effect of higher voltages on the separation was examined. The experimental conditions for this investigation are listed in Table III.

The results obtained are shown in Fig. 4. The migration order was observed to be the same for all four sets of experiments and the order is governed by the log P values. Sharper peaks were observed at higher voltages. The increase in efficiency due to the higher voltages seems to improve the overall peak shape and resolution. It is worth

TABLE II

EXPERIMENTAL CONDITIONS EMPLOYED TO INVESTIGATE THE EFFECT OF VARYING SDS CONCENTRATION ON THE SEPARATION OF PHTHALATES AND EXPERIMENTAL t_0/t_{mc} RATIOS

Parameter	Experiment No.		
	3	5	6
SDS concentration (mM)	10	20	30
Applied voltage (kV)	15	15	15
Length (cm)	50	50	50
Tubing I.D. (μm)	50	50	50
pH	7.0	7.0	7.0
Electrophoretic solution	0.1 M borate–0.05 M phosphate buffer		
t_0/t_{mc}	0.20	0.19	0.17

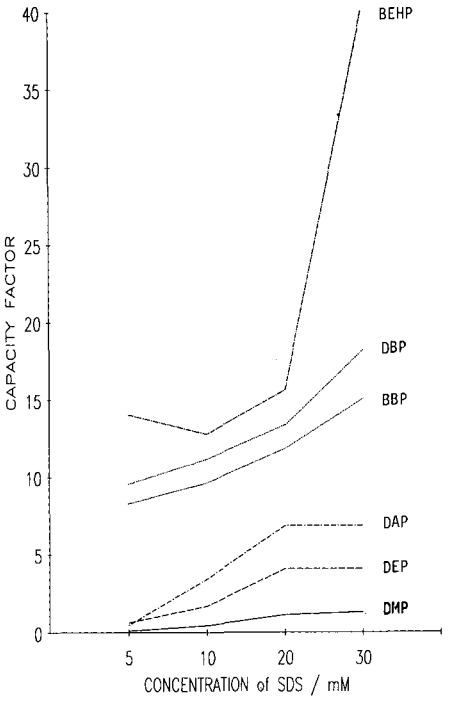

Fig. 3. Plot of capacity factors *versus* SDS concentration. Other conditions are given in Table II.

noting that the values of the ratio t_0/t_{mc}, obtained for experiments conducted at higher voltages (see Table III) are generally smaller than those shown in Tables I and II. The ratio t_0/t_{mc} indicates the elution range for the solute under a given set of experimental conditions. A smaller t_0/t_{mc} ratio offers a wider elution range, which to a certain extent enhances the separation of peaks [12]. Therefore, it is expected that the experiments performed at higher voltages would give better separations. In fact, the two experiments conducted at 25 and 30 kV have the smallest t_0/t_{mc} values and complete separation of all six phthalates was achieved.

The corresponding chromatograms are shown in Figs. 5 and 6. From Fig. 5, it can be seen that all six phthalates are satisfactorily separated within 40 min. However, at 30 kV, even though all six phthalates were satisfactorily separated, an additional peak (peak 7 in Fig. 6) was observed. This could be due to the stronger electric field at the higher voltage, which tends to produce excessive Joule heat [14]. The excessive heat generated at such a high potential could have promoted the hydrolysis of the phthalate ester to give an alcohol and an acid (probably phthalic acid).

Amongst the six phthalates, it seems that bis(2-ethylhexyl) phthalate is the one most prone to hydrolysis at the higher voltage. This is probably due to its bulky substituent groups which make it very unstable. After further investigation, it was found that the extra peak was indeed due to phthalic acid, the hydrolysed product of bis(2-ethylhexyl) phthalate. Hence, even though the higher voltage of 30 kV resulted in a higher efficiency, because of the possibility of side-reactions (hydrolysis) occurring

TABLE III

EXPERIMENTAL CONDITIONS EMPLOYED TO INVESTIGATE THE EFFECT OF VOLTAGE ON THE SEPARATION OF PHTHALATES AND EXPERIMENTAL t_0/t_{mc} RATIOS

Parameter	Experiment No.			
	1	7	8	9
Applied voltage (kV)	15	20	25	30
Length (cm)	50	50	50	50
Tubing I.D. (μm)	50	50	50	50
pH	6.0	6.0	6.0	6.0
Electrophoretic solution	10 m*M* SDS in 0.1 *M* borate–0.05 *M* phosphate buffer			
t_0/t_{mc}	0.21	0.18	0.14	0.12

during the separation, the optimum voltage for the separation of the phthalates was found to be 25 kV in these experiments.

It should be noted that generally with increasing applied voltage, a corresponding decrease in migration time would be expected for most solutes. This observation can be accounted for by the fact that at a higher voltage, the electroosmotic velocity (V_{os}) would be increased. At the same time, a corresponding increase in the electrophoretic velocity (V_{ep}) would also be observed. However, it was found that in most instances, under normal circumstances the increase in V_{os} is often

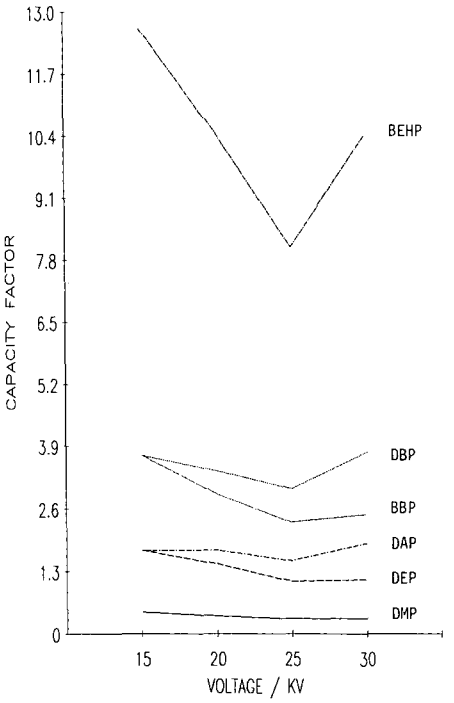

Fig. 4. Plot of capacity factors *versus* voltage. Other conditions are given in Table III.

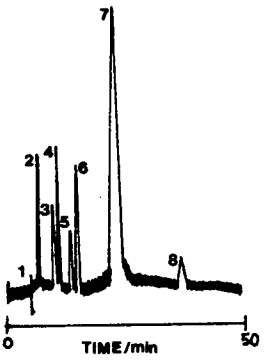

Fig. 5. Electrokinetic chromatogram of the six phthalate esters: 1 = methanol; 2 = DMP; 3 = DEP; 4 = DAP; 5 = BBP; 6 = DBP; 7 = phthalic acid; 8 = BEHP; 9 = Sudan III. Conditions as in Fig. 5, except voltage = 30 kV.

more pronounced than V_{ep}. Consequently, an overall decrease in migration time is expected. The results of our study, with the exception of those obtained using 30 kV, seem to be in agreement with the above trend. At 30 kV, a reversal in this trend was observed for most of the phthalates. A possible reason could be the heat generated at the relatively higher applied voltage. It is known that in such a system, V_{ep} would be affected such that the electrophoretic mobility would be increased. In fact, it was found that V_{ep} increases at a rate of *ca.* 2%/°C [15]. Therefore, in this instance, the increase in V_{os} in the system can no longer compensate for the larger increase in V_{ep}. Consequently, there is an overall increase in the migration times for the phthalates at 30 kV. From Fig. 4 it was noted that the increase is less apparent for those phthalates with shorter migration times. This is expected, as the fact that these phthalates are eluted earlier suggests that they are not much influenced by the electrophoretic interaction. Hence it would be reasonable to expect that any changes in V_{ep} would not be significant enough to cause any drastic change in their migration times.

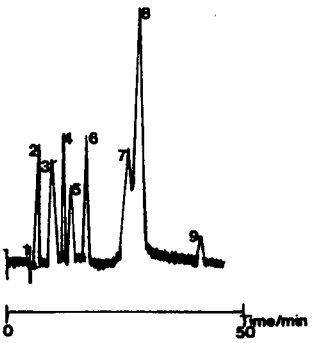

Fig. 6. Electrokinetic chromatogram of the six phthalate esters: 1 = methanol; 2 = DMP; 3 = DEP; 4 = DAP; 5 = BBP; 6 = DBP; 7 = BEHP; 8 = Sudan III. Electrophoretic solution, 10 m*M* SDS in 0.1 *M* borate–0.05 *M* phosphate buffer; pH, 6.0; separation tube, 50 cm × 50 μm I.D. fused-silica capillary; voltage, 25 kV; detection wavelength, 210 nm; volume of sample injected, 1.5 nl.

This work has successfully demonstrated the use of MEKC for the separation of priority phthalates. By optimizing parameters such as the pH and SDS concentration of the electrophoretic media and the voltage across the capillary tubing, high-resolution separations can be easily achieved. From the promising results obtained, it is believed that this technique can be extended to the analysis of other groups of priority pollutants.

ACKNOWLEDGEMENT

We thank the National University of Singapore for financial support.

REFERENCES

1 S. Terabe, K. Otsuka and T. Ando, *Anal. Chem.*, 56 (1984) 111.
2 J. M. Jorgenson and K. D. Lukacs, *Science (Washington, D.C.)*, 222 (1983) 266.
3 J. W. Jorgenson and K. D. Lukacs, *Anal. Chem.*, 57 (1985) 834.
4 F. L. Mayer, Jr., D. L. Stanlly and J. L. Johnson, *Nature (London)*, 238 (1972) 411.
5 J. L. Marx, *Science*, 178 (1972) 46.
6 A. Arbin and J. Osetelius, *J. Chromatogr.*, 193 (1980) 405.
7 M. Ishida, K. Suyama and S. Adachi, *J. Chromatogr.*, 294 (1984) 339.
8 M. R. Khan, C. P. Ong, S. F. Y. Li and H. K. Lee, *J. Chromatogr.*, 513 (1990) 360.
9 M. R. Khan, C. P. Ong, Y. J. Yao, S. F. Y. Li and H. K. Lee, *Environ. Monit. Assess.*, in press.
10 S. Kobayashi, T. Ueda and M. Kikumoto, *J. Chromatogr.*, 480 (1989) 179.
11 K. Otsuka, S. Terabe and T. Ando, *J. Chromatogr.*, 348 (1985) 39.
12 S. Terabe, K. Otsuka and T. Ando, *Anal. Chem.*, 57 (1985) 834.
13 H. Nishi, N. Tsumagari and S. Terabe, *Anal. Chem.*, 61 (1989) 2434.
14 S. Terabe, *Trends Anal. Chem.*, 8 (1989) 129.
15 R. J. Wieme, in E. Heftmann (Editor), *Chromatography: a Laboratory Handbook of Chromatographic and Electrophoretic Methods*, Van Nostrand Reinhold, New York, 1975, ch. 10.

Journal of Chromatography, 542 (1991) 483–501
Elsevier Science Publishers B.V., Amsterdam

CHROM. 23 052

Analysis of paralytic shellfish poisons by capillary electrophoresis[a]

P. THIBAULT*, S. PLEASANCE[b] and M. V. LAYCOCK
Institute for Marine Biosciences, National Research Council of Canada, 1411 Oxford Street, Halifax, Nova Scotia B3H 3Z1 (Canada)
(First received October 3rd, 1990; revised manuscript received December 3rd, 1990)

ABSTRACT

A capillary electrophoresis (CE) method with UV detection is described for the separation and determination of underivatized toxins associated with paralytic shellfish poisoning (PSP). Confirmation of the electrophoretic peaks was facilitated by mass spectrometric (MS) detection using an ionspray CE–MS interface and by high-performance liquid chromatography with fluorescence detection. The determination of PSP toxins, such as saxitoxin and neosaxitoxin, in toxic dinoflagellates and scallops is demonstrated and comparisons are made with existing techniques.

INTRODUCTION

Paralytic shellfish poisoning (PSP) is a severe form of seafood poisoning which results from the ingestion of contaminated shellfish [1–4]. It presents a real threat to public health as no antidote has yet been found and it is not possible to detoxify the contaminated shellfish efficiently. Symptoms of PSP are primarily neurological and can vary from facial paresthesis, nausea and vomiting to death resulting from respiratory paralysis, which can occur within 12 h after ingestion of toxic shellfish.

Toxic phytoplankton blooms, which occur sporadically along many coasts around the world, are the primary source for the toxification of filter-feeding shellfish [3]. Toxicity and toxin profiles vary widely among PSP-producing dinoflagellates and as much as 20 fmol per cell of the potent saxitoxin (STX) has been reported for a Bay of Fundy strain of *Alexandrium tamarensis* [5]. Toxins associated with PSP include STX, neosaxitoxin (NEO) and a complex suite of sulfate and N-sulfonate analogues [1]. Their structures are characterized by a five-membered ring fused on a perhydropurine skeleton (Fig. 1).

The development of reliable analytical techniques for the detection of these toxins has become important not only in view of the small amounts of toxins reported to cause illness (6–40 μg/kg [6,7]) but also for a greater understanding of the biogen-

[a] NRCC No. 31946.

[b] Under contract from SCIEX, 55 Glen Cameron Road, Thornhill, Ontario, L3T 1P2.

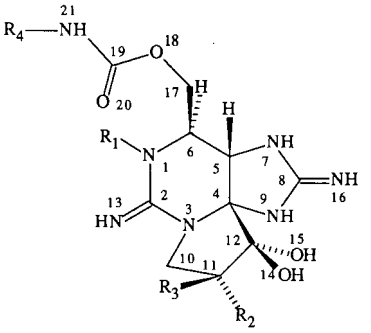

R_1	R_2	R_3	R_4	
H	H	H	H	STX
OH	H	H	H	NEO
H	H	H	SO_3H	B_1
OH	H	H	SO_3H	B_2
H	H	OSO_3H	H	GTX_2
H	OSO_3H	H	H	GTX_3
OH	H	OSO_3H	H	GTX_1
OH	OSO_3H	H	H	GTX_4
H	H	OSO_3H	SO_3H	C_1
H	OSO_3H	H	SO_3H	C_2
OH	H	OSO_3H	SO_3H	C_3
OH	OSO_3H	H	SO_3H	C_4

Fig. 1. Structures of toxins associated with paralytic shellfish poisoning.

esis and metabolic pathways of the toxins involved. At present the official analytical procedure which supports the majority of toxin-monitoring programs in shellfish is the mouse bioassay [8,9]. This procedure allows the determination of the "total toxicity" of a biological extract and provides adequate sensitivity with respect to the permissible limit for human consumption (80 μg per 100 g of shellfish meat) [3]. However, its narrow dynamic range, coupled with its wide variability (effects of salts, susceptibility to mouse strains), difficulties in the supportive logistics and increasing pressure to discontinue the use of animal bioassays have stimulated the development of alternative methods [10].

The detection of PSP toxins has provided a considerable challenge to the development of analytical techniques. The lack of useful UV chromophores absorbing above 220 nm [11] and the low volatility and highly polar nature of these compounds are some of the difficulties that prevent their separation and detection by conventional techniques. In spite of these obstacles, a variety of separation procedures have been reported for the isolation and determination of PSP toxins, including column chromatography [12,13], thin-layer chromatography [14] and cellulose acetate electrophoresis [15]. The instrumental technique most commonly used for the routine determination of PSP toxins involves reversed-phase high performance liquid chromatography using ion-pairing reagents and post-column reaction permitting fluorescence detection (HPLC–FLD) [16]. The post-column reaction system consists of an alkaline oxidation reaction which converts the native toxins into their corresponding fluorescent derivatives [16]. Although the method offers good sensitivity and dynamic range for the separation and detection of different PSP toxins, the sensitivity is dependent on parameters such as reagent concentrations, reaction times, pH and temperature of the oxidation reaction [17]. In addition to the elaborate procedure required to achieve reliable and reproducible results, a significant drawback of the alkaline oxidation reaction is the reliance on fluorescence response factors for the different PSP toxins based on that of the only commercially available standard, STX [16,18].

The successful separation of these marine toxins by both ion-exchange chromatography and cellulose acetate electrophoresis [15] prompted us to investigate the

application of capillary electrophoresis (CE) for their analysis. Also, the recent investigation of ionspray mass spectrometry of marine toxins [19] using flow-injection analysis indicated a useful detection limit for STX (30 pg) and suggested that mass spectral detection of PSP toxins following separation by CE would be practical, provided that a suitable interface is built. Owing to its high-resolution separation capability (up to 10^6 theoretical plates in less than 20–25 min [20–22]) and its ease of operation, the CE technique has aroused considerable interest for the analysis of complex polar biomolecules including marine toxins. Wright *et al.* [23] recently demonstrated the applicability of CE using laser-induced fluorescence detection for the analysis of derivatives of marine toxins including STX. The method has permitted high-resolution separations, with an attomole-range detection limit for the *o*-phthaldialdehyde derivative of STX [23]. However, in view of the desired application to the analysis of biological extracts, the use of chemical derivatives could potentially lead to problems of highly variable response factors, interferences due to reagents and other non-PSP compounds and complications arising from the instability of the derivative and the extensive work-up required.

This paper describes the application of CE with UV detection to the determination of PSP toxins in marine samples. Confirmation of the chemical identities of electrophoretic peaks is made using an improved mass spectrometric interface. A preliminary evaluation of the factors affecting the separation and detection of these toxins is also reported.

EXPERIMENTAL

Chemicals

Saxitoxin was obtained from Calbiochem Biochemicals (San Diego, CA, U.S.A.) as a 1 μmol/ml solution in 0.01 *M* acetic acid and used without further purification. Analytical reagent grade acetic acid (Caledon Laboratories, Georgetown, Ont., Canada), sodium citrate (Sigma, St. Louis, MO, U.S.A.) and water purified with a Milli-Q system (Millipore, Bedford, MA, U.S.A.) were used to prepare the buffer solutions.

Biological samples

Toxins from either cultured algal cells (1–10 g wet weight) or homogenized scallop livers (15 g wet weight) were extracted by sonication in 0.1 *M* acetic acid. Freeze-dried cells of the cyanobacterium *Aphanizomenon flos-aquae* were provided from Dr. W. W. Carmichael (Wright State University, Dayton, OH, U.S.A.). Cell and tissue debris were removed by centrifugation at 20 000 *g* for 30 min and the supernatant fluid was then freeze-dried. The resulting solid was dissolved in 5 ml of 0.1 *M* acetic acid, adjusted to pH 5 and then passed through a 90 × 1.6 cm I.D. Bio-Gel P-2 column (Bio-Rad Labs., Mississauga, Ont., Canada) previously equilibrated with water and eluted with 0.1 *M* acetic acid. Fractions of 1.5 ml were collected and subsequently analysed by high-voltage paper electrophoresis (HVPE).

High-voltage paper electrophoresis

HVPE was conducted in a similar manner to that described by Leggett-Bailey [24]. Aliquots of 10–20 μl of each fraction were spotted across a sheet of Whatman

No. 1 paper (46 × 57 cm). After drying of the sample line, the paper was wetted with the electrolyte [10% (v/v) acetic acid] on either side of the origin and excess of electrolyte was removed with blotting paper. A glass chromatographic tank (Shandon, London, U.K.) containing 5 l of the electrolyte as the anode reservoir was used for electrophoresis. The paper was suspended from the cathode at the top of the tank. The remainder was filled with toluene cooled by a convoluted glass tube through which cold tap-water flowed. Electrophoresis was conducted at 3 kV for 30 min, after which the paper was dried in a vented oven at 100°C. PSP toxins were detected with a long-wavelength UV light source after spraying with 1% hydrogen peroxide solution and heating for 5 min at 100°C.

Capillary electrophoresis

An Applied Biosystems (Foster City, CA, U.S.A.) Model 270A capillary electrophoresis system was used for all CE experiments. An untreated fused-silica capillary column (Polymicro Technologies, Phoenix, AZ, U.S.A.) of 50 μm I.D. and length 90 cm (68 cm to the detector) was used in all separations. Sample introduction was performed using either hydrodynamic (vacuum) or electrokinetic (voltage) injections. In hydrodynamic injection, a preset vacuum (17 kPa) was applied to the detector end of the capillary for 3 s, whereas electrokinetic injection used a potential of 5 kV applied to the capillary end for 30 s. Unless specified otherwise, electrophoretic separations were carried out in either 20 m*M* sodium citrate buffer (pH 2) or 0.1 *M* acetic acid (pH 2.9). UV detection was performed at 200 nm. Data acquisition and handling were accomplished using a Hewlet-Packard HP 3396A integrator linked to an MS-DOS microcomputer using the Chromperfect data acquisition–processing software package (Justice Innovations, Palo Alto, CA, U.S.A.).

Mass spectrometry

All mass spectrometric experiments were performed on a SCIEX (Thornhill, Ont., Canada) API III triple quadrupole mass spectrometer equipped with an atmospheric pressure ionization (API) source operated in the ionspray mode. For flow-injection analyses (FIA) samples were injected via a 0.1-μl loop Valco injector (Chromatographic Specialties, Brockville, Ont., Canada) into a stream of acetonitrile–water (1:1) containing 0.1% trifluoroacetic acid, delivered by a Brownlee syringe pump operating at a flow-rate of 50 μl/min.

The CE–MS interface is shown schematically in Fig. 2. The interface was constructed from a modified commercial IonSpray (ISP) probe and was based on a co-axial column arrangement, similar in design to that described by Smith *et al.* [25]. The CE fused-silica column (90 cm × 50 μm I.D. × 350 μm O.D.) was connected to the interface via a zero dead volume (ZDV) tee, mounted externally on the pressurized probe handle. A make-up solution (0.1 *M* acetic acid) was delivered at a flow-rate of 20 μl/min to the probe tip via the interspace between the CE capillary and the outer capillary (42 cm × 400 μm I.D. × 530 O.D.) using a syringe pump (Harvard Apparatus, Southnatick, MA, U.S.A.). Optimization of the CE–MS system was achieved by injecting a standard into the make-up flow stream using a 0.1-μl loop Valco injector as described above. The ISP probe tip consisted of a 20-gauge stainless-steel tube and was held at a potential of *ca.* 6 kV. Air was used as a nebuliser gas at a flow-rate of 1.5–2.0 l/min. The potential difference between the CE electrode and the ISP needle

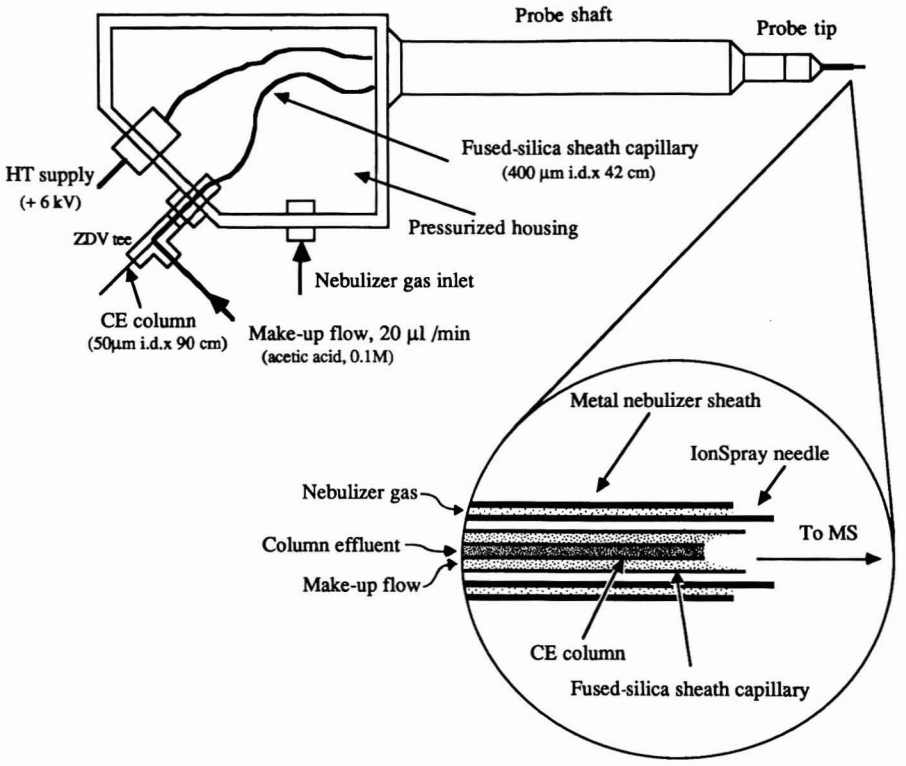

Fig. 2. Schematic diagram of the CE–MS interface.

therefore defined the CE field gradient. Electrokinetic injections (30 s) were made in all CE–MS experiments. The CE column terminated *ca.* 0.5 mm inside the ISP needle. This arrangement minimized column peak broadening and ensured good electrical contact between the ISP needle and the CE electrolyte. Mass spectral acquisition was performed using dwell times of 5 and 200 ms per channel for full mass scan (either 50-350 dalton in CE–MS or 200–500 dalton in FIA–ISP-MS analyses) and selected ion monitoring (SIM) experiments, respectively. A Macintosh IIx computer was used for instrument control, data acquisition and data processing.

RESULTS AND DISCUSSION

Determination of PSP toxins by CE–UV following sample fractionation

With the exception of C compounds (Fig. 1), PSP toxins have an overall positive charge under acidic conditions, making them ideal candidates for separation based on ionic state. Their basic nature is attributed to the delocalized guanidinium groups, centered on C_8 and C_2, which have pK_a values of 8.22 and 11.28 in the case of STX [26]. In this study, electrophoretic separation of PSP toxins by HVPE was conducted to establish toxin profiles as they eluted from the Biogel P-2 gel permeation column. This method is similar to that previously reported using cellulose acetate

electrophoresis [15], except that the acetic acid buffer system chosen here facilitates solvent evaporation and its larger scale allows 50–100 samples to be run simultaneously. Further, the time for electrophoresis was typically 30 min compared with 3 h on cellulose acetate [15]. The P-2 column was used prior to electrophoresis as PSP toxins could easily be separated from salts, proteins, carbohydrates and most non-PSP compounds present in plankton and more particularly in scallop extracts.

A typical two-dimensional analytical chromatogram (P-2 column fractions on the horizontal axis with electrophoretic separation on the vertical axis) of PSP toxins is presented in Fig. 3 for the analysis of an extract isolated from 10 g of sonicated cells of *Alexandrium tamarensis*. Most non-PSP compounds were found in fractions 15–30 and did not show any fluorescence on oxidation with hydrogen peroxide but stained strongly with ninhydrin. PSP toxins eluted later in fractions 40–104, which exhibited a blue fluorescence on oxidation and drying. Based on a previous report [27], these different migration bands can be separated into three main toxin groups in descending order of net charge: fractions 40–58 containing both STX and NEO (2+), fractions 52–66 containing the GTX toxins (1+) and fractions 80–104 containing the C

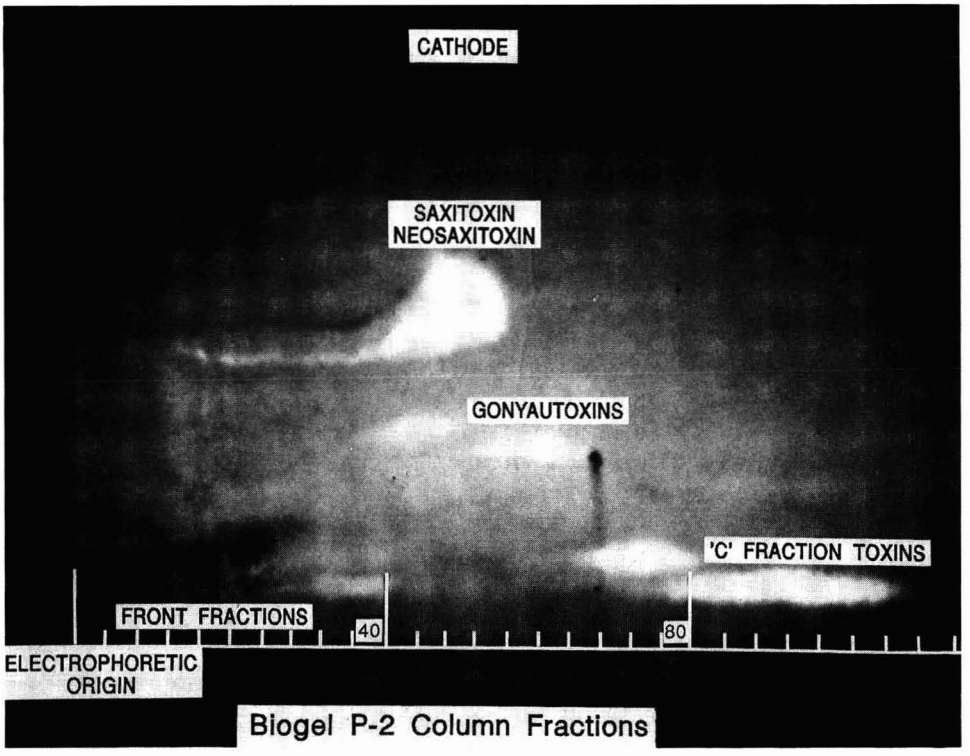

Fig. 3. High-voltage paper electrophoretic separation of PSP toxins following Bio-Gel P-2 column fractionation. Electrophoresis was conducted at 3 kV for 30 min on Whatman No. 1 paper (46 × 57 cm) using 10% (v/v) acetic acid electrolyte. PSP toxins were identified as a blue fluorescent band after H_2O_2 oxidation and heating at 100°C for 5 min. Non-PSP compounds were found in fractions 14–18. STX and NEO were found in fractions 21–24 and did not separate from each other. GTX toxins eluted in fractions 24–27 and the C toxins appeared in fractions 30–37.

toxins (no net charge). Although the C toxins have no net charge in dilute acetic acid, they do migrate from the electrophoretic origin owing to the electroendosmotic flow. Fractions corresponding to each of these three groups were also analyzed by ionspray mass spectrometry in order to validate this qualitative assignment (see below). The fluorescent band seen in fractions 68–80, having a mobility slightly higher than the electroendosmotic flow, was not identified but may be due to a PSP degradation product.

Although the separation of PSP toxins into three groups was readily achieved on the P-2 column and by HVPE, it was anticipated that CE would provide more efficient separation. However, some of the inherent difficulties in analyzing such compounds are the lack of a chromophore absorbing in the usual UV range and the unavailability of standards to confirm the electrophoretic peak identity. With respect to the detection capability, it is expected that PSP detection using a conventional deuterium lamp would be difficult if not impossible, in view of the low molar absorptivities (e.g., $< 1 \cdot 10^{-3}$ mol/cm above 220 nm for STX [11]). However, STX shows a rise in its molar absorptivity below 220 nm [11]. This, coupled with the fact that the signal-to-noise characteristics of the UV detector used in this present study provide better sensitivity at 200 nm on compounds such as peptides [28], prompted us to investigate the practical applications of this instrument to PSP toxins.

In situations where the electrophoretic peak identity could present some uncertainties, or if standards are not available to correlate with the peak of interest, it is desirable to use a complementary technique. Mass spectrometric detection using nebulizer-assisted electrospray ionization (ionspray) was chosen for this purpose, as its excellent sensitivity observed for PSP and other marine toxins [19] renders detection of STX possible within the concentration and injection volumes used in the CE experiment. A CE–MS interface inspired by a co-axial capillary arrangement carrying both the CE buffer and make-up flow initially described by Smith *et al.* [25] was designed and constructed in this laboratory. Although other CE-MS interfaces using a "liquid junction" remote from the ion source have been demonstrated successfully [29,30], the co-axial design has the advantage of removing dead volume associated with the "liquid junction" in addition to minimizing band broadening arising from the dynamic mixing of the make-up flow and CE stream [31].

Initial investigations of PSP toxin analysis by CE were made using a buffer system similar to that used in the HVPE experiment. In addition to enhancing protonation, the acetic acid buffer has the advantage of being compatible with the CE–MS interface and can also be used as make-up flow, thus preventing changes in the CE buffer composition during a run. The results of analyses of an extract of *A. tamarensis* by CE–UV and CE–MS are presented in Fig. 4. The sample chosen for the CE experiment originated from fraction 52 from the Bio-Gel P-2 column separation and showed a fluorescent band in the NEO–STX region of the HVPE analysis. The electropherogram of fraction 52, using UV detection at 200 nm, is shown in Fig. 4a. This separation corresponds to an electrokinetic injection of 30 s and was achieved at a field strength of 220 V/cm. As indicated in Fig. 4a, three major components are observed at 7.41, 7.46 and 7.58 min. The resolution of the last two peaks was estimated to be only 0.50.

The analysis of fraction 52 by CE–MS is presented in Fig. 4b and c, corresponding to the reconstructed ion electropherograms of the protonated molecules (MH^+)

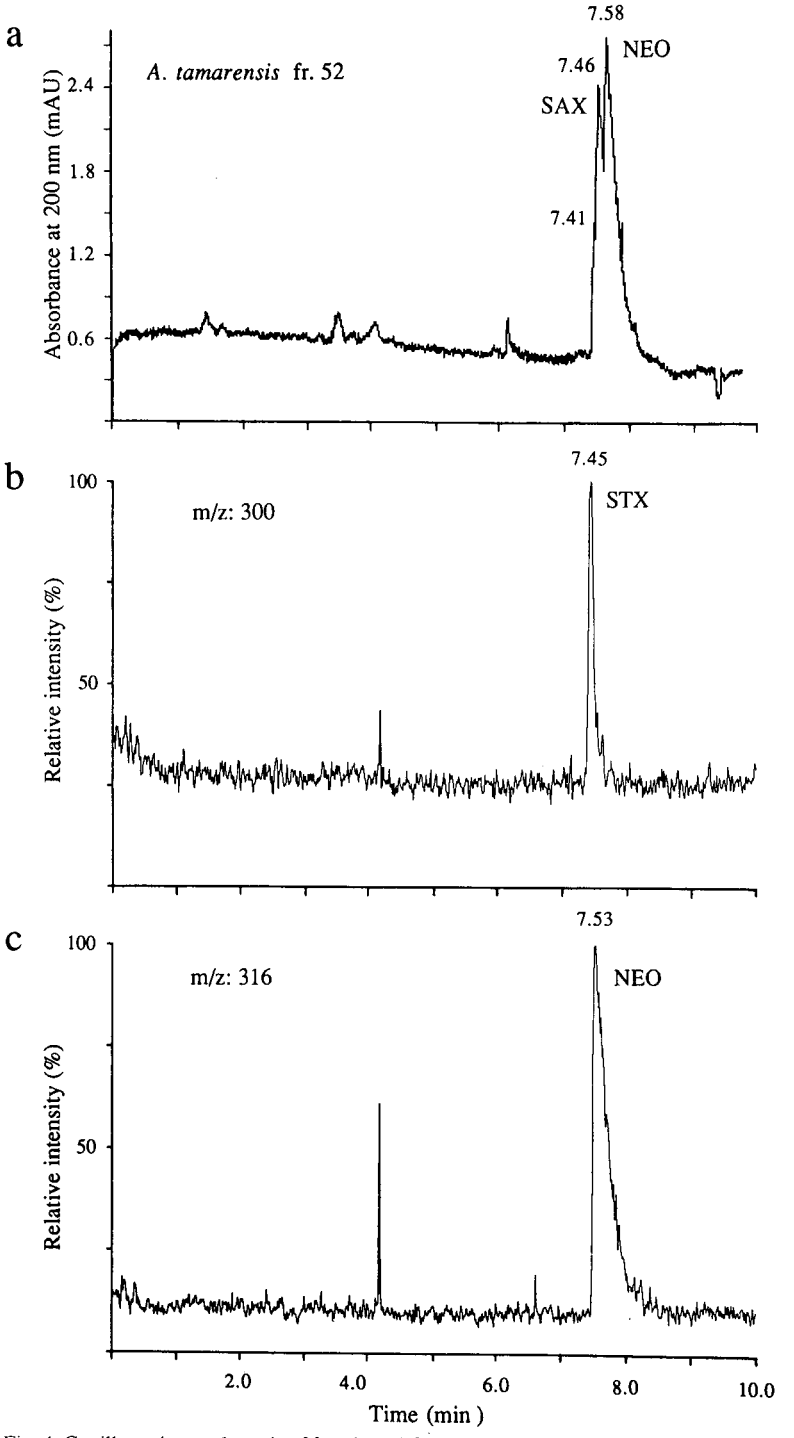

Fig. 4. Capillary electrophoresis of fraction 52 from the *A. tamarensis* extract. (a) Analysis performed using UV detection at 200 nm, 30-s electrokinetic injection, +20 kV, 0.1 *M* acetic acid buffer. Injection of *ca.* 0.5 and 1.3 ng of STX and NEO, respectively. Reconstructed ion electropherogram for (b) *m/z* 300 and (c) *m/z* 316, 30-s electrokinetic injection, +25 kV applied at injector end, +5.6 kV on ionspray probe tip.

of STX and NEO, respectively. The migration times observed for the two toxins are remarkably close to those observed in the CE–UV experiment and confirmed the identity of the two electrophoretic peaks. Independent injections of STX standard, using both CE–UV and CE–MS with full mass acquisition of *m/z* 100–400 dalton (data not shown), provided additional evidence of the peak identity. In addition to the good correlation of migration times observed in the two experiments, it is noteworthy that the peak widths at half-height differed by at most 3 s in the two experiments, indicating that loss of separation efficiency due to large dead volume was minimal with this CE–MS interface. As a result, the resolution for STX and NEO obtained in the CE–MS analysis was similar to that observed with the CE–UV; a value of *ca.* 0.7 was obtained for the former technique as opposed to 0.5 in the latter.

Although no effort was made to improve the detection limit of the CE–MS interface, adequate signal-to-noise ratios were obtained in the analysis of fraction 52. As will be described later, this fraction contained STX and NEO in concentrations of 32 and 83 μg/ml, respectively. The amount of sample loaded on the CE column by electrokinetic injection was established by comparing area counts with those obtained using vacuum injection, the latter being calibrated by measuring the amount of sample drawn into the cappillary using a coloring agent prepared with the sample solvent. These experiments indicated that *ca.* 500 pg of STX were loaded on the column during the CE–MS experiment. For such amounts a signal-to-noise ratio of 15:1 was obtained, suggesting that an instrumental detection limit of *ca.* 100 pg is achievable. This result is consistent with data obtained independently with flow-injection analysis of STX using ionspray [19], where a detection limit of 30 pg was obtained with a signal-to-noise valid ratio of 2. The difference in sensitivity can be explained by the larger peak width observed with the combined CE–MS technique.

Determination of STX and NEO concentrations in biological extracts

Further to the preliminary work on the separation of NEO and STX described above, work was needed to enhance the separation efficiency of the CE technique and to facilitate the confirmation and determination of these toxins in natural extracts. Buffer composition and acidity were investigated to establish their effects on plate counts, resolution and background contribution.

Variation of the buffer acidity had a considerable effect on the separation of NEO and STX. Increasing the acetic acid content of the buffer from 0.1 to 5.0 *M* resulted in a pH change from 2.9 to 1.9. Using a field strength and capillary identical with those described in Fig. 4, it was observed that the resolution improved progressively with decreasing pH up to the point where these peaks were resolved completely. For example, using solutions of approximately equal concentration of STX and NEO, pH values of 2.9, 2.4 and 1.9 resulted in resolution values (R_s) of 0.5, 1.6 and 2.7, respectively. At pH 1.9 the efficiency of separation (N) obtained from the conventional equation for plate numbers using peak widths at half-height was 53 800, an improvement of *ca.* 2-fold over the same analysis conducted at pH 2.9.

Lowering the pH of the buffer also affected the analysis time. At pH 1.9 the migration of both STX and NEO was completed in 24 min as opposed to 8 min at pH 2.9. This increase in migration time is due to electroendosmosis where the bulk flow of liquid progressively increases with increasing pH. The electroendosmotic flow arises from solvated cations from the double layer adjacent to the capillary wall migrating

to the cathode. At low pH, where the silanol groups of the capillary wall are protonated, there is very little coulombic interaction between the analyte cations, buffer ions and the capillary wall, hence decreasing the electroendosmotic flow [32,33].

Other buffer systems were also investigated in an attempt to improve the separation efficiency. Better resolution and sensitivity were achieved by changing the buffer to a 20 m*M* solution of sodium citrate adjusted to pH 2.1. An example of such a separation is presented in Fig. 5 for the analysis of fraction 52 from the *A. tamarensis* extract. The CE analysis performed under these conditions yielded three distinct peaks with an R_s value of 2.6 for NEO and STX. The identity of the first peak observed at 14.68 min is unknown. However, this compound is not an isomer of either STX or NEO as no corresponding signal was observed in the SIM traces in Fig. 4b or c. Owing to the low concentration of this component and the amount of sample that could be loaded on the capillary, the identification of this compound using CE–MS with full mass scan acquisition was not possible. It is possible that this compound is a decarbamoyl derivative of STX which was previously found to have a mobility slightly higher than that of STX [15].

In terms of separation efficiencies, the number of theoretical plates achieved with the sodium citrate buffer was *ca.* 46 000. Although this is less than that with the acetic acid buffer of pH 1.9, the use of sodium citrate buffer has the advantage of reducing the analysis time to 18 min, in addition to providing better signal-to-noise ratios (typically four times better than with acetic acid at pH 1.9). It is noteworthy that a gain of a factor of 2 in sensitivity could be achieved by setting the UV detector

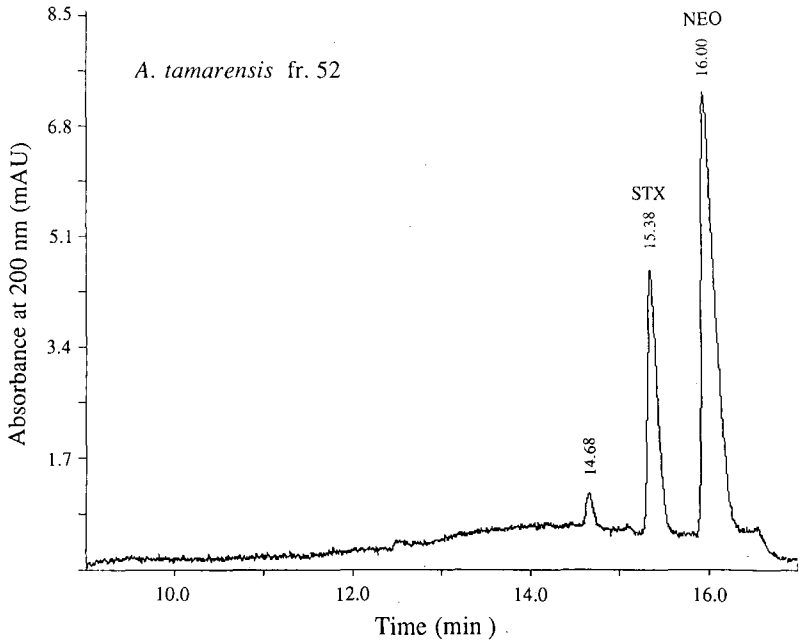

Fig. 5. Capillary electrophoresis of fraction 52 from the *A. tamarensis* extract using UV detection at 200 nm, 3-s vacuum injection, +20 kV, 20 m*M* sodium citrate buffer. The electropherogram represents an injection of 320 and 830 pg of STX and NEO, respectively.

to 190 nm instead of 200 nm. However, in view of the stability of the baseline noise over a day-long operation, analysis at 200 nm was preferred.

In order to improve the separation efficiency and reduce the analysis time still further for routine analysis, the CE separation was carried out at 30 kV using the sodium citrate buffer. Under these conditions, migration of STX was achieved within 10 min with N values at least 4–5 times greater than those obtained in the same experiment performed at 20 kV. Reproducibility of migration times was adequate to ensure proper peak assignment; extremes of migration times varied by no more than 2% on a daily basis. These fluctuations could also be corrected by using a mobility standard such as lysine, thereby reducing these variations to less than 1%. In terms of reproducibility for determination, replicate injections ($n = 6$) of solutions containing both STX and NEO indicated that the standard deviation of the integrated areas was *ca.* 4% for each compound.

The CE separation developed here for the determination of STX and NEO also provided good linearity over the concentration range 1.5–300 μg/ml. A typical calibration graph for STX is presented in Fig. 6. This graph shows a good linear response over at least two orders of magnitude, with a correlation coefficient of 0.998. The mass detection limit was reached for a *ca.* 15-pg injection of STX. The inset in Fig. 6 shows the CE analysis achieved at this detection limit for STX with a signal-to-noise ratio of 2.

We found that the response for NEO at 200 nm is slightly lower than that for STX. Studies performed using NMR [34] established the molar ratio of NEO and STX in a synthetic mixture of these two toxins. Results from analytical techniques such as FIA–ISP-MS and CE–UV were compared with data obtained from NMR

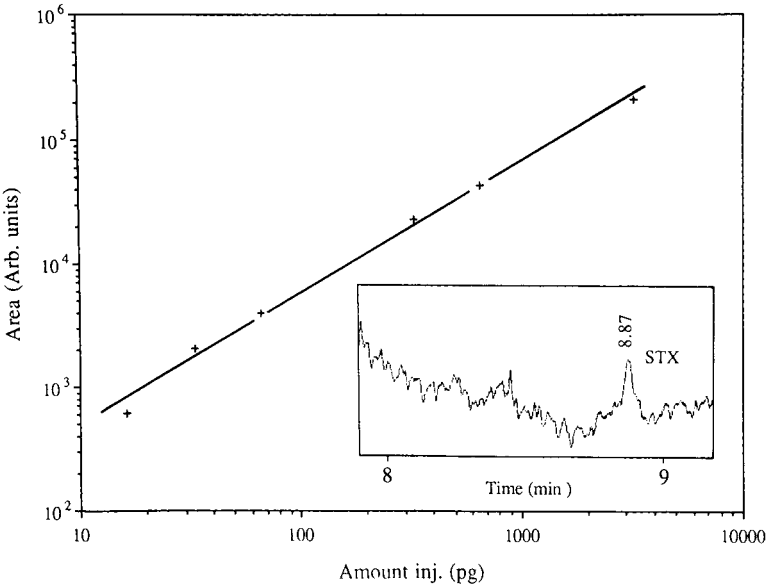

Fig. 6. Calibration curve for STX in the concentration range 1.5–300 μg/ml. Conditions: UV detection at 200 nm, 3-s vacuum injection, +30 kV, 20 mM sodium citrate buffer. The mass detection limit was reached for a *ca.* 15-pg injection of STX. The inset shows the CE analysis achieved at the detection limit for STX with a signal-to-noise ratio of 2.

spectroscopy. Correlations amongst these different techniques indicated that the response observed for NEO should be corrected by a factor of 1.18 in order to compensate for the lower sensitivity of this compound with UV detection at 200 nm. Based on this information, it was possible to determine the amount of STX and NEO present in fraction 52 from the *A. tamarensis* extract (Fig. 5). This quantitative analysis revealed that the concentrations of STX and NEO were 32 ± 1 and 83 ± 2 μg/ml, respectively.

The results from applying the CE–UV determination of STX and NEO to fractions from phytoplankton, a cyanobacterium and contaminated scallops are presented in Fig. 7. The sample of contaminated scallop livers was from a material

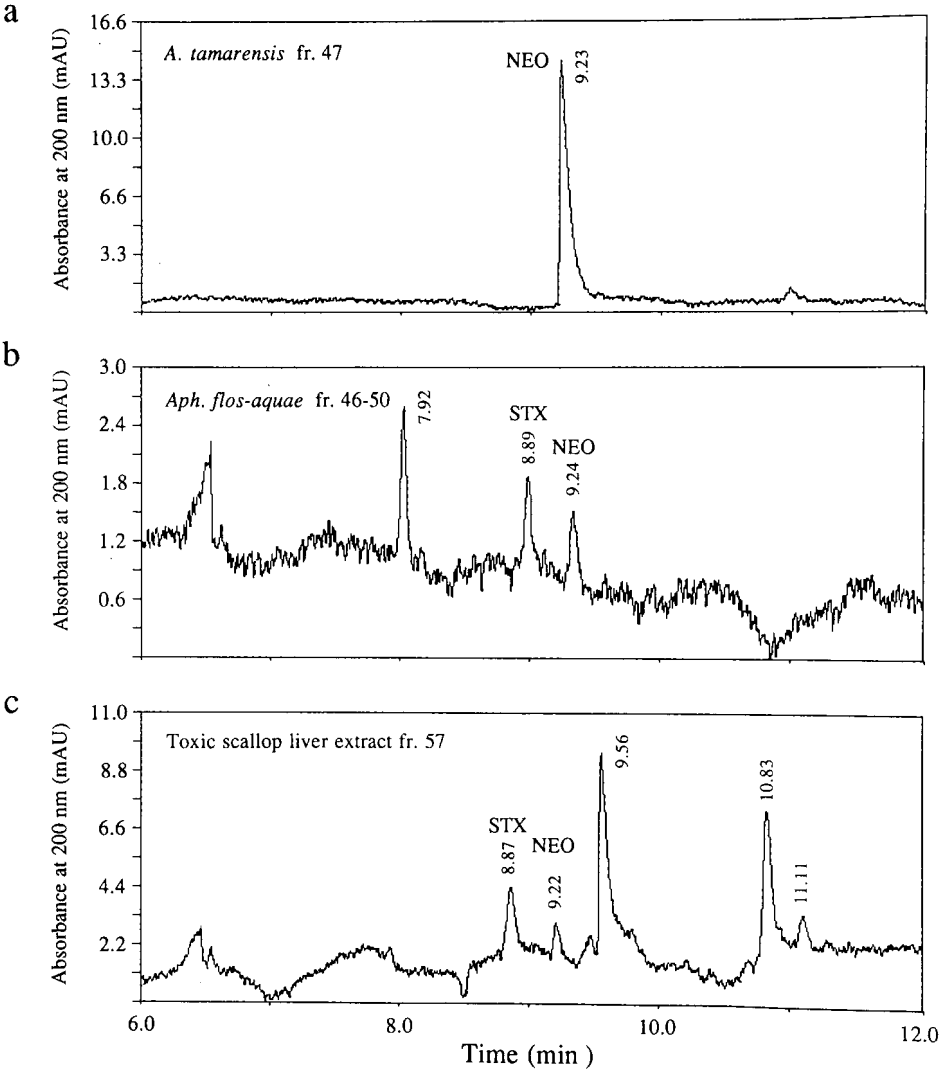

Fig. 7. CE analysis of toxin fractions isolated from different matrices. (a) Fraction 47 from an extract of sonicated cells of *A. tamarensis*; (b) combined fractions 46–50 from an extract of sonicated cells of *Aph. flos-aquae*; (c) fraction 57 from toxic scallop liver extract. Conditions: detection at 200 nm, 3-s vacuum injection, +30 kV, 20 m*M* sodium citrate buffer.

currently under evaluation for its suitability as a PSP reference material. In each instance extracts from sonicated cells were fractionated using a Bio-Gel P-2 column as described previously. Fig. 7 illustrates the electropherograms obtained for three arbitrarily chosen fractions of each biological matrix. The migration times observed for STX and NEO were consistent with those previously obtained on different samples. Although the presence of a high salt content (possibly sodium) could be detected easily by the fronting peak at 6.5 min in Fig. 7b and c, the migration times were reproducible to within 2% on any given day. In addition to observing STX and NEO at the correct migration times, several unknown compounds (possibly amino acids or other dicationic PSP toxins) were also detected, as illustrated in Fig. 7b and c.

Although the migration times for STX and NEO were consistent for all samples analysed, it was observed that high salinity of the sample could complicate the peak assignment. In experiments using solutions of STX prepared in buffers of various salinities, ranging from 0 to 0.5 *M* NaCl, it was found that variation of migration times of more than 2% was observed only when the sample contained more than *ca.* 0.3 *M* NaCl. Above this concentration, loss of resolution between STX and NEO and increased background contribution were also noted. These observations can be explained by the rise in electrophoretic current with increasing salt concentration, resulting in changes in temperature and consequent effects including convection.

The determination of STX and NEO in the fractions from biological extracts presented in Fig. 7 is summarized in Table I. Where possible, the results from the quantitative analysis obtained using CE–UV were correlated with those given by FIA–ISP-MS [19]. However, the latter technique can be used only with relatively pure samples of STX and NEO, as salts and other contaminants present in the fraction interfere in the analysis by forming adduct ions, which reduce the abundance of the protonated molecular ion. In spite of this limitation, useful comparisons were obtained for samples of low salt content, such as fraction 47 from the *A. tamarensis* extract (Fig. 7a). In this instance the two techniques yielded comparable results for the determination of NEO, *i.e.*, 115 ± 5 μg/ml by CE–UV compared with 121 ± 2 μg/ml by FIA–ISP-MS.

Table II illustrates the detection limits for NEO and STX using different analytical techniques for PSP toxin monitoring. It can be seen that in terms of mass detec-

TABLE I

DETERMINATION OF STX AND NEO IN ALGAL AND MOLLUSC EXTRACTS USING CE–UV

Detection at 200 nm, 3-s vacuum injection, +30 kV, 20 m*M* sodium citrate buffer.

Sample	Concentration (μg/ml)	
	NEO[a]	STX
A. tamarensis, Fraction 47	115 ± 5[d]	n.o.[b]
Aph. flos-aquea, Fractions 46-50	4.1 ± 0.1[d]	3.7 ± 0.1[d]
Toxic scallop liver, Fraction 57	6.4 ± 0.3[c,d]	14.9 ± 0.8[d]

[a] Corrected response for NEO.
[a] Corresponds to *ca.* 5.1 μg/g of wet liver tissue.
[c] Not observed (< 1.5 μg/ml).
[d] Standard deviation, $n = 3$.

TABLE II

DETECTION LIMITS OF STX AND NEO USING DIFFERENT TECHNIQUES

Technique	NEO		STX	
	Concentration (μM)	Amount injected (ng)	Concentration (μM)	Amount injected (ng)
Mouse bioassay [35][a]	0.4	120	0.5	150
HPLC–FLD [35][b]	0.065	0.39	0.014	0.08
FIA–ISP-MS [19]	–	–	0.1	0.03
CE–UV (this study)	5.6	0.018	5.0	0.015

[a] Based on a 1-ml injection.
[b] Based on a 20-μl injection.

tion limits CE–UV is considerably more sensitive than the mouse bioassay. It also offers better detection limits than HPLC–FLD [16,35] and flow-injection analysis using FIA–ISP-MS. However, owing to the limited sample (a few nanolitres) which can be loaded on the CE column, the CE–UV technique lacks the ability to provide good detection limits for samples of low concentration (sub-micromolar range). From a practical standpoint, this limitation can be circumvented by concentrating the sample before analysis by CE–UV, as only a limited amount of sample is required. Further, in situations where the sample is dissolved in a solution of lower conductivity than the running buffer, one can apply sample "stacking", where a large volume of a dilute solution is injected on the CE capillary [28]; this permits injection of a solution typically 3–5 times less concentrated without degradation of signal-to-noise ratios or loss of resolution [28].

Application of CE–UV to the determination of GTX and C-type PSP toxins

In addition to STX and NEO, GTX toxins (Fig. 1), more specifically GTX_2 and GTX_3, are often found in toxic shellfish and dinoflagellates [2,14]. During the analysis of biological extracts by CE–UV, GTX toxins migrated more slowly than STX and NEO as they have an overall charge of + 1 under the electrophoretic conditions used. An electropherogram corresponding to the analysis of a purified fraction of GTX toxins isolated from *A. tamarensis* is presented in Fig. 8a. This sample contained a high proportion of GTX toxins, as indicated by the peaks in the region of 16 min. A small amount of NEO (4.4 μg/ml) was also found in the same sample, as evidenced by a peak at 9.17 min. The ionspray mass spectrum of the same fraction is presented in Fig. 8b. An abundant protonated molecular ion was observed at m/z 396, which confirmed the presence of the GTX toxins. Fig. 8a also shows a prominent ion at m/z 316, thought to be a fragment ion corresponding to the loss of an SO_3 group from m/z 396. Although the ion at m/z 316 also corresponds to the MH^+ of NEO, the low concentration of this compound found in the CE–UV trace (Fig. 8a) could not account for such an intense peak in the mass spectrum. The assignment of the ion at m/z 316 was confirmed by tandem mass spectrometry (MS–MS), which showed that this ion is indeed a fragment ion of GTX toxins, rather than the MH^+ ion of NEO.

Owing to the unavailability of standards, the assignment of individual GTX

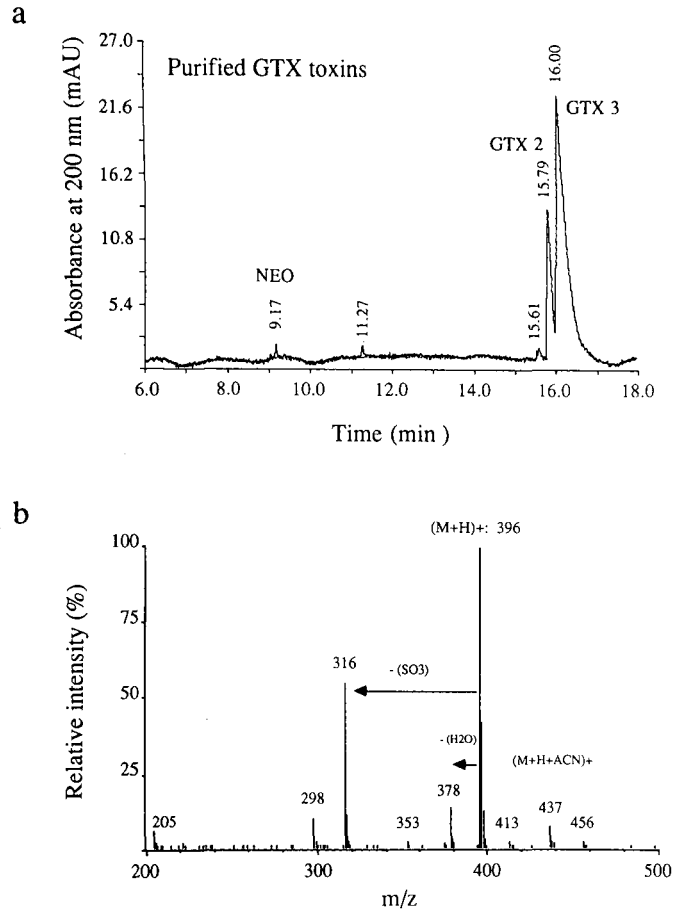

Fig. 8. Analysis of a purified fraction of GTX toxins by (a) CE–UV (conditions as in Fig. 7) and (b) FIA–ISP-MS [0.1-μl injection, flow-rate 50 μl/min, acetonitrile–water (1:1), 0.1% trifluoroacetic acid].

toxins remains difficult at this stage. In order to facilitate the assignments, the peak areas observed in the electropherogram in Fig. 8a were correlated with the results from the HPLC–FLD analysis using post-column reaction modification [16]. Using the latter technique it was found that the purified fraction of GTX toxins contained mainly GTX_3 and GTX_2, at concentrations of 320 and 130 μg/ml, respectively (molar ratio 2.5:1). This result is in reasonably good agreement with that observed in the CE–UV analysis, where a molar ratio of 3.8:1 was obtained for GTX_3:GTX_2. Based on this observation, it was deduced that the early migrating peak at 15.79 min was GTX_2, followed by GTX_3 at 16.00 min.

The preliminary work described above indicates that GTX, NEO and STX toxins can all be identified in a single CE–UV experiment within less than 20 min. However, the conditions chosen here for the analysis of these toxins do not permit the detection of the C toxins as these compounds have no net charge at pH 2.1, and thus

would migrate only with the electroendosmotic flow. The inability to separate the different C toxins is also encountered with the HPLC–FLD method [16], where these compounds are not retained by the column and elute with the solvent front. Work is in progress to establish a direct CE–UV method for the detection of these electrically neutral toxins.

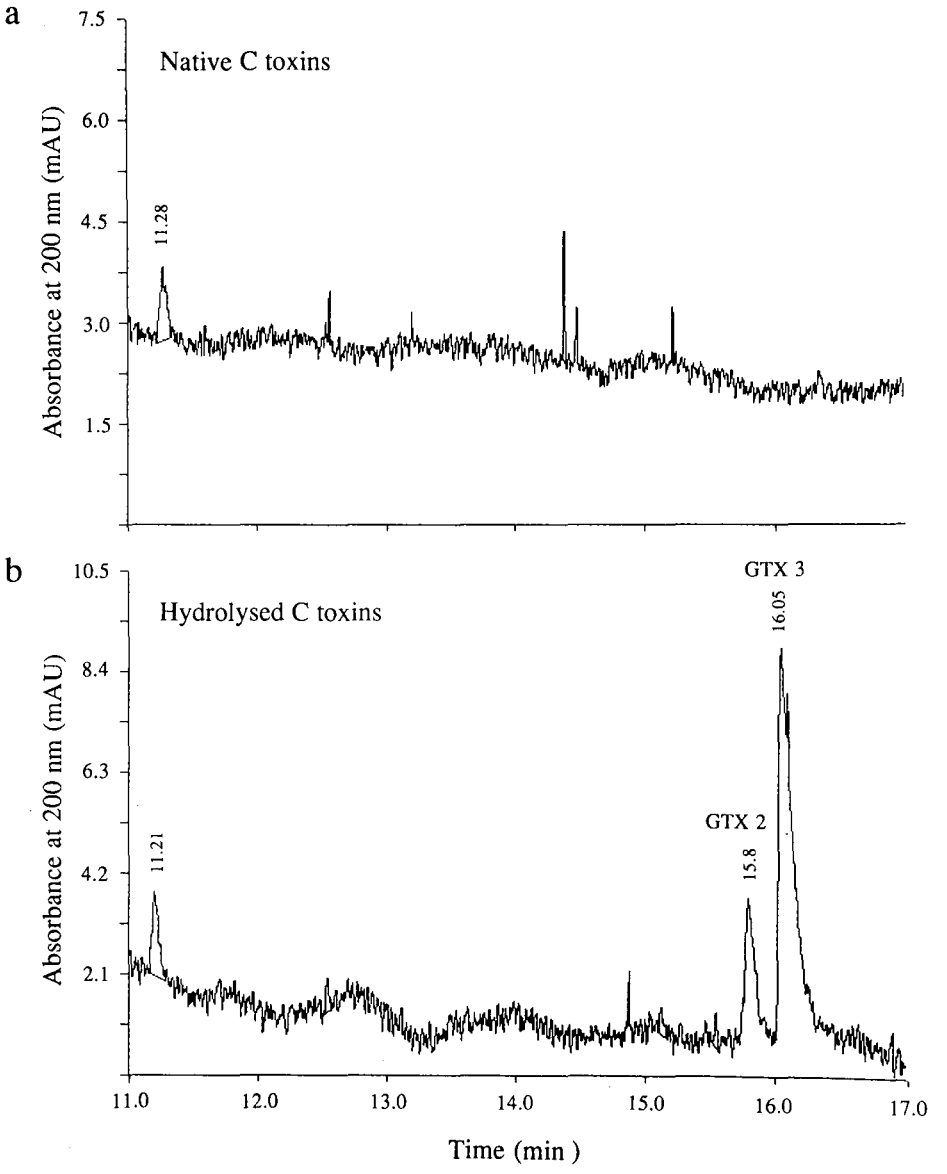

Fig. 9. Analysis of a fraction of C toxins isolated from *A. tamarensis*. Capillary electrophoretic separation of C toxins (a) before and (b) after hydrolysis to the corresponding GTX toxins. Hydrolysis performed with 0.1 *M* HCl at 100°C for 10 min. Electrophoretic conditions as in Fig. 7.

Indirect determination of the C toxins by CE–UV can be achieved by measuring their hydrolytic products. Conversion of the C toxins into the corresponding GTX forms is achieved by briefly heating in 0.2 *M* hydrochloric acid [17]. This procedure is used in the standard AOAC mouse bioassay method [8], which converts the latent C toxins into the more toxic GTX forms. A pooled fraction containing mostly C toxins was divided into two equal samples, one of which was subsequently hydrolyzed with 0.1 *M* hydrochloric acid at 100°C for 10 min whereas the other was left intact. The CE–UV trace corresponding to the native C fraction is presented in Fig. 9a, and shows that no GTX toxins are observed at 16 min. However, this sample contained an unknown constituent at 11.28 min, which could be a degradation product of C toxins resulting in the formation of a dicationic product. In comparison, the hydrolyzed fraction of C toxins (Fig. 9b) clearly shows two peaks at 15.80 and 16.05 min, which correspond to GTX_2 and GTX_3, respectively. The ratio of the areas of these two peaks is 0.22. From the hydrolytic products of this reaction it was concluded that the pooled C fraction contained mainly C_1 and C_2 toxins.

The sample corresponding to the hydrolyzed C toxins was later subjected to the HPLC–FLD analysis to establish the toxin concentrations. This analysis confirmed the presence of GTX_2 and GTX_3 at concentrations of 29 and 70 μg/ml, respectively, a ratio of 0.41. Assuming that the concentrations of the GTX toxins are accurate, in the absence of pure standards the electropherogram in Fig. 9b corresponds to injections of *ca.* 290 and 700 pg of GTX_2 and GTX_3, respectively. For this analysis the signal-to-noise ratio observed with GTX_2 was *ca.* 8:1, indicating that the method appears to be less sensitive for the detection of GTX toxins than for NEO and STX. This observation is consistent with the sensitivity loss expected as the migration time is increased.

CONCLUSIONS

The work outlined above demonstrates the potential of CE combined with either UV or MS detection for the rapid and efficient determination of PSP toxins. Identification of the electrophoretic peak observed with UV detection was confirmed by MS using ionspray ionization. Although these compounds do not contain a chromophore with a significant molar absorptivity in the wavelength range 220–500 nm, the high sensitivity of the detector used permitted detection limits of 15 and 18 pg for underivatized STX and NEO, respectively, at 200 nm. Owing to the small volume of sample that can be injected onto the capillary (a few nanolitres), the concentration detection limit is of the order of 5 μ*M* for these two toxins. It is expected that improvements in sensitivity could be achieved by using pre- or post-column fluorescent derivatization.

Application of the CE–UV method has been demonstrated for the separation of PSP toxins and for the determination of STX and NEO found in plankton and in scallop liver extracts. In the presence of high salt concentrations in the sample (up to 0.3 *M* NaCl), the CE method reported here yielded reproducible results in terms of both migration times and sensitivity. Further investigations are in progress to evaluate the sample treatment required to analyse raw extracts from different sources and the results will be reported separately.

In comparison with existing techniques such as the mouse bioassay and HPLC

using fluorescence detection, the determination of PSP toxins by CE–UV holds promise for the routine screening of these compounds in natural extracts. Particularly attractive are its ease of operation, small sample consumption, speed of analysis, separation efficiency and the potential for automation.

ACKNOWLEDGEMENTS

The authors are grateful to Drs. A. S. W. de Freitas and P. Wangersky for providing the plankton cells, to Dr. S. W. Ayer and T. J. Uher for the analyses of PSP toxins using HPLC–FLD and to P. Blay for technical assistance. They also thank Drs. R. K. Boyd, M. A. Quilliam, P. G. Sim and J. L. C. Wright for helpful discussions.

REFERENCES

1 Y. Shimizu, in A. T. Tu (Editor), *Handbook of Natural Toxins*, Vol. 3, Marcel Dekker, New York, 1988, p. 63.
2 Y. Shimizu, M. Alam, Y. Oshima and W. E. Fallon, *Biochem. Biophys. Res. Commun.*, 66 (1975) 731.
3 G. L. Boyer, C. Fix-Wichmann, J. Mosser, E. J. Schantz and H. K. Schnoes, in D. L. Taylor and H. H. Seliger (Editors), *Toxic Dinoflagellate Blooms*, Elsevier, Amsterdam, 1979, p. 373.
4 Y. Shimizu, in W. Herz, H. Grisebach and G. W. Kirby (Editors), *Progress in the Chemistry of Organic Natural Products*, Vol. 45, Springer, New York, 1984, p. 235.
5 A. D. Cembella, J. J. Sullivan, G. L. Boyer, F. J. R. Taylor and R. J. Andersen, *Biochem. Syst. Ecol.*, 15 (1986) 171.
6 R. Fortuine, *Alaska Med.*, 17 (1975) 71.
7 W. W. Carmichael, *Adv. Bot. Res.*, 12 (1986) 47.
8 *Official Methods of Analysis of the Association of Official Analytical Chemists*, Association of Official Analytical Chemists, Arlington, VA, 1984, 18.086–18.092.
9 *Recommended Procedures for Examination of Sea Water and Shellfish*, American Public Health Association, New York, 4th ed., 1970, p. 61.
10 J. J. Sullivan, M. M. Wekell and S. Hall, in A. T. Tu (Editor), *Handbook of Natural Toxins*, Vol. 3, Marcel Dekker, New York, 1988, p. 87.
11 E. J. Shantz, J. D. Mold, W. L. Howard, J. P. Bowden, D. W. Stanger, J. M. Lynch, O. P. Wintersteiner, J. D. Dutcher, D. R. Walters and B. Riegel, *Can. J. Chem.*, 39 (1961) 2117.
12 Y. Oshima, L. J. Buckley, M. Alam and Y. Shimizu, *Comp. Biochem. Physiol.*, 57c (1977) 31.
13 L. J. Buckley, Y. Oshima and Y. Shimizu, *Anal. Biochem.*, 85 (1978) 187.
14 L. J. Buckley, M. Ikawa and J. J. Sasner, *J. Agric. Food Chem.*, 24 (1976) 107.
15 W. E. Fallon and Y. Shimizu, *J. Environ. Sci. Health*, A12(9) (1977) 455.
16 J. J. Sullivan and W. T. Iwaoka, *J. Assoc. Off. Anal. Chem.*, 66 (1983) 297.
17 J. J. Sullivan, in S. Hall and G. Strichartz (Editors), *Marine Toxins, Origin, Structure, and Molecular Pharmacology, (ACS Symp. Ser.*, Vol. 418), American Chemical Society, Washington, DC, 1990, p. 66.
18 J. J. Sullivan and M. M. Wekell, in E. P. Ragelis (Editor), *Seafood Toxins (ACS Symp. Ser.*, Vol. 262), American Chemical Society, Washington, DC, 1984, p. 197.
19 M. A. Quilliam, B. A. Thomson, G. J. Scott and K. W. M. Siu, *Rapid Commun. Mass Spectrom.*, 3 (1989) 145.
20 J. W. Jorgenson and K. D. Lukacs, *Anal. Chem.*, 53 (1981) 1298.
21 J. W. Jorgenson and K. D. Lukacs, *Science*, 22 (1983) 266.
22 A. G. Ewing, R. A. Wallingford and T. M. Olefirowicz, *Anal. Chem.*, 61 (1989) 292.
23 B. W. Wright, G. A. Ross and R. D. Smith, *J. Microcolumn Sep.*, 1 (1989) 85.
24 J. Leggett-Bailey, *Techniques in Protein Chemistry*, Elsevier, London, 2nd ed., 1967, p. 41.
25 R. D. Smith, J. A. Loo, C. J. Barinaga, C. G. Edmonds and H. R. Udseth, *J. Chromatogr.*, 480 (1989) 211.
26 R. S. Rogers and H. Rapaport, *J. Am. Chem. Soc.*, 102 (1980) 7335.
27 S. Hall, P. B. Reichardt and R. A. Neve, *Biochem. Biophys. Res. Commun.*, 97 (1980) 649.

28 P. D. Grossman, H. H. Lauer, S. E. Moring, D. E. Mead, M. F. Oldman, J. H. Nickel, J. R. P. Goudberg, A. Krever, D. H. Ransom and J. C. Colburn, *Am. Biotechnol. Lab.*, Feb. (1990) 35.
29 E. D. Lee, W. Müch, J. D. Henion and T. R. Covey, *Biomed. Environ. Mass Spectrom.*, 18 (1989) 844.
30 N. J. Reinhoud, W. M. A. Niessen, U. R. Tjaden, L. G. Gramberg, E. R. Verheij and J. van der Greef, *Rapid Commun. Mass Spectrom.*, 3 (1989) 348.
31 M. J. F. Suter and R. M. Caprioli, in *Proceedings of the 39th ASMS Conference on Mass Spectrometry and Allied Topics, Tucson, AZ, June 3–8, 1990*, p. 1331.
32 P. D. Grossman, K. J. Wilson, G. Petrie and H. L. Lauer, *Anal. Biochem.*, 173 (1988) 265.
33 K. D. Altria and C. F. Simpson, *Chromatographia*, 24 (1988) 527.
34 J. Walter, S. W. Ayer, S. Pleasance, M. A. Quilliam, P. Thibault and J. L. C. Wright, personal communication.
35 J. J. Sullivan, M. M. Wekell and L. L. Kentala, *J. Food Sci.*, 50 (1985) 26.

Journal of Chromatography, 542 (1991) 502–507
Elsevier Science Publishers B.V., Amsterdam

CHROM. 23 068

Short Communication

Preparative liquid chromatographic separation of isomers of 4-amino-3-(4-chlorophenyl)butyric acid

CLAUDE VACCHER, PASCAL BERTHELOT, NATHALIE FLOUQUET and MICHEL DEBAERT*

Laboratoire de Pharmacie Chimique, Université de Lille II, 3 Rue du Pr. Laguesse, 59045 Lille Cédex (France)

(First received September 12th, 1990; revised manuscript received December 4th, 1990)

ABSTRACT

A liquid chromatography method was developed for the chiral resolution of [4-amino-3-(4-chlorophenyl)butyric acid isomers. The compound was derivatized in two steps: protection of the amino group with di-*tert.*-butyl carbonate and reaction with (*S*)-α-methyl benzyl amine to obtain the diastereomeric mixture *RS* and *SS*. Chromatography was carried out on silica gel (5–20 μm) employing *n*-hexane–ethyl acetate as eluent. ^{1}H NMR spectroscopy and analytical high-performance liquid chromatography indicated that the separated fractions were pure.

INTRODUCTION

We are particularly interested in the synthetic preparation of GABA derivatives and especially in GABA-B analogues such as baclofen [4-amino-3-(4-chlorophenyl) butyric acid; β-(*p*-chlorophenyl)-GABA] [1]. Baclofen is used to relieve symptoms of spasticity in patients suffering from sclerosis and spinal lesions [2–5]. The enantiomers were found to have different properties, so the optical resolution of racemates is essential [6]. β-Phenyl-GABA have been resolved by fractional crystallization of cinchonidine [7] or α-methylbenzylamine [8] salts. Resolution based on diastereoisomeric salt has the disadvantage that crystallization is crucial and that the optical purity of the salts relies mainly on chiroptical measurements depending of the concentration of the analyte, solvent and temperature. In high-performance liquid chromatography (HPLC), optical resolution of baclofen enantiomers for preparatives purposes was achieved using a chiral mobile phase [9]. The same resolution by the liquid chromatographic separation of diastereoisomers has been suggested but literature data on the subject are incomplete [5]. Preparative high-performance liquid chromatography (HPLC) seemed the most appropriate method for this purpose in

0021-9673/91/$03.50

order to avoid the disadvantage of crystallization and to perform an easy work-up, with a view to extending it to various GABA derivatives. In this paper we describe the results for the HPLC resolution of baclofen after derivatization. A direct scale-up from the analytical to the preparative mode was achieved with only slight changes in the chromatographic conditions. Unmodified silica was used as the stationary phase and *n*-hexane–ethyl acetate as the mobile phase, with UV detection.

EXPERIMENTAL

Baclofen was kindly supplied by Ciba-Geigy.

Analytical HPLC was carried out with an LKB Model 2249 metering pump at a flow-rate of 1 or 1.5 ml/min with an injection valve (20-μl loop). Detection was performed with an HP 1040 photodiode-array spectrophotometer connected to an HP 9000 S300 computer. UV spectral characteristics were measured by HPLC with diode-array detection to confirm peak homogeneity and purity. A Spherisorb 5 Sil (5 μm) column (250 mm × 4.6 mm I.D.) from Laboratory Data Control (LDC) was used with *n*-hexane–ethyl acetate in various proportions as the eluent. The samples were dissolved in ethyl acetate. Preparative HPLC separations were made with an LDC Constametric III metering pump at a flow-rate of 6 ml/min on a 40 mm I.D. column of silica gel (5–20 μm; 100 g), with *n*-hexane–ethyl acetate in various proportions as the eluent. Detection was performed with an LDC multi-wavelength spectromonitor D at 260 nm. Three samples (mass injected = 300, 380 and 438 mg) were dissolved in 10 ml of pure ethyl acetate, owing to their low solubility in *n*-hexane. All experiments were performed at ambient temperature. The solvents used were of analytical-reagent grade from Merck.

Derivatization was undertaken in two steps (Fig. 1): the first involved treatment of baclofen with di-*tert.*-butyl carbonate to protect the amino group [10], and the second was reaction with (*S*)-α-methylbenzlamine according to the mixed anhydride method [11]. This furnished a mixture of *RS* (compound 1) and *SS* (compound 2) diastereomers, resolved by chromatography. This pathway has been reported previously but no experimental details were given [5].

The purity of the separated components was checked by thin-layer chromatography (TLC), analytical HPLC and routine ^{1}H NMR spectroscopy at 80 MHz. The different fractions were compared with pure *RS* and *SS* compounds prepared unambiguously from the corresponding *R* and *S* isomers of baclofen following the same reaction scheme.

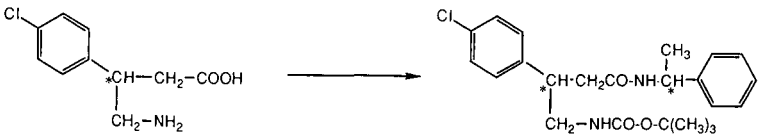

Baclofen

RS 1
SS 2

Fig. 1. Scheme of the reaction.

RESULTS

Analytical HPLC resolution of baclofen isomers has been widely published [12–14] but preparative HPLC has not been extensively studied [5,6,9], and this justified our work to set up a procedure and to optimize the resolution.

Derivatization of baclofen in two steps gave a mixture of diastereoisomers as a glassy viscous oil. The enantiomeric ratios of the starting racemate 1 and 2, obtained by NMR and HPLC, are similar (ratio $\approx$ 1). At 80 MHz the diastereomers were readily distinguished by their spectra in that the chemical shifts for the $CH(CH_3)$ methyl doublets differed by 0.10 ppm: δ = 1.28 ppm (d, J = 6.9 Hz, compound 1, *RS*) and 1.38 ppm (d, J = 6.9 Hz, compound 2, *SS*). More complete data at 300 MHz will be published elsewhere. The analytical HPLC data are summarized in Table I. An example of an analytical chromatogram is given in Fig. 2: the *RS* isomers (compound 1) is eluted before the *SS* isomer (compound 2). An analytical HPLC study of the effect of the percentage of *n*-hexane (20–60%) on the capacity factors (identification), selectivity of resolution (α) and resolution (R) was undertaken. An increase in *n*-hexane concentration (at a flow-rate of 1.5 ml/min) resulted in a corresponding increase in retention. The changes in identification (k'_1, 0.64–4.79; k'_2, 1.20–10.05) α (1.80–2.10) and R (2.52–5.74) are significant. When developing an analytical method for scale-up to the preparative mode, it is desirable to have an analytical resolution (R) greater than 2 and a capacity factor (identification) of less than 5, the latter because of the shorter run times obtained and a corresponding increase in the throughput (mg/h of chemical) for the purification. In fact, for an *n*-hexane–ethyl acetate (60:40) mobile phase, where k'_1 = 4.79 and k'_2 = 10.05, the retention times in the preparative HPLC become prohibitive, with t_1 = 220 and t_2 = 501 min.

The first attempted resolution by recrystallization of the diastereomeric mixture in various solvents such as *n*-hexane or diisopropyl ether was unsuccessful, leading only to enrichment of some of the diastereomers; thus from the starting material (mass m = 1118 mg; ratio $\approx$ 1) we collected three fractions (m = 300, 380 and 438 mg) with the corresponding ratios 0.55, 0.59 and 2.00.

In a second attempt, using those fractions, we undertook a preparative separation by chromatography and tried to optimize the conditions by modifying the

TABLE I

ANALYTICAL HPLC: CAPACITY FACTORS (k') SELECTIVITY OF RESOLUTION (α) AND RESOLUTION (R) OF COMPOUNDS 1 AND 2 (*RS* AND *SS*)

Capacity factor identification = $(t_x - t_0)/t_0$; separation factor $\alpha = (t_2 - t_0)/(t_1 - t_0)$; peak resolution $R = 2(t_2 - t_1)/(w_1 + w_2)$; w = width at baseline; t_0 = retention time of an unretained compound; t_x = retention time of compound 1 or 2.

Mobile phase (*n*-hexane–ethyl acetate)	Flow-rate (ml/min)	k'_1	k'_2	α	R
20:80	1	0.65	1.22	1.87	2.66
20:80	1.5	0.64	1.20	1.80	2.52
50:50	1.5	2.68	5.49	2.05	3.93
60:40	1.5	4.79	10.05	2.10	5.74

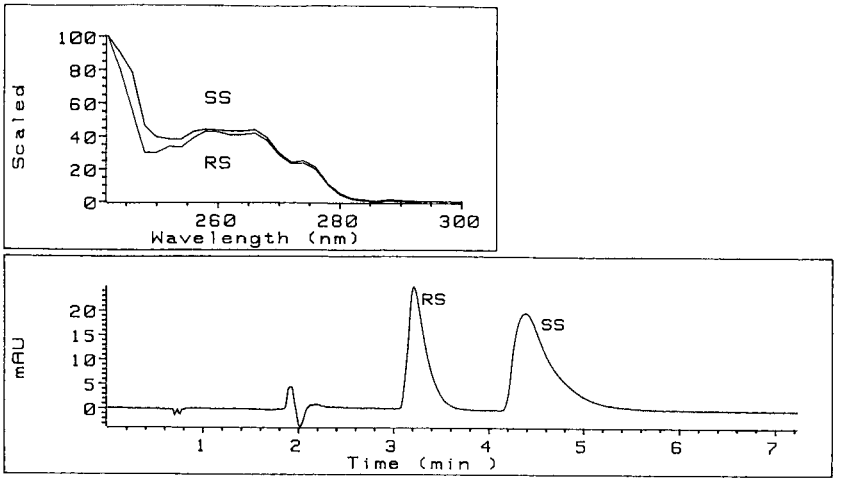

Fig. 2. Analytical HPLC of starting material and UV spectrum of each diastereomer. Eluent, *n*-hexane–ethyl acetate (20:80). Detection at 260 nm.

mobile phase composition. The preparative data are given in Table II. A chromatogram of a preparative separation is shown in Fig. 3. The average recovery of the preparative procedure, calculated on three injections, was 86% with a mean injected mass of 370 mg. The average isomer ratio, calculated on three injections, was 0.97 (*RS*/*SS*). No conclusion can be drawn from the loading effects; the injected masses are too close, as also are the yields observed. Nevertheless, the lower yield (74%) is certainly due to the tailing of the peaks caused by a much less effective eluting solvent, *n*-hexane–ethyl acetate (60:40). This gives rise to a higher loss of compounds during the fractionation. Much larger loadings could be made by using a less effective eluting solvent [*e.g.*, *n*-hexane–ethyl acetate (60:40)] but with the disadvantage of a higher run time (*e.g.*, $t_1 = 220$, $t_2 = 501$ min).

TABLE II

PREPARATIVE HPLC: RETENTION TIMES (t_1 AND t_2) OF COMPOUNDS 1 AND 2 (*RS* AND *SS*)

Flow-rate, 6 ml/min; m_{1+2}, m_1, m_2 = collected masses of compounds 1+2, 1 and 2.

Mobile phase composition (*n*-hexane–ethyl acetate)	Retention time (min)		Mass injected (mg)	Ratio[b]	Mass recovered (mg)			Ratio[a]
	t_1	t_2			m_{1+2}	m_1	m_2	
20:80	41	67	438	2.09	420 (96)[c]	284	135	2.10
40:60	70	106	380	0.52	308 (81)[c]	108	200	0.51
60:40	220	501	300	0.55	221 (74)[c]	75	146	0.54

[a] Ratio defined as m_1/m_2 (*RS*/*SS*).
[b] Initial ratio calculated from analytical HPLC.
[c] Yield (%) in parentheses.

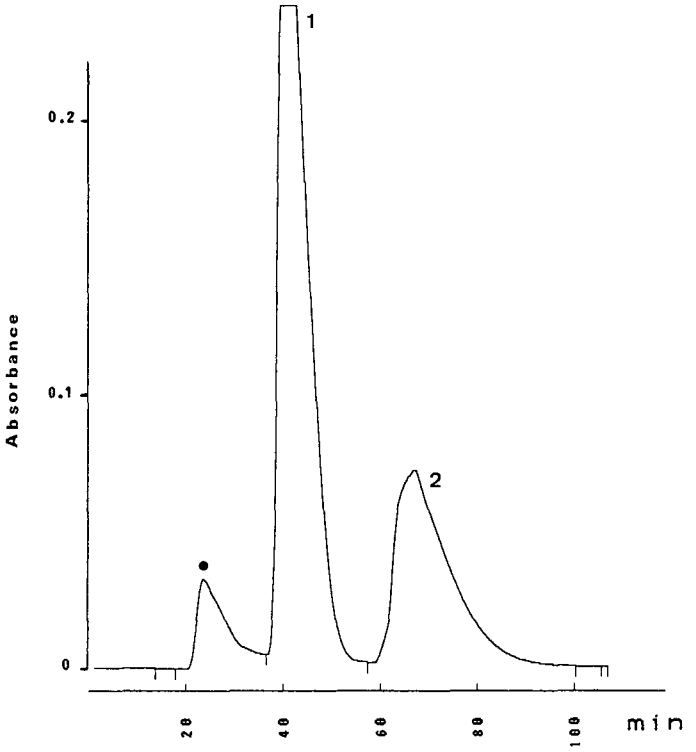

Fig. 3. Preparative chromatogram. Eluent, *n*-hexane–ethyl acetate (20:80). Detection at 260 nm. Mass injected = 438 mg; volume injected = 10 ml; ratio m_1/m_2 = 2.10. ● = Impurity.

It was possible to demonstrate by ^{1}H NMR spectroscopy and analytical HPLC that the separated fractions were pure (>99%). Preparative HPLC proved to be a rapid and economic method for isolating the isomers of GABA analogues. Hydrolysis of the diastereomers in hydrochloric acid medium leads to the enantiomers [6,15].

ACKNOWLEDGEMENTS

We gratefully acknowledge Ciba-Geigy (Rueil-Malmaison, France; Basle, Switzerland) for the generous provision of (±)-(*RS*)-baclofen, (−)-(*R*)-blaclofen hydrochloride and (+)-(*S*)-baclofen hydrochloride.

REFERENCES

1 P. Berthelot, C. Vaccher, A. Musadad, N. Flouquet, M. Debaert and M. Luyckx, *J. Med. Chem.*, 30 (1987) 743.
2 N. G. Bowery, *Trends Pharmacol. Sci.*, 3 (1982) 400.
3 D. R. Hill and N. G. Bowery, *Nature (London)*, 290 (1981) 149.
4 N. G. Bowery, *Trends Pharmacol. Sci.*, 10 (1989) 401.

5 H. R. Olpe, H. Demiéville, V. Baltzer, W. L. Bencze, W. P. Koella, P. Wolf and H. L. Hass, *Eur. J. Pharmacol.*, 52 (1978) 133.
6 R. D. Allen, M. C. Bates, C. A. Drew, R. K. Dukes, T. W. Hambley, G. A. R. Johnston, K. N. Mewett and I. Spence, *Tetrahedron*, 46 (1990) 2511.
7 M. Sobocinska, G. Kupryszewski and M. M. Zobaczewa, *Rocz. Chem.*, 17 (1974) 461.
8 N. A. Sirov, R. A. Gracheva, V. M. Potapov, L. G. Polevoi and I. P. Neumyvakin, *Otkytiya, Izobret., Prom. Obraztsy. Tovarnye Znaki.*, 17 (1981) 88.
9 R. P. Weatherby, R. D. Allen and G. A. R. Johnston, *J. Neurosci. Methods*, 10 (1984) 23.
10 L. Moroder, A. Hallett, E. Wunsch, O. Keller and G. Wessin, *Hoope Seyler's Z. Physiol. Chem.*, 357 (1976) 1651.
11 C. Vaccher, P. Berthelot, N. Flouquet and M. Debaert, *Synth. Commun.*, 19 (1989) 3535.
12 E. W. Wuis, E. W. J. Beneken Kolmer, L. E. C. Van Beijsterveldt, R. C. M. Burgers, T. B. Vree and E. Van der Kleyn, *J. Chromatogr.*, 415 (1987) 419.
13 A. M. Rustum, *J. Chromatogr.*, 487 (1989) 107.
14 H. Spahn, D. Krauss and E. Mutschler, *Pharm. Res.*, 5 (1988) 107.
15 R. N. Comber and W. J. Brouillette, *J. Org. Chem.*, 52 (1987) 2311.

Journal of Chromatography, 542 (1991) 508–514
Elsevier Science Publishers B.V., Amsterdam

CHROM. 23 106

Short Communication

Rapid isolation of a neurohormone from mosquito heads by high-performance liquid chromatography

GEOFFREY D. WHEELOCK and KLAUS P. SIEBER
Department of Entomology, Cornell University, Ithaca, NY 14853 (U.S.A.)
and
HENRY H. HAGEDORN*
Department of Entomology and Center for Insect Science, University of Arizona, Tucson, AZ 85721 (U.S.A.)
(First received June 11th, 1990; revised manuscript received January 3rd, 1991)

ABSTRACT

Methods were developed for the isolation of the egg development neurosecretory hormone, EDNH, from heads of the mosquito *Aedes aegypti*. This hormone stimulates ecdysone production by ovaries. Methods used for the successful isolation of insulin-like peptides from vertebrate tissues were modified to develop a four-step procedure involving extraction in acidified ethanol, precipitation by neutralization, followed by sequential separation on size-exclusion, ion-exchange and reversed-phase high-performance liquid chromatography columns.

INTRODUCTION

The egg development neurosecretory hormone (EDNH), first identified in the mosquito by Lea [1], is necessary for egg development to occur normally after a blood meal. This hormone is produced by neurosecretory cells in the medial portion of the brain and released from neurohemal sites lying along the aorta [2]. We have shown that EDNH stimulates the ovary to produce ecdysone [3]. Several attempts have been made to isolate EDNH [4–8]. A functionally related molecule, Bombyxin (which was earlier known as 4K-PTTH), was isolated from *Bombyx mori* on the basis of the fact that it stimulated ecdysone production by the prothoracic glands of *Samia cynthia ricini* [9–10]. However, it has no effect on *B. mori* glands, and it has been suggested that its role in *B. mori* is to stimulate ecdysone production by the ovary [11]. Bombyxin is closely related to insulin [9]. This line of reasoning led us to consider whether methods used for the isolation of hormones related to insulin from vertebrate tissues might work in the isolation of EDNH. We report here that techniques developed for the initial extraction of insulin-like peptides were useful for extracting EDNH. In

0021-9673/91/$03.50

addition we report on improved techniques for using high-performance liquid chromatography (HPLC) to isolate EDNH.

EXPERIMENTAL

Animals

Larval mosquitoes (*Aedes aegypti* derived from the Rock strain) were mass reared at 26.5 ± 0.5°C in 20 shallow pans (38 × 144 cm) containing $1\frac{1}{2}$ cm of water and approximately 2000 larvae. They were fed on a solution containing 45 g mouse and hamster chow (Agway 32000 meal), 35 yeast hydrolysate and 45 g lactalbumin hydrolysate suspended in 1 liter of distilled water, the whole autoclaved before use. The feeding schedule was:

Day	1	2	3	4	5	6	7
ml	20	10	0	30	30	10–50	0–50

Pupae were collected on day 8 and adults emerged on days 9–11. Adults were maintained on a 3% sucrose solution in 12 l containers and harvested on day 16.

Preparation of heads

Adults were collected by gentle vacuuming and frozen at −70°C. Heads were isolated by shaking frozen adults in a chilled erlenmeyer flask and sieving the body parts through U.S.A. Standard testing sieves. Sieves 20 and 25 contained thoraces and abdomens while sieve 40 contained female and male heads and legs. Heads were separated from legs by letting them roll to the side of the sieve and aspirating them into a collection flask. Contamination with other body parts was negligible. Heads were lyophilized and stored at −70°C.

Solutions

Extraction buffer: 1 ml conc. HCl was added to 40 ml absolute ethanol, water was then added to a total volume of 50 ml. Size-exclusion chromatography (SEC) buffer: 20 m*M* phosphate buffer (HPLC-grade phosphoric acid adjusted to pH 6.5 with 1 *M* NaOH) containing 200 m*M* NaCl, 1 m*M* thiodiglycol and 1 m*M* EDTA (thiodiglycol is added just prior to use)). Ion-exchange chromatography (IEX) buffers: 50 m*M* Tris stock (pH 7.2 obtained by mixture of Tris base and Tris acid); IEX buffer A = 200 ml Tris stock, 100 ml isopropanol diluted to 1 l and filtered; IEX buffer B = IEX buffer A plus 500 m*M* NaCl. Analytical reversed-phase (ARP) buffers: ARP buffer A = m*M* phosphate (HPLC-grade phosphoric acid adjusted to pH 6.5 with 1 *M* NaOH) containing 150 m*M* NaCl; ARP buffer B = equal volumes of ARP buffer A and isopropanol. Microbore reversed-phase (MRP) buffers: MRP buffer A = 0.01% trifluoroacetic acid; MRP buffer B = 60% acetonitrile in 0.01% trifluoacetic acid, (TFA). Solvents were HPLC grade. Buffers and solvents were filtered through a 0.2-μm filter and degassed with helium prior to use.

Extraction of heads

In a standard preparation, 0.5 g of lyophilized heads (about 14 000 heads) were homogenized in 20 ml of ice cold extraction buffer using a motor driven 50-ml PTFE

homogenizer for about 25 strokes. The extract was centrifuged at 4°C at 15 000 *g* for 10 min. The pellet was reextracted in 10 ml of extraction buffer. The two supernatants were combined and centrifuged again. While keeping the extract on ice, 600 μl of 500 m*M* Tris pH 7.7 was added and the pH was adjusted to 7.5 to 8.0 by slowly adding 1 *M* NaOH. The pH was checked for stability after 10 min. Absolute ethanol was added to a final concentration of *ca.* 95% and the solution was held on ice overnight. The precipitate containing EDNH activity was removed by centrifugation at 15 000 *g* and dried under vacuum. The precipitate was then homogenized in 5 ml of 6 *M* urea prepared just before use and deionized by stirring with 1/5 volume of Dowex MR-3 ion exchanger (Sigma). The homogenate was mixed for 30–45 min by gentle shaking at room temperature. The non-solubilized material was pelleted and the supernatant was recentrifuged.

High-performance liquid chromatography

Instrumentation. LKB Ultra Chrom GT; BioSeparation System (Pharmacia LKB, Piscataway, NJ, U.S.A.).

Programmed gradients. Program No. 1 (ion exchange): 0–100% IEX buffer B in 50 min starting 5 min after injection, flow-rate 0.5 ml/min. Progam No. 2 (analytical reversed phase): 0–10% ARP buffer B in 13 min, 10–36% ARP buffer B in 2 min, 36–56% ARP buffer B in 30 min, 56–100% ARP buffer B in 22 min, flow-rate 1 ml/min. Program No. 3 (microbore reversed-phase column): 0–8% MRP buffer B in 5 min, 8–100% MRP buffer B in 55 min, flow-rate 1 ml/min.

Size-exclusion chromatography. Column: Altex Spherogel TSK-G 2000 SWg, 30 cm × 21.5 mm (Beckman, San Ramon, CA, U.S.A.). Conditions: The column was equilibrated for 18 h with 500 ml SEC buffer. The head extract (3 ml) was prepared by centrifuging in a microfuge 2 × for 10 min and injected at a flow-rate of 1 ml/min for 5 min and then 1.5 ml/min for the remainder of the run. Fractions of 3 ml were collected. Active fractions were concentrated in a dialysis bag (3500 cut off) against polyethylene glycol compound (Sigma) at 4°C until the volume was reduced to 0.5 ml. They were then dialyzed against IEX buffer A for 2 h.

Ion-exchange chromatography. Column: Altex Spherogel (DEAE-55W, 7.5 cm × 7.5 mm, 10 μm (Beckman). Conditions: The column was equilibrated with IEX buffer B at 0.5 ml/min for 30 min followed by buffer A at 0.5 ml/min for 2 h. The sample was prepared for injection by removing the sample, including the precipitate, from the dialysis bag. The sample was diluted to 3 ml with buffer A, and mixed gently for 15 min at room temperature. After centrifugation in a microfuge for 10 min the sample was injected at 0.5 ml/min and eluted using program No. 1. Five minutes after starting the gradient, the loop was disconnected from the buffer flow. Fractions of 2 ml were collected. Neurotensin (20 μg) was added to the active fractions as a carrier.

Analytical reversed-phase chromatography. Column: Analytical Vydac C_8 pH stable 25 cm × 2.1 mm (Alltech, Deerfield, IL, U.S.A.). The column was equilibrated at 1 ml/min with methanol for 30 min, water for 10 min and then ARP buffer A for 30–60 min. Prior to the run, 20 μg of neurotensin (40 μg/ml) was injected for 2 min at 1 ml/min and eluted using program No. 2. After elution of neurotensin (which was saved for later use), the active fraction from the IEX column was injected and eluted as described above. Fractions of 3 ml were collected. Purified neurotensin (20 μg) was added to the active fractions which were then frozen.

Microbore reversed-phase chromatography. Column: Brownlee Aquapore RP-300 C_8, 30 × 2.1 mm column in an HPLC cartridge (Raining, Woburn, MA, U.S.A.). The column was washed with 5 ml of buffer B and then equilibrated with buffer A. Neurotensin, purified on a reversed-phase column, was injected in 0.01% TFA and eluted using program No. 3. Fractions containing activity from the analytical reversed-phase column were reduced in volume by lyophilization and made up to 0.01% TFA by adding 0.1% TFA, injected onto the column and eluted using program No. 3. Fractions of 3 ml were collected and 15 μg of BSA in water were added to fractions which were then frozen and lyophilized prior to bioassay.

Bioassay of fractions

Ovaries were dissected from 3–6 day old mosquitoes, rinsed five times with sterile saline and divided into groups of 20 ovaries which were incubated for 6 h at 25°C in 50 μl of saline containing a dilution of the fraction being tested. Fractions were assayed in duplicate. The incubation medium was then assayed for the presence of ecdysone using a radioimmunoassay [3]. As high doses of EDNH are inhibitory [3], several doses were assayed to ensure that the linear portion of the response was obtained. Protein content of the fractions was determined using the method of Bradford [12] using BSA as a standard, or, for the microbore column, by area of the peak using neurotensin as a standard. To show that fractions active in the ovary bioassay also stimulated egg development *in vivo*, extracts were injected into blood-fed, decapitated, females as described by Wheelock and Hagedorn [13].

RESULTS

Previous studies had shown that EDNH retains activity after boiling, is fairly hydrophobic and contains disulfide bonds [4]. Although boiling achieved some degree of purification we wanted to avoid boiling because it caused erratic chromatographic behavior. Extraction with saline exposes the peptide to enzymatic acitivity and is not selective. We therefore extracted in acid ethanol which has been used in purification of insulin-like growth factors [14]. Acid–ethanol extracts molecules in the size range of EDNH; it is therefore somewhat selective. The pellet containing EDNH activity was extracted with 6 *M* urea to avoid non-specific interaction of EDNH with other proteins, as suggested by work with relaxin [15]. Using this technique, over 90% of the activity was extracted and 3- to 6-fold purification was achieved, as compared to saline extracts. The specific activity of the extract was 2 to 4 head equivalents/μg of protein. Acetone extracts were less successful. Although high recoveries were achieved with acetone, subsequent elution patterns on columns were not reproducible.

Having developed an efficient method for the initial extraction we then turned to methods for isolating EDNH from the acid–ethanol–urea extract. After trying a number of columns and elution techniques, we developed a purification scheme that involved the sequential use of size exclusion, ion exchange, and C_8 reversed-phase HPLC columns.

SEC of the initial extract showed that the acid–ethanol method removed the bulk of the proteins leaving only molecules in the size range of EDNH (Fig. 1A). Despite the coelution of EDNH activity with the major peak of protein, this column

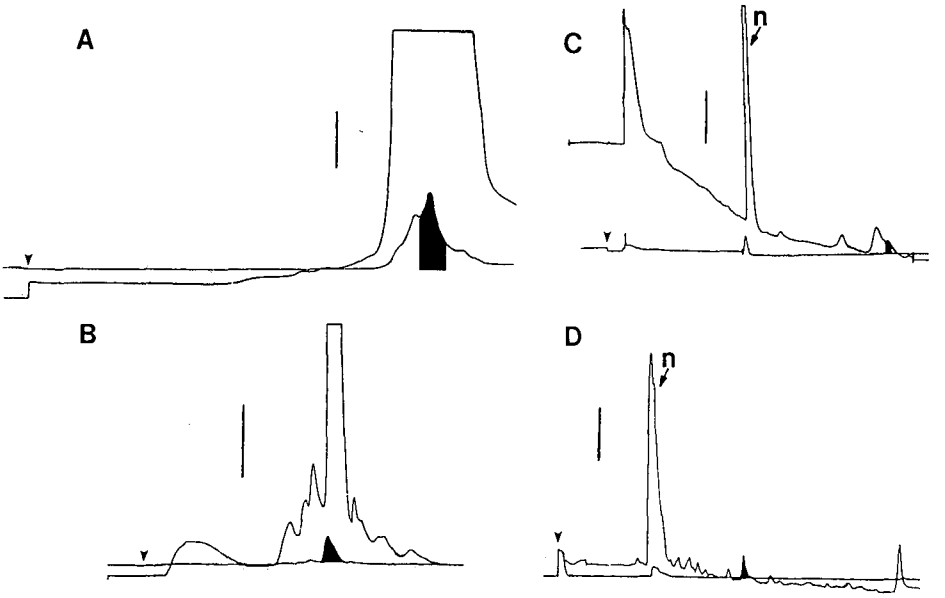

Fig. 1. Separation of EDNH activity from head extracts of *Aedes aegypti* using a size-exclusion column (A), ion-exchange column (B), analytical reversed-phase C_8 column (C), and a microbore reversed-phase C_8 column (D). The arrow head indicates the time of injection; n = neurotensin, an added carrier. The traces represent absorbance at 280 (A and B) and 206 (C and D) nm at two different sensitivities. The bar on the left of each figure represents 0.2 absorbtion units. Shaded areas indicate fractions with EDNH activity.

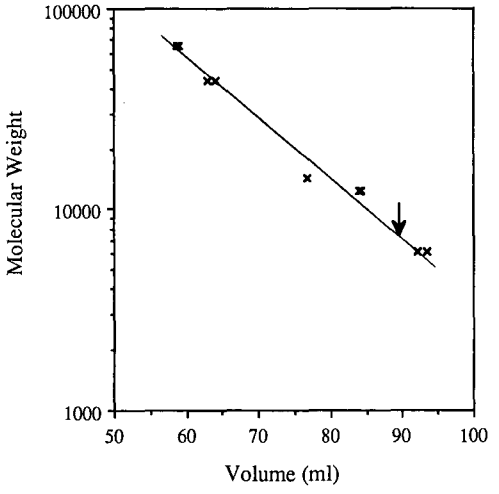

Fig. 2. Molecular weight determination by size-exclusion chromatography. Standards used included bovine serum albumin (65 000 dalton), ovalbumin (43 500), soybean trypsin inhibitor (14 300), cytochrome *c* (12 400), and insulin (6100). Points indicate results from two separate experiments. The arrow indicates the elution of EDNH activity.

achieved 3- to 7-fold purification with up to 90% recovery of acitivity. The specific activity of the active fractions from the SEC column in several experiments ranged between 8 and 25 head equivalents/μg of protein. The elution of the active fraction indicated an approximate molecular weight of 7500 (Fig. 2) in agreement with previous results [4].

The IEX column (Fig. 1B) achieved an 8-fold purification while allowing the recovery of up to 80 to 100% of the EDNH activity. The specific activity increased to 100 to 200 head equivalents/μg of protein.

Losses were greater on the analytical C_8 column (Fig. 1C) with recoveries of about 50%. But the specific activity of the active fraction of this column rose to over 600 head equivalents/μg of protein, and a 30-fold purification was achieved in this step. At this stage a greater than 10 000-fold purification had been achieved with recoveries of about 25%. Injection of 1.0 μl of the active fraction into females that were blood fed and decapitated caused egg maturation in 14 out of 17 injected females, thus showing that the purified material had the expected effects *in vivo* [13].

The active fraction from the C_8 column was still not pure as shown by the presence of multiple peaks in a subsequent separation of the active fraction on a microbore C_8 column (Fig. 1D). This column is a good candidate for the final step in isolation of EDNH.

DISCUSSION

The size and characteristics of EDNH, and the fact that the only source of this hormone is whole heads of mosquitoes, have made this a very difficult molecule to isolate and characterize. Nevertheless, EDNH is clearly an important insect hormone. In the mosquito is is thought to be released within hours after a blood meal where upon it stimulates the production of ecdysone by the ovary, thus beginning the process of vitellogenin synthesis [13]. The ovaries of many insects have been shown to produce ecdysteroids at some stage during the growth of the oocyte and the presence of factors with activities similar to EDNH have been detected.

Several groups have attempted to isolate EDNH with varying degrees of success [4–8, 13]. Our first effort, utilizing classical liquid chromatography, was hampered by lack of separation power of the techniques [4]. Separations were greatly improved by the development of HPLC [5], but recoveries were very low. As reported here, the development of HPLC columns specifically designed for peptide and protein separations our recoveries improved, but we also believe that the use of carrier protein avoids losses during the final steps of the isolation procedures. Neurotensin was added to the active fractions from the ion-exchange columns and the C_8 column. Neurotensin was chosen as a carrier because it elutes long before EDNH in both the ion-exchange and C_8 columns. We also found it important to add bovine serum albumin as a carrier to fractions that were to be bioassayed.

EDNH is functionally related to the prothoracicotropic hormone (PTTH) that stimulates ecdysone production by the prothoracic glands in immature insects. Definitive evidence that they are related awaits a sequence of EDNH. A hormone isolated from heads of adult *B. mori* was originally described as PTTH [10] but may, in fact, be more related to EDNH [11]. This molecule, recently renamed bombyxin, is closely related to insulin both in primary and secondary structure [9]. The work on Bombyx-

in suggested to us that methods used to isolate insulin-like peptides [14,15] might be successfully used for the isolation of EDNH. We have found that this was indeed true for both the acid–ethanol extraction of whole heads [14], and the use of urea to reduce hydrophobic interactions between EDNH and other molecules [15]. Another advantage of these techniques is that they avoid the use of a boiling step which we [4], and others [8], have used in the past and which may adversly affect the peptide.

The methods presented here for isolation of EDNH are relatively rapid compared to the more complex methods that have been used in the past [8,9]. It takes less than a week from extraction of the heads to the microbore C_8 column. Doing the bioassay after each column run will add several days per assay. We found, however, that the pattern of UV absorbance is a reproducible guide to active peaks, so that once the active peaks have been identified, the bioassay need not be done each time.

ACKNOWLEDGEMENTS

This work was supported in part by National Institutes of Health grant AI 14771 to H.H.H. and by the New York Agricultural Experiment Station (project 420).

REFERENCES

1 A. O. Lea, *J. Insect Physiol.*, 13 (1967) 419.
2 S. M. Meola and A. O. Lea, *Gen. Comp. Endocrinol.*, 18 (1972) 210.
3 H. H. Hagedorn, J. P. Shapiro and K. Hanaoka, *Nature (London)*, 282 (1979) 92.
4 K. Hanaoka and H. H. Hagedorn, in J. A. Hoffmann, (Editor), *Progress in Ecdysone Research*, Elsevier/North Holland Biomedical Press, Amsterdam, 1980, p. 467.
5 E. P. Masler, H. H. Hagedorn, D. H. Petzel and A. B. Borkovec, *Life Sci.*, 33 (1983) 1925.
6 D. Borovsky and B. R. Thomas, *Arch. Insect Biochem. Physiol.*, 2 (1985) 265.
7 L. R. Whisenton, T. J. Kelly and W. E. Bollenbacher, *Mol. Cell. Endocrinol.* 54 (1987) 171.
8 S. Matsumoto, M. R. Brown, A. Suzuki and A. O. Lea, *Insect Biochem.*, 19 (1989) 651.
9 M. Iwami, A. Kawakami, H. Ishizaki, S. Y. Takahashi, T. Adachi, Y. Suzuki, H. Nagasawa and A. Suzuki, *Develop. Growth Diff.*, 31 (1989) 31.
10 H. Nagasawa, H. Kataoka, A. Isogai, S. Tamura, A. Suzuki, A. Mizoguchi, Y. Fujiwara, A. Suzuki, S. Y. Takahashi and H. Ishizaki, *Proc. Nat. Acad. Sci. U.S.A.*, 83 (1986) 5840.
11 L. I. Gilbert, W. E. Bollenbacher, N. Agui, N. A. Granger, B. J. Sedlak, S. D. Gibb and C. M. Buys, *Am. Zool.*, 21 (1981) 641.
12 M. M. Bradford, *Anal. Biochem.*, 72 (1976) 248.
13 G. D. Wheelock and H. H. Hagedorn, *Gen. Comp. Endocrinol.*, 60 (1985) 196.
14 J. F. Cutfield, S. M. Cutfield, A. Carne, S. O. Emdin and S. Falkmer, *Europ. J. Biochem.*, 158 (1986) 117.
15 E. E. Büllesbach, L. K. Gowan, C. Schwabe, B. G. Steinetz, E. O'Brian and I. P. Callard, *Euro. J. Biochem.*, 161 (1986) 335.

Journal of Chromatography, 542 (1991) 515–520
Elsevier Science Publishers B.V., Amsterdam

CHROM. 23 059

Short Communication

Simultaneous determination of chloramphenicol and benzocaine in topical formulations by high-performance liquid chromatography

G. S. SADANA* and A. B. GHOGARE
Department of Chemistry, G. N. Khalsa College, King's Circle, Matunga, Bombay 400 019 (India)
(First received September 10th, 1990; revised manuscript received December 10th, 1990)

ABSTRACT

A reversed-phase high-performance liquid chromatographic method was developed for the simultaneous determination of chloramphenicol and benzocaine in topical solutions and suppositories. The method was statistically evaluated for its accuracy and precision in the assay of chloramphenicol and benzocaine in commercial pharmaceutical preparations. Excipients and impurities normally present did not interfere, and the mean recoveries were 99.68% (R.S.D. = 1.20%) for benzocaine and 99.96% (R.S.D. = 0.66%) for chloramphenicol. A Waters Assoc. Guard-Pak precolumn module with a μBondapak C_{18} precolumn was utilized to protect the analytical column from contamination. The ratio-plotting technique was used to confirm the non-interference of excipients and other impurities with the peak of interest from formulations, and for validation of the method.

INTRODUCTION

Topical solutions and suppositories of chloramphenicol are widely used clinically in bacterial infections of the ear and eyes. The topical solutions are formulated with a local anaesthetic to avoid local irritation produced by chloramphenicol [1]. Benzocaine is commonly used in combination with chloramphenicol in formulations of topical solutions and suppositories.

Topical solutions and suppositories usually consist of large amounts of a non-polar, lipophilic material such as petrolatum, mineral oil or waxes. Prior to analysis, the active ingredients from pharmaceutical preparations normally have to be separated from the complex formulation matrices and analysed individually by conventional pharmacopoeial or literature procedures.

There are various methods for the individual determination of chloramphenicol [2–7] and benzocaine [8–12] in pharmaceutical preparations and biological fluids, but the only procedure reported for the simultaneous determination of these drugs is that

0021-9673/91/$03.50

by Kannan *et al.* [13], using differential spectrophotometry. This procedure involves reduction of the nitro group of chloramphenicol with zinc and hydrochloric acid. Benzocaine and unreacted chloramphenicol were determined by use of differential spectrophotometry. The method is laborious and non-specific.

Hence there is a need for a faster, specific and accurate method for the simultaneous determination of benzocaine and chloramphenicol in topical solutions in a single run, and high-performance liquid chromatography (HPLC) is the method of choice.

EXPERIMENTAL

Chemicals

Chloramphenicol and benzocaine (reference compounds) were donated by Parke-Davis Pharmaceuticals (Bombay, India). The internal standard, sulphamethoxazole, was obtained from Ana-Lab (Bombay, India) and acetonitrile (HPLC grade) from Glaxo Chemicals (Bombay, India). Formulations were obtained from commercially available sources.

Apparatus

The liquid chromatograph consisted of a dual-piston constant-flow pump (Model 510A solvent-delivery system), a programmable multi-wavelength detector with a four-channel monitoring system (Model 490), an autosampler (Model 712 WISP) and a data station (Model 840 with a Model 350 computer) with a Quickset HPLC programme, all from Waters Assoc. (Milford, MA, U.S.A.)

Chromatographic conditions

A reversed-phase 10-μm μBondapak C_{18} column (30 cm $\times$ 3.9 mm I.D.) was used together with a Guard-Pak precolumn module equipped with a disposable μBondapak C_{18} precolumn (Waters Assoc.) at ambient temperature (24 $\pm$ 2°C). The mobile phase was acetonitrile–water (35:65, v/v), filtered and deaerated before use. The flow-rate was 1.4 ml/min at a back-pressure of 1800 MPa. The detector was set at 280 nm (0.05 a.u.f.s.).

Ratio plotting

The other channel of the programmable multi-wavelength detector was set with a ratio-plotting programme with 280 nm as the observation wavelength and 240 nm as the master wavelength. The ratio observation maxima were set at 10% full scale of the recorder response with 0.05 a.u.f.s. detector sensitivity.

Stock solutions

Stock solutions in methanol of chloramphenicol (2.5 mg/ml) (stock solution I), benzocaine (1.0 mg/ml) (stock solution II) and sulphamethoxazole (2.0 mg/ml) (internal standard solution) were prepared.

A 2.0-ml volume of chloramphenicol stock solution I and 1.0 ml of benzocaine stock solution II were pipetted into a 25-ml volumetric flask, followed by addition of 2 ml of internal standard solution and dilution to volume with the mobile phase. The solution was mixed well and 20-μl aliquot of this standard preparation were used in the HPLC assay.

Sample preparations

Ear and eye drops. After shaking thoroughly, the topical solution equivalent to 5 mg of benzocaine or 25 mg of chloramphenicol was accurately pipetted into a 25-ml volumetric flask and diluted to volume with methanol, the vortex mixed for 5 min. A 2.0-ml volume of this solution ws transferred into a 25-ml volumetric flask, followed by addition of 2.0 ml of internal standard solution, and diluted to volume with the mobile phase. Aliquots of 20 μl were used in the HPLC assay.

Ointment. A cream equivalent to 25 mg of chloramphenicol was weighed into a 25-ml volumetric flask, dissolved in methanol, vortex mixed for 15 min and the insoluble excipients were allowed to settle. A 2.0-ml volume of the supernatant was transferred into a 25-ml volumetric flask, followed by addition of 2.0 ml of internal standard solution, and diluted to volume with the mobile phase. It was mixed well and 20-μl aliquots were used directly in the HPLC assay.

Assay procedure

The column was flushed with the mobile phase under the HPLC operating conditions until a stable baseline was obtained. Volumes of 20 μl each of the standard preparation and sample preparations were injected in triplicate at intervals of 15 min. The peak-area ratios of chloramphenicol and benzocaine with respect to the internal standard were calculated. By comparing the peak-area ratios for the standard and sample preparations the amount of each drug could be calculated.

Linearity

Linearity of detection was determined from the calibration graph. Triplicate samples of each of five concentrations of chloramphenicol and benzocaine containing the internal standard were injected onto the HPLC column. A linear correlation was observed between the peak-area ratios of the drug to the internal standard and the concentration of each active ingredient. The method found to be linear over the concentration range 0.04 –0.2 mg/ml for benzocaine and 0.12–0.6 mg/ml for chloramphenicol. The straight lines passed through the origin with a correlation coefficient of 0.9978 for chloramphenicol and 0.9997 for benzocaine.

Recovery

To study the accuracy, precision and reproducibility of the method, a recovery experiment was carried out. To a preanalysed sample, a known amount of standard drug was added at four different levels and each level was analysed at least seven times. From the amount of drug found by the proposed method, the percentage recovery (R) was calculated using the equation $R = 1/N \Sigma [100(Y - Z/X]$, where X is the amount of drug added, Y the amount of drug found, Z the amount of drug in the preanalysed sample and N the number of observation.

RESULTS AND DISCUSSION

The applicability of the proposed method was tested by determining chloramphenicol and benzocaine simultaneously in commercially available combined pharmaceutical preparations, or individually in combination with other ingredients, and the results are presented in Table I. Table II shows the recovery for added drug

TABLE I

HPLC ASSAY OF CHLORAMPHENICOL AND BENZOCAINE IN FORMULATIONS

Sample No.[a]	Formulation	Ingredients	Claimed (mg/ml)	Found (mg)	S.D.[b] (mg)	Recovery (%)
1	Ear drops	Chloramphenicol	50.0	50.06	0.38	100.12
		Benzocaine	10.0	9.82	0.45	98.20
2	Ear drops	Chloramphenicol	50.0	48.93	0.27	97.86
		Benzocaine	10.0	10.14	0.51	101.40
3	Ear drops	Chloramphenicol	50.0	49.18	0.48	98.36
		Prednisolone	5.0	–	–	–
		Lignocaine · HCl	20.0	–	–	–
4	Eye drops	Chloramphenicol	10.0	9.96	0.33	99.60
		Dexamethasone	1.0	–	–	–
5	Eye drops	Chloramphenicol	4.0	4.02	0.56	100.50

[a] Formulation 1 is from Parke-Davis Pharmaceuticals (Bombay, India), 2 from Juggat Pharma (Bangalore, India) and 3–5 are from FDC Pharmaceuticals (Bombay, India). Formulations 1, 2, 3 and 5 contain propylene glycol as vehicle and 4 contains water as vehicle.

[b] $n = 3$.

standards in preanalysed samples of suppositories. A 99.96% recovery (R.S.D. = 0.66%) for chloramphenicol and 99.68% (R.S.D. = 1.20%) for benzocaine indicate non-interference from excipients and high precision of the method. The method is easy to apply as it does not involve the use of any solid buffer for preparation of the mobile phase. Sample preparation is also simple and does not involve labour-intensive extraction for separation of the ingredients or any chemical modification prior to analysis. The proposed method is efficient and fast, as elution of drugs and internal standard is completed within 12 min and the peaks obtained are symmetrical with good resolution between the drugs and the internal standard (Fig. 1a).

Compared with other techniques, the proposed method is highly selective. The use of this method for the simultaneous determination of these drugs is advantageous as both the components have the same absorption maxima and the response of ben-

TABLE II

RECOVERY STUDIES AND STATISTICAL EVALUATION OF THE HPLC METHOD

Level No.	Benzocaine					Chloramphenicol				
	Amount added (mg)	Amount found (mg)	S.D. (mg) ($n=7$)	R.S.D. (%)	Recovery (%)	Amount added (mg)	Amount found (mg)	S.D. (mg) ($n=7$)	R.S.D. (%)	Recovery (%)
1[a]	0	9.86	–	–	–	0	49.31	–	–	–
2	1.12	10.96	0.16	1.46	99.81	4.21	53.45	0.31	0.58	99.86
3	2.24	12.14	0.11	0,99	100.36	8.42	57.59	0.46	0.81	99.76
4	3.36	13.15	0.19	1.44	99.47	12.63	62.08	0.38	0.61	100.23
5	4.48	14.21	0.13	0.91	99.09	16.84	66.11	0.43	0.65	99.94

[a] Preanalysis sample of a topical solution of chloramphenicol and benzocaine in combination.

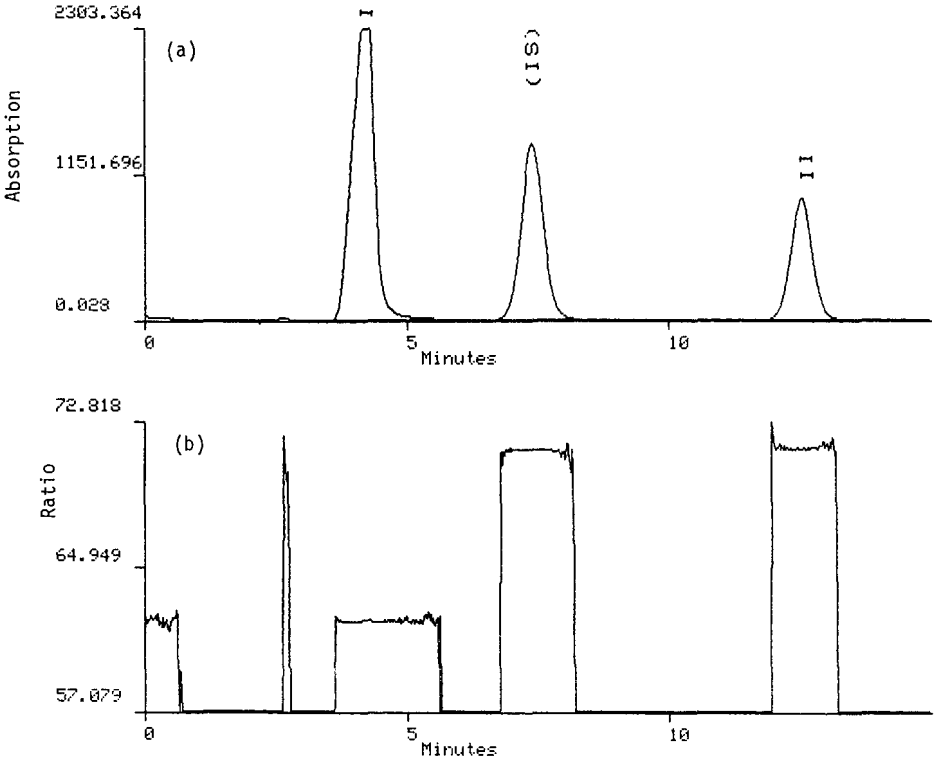

Fig. 1. (a) Typical HPLC trace for chloramphenicol (I, 0.8 mg/ml) and benzocaine (II, 0.18 mg/ml) in pharmaceutical preparations with sulphamethoxazole (IS, 0.4 mg/ml) as an internal standard. Detection, UV, absorption at 280 nm. (b) Ratiogram at observation wavelength 280 nm and master wavelength 240 nm.

zocaine at the observation wavelength, which is approximately five times greater than that of chloramphenicol, compensates for the concentration difference in commercially available combined formulations of these two ingredients. The flat top on the peaks for the drugs and internal standard in the ratiogram of the formulation (Fig. 1b) indicates non-interference from excipients or other impurities from pharmaceutical preparations [14].

Two lots of different formulations containing 0.5% of chloramphenicol and 0.1% of benzocaine were assayed with and without a μBondapak C_{18} precolumn. The retention time, resolution factors and tailing factors were not affected by incorporating the precolumn as an on-line column clean-up system [15]. In our study, we observed that one precolumn can efficiently protect the column during 70–75 sample injections of ointment and 100–110 sample injections of topical solutions. Hence the proposed method can be used for routine quality control analysis of these drug formulations, either for individual drug formulations or in combined dosage forms.

ACKNOWLEDGEMENT

The authors are grateful to the management of Hoechst India Bombay, for providing the instrumental facilities for this work.

REFERENCES

1 N. W. Blacow (Editor), *Martindale, The Extra Pharmacopoeia*, Pharmaceutical Press, London, 26th ed., 1972, pp. 1339–1344.
2 C. S. Sastry, B. G. Rao and K. V. Murthy, *J. Indian Chem. Soc.*, 59 (1982) 1107.
3 H. Tokunaga, T. Kimura and J. Kawamura, *Yakugaku Zasshi*, 100 (1980) 200.
4 N. M. Sanghvi, N. H. Sathe and M. M. Phadki, *Indian Drugs*, 20 (1983) 341.
5 J. Yang, *Yaowa Fenxi Zazhi*, 8 (1988) 40.
6 A. Hulshoff and O. A. Lake, *Chromatographia*, 16 (1982) 247.
7 J. Gal and S. Mayer Lehnert, *J. Pharm. Sci.*, 77 (1988) 1062.
8 S. M. Khanna, Y. K. Agrawal and S. K. Banerjee, *Anal. Lett.*, 15 (1982) 1073.
9 M. E. El-Kammos and K. M. Emara, *Analyst (London)*, 112 (1987) 1253.
10 K. W. Jun, *Pharm. Acta Helv.*, 57 (1982) 290.
11 F. T. Nuggle and C. R. Clark, *J. Assoc. Off. Anal. Chem.*, 66 (1983) 151.
12 T. G. Hurdley, R. M. Smith, R. Gill and A. C. Moffat, *Anal. Proc.*, 23 (1986) 161.
13 K. Kannan, R. Manavalan and A. K. Kelkar, *Indian Drugs*, 25 (1987) 128.
14 A. Drouen, H. Billiet and L. de Galan, *Anal. Chem.*, 56 (1984) 971.
15 N. Maron, E. A. Crasto and A. A. Ramos, *J. Pharm. Sci.*, 77 (1988) 638.

Journal of Chromatography, 542 (1991) 521–525
Elsevier Science Publishers B.V., Amsterdam

CHROM. 23 073

Short Communication

Determination of three active principles in licorice extract by reversed-phase high-performance liquid chromatography

TUNG-HU TSAI
National Research Institute of Chinese Medicine, Taipei (Taiwan)
and
CHIEH-FU CHEN*
Institute and Department of Pharmacology, National Yang-Ming Medical College, Shih-Pai, Taipei 11221 (Taiwan)
(First received October 23rd, 1990; revised manuscript received December 20th, 1990)

ABSTRACT

An improved high-performance liquid chromatographic technique with a photodiode-array detection system for the determination of the active principles of licorice extract such as glycyrrhizin or glycyrrhizic acid (GL), 18α-glycyrrhetinic acid (18α-GA) and 18β-glycyrrhetinic acid (18β-GA) is presented. A reversed-phase column (LiChrospher RP-18, 5 μm) was eluted with a linear gradient of methanol–perchlorate buffer (pH 7.5–7.7) from 1:9 to 10:0 in 120 min. It was found that 58.53 ± 9.14 mg of GL, 5.94 ± 1.60 μg of 18α-GA and 95.25 ± 27.20 μg of 18β-GA were contained in the aqueous extract of 1 g of licorice. The method can determine these components in one analytical step without any pretreatment of the tested sample. Hence this simple method can be used to determine GL and stereoisomers of glycyrrhetinic acid in any licorice extract and traditional Chinese prescriptions.

INTRODUCTION

Licorice or Glycyrrhizae Radix (Chinese name: Gancao), the root of *Glycyrrhiza uralensis* Fisch. (Leguminosae), is one of the most commonly used herbal medicines in traditional Chinese prescriptions. It is also used as a sweetener [1]. Glycyrrhizin or glycyrrhizic acid (GL), one of the active principles in licorice, is applied in cosmetic lotions [2] and as a vehicle in pharmaceutical preparations [3]. GL is hydrolysed to 18β-glycyrrhetinic acid (18β-GA) and two molecules of glucuronic acid after being absorbed from the gastrointestinal tract. Because of the similarity in chemical structure to steroids, GL and its hydrolysate produce mineralocorticoid-like effects [4]. They also inhibit the metabolic enzymes for adrenocorticosteroids [5]. Determination of the GL content in licorice has been reported [6–11]. However, the simultaneous determination of GL, 18α-glycyrrhetinic acid (18α-GA) and 18β-GA in licorice by

0021-9673/91/$03.50

high-performance liquid chromatography (HPLC) has not been described. In this work, an HPLC technique was developed to determine simultaneously the contents of GL, 18α-GA and 18β-GA in licorice extract in one analytical step.

EXPERIMENTAL

Materials and reagents

Licorice (*Glycyrrhiza uralensis* Fisch.) was purchased from a traditional Chinese pharmaceutical company in Taipei. GL, 18α-GA and 18β-GA were obtained from Sigma (St. Louis, MO, U.S.A.) and perchloric acid (70%), ammonia solution (32%) and methanol from E. Merck (Darmstadt, Germany).

Apparatus

The HPLC system (Waters Assoc., Milford, MA, U.S.A.) consisted of a Model U6K injector, two Model 510 pumps, a Model 441 detector, a Model 990 photodiode-array detector and a Model 740 integrator. Elution was carried out on a LiChrospher 100 RP-18 (5 μm) end-capped column (125 × 4 mm I.D.) (E. Merck) connected to a guard column (5 μm) (4 × 4 mm I.D.) (E. Merck). The detection wavelength was set at 254 nm. The mobile phase consisted of methanol (solvent A) and 0.1% perchloric acid (solvent B, adjusted to pH 7.5–7.7 with ammonia solution) and samples (10 μl) were eluted with a linear gradient of solvent A–solvent B from 1:9 to 10:0 in 120 min. The flow-rate was 1.0 ml/min.

Preparation of licorice extract

Licorice (10 g) was cut into coarse pieces and refluxed at 50°C with 50 ml of the extraction solution (water, 0.05 *M* NaOH, 50% ethanol, 95% ethanol or methanol) for 30 min. This procedure was repeated twice. The two solvent filtrates were combined, condensed under reduced pressure, dried by lyophilization and stored at −20°C to maintain stability. The lyophilized samples were reconstituted with their respective extraction solutions before being subjected to HPLC. To minimize the effect of the solvent (0.05 *M* NaOH) on the analytical column, we restricted the injection volume to 10 μl.

Determination of GL, 18α-GA and 18β-GA

Calibration graphs for GL, 18α-GA and 18β-GA dissolved in methanol were constructed by HPLC of various amounts of these compounds (0.2, 0.5, 1, 2 and 5 μg for GL; 10, 20, 40 and 100 ng for 18α-GA or 18β-GA). The contents of GL, 18α-GA and 18β-GA in the crude extract of licorice were determined from the regression equation lines constructed for the three compounds.

RESULTS AND DISCUSSION

A typical elution profile of a mixture of GL, 18α-GA and 18β-GA is shown in Fig. 1. It should be mentioned the pH of the mobile phase is very important for good resolution. When the pH of solvent B was decreased, the retention time for the three compounds increased and the peaks for the stereoisomers of glycyrrhetinic acids overlapped. In addition, the peak for GL merged with those of other components of

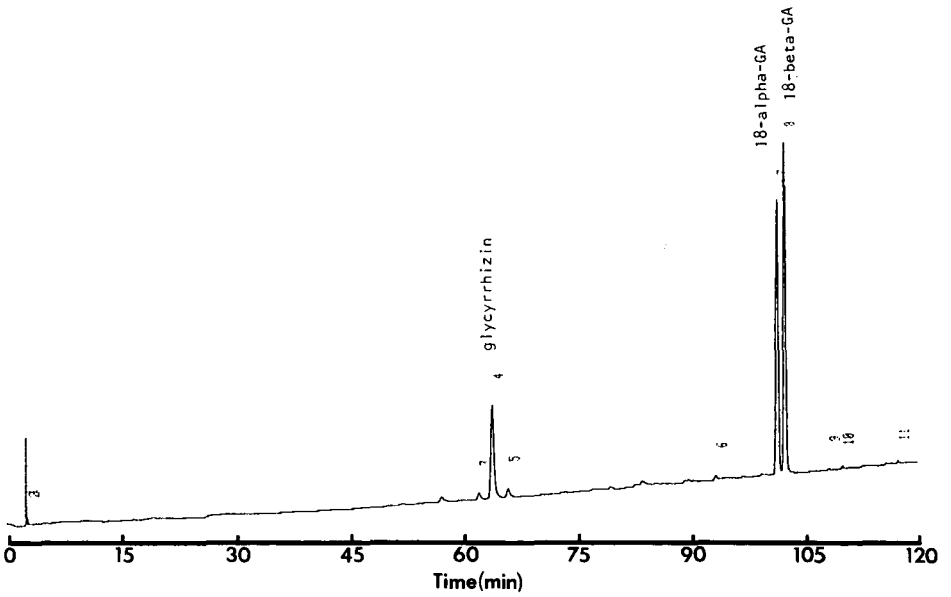

Fig. 1. Chromatogram of glycyrrhizin, 18α-GA and 18β-GA.

the licorice extract. The optimum pH for solvent B was 7.5–7.7. Under this condition, the retention tims for GL, 18α-GA and 18β-GA were 63.9, 101.4 and 102.5 min, respectively. Fig. 2 shows the chromatogram of a 50% ethanol extract of licorice. The peaks corresponding to GL, 18α-GA and 18β-GA were confirmed by the retention times and the spectra from photodiode-array detection. The content of each compound in the licorice extract was determined from the linear regression equation of the calibration graph for each compound. The equations for GL, 18α-GA and 18β-GA were $y = 6919 + 782152x$ ($r = 0.999$), $y = 103 + 1666x$ ($r = 0.999$) and $y = -530 + 1287x$ ($r = 0.999$), respectively, where x is amount of compound analyzed and y is response in peak area.

Table I gives the contents of GL, 18α-GA and 18β-GA in different licorice extracts. It appears that 0.05 *M* NaOH is best for the extraction of GL and methanol is best for the extraction of 18α-GA and 18β-GA from licorice.

A number of techniques, such as thin-layer chromatography [6], three-dimensional HPLC [7], HPLC [8,9], spectrophotometry [10] and infrared spectrometry [11], have been used to determine the GL content in licorice or its preparations. However, there has been no report of the simultaneous determination of GL, 18α-GA and 18β-GA in licorice extract. The proposed reversed-phase HPLC technique provided an excellent separation of GL, 18α-GA and 18β-GA and can determine the contents of these three compounds in licorice extracts without any pretreatment of the tested samples. Hence, this technique should be useful for the quality control of licorice, for stability testing and for the pharmacokinetic study of the three compounds.

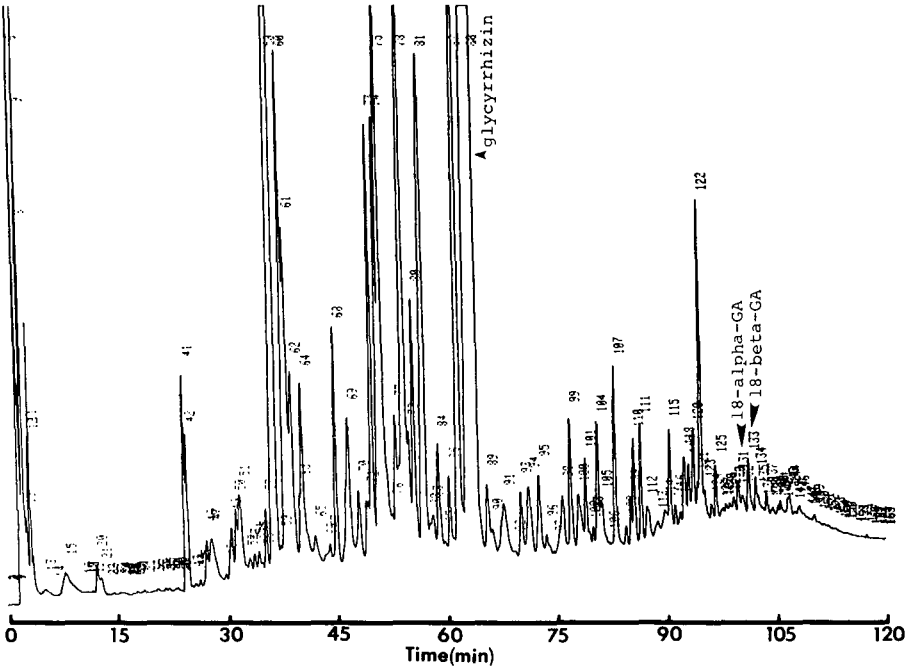

Fig. 2. Chromatogram of the 50% ethanol extract of licorice.

TABLE I

CONTENTS OF GL, 18α-GA AND 18β-GA IN DIFFERENT LICORICE EXTRACTS

Contents in 11 g of licorice. Data are expressed as mean ± standard error (n = 4).

Extracted solution	GL (mg)	18α-GA (μg)	18β-GA (μg)
0.05 *M* NaOH	83.25 ± 4.98	9.96 ± 2.03	76.14 ± 17.32
Water	58.35 ± 9.14	5.94 ± 1.60	95.25 ± 27.20
Ethanol (50%)	81.39 ± 4.72	119.61 ± 26.23	450.81 ± 38.72
Methanol	26.79 ± 2.61	550.56 ± 34.82	1273.47 ± 63.66
Ethanol (95%)	8.52 ± 0.90	479.94 ± 91.91	1118.07 ± 74.98

ACKNOWLEDGEMENTS

This work was supported by Research Grant NSC78-0412-B-077-01 from the National Science Council, Taiwan. The authors are grateful to Professor Chun-Ching Lin for the identification of *Glycyrrhiza uralensis* Fisch.

REFERENCES

1 H. Jiang, Y. Ma and S. Zhao, *Shipin Kexue*, 83 (1986) 10.
2 E. Nikami, S. Yamada, J. Hayakawa and M. Yamada, *Eisei Kagaku*, 34 (1988) 466.
3 R. Segal and S. Pisanty, *J. Clin. Pharmacol. Ther.*, 12 (1987) 165.

4 R. Takeda, I. Miyamori, R. Soma, T. Matsubara and M. Ikeda, *J. Steroid Biochem.*, 27 (1987) 845.
5 S. Shibata, K. Takahashi, S. Yano, M. Harada, H. Saito, Y. Tamura, A. Kumagai, K. Hirabayashi, M. Yamamoto and N. Nagata, *Chem. Pharm. Bull.*, 35 (1987) 1910.
6 M. Alam, M. Umar and F. Dar, *J. Pharm.*, 7 (1986) 21.
7 S. Shibata and T. Hiraka, *Pharm. Tech. Jpn.*, 2 (1986) 569.
8 N. Sadlej-Sosnowska, *J. Pharm. Biomed. Anal.*, 5 (1987) 289.
9 R. C. Li, Q. H. Wang, J. Y. Dou and Y. Q. Pei, *Zhongcaoyao*, 18 (1987) 157.
10 J. Y. Du, Q. H. Wang, Y. Q. Pei and R. C. Li, *Yiyao Gongye*, 18 (1987) 451.
11 J. H. Ma, *Fenxi Huaxue*, 16 (1988) 188.

Journal of Chromatography, 542 (1991) 526–530
Elsevier Science Publishers B.V., Amsterdam

CHROM. 23 033

Short Communication

Gas chromatographic determination of aldicarb and its metabolites in urine

DAI XIU LIAN*, LUAN YANG, WANG XIAO YUN, SHAO HUA and CHENG HU
Shandong Academy of Medical Science, Jing-Shi Road, Jinan, Shandong (China)
(First received August 24th, 1990; revised manuscript received December 13th, 1990)

ABSTRACT

A method is described for the determination of aldicarb and its metabolites (the sulphoxide and sulphone) in urine by gas chromatography with flame photometric detection (GC–FPD). The sample was concentrated with a column containing activated charcoal and Florisil, and then eluted with dichloromethane–acetone (1:1, v/v). The aldicarb and aldicarb sulphoxide in the eluate solution were oxidized to aldicarb sulphone and the total sulphone concentration was determined by GC–FPD after extraction with dichloromethane and clean-up with an activated charcoal column. The detection limit was 0.0024 mg/l. The mean recoveries from spiked urine in the range 0.04–0.12 mg/l were 90.9%, 86.6%, 92.6% for aldicarb, aldicarb sulphoxide and aldicarb sulphone, respectively.

INTRODUCTION

Aldicarb [2-methyl-2-(methylthio)propionaldehyde-O-(methylcarbamoyl)-oxime] is a highly effective and highly poisonous broad-spectrum N-methylcarbamate insecticide. It can be degraded by oxidation into aldicarb sulphoxide and sulphone in human and animal body tissue. Wagner [1] reported that 80% of aldicarb and its metabolites are excreted in the urine by 24 h after external exposure. Because aldicarb and the sulphoxide and sulphone are toxic with potential risks for human health, it is important to be able to determine the levels of all three compounds in urine for biological monitoring of workers' exposure to aldicarb.

A number of methods have been reported for the determination of aldicarb residues but there have been few papers on its determination in urine. On the basis of published work [2–4], we developed an method for the determination of aldicarb and its metabolites in urine by gas chromatography with flame photometric detection (GC–FPD). This method involves determining aldicarb sulphone in urine from rats dosed with aldicarb orally. The results showed that the method is an efficient technique for biological monitoring of exposure to aldicarb.

0021-9673/91/$03.50

EXPERIMENTAL

Equipment

A Shimadzu GC-RIA gas chromatograph equipped with a flame photometric detector and a sulphur filter was used. The glass column (2.1 m × 2.7 mm I.D.) was packed with 3% polyethylene glycol 20M–Gas-Chrom Q (80–100 mesh). A glass chromatographic column (20 cm × 1.0 cm I.D.) with a stopcock was also used.

Reagents

Acetone and dichloromethane (analytical-reagent grade) were glass distilled. Florisil (pure reagent grade, 60–80 mesh) was heated in an oven at 400°C for 4 h prior to use. Activated charcoal (60–80 mesh) was obtained from the Berjing Guang Hua Wood Factory.

The oxidizing reagent was prepared by mixing 0.1 ml of concentrated sulphuric acid with 10 ml of 30% hydrogen peroxide and 10 ml of glacial acetic acid. The mixture was placed in a refrigerator and allowed to stand overnight. This solution could be used for 1 week.

A standard solution was prepared by dissolving appropriate amounts of aldicarb, aldicarb sulphoxide and aldicarb sulphone (Union Carbide Agricultural Products) in methanol.

Procedure

Concentration. The column was prepared by insterting glass-wool at the bottom, adding 1.0 g of activated charcoal and 1.0 g of Florisil, tapping it gently, then plugging with glass-wool at the top of the column. The column was washed with 30 ml of distilled water. A 50-ml urine sample was passed through the column at a flow-rate of 1 ml/min and the eluate was discarded. The column was then cleaned up with 40 ml of acetone–water (1:30). Finally, the analyte on the column was eluted with 20 ml of acetone–dichloromethane (1:1) and collected in a 50-ml beaker. The eluate was evaporated to dryness on a water-bath (40°C). The residue was then ready for oxidation.

Oxidation. A beaker containing 20 ml of distilled water was placed on a magnetic stirrer, then 25 ml of oxidizing reagent were added. The reaction mixture was stirred for 30 min, then the pH was adjusted to 6–7 with 10% sodium hydrogencarbonate solution and the mixture was stirred for a further 20 min. The mixture was transferred into a 150-ml separating funnel and aldicarb sulphone was extracted with three 30-ml portions of dichloromethane. The dichloromethane extracts were combined and evaporated to dryness and the residue was dissolved in 10 ml of distilled water.

Clean-up. The chromatographic column was prepared by adding 1.0 g of activated charcoal and pretreated by passing 20 ml distilled water through the column. The sample extract from the oxidation step was then passed through the column at flow-rate of 1 ml/min and eluted with 10 ml of acetone–dichloromethane (1:1). The eluate was evaporated to dryness and the residue was dissolved in and diluted to 1.0 ml with methanol. The solution was then ready for GC analysis.

GC analysis. Quantitative analysis was performed according to the external standard method. A calibration graph was prepared in the range 2 ng–10 ng. The GC conditions were as follows: injector temperature, 220°C; detector temperature, 220°C;

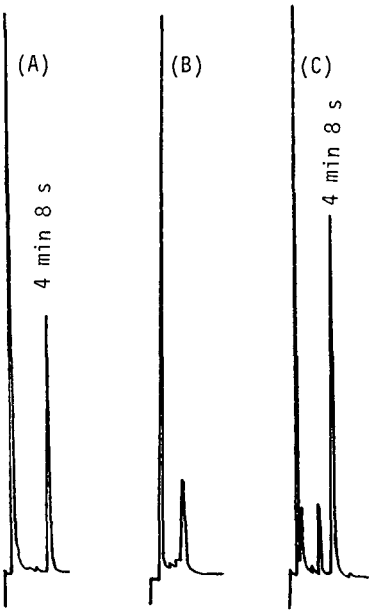

Fig. 1. Gas chromatograms of standard and urine samples spiked with aldicarb. (A) Aldicarb sulphone standard; (B) urine blank; (C) urine from rats dosed with aldicarb.

column temperature, 160°C; flow-rates, hydrogen 50 ml/min, air 52 ml/min and nitrogen 45 ml/min; and injection volume, 5 μl.

RESULTS AND DISCUSSION

Because some co-extracted impurities in the dichloromethane extract interfere in the determination of aldicarb sulphone it is necessary for the extract to be cleaned up with an activated charcoal column. After treatment with this column, the peaks of both aldicarb sulphone and the impurities can be separated at the baseline (see Fig. 1). The retention time for aldicarb sulphone was 4 min 8 s.

TABLE I

PRECISION OF THE METHOD [RELATIVE STANDARD DEVIATION (R.S.D.) (n=6)]

Parameter	Spiking level (μg per 50 ml)		
	2	4	6
Single day			
S.D. (μg per 50 ml)	0.08	0.14	0.23
R.S.D. (%)	4.0	3.5	3.8
Different days			
S.D. (μg per 50 ml)	0.15	0.30	0.35
R.S.D. (%)	7.5	7.5	5.8

TABLE II

RECOVERIES OF ALDICARB, ALDICARB SULPHOXIDE AND ALDICARB SULPHONE FROM SPIKED URINE SAMPLES

Pesticide	Amount added (μg per 50 ml)	Amount found (μg per 5 ml)	Mean recovery (%) ($n=6$)	R.S.D. (%)
Aldicarb	2	1.82	91.0	4.5
	4	3.71	92.8	3.5
	6	5.34	89.0	5.3
Aldicarb sulphoxide	2	1.72	86.0	3.0
	4	3.57	89.3	3.3
	6	5.11	85.1	5.5
Aldicarb sulphone	2	1.87	93.5	2.5
	4	3.76	94.0	4.3
	6	5.44	90.7	4.3

The relative standard deviations obtained with the method were 4.0–3.5% for analyses on a single day and 5.8–7.5% for analyses on different days for urine spiked with aldicarb sulphone in the range 2–6 μg per 50 ml (Table I). The detection limit was 0.0024 mg/l.

The recoveries of aldicarb, aldicarb sulphoxide and aldicarb sulphone spiked in urine at three levels (2 μg, 4 μg and 6 μg per 50 ml) were determined and the results are given in Table II. The recoveries ranged from 89% to 92.8% for aldicarb, 85.1% to 89.3% for aldicarb sulphoxide and 90.7% to 94% for aldicarb sulphone, with relative standard deviations of 3.5–5.3%, 3.0–5.5% and 2.5–4.3%, respectively.

Urine samples were collected from rats dosed with aldicarb orally at 0–24 h and 24–48 h after dosing and after oxidation the total amount of aldicarb sulphone was determined. The results are given Table III.

TABLE III

RESULTS FOR DETERMINATION OF ALDICARB SULPHONE IN RAT URINE

Dose (μg)	No. of rats	Found (μg)	
		0–24 h	24–48 h
0.168	3	35.3	2.3
0.125	3	25.8	1.8
0.080	4	15.5	1.2
0.050	4	9.9	1.1
0.000	2	0.0	0.0

CONCLUSION

The method described is sensitive, inexpensive and efficient. It has potential use for biological monitoring of aldicarb and its metabolites in the urine of workers who are exposed to aldicarb for estimating occupational exposure levels.

ACKNOWLEDGEMENTS

The authors thank Dr. C. R. J. Chipeta and Joseph Lau for their invaluable advice and assistance in preparing this paper.

REFERENCES

1 S. L. Wagner, *Clinical Toxicology of Agricultural Chemicals*, Noyes Data, Park Ridge, NJ, 1983.
2 D. W. Woodham, R. R. Edwards, R. G. Reeves and R. L. Schutzmann, *J. Agric. Food Chem.*, 21 (1973) 303.
3 C. J. Miles and J. J. Delfino, *J. Chromatogr.*, 299 (1984) 275.
4 R. X. Ma, Z. Q. Yun, X. W. Chen, W. X. Sun and W. E. Lin, *Huang Jing Ke Xiu*, 7, No. 2 (1986) 80.
5 H. H. Mo, F. C. An, W. E. Lin and X. W. Chen, *Huan Jing Ke Xiu*, 8, No. 2 (1987) 73.

Journal of Chromatography, 542 (1991) 531–536
Elsevier Science Publishers B.V., Amsterdam

CHROM. 23 047

Short Communication

Thin-layer chromatography of thiazolidinones. I

RAJ KUMAR UPADHYAY*, NAMITA AGARWAL and NEELU GUPTA
Chemistry Department, NREC College, Khurja-203131 (India)
(First received June 20th, 1989; revised manuscript received October 31st, 1990)

ABSTRACT

1,4-Thiazolidinones, the cyclocondensation products of ketoanils with thioglycolic acid, including isomers, have been chromatographed on starch bound silica gel thin-layers using one- and two-component solvent systems and effects of various properties of developing solvents and migrating species on R_F values have been investigated beside the separation, identification and estimation.

INTRODUCTION

Although thin-layer chromatographic (TLC) and paper chromatographic studies on heterocyclic organic compounds are well documented and numerous reports are also available on isomers, 1,4-thiazolidinones have not previously been investigated. This led us to carry out TLC studies, as this technique is superior to others in providing rapid and better separation, on a few 1,4-thiazolidinones including their isomers. The effects of various properties of developing solvents and thiazolidinones on R_F values and the separation of isomers were investigated. The relationship between the infrared spectral frequencies of characteristic groups and R_F values in different solvents were used for the identification of compounds.

EXPERIMENTAL

Materials

1,4-Thiazolidinones were obtained by reaction of ketoanils [1] with thioglycolic acid in dry benzene followed by refluxing for 15–20 h and neutralizing the reaction mixture with sodium hydrogencarbonate. The composition of each product, purified by column chromatography using silica gel G as sorbent and acetone as solvent, was confirmed by elemental analysis and infrared spectrometry, as reported elsewhere [2].

In synthetic work reagent-grade chemicals were used as received whereas in TLC studies they were used after purification involving drying and distillation.

0021-9673/91/$03.50

Procedure

For coating the plates an aqueous slurry containing a homogeneous mixture of silica gel G (BDH) and starch (19:1, w/w) was spread on glass plates (18 × 10 cm) with a laboratory-built applicator [3]. The coated plates were dried in air. Both sides of the gel layer were scraped off to a width of about 5 mm. Before use the coated plates were activated by heating at *ca.* 100°C for 1 h.

For qualitative studies warm plates (with a 0.10-cm thick layer), to ensure compactness of spots, were spotted with standard solutions of samples in acetone as small drops using glass capillaries whereas in quantitative work known volumes of solutions were applied with a micropipette to a 0.15-cm thick gel layer. Sample solutions were applied as series of spots or bands in a line 2 cm from the edge of the plate. The oven-dried loaded plates were developed in rectangular glass chambers with ground-in-lids by the ascending technique. To obtain reproducible results the development chambers were saturated with solvent before use. When development had proceeded for *ca.* 8 cm the plate was removed from the chamber. Owing to the dark colours produced by the analytes their spots were readily discernible in daylight.

For quantification the component bands were scraped off, treated with 15–20 ml of acetone to extract the thiazolidinones and the solutions were evaporated to 5 ml. The absorbances of the solutions were measured on a Bausch and Lomb Spectronic-20 spectrophotometer at the wavelengths of maximum absorption of the solutes and the concentrations were calculated from linear calibration graphs obtained in the range 0–500 μg under identical conditions of medium (acetone) and temperature (27 ± 2°C).

RESULTS AND DISCUSSION

Effects of various parameters on R_F values

The effects of the development rate, gel layer thickness and the presence of other compounds on the R_F values were examined for some thiazolidinones as migrating spots in selected solvents. The R_F values determined at two development rates (measured at plate angles of 80° and 50° from the horizontal plane) are given in Table I. As can be seen, the R_F values were independent of development rate. Almost identical R_F values obtained when the compounds migrated individually (Table II) and in mixtures (containing up to six compounds); hence the migration is independent of the presence of other compounds. The R_F data for ternary and binary mixtures of isomers in Tables II and III show a lowering of R_F values with increase in gel layer thickness.

The effect of solvent polarity on R_F values was studied with all the thiazolidinones in both oxygen-containing and non-oxygen-containing solvents. The R_F orders, isobutanol < *n*-butanol, *n*-butanol < ethanol and carbon tetrachloride < dichloromethane < chloroform, corresponding to the solvent polarities, show that the R_F values and their sequences are governed by the solvent polarity.

TLC studies of isomeric ternary nitro- and methoxythiazolidinone mixtures and binary naphthyl compound mixtures revealed particular R_F orders depending on the nature of the solvent, *i.e.*, whether oxygen-containing or non-oxygen-containing, alcoholic or ketonic, or a one- or two-component system.

To study the effect of the nature of substituents on R_F values, *para*-substituted

TABLE I

EFFECT OF DEVELOPMENT RATE ON R_F VALUES

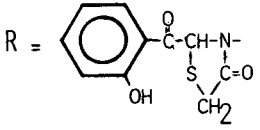

Developing solvent	Development rates (mm/h)[a]	$R_F \times 100$[a]				
		RC_6H_5	RC_6H_4SH-*o*	$RC_6H_4NO_2$-*o*	$RC_6H_4NO_2$-*m*	$RC_6H_4NO_2$-*p*
Acetone	69(43)	94(94)	93(93)	92(92)	89(90)	92(92)
n-Butanol	45(30)	94(94)	95(94)	94(94)	87(87)	90(90)
Chloroform	107(67)	00(00)	63(63)	43(43)	53(53)	63(63)
Dioxane	71(45)	93(92)	98(98)	99(98)	94(94)	97(97)
Diethyl ether	156(98)	00(00)	96(96)	86(86)	62(62)	62(62)
Benzene–ethanol (7:3, v/v)	107(70)	70(70)	93(93)	78(78)	72(72)	65(65)
Benzene–ethanol (2:3, v/v)	86(54)	97(98)	98(99)	94(93)	93(93)	98(97)

[a] First and second (in parentheses) values were measured at plate angles of 80° and 50° respectively.

TABLE II

SPOT COLOURS, SPECTRAL PARAMETERS AND $R_F \times 100$ VALUES FOR THIAZOLIDINONES

Compound	Spot colour	IR frequencies (cm^{-1})		$R_F \times 100$								
		ν C–N	ν C=O (ring)	Diethyl ether	Isobutanol	Ethyl acetate	Benzene	Toluene	Chloroform	Benzene–ethanol		
										7:3 (v/v)	1:1 (v/v)	24:1 (v/v)
RC_6H_5	Light brown	1590	1720	00	80	94	00	00	00	70	87	–
RC_6H_4SH-*o*	Light brown	1600	1690	96	95	85	84	00	–[a]	90	100	–
RC_5H_4N-*o*	Dark brown	1590	1695	00	00	00	00	00	00	–	–	–
$RC_6H_4NO_2$-*o*	Light yellow	1600	1780	86	92	75	35	25	43	78	100	66
$RC_6H_4NO_2$-*m*	Yellow	1600	1740	62	85	70	19	14	53	72	100	50
$RC_6H_4NO_2$-*p*	Yellow	1600	1720	62	85	72	19	8	63	65	100	30
$RC_6H_4OCH_3$-*o*	Light yellow	1585	1780	00	92	82	00	00	00	91	100	–
$RC_6H_4OCH_3$-*m*	Brownish yellow	1585	1775	00	92	00	00	00	00	84	100	–
$RC_6H_4OCH_3$-*p*	Brownish yellow	1580	1760	00	89	84	67	1	00	89	100	–
$RC_{10}H_9$-α	Light brown	1630	1800	00	85	97	50	00	00	100	100	–
$RC_{10}H_9$-β	Red-brown	1600	1720	00	85	95	50	46	00	93	87	–
RC_6H_4Cl-*p*	Yellowish brown	1580	1770	00	89	86	67	00	00	98	100	–
RC_6H_4Br-*p*	Brownish yellow	1585	1680	00	89	85	67	00	00	95	100	–
RC_6H_4I-*p*	Brown	1590	1780	00	89	85	67	00	00	96	100	–
$RC_6H_4N(C_2H_5)_2$-*p*	Purple-brown	1590	1690	00	00	00	00	00	00	–	90	–
$RC_6H_4CH_3$-*p*	Yellowish brown	1590	1690	98	78	94	67	00	00	75	92	–
RC_6H_4R-*p*	Yellowish brown	1580	1680	00	00	00	00	00	00	80	85	–
$RC_6H_4C_6H_4R$-*p*	Light brown	1575	1760	–	00	79	67	00	00	82	79	–

[a] Dashes denote spreading of spots.

TABLE III

QUANTITATIVE ANALYSIS OF ISOMERIC THIAZOLIDINONE MIXTURES

Isomeric thiazolidinones in mixture	Experiment 1[a]							
	Amount loaded (μg)	Amount recovered (μg)	M.D. (μg)	S.D. (μg)	R.S.D. (%)	Error (%)		
$RC_6H_4NO_2$-*o*	150	148,149,148.5	0.33	0.41	0.28	1.00		
$RC_6H_4NO_2$-*m*	150	149,149.5,150	0.33	0.41	0.27	0.33		
$RC_6H_4NO_2$-*p*	150	150.5,148.5,149	0.78	0.85	0.57	0.45		
$RC_6H_4OCH_3$-*o*	100	99,99.5,100.5	0.55	0.62	0.63	0.34		
$RC_6H_4OCH_3$-*m*	100	100,99.5,99.5	0.22	0.24	0.24	0.34		
$RC_6H_4OCH_3$-*m*	100	99.5,99,99	0.22	0.24	0.23	0.83		
$RC_6H_4OCH_3$-*p*	100	99.5,98.5,99.5	0.44	0.47	0.48	0.83		
$RC_{10}H_9$-α	100	99,99,99	0.00	0.00	0.00	1.00		
$RC_{10}H_9$-β	60	59.5,59.5,58.5	0.44	0.47	0.80	1.39		
Isomeric thiazolidinones in mixture	Experiment 2[a]							
	Amount loaded (μg)	Amount recovered (μg)	M.D. (μg)	S.D. (μg)	R.S.D. (%)	Error (%)		
$RC_6H_4NO_2$-*o*	150	148.5,149.5,148.5	0.44	0.47	0.32	0.78		
$RC_6H_4NO_2$-*m*	300	298,298.5,298	0.12	0.23	0.08	0.61		
$RC_6H_4NO_2$-*p*	300	299,299.5,300	0.33	0.41	0.14	0.17		
$RC_6H_4OCH_3$-*o*	100	99.5,99.5,99.5	0.00	0.00	0.00	0.50		
$RC_6H_4OCH_3$-*m*	60	60.5,59,59.5	0.55	0.62	1.04	0.57		
$RC_6H_4OCH_3$-*m*	120	119.5,120,119	0.33	0.41	0.34	0.42		
$RC_6H_4OCH_3$-*p*	60	59,59,59.5	0.12	0.23	0.40	1.39		
$RC_{10}H_9$-α	60	59,60,59	0.44	0.47	0.79	1.12		
$RC_{10}H_9$-β	100	99,98.5,99.5	0.33	0.41	0.41	1.00		
Isomeric thiazolidinones in mixture	Experiment 3[a]						$R_F \times 100$	Resolving solvent
	Amount loaded (μg)	Amount recovered (μg)	M.D. (μg)	S.D. (μg)	R.S.D. (%)	Error (%)		
$RC_6H_4NO_2$-*o*	–	–	–	–	–	–	65	Benzene–ethanol (24:1, v/v)
$RC_6H_4NO_2$-*m*	–	–	–	–	–	–	49	
$RC_6H_4NO_2$-*p*	–	–	–	–	–	–	29	
$RC_6H_4OCH_3$-*o*	–	–	–	–	–	–	80	Ethyl acetate
$RC_6H_4OCH_3$-*m*	–	–	–	–	–	–	00	
$RC_6H_4OCH_3$-*m*	160	159,158.5,158.5	0.12	0.23	0.15	0.83	00	
$RC_6H_4OCH_3$-*p*	120	119,119.5,118.5	0.33	0.41	0.34	0.83	82	
$RC_{10}H_9$-α	–	–	–	–	–	–	00	Toluene
$RC_{10}H_9$-β	–	–	–	–	–	–	45	

[a] M.D. = Mean or average deviation; S.D. = standard deviation; R.S.D. = relative standard deviation.

thiazolidinones were chosen, as in this position steric effects are smaller than in other positions and the nature of the substituent group predominates. The R_F values of substituted compounds were compared with that of unsubstituted phenylthiazolidinone. In most of the developing solvents examined the R_F values of the substituted phenylthiazolidinones were generally higher than that of the unsubstituted compound, irrespective of the nature of the substituent in the phenyl group, whether electron donating [CH_3, R, C_6H_4R, I or $N(C_2H_5)_2$] or electron withdrawing (NO_2, OCH_3, Br or Cl).

The IR stretching frequencies of the characteristic C–N and C=O (ring) groups of thiazolidinones, being highly sensitive to the nature and position of substituents, were correlated with the R_F values in almost all of the developing solvents. In *para*-thiazolidinones both spectral parameters, which are in accord with the electron-repelling ability of the substituents, fall in the orders opposite to those of the R_F values. In isomers the retention orders were different in different systems and similar or opposite to the order of the IR frequencies.

Separation, identification and determination of thiazolidinones in mixtures

Among different solvents tried for the separation of thiazolidinones, benzene showed the highest resolving capacity as it could resolve several mixtures of six compounds; the best resolution of five or less compounds, however, could only be achieved in toluene. For the ternary mixture of nitrothiazolidinones and binary mixtures of naphthyl- and methoxythiazolidinones benzene–ethanol (24:1, v/v)) and toluene and ethyl acetate, respectively, are the best resolving solvents. Spectral and R_F correlations were used for the identification of mixture components after separation.

In addition to the solvents listed in Table II, several others were also tried. In acetone, ethanol, acetic acid, dioxane and benzene–ethanol (3:2, 1:1 and 2:3) all the substances had very high R_F values and in carbon tetrachloride and dichloromethane all substances, except the *o*-nitrophenyl compound (R_F 0.07) and all three nitrophenyl compounds (R_F 0.44), respectively remained at the origin.

In order to test the application of the TLC method in the analysis of thiazolidinones, various mixtures were resolved qualitatively on 0.10-cm thick layers (Table II) and a few typical mixtures of isomeric compounds including a ternary mixture of nitrothiazolidinones in benzene–ethanol (24:1, v/v), and binary mixtures of naphthyl- and methoxythiazolidinones in toluene and ethyl acetate, respectively, were analysed quantitatively on 0.15-cm thick layers (Table III). The highest amounts of isomers resolved (Table III) from their mixtures reveal the maximum separation limits of this method. The reproducibility of the results, as can be seen from Table III, is good.

ACKNOWLEDGEMENTS

We are grateful to Dr. G. S. Vashishtha, Principal, for providing facilities for this work; N. A. also extends thanks to CSIR, New Delhi, for the award of a Junior Research Fellowship.

REFERENCES

1 R. K. Upadhyay and N. Agarwal, *J. Indian Chem. Soc.*, submitted for publication.
2 R. H. Upadhyay and N. Agarwal, *Acta Chim. Hung.*, submitted for publication.
3 E. Stahl, *Thin-Layer Chromatography*, Springer, Berlin, 2nd ed., 1966, p. 56.

Journal of Chromatography, 542 (1991) 537–544
Elsevier Science Publishers B.V., Amsterdam

CHROM. 23 067

Short Communication

Ionophoretic studies on mixed complexes

Metal–nitrilotriacetate–penicillamine system

B. B. TIWARI*, R. K. P. SINGH and K. L. YADAVA
Electrochemical Laboratories, Department of Chemistry, University of Allahabad, Allahabad-211 002 (India)
(First received April 3rd, 1990; revised manuscript received November 29th, 1990)

ABSTRACT

A method involving the use of paper electrophoresis is described for the study of equilibria in mixed-ligand complex systems in solution. The technique is based on the movement of a spot of metal ion under an electric field with the complexants added to the background electrolyte at pH 8.5. The stability constants of the complexes were found to be 5.28, 5.15 and 4.97 (log K values) for Hg(II), Be(II) and Ni(II) complexes, respectively, at $\mu = 0.1$ and 35°C.

INTRODUCTION

The properties and chemical reactions of naturally occurring D-penicillamine have already been subjected to wide investigation. The most important reactions are processes involving participation of the mercapto group, and the main biochemical aspects have been reviewed by Jocelyn [1]. The complex chemical significance of these amino acids is determined by the mercapto sulphur donor atom, which is very soft in character. Great biological importance is attached to the study of metal–sulphur bonds formed in such processes, primarily in the non-haeme iron proteins [2] and the blue copper proteins [3]. The significance of this amino acid is enhanced by the fact that it displays independent therapeutic activity. Its most valuable use is for the treatment of Wilson's disease, caused by accumulation of copper. As a consequence of its property of forming stable complexes, it can also be employed to advantage for the elimination of other heavy metals (*e.g*, Pb, Hg) from the organism. It has been utilized in connection with rheumatoid arthritis and neonatal jaundice. Sorensen [4] has demonstrated the anti-inflammatory activity of copper—D-penicillamine.

Czakis-Sulikowska [5] studied the formation of mixed halide complexes of Hg(II). We previously described [6,7] a method for the study of mixed complexes. This

0021-9673/91/$03.50

work is an extension of the technique and reports our observations on mixed systems, *viz.*, Hg(II)–, Be(II)- and Ni(II)–nitrilotriacetate (NTA)–penicillamine.

EXPERIMENTAL

Instruments

A Systronics Model 604 electrophoresis equipment system was used, which has a built-in power supply (a.c.–d.c.) that is fed directly to paper electrophoretic tanks. In order to maintain the temperature constant, two hollow metallic plates coated with thin plastic paper on the outer surface were used for sandwiching paper strips and thermostated water (35°C) was circulated through them. pH meaurements were made with an Elico Model L_{1-10} pH meter using-glass electrode.

Chemicals

Mercury(II), beryllium(II) and nickel(II) perchlorate solutions were prepared by precipitating the corresponding carbonates from solutions of the nitrates (analytical-reagent grade) with sodium hydrogencarbonate, washing the precipitates thoroughly with boiling water and treating them with a suitable amount of 1% perchloric acid. The resulting mixtures were heated to boiling on a water-bath and then filtered. The solutions were standardized and diluted to $5.0 \cdot 10^{-3}$ *M*.

Metal spots were detected on the paper using hydrogen sulphide [for Hg(II)], aluminon [for Be(II)] and dimethylglyoxime [for Ni(II)]. Silver nitrate in alkaline acetone was used for glucose.

Background electrolyte

The background electrolyte in the study of binary complexes consisted of 0.1 *M* perchloric acid and $1.0 \cdot 10^{-2}$ *M* penicillamine. It was maintained at pH 8.5 by addition of sodium hydroxide. Each solution was standardized as usual. Stock solutions of 9.0 *M* perchloric acid, 2.0 *M* sodium hydroxide and 0.5 *M* penicillamine were prepared from AnalaR reagents (BDH, Poole, U.K.). A 0.01 *M* nitrolotriacetic acid solution was prepared from a sample obtained from E. Merck (Darmstadt, Germany).

Procedure

The hollow base plate in the instrument was made horizontal with a spirit level. A 150-ml volume of background electrolyte was placed in each tank of the electrophoretic apparatus. Paper strips (Whatman No. 1, 30 × 1 cm) in duplicate were spotted with metal ions and glucose in the centre with a micropipette and were subsequently placed on the base plate and sandwiched under the upper hollow metallic plate with the ends of the strips immersed in the tank solutions on both sides. Then a potential difference of 200 V was applied between the tank solutions and electrophoresis was carried out for 60 min. Subsequently the strips were removed and the spots were detected. The averages for duplicate strips were noted for calculations and movement of the glucose spot was used as a correction factor. The mobilities were calculated by dividing the movement by the potential gradient and expressed in cm^2 V^{-1} min^{-1}.

RESULTS AND DISCUSSION

Metal–penicillamine binary system

The plot of ionophoretic mobility of a metal spot against pH gives a curve with a number of plateaus as shown in Fig. 1. A plateau is obviously an indication of a pH range where the speed is virtually constant and indicates the formation of a certain complex species. The first corresponds to a region in which metal ions are uncomplexed. Fig. 1 reveals a second plateau in each instance with zero mobility, indicating the formation of neutral 1:1 complexes. With a further increase in pH, the mobility decreases, giving rise to a third plateau in a negative region, indicating an anionic nature of the metal complex. Prominent liganding properties of unprotonated anionic species of penicillamine ruling out the involvement of a zwitterion have been reported [8]. Further increase in pH has no effect on the mobility of metal ions.

In view of the above observations, the complexation of metal ions with the penicillamine anion [L^{2-}] may be represented by

$$M^{2+} + L^{2-} \underset{K_2}{\overset{K_1}{\rightleftharpoons}} ML \tag{1}$$

$$ML + L^{2-} \rightleftharpoons ML_2^{2-} \tag{2}$$

where M represents Ni, Be and Hg and ML and ML_2^{2-} are their complexes with penicillamine.

The metal spot on the paper is thus a conglomeration of uncomplexed metal

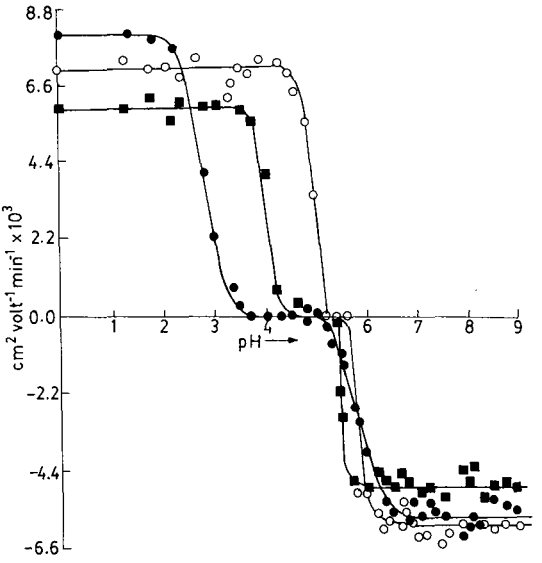

Fig. 1. Mobility curve for M–penicillamine systems. ○ = Ni(II)–penicillamine; ■ = Be(II)–penicillamine; ● = Hg(II)–penicillamine.

ions, a 1:1 complex and a 1:2 complex. This spot is moving under the influence of the electric field, and its overall mobility, U, can be represented by the equation

$$U = \sum_n u_n f_n \tag{3}$$

where u_n and f_n are the mobility and mole fraction, respectively, of particular complex species. On taking into consideration the different equilibria, this equation is transformed into

$$U = \frac{u_0 + u_1 K_1 [L^{2-}] + u_2 K_1 K_2 [L^{2-}]^2}{1 + K_1 [L^{2-}] + K_1 K_2 [L^{2-}]^2} \tag{4}$$

where u_0, u_1 and u_2 are mobility of the uncomplexed metal ion, the 1:1 metal complex and the 1:2 metal complex respectively.

Eqn. 4 was used for the determination of the stability constants of metal ions with penicillamine. For calculating the first stability constant, K_1, the region between the first and second plateaus is pertinent. The overall mobility U will be equal to the arithmetic mean of the mobility of the uncomplexed metal ion, u_0, and that of the first complex, u_1, at a pH where, $K_1 = 1/[L^{2-}]$. With the help of the dissociation constants of penicillamine ($k_1 = 10^{1.90}$, $k_2 = 10^{7.85}$, $k_3 = {}^{10.55}$) [9,10], shown in Fig. 2, the concentration of the penicillamine anion $[L^{2-}]$ is determined for the pH using the following equation, from which K_1 can be calculated:

$$[L^{2-}] = \frac{[L_T]}{1 + \frac{[H]}{k_3} + \frac{[H]^2}{k_2 k_3} + \frac{[H]^3}{k_1 k_2 k_3}} \tag{5}$$

where $[L_T]$ = total concentration.

The stability constant of the second complex, K_2 can be calculated by taking into consideration the region between the second and third plateaus of the mobility curve. These calculated values are given in Table I.

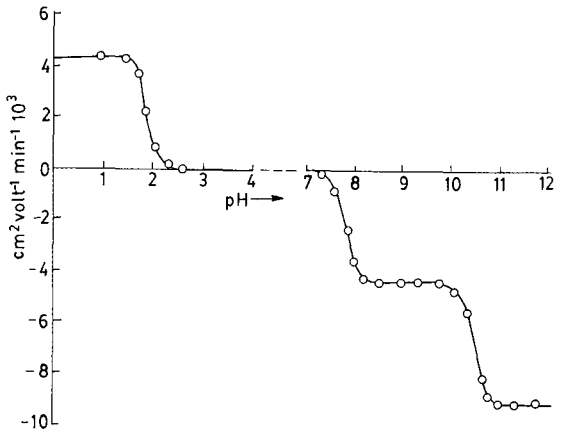

Fig. 2. Mobility curve for H^+–penicillamine.

TABLE I

STABILITY CONSTANTS OF SOME BINARY AND TERNARY COMPLEXES OF Hg(II), Be(II) AND Ni(II)

Ionic strength, μ = 0.1; temperature = 35°C. NTA anion = $N(CH_2COO)_3^{3-}$. Penicillamine anion = $(CH_3)_2C(S^-)CH(NH_2)COO^-$.

Metal ions	Calculated values of stability constants[a]				Literature values of stability constants[a]			
	Log $K_{1_{ML}}^{M}$	Log $K_{2_{ML_2}}^{M}$	Log $K_{M\text{-}NTA}^{M}$	Log $K_{M\text{-}NTA\text{-}L}^{M\text{-}NTA}$	Log $K_{1_{ML}}^{M}$	Log $K_{2_{ML_2}}^{M}$	Log $K_{M\text{-}NTA}^{M}$	Log $K_{M\text{-}NTA\text{-}L}^{M\text{-}NTA}$
Hg(II)	14.95	23.85	13.30	5.28	17.50[10]	23.5[10]	14.6[12]	–
					16.15[10]			–
					16.10[11]			
Be(II)	12.50	22.70	7.10	5.15	–	–	7.10[11]	–
							7.11[13]	
Ni(II)	10.53	19.43	11.49	4.97	11.40[10]	22.30[10]	10.80[12]	–
					11.11[10]	21.79[10]		
					10.75[10]	22.89[10]		
					10.63[9]	23.02[9]	11.90[12]	–
					10.63[11]	23.37[11]		
					10.75[11]	–		

[a] $K_{1_{ML}}^{M} = \frac{[ML]}{[M][L]}$; $K_{2_{ML_2}}^{M} = \frac{[ML_2]}{[ML][L]}$; $K_{M\text{-}NTA}^{M} = \frac{[M\text{-}NTA]}{[M][NTA]}$; $K_{M\text{-}NTA\text{-}L}^{M\text{-}NTA} = \frac{[M\text{-}NTA\text{-}L]}{[M\text{-}NTA][L]}$.

Metal–NTA–binary system

The overall mobilities of metal spots in the presence of NTA at different pH values are shown in Fig. 3. The mobility of the last plateau in the case of Hg(II), Be(II) and Ni(II) is negative, showing the anionic nature of Hg(II)–, Be(II)– and Ni(II)–NTA complexes. Hence only one NTA anion, $(NTA)^{-3}$, is assumed to combine with metal ions to give 1:1 complexes, which is in conformity with the findings of others [14]. The stability constants of complexes with NTA were calculated as described in the preceding paragraph. The calculated values are given in Table I.

Metal–NTA–penicillamine ternary system

The study of this system was made at pH 8.5. It was observed from the mobility curves for the metal–penicillamine and M–NTA binary systems that binary complexes are formed at a pH < 8.5. Hence it was considered appropriate to study the transformation of M–NTA complexes into M–NTA–penicillamine complexes at pH. 8.5 in order to avoid any side interactions.

The plot of mobility against logarithm of concentration of added penicillamine gives a curve (Fig. 4) containing two plateaus, one at the beginning and the other at the end. The mobility of the range of the first plateau corresponds to the mobilities of 1:1 M–NTA complexes, as also observed in the study of M–NTA complexes. The mobility of the last plateau is more negative than the mobility of a pure M–NTA complex. Further, as the mobility of the last plateau does not agree with the mobility of 1:1 and 1:2 metal–penicillamine complexes (observed in the study of binary M–NTA systems),

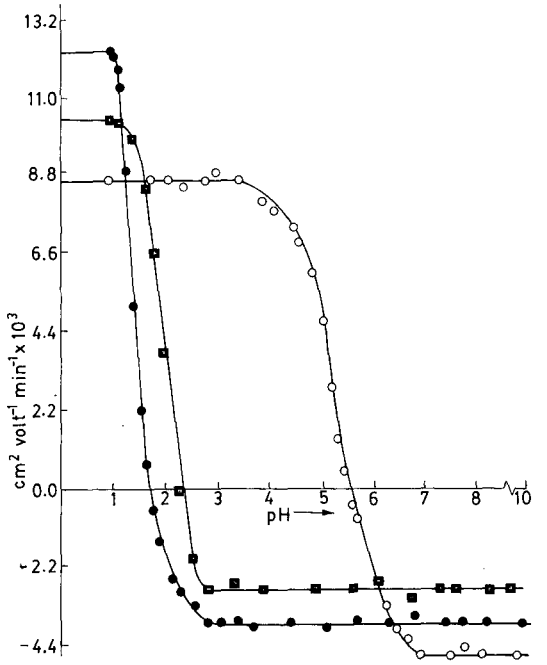

Fig. 3. Mobility curve for M–NTA systems. ■ = Ni(II)–NTA; ● = Hg(II)–NTA; ○ = Be(II)–NTA.

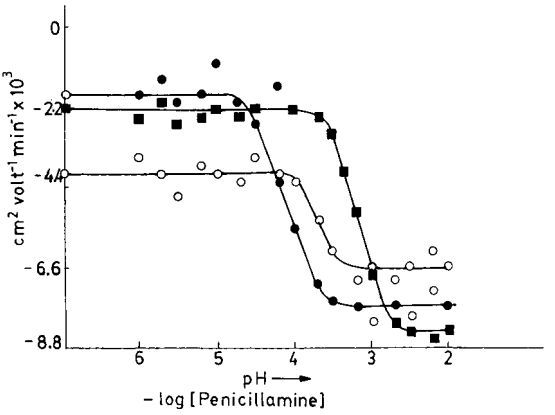

Fig. 4. Mobility curves for M–NTA–penicillamine systems. ○ = Be(II)–NTA–penicillamine; ● = Hg(II)–NTA–penicillamine; ■ = Ni(II)–NTA–penicillamine.

it is inferred that the moiety in the last plateau is due to coordination of the penicillamine anion with a 1:1 M–NTA moiety, resulting in the formation of a 1:1:1 M–NTA–penicillamine mixed complex:

$$\text{M–NTA}^- + \text{L}^{2-} \overset{K'}{\rightleftharpoons} \text{M–NTA–L}^{3-} \tag{6}$$

In the present electrophoretic study, the transformation of a simple complex into a mixed complex took place, the overall mobility being given by

$$U = u_0 f_{\text{M-NTA}} + u_1 f_{\text{M-NTA-L}} \tag{7}$$

where u_0, u_1 and $f_{\text{M-NTA}}, f_{\text{M-NTA-L}}$ are the mobilities and mole fractions of the M–NTA and M–NTA–L complexes, respectively. The above on adding the values of mole fractions, this equation becomes

$$U = \frac{u_0 + u_1 K' [\text{L}^{2-}]}{1 + K' [\text{L}^{2-}]} \tag{8}$$

where u_0 and u_1 are the mobilities in the regions of the two plateaus of the curve. The concentration of penicillamine at which the overall mobility is the mean of the mobilities of the two plateaus is determined from Fig. 4. The concentration of the penicillamine anion at pH 8.5 for this penicillamine concentration was calculated. K' is obviously equal to $1/[\text{L}^{2-}]$. All these values of K' are given in Table I.

REFERENCES

1 C. P. Jocelyn, *Biochemistry of the SH Group*, Academic Press, London and New York, 1972.
2 R. G. Moore and P. J. R. Williams, *Coord. Chem. Rev.*, 18 (1976) 125.
3 A. J. Fee, *Struct. Bonding*, 23 (1975).
4 R. J. Sorensen, *J. Med. Chem.*, 19 (1976) 135.

5 M. Czakis-Sulikowska, *Zesz. Nauk, Politech. Lodz, Chem.*, (1965) 23; *C.A.*, 65 (1966) 1746e.
6 P. C. Yadava, A. K. Ghose, K. L. Yadava and A. K. Dey, *J. Chromatogr.*, 9 (1976) 416.
7 J. R. Yadava, J. K. Sirkar and K. L. Yadava, *Electrochim. Acta*, 26 (1981) 391.
8 J. R. Blackburn and M. M. Jones, *J. Inorg. Nucl. Chem.*, 35 (1973) 1605.
9 D. D. Perrin, *Stability Constants of Metal Ion Complexes, Part B (Organic Ligands) (IUPAC Chemical Series*, No. 22), Pergamon Press, Oxford, 1979.
10 A. E. Martell and R. M. Smith, *Critical Stability Constants, Vol. 1 (Amino Acids)*, Plenum Press, New York and London, 1977.
11 L. G. Sillen and A. E. Martell, *Stability Constants of Metal Ion Complexes (Special Publication*, No. 17), Chemical Society, London, 1964.
12 D. D. Perrin, *Stability Constants of Metal Ion Complexes, Part B (Organic Ligands) (IUPAC Chemical Series*, No. 22), Pergamon Press, Oxford, 1979, p. 417.
13 A. E. Martell and R. M. Smith, *Critical Stability Constants, Vol. 1 (Amino Acids)*, Plenum Press, New York and London, 1977, p. 139.
14 N. G. Elenkova and R. A. Tesoneva, *J. Inorg. Nucl. Chem.*, 35 (1973) 841.

Journal of Chromatography, 542 (1991) 545–546
Elsevier Science Publishers B.V., Amsterdam

CHROM. 23 184

Book Review

Gas chromatography: A practical course, by G. Schomburg, VCH, Weinheim, 1990, XIV + 320 pp., price DM 76.00, ISBN 3-527-27879-6.

Currently a plethora of texts covering the various aspects of chromatography is available. At the same time, the demands on library budgets, due to the inexorable increase of the cost of journals and textbooks, are such that one cannot afford to purchase each new book as it is released onto the market. Today librarians are required to be much more selective about the additions to their stocks. No longer can one expect to simply send off a chitty for that book to appear, instead it is necessary to provide good reasons to support an intended purchase. The present text, notwithstanding its rather general title, can be regarded as an essential purchase if you are looking for an update on contemporary capillary gas chromatography (GC).

Professor Gerhard Schomburg is an esteemed analytical chemist, who has gained international recognition as an exponent of the art of chromatography. In particular he is known for his elegant and innovative work in the field of capillary GC. Knowledge gained through his research and years of experience of solving real analytical problems are combined to generate a highly readable and authorative text, which is thoroughly recommended.

The book consists of twelve chapters, the first five of which are devoted to a discussion of the fundamentals of capillary GC. Topics covered include the role of the technique in chemical analysis, the design fundamentals of the gas chromatograph and the essentials of the theory of GC resolution. The account of GC instrumentation is largely concerned with capillary instruments and contains a wealth of detail concerning the design and operation of vital components, such as injectors and detectors. Many readers will find the table on p. 33 helpful, where the graphic symbols used for the components of the gas chromatograph are given. Such information is seldom included in GC texts.

The strategies of peak identification and analyte determination applicable to GC are reviewed in Chapter 6. The discussion of retention coincidence contrasts the roles of absolute and relative retentions and emphasises the importance of Kováts' retention index in this context. A number of useful tips are given which should enable the beginner to avoid some of the pitfalls associated with peak identification by retention coincidence. Similar comments apply to the treatment of quantitative analysis where much sound advice is given, particularly on the measurement and use of response factors.

A variety of auxiliary techniques associated with capillary GC are reviewed in Chapter 7. Discussions include topics such as high-temperature operation, analyte derivatization, automated systems and the full-spectrum of dual column/multi-

dimensional GC techniques. The less familiar topics of reaction GC and pre-column reaction GC also are described.

Instrumental and column variables which can affect the quality of GC analysis are reviewed in Chapter 8. Special attention is paid to the recognition and elimination of sources of analytical error. The part of the book is commended to both beginners and established exponents of the art.

Chapter 9 consists of a brief introduction to capillary supercritical fluid chromatography. In the reviewer's opinion its inclusion does not serve a very useful purpose. Likewise Chapter 10 is very brief and it is surprising that the author did not choose to include the coupling of liquid chromatography with GC with the auxiliary techniques chapter.

A substantial part of the book is devoted to descriptions of a wide range of analyses which illustrate the wide scope of contemporary GC. Each example is illustrated by representative chromatograms which could prove to be invaluable performance indicators to analysts faced with similar problems.

The book is concluded by a resumé of the terminology of GC and a selection of the more important equations.

The book is nicely presented and it is modestly priced by today's standards. For those people who are either using or contemplating the use of capillary GC it may be regarded to be a vital acquisition.

Hatfield (U.K.) MICHAEL B. EVANS

Journal of Chromatography, 542 (1991) 547–548
Elsevier Science Publishers B.V., Amsterdam

CHROM. 23 127

Book Review

Continuous-flow fast atom bombardment mass spectrometry, edited by R. M. Caprioli, Wiley, Chichester, VIII + 189 pp., price £ 27.50, ISBN 0-471-92863-1.

The continuous-flow fast atom bombardment (CF-FAB) technique provides a basis for coupling liquid chromatography (LC) and capillary electrophoresis with the highly selective, information-rich mass spectrometric (MS) detector. The CF-FAB method is a dynamic variation upon FAB methods which blossomed during the 1980s into one of the most widely utilized of MS methods. The first generations of LC–MS coupling methods, based upon direct liquid introduction and moving belt technologies, have now been largely supplanted by "second generation" thermospray and, more recently, particle beam interfaces. The use of CF-FAB for LC coupling is probably more attractive from the mass spectrometrists' viewpoint, since it represents a variation on a routine method (*i.e.*, FAB). In fact, the most significant advantages of CF-FAB are most evident in the reduced background and discrimination effects compared to conventional FAB methods. Thus, the role of CF-FAB must be viewed from a larger perspective than chromatographic interfacing. This is consistent with the emphasis of the volume edited by Professor Richard Caprioli, approximately one third of which is devoted to LC or capillary electrophoresis with CF-FAB.

This relatively short book (189 pages) is largely based upon an *American Society for Mass Spectrometry Workshop* held in November 1989, and is clearly aimed at mass spectrometrists and those already familiar with FAB and basic MS methods. The various chapters offer a range of experimental detail, "tricks", and practical insights which would be useful to the novice trying to implement the new methods. Largely absent are descriptions of the FAB process and other physical and chemical phenomena underlying these methods. This deliberate limitation of scope keeps the book focused on the issues at hand; providing several different perspectives on the relative advantages and disadvantages of the method. Like most new methods, particularly those involving the tools of microcolumn separations, there is a substantial component of "art" which must be learned for successful operation. The value of the book is in communicating this art.

The general subject of CF-FAB is covered in the first three chapters by Caprioli, Gaskell and Orkiszewski, and Markey and Shih. Chapter 4 (Caprioli) describes application for the direct analysis or monitoring of biological processes. Flow injection analysis, on-line reaction monitoring and microdialysis combined with CF-FAB are described. Chapter 5 (Caprioli and Tomer) describes microbore LC and open tubular capillary LC (10 μm I.D.) coupling with CF-FAB. Chapter 6 (Tomer and Moseley) describes equivalent results with capillary zone electrophoresis–MS coupling. Chapter 7 (D. L. Smith) describes the application of CF-FAB for non-volatile low-polarity substances. The final chapter of the book is divided into five

short "miscellaneous" sections; two of which describe research with packed capillary and microbore LC coupling with CF-FAB.

This book is essential reading for the mass spectroscopist who uses, or is considering use of, the CF-FAB technique. Careful reading, sometimes between the lines, provides one with a good perspective on both the advantages and the disadvantages of the method. Clearly CF-FAB does not provide a good basis for routine LC–MS coupling. The low flow-rates tolerated by the method, *ca.* 10 μl/min, provide some obvious limitations. However, substantial success has been demonstrated using microcolumn separations given practical detection limits (picomole-femtomole range). Unfortunately, little is said about alternative methods for coupling microcolumn LC and capillary electrophoresis to MS, such as those based upon electrospray ionization, and little guidance is given for those trying to compare alternative methods. This is a relatively minor flaw, given the book's audience, however, since it is clearly aimed at mass spectrometrists wielding a particular hammer. A powerful hammer indeed.

Richland, WA (U.S.A) RICHARD D. SMITH

Journal of Chromatography, 542 (1991) 549
Elsevier Science Publishers B.V., Amsterdam

CHROM. 23 128

Book Review

Polymer thermodynamics by GC, by R. Vilcu and M. Leca, Elsevier, Amsterdam, 1990, VIII + 204 pp., price Dfl 190.00, ISBN 0-444-98857-2.

This slim work consists of five chapters and seeks to comprehensively review the thermodynamic characterization of polymers using gas chromatographic techniques. The first introductory chapter, while very short (9 pages), classifies chromatographic methods, most of which are not relevant to the present work, and summarizes the principles of construction of gas chromatographs, material hardly appropriate to the treatment of thermodynamics.

Chapter Two, with the quaint title "Elements of chromatography with gas mobile phase" in about 20 pages outlines much of the theory and terminology of gas chromatography but is largely unrelated to the application of thermodynamics to polymers. Clearer treatments appear in many textbooks on gas chromatography, the recent of these presentations have more timely treatments as the most recent literature reference is 1977.

The third chapter "Thermodynamics of solution as related to gas–liquid chromatography" outlines the relevant fundamentals of thermodynamics and gas chromatography, the quantities of solution thermodynamics, statistical models of solution and finally the application of models to gas–liquid chromatography.

Chapter Four is entitled "Thermodynamics of direct gas chromatography" and considers the thermodynamics of dissolution, adsorption at a gas–solid interface vaporization and finally the molecular properties of single substances.

The final chapter which makes up about one third of the work, considers inverse gas chromatography and polymers. The earlier treatment of dissolution and adsorption is developed. The determination of phase transitions and glass transitions is outlined with many examples while almost single page treatments of second order transition in polymers, determination of diffusion coefficient, segregation of block copolymers and other applications of inverse gas chromatography follow.

Like many books from Eastern Europe the work is hopelessly out of date and is of little use to workers seeking a current treatment. While the work contains over 500 literature references the most recent is 1984 while only about 30 or 6% date from 1980 or later. The work is quite well produced and contains valuable and extensive listing of the symbols used which covers almost ten pages.

It is difficult to see a niche for the work as most of the subject matter has been treated more elegantly in other works which have not suffered from the unacceptable time delays.

Kensington (Australia) J. K. HAKEN

Author Index

PUBLICATION SCHEDULE FOR 1991

Journal of Chromatography and Journal of Chromatography, Biomedical Applications

MONTH	D 1990	J	F	M	A	M	
Journal of Chromatography	535/1 + 2	536/1 + 2 537/1 + 2 538/1	538/2 539/1 539/2	540/1 + 2 541/1 + 2 542/1	542/2 543/1	543/2 544/1 + 2 545/1	the publication schedule for further issues will be published later
Cumulative Indexes, Vols. 501–550							
Bibliography Section				560/1			
Biomedical Applications		562/1 + 2 563/1	563/2	564/1	564/2 565/1 + 2	566/1 566/2	

INFORMATION FOR AUTHORS

(Detailed *Instructions to Authors* were published in Vol. 522, pp. 351–354. A free reprint can be obtained by application to the publisher, Elsevier Science Publishers B.V., P.O. Box 330, 1000 AH Amsterdam, The Netherlands.)

Types of Contributions. The following types of papers are published in the *Journal of Chromatography* and the section on *Biomedical Applications:* Regular research papers (Full-length papers), Review articles and Short Communications. Short Communmications are usually descriptions of short investigations, or they can report minor technical improvements of previously published procedures; they reflect the same quality of research as Full-length papers, but should preferably not exceed six printed pages. For Review articles, see inside front cover under Submission of Papers.

Submission. Every paper must be accompanied by a letter from the senior author, stating that he/she is submitting the paper for publication in the *Journal of Chromatography*.

Manuscripts. Manuscripts should be typed in double spacing on consecutively numbered pages of uniform size. The manuscript should be preceded by a sheet of manuscript paper carrying the title of the paper and the name and full postal address of the person to whom the proofs are to be sent. As a rule, papers should be divided into sections, headed by a caption (*e.g.*, Abstract, Introduction, Experimental, Results, Discussion, etc.). All illustrations, photographs, tables, etc., should be on separate sheets.

Introduction. Every paper must have a concise introduction mentioning what has been done before on the topic described, and stating clearly what is new in the paper now submitted.

Abstract. All articles should have an abstract of 50–100 words which clearly and briefly indicates what is new, different and significant.

Illustrations. The figures should be submitted in a form suitable for reproduction, drawn in Indian ink on drawing or tracing paper. Each illustration should have a legend, all the *legends* being typed (with double spacing) together on a *separate sheet*. If structures are given in the text, the original drawings should be supplied. Coloured illustrations are reproduced at the author's expense, the cost being determined by the number of pages and by the number of colours needed. The written permission of the author and publisher must be obtained for the use of any figure already published. Its source must be indicated in the legend.

References. References should be numbered in the order in which they are cited in the text, and listed in numerical sequence on a separate sheet at the end of the article. Please check a recent issue for the layout of the reference list. Abbreviations for the titles of journals should follow the system used by *Chemical Abstracts*. Articles not yet published should be given as "in press" (journal should be specified), "submitted for publication" (journal should be specified), "in preparation" or "personal communication".

Dispatch. Before sending the manuscript to the Editor please check that the envelope contains four copies of the paper complete with references, legends and figures. One of the sets of figures must be the originals suitable for direct reproduction. Please also ensure that permission to publish has been obtained from your institute.

Proofs. One set of proofs will be sent to the author to be carefully checked for printer's errors. Corrections must be restricted to instances in which the proof is at variance with the manuscript. "Extra corrections" will be inserted at the author's expense.

Reprints. Fifty reprints of Full-length papers and Short Communications will be supplied free of charge. Additional reprints can be ordered by the authors. An order form containing price quotations will be sent to the authors together with the proofs of their article.

Advertisements. Advertisement rates are available from the publisher on request. The Editors of the journal accept no responsibility for the contents of the advertisements.

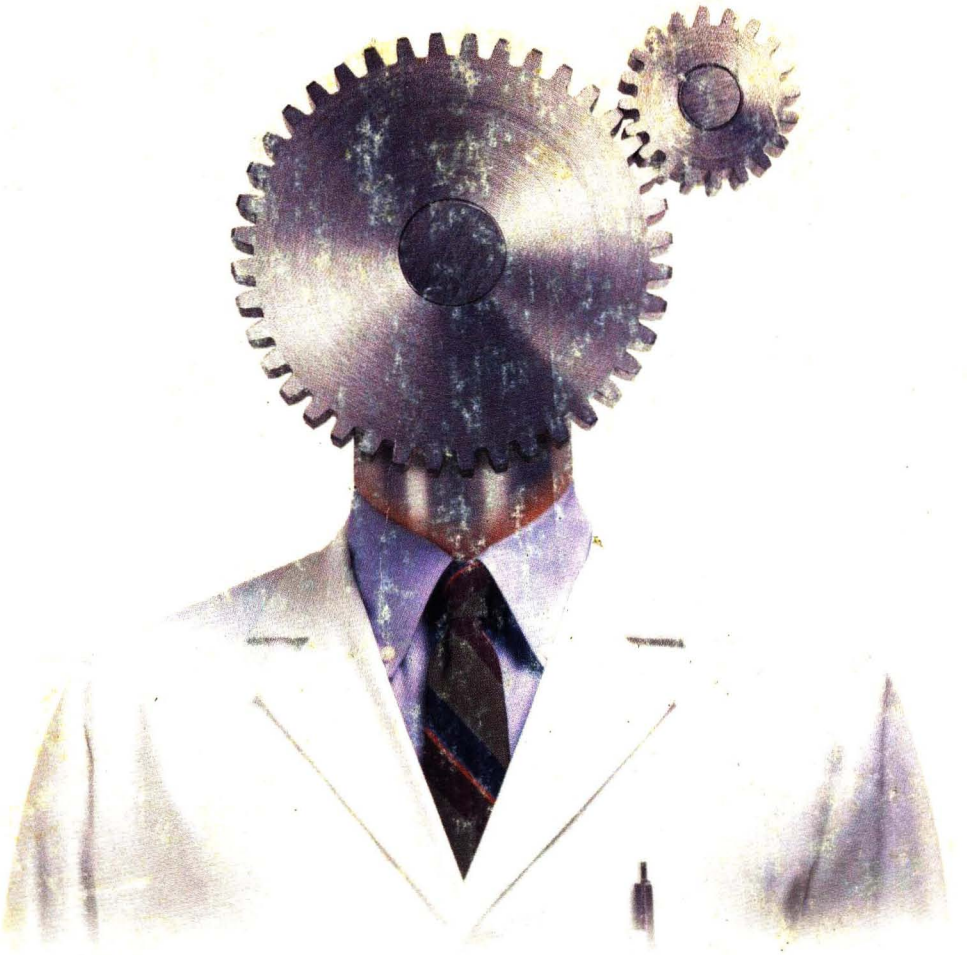

There's more to our CE autosampler than automation.

On the new Model 270A-HT High Throughput Capillary Electrophoresis System, a unique sample cooling system minimizes sample degradation. Our special design eliminates evaporation. Ion replenishment can be fully automated with the multiple buffer system. The software makes it easy to custom-tailor analysis parameters to each sample...Whether you need unattended overnight operation on 50 samples or just a few, optimal performance is ensured. The Model 270A-HT High Throughput Capillary Electrophoresis System. Higher sensitivity, greater reliability and more performance than ever. Contact Applied Biosystems today.

Applied Biosyste

Foster City, U.S.A. Tel: (415) 570-6667. Telex: 470052 APBIO UI. Fax: (415) 572-2743.
Mississauga, Canada. Tel: (416) 821-8183. Fax: (416) 821-8246.
Warrington, U.K. Tel: 0925-825650. Telex: 629611 APBIO G. Fax: 0925-828196.
Weiterstadt, Germany. Tel: 06151-87940. Telex: 4197318 Z ABI D. Fax: 06151-84899.
Paris, France. Tel: (1) 48 63 24 44. Telex: 230458 ABIF. Fax: (1) 48 63 22 82.
Milan, Italy. Tel: (0)2 89404561. Fax: (0)2 8321655.
Maarssen, The Netherlands. Tel: (0) 3465-74868. Telex: 70896. Fax: (0) 3465-74904.
Burwood, Australia. Tel: (03) 808-7777. Fax: (03) 887-1469.
Tokyo, Japan. Tel: (03) 699-0700. Fax: (03) 699-0733.